

**ANTIPLASMODIAL AND ANTIOXIDANT ALKALOIDS
FROM TWO LAURACEAE SPECIES, *ALSEODAPHNE
CORNERI* AND *DEHAASIA LONGIPEDICELLATA*, AND
THE ACID DISSOCIATION CONSTANT OF SELECTED
BIOACTIVE ALKALOIDS**

AZEANA ZAHARI

**FACULTY OF SCIENCE
UNIVERSITY OF MALAYA
KUALA LUMPUR**

2016

**ANTIPLASMODIAL AND ANTIOXIDANT ALKALOIDS
FROM TWO LAURACEAE SPECIES, *ALSEODAPHNE
CORNERI* AND *DEHAASIA LONGIPEDICELLATA*, AND
THE ACID DISSOCIATION CONSTANT OF SELECTED
BIOACTIVE ALKALOIDS**

AZEANA ZAHARI

**THESIS SUBMITTED IN FULFILMENT OF THE
REQUIREMENTS FOR THE DEGREE OF
DOCTOR OF PHILOSOPHY**

**FACULTY OF SCIENCE
UNIVERSITY OF MALAYA
KUALA LUMPUR**

2016

ABSTRACT

Preliminary survey of crude extracts of two Lauraceae species possessed potent antiplasmodial activities; *Dehaasia longipedicellata* (IC₅₀=1.30 µg/mL), and *Alseodaphne corneri* (IC₅₀=2.78 µg/ml). Twenty two compounds were successfully isolated and purified using extensive chromatography techniques. Purification of all alkaloids from crude extract of *Alseodaphne corneri* yielded sixteen alkaloids; reticuline **8**, gyrolidine **18**, 3', 4'-dihydronorstephasubine **19**, norstephasubine **20**, *N*-methyllaurotetanine **26**, laurotetanine **27**, isocorydine **41**, norisocorydine **42**, thalrugosine **71**, *O*-methyllimacusine **118**, 2-norobaberine **115**, 3', 4'-dihydropstephasubine **119**, stephasubine **120**, stephasubimine **121**, *N*-methyllindcarpine **123**, and one new compound; cornerin A **124**, while, *Dehaasia longipedicellata* afforded eight alkaloids namely; reticuline **8**, laurotetanine **27**, norboldine **36**, boldine **37**, sinoacutine **29**, milonine **46**, sebiferine **47**, and *O-O*-dimethylgrisabine **48**. The structural elucidation of all the alkaloids were done by using spectroscopic techniques such as 1D-NMR (¹H, ¹³C, DEPT), 2D-NMR (COSY, NOESY, HMQC, HMBC), UV, IR, MS and by comparison with the literature data. All compounds with sufficient amount (**8**, **18**, **20**, **27**, **36**, **37**, **41**, **42**, **46**, **47**, **48**, **115**, **118**, **120**) were tested for antiplasmodial and antioxidant activities. As a result, norstephasubine **20** (0.116 µM), *O-O*-dimethylgrisabine **48** (0.031 µM) and laurotetanine **27** (0.189 µM) showed potent antiplasmodial activities. **48** had a higher potency with a lower IC₅₀ value compared to the antimalarial drug, chloroquine, 0.090 µM. Antioxidant properties of a drug are beneficial to the host (human) as it could help as an additive therapy to reduce the side effects of malaria disease. Thus, these alkaloids have also been tested for their antioxidant activities using DPPH, FRAP and metal chelating assay. **48** showed the highest scavenging activity with an IC₅₀ value of 28.75 µM when compared to the standard, BHA (77.73 µM). Furthermore, the most potent alkaloid, **48** apart from being potent antiplasmodial and antioxidant agents, is also not toxic towards normal pancreatic cell line, which makes it a good candidate for the drug development of malarial compounds. Three of the bioactive and highest yield alkaloids; **37**, **41** and **42**, were studied for acid dissociation constant using UV-vis spectrophotometry. The *pK_a* values of isocorydine **41** and norisocorydine **42** were 11.75 and 12.11, respectively. Meanwhile, boldine **37** gave two *pK_a* values of 9.12 and 10.44. The *pK_a* values of all alkaloids were stable at physiological pH; thereby all of them will not ionize at physiological pH, thus permitting the basic nitrogen to be protonated and accumulated within the parasite acidic food vacuole of *Plasmodium* via pH trapping. Acidic food vacuoles that have been neutralized by alkaloids would result in the enhancement of the antiplasmodial activity. Interestingly, these alkaloids also possessed antioxidant activities that might prevent oxidative damage to the host by binding to free heme and neutralizing the electrons produced during the *P. falciparum* mediated haemoglobin destruction in the host. Based on pharmacodynamics and pharmacokinetic characteristics, it is noteworthy that slightly basic properties of the aforementioned alkaloids, along with their antioxidant activities are advantageous in improving the suppression of malaria infection that cause less damage to the host.

ABSTRAK

Kajian awal ekstrak pokok telah menunjukkan dua spesies Lauraceae mempunyai aktiviti antiplasmodial yang bagus; *Dehaasia longipedicellata* ($IC_{50}=1.30 \mu\text{g/mL}$), dan *Alseodaphne corneri* ($IC_{50}=2.78 \mu\text{g/ml}$). Dua puluh dua sebatian alkaloid telah berjaya diasingkan dan dituliskan menggunakan pelbagai teknik kromatografi. Penulenan semua alkaloid dari ekstrak *Alseodaphne corneri* menghasilkan enam belas alkaloid. Alkaloid itu terdiri daripada; girolidina **18**, 3', 4'-dihydonorstephasubina **69**, norstephasubina **20**, *N*-metillaurotetanina **26**, laurotetanina **27**, norboldina **36**, boldina **37**, isokoridina **41**, norisokoridina **42**, thalrugosina **71**, *O*-metillimakusina **118**, 2-norobaberina **115**, 3', 4'-dihydo-stephasubina **119**, stephasubina **120**, stephasubimina **121**, *N*-metillindkarpina **123** dan sebatian baru; cornerin A **124**, manakala, *Dehaasia longipedicellata* menghasilkan lapan alkaloid iaitu; retikulina **58**, norboldina **36**, boldina **37**, sinoakutina **29**, milonina **46**, sebiferina **47**, dan *O,O*-dimethylgrisabina **48**. Penentuan struktur organik semua alkaloid telah dikenalpastikan dengan menggunakan teknik-teknik spektroskopi seperti 1D-NMR (^1H , ^{13}C , DEPT), 2D-NMR (COSY, NOESY, HMQC, HMBC), UV, IR, MS dan perbandingan dengan kajian-kajian terdahulu. Semua sebatian yang mempunyai jumlah yang mencukupi (**8**, **18**, **20**, **27**, **36**, **37**, **41**, **42**, **46**, **47**, **48**, **115**, **118**, **120**) telah diuji untuk aktiviti antiplasmodial dan antioksidan. Hasil kajian mendapati norstephasubina **20** ($0.116 \mu\text{M}$), *O,O*-dimetilgrisabina **48** ($0.031 \mu\text{M}$) dan laurotetanina **27** ($0.189 \mu\text{M}$) menunjukkan potensi yang bagus untuk aktiviti antiplasmodial. **48** mempunyai potensi yang lebih tinggi dengan nilai IC_{50} yang lebih rendah berbanding dengan ubat anti malaria, chlorokuina, $0.090 \mu\text{M}$. Ciri-ciri antioksidan memberi manfaat kepada tuan rumah (manusia) kerana ia boleh membantu sebagai terapi tambahan untuk mengurangkan kesan-kesan sampingan penyakit malaria. Oleh itu, alkaloid ini juga telah diuji untuk aktiviti antioksidan dengan menggunakan DPPH, FRAP dan esei logam pengikatan. **48** menunjukkan aktiviti memerangkap tertinggi dengan nilai IC_{50} $28.75 \mu\text{M}$ berbanding dengan piawaian, BHA ($77.73 \mu\text{M}$). Menariknya, keputusan menunjukkan hubungan yang positif antara aktiviti antiplasmodial dan antioksidan untuk semua alkaloid. Tambahan pula, alkaloid yang paling aktif, **48** selain daripada menjadi ejen antiplasmodial dan antioksidan, ia juga tidak toksik kepada sel pankreas biasa, yang menjadikan ia struktur yang terbaik untuk pembangunan ubat-ubatan malaria. Tiga daripada bioaktif dan kadar kuantiti alkaloid yang banyak; **37**, **41** dan **42** telah dikaji untuk pemalar penceraian asid menggunakan UV-vis spektrofotometri. Nilai pK_a bagi isokoridina **41** dan norisokoridina **42** adalah masing-masing 11.75 dan 12.11. Manakala, boldina **37** memberikan dua nilai pK_a ; 9.12 dan 10.44. Nilai pK_a semua alkaloid adalah stabil pada pH fisiologi; dengan itu semua alkaloid tidak akan mengion pada pH fisiologi dan seterusnya membenarkan nitrogen berbes untuk pemindahan proton dan terkumpul dalam *Plasmodium* vakuol makanan berasid melalui pH memerangkap. Vakuol makanan berasid yang telah dineutralkan oleh alkaloid akan menyebabkan peningkatan aktiviti antiplasmodial. Ciri-ciri antioksidan alkaloid dalam kajian menunjukkan bahawa sebagai tambahan kepada aktiviti antiplasmodial, alkaloid juga mungkin menghalang kerosakan oksidatif. Ia boleh dihalang dengan mengikat heme bebas dan meneutralkan elektron yang dihasilkan semasa *P. falciparum* menjadi pengantara kepada pemusnahan hemoglobin dalam perumah. Berdasarkan ciri-ciri farmakodinamik dan farmakokinetik, ia perlu diberi perhatian bahawa ciri-ciri alkaloid yang berbes seperti yang dinyatakan di atas, bersama-sama dengan aktiviti antioksidan adalah bermanfaat dalam meningkatkan perencatan jangkitan malaria yang menyebabkan kurang kerosakan kepada perumah.

ACKNOWLEDGEMENTS

In the name of Allah, most Gracious, most Merciful. Firstly, I would like to thank my supervisors; Professor Khalijah Awang and Professor Mohammad Niyaz Khan for their dedication and supervision throughout my study. Respectable Professor Khalijah Awang, thanks for accepted me to be under your supervision, you have an amazing knowledge of chemistry and your passion in this field is admirable. You have taught me much more than just chemistry; I have acquired many skills needed to grow as a chemist by just observing your working attitudes and listening to your guidance. I wish to forward my greatest appreciation to Professor Niyaz for his patience, guidance throughout new field area that I have to learn to complete my knowledge.

My appreciation extended to my friends for making my study such an enjoyable time in phytochemistry laboratory; Nurul, Momo, Joey, Pae, Fadzli, Chong, Hazrina, Dewi, Norsita, Aimi, Aza, Hafiz, Maryam, Azrul, Aqmal, Rosalind, Azmi, Julia, linda, Umar, Ahmad, Arshia, Tien, Shelly, Noridayu, Ayu, Dr Jamal, Dr Yasodha and others for their kind help, support and friendship.

I also would like to thank herbarium staffs; Mr. Pok din, Mr. Teo, Mr. Ujang, and Mr. Rafly for their sample collection, the NMR and GC-MS staffs; Mr. Nordin, Ms Norzalida, Mrs. Fiona, Mr. Fateh and Mr. Siew for recording the spectra. Without their helps, this research work could not be completed.

I would like to dedicate this thesis to my late mum Nor Azaliah Ishak, father and all my family members for your supports and encouragement over the past years. I also would like to thank to my husband Ibrahim Ramli for your support and patience during my study. Last but not least I would like to thank my incredible late supervisor Professor Madya Dr Mat Ropi Mukhtar for all his guidance throughout my beginning journey in the chemistry field.

TABLE OF CONTENTS

Abstract	iii
Abstrak	iv
Acknowledgements	v
Table of Contents	vi
List of Schemes	x
List of Figures	xi
List of Tables.....	xv
Abbreviations	xvii
List of Appendices	xx
CHAPTER 1: INTRODUCTION.....	1
1.1 General	1
1.2 Lauraceae: Morphology and Distribution.	3
1.3 Classification of the Lauraceae	4
1.4 Botany and Morphology of <i>Alseodaphne</i> and <i>Dehaasia</i>	5
1.5 <i>Alseodaphne corneri</i> Kosterm.....	6
1.6 <i>Dehaasia longipedicellata</i> (Ridl.) Kosterm	8
1.7 Medicinal Uses of the Lauraceae	9
1.8 Objectives of the Study	11
CHAPTER 2: GENERAL CHEMICAL ASPECTS.....	12
2.1 Alkaloid	12
2.2 Alkaloid Classification	12
2.3 Alkaloids from the Lauraceae	19
2.4 Alkaloids from the Genus <i>Alseodaphne</i>	19
2.5 Alkaloids from the Genus <i>Dehaasia</i>	22
2.6 Biosynthesis of Isoquinoline Alkaloids.....	33
2.6.1 Benzyloisoquinolines	37
2.6.2 Bisbenzyloisoquinolines	37
2.6.3 Morphinanandienones	42

2.6.4	Aporphines	45
2.7	Structural Elucidation of Alkaloids	46
2.7.1	Benzyloisoquinoline.....	46
2.7.2	Bisbenzyloisoquinolines	49
2.7.3	Morphinanandienones	57
2.7.4	Aporphines	59
2.8	Pharmacological Importance of Isoquinoline Alkaloids	63
2.8.1	Benzyloisoquinolines	63
2.8.2	Bisbenzyloisoquinolines	64
2.8.3	Morphinanandienones	65
2.8.4	Aporphines	65
CHAPTER 3: RESULTS AND DISCUSSION		66
3.1	General	66
3.1.1	Reticuline 8	69
3.1.2	2-Norobaberine 115	78
3.1.3	Gyrolidine 18	89
3.1.4	<i>O</i> -methyllimacusine 118	95
3.1.5	3', 4'-Dihydronorstephasubine 19	101
3.1.6	3', 4'-Dihydrostephasubine 119.....	107
3.1.7	Norstephasubine 20.....	112
3.1.8	Stephasubine 120	117
3.1.9	Stephasubimine 121	122
3.1.10	Thalrugosine 71.....	127
3.1.11	Isocorydine 41	136
3.1.12	Norisocorydine 42.....	144
3.1.13	<i>N</i> -methyl lindcarpine 123.....	148
3.1.14	<i>N</i> -methyllaurotetanine 26.....	152
3.1.15	Laurotetanine 27.....	160
3.1.16	Norboldine 36	165
3.1.17	Boldine 37	169
3.1.18	Milonine 46	173
3.1.19	Sinoacutine 29.....	181
3.1.20	Sebiferine 47	185

3.1.21	<i>O-O</i> -dimethylgrisabine 48	190
3.1.22	Cornerin A 124.....	196
CHAPTER 4: BIOACTIVITY		206
4.1	Introduction	206
4.2	Life Cycle of Malaria	208
4.3	Oxidative Stress.....	210
4.4	Drugs Used in the Malaria Treatment	211
4.5	Antiplasmodial Activities.....	214
4.5.1	Antiplasmodial Assay	214
4.5.2	Results	215
4.6	Antioxidant Activities	216
4.6.1	DPPH	217
4.6.2	Ferric Reducing Antioxidant Power Assay (FRAP).....	218
4.6.3	Metal Chelating Activity Assay	218
4.6.4	Results.....	220
4.7	Cytotoxic Activities.....	221
4.7.1	Cytotoxic Assay	221
4.7.2	Results.....	222
4.8	Discussion	223
CHAPTER 5: ACID-BASE EQUILIBRIA		225
5.1	Introduction	225
5.2	Experimental	228
5.2.1	Reagents and Materials	228
5.2.2	Instrumentation	229
5.2.3	pH Measurement	229
5.2.4	Acid and Bases	230
5.2.5	Determination of Acidity Constants	231
5.2.6	Temperature Variation and Acid Base Equilibria.....	232
5.3	Results	233
5.3.1	Acid Dissociation Equilibria.....	233
5.3.2	Electronic Spectra	234
5.4	Discussion	241

CHAPTER 6: CONCLUSION.....	243
6.1 Future work	245
CHAPTER 7: EXPERIMENTAL	246
7.1 Plant Material	246
7.2 Instrumentation.....	246
7.3 Solvent.....	247
7.4 Chromatography.....	247
7.4.1 Thin Layer Chromatography (TLC)	247
7.4.2 Column Chromatography (CC).....	247
7.4.3 Preparative Thin Layer Chromatography (PTLC).....	248
7.4.4 Recycle High Performance Liquid Chromatography (RHPLC).....	248
7.4.5 High Performance Liquid Chromatography (HPLC).....	248
7.5 Reagents	248
7.5.1 Mayer's Reagent (Potassium Mercuric Iodide)	249
7.5.2 Dragendorff's Reagent (Potassium Bismuth Iodide)	249
7.6 Extraction of the Bark	249
7.7 Extraction of the Leaves.....	250
7.8 Isolation and Purification	250
7.9 Physical and Spectral Data of the Isolated Compounds.....	261
References	269
List of Publications and Papers Presented	286
Appendix.....	288

LIST OF SCHEMES

Scheme 1.1 : Classification of Genera	4
Scheme 2.1 : Proposed Biosynthesis of BIQ and BBIQ from Tyrosine Amino Acid ...	34
Scheme 2.2 : Proposed Biosynthesis of Various Alkaloids from (<i>S</i>)-Reticuline.....	36
Scheme 2.3 : Proposed Biosynthesis of Bisbenzylisoquinolines	41
Scheme 2.4 : Proposed Biosynthesis of Sinoacutine 29 and Salutaridine 100	43
Scheme 2.5 : Proposed Biosynthesis of Morphinan Alkaloid	44
Scheme 2.6 : Proposed Biogenesis of Aporphine	46
Scheme 2.7 : Proposed Fragmentation Pattern of Benzylisoquinoline	49
Scheme 2.8 : Proposed Mass Fragmentation of Type I Bisbenzylisoquinolines	55
Scheme 2.9 : Proposed Mass Fragmentation of Type VI Bisbenzylisoquinolines	56
Scheme 2.10: Proposed Mass Fragmentation of Type VIII Bisbenzylisoquinolines	56
Scheme 2.11: Proposed Mass Fragmentation Pattern of an Aporphines	62
Scheme 7.1 : Isolation of Alkaloids from the Leaves of <i>Alseodaphne corneri</i> Kosterm.	255
Scheme 7.2 : Isolation of Alkaloids from the Bark of <i>Alseodaphne corneri</i> Kosterm.	256
Scheme 7.3 : Isolation of Alkaloids from the Leaves of <i>Dehaasia longipedicellata</i> ..	257
Scheme 7.4 : Isolation of Alkaloids from the Bark of <i>Dehaasia longipedicellata</i>	258

LIST OF FIGURES

Figure 1.1 : <i>Alseodaphne corneri</i> Kosterm	7
Figure 1.2 : <i>Dehaasia longipedicellata</i> (Ridl.) Kosterm	8
Figure 2.1 : Alkaloids Isolated from the Genus <i>Alseodaphne</i> and <i>Dehaasia</i>	32
Figure 2.2 : The Circulation of the π - electrons around a Benzene Ring Produces a Magnetic Field: Deshielding (A) and Shielding (B) Zones around the Benzene Ring.....	60
Figure 3.1 : ^1H - ^{13}C Correlations Observed in the HMBC spectrum of Reticuline 8	71
Figure 3.2 : LCMS Spectrum of Reticuline 8	72
Figure 3.3 : ^1H NMR Spectrum of Reticuline 8	73
Figure 3.4 : ^{13}C NMR Spectrum of Reticuline 8	74
Figure 3.5 : COSY Spectrum of Reticuline 8	75
Figure 3.6 : HSQC Spectrum of Reticuline 8	76
Figure 3.7 : HMBC Spectrum of Reticuline 8	77
Figure 3.8 : ^1H NMR and HMBC Correlations of (+)-2-norobaberine 115 and (+)-2'-norobaberine 116	81
Figure 3.9 : LCMS Spectrum of 2-norobaberine 115	83
Figure 3.10: ^1H NMR Spectrum of 2-norobaberine 115	84
Figure 3.11: ^{13}C NMR Spectrum of 2-norobaberine 115	85
Figure 3.12: COSY Spectrum of 2-norobaberine 115	86
Figure 3.13: HSQC Spectrum of 2-norobaberine 115	87
Figure 3.14: HMBC Spectrum of 2-norobaberine 115	88
Figure 3.15: ^1H NMR and HMBC Correlations of (-)-Gyrolidine 18 , (+)-Obaberine 62 and (-)-Gyrocarpine 117	91
Figure 3.16: ^1H NMR Spectrum of Gyrolidine 18	93
Figure 3.17: ^{13}C NMR Spectrum of Gyrolidine 18	94
Figure 3.18: ^1H NMR Spectrum of <i>O</i> -methyllimacusine 118	98
Figure 3.19: ^{13}C NMR Spectrum of <i>O</i> -methyllimacusine 118	99
Figure 3.20 NOESY Spectrum of <i>O</i> -methyllimacusine 118	100
Figure 3.21: ^1H NMR and HMBC Correlations of (+) - 3', 4'- dihydronorstephasubine 19 and Pangkorimine 69	103
Figure 3.22: ^1H NMR Spectrum of 3',4'-dihydronorstephasubine 19	105
Figure 3.23: ^{13}C NMR Spectrum of 3',4'-dihydronorstephasubine 19	106
Figure 3.24: ^1H NMR and HMBC Correlations of (+)-3', 4'-dihydrostephasubine 119	108
Figure 3.25: ^1H NMR Spectrum of 3',4'-dihydrostephasubine 119	110
Figure 3.26: ^{13}C NMR Spectrum of 3',4'-dihydrostephasubine 119	111
Figure 3.27: ^1H NMR Spectrum of Norstephasubine 20	115

Figure 3.28: ^{13}C NMR Spectrum of Norstephasubine 20	116
Figure 3.29: ^1H NMR and HMBC Correlations of (+)-Stephasubine 120	118
Figure 3.30: ^1H NMR Spectrum of Stephasubine 120	120
Figure 3.31: ^{13}C NMR Spectrum (inset: DEPT spectrum) of Stephasubine 120	121
Figure 3.32: ^1H NMR and HMBC Correlations of Stephasubimine 121	123
Figure 3.33: ^1H NMR Spectrum of Stephasubimine 121	125
Figure 3.34: ^{13}C NMR Spectrum of Stephasubimine 121	126
Figure 3.35: ^1H NMR and HMBC Correlations of (+)-Thalrugosine 71 and (-)- Limacine 122	129
Figure 3.36: ^1H NMR Spectrum of Thalrugosine 71	131
Figure 3.37: ^{13}C NMR Spectrum of Thalrugosine 71	132
Figure 3.38: COSY Spectrum of Thalrugosine 71	133
Figure 3.39: HSQC Spectrum of Thalrugosine 71	134
Figure 3.40: HMBC Spectrum of Thalrugosine 71	135
Figure 3.41: ^1H - ^{13}C Correlations Observed in HMBC Spectrum of isocorydine 41	137
Figure 3.42: HREIMS Spectrum of Isocorydine 41	139
Figure 3.43: ^1H NMR Spectrum of Isocorydine 41	140
Figure 3.44: ^{13}C NMR Spectrum of Isocorydine 41	141
Figure 3.45: HSQC Spectrum of Isocorydine 41	142
Figure 3.46: HMBC Spectrum of Isocorydine 41	143
Figure 3.47: ^1H - ^{13}C Correlations Observed in HMBC Spectrum of Norisocorydine 42	145
Figure 3.48: ^1H NMR Spectrum of Norisocorydine 42	146
Figure 3.49: ^{13}C NMR Spectrum of Norisocorydine 42	147
Figure 3.50: ^1H NMR Spectrum of <i>N</i> -methyllindcarpine 123	150
Figure 3.51: ^{13}C NMR Spectrum of <i>N</i> -methyllindcarpine 123	151
Figure 3.52: HREIMS Spectrum of <i>N</i> -methyllaurotetanine 26	155
Figure 3.53: ^1H NMR Spectrum of <i>N</i> -methyllaurotetanine 26	156
Figure 3.54: ^{13}C NMR Spectrum of <i>N</i> -methyllaurotetanine 26	157
Figure 3.55: HSQC Spectrum of <i>N</i> -methyllaurotetanine 26	158
Figure 3.56: HMBC Spectrum of <i>N</i> -methyllaurotetanine 26	159
Figure 3.57: ^1H - ^{13}C Correlations Observed in HMBC Spectrum of Laurotetanine 27	161
Figure 3.58: ^1H NMR Spectrum of Laurotetanine 27	163
Figure 3.59: ^{13}C NMR Spectrum of Laurotetanine 27	164
Figure 3.60: ^1H NMR Spectrum of Norboldine 36	167
Figure 3.61: ^{13}C NMR Spectrum of Norboldine 36	168
Figure 3.62: ^1H NMR Spectrum of Boldine 37	171
Figure 3.63: ^{13}C NMR Spectrum of Boldine 37	172

Figure 3.64: ^1H - ^{13}C Correlations Observed in HMBC Spectrum of Milonine 46	175
Figure 3.65: IR Spectrum of Milonine 46	176
Figure 3.66: ^1H NMR Spectrum of Milonine 46	177
Figure 3.67: DEPT NMR Spectrum of Milonine 46	178
Figure 3.68: COSY Spectrum of Milonine 46	179
Figure 3.69: HMBC Spectrum of Milonine 46	180
Figure 3.70: NOESY Correlation of Sinoacutine 29	182
Figure 3.71: ^1H NMR Spectrum of Sinoacutine 29	183
Figure 3.72: ^{13}C NMR Spectrum of Sinoacutine 29	184
Figure 3.73: ^1H NMR Spectrum of Sebiferine 47	188
Figure 3.74: ^{13}C NMR Spectrum of Sebiferine 47	189
Figure 3.75: ^1H NMR Spectrum of <i>O-O</i> -dimethylgrisabine 48	193
Figure 3.76: ^{13}C NMR Spectrum of <i>O-O</i> -dimethylgrisabine 48	194
Figure 3.77: COSY Spectrum of <i>O-O</i> -dimethylgrisabine 48	195
Figure 3.78: EIMS Spectrum of Cornerin A 124	199
Figure 3.79: Infrared Spectrum of Cornerin A 124	200
Figure 3.80: ^1H NMR Spectrum of Cornerin A 124	201
Figure 3.81: ^{13}C NMR Spectrum of Cornerin A 124	202
Figure 3.82: NOESY Spectrum of Cornerin A 124	203
Figure 3.83: HSQC Spectrum of Cornerin A 124	204
Figure 3.84: HMBC Spectrum of Cornerin A 124	205
Figure 4.1 : Vector-borne Disease from Mosquito.	206
Figure 4.2 : Percentage of Malaria Based on <i>Plasmodium</i> Parasite, 2004-2013.	208
Figure 4.3 : Life Cycle of Malaria Transmission (Malaria, 2015).....	209
Figure 4.4 : Structures Natural/ Naturally Derived Compounds from Plants Discovered in Antimalarial Drug Research.....	212
Figure 5.1 : Structure of Drugs Consist of Nitrogen Atom and Phenolic Function.....	225
Figure 5.2 : General Acid-base Equilibria for Boldine 37	233
Figure 5.3 : General Acid-base Equilibria for Isocorydine 41 , Norisocorydine 42	234
Figure 5.4 : The UV Absorption of 2×10^{-4} M Isocorydine 41 (blue), Norisocorydine 42 (red), Boldine 37 (green) in Acetonitrile.	234
Figure 5.5 : The UV Absorption Spectra of 2×10^{-4} M Isocorydine 41 in 2% v/v Acetonitrile at pH 1-13.5. Inset Shows the pH-dependence of the Absorbance at 338 nm.	236
Figure 5.6 : The UV Absorption Spectra of 2×10^{-4} M Norisocorydine 42 in 2% v/v Acetonitrile at pH 1-13.5. Inset Shows the pH-dependence of the Absorbance at 338 nm.	236

Figure 5.7 : The UV absorption Spectra of 2×10^{-4} M Boldine 37 in 2% v/v Acetonitrile at pH 1-13.5. Inset Shows the pH-dependence of the Absorbance at 295 and 332 nm.	237
Figure 5.8 : Graph of pK_a of Norisocorydine 42 (2×10^{-4} M) in Water/acetonitrile, $I = 0.1$ M (NaCl) versus Different Temperature 30- 50 °C	240
Figure 5.9 : The UV Absorption Spectra of 2×10^{-4} M Norisocorydine 42 in 2% v/v Acetonitrile at pH 12.0 for Different Temperature 30- 50 °C.	241
Figure 7.1 :HPLC Chromatogram of Fraction 61-140 from <i>D. longipedicellata</i> for Norboldine 36	252
Figure 7.2 : RHPLC Chromatogram of Fraction from <i>A. corneri</i> for A (Gyrolidine 18) and B (Stephasubimine 121).....	253

University of Malaya

LIST OF TABLES

Table 1.1 : <i>Alseodaphne</i> Species Found in Malaysia.....	6
Table 1.2 : <i>Dehaasia</i> Species Found in Malaysia	6
Table 1.3 : Selected Vegetative Characters of <i>Alseodaphne</i> and <i>Dehaasia</i>	6
Table 2.1 : Main Types of Alkaloids and Their Chemical Groups.....	14
Table 2.2 : Alkaloids from the Genus <i>Alseodaphne</i> and Their Biological Activities....	20
Table 2.3 : Alkaloids from the Genus <i>Dehaasia</i> and Their Biological Activities	22
Table 2.4 : General Chemical Shifts of the ^1H and ^{13}C NMR Spectral Data of BIQ.....	48
Table 2.5 : General Chemical Shifts of the ^1H and ^{13}C NMR Spectral Data of BBIQ..	53
Table 2.6 : General Chemical Shifts of the ^1H and ^{13}C NMR of Morphinanandienones	58
Table 2.7 : ^1H and ^{13}C NMR Data (δ) of Aporphine Alkaloids in CDCl_3	61
Table 2.8 : Ultraviolet Spectroscopy of Aporphine Type Alkaloids.	63
Table 3.1 : The Alkaloids Isolated from <i>Alseodaphne corneri</i> and <i>Dehaasia longipedicellata</i>	67
Table 3.2 : ^1H and ^{13}C -NMR Data of Reticuline 8 in CDCl_3	71
Table 3.3 : ^1H , ^{13}C -NMR and HMBC Data of 2-norobaberine 115	82
Table 3.4 : ^1H , ^{13}C -NMR and HMBC Data of Gyrolidine 18	92
Table 3.5 : ^1H , ^{13}C -NMR and HMBC Data of <i>O</i> -methyllimacusine 118	97
Table 3.6 : ^1H , ^{13}C -NMR and HMBC Data of 3',4'-dihydronorstephasubine 19	104
Table 3.7 : ^1H and ^{13}C -NMR Data of 3',4'-dihydrostephasubine 119	109
Table 3.8 : ^1H , ^{13}C -NMR and HMBC Data of Norstephasubine 20	114
Table 3.9 : ^1H and ^{13}C -NMR Data of Stepasubine 120	119
Table 3.10: ^1H , ^{13}C -NMR and HMBC Data of Stepasubimine 121	124
Table 3.11: ^1H and ^{13}C -NMR Data of Thalrugosine 71	130
Table 3.12: ^1H and ^{13}C -NMR Data of Isocorydine 41	138
Table 3.13: ^1H and ^{13}C -NMR Data of Norisocorydine 42	145
Table 3.14: ^1H and ^{13}C -NMR Data of <i>N</i> -methyllindcarpine 123	149
Table 3.15: ^1H , ^{13}C -NMR and HMBC Data of <i>N</i> Me-laurotetanine 26	154
Table 3.16: ^1H , ^{13}C -NMR and HMBC Data of Laurotetanine 27	162
Table 3.17: ^1H and ^{13}C -NMR Data of Norboldine 36	166
Table 3.18: ^1H and ^{13}C -NMR Data of Boldine 37	170
Table 3.19: ^1H and ^{13}C -NMR Data of Milonine 46	175
Table 3.20: ^1H and ^{13}C -NMR Data of Sinoacutine 29	182
Table 3.21: ^1H and ^{13}C -NMR Data of Sebiferine 47	187
Table 3.22: ^1H and ^{13}C -NMR Data of <i>O</i> - <i>O</i> -dimethylgrisabine 48	192
Table 3.23: ^1H , ^{13}C -NMR and HMBC Data of Cornerin A 124	198

Table 4.1 : Antiplasmodial Activities of Isolated Alkaloids.....	216
Table 4.2 : Antioxidant Activities of Isolated Alkaloids.	221
Table 4.3 : Cytotoxicity Activities of Isolated Alkaloids.	223
Table 5.1 : The List of Alkaloids Studied in Acid-base Equilibria.....	228
Table 5.2 : List of Chemicals Used in the Acid-base Equilibria.....	228
Table 5.3 : The List of Buffer Solution and its pH Range.	229
Table 5.4 : Values of Ionization Constant for Alkaloids 37 , 41 , 42 (2×10^{-4} M) in 2% v/v Acetonitrile, $I = 0.1$ M (NaCl), at 35°C.	239
Table 5.5 : Values of Ionization Constant for Norisocorydine 42 (2×10^{-4} M) in 2% v/v Acetonitrile, $I = 0.1$ M (NaCl), at 30- 50 °C.	240
Table 7.1 : Plant Species and Locality.....	246
Table 7.2 : Yield of Crude Extracted from Plants.....	250
Table 7.3 : Solvent Systems for the Isolation and Purification of CH ₂ Cl ₂ Crude Alkaloid.....	251
Table 7.4 : HPLC Solvent System of Fraction from <i>D. longipedicellata</i> for Norboldine 36	252
Table 7.5 : RHPLC Solvent System of Fraction from <i>A. corneri</i> for Gyrolidine 18 and Stephasubimine 122	252
Table 7.6 : List of Eluent and Fractions of Respective Alkaloids from the Leaves of <i>Alseodaphne corneri</i> Kosterm	259
Table 7.7 : List of Eluent and Fractions of Respective Alkaloids from the Bark of <i>Alseodaphne corneri</i> Kosterm	259
Table 7.8 : List of Eluent and Fractions of Respective Alkaloids from the Leaves of <i>Dehaasia longipedicellata</i>	260
Table 7.9 : List of Eluent and Fractions of Respective Alkaloids from the Bark of <i>Dehaasia longipedicellata</i>	260

ABBREVIATIONS

ACN	: Acetonitrile
BBIQ	: Bisbenzylisoquinoline
BHA	: Butylated hydroxyanisole
BHT	: Butylated hydroxytoluene
BIQ	: Benzylisoquinoline
Calcd.	: Calculated
CC	: Column chromatography
CDCl ₃	: Deuterated chloroform
CH	: Methine
CHCl ₃	: Chloroform
CH ₂	: Methylene
CH ₂ Cl ₂	: Dichloromethane
CH ₃	: Methyl group
CO ₂	: Carbon dioxide
COSY	: ¹ H- ¹ H correlation spectroscopy
<i>d</i>	: Doublet
<i>dd</i>	: Doublet of doublets
<i>ddd</i>	: Doublet of doublet of doublets
<i>dddd</i>	: Doublet of doublet of doublet of doublets
<i>ddt</i>	: Doublet of doublet of triplets
DEPT	: Distortion enhancement of polarisation transfer
DMSO	: Dimethyl sulfoxide
DPPH	: di(phenyl)-(2,4,6-trinitrophenyl)iminoazanium
EDTA	: Ethylenediaminetetraacetic acid

EIMS	:	Electron ionization mass spectroscopy
FA	:	Formic acid
FRAP	:	Ferric reducing power assay
GCMS	:	Gas chromatography mass spectrometry
H ₂ O ₂	:	Hydrogen peroxide
H ₂ SO ₄	:	Sulfuric acid
HCl	:	Hydrochloric acid
HMBC	:	Heteronuclear multiple bond coherence
HMQC	:	Heteronuclear multiple quantum coherence
HPLC	:	High-performance liquid chromatography
HRESIMS	:	High-resolution electrospray ionisation mass spectrometry
IC ₅₀	:	Concentration required to inhibit of 50 % activity
IR	:	Infrared
KCl	:	Potassium chloride
LCMS	:	Liquid chromatography mass spectrometry
LCMS-IT-TOF	:	Liquid chromatography mass spectrometry ion-trap and time-of-flight
<i>m</i>	:	Multiplet
MeOH	:	Methanol
MgSO ₄	:	Magnesium sulphate
MS	:	Mass Spectrometry
m/z	:	Mass/charge ratio
Na ₂ SO ₄	:	Sodium sulphate
NaCl	:	Sodium chloride
NMR	:	Nuclear magnetic resonance
NOESY	:	Nuclear overhauser effect spectroscopy

OCH ₃	:	Methoxyl group
OH	:	Hydroxyl group
PTLC	:	Preparative thin layer chromatography
R _f	:	Retention factor
rt	:	Room temperature
ROS	:	Reactive oxygen species
<i>s</i>	:	Singlet
SOD	:	Superoxide dismutase
<i>t</i>	:	Triplet
TLC	:	Thin layer chromatography
UV	:	Ultraviolet

University of Malaya

LIST OF APPENDICES

List of Publication and Paper Presented	286
Appendix A	288
Appendix B	321
Appendix C	335

University of Malaya

CHAPTER 1: INTRODUCTION

1.1 General

Tropical rainforest are the home of higher plants that produce most of the drugs we used nowadays. Rainforest plants are rich in secondary metabolites, particularly alkaloids. Only recently, we have gained precise knowledge about the chemical structures of interesting compounds present in the plants that exhibit medicinal properties. In spite of the large diversity of higher plants with 250,000 species that exist to date, only 12% of these species have been screened for medicinal use (Cordell, 2014; Sarker et al., 2007). Thus, the biological studies of natural compounds are in great demand. It is bonus to evaluate the different types of biological activities of these compounds and to study the relationship as to whether it acts in synergy or neutralize the side effects of the disease. In developing countries, 80% of the population relies on traditional remedies for the treatment of illness (Bowsher et al., 2008). This can be seen by a totalled of 16 billion dollars in sales for the 8 top selling plant-derived drugs (Sarker et al., 2007).

In the modern world, vector-borne diseases still posed a great threat to human health. The impact of vector-borne diseases from mosquitos has killed millions of human beings every year. Malaria is one of the serious vector-borne diseases that people get after being bitten by the *Anopheles* mosquito that is infected with a parasite called *Plasmodium*. There are four different types of *Plasmodium* parasites (*P. falciparum*, *P. vivax*, *P. ovale*, and *P. malariae*) which affect humans. In 2013, World Health Organization (WHO) estimated 198 million malaria cases reported, with 584,000 deaths globally and it is endemic throughout tropical and subtropical countries (WHO, 2014). Among that, 3,850 cases were reported with 14 deaths in Malaysia for malaria infection transmitted by *Anopheles leucosphyrus* mosquitoes (William et al., 2013; Yusof et al.,

2014). Global warming could increase malaria by expanding the area in which the ambient temperature and climate conditions are suitable. This could lead to the resistance of common antimalarial drugs such as artemisinin-based monotherapies. Parasite resistance to artemisinin has now been detected in 4 countries: Cambodia, Myanmar, Thailand, and Vietnam (WHO, 2014). Thus, there is urgency for research to be done on new antimalarial drugs from natural resources.

The tropical rain forest of Malaysia is one of the 17-mega biodiversity countries in the world (Ali et al., 2013). In 2012, nearly 21.01 million hectares or 63% of Malaysia remains forested. Its forests are a unique natural heritage which has evolved over 130 million years, resulting in very rich flora and fauna (Environment, 2014). Approximately, 15,000 species of vascular plants are found abundantly in the forest of Malaysia. As a tropical rainforest, it lies within the equatorial zone with the temperature throughout Malaysia varying from 21.0 to 32.0 °C. The temperature and humidity of forest in Malaysia suitable for growing various sources of families plants such as Rubiaceae, Melicaceae, Apocynaceae and Lauraceae (Ong et al., 2009). The rich diversity of the plants produce vast array for chemical entities with different skeletal types for the evaluation of biological activities.

Lauraceae is one of the largest and important families of trees and shrubs throughout the Malaysian reserve forest. It consists of 2500-3000 species within 68 genera all over the world, while in Malaysia; there are 16 genera and 287 species (Custodio & Florencio da Veiga Junior, 2014; Julia et al., 2009; Ng, 1989). Among the 16 genera, *Alseodaphne* and *Dehaasia* have been studied in this investigation. Both genera are known to be rich in isoquinoline alkaloids that contain various interesting biological activities such as antihypertensive (Mukhtar et al., 2009) cytotoxic and antimicrobial (Parvin et al., 1988). However, very few phytochemical and biological activity studies

have been carried out until now. Hence, the investigation of the alkaloids from *A. corneri* Kosterm. and *D. longipedicellata* Ridl. as well as their biological activities; antiplasmodial and antioxidant together with the acid dissociation constant study were attempted.

1.2 Lauraceae: Morphology and Distribution.

The name of Lauraceae was derived from the prominent member, the Grecian laurel, *Laurus nobilis*. It was characterized by the presence of aromatic substances in the leaves, wood and fruits that smelt like resin, turpentine, citronella, cloves and cinnamon. (Corner, 1951; Thakur et al., 2012).

In Malaysia, the members of the Lauraceae are known as “*Medang*” or “*Tejur*” and grow either on lowlands or highlands. In the lowlands, they are typically small trees of the lower canopy, whereas in the highlands the Lauraceae becomes more abundant as they reach the top of the forest canopy. Therefore, the term “oaks laurels forest” is given to this vegetation which lies at 1200-1600 m that features the mountain of tropical Asia from the Himalayas to New Guinea (Corner, 1951).

The leaves of this family are simple, variously arranged but generally spiral, rarely opposite or sub opposite. It usually gives a spider web effect when closely set parallel veinlet between the main veins of the leaf. Most of them are evergreen, though seasonal in flowering and in the development of new leaves (Ridley, 1967).

The bark is usually very thick with yellowish brown to reddish brown colour. It is typically smooth, rarely tissues, scaly or dappled, often covered with large lenticels. The inner bark is also very thick with granular, mottled or laminated, followed by strong aromatic smell (Whitmore & Ng, 1989).

The flowers are small, regular with greenish white or yellow colour. It is pollinated predominantly by flies and beetles that are attracted by the smell which varies from sweetly fragrant to foul as rancid fat (Corner, 1951).

1.3 Classification of the Lauraceae

The classification of the Lauraceae is illustrated in the list below. The classification includes 68 genera which are found mainly in the Southeast Asia and Latin America (Sakurai et al., 2015; Thakur et al., 2012).

Kingdom: Plantae

Division: Magnoliophyta

Class: Magnoliopsida

Order: Laurales

Family: Lauraceae

Genera:

<i>Actinodaphne</i>	<i>Aiouea</i>	<i>Alseodaphne</i>	<i>Aniba</i>
<i>Apollonias</i>	<i>Aspidostemon</i>	<i>Beilschmiedia</i>	<i>Camphora</i>
<i>Caryodaphnopsis</i>	<i>Cassytha</i>	<i>Chlorocardium</i>	<i>Cinnadenia</i>
<i>Cinnamomum</i>	<i>Cryptocarya</i>	<i>Dehasia</i>	<i>Dicypellium</i>
<i>Dodecadenia</i>	<i>Endiandra</i>	<i>Endlicheria</i>	<i>Eusideroxylon</i>
<i>Gamanthera</i>	<i>Hufelandia</i>	<i>Hypodaphnis</i>	<i>Iteadaphne</i>
<i>Kubitzkia</i>	<i>Laurus</i>	<i>Licaria</i>	<i>Lindera</i>
<i>Litsea</i>	<i>Machilus</i>	<i>Malapoenna</i>	<i>Mespilodaphne</i>
<i>Mezilaurus</i>	<i>Misanteca</i>	<i>Mochinnodaphne</i>	<i>Mutisiopersea</i>
<i>Nectandra</i>	<i>Neocinnamomum</i>	<i>Neolitsea</i>	<i>Notaphoebe</i>
<i>Nothaphoebe</i>	<i>Ocotea</i>	<i>Oreodaphne</i>	<i>Paraia</i>
<i>Parrasassafras</i>	<i>Parthenoxylon</i>	<i>Persea</i>	<i>Phoebe</i>
<i>Phyllostemonodaphne</i>	<i>Pleurothyrium</i>	<i>Polyadenia</i>	<i>Potomeia</i>
<i>Potoxylon</i>	<i>Povedadaphne</i>	<i>Ravensara</i>	<i>Rhodostemonodaphne</i>
<i>Sassafras</i>	<i>Schauera</i>	<i>Sextonia</i>	<i>Sinopora</i>
<i>Sinosassafras</i>	<i>Syndiclis</i>	<i>Systemonodaphne</i>	<i>Tetranthera</i>
<i>Umbelluraria</i>	<i>Urbanodendron</i>	<i>Williamodendron</i>	<i>Yasunia</i>

Scheme 1.1: Classification of Genera

1.4 Botany and Morphology of *Alseodaphne* and *Dehaasia*

The genus *Alseodaphne* was first described by Nees in 1831 (Julia et al., 2009) and distributed in the tropical belt of Cambodia, China, Indonesia, Laos, Malaysia, Myanmar, Philippines, Sri Lanka, Thailand, Vietnam and India (Julia et al., 2009). It comprises 57 species throughout the tropical belt out of which 19 species (Table 1.1) are found only in Malaysia (Sakurai et al., 2015; Whitmore & Ng, 1989). The genus consists of small to medium sized trees of 5-35 meters in height in wet evergreen tropical forest. Most of the species are distributed in the lowlands and become more abundant as they reach the top layer of the canopy between 1200-1600 m in altitude (Thakur et al., 2012).

Dehaasia was founded by Blume in 1836 (Whitmore & Ng, 1989). It comprises about 38 species (Table 1.2), which are distributed in Burma, China, Thailand, and Indo-China, Malaysia to New Guinea. Out of these, 9 were reported from Malaysia (Sakurai et al., 2015; Whitmore & Ng, 1989). *Dehaasia* consist of small to medium sized trees with various names such as 'gajus hutan' or 'pekan' given by the Malays.

The *Alseodaphne* and *Dehaasia* genera are morphologically similar such as the non-perulate terminal vegetative buds and the leaves are pinnately veined and usually crowded at the end of the upright twig (Julia et al., 2009). Table 1.3 showed selected vegetative characteristic to distinguish between both genera. In this context, most of the *Alseodaphne* species can be distinguished from *Dehaasia* by combination of the respective characters: lateral flowers of the terminal cymes non-opposite (vs strictly opposite) and also the anther 4-locular (vs mostly 2-locular) (Whitmore & Ng, 1989). In addition, there are no traditional medicine usage have been reported from both species.

Table 1.1: *Alseodaphne* Species Found in Malaysia

Genus: <i>Alseodaphne</i>	
<i>A. albifrons</i>	<i>A. bancana</i>
<i>A. corneri</i>	<i>A. dura</i>
<i>A. foxiana</i>	<i>A. garciniicarpa</i>
<i>A. insignis</i>	<i>A. intermedia</i>
<i>A. macrantha</i>	<i>A. micrantha</i>
<i>A. nigrescens</i>	<i>A. oblanceolata</i>
<i>A. paludosa</i>	<i>A. peduncularis</i>
<i>A. pendulifolia</i>	<i>A. perakensis</i>
<i>A. ridleyi</i>	<i>A. rubrolignea</i>
<i>A. wrayi</i>	

Table 1.2: *Dehaasia* Species Found in Malaysia

Genus: <i>Dehaasia</i>	
<i>D. candolleana</i>	<i>D. cuneata</i>
<i>D. incrassata</i>	<i>D. lancifolia</i>
<i>D. longipedicellata</i>	<i>D. longipetiolata</i>
<i>D. pauciflora</i>	<i>D. polyneura</i>
<i>D. tomentosa</i>	

Table 1.3: Selected Vegetative Characters of *Alseodaphne* and *Dehaasia*

Character/species	<i>Alseodaphne</i>	<i>Dehaasia</i>
Terminal (bud)	Not or rarely perulate	Not perulate
Leaves (arrangement)	Alternate or sub opposite Usually crowded at the end of twig, sometimes not crowded	Alternate Crowded at the end of twig or rarely not crowded
Petiole		
Lateral flowers of terminal cymes	Not opposite	Strictly opposite
Relative length of inflorescence compared to leaves	Usually longer, rarely shorter or as long as leaves	Shorter or as long as leaves
Number of anther locules	4	2
Filaments		
Relative length	Usually shorter	Usually longer
Fruits		
Shape	Rounded, ellipsoid, oblong or obovate	Obovate, ellipsoid, oblong or rounded

1.5 *Alseodaphne corneri* Kosterm.

Alseodaphne corneri Kosterm (Figure 1.1) exists as small trees of about 6 m tall in height. Terminal buds are covered with 1 cm long scales. Their twigs are stout, grey with prominent leaf scars. Leaves are closely spirally arranged at the ends of the twigs with a stalk of about 3-4 cm in length, the blade is thickly leathery, obovate to elliptical

in shape with a size of between 28-52 × 12-16 cm. Inflorescence in particles clustered below the apical bud and axillaries up to 14 cm long, unbranched, smooth, greyish-green colour, bracts up to 8 mm long and persistent. The flowers are up to 14 mm long, perianth lobes equal, oblong and 5mm long. The fruit of this species are ellipsoid; up to 3×2 cm seated on very thick, rough, in the form of inverted cone 2-3 cm long pedicles with persistent perianth lobes (Ng, 1989).

It is worthy to note that only one biological activity has been carried out on this species and it was from our group (Mukhtar et al., 2009) which was on vasorelaxant assay.



Figure 1.1: *Alseodaphne corneri* Kosterm

1.6 *Dehaasia longipedicellata* (Ridl.) Kosterm

Dehaasia longipedicellata (Figure 1.2) is a small or medium sized tree up to 12 m in height and 30 cm girth. The leaves are 1-2.5 cm long, hairy, broadly elliptic to obovate, apex pointed, base rounded to sub cordate, unequal, midrib sunken above. It also has 10-14 pairs of secondary nerves, raised below, faint above, tertiary nerves and reticulation visible on both surfaces. Fruits of this species are globose with depressed or flattened apex with 5.5 cm across on 3.5 cm long swollen stalk (Whitmore & Ng, 1989).



Figure 1.2: *Dehaasia longipedicellata* (Ridl.) Kosterm

1.7 Medicinal Uses of the Lauraceae

Long before Lauraceae plants are known to have medicinal values, the ancient Greeks have been using the leaves of *Laurus nobilis* L. to make wreaths for their victorious heroes and athletes. Nowadays, the word 'laureate' is used for the winners of the Nobel Prize to indicate academic honours. The Lauraceae plants have renowned oil cells in the leaves, wood and fruits. These oils are mostly aromatic, thus provide a number of flavouring spices and essential oils. Among that, the most widely use spices for cooking in Asia is cinnamon. Cinnamon is isolated from *Cinnamomum zeylanicum* Blume produced in Ceylon (Schroeder, 1976).

Another important spice isolated from the Lauraceae family that has a strong aromatic odour is camphor. The major source of camphor is *Cinnamomum camphora* (L.) J.Presl found abundantly in China and Japan. Camphor can be made into camphor oil and mothballs. Camphor is also taken orally to calm hysteria, nervousness, neuralgia and to treat serious diarrhoea. Camphor is also known to be effective in treating colds and chills. In the Holy Quran verse 76:5, camphor is used to flavour drinks. Nowadays, the Arabic community use it widely in the cooking ingredients (Schroeder, 1976).

Another ingredient from Lauraceae to flavour tea is isolated from *Sassafras albidum* (Nutt.) Nees. It is regularly grown as an ornamental tree for its unusual leaves and aromatic odour. The Native American people use the leaves of sassafras to treat wounds by rubbing the leaves directly on the wound and as an ingredient in cooking. The bark of this plant produces essential oils that are used as fragrances and aromatherapy in perfumes and soaps. The rosewood odour isolated from *Aniba duckei* Kosterm. is also used as perfume oils (Schroeder, 1976).

The durable and beautiful wood of the Lauraceae plants have been utilized in construction, shipbuilding and furniture-making in North America, Asia, and Europe. The most renowned timber tree is *Eusideroxylon zwageri* Teijsm. & Binn. or recognized as iron-wood is found in Indonesia for many uses as mentioned earlier. The other well-known and valuable timber trees in the Laurel-family are *Ocotea bullata* Burch. and *Mezilaurus ita-uba* (Meisn.) Taub. ex Mez which are found in South Africa and Brazil respectively (Gottlieb, 1972; Schroeder, 1976).

Recently, the Lauraceae plants; *Litsea cubeba* (Lour.) Pers. and *Lindera melissifolia* (Walter) Blume are used as repellents against mosquito and ticks (Oh et al., 2012; Vongsombath et al., 2012). The Bangladesh community are known to use *Cinnamomum tamala* (Buch.-Ham.) T.Nees & Eberm. and *Cinnamomum verum* J.Presl as medicine against influenza and gonorrhoea (Kalita et al., 2015; Rahmatullah et al., 2012).

In Malaysia, the genus of *Alseodaphne hainanensis* Merr., *A.oblanceolata* (Merr.) Kosterm. and *A.perakensis* (Gamble) Kosterm. are commercialized as timber. They are utilised in plywood manufacture as decorative work, as furniture and in cabinet-making (Ng, 1989). The Indonesian community uses the bark of *A.coriaceae* Kosterm. as mosquito repellent coils (Suyanto et al., 2009). As for the Indian community, they use the bark of *A.semicarpifolia* Nees for dysentery in cattle's and leaches bite treatment. The bark and fruits of this plant are also used in the treatment of cholera-like illness (Charles et al., 2013).

In Bangladesh, the Chakma tribe uses the leaves and roots of *Dehaasia kurzii* King ex Hook.f. to treat vaginal infection known as leucorrhoea (Hossan et al., 2010). They also use it to reduce pain in the neck and treat heat stroke (Rahmatullah et al., 2011). There is very little information available on the medicinal use of the plants of the *Dehaasia* and *Alseodaphne*. Therefore, the biological activitiy studies for these two

genera; *Alseodaphne* and *Dehaasia* are in high demand to complement the exquisiteness of the plant-derived drugs.

1.8 Objectives of the Study

The focus of this phytochemical investigation was two plant samples; *Dehaasia longipedicellata* and *Alseodaphne corneri* (Lauraceae). The objectives of this study are outlined as follows:

1. To isolate the alkaloids from *A. corneri* and *D. longipedicellata* by using chromatographic methods such as column chromatography (CC), preparative thin layer chromatography (PTLC), high performance liquid chromatography (HPLC) and recycle high performance liquid chromatography (RHPLC).
2. To elucidate and characterize the structures of the isolated alkaloids using spectroscopic methods such as 1D-NMR (^1H , ^{13}C and DEPT-135), 2D-NMR (COSY, HMBC, HSQC), ultraviolet (UV), Infrared (IR), and MS (LCMS-IT-TOF, HRESIMS) analysis.
3. To investigate and evaluate the antiplasmodial effects of extract and pure alkaloids from *A. corneri* and *D. longipedicellata*.
4. To evaluate the antioxidative activities (DPPH, FRAP, ferum chelating) of the isolated alkaloids from *A. corneri* and *D. longipedicellata*.
5. To determine the acid dissociation constant of selective bioactive isoquinoline alkaloids in order to investigate the nature of their existences (ionised and non-ionised form) at physiological pH.

CHAPTER 2: GENERAL CHEMICAL ASPECTS

2.1 Alkaloid

In 1819, Carl Meissner a pharmacist from Halle, Germany, proposed the term of “alkaloid” or “alkali-like” for alkaline nitrogen-containing compounds. Another definition that is still being used until now which was suggested by (Winterstein & Tier, 1910) is alkaloids are compounds with heterocyclic bound nitrogen atoms. They have complex molecular structure with pronounced physiological actions and are found in plants (and animals) (Zenk & Juenger, 2007). They contain one or more nitrogen atoms, which are belong to primary, secondary or tertiary amines, and this usually deliberates basicity on the alkaloid, in turn assisting isolation and purification. The degree of basicity varies greatly, depending on the location and the type of substituents presents in the molecule (Dewick, 2009). Alkaloids are usually neutralized with acid to form salts that may be converted into the corresponding free base by the cautious addition of a selective weak base, such as ammonia, sodium carbonate or calcium hydroxide. Alkaloids having low pK_a values require a high acidic medium to form their respective salts with the corresponding acid, and vice versa. There are some alkaloids which are amphoteric in nature, whereby they are neither acidic nor basic in character, and this is due to the presence of a phenolic moiety (Kumar, 2014).

2.2 Alkaloid Classification

Alkaloids are generally classified by their common molecular precursors, based on their biosynthetic pathway used to construct the molecule. The nitrogen atoms in alkaloids originate from an amino acid, and in general, the carbon skeleton of the particular amino acid precursor remains intact in the alkaloid structure. There are three main types of alkaloids namely (1) true alkaloids (2) protoalkaloids and (3)

pseudoalkaloids (Table 2.1). True alkaloids are derived from amino acids and shared a heterocyclic ring with the nitrogen. Protoalkaloids are compounds which are derived from amino acids but the amino acid nitrogen is not within the heterocyclic ring. Pseudoalkaloids are compounds whereby their basic carbon skeletons not derived from amino acids. Alkaloids also can be classified in terms of their biosynthetic, chemical, pharmacological and taxonomic classification. Names of chemically derived alkaloids are based on the skeletal features of the parent compounds and are widely accepted for classification. However, it is not common practise to classify alkaloids according to their pharmacological characteristics. Table 2.1 list the type of alkaloids along with the amino acids which they were derived from. The above mentioned alkaloids possess different taxonomic distribution and pharmacological activities (Aniszewski, 2007; Dewick, 2009; Pelletier, 1970).

Table 2.1: Main Types of Alkaloids and Their Chemical Groups

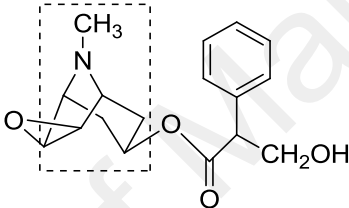
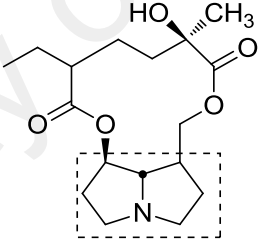
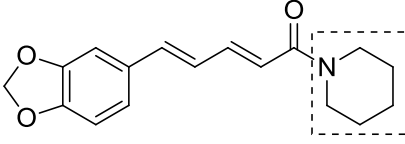
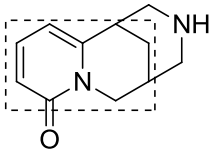
Alkaloid type	Precursor compound	Chemical group of alkaloids	Parent compounds	Example of alkaloids	Pharmacological activities
True Alkaloid	L-ornithine	Tropane alkaloids	Tropane	Hyoscyamine 	Hyoscyamine alkaloids extracted from <i>Atropa belladonna</i> (Solanaceae) exhibits antispasmodic action on the gastrointestinal tract, antisecretory effect controlling salivary secretions during surgical operations and as mydriatics to dilate the pupil of the eye.
		Pyrrolizidine alkaloids	Pyrrolizidine	Senecionine 	Many pyrrolizidine alkaloids are known to cause hepatic toxicity. Prolonged used may lead to liver damage.
	L-lysine	Piperidine alkaloids	Piperidine	Piperine 	The pungency of the fruits of black pepper from <i>Piper nigrum</i> (Pipereceae), a widely used condiment, is mainly due to the piperidine alkaloid, piperine.
		Quinolizidine alkaloids	Quinolizidine	Cytisine 	Cytisine can be obtained in large amounts from the seeds of <i>Laburnum anagyroides</i> (Leguminosae). It is a potent agonist for nicotinic acetylcholine receptors which in turn helps stop smoking.

Table 2.1: (continued).

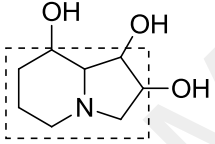
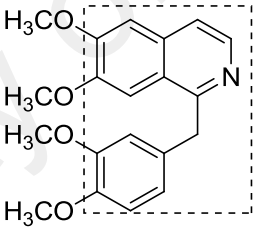
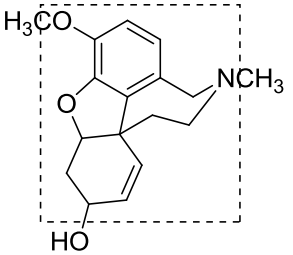
Alkaloid type	Precursor compound	Chemical group of alkaloids	Parent compounds	Example of alkaloids	Pharmacological activities
True Alkaloid	L-lysine	Indolizidine alkaloids	Indolizidine	Swansonine 	Swainsonine from <i>Swainsona canescens</i> (Leguminosae) displays activity against HIV virus, by its ability to inhibit glycoside enzymes involved in glycoprotein biosynthesis.
	L-tyrosine	Simple tetrahydroisoquinoline alkaloids	Benzyl tetrahydroisoquinoline	Papaverine 	Papaverine is a benzylisoquinoline that is found in opium or <i>Papaver somniferum</i> (Papaveraceae). It relaxes the smooth muscles in blood vessels. It is sometimes used as an effective treatment for male impotence.
		Phenylethylisoquinoline alkaloids	Amaryllidaceae alkaloids	Galanthamine 	Galanthamine was extracted from <i>Narcissus pseudonarcissus</i> (Amaryllidaceae). It is used as a centrally acting competitive and reversible inhibitor of acetylcholinesterase, and enhances cognitive function in the treatment of Alzheimer disease

Table 2.1: (continued).

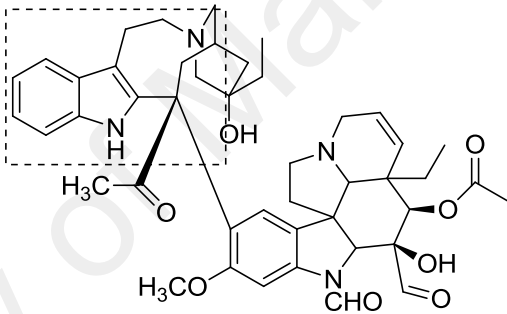
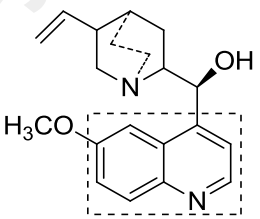
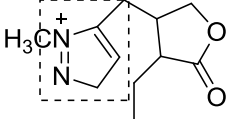
Alkaloid type	Precursor compound	Chemical group of alkaloids	Parent compounds	Example of alkaloids	Pharmacological activities
True Alkaloid	L-tryptophan	Indole alkaloids	Terpenoid alkaloids indole	Vincristine 	Vincristine was isolated from <i>Catharanthus roses</i> (Apocynaceae). It is useful in the treatment of leukaemia, small-cell lung cancer, cervical and breast cancer. It has been introduced to cancer chemotherapy and has proven to be an extremely valuable drug.
		Quinoline alkaloids	Quinoline	Quinine 	Quinine was isolated from <i>Cinchona</i> species (Rubiaceae) that has been used for many years in the treatment of malaria. It also has a skeletal muscle relaxant effect to prevent and treat leg cramps.
	L-histidine	Imidazole alkaloids	Imidazole	Pilocarpine 	Pilocarpine was isolated from <i>Pilocarpus microphyllus</i> (Rutaceae). It is used as eye drops for miotics and for the treatment of glaucoma. In addition, it is also used for patients undergoing radiotherapy to give relief for dryness of the mouth.

Table 2.1: (continued).

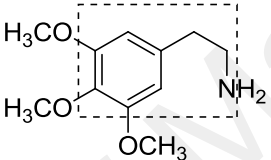
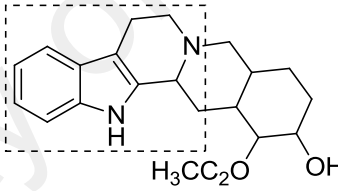
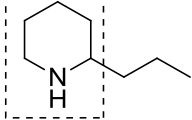
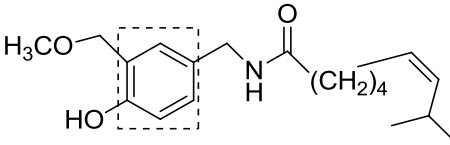
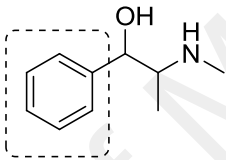
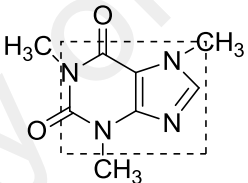
Alkaloid type	Precursor compound	Chemical group of alkaloids	Parent compounds	Example of alkaloids	Pharmacological activities
Proto Alkaloid	L-tyrosine	Phenylethylamino alkaloids	Phenylethylamine	Mescaline 	Mescaline was isolated from <i>Lophophora williamsii</i> (Cactaceae). It has been used as a hallucinogen in experimental psychiatry.
	L-tryptophan	Terpenoid indole alkaloids	Indole	Yohimbine 	Yohimbine is found in <i>Pausinystalia yohimbe</i> (Rubiaceae) and has been used in folk medicine as an aphrodisiac. It is also known to dilate blood vessels.
Pseudo Alkaloid	Acetate	Piperidine alkaloids	Piperidine	coniine 	Coniine was isolated from <i>Conium maculatum</i> (Umbelliferae). The ancient Greeks used it as a poison hemlock for prisoners. The poison causes gradual muscular paralysis followed by convulsion and death from respiratory paralysis.
	Ferrulic acid	Aromatic alkaloids	phenyl	Capsaicin 	Capsaicin or chilli peppers isolated from <i>Capsicum annuum</i> (Solanaceae) are used worldwide spices in cooking.

Table 2.1: (continued).

Alkaloid type	Acid amino precursor	Chemical group of alkaloids	Parent compounds	Example of alkaloids	Pharmacological activities
Pseudo Alkaloid	Pyruvic Acid	Ephedra Alkaloids	Phenyl	Ephedrine 	Ephedrine was isolated from <i>Ephedra sinica</i> (Ephedraceae). It acts as an adrenergic receptor, exhibits bronchodilator activity and gives relief for asthma.
	Adenine	Purine alkaloids	Purine	Caffeine 	Caffeine occurs naturally in coffee beans, tea leaves, cocoa pods and kola nuts. Caffeine is used medically as a central nervous stimulant. It is usually combined with therapeutics as an analgesic, as well as reduces blood pressure and headache symptoms.

2.3 Alkaloids from the Lauraceae

The Lauraceae family which has diverse chemical structures and interesting biological activities has been chosen for many phytochemicals and biological investigations. Majority of the alkaloids isolated from this family were identified in the stem bark. Several studies have also reported them being presents in the leaves and roots.

The Lauraceae which comprises 21 genera is characterized by 300 different alkaloids. In addition, neolignan and essential oils were also isolated from this family. Isoquinolines are the main class reported in the literatures with 287 structures distributed among all the genera within the Lauraceae. Subsequently, these isoquinolines were divided into subclasses inclusive of 148 aporphines, 47 benzyloisoquinolines, 23 pavinines, 21 bisbenzyloisoquinolines, 21 proaporphines, 18 morphinandienones, 4 phenanthrenes and 5 simple isoquinolines. The most frequently detected alkaloids in the Lauraceae are those with the aporphine skeleton, namely; laurotetanine, *N*-methyllaurotetanine, norboldine, boldine, isoboldine, isocorydine, actinodaphne, dicentrine, and one benzyloisoquinoline; reticuline (Custodio & Florencio da Veiga Junior, 2014).

The following sections will discuss briefly on the literature review of the alkaloids isolated from the genera *Alseodaphne* and *Dehaasia* along with their biological activities.

2.4 Alkaloids from the Genus *Alseodaphne*

Among 57 species (section 1.4, page 5), only 8 species of *Alseodaphne*; *A. andersonii*, *A. archboldiana*, *A. hainensis*, *A. semicarpifolia*, *A. corneri*, *A. perakensis*, have been phytochemically investigated. These plants are reported to contain

aporphines, lactones, furanones, phenanthrenes, benzyloisoquinolines (BIQ), bisbenzyloisoquinolines (BBIQ) and morphinandienone alkaloids (Table 2.2). Although there are reports on the crude extracts of these species exhibiting immunomodulatory, antifungal, antibacterial, anti-inflammatory, antimicrobial, antioxidant and vasorelaxant activities, however, the number of active compounds isolated from them are still limited.

Table 2.2: Alkaloids from the Genus *Alseodaphne* and Their Biological Activities

Plant	Plant part	Compounds isolated	Skeletal Type	Biological activities
<i>Alseodaphne andersonii</i> (King Hook.f.) Kosterm	Roots and stems	Dihydroisoobtusilactone 1 Dihydroobtusilactone 2 3-Epilitsenolide D1 3 3-Epilitsenolide D2 4 Alseodofuranone 5 (Lee et al., 2001)	Lactones	The crude extract of this species showed immunomodulatory (Gupta & Bhagat, 2010), antifungal (Kaushik et al., 2010), antibacterial (Parcha et al., 2007), anti-inflammatory and central nervous system (CNS) stimulating activities (Dhillon et al., 2009).
<i>Alseodaphne archboldiana</i> (C.K.Allen) Kosterm	Bark	Coclaurine 6 <i>N</i> -norarmepavine 7 Reticuline 8 (Johns et al., 1967)	BIQ type I	None reported
<i>Alseodaphne hainanensis</i> Merr.	Bark	Neolignan Eusiderin A 9 (6,7-dimethoxyisoquinoliny)- (4'-methoxyphenyl) methanone 10 (6,7-methylenedioxyisoquinoliny)- (4'-methoxyphenyl) methanone 11 4-hydroxy-3-methoxy benzoic acid 12 (Haitao et al., 1999)	Lignan BIQ type I Benzoic acid	None reported

Table 2.2: (continued).

Plant	Plant part	Compounds isolated	Skeletal Type	Biological activities			
<i>Alseodaphne hainanensis</i>	Bark	Xylopinine 13 Armepavine 14 Doryafranine 15 1-(4-methoxybenzyl)-6,7-methylenedioxy-1,2,3,4,-tetrahydroisoquinoline 16 (Haitao et al., 1999; Zhang et al., 1988)	Protoberberine BIQ type I	None reported			
<i>Alseodaphne semicarpifolia</i> Nees	Leaves	Srilankine 17 (Smolnycki et al., 1978)	1, 2, 9, 10-tetrasubstituted aporphine	The crude extract of this species has been tested for antimicrobial (Charles & Ramani, 2011) and antioxidant (Charles et al., 2012) activities.			
<i>Alseodaphne corneri</i> Kosterm	Bark	Gyrolidine 18 3'-4'-dihydronorstephasubine 19 Norstephasubine 20 (Mukhtar et al., 2009)	Type VI BBIQ	The first biological activity carried out on this species was reported by our research group on the vasorelaxant activity on isolated rat aorta			
<i>Alseodaphne perakensis</i> (Gamble) Kosterm.	Bark	α -oxoperakensimines A 21 α -oxoperakensimines B 22 α -oxoperakensimines C 23 (Mukhtar et al., 2009)	Type I BBIQ	Moderate vasorelaxant activity on isolated rat aorta (Mukhtar et al., 2009; Nafiah et al., 2011)			
		Leaves			Perakensol 24 (Mahmud et al., 1992)	Phenanthrenoid	None reported
		Bark			<i>N</i> -cyanomethylnorboldine 25 <i>N</i> -methy-laurotetanine 26 (Nafiah et al., 2011)	1, 2, 9, 10-tetrasubstituted aporphine	

2.5 Alkaloids from the Genus *Dehaasia*

Among 38 species (section 1.4, page 5), only six species of *Dehaasia*; *D. hainanensis*, *D. kurzii*, *D. incrassate*, *D. longipedicellata*, *D. candolleana* and *D. triandra* have been studied phytochemically. Interestingly, these plants have been reported to consist of morphinandienones which are found abundantly in opium. In addition, BBIQ, phenanthrene and aporphine alkaloids have also been isolated from these plants (Table 2.3). Only antiplasmodial and antibacterial activities have been reported throughout centuries. Therefore, it is important to further explore their pharmacological activities due to their very interesting structures.

Table 2.3: Alkaloids from the Genus *Dehaasia* and Their Biological Activities

Plant	Plant part	Compounds isolated	Skeletal type	Biological activities
<i>Dehaasia hainanensis</i> Kosterm	Leaves	(+)-Laurotetanine 27	1, 2, 9, 10-tetrasubstituted aporphine	None reported
		(-)- <i>N-N'</i> -dimethylindoldhamine 28	Type I BBIQ	
		(-)-Sinoacutine 29	Metaphenine morphinandienone	
		(-)-Ocobotrine 30	Isosinomenine morphinandienone	
		(+)-Roefractine 31	Type I BIQ	
		(+)-Reticuline <i>N</i> -oxide 32		
		<i>O</i> -methylarmepavine 33	1, 2, 10, 11-tetrasubstituted aporphine	
		(+)-Corydine 34		
		(+)-Lindcarpine 35	1, 2, 9, 10-tetrasubstituted aporphine	
		(+)-Norboldine 36		
(C.-K. Chen et al., 2007)				

Table 2.3: (continued).

Plant	Plant part	Compounds isolated	Skeletal type	Biological activities
<i>Dehaasia kurzii</i> King ex Hook.f.	Bark	(+)-Boldine 37 (Hasan et al., 1987)	1, 2, 9, 10-tetrasubstituted aporphine	The crude extract of this species showed <i>in vitro</i> antibacterial activity against <i>Shigella flexneri</i> . Boldine showed cytotoxic activity towards human epidermoid carcinoma of the larynx (HEp-2 cells)
	Bark	Dehassiline 38 (Atta-Ur-Rahman et al., 1990)	Type I BIQ	
	Aerial	Phenolic alkaloid 39 (Abdur & Aftaf, 1988) n-nonacosane 40 (Abdur & Anwar, 1987)	Phenolic Straight-chain hydrocarbon	
<i>Dehaasia incrassate</i> (Jack) Kosterm.	Leaves	(+)-Isocorydine 41 (+)-Norisocorydine 42 Oxycanthine 43 (Said et al., 1991)	1, 2, 10, 11-tetrasubstituted aporphine	The crude extract was screened for antimalarial activity.
<i>Dehaasia longipedicellata</i> (Ridl.) Kosterm.	Leaves	2,7-dihydroxy-3,6-dimethoxyphenanthrene 44 (Mukhtar et al., 2008)	Phenanthrene	None reported
	Leaves	(+)-Pallidine 45 (+)-Milonine 46 (Mukhtar et al., 2004)	Isosinomenine morphinandienone	The crude extract showed antiplasmodial activity against <i>Plasmodium falciparum</i>
<i>Dehaasia candolleana</i> (Meisn.) Kosterm	Bark	Sebiferine 47 <i>O-O</i> -dimethylgrisabine 48 Grisabine 49 (Hadi et al., 2008)	Metaphenine morphinandienone	Alkaloids isolated have been tested for antiplasmodial activities against D10 and Gombak A strains

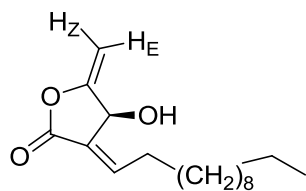
Table 2.3: (continued).

Plant	Plant part	Compounds isolated	Skeletal type	Biological activities
<i>Dehaasia triandra</i> Merr	Leaves	Isocorydione 50 Norisocorydione 51 Dehatriphine 52 (Lee et al., 1996)	Aporphine Dimeric aporphine	None reported
	Leaves	Secoxanthoplanine 53 Dehydroisocorydione 54 (8,8'- <i>R</i>)- bisisocorydine 55 (8,8'- <i>S</i>)- bisisocorydine 56 11,8'- <i>O</i> -bisisocorydine 57 (Lee et al., 1996)	Phenanthrene Aporphine Dimeric aporphine	
	Leaves Trunk	Corytuberine 58 Atheroline 59 Nantenine 60 Xanthoplanine 61 Obaberine 62 Dehatridine 63 Dehatrine 64 (Lu et al., 1989)	1, 2, 10, 11- tetrasubstituted aporphine Aporphine 1, 2, 9, 10- tetrasubstituted aporphine Type VI BBIQ Type VIII BBIQ	
	Leaves	(+)-Homoaromoline 65 (+)-Daphnandrine 66 (+)-Aromaline 67 (+)-Daphnoline 6	Type VI BBIQ Type VIII BBIQ	

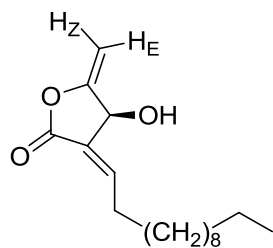
Table 2.3: (continued).

<i>Dehaasia triandra</i> Merr	(+)-Pangkorimine 69	Type VIII BBIQ
	Colorflammimine 70	
	(+)-Thalrugosine 71	
	(+)-Obamegine 72	
	(+)-2-norobamegine 73	
	1,2-dehydroapateline 74	
	(C.-K. Chen et al., 2003)	

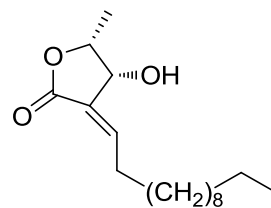
University of Malaya



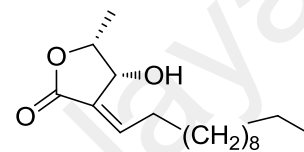
1



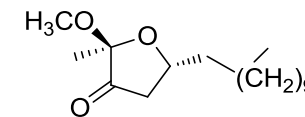
2



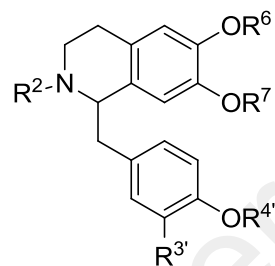
3



4



5



6

7

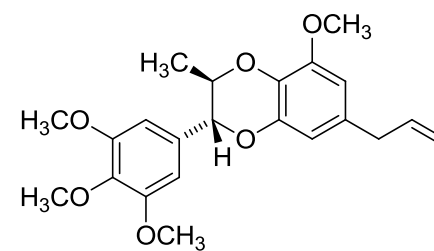
8

14

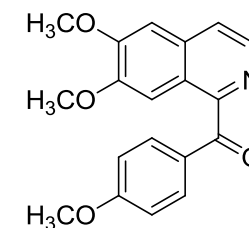
31

33

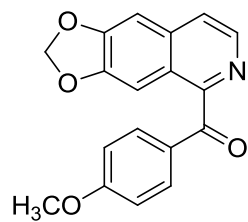
	6	7	8	14	31	33
R ²	H	H	CH ₃	CH ₃	CH ₃	CH ₃
R ³	H	H	OH	H	H	H
R ⁴	H	H	CH ₃	H	CH ₃	CH ₃
R ⁶	CH ₃	CH ₃	CH ₃	CH ₃	H	CH ₃
R ⁷	H	CH ₃	H	CH ₃	CH ₃	CH ₃



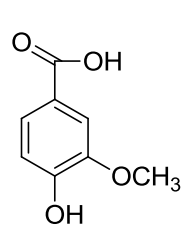
9



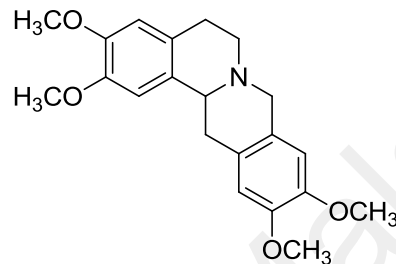
10



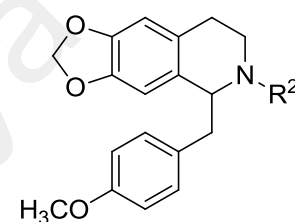
11



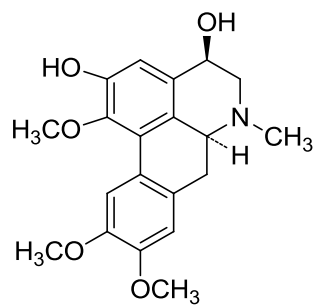
12



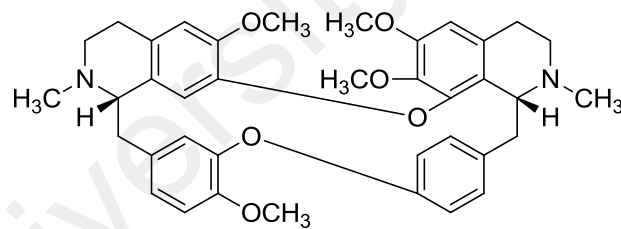
13



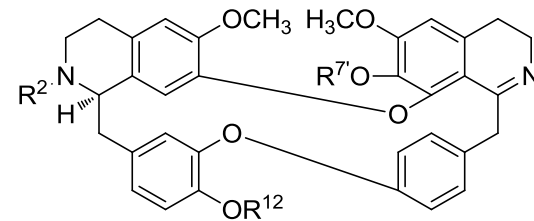
	15	16
R ²	CH ₃	H



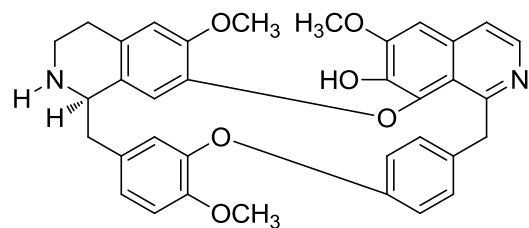
17



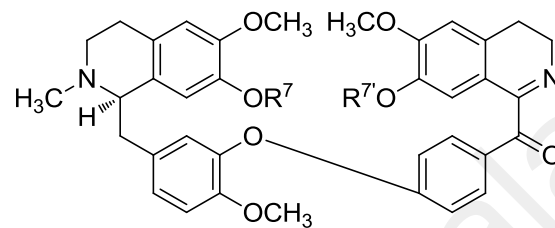
18



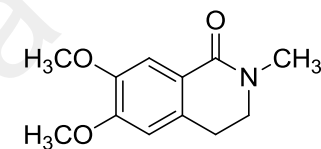
	19	69
R ²	H	H
R ^{7'}	H	H
R ¹²	CH ₃	H



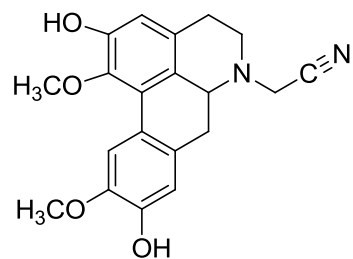
20



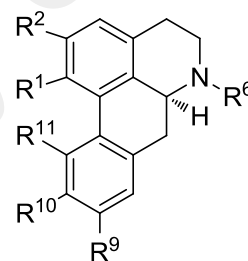
	21	22	23
R ⁷	H	CH ₃	H
R ^{7'}	CH ₃	H	H



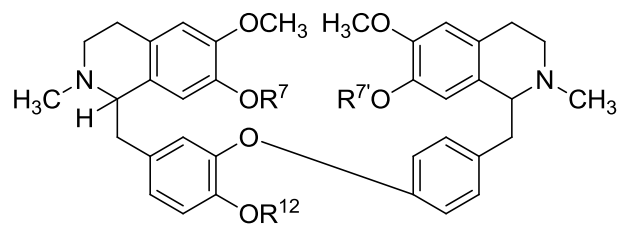
24



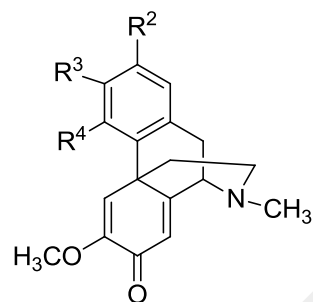
25



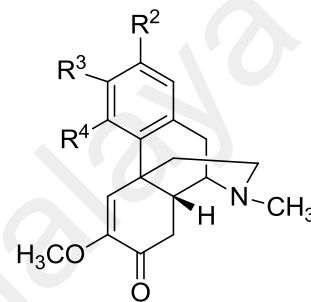
	26	27	29	34	36	37	41	42	58	61
R ¹	OCH ₃	OCH ₃	OH	OCH ₃	OH	OCH ₃	OCH ₃	OCH ₃	OH	OCH ₃
R ²	OCH ₃	OCH ₃	OCH ₃	OH	OCH ₃	OH	OCH ₃	OCH ₃	OCH ₃	OCH ₃
R ⁶	CH ₃	H	CH ₃	H	H	CH ₃	CH ₃	H	CH ₃	(CH ₃) ₂
R ⁹	OH	OH	H	H	OH	OH	H	H	H	OH
R ¹⁰	OCH ₃	OCH ₃	OCH ₃	OCH ₃	OCH ₃	OCH ₃	OCH ₃	OCH ₃	OCH ₃	OCH ₃
R ¹¹	H	H	OCH ₃	OH	H	H	OH	OH	OH	H



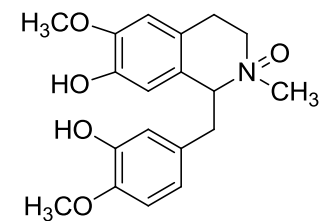
	28	48	49
R ⁷	H	CH ₃	H
R ^{7'}	H	CH ₃	H
R ¹²	H	CH ₃	CH ₃



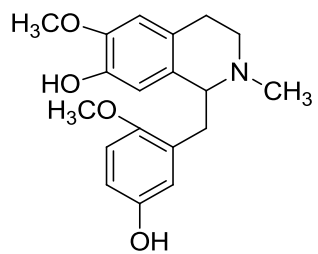
	29	47
R ²	H	OCH ₃
R ³	OCH ₃	OCH ₃
R ⁴	OH	H



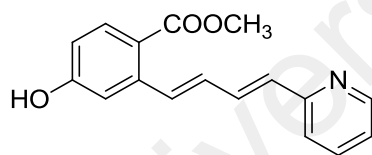
	30
R ²	H
R ³	OCH ₃
R ⁴	OH



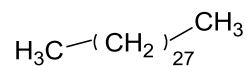
32



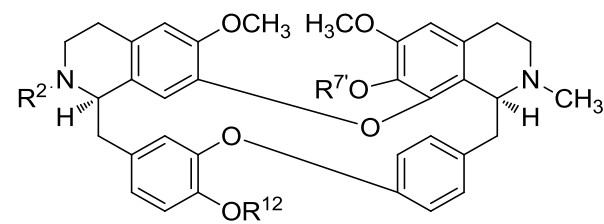
38



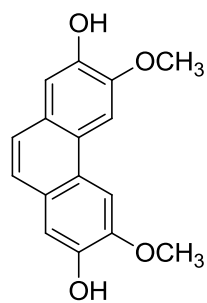
39



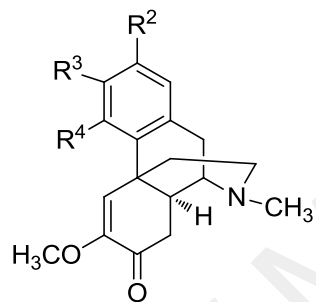
40



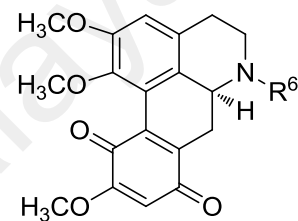
	43	62	65	66	67	68
R ²	CH ₃	CH ₃	CH ₃	H	CH ₃	H
R ^{7'}	CH ₃	CH ₃	H	H	H	H
R ¹²	H	CH ₃	CH ₃	CH ₃	H	H



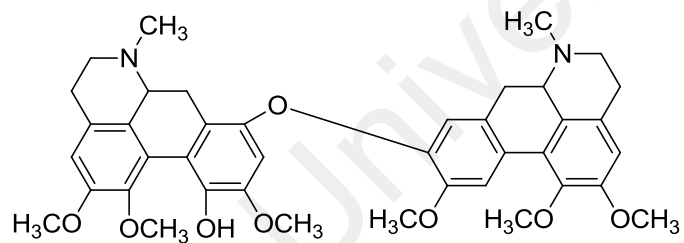
44



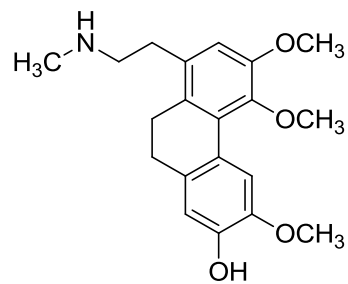
	45	46
R ²	OH	H
R ³	OCH ₃	OCH ₃
R ⁴	H	OH



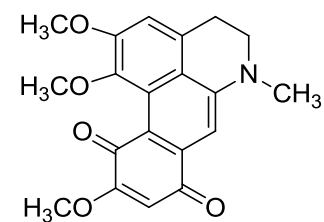
	50	51
R ⁶	CH ₃	H



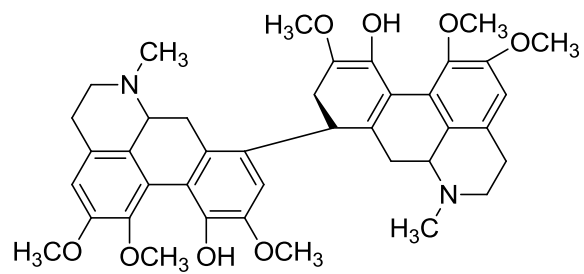
52



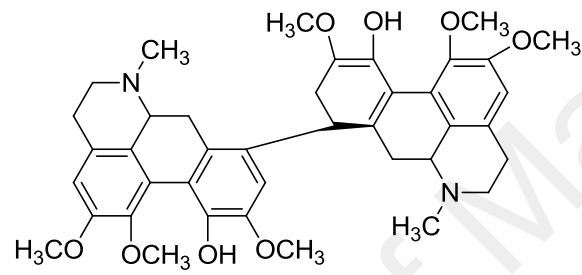
53



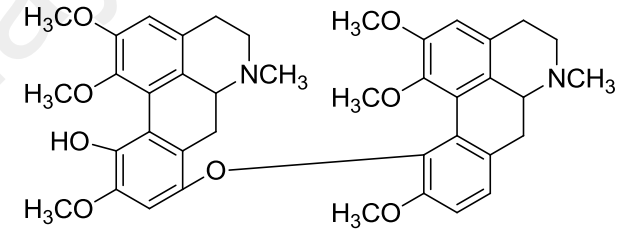
54



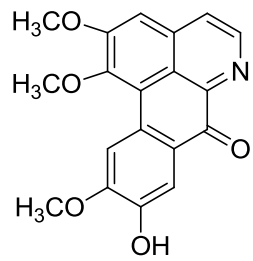
55



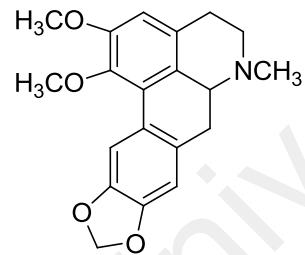
56



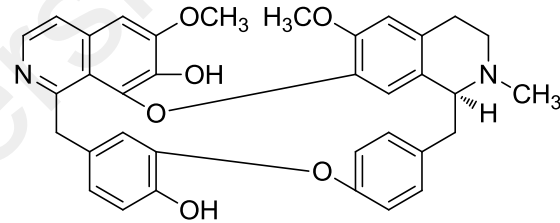
57



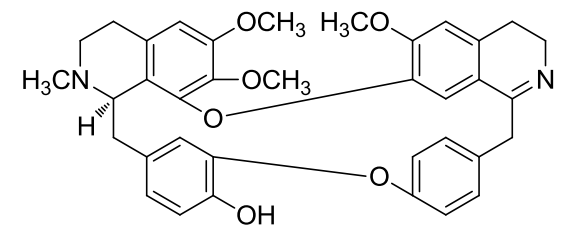
59



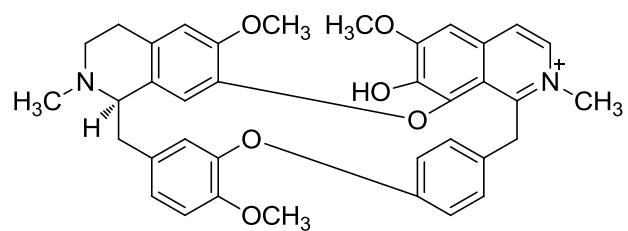
60



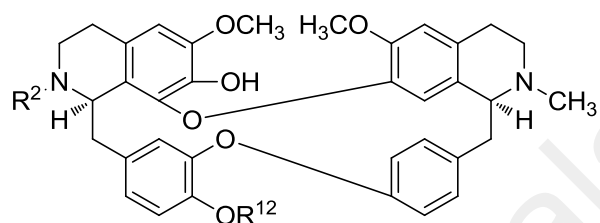
63



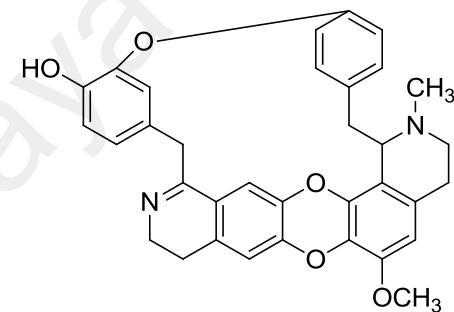
64



70



	71	72	73
R ²	CH ₃	CH ₃	H
R ¹²	CH ₃	H	H



74

Figure 2.1: Alkaloids Isolated from the Genus *Alseodaphne* and *Dehaasia*

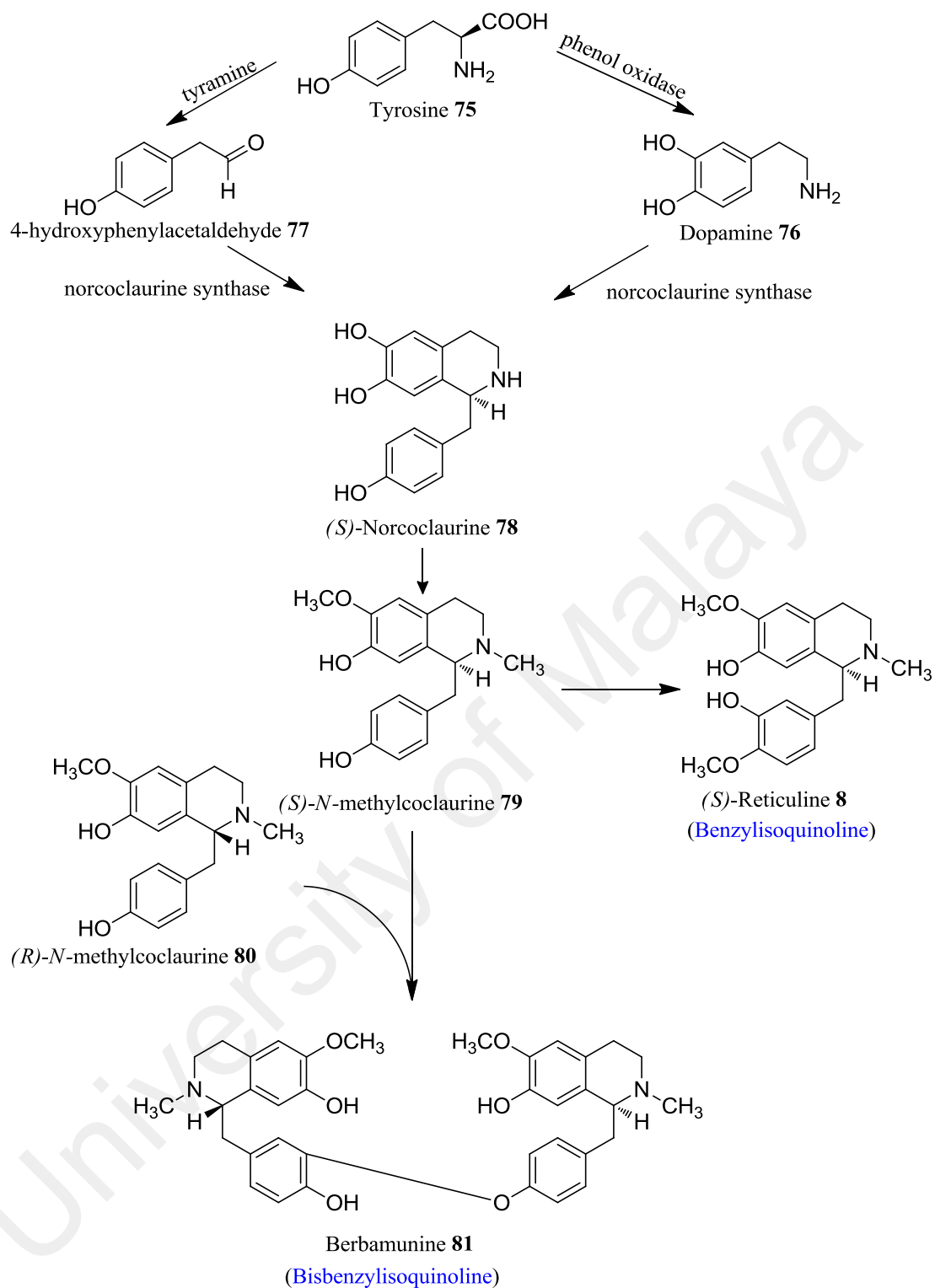
2.6 Biosynthesis of Isoquinoline Alkaloids

The genera *Alseodaphne* and *Dehaasia* produce BIQ, BBIQ, morphinandienone and aporphine type alkaloids. The biosynthesis of these types of alkaloids is presented in the following sub-sections.

The biosynthesis of alkaloids has evolved from the use of potential precursors to radio- and then stable-isotope studies, to the isolation of crude and then purified enzyme systems. Recently, studies are typically providing important information regarding the functionality of the genes which are responsible for the biosynthetic enzymes of alkaloid pathways (Cordell, 2013; Zenk, 1991; Zenk & Juenger, 2007). As a result of all these studies, many alkaloids have been shown to be synthesized by amino acids. Isoquinoline alkaloids are derived from the amino acid tyrosine **75** (Scheme 2.1).

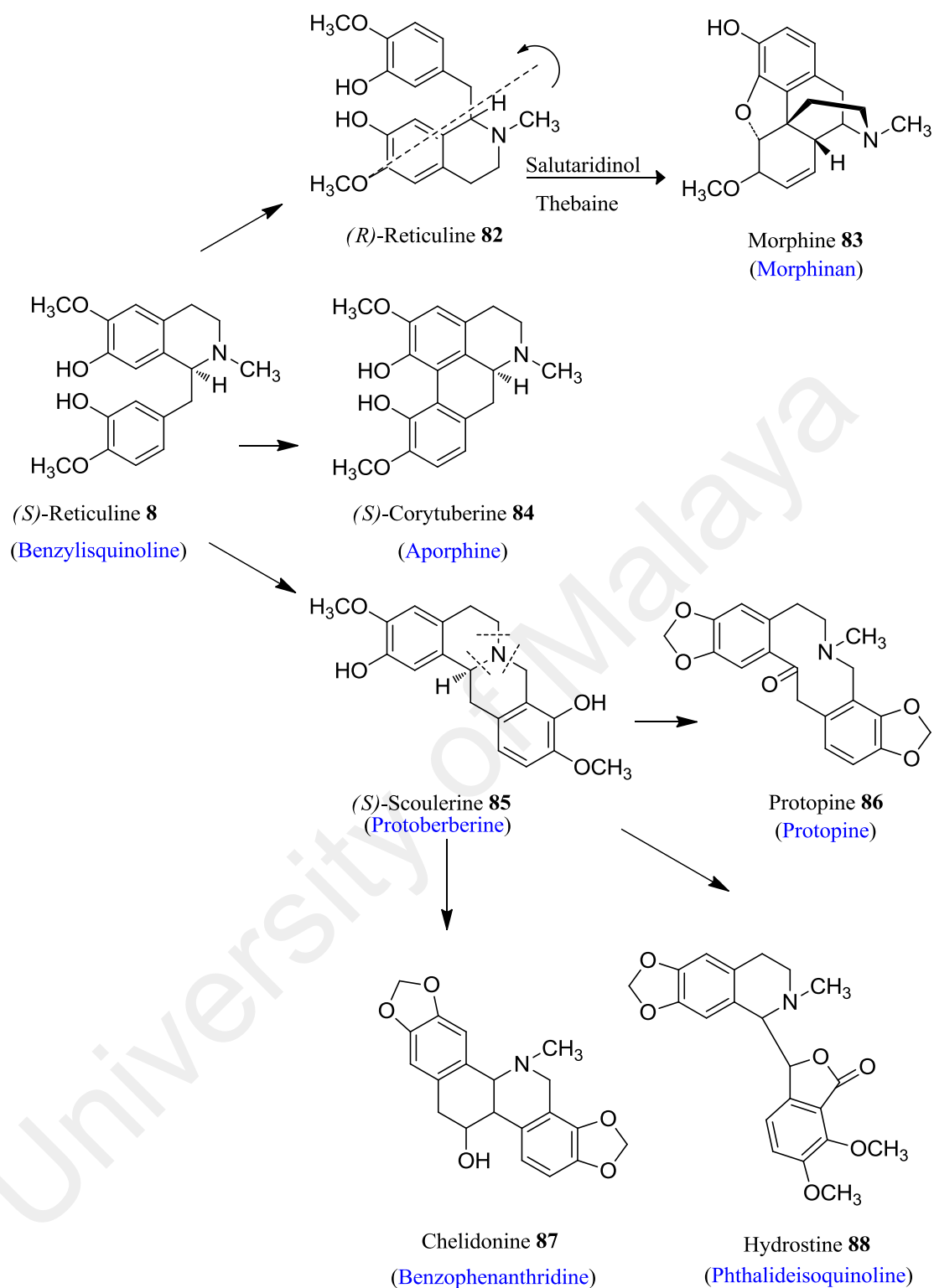
Two tyrosine **75** molecules are used in the biosynthetic pathway; one is converted to dopamine **76** via a phenol oxidase and a decarboxylation reaction, while the other is decarboxylated to the amine, tyramine to give 4-hydroxyphenylacetaldehyde **77**. The important intermediates that act as precursors of all the alkaloids in this group are (*S*)-norcoclaurine **78** and (*S*)-reticuline **8**.

The central intermediate, (*S*)-norcoclaurine **78** is formed from the condensation of dopamine **76** and 4-hydroxyphenylacetaldehyde **77** in a reaction catalysed by norcoclaurine synthase. Two methylation reactions convert (*S*)-norcoclaurine **78** to (*S*)-*N*-methylcoclaurine **79**, which has two potential branches. One of the branches is when (*S*)-*N*-methylcoclaurine **79** reacts with its isomer (*R*)-*N*-methylcoclaurine **80** to form the bisbenzylisoquinoline precursor, berbamunine **81**. Alternatively, (*S*)-*N*-methylcoclaurine **79** can be converted to (*S*)-reticuline **8** by hydroxylation and methylation reactions (Scheme 2.2).



Scheme 2.1: Proposed Biosynthesis of BIQ and BBIQ from Tyrosine Amino Acid

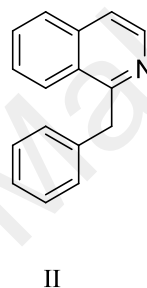
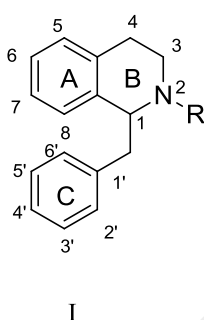
In brief, the pathway is branched in several places, depending on the species of the plant, which undergo further modification to produce a wide range of isoquinolines. Scheme 2.2 reveals that the most important branch is from the precursor (*S*)-reticuline **8** that will be used to form various skeletal types. Firstly, it can be converted to (*R*)-reticuline **82** via oxidation-reduction process. This (*R*)-reticuline **82** forms the morphinan alkaloid **83** by conversion into salutaridinol and thebaine via intramolecular carbon-carbon bonding between aromatic rings. (*S*)-Reticuline **8** forms the aporphine alkaloid, (*S*)-corytuberine **84** via enzyme catalysing oxidative coupling. (*S*)-reticuline **8** to (*S*)-scoulerine **85** (protoberberine) by cleavage of the heterocyclic systems adjacent to the nitrogen atom sits at another branch point leading to three subgroups; protopine **36**, benzophenanthridine **87** and phthalideisoquinoline **88** alkaloids (Bowsher et al., 2008; Dewick, 2009).



Scheme 2.2: Proposed Biosynthesis of Various Alkaloids from (*S*)-Reticuline

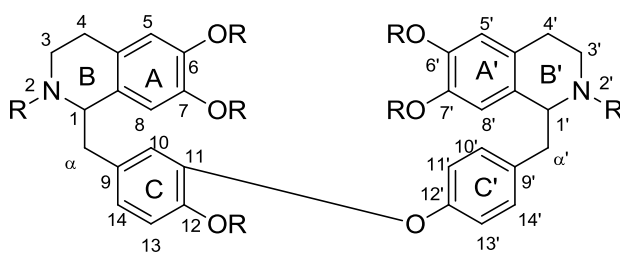
2.6.1 Benzyloquinolines

Benzyloquinoline (BIQ) is found mainly in Papaveraceae, Fumariceae, Ranunculaceae, Berberidaceae and Menispermaceae with over 2500 alkaloids belong to this group (Dewick, 2009). The BIQ alkaloids are classified into two types of skeletons; BIQ type I and BIQ type II as depicted below (Pelletier, 1970). BIQ consists of 3 rings (A, B, C) and mostly the skeletons contain *ortho*-deoxygenation substituents in each aromatic ring.



2.6.2 Bisbenzyloquinolines

Bisbenzyloquinolines (BBIQ) are dimer alkaloids that built up from two monomer of benzyloquinoline (BIQ) units linked by one or more ether bridges. Most of them have been isolated from Menispermaceae, Berberidaceae, Monimaceae and Ranunculaceae (Philipson et al., 1985). BBIQ consists of six rings (A, B, C, A', B', C'). The 'prime' superscript in the numbering of BBIQ is reserved for the right hand BIQ unit and all of the oxygenated substituents will always be located in ring C rather than in the ring C' (Guinaudeau et al., 1986). Generally, the numbering scheme is represented by the structure below.

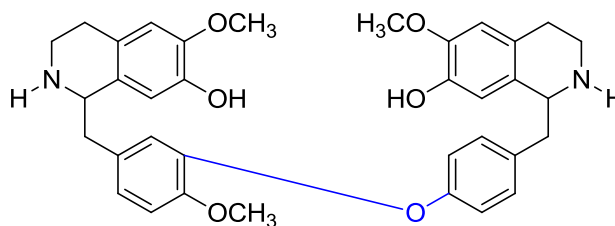


The isoquinoline portion is considered as the ‘head’ of the monomer and the benzyl portion as the ‘tail’ of monomer. The substituents on the aromatic rings could either be a hydroxyl, a methoxyl or a methylenedioxy group (Philipson et al., 1985). Interestingly, BBIQs usually have two asymmetric centres and these will give four stereochemical configurations that can be referred to as ‘*anti*’ for (1*R*, 1’*R*), (1*S*, 1’*S*) dimers and ‘*syn*’ for (1*R*, 1’*S*), (1*S*, 1’*R*) dimers. These variations in stereochemistry at C-1 and C-1’ make each group differ from one another in the identification and classification of BBIQs (Guinaudeau et al., 1986).

Based on the differences in stereochemistry, substituents, numbers of ether linkages and type of bridges linking the two monomers (diaryl ether or benzyl phenyl ether), the BBIQ alkaloids are classified into 5 groups and 27 subgroups (Guinaudeau et al., 1986; Philipson et al., 1985). These examples (**92**, **93**, **94**, **95**, **96**, **97**, **98**) represent each subgroup as listed:

- A. Alkaloids containing one diaryl ether linkage between C11 and C12’. This group belongs to the subgroups of type I, Ia, II, III, IV, V BBIQ.

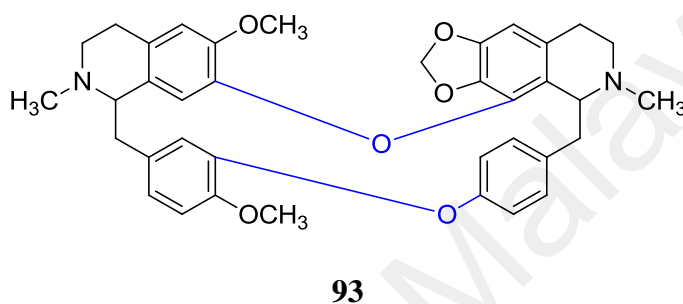
Type I: Costaricine (tail to tail C11-O-C12’)



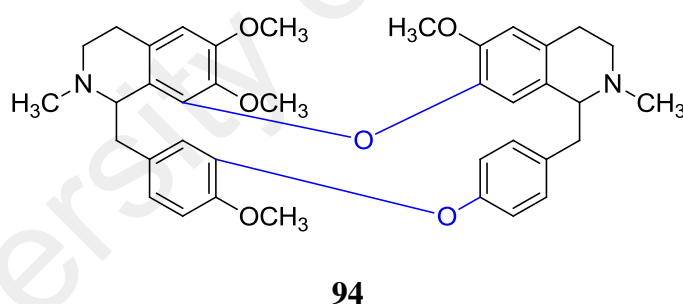
92

- B. Alkaloids containing two diaryl ether linkages. All these types of the BBIQ alkaloids contain ether linkages between the aromatic rings of the tetrahydroisoquinoline component and the benzyl rings. This group belongs to the subgroups of type VI, VII, VIII, IX, X, XI, XII, XIII, XIV, XV, XVI, XVII, XVIII, XIX, XX and XXI BBIQ.

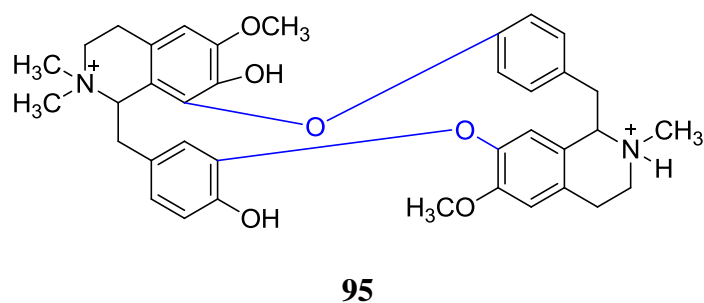
Type VI: Cepharanthine (head to head C7-O-C8' and tail to tail C11-O-C12')



Type VIII : Tetrandrine (head to head C8-O-C7' and tail to tail C11-O-C12')

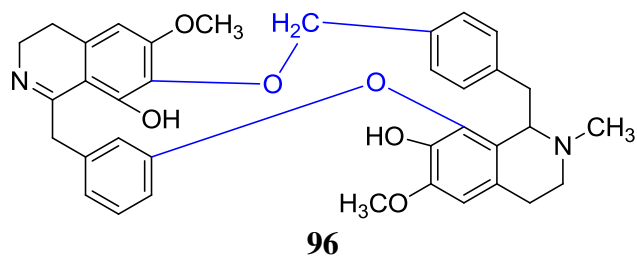


Type XXI : Tubocurarine (head to tail)



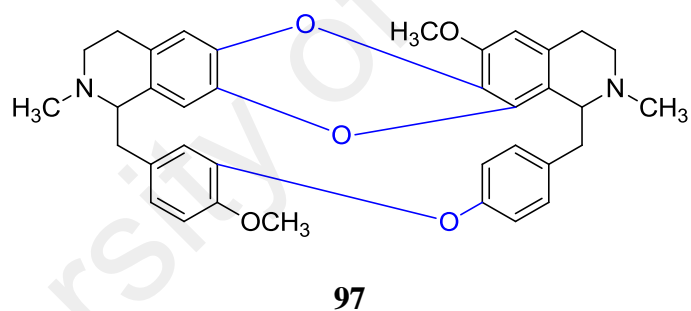
- C. Alkaloids with one diaryl ether and one benzyl phenyl ether linkages. This group belongs to the subgroups of type XXII BBIQ.

Type XXII : Warifteine



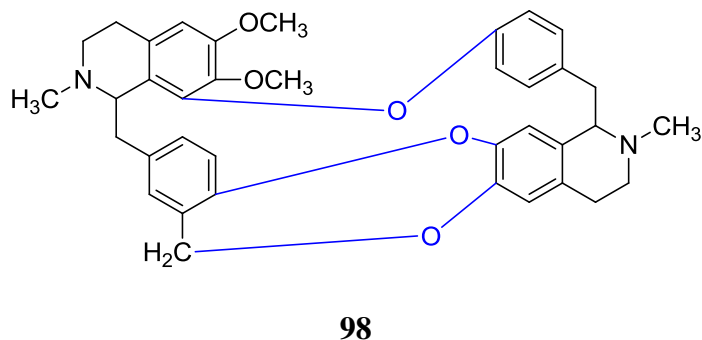
- D. Alkaloids with three ether linkages. This group belongs to the subgroups of type XXIII and XXIV BBIQ.

Type XXI : 2-N-methyltelobine



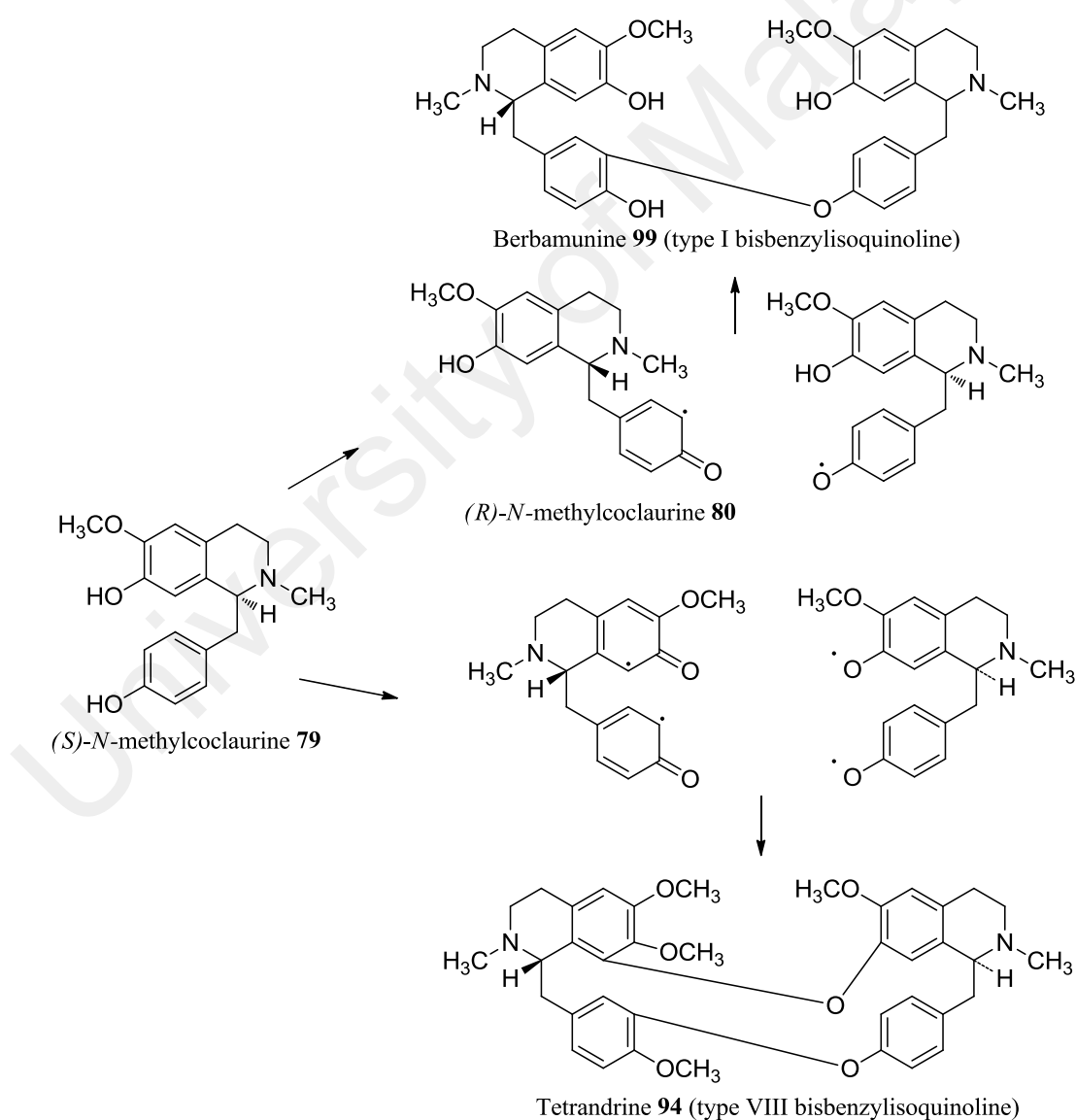
- E. Alkaloids containing two diaryl ether and one diphenyl benzyl ether linkages. This group belongs to the subgroups of type XXV and XXVI BBIQ.

Type XXVI : Insularine



Biosynthesis of Bisbenzylisoquinolines

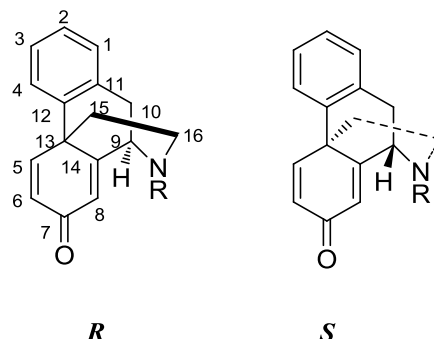
Biosynthesis for BBIQ is shown in Scheme 2.3. Berbamunine **99**, type I BBIQ that has a single ether linkage is derived from (*S*)-*N*-methylcoclaurine **79** and (*R*)-*N*-methylcoclaurine **80** by phenolic oxidative coupling in a regiospecific and stereospecific manner. Meanwhile, two (*S*)-*N*-methylcoclaurine **79** are linked together via a phenolic oxidative coupling to form tetrandrine **94**, type VIII BBIQ. The two diradicals formed couple to give an ether linkage by one electron oxidation of a free phenol group in each ring and the product is then methylated to give tetrandrine **94**.



Scheme 2.3: Proposed Biosynthesis of Bisbenzylisoquinolines

2.6.3 Morphinanandienones

The numbering scheme of the morphinanandienone skeleton is generally represented as shown below (Blasko & Cordell, 1988).



Biosynthesis of Morphinanandienones

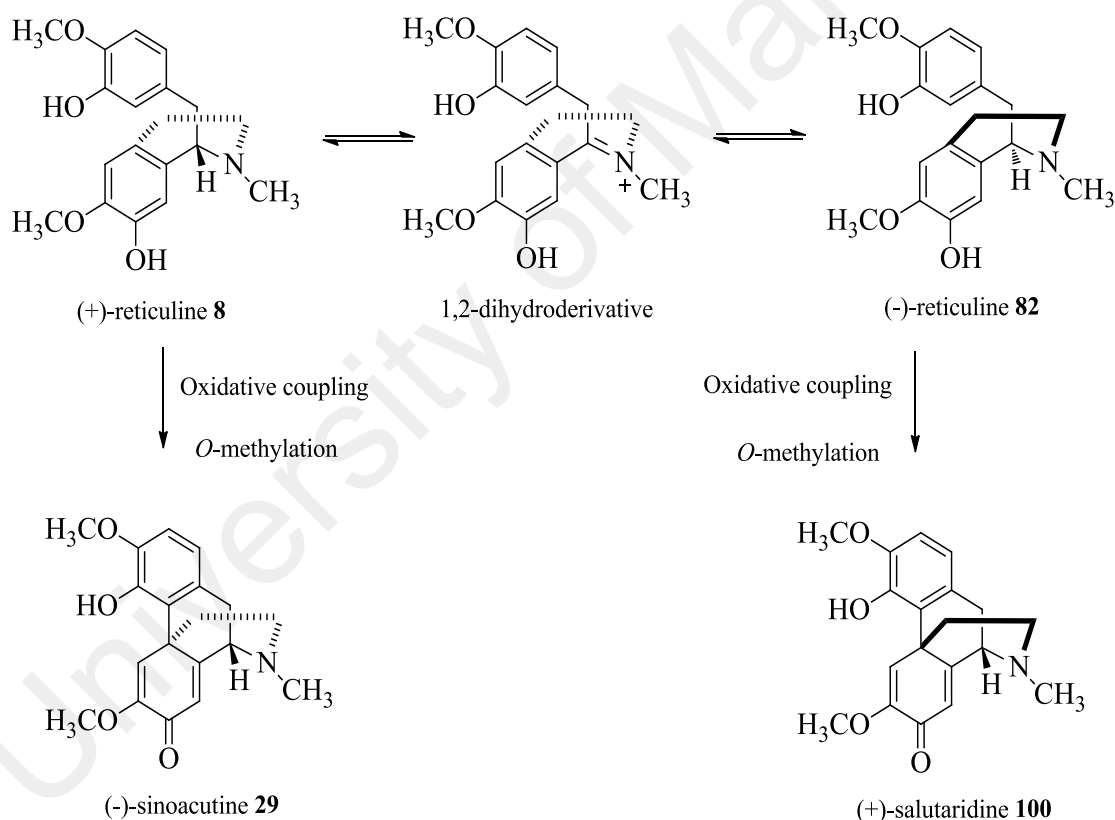
Surprisingly, mostly morphinan alkaloids are derived from (*R*)-reticuline / (-)-reticuline **82** rather than (*S*)-reticuline / (+)-reticuline **8**. The change in configuration is known to be achieved by oxidation-reduction process presumably via the 1, 2-dihydro-derivative. Several studies have also shown that morphinan can exist in two enantiomer forms; (-)-sinoacutine **29** and (+)-salutaridine **100** from different precursor; (+)-reticuline **8** and (-)-reticuline **82** respectively as shown in Scheme 2.4.

In Scheme 2.5, (*R*)-reticuline **82** is converted to salutaridine **100** by one-electron oxidation of phenol groups to give resonance-stabilized radicals. Salutaridine **100** can be used to form diverse branches to form various types of morphinan groups. According to (Barton et al., 1968), Salutaridine **100** can be converted to hasubanonine **101** and metaphenine **102** via phenolic oxidative coupling. Next, it also can be used to form sinomenine **104** through isosinomenine **103** by phenolic oxidative coupling.

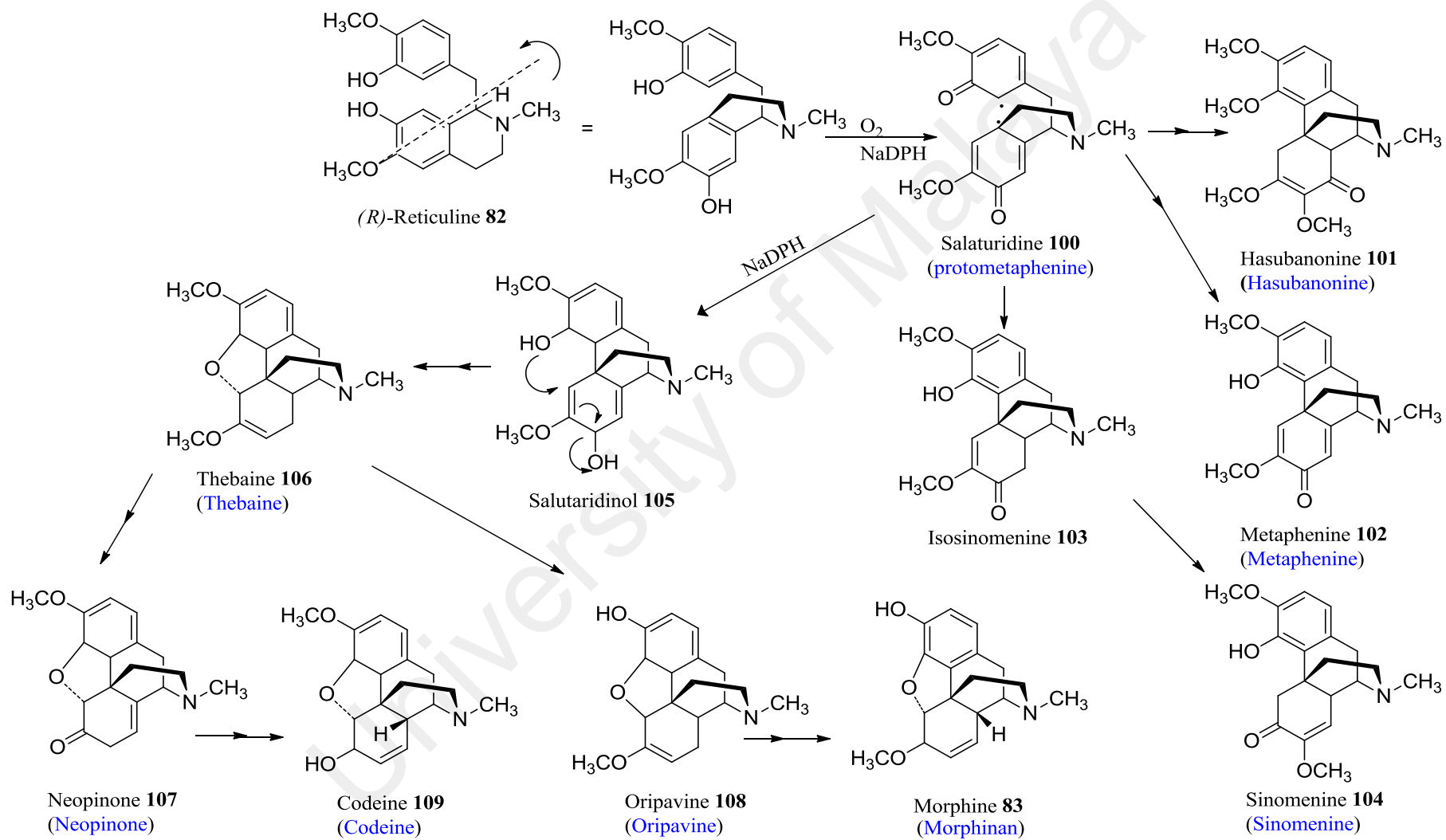
Subsequent reactions involve stereospecific reduction to salutaridinol **105**. Then, salutaridinol **105** spontaneously degrades to thebaine **106**. Thebaine **106** sits at another

branch point leading either to the codeine **109** or morphine **83** production (Bowsher et al., 2008; Dewick, 2009).

The morphine structure can be divided into two subgroups according to which family it was originated. One afforded from genera *Sinomenium* and *Stephania* (Lauraceae family), namely, salutaridine **100**, hasubanonine **101**, metaphenine **102** and morphine **83**. Another one, were isolated from *Papaver* genus (Papaveraceae family); thebaine **106**, neopinone **107**, oripavine **108**, codeine **109** and morphine **83** (Pelletier, 1970).



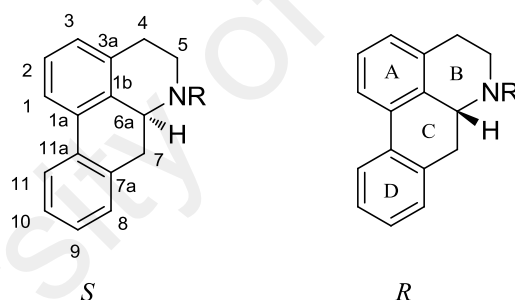
Scheme 2.4: Proposed Biosynthesis of Sinoacutine **29** and Salutaridine **100**



Scheme 2.5: Proposed Biosynthesis of Morphinan Alkaloid

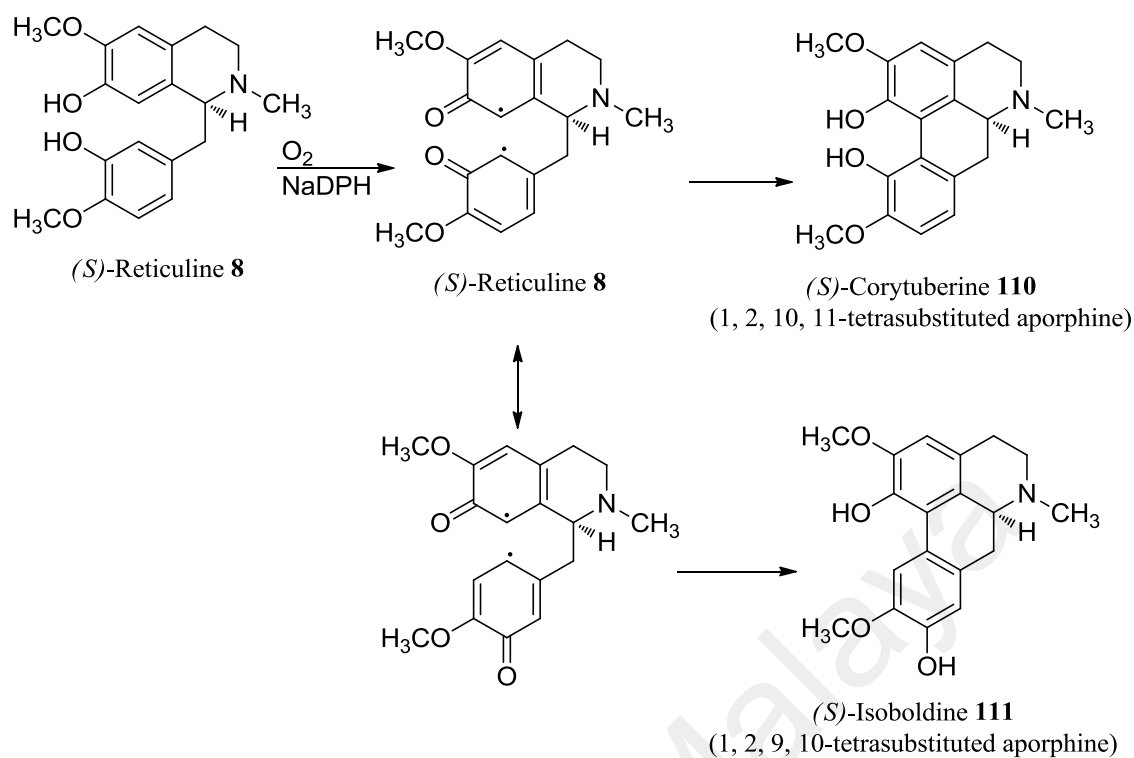
2.6.4 Aporphines

Aporphine alkaloids found abundantly in Papaveraceae, Fumariceae, Lauraceae and Ranunculaceae families (Shamma & Moniat, 1978). The aporphine alkaloids contain a twisted biphenyl system. The numbering scheme of an aporphine skeleton is generally represented by the structure below. In the naturally occurring aporphine alkaloids, positions 1 and 2 are always oxygenated and frequently other positions are also substituted either with hydroxyl, methoxyl, or methylenedioxy groups. The structure is proven to be optically active, possessing either the *R* or *S* absolute configuration. Aporphines substituted at both C-2 and C-11 or both C-9, C-10 are usually (*S*)-isomers, while aporphines unsubstituted or monosubstituted at their ring D can either be a (*S*)-isomer or (*R*)-isomer (Pelletier, 1970; Philipson et al., 1985; Shamma & Moniat, 1978).



Biosynthesis of Aporphine

Scheme 2.6 shows the biosynthesis for different types of aporphines belonging to the 1, 2, 10, 11- tetrasubstituted aporphine and 1, 2, 9, 10- tetrasubstituted aporphine. (*S*)-Reticuline **8** changes to either (*S*)-corytuberine **110** or (*S*)-Isoboldine **111** via two diradicals oxidative coupling. (Dewick, 2009).

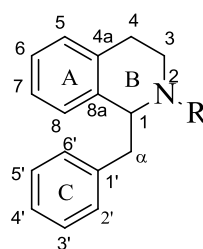


Scheme 2.6: Proposed Biogenesis of Aporphine

2.7 Structural Elucidation of Alkaloids

In the following section, the general spectral features of benzyloquinolines, bisbenzyloquinolines, aporphines and morphinandienones will be discussed briefly.

2.7.1 Benzyloquinoline



I

¹H NMR of Benzyloisoquinolines

The literature survey on Lauraceae plants produced abundantly type I benzyloisoquinoline (BIQ). Thus, this section will discuss generally ¹H and ¹³C NMR for this type.

Rings A and C are always lying on the same side of the molecule. All BIQs are substituted at positions 6, 7 as a mono- or di- substituted moiety. The asymmetric centre at C-1 bears a proton, H-1, which appears as either a triplet or doublet-doublet between δ_{H} 3.60- 3.70 ($J=6.0, 13.0$ Hz) in CDCl₃ solution. Aliphatic protons of H-3, H-4 and H- α normally appear as multiplets at δ_{H} 2.50-3.50. The methoxyl groups resonate between δ_{H} 3.50-4.00, while the *N*-methyl groups at δ_{H} 2.40-2.60. Table 2.4 lists the general chemical shifts of a ¹H NMR spectra of type I BIQ (Janssen et al., 1989).

¹³C NMR of Benzyloisoquinolines

In the ¹³C NMR spectra, generally, C-1 resonates at δ_{C} 52.0-58.0, but it will be more deshielded (δ_{C} 60.0-68.0) in the presence of an *N*-methyl group. *N*-methyl and methoxyl substituents always appear respectively at δ_{C} 40.0-45.0, and δ_{C} 52.0-63.0. The quaternary carbons at position C-4a, C-8a and C-1' resonate between δ_{C} 115.0-135.0, while quaternary carbons (C-6, C-7, C-3', C-4') attached to methoxyl or hydroxyl groups appear between δ_{C} 140.0-152.0. The methylene C- α usually appears at δ_{C} 40.0-45.0. Table 2.4 shows the general chemical shifts of a ¹³C NMR spectra for type I BIQ (Janssen et al., 1989; Marsaioli et al., 1978).

Ultraviolet Spectra of Benzyloisoquinolines

The ultraviolet spectra showed absorption maxima at λ_{max} between 285 and 291 nm which was an effect due to conjugate aromatic substitution (Shamma, 1972).

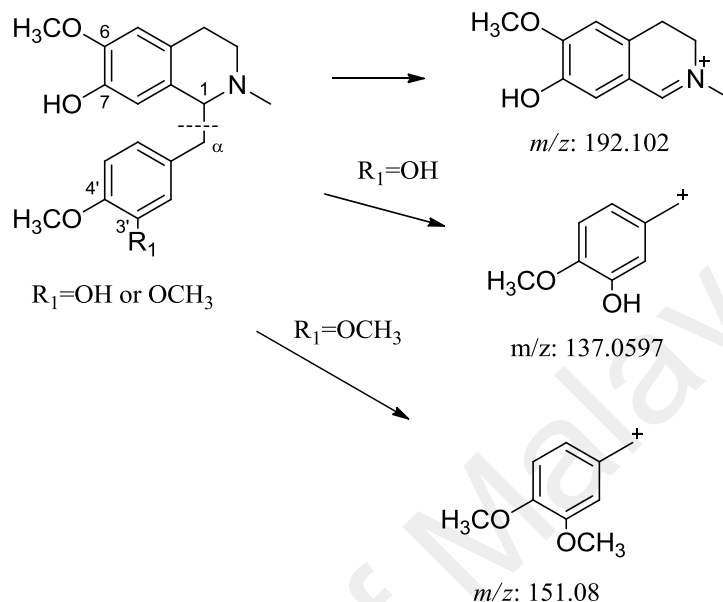
Table 2.4: General Chemical Shifts of the ¹H and ¹³C NMR Spectral Data of BIQ.

Position/(δ) CDCl ₃	Methoxy Group (δ) (Janssen et al., 1989)	Aromatic proton (δ) (Janssen et al., 1989)	<i>N</i> -methyl Group (δ) (Janssen et al., 1989)	Aliphatic Group (δ) (Janssen et al., 1989)	¹³ C- NMR (δ) (Janssen et al., 1989)
1				3.60-3.70	52-68
3				2.50-3.50	40-50
4				2.50-3.50	23-29
4a					115-135
5		6.00-7.00			110-125
6	3.50-4.00				140-152
7	3.50-4.00				140-152
8		6.00-7.00			110-125
8a					115-135
α				2.50-3.50	40-45
1'					115-135
2'		6.00-7.00			110-125
3'	3.50-4.00				140-152
4'	3.50-4.00				140-152
5'		6.00-7.00			110-125
6'		6.00-7.00			110-125
6-OCH ₃					52-63
7-OCH ₃					52-63
3'-OCH ₃					52-63
4'-OCH ₃					52-63
<i>N</i> -CH ₃			2.40-2.60		40-45

Mass Spectra of Benzylisoquinolines

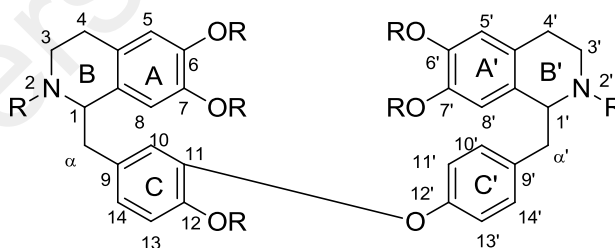
In the mass spectra, the main cleavage occurs between C-1 and C- α to form an imine ion. The fragmentation at m/z 192 will appear as a base peak indicating that the carbons C-6 and C-7 were substituted with methoxyl and hydroxyl groups that possessed an *N*-methyl group in the structure (Tomita et al., 1966).

BIQs having methoxyl and hydroxyl groups at C-3' and C-4' in their ring C will display a peak at m/z 137. Meanwhile, if two methoxyl groups are attached to it, the fragmentation peak changes to m/z 151 (Scheme 2.7) (Tomita et al., 1966).



Scheme 2.7: Proposed Fragmentation Pattern of Benzyloisoquinoline

2.7.2 Bisbenzyloisoquinolines



^1H NMR of Bisbenzyloisoquinolines

Since the Lauraceae plants usually produce three types of bisbenzyloisoquinoline (BBIQ); I, VI, VIII. This section will discuss briefly on general ^1H NMR spectra features of this types.

Type I BBIQ has one ether linkage at (C₁₁-O-C_{12'}), while, types VI and VIII BBIQ have two diphenyl ether linkages. Type VI BBIQ has diaryl ether linkages at (C_{7'}-O-C₈) and (C₁₁-O-C_{12'}), whereas, type VIII has diaryl ether linkages at (C₈-O-C_{7'}) and (C₁₁-O-C_{12'}). The presence of the two chiral carbons at C-1 and C-1' proved that this structure could give rise to four different configurations; 'anti'; (1*R*, 1'*R*), (1*S*, 1'*S*) dimers or 'syn'; (1*R*, 1'*S*), (1*S*, 1'*R*) dimers. The positive optical rotation values indicate structures to have either (1*R*, 1'*S*) or (1*R*, 1'*R*) configuration, while, negative optical rotation values indicate structures to have either (1*S*, 1'*R*) or (1*S*, 1'*S*) configuration. Different types of BBIQ have different ¹H NMR spectra characteristics depending upon the relative stereochemistry at C-1 or C-1' of the 'syn' or 'anti' configurations as shown in Table 2.5 (Guinaudeau et al., 1986).

¹H NMR spectra display similar pattern of coupling constant for aromatic protons of the lower path of BBIQ for type I, VI and VIII due to the same (C₁₁-O-C_{12'}) linkage. Generally, ABX and AA'BB' spin systems are assigned to H-10, H-13, H-14 (ring C) and H-10', H-11', H-13', H-14' (ring C') respectively. H-10 is either a broad singlet or a poorly defined doublet. The signals for H-13, H-14 are similar and appear as asymmetric doublets or broad singlets. In ring C', the four protons resonate as doublet of doublets (*dd*). Replacement of the *N*-methyl group with the *N*-H group resulting in H-1 or H-1' become more deshielded (Guinaudeau et al., 1986).

Type I BBIQ NMR spectra are nearly independent of the stereochemistry at C-1 and C-1'. The spectrum shows the superimposition of the two monomers of the benzyloquinoline (BIQ) spectra. The *N*-methyl groups usually appear at δ_H 2.50. H-8 is slightly shielded compared to the normal aromatic proton at δ_H 5.95-6.35. The actual chemical shift for H-8 depends on the substituents attached to C-7. If a methoxyl group is present at that site, the resonance for H-8 appears near δ_H 6.00. On the other hand, if a

hydroxyl group is at C-7, H-8 will be slightly more deshielded and moves to δ_{H} 6.30. The same rules apply to the other monomer (Guinaudeau et al., 1986).

Type VI BBIQ spectra will show two *N*-methyl peaks resonating close to each other at δ_{H} 2.50. The characteristic feature of the spectra which defines the *syn* or *anti* configurations for type VI depends on the H-10, H-8, 7'-OMe and 6-OMe peaks. For the *syn* configuration, H-10 appears more shielded as a broad singlet at δ_{H} 5.40- 5.65 ($J = 1.6$ Hz). For the *anti*-configuration, H-10 resonates between δ_{H} 6.55-6.75. Meanwhile, H-8 in the *syn* configuration is situated around δ_{H} 6.60-6.75. For the *anti*-configuration, the corresponding peak is further shielded (δ_{H} 6.45-6.60). In special cases, both H-10 and H-8 are further shielded and resonate at δ_{H} 4.75-4.90 and δ_{H} 6.00, respectively, due to the presence of the imine function in ring B'. 7'-OMe always resonates at δ_{H} 3.15-3.25 for the *syn* series, while for the *anti*-series it is further shielded (δ_{H} 2.95-3.10). 6-OMe resonates at δ_{H} 3.60-3.70, which is indicative of the *syn*-series, while the appearance of a shielded signal between δ_{H} 3.35-3.50 is typical of the *anti*-series (Guinaudeau et al., 1986).

In contrast to the alkaloids of type VI bisbenzylisoquinoline, the signals for the two *N*-methyl groups in the spectra for type VIII are at distinctly different positions. The *N*-methyl and *N'*-methyl each resonate between δ_{H} 2.25-2.35 and δ_{H} 2.50-2.65 respectively. The resonances of the H-10, H-8', 6'-OMe and H-10' protons will determine the *syn* or *anti* configurations for type VIII. H-10 resonates between δ_{H} 6.15-6.45 for the *syn* configuration, while for the *anti*-configuration, it resonates between δ_{H} 6.45-6.60. The singlet for H-8', on the other hand, appears close to δ_{H} 6.00, and is mostly not susceptible to stereochemical factors. 6'-OMe appears as a singlet in the range of δ_{H} 3.60-3.80 for the *syn* series, but it is appreciably shielded (δ_{H} 3.20-3.40) for the *anti*-series. In the ring C', H-10' will always appear shielded, around δ_{H} 6.40 for the

syn configuration and even further shielded, near δ_{H} 6.25, for the *anti*-configuration. The signal for H-1' always appears as a doublet of doublets, while that of H-1 as a singlet or a doublet (Guinaudeau et al., 1986).

^{13}C NMR of Bisbenzylisoquinolines

^{13}C NMR provides useful data (Table 2.5) on the types of BBIQ alkaloids. The methylene sp^3 carbons; C-4, C- α , C-3 usually appear between δ_{C} 22.0-50.0. The methoxyl carbon signals resonate at δ_{C} 56.0 except for those which are attached to C-7' (type VI) and C-7 (type VIII) which are further deshielded (δ_{C} 60.0) (Mahiou et al., 2000).

The *N*-methyl group resonates at δ_{C} 40.0-45.0 and it is practically equivalent in all BBIQs. In the presence of an imine functions at ring B or B', C-1 or C-1' which are attached to the imine group appear further downfield at δ_{C} 160.0- 165.0. The quaternary carbons, C-4a, C-4a', C-8a, C-8a', C-9 and C-9' resonate in the range of δ_{C} 125.0-135.0 (Mahiou et al., 2000).

The aromatic carbons (rings B, B', C, C') resonate between δ_{C} 120.0-130.0. However, the aromatic carbon resonates further shielded at δ_{C} 115.0-119.0 inferred to aromatic proton attached to C-8 (type VI) and C-8' (type VIII). The presence of an oxygenated substituent attached to C-6, C-6', C-7, C-7' and C-12 cause their signals to resonate further deshielded at δ_{C} 140-150 (Lin et al., 1993; Mahiou et al., 2000).

Table 2.5: General Chemical Shifts of the ^1H and ^{13}C NMR Spectral Data of BBIQ

Position	Unit	^1H - NMR General BBIQ (δ) (Guinaudeau et al., 1986)	^1H - NMR differences (δ)	^{13}C - NMR General BBIQ (δ) (Guinaudeau et al., 1986)	BBIQ Type
1	CH	4.00-5.00		55.0-65.0	
<i>N</i> -Me	<i>N</i> -CH ₃	2.50	3.60-4.05	40.0-45.0	VIII
3	CH ₂	2.50-3.50	2.25-2.35	22.0-50.0	VIII
4	CH ₂	2.50-3.50		22.0-50.0	
4a	C			125.0-135.0	
5	CH	6.20-7.60		120.0-130.0	
6	C			140.0-150.0	
6-OMe	O-CH ₃	3.00-3.90		56.0	
			3.60-3.70		IV <i>syn</i>
			3.35-3.50		IV <i>anti</i>
7	C			140.0-150.0	
7-OMe	O-CH ₃		3.10-3.20	60.0	VIII
8	CH	6.20-7.60		120.0-130.0	
			5.95-6.35		I
			6.60-6.75	115.0-119.0	IV <i>syn</i>
			6.45-6.60	115.0-119.0	IV <i>anti</i>
8a	C			125.0-135.0	
α	CH ₂	2.50-3.50		22.0-50.0	
9	C			125.0-135.0	
10	CH	5.50-6.50		120.0-130.0	
			5.40-5.60		IV <i>syn</i>
			6.45-6.60		IV <i>anti</i>
			6.15-6.45		VIII <i>syn</i>
			6.45-6.60		VIII <i>anti</i>
11	C			140.0-150.0	
12	C			140.0-150.0	
12-OMe	O-CH ₃	3.00-3.90		56.0	
13	CH	6.20-7.60		120.0-130.0	
14	CH	6.20-7.60		120.0-130.0	
1'	CH	4.00-5.00		55.0-65.0	
			3.60-4.05		VIII
<i>N'</i> -Me	<i>N'</i> -CH ₃	2.50		40.0-45.0	
			2.50-2.65		VIII
3'	CH ₂	2.50-3.50		22.0-50.0	
4'	CH ₂	2.50-3.50		22.0-50.0	
4a'	C			125.0-135.0	
5'	CH	6.20-7.60		120.0-130.0	
6'	C			140.0-150.0	
6'-OMe	O-CH ₃	3.00-3.90		56.0	
			3.60-3.80		VIII <i>syn</i>
			3.20-3.40		VIII <i>anti</i>
7'	C			140.0-150.0	
7'-OMe	O-CH ₃	3.00-3.90		60.0	IV <i>syn</i>
			2.95-3.10		IV <i>anti</i>

Table 2.5: (continued).

Position	Unit	¹ H- NMR General BBIQ (δ (Hz))	¹ H- NMR differences (δ)	¹³ C- NMR General BBIQ (δ)	BBIQ Type
8'	C			140.0-150.0	VIII
	CH		6.00	115.0-119.0	
8a'	C			125.0-135.0	
α'	CH ₂	2.50-3.50		22.0-50.0	
9'	C			125.0-135.0	VIII <i>syn</i> VIII <i>anti</i>
10'	CH			120.0-130.0	
		6.20-7.60	6.40 6.25		
11'	CH	6.20-7.60		120.0-130.0	
12'	C			140.0-150.0	
13'	CH	6.20-7.60		120.0-130.0	
14'	CH	6.20-7.60		120.0-130.0	

Mass Spectra of Bisbenzyisoquinolines

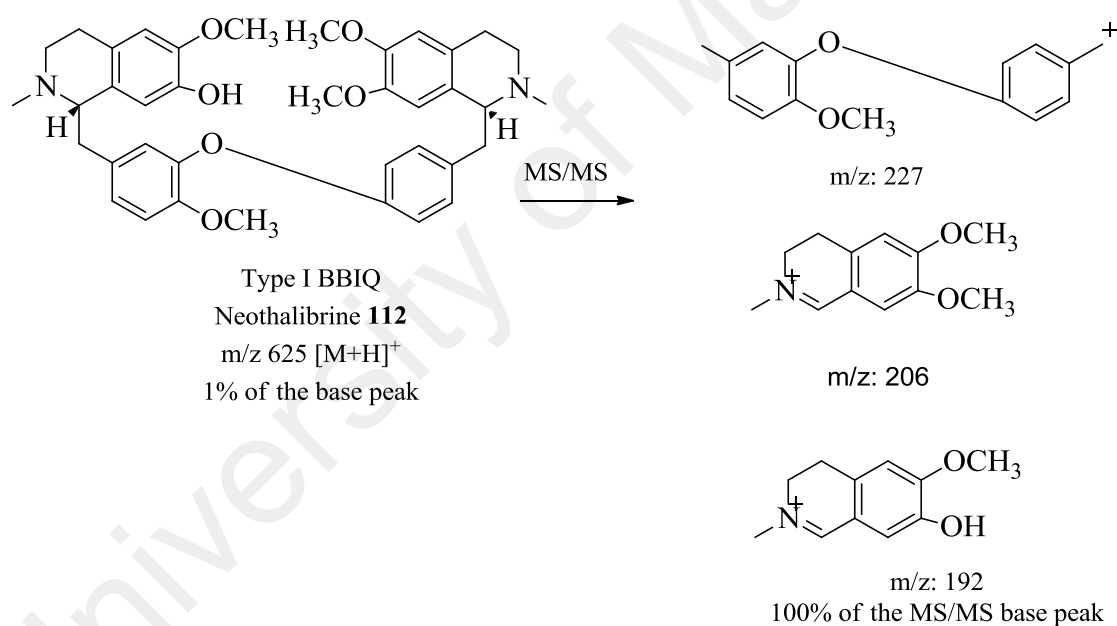
The mass spectra of the BBIQs type I include a weak peak for the molecular ion which is 0.5 to 5% of the base peak. This base peak and the next intense peak correspond to rings A and B or (rings A' and B') of the BIQ moieties. If the substitution patterns for these four rings are identical, the base peak will stand alone, and there will be no other peak of nearly equal intensity. In the mass spectrum of neothalibrine **112**, it reveals a weak protonated molecular ion at m/z 625 and a doubly-protonated molecular ion at m/z 335 which is 100% of the base peak. The MS/MS of the protonated molecular ion is shown in Scheme 2.8 (Wu & Moyer, 2004).

Type VI bisbenzyisoquinolines mass spectra shows 40 to 60% of the base peak and is always accompanied by $[M + H]^+$ peaks. The base peak originates from the top half of the dimer, and gives an indication of the substitution pattern of rings A, B, A' and B'. By subtraction, it is possible to gain information on the nature of the substituents in the rings. Oxycanthine **43** reveals an intense protonated molecular ion peak at m/z 609. The MS/MS analysis of the protonated molecular ion provides important product ions as seen in Scheme 2.9 (Wu & Moyer, 2004).

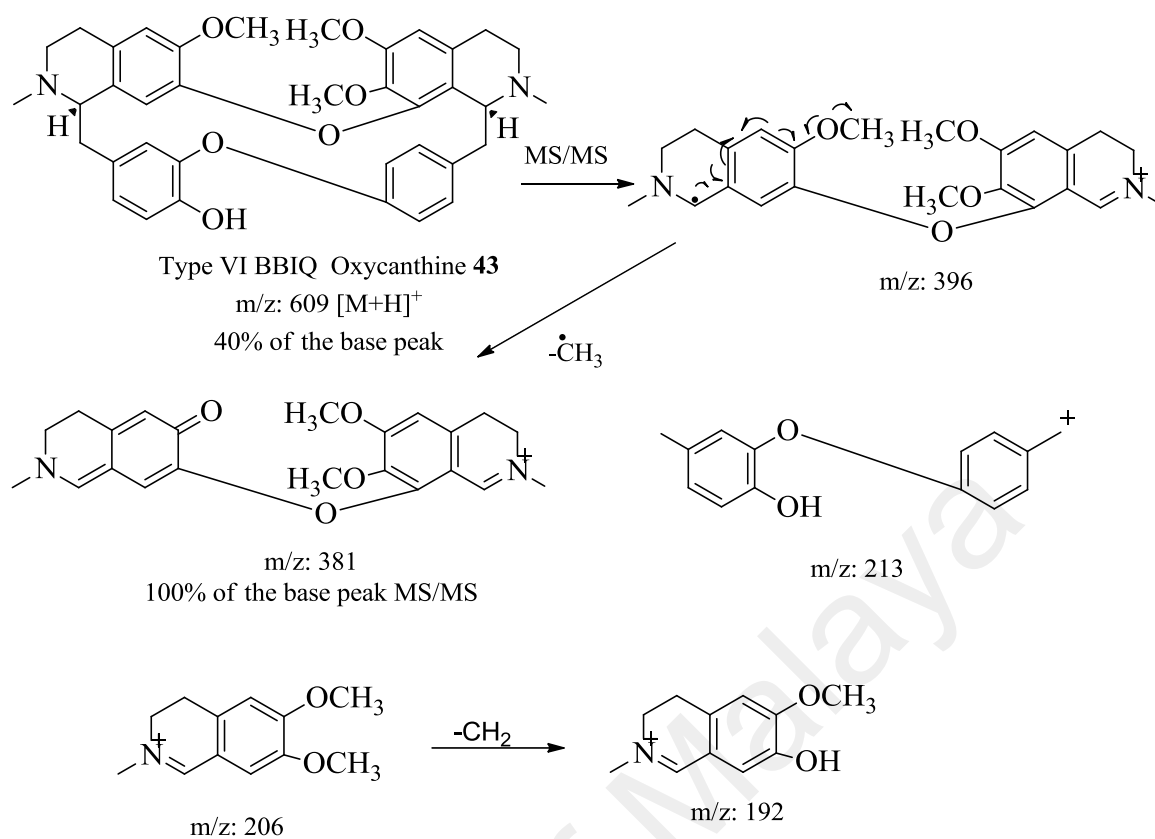
The mass fragmentation for BBIQs type VIII is essentially the same as for those of type VI. Thalrugosine **71** exhibits an apparent molecular ion at m/z 609. Thalrugosine **71** (type VIII) and oxycanthine **43** (type VI) have the same molecular ion, but the MS/MS results in different product ions depending on the position of the substituents. Scheme 2.10 shows the MS/MS fragment of the molecular ion of thalrugosine **71** (Guinaudeau et al., 1986; Wu & Moyer, 2004).

UV-Vis spectroscopy of Bisbenzylisoquinolines

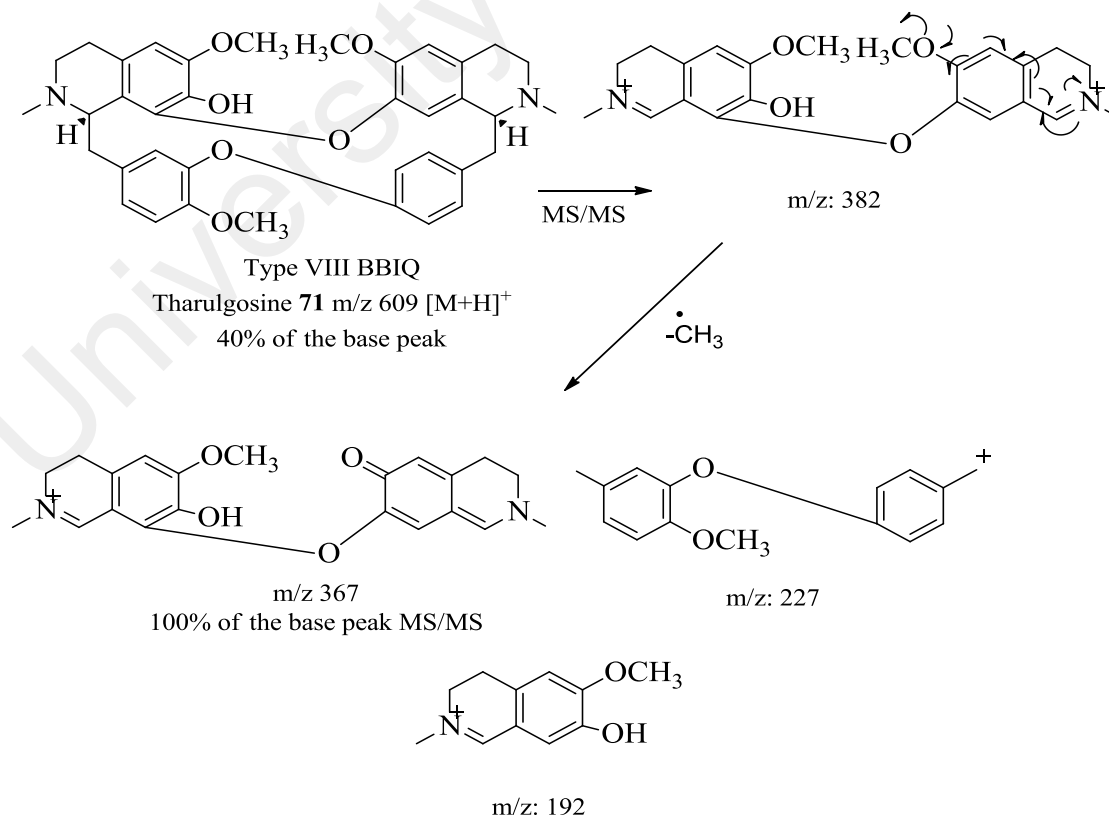
The UV absorption spectra of BBIQs are broad structureless bands with λ_{\max} 283 nm (Gibson & Turnbull, 1980; Sangster & Stuart, 1965).



Scheme 2.8 : Proposed Mass Fragmentation of Type I Bisbenzylisoquinolines

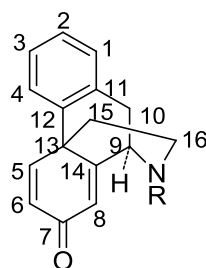


Scheme 2.9: Proposed Mass Fragmentation of Type VI Bisbenzylisoquinolines



Scheme 2.10: Proposed Mass Fragmentation of Type VIII Bisbenzylisoquinolines

2.7.3 Morphinandienones



¹H NMR of Morphinandienones

Discussion will be based on metaphenine **102** and isosinomenine (8, 14-dihydromorphinandienones) **103** (Scheme 2.5) since literature survey of *Dehaasia* frequently isolated these two types of morphinandienones alkaloids (Table 2.3).

Generally the ¹H NMR spectral data of morphinandienones contains three to four singlets of the aromatic protons between δ_{H} 6.50-7.00. The H-5 cross-conjugated cyclohexadienone protons are observed around δ_{H} 7.00 for metaphenine **102**, whereas for isosinomenine **103** it further deshielded appearing at δ_{H} 8.30. The methoxyl groups resonate at δ_{H} 3.00-4.00. The presence of three sets of resonances belonging to H-9, H-10 α and H-10 β are typical of the morphinandienone skeleton. H-9 appears as a doublet ($J= 5.6$ Hz) at δ_{H} 2.50-4.00. H-10 α resonates as a doublet ($J= 17.6$ Hz) while its geminal partner, H-10 β , as doublet of doublets ($J= 17.6, 5.6$ Hz) between δ_{H} 2.00-3.50. In addition, the multiples around δ_{H} 1.00-2.00 are assigned to the methylene protons of H-15 and H-16 (De Freitas et al., 1995; Roblot et al., 1984). General chemical shifts of the ¹H-NMR spectra are shown in Table 2.6.

¹³C NMR of Morphinandienones Alkaloids

The ¹³C NMR spectroscopic features of morphinandienones are the presence of quaternary aliphatic carbon around δ_{C} 40.0-45.0 and a conjugated ketonic carbonyl at δ_{C}

180.0-190.0 (Suau et al., 1991). General chemical shifts of the ^{13}C -NMR spectra are shown in Table 2.6.

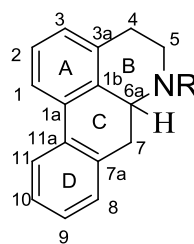
UV Spectra of Morphinandienones Alkaloids

Morphinandione alkaloids have an α, β -unsaturated carbonyl moiety. The spectrum is characterized by λ_{max} at 232 nm and a broad band at 265 nm (Kashiwaba et al., 1996; Sangster & Stuart, 1965).

Table 2.6: General Chemical Shifts of the ^1H and ^{13}C NMR of Morphinandienones

Position	Unit	^1H - NMR General Morphinanandienones δ (J, Hz) (De Freitas et al., 1995)	^{13}C - NMR General Morphinanandienones δ (Suau et al., 1991)
1	CH	6.50-7.00	110.0-120.0
2	CH	6.50-7.00	110.0-120.0
3	C		125-160
3-OMe	OCH ₃	3.00-4.00	56.0
4	C		125-160
5	CH	6.50-7.00 7.00 (metaphenine) 8.30 (isosinomenine)	110.0-120.0
6	C		125-160
6-OMe	OCH ₃	3.00-4.00	56.0
7	C=O		180.0-190.0
8	CH	6.50-7.00	110.0-120.0
9	CH	2.50-4.00 (<i>d</i> , 5.6)	60.0
10	CH ₂	α 2.00-3.50 (<i>d</i> , 17.6) β 2.00-3.50 (<i>dd</i> , 17.6, 5.6)	35.0-50.0
11	C		125-160
12	C		125-160
13	C		40.0-45.0
14	C		125-160
15	CH ₂	1.00-2.50	35.0-50.0
16	CH ₂	1.00-2.50	35.0-50.0
NCH ₃	NCH ₃	2.50	40.0-45.0

2.7.4 Aporphines



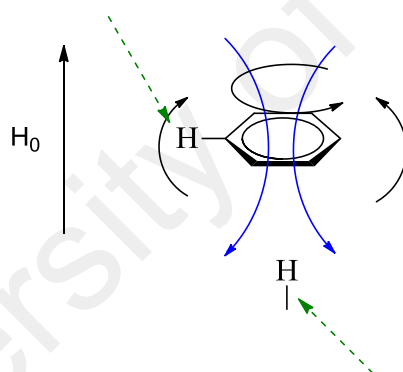
¹H NMR of Aporphines

The ¹H-NMR spectral data (Table 2.7) of aporphines consist; three to four aromatic signals (H-3, H-8, H-9 and H-11), one methine (H-6a), three methylenes (H-4, H-5, H-7), one *N*-CH₃ or NH group and substituents belonging to either methoxyl or hydroxyl groups attached to C-1, C-2, C-9, C-10 or C-11. Lauraceae plants abundantly afforded two types of aporphines; 1, 2, 9, 10-tetrasubstituted aporphines and 1, 2, 10, 11-tetrasubstituted aporphines. Different coupling patterns can be seen for aromatic protons of both types, in which; H-3, H-8 and H-11 display as a singlets, proving that it belong to 1, 2, 9, 10-tetrasubstituted aporphine. On the other hand, for a 1, 2, 10, 11-tetrasubstituted aporphine type, H-3 resonates as a singlet and H-8 and H-9 as a pair of doublets ($J=8.0$ Hz). The *N*-methyl resonates between δ_{H} 2.50-2.60 and the aliphatic protons of H-4, H-5, H-6a and H-7 displayed complex splitting patterns between δ_{H} 2.40-4.44 (Baarschers et al., 1964).

Aromatic hydrogens; H-3, H-8, H-9 are located between δ_{H} 6.38-7.00. Meanwhile, H-11 usually resonates more deshielded as a singlet at δ_{H} 7.68-8.75 with the presence of substituents at C-1. The methoxyl attached to C-1 normally resonates at δ_{H} 3.55 in comparison to other methoxyls (δ_{H} 3.65-3.90). The relatively more shielded methoxyl is due to the anisotropic character of the benzene ring. In the benzene rings, the π -electron delocalized over the ring atoms are induced to circulate above or below the plane of the

ring. This circulation is such to oppose the applied magnetic field at the centre of the ring but reinforce it in the region where the aromatic protons are located. This results in a strong deshielding of the aromatic protons, H-11, nevertheless, if a nucleus is held above the centre of the aromatic ring, it will be strongly shielded, thus explaining the upfield shift of C-1. Normally, when both positions C-1 and C-11 are substituted; C-2 is substituted too. Thereby, the methoxyl group attached to C-1 will be sterically hindered, therefore resulting in the push of the 1-OMe proton out of the ring plane A, which in a shielded zone (B) (Figure 2.2). Furthermore, the ring A and ring D are facing each other; hence the methoxyl proton can rearrange them on the adjacent ring, which happened to be a shielded zone (B) (Baarschers et al., 1964).

The local magnetic field is higher here, so lower external field (downfield) is needed to achieve resonance: deshielding zone (A)



The local magnetic field is lower here, so higher external field (upfield) is needed to achieve resonance: shielding zone (B)

Figure 2.2: The Circulation of the π - electrons around a Benzene Ring Produces a Magnetic Field: Deshielding (A) and Shielding (B) Zones around the Benzene Ring.

^{13}C NMR of Aporphines

In the ^{13}C NMR spectra, sp^2 carbons bearing aromatic protons normally resonate at δ_{C} 105.0-112.0, while the sp^2 quaternary carbons at position C-1a, C-1b, C-3a, C-7a, and C-11a appear between δ_{C} 119.0-130.0. The sp^3 methylene carbon at C-4 displays a peak at δ_{C} 28.0-30.0; C-7 resonates at δ_{C} 35.0; C-5 and C-6a δ_{C} 42.0 and δ 52.0, respectively.

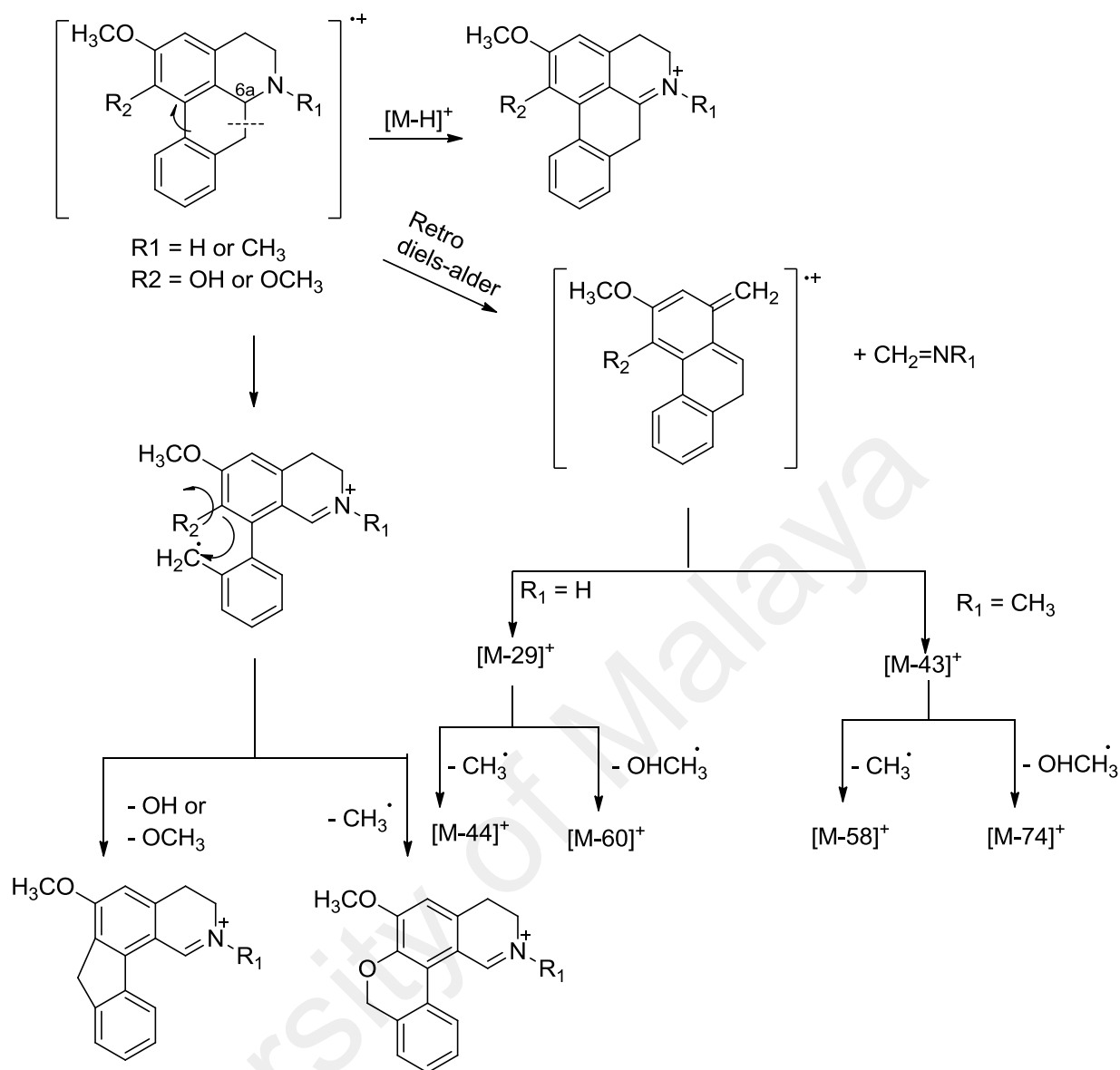
The *N*-methyl group resonates at δ 43.0. The methoxyl carbon signal appears between δ_C 56.0-62.0 (Jackman et al., 1979).

Table 2.7: ^1H and ^{13}C NMR Data (δ) of Aporphine Alkaloids in CDCl_3

Position	Methoxy Group (Baarschers et al., 1964)	Aromatic Proton (δ) (Baarschers et al., 1964)	<i>N</i> -methyl Group (δ) (Baarschers et al., 1964)	Aliphatic Group (δ) (Baarschers et al., 1964)	^{13}C NMR (δ) (Jackman et al., 1979)
1-OMe	3.55-3.65				56.0-62.0
1a					119.0-130.0
1b					119.0-130.0
2-OMe	3.65-3.90				56.0-62.0
3		6.38-7.00			105.0-112.0
3a					119.0-130.0
4				2.40-4.44	28.0-30.0
5				2.40-4.44	42.0
6- <i>N</i> Me			2.50-2.60		43.0
6a				2.40-4.44	52.0
7				2.40-4.44	35.0
7a					119.0-130.0
8		6.38-7.00			105.0-112.0
9	3.65-3.90	6.38-7.00			105.0-112.0
10	3.65-3.90				56.0-62.0
11	3.65-3.90	7.68-8.75			105.0-112.0
11a					119.0-130.0

Mass Spectroscopy of Aporphines

In the mass spectrum, the fragmentations of the aporphines are mainly due to the loss of the hydrogen attached to C-6a. The $[\text{M}-1]^+$ peak always serves as the base peak of the molecule. Next, the fragment loss is due to the methylene imine group ($\text{CH}_2=\text{NR}$) which is expelled via a Retro-Diels Alder mechanism. Aporphine compounds having either *N*-H or *N*- CH_3 groups will display peaks at $[\text{M}-29]^+$ and $[\text{M}-43]^+$, respectively. The ion formed can further lose another methyl or methoxyl to produce peaks at $[\text{M}-74]^+$, $[\text{M}-58]^+$, $[\text{M}-60]^+$ and $[\text{M}-44]^+$ peaks. The fragmentation patterns are shown in Scheme 2.11 (Jackson & Martin, 1966).



Scheme 2.11: Proposed Mass Fragmentation Pattern of an Aporphines

Ultraviolet Spectroscopy of Aporphines

Most aporphine alkaloids are substituted at C-10 or C-11 (ring D) and are variably substituted at C-1 and C-2 (ring A). The zone of absorption in the ultraviolet region for the skeleton depends on the substitution of ring D. Ultraviolet spectra of an aporphine can be classified into two main ultraviolet absorptions. For aporphines substituted at C-10, they show maxima at λ_{max} 282 and 303-310 nm of about equal intensities. Meanwhile, for aporphines substituted at C-11, they show maxima at λ_{max} 268-272 nm

and other absorption with lowered intensity at λ_{\max} 303-310 nm (Sangster & Stuart, 1965). The general observations are listed in Table 2.8 (Pelletier, 1970).

Table 2.8: Ultraviolet Spectroscopy of Aporphine Type Alkaloids.

Substitution Pattern	Maximum Absorption (nm)
1, 2	234, 273, 312
1, 2, 9	233, 280, 305
1, 2, 10	226, 266, 275, 305
1, 2, 11	220, 265, 272, 300
1, 2, 9, 10	220, 282, 305
1, 2, 10, 11	220, 270, 305

2.8 Pharmacological Importance of Isoquinoline Alkaloids

Numerous investigations have demonstrated that certain isoquinoline structures such as BIQs, BBIQs, morphinandienones and aporphines have potent medicinal values. This section discusses the latest discoveries regarding the respective skeletons with their medicinal properties.

2.8.1 Benzyloisoquinolines

(*S*)-reticuline **8** has been found to stimulate the growth of cultured hair cells of mice and it is currently being tested as a potential treatment for baldness. (*S*)-reticuline **8** can also be used as a precursor for the synthetic production of other pharmaceutical products (Bowsher et al., 2008). Recently, (Kashiwada et al., 2005) has found that (*S*)-norcoclaurine **78** possess anti HIV activity.

Papaverine **89** is the most important benzyloisoquinoline alkaloid from a pharmacological point of view. It has little or no analgesic properties. It exerts a strong spasmolytic action on uterus of the pregnant woman; it is also used as a coronary and

peripheral vasodilator. In addition, papaverine **89** also has been used in expectorant preparation, and in the treatment of gastrointestinal spasm. Sometimes it is also used as an effective treatment for male impotence (Dewick, 2009).

2.8.2 Bisbenzylisoquinolines

Several bisbenzylisoquinolines exhibit potent *in vitro* antiplasmodial activities such as costaricine **92** isolated from *Nectandra salicifolia* (Kunth) Nees (Böhlke et al., 1996), and cepharanthine **93** from *Stephania erecta* Craib. (Tamez et al., 2005) which showed antiplasmodial activities against both *P. falciparum* clones the D6 and W2 strains. 2-*N*-methyltelobine **97** (Saxena et al., 2003) and insularine **98** (Marshall et al., 1994) also exhibit antiplasmodial activities.

Tetrandrine **94** isolated from the roots of *Stephania tetrandra* S.Moore. also possessed antimalarial activity (Zuguang & Knox, 1989) and it is also used to treat hypertension (Wong et al., 2000), as well as it exhibits anti-inflammatory (Serck et al., 2000), antiproliferative (Teik et al., 2006) and antioxidant (Cao, 1996) activities. Recently, tetrandrine **94** has also been reported to have activity against Ebola virus (Sakurai et al., 2015) and Arenavirus (Rathbun et al., 2015) by inhibiting viruses from human haemorrhagic fever.

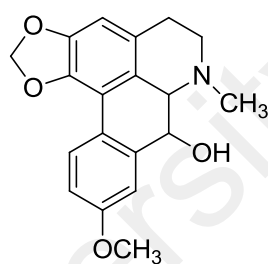
Moreover, cepharanthine **93** possess cytotoxic activity against three human cancer cells line; HT29 (colon adenocarcinoma), LS174T (colon adenocarcinoma), and HepG2 (hepatocellular carcinoma) (Bun et al., 2009). Tubocurarine **95**, the active component in the arrow poison curare from *Chondrodendron tomentosum* is injected as a muscle relaxant in surgical operations, thus reducing the need for deep anaesthesia (Dewick, 2009). Warifteine **96** inhibited spasmolytic effect, antileishmanial and muscle relaxant in the guinea-pig trachea (Cavalcanti da Silva et al., 2012; Cortes et al., 1995).

2.8.3 Morphinanandienones

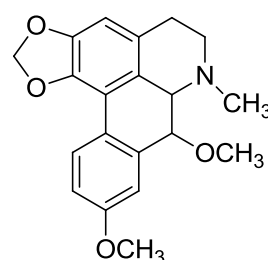
Morphine **83** is a powerful analgesic and narcotic, and remains one of the most valuable analgesics for relieve of severe pain. It also induces a state of euphoria and mental detachment, together with nausea, vomiting, constipation, tolerance and addiction. Codeine **109** is also used as an analgesic and antitussive action, helps to relieve and prevent cough (Dewick, 2009).

2.8.4 Aporphines

Oliveridine **113** and oliverine **114** isolated from Annonaceae family is being test for anti-parkinson and hypotension in mice model (Shamma & Moniat, 1978). (Naaz et al., 2013) reported that Oliveridine **113** also demonstrated *in silico* anti-cholinesterase agent for Alzhemier disease.



113



114

CHAPTER 3: RESULTS AND DISCUSSION

3.1 General

Chemical screening of the leaves and bark of *Alseodaphne corneri* and *Dehaasia longipedicellata*, belonging to the Lauraceae family were studied in detail for their alkaloidal contents. The extraction and isolation procedures of the alkaloids from these two species are described in chapter 7. The following sub-chapters will focus primarily on the structural elucidation of the isolated alkaloids. Their structures were established through several spectroscopic methods; UV, IR, MS, 1D-NMR, 2D-NMR and also upon comparison with those reported in the literature.

The leaves and bark of *A. corneri* in total yielded sixteen alkaloids (Table 3.1). One benzylisoquinoline; reticuline **8** and four aporphine alkaloids namely; *N*-methyl-laurotetanine **26**, isocorydine **41**, norisocorydine **42** and *N*-methyl-lindcarpine **123** were isolated from the leaves. The bark also afforded aporphine alkaloid; laurotetanine **27** and a new compound; cornerin A **124** together with ten bisbenzylisoquinoline alkaloids namely 2-norobaberine **115**, 3', 4'-dihydonorstephasubine **19**, 3', 4'-dihydo-stephasubine **119**, gyrolidine **18**, norstephasubine **20**, *O*-methyllimacusine **118**, *O*, *O*-dimethylgrisabine **48**, stephasubimine **121**, stephasubine **120** and thalrugosine **71**. All of these bisbenzylisoquinolines belong to either types IV or VIII which will be discussed in the following sub-chapters. The chemical study of *D. longipedicellata* yielded eight known alkaloids (Table 3.1) with milonine **46** and sebiferine **47** found in both the leaves and bark. The investigation of the leaves afforded two morphinandienones; **46** and **47**, one benzylisoquinoline; reticuline **8** and one aporphine; laurotetanine **27**. Subsequently, two aporphines; norboldine **36** and boldine **37**, three morphinandienones; sinoacutine **29**, milonine **46** and sebiferine **47** and a bisbenzylisoquinoline; *O*, *O*-dimethylgrisabine **48**, were isolated from the bark.

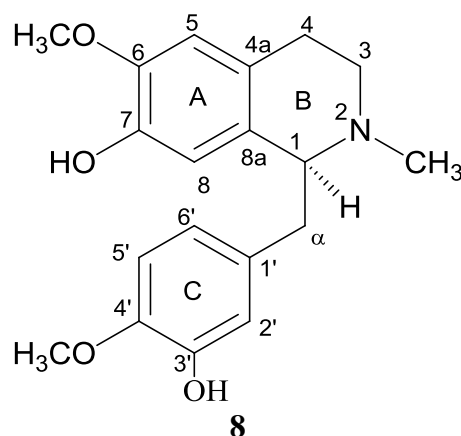
Table 3.1: The Alkaloids Isolated from *Alseodaphne corneri* and *Dehaasia longipedicellata*

No.	Alkaloids	Plant	Plant part	Type	Carbon Skeleton	Page No.
1	2-norobaberine 115	<i>A. corneri</i>	Bark	Bisbenzylisoquinoline	Type VI (two ether linkages between 7-8', 11-12') BBIQ	78
2	3', 4'-dihydonorstephasubine 19	<i>A. corneri</i>	Bark	Bisbenzylisoquinoline	Type VI (two ether linkages between 7-8', 11-12') BBIQ	101
3	3', 4'-dihydropstephasubine 119	<i>A. corneri</i>	Bark	Bisbenzylisoquinoline	Type VI (two ether linkages between 7-8', 11-12') BBIQ	107
4	Boldine 37	<i>D. longipedicellata</i>	Bark	Aporphine	1, 2, 9, 10-tetrasubstituted aporphine	169
5	Cornerin A 124	<i>A. corneri</i>	Bark	Benzyltetrahydroisoquinoline	Benzyltetrahydroisoquinoline	196
5	Gyrolidine 18	<i>A. corneri</i>	Bark	Bisbenzylisoquinoline	Type VI (two ether linkages between 7-8', 11-12') BBIQ	89
6	Isocorydine 41	<i>A. corneri</i>	Leaves	Aporphine	1, 2, 10, 11-tetrasubstituted aporphine	136
7	Laurotetanine 27	<i>A. corneri</i>	Bark	Aporphine	1, 2, 9, 10-tetrasubstituted aporphine	160
8	Milonine 46	<i>D. longipedicellata</i>	Leaves			
		<i>D. longipedicellata</i>	Bark	Morphinandienone	Isosinomenine	173
9	<i>N</i> -methyllaurotetanine 26	<i>A. corneri</i>	Leaves	Aporphine	1, 2, 9, 10-tetrasubstituted aporphine	152
10	<i>N</i> -methyllindcarpine 123	<i>A. corneri</i>	Leaves	Aporphine	1, 2, 10, 11-tetrasubstituted aporphine	148
11	Norbaldine 36	<i>D. longipedicellata</i>	Bark	Aporphine	1, 2, 9, 10-tetrasubstituted aporphine	165
12	Norisocorydine 42	<i>A. corneri</i>	Leaves	Aporphine	1, 2, 10, 11-tetrasubstituted aporphine	144
13	Norstephasubine 20	<i>A. corneri</i>	Bark	Bisbenzylisoquinoline	Type VI (two ether linkages between 7-8', 11-12') BBIQ	112

Table 3.1: (continued).

No.	Alkaloids	Plant	Plant part	Type	Carbon Skeleton	Page No.
14	<i>O</i> -methyllimacusine 118	<i>A. corneri</i>	Bark	Bisbenzylisoquinoline	Type VI (two ether linkages between 7-8', 11-12') BBIQ	95
15	<i>O-O</i> -dimethylgrisabine 48	<i>D. longipedicellata</i>	Bark	Bisbenzylisoquinoline	Type I (two ether linkages between 8-7', 11-12') BBIQ	190
16	Reticuline 8	<i>A. corneri</i>	Leaves	Benzylisoquinoline	3', 4', 6, 7-benzyltetrahydroisoquinoline	69
		<i>D. longipedicellata</i>	Bark			
17	Sebiferine 47	<i>D. longipedicellata</i>	Bark	Morphinandienone	Protometaphenine	185
			Leaves			
18	Sinoacutine 29	<i>D. longipedicellata</i>	Bark	Morphinandienone	Protometaphenine	181
19	Stephasubimine 121	<i>A. corneri</i>	Bark	Bisbenzylisoquinoline	Type VI (two ether linkages between 7-8', 11-12') BBIQ	122
20	Stephasubine 120	<i>A. corneri</i>	Bark	Bisbenzylisoquinoline	Type VI (two ether linkages between 7-8', 11-12') BBIQ	117
21	Thalrugosine 71	<i>A. corneri</i>	Bark	Bisbenzylisoquinoline	Type VIII (two ether linkages between 8-7', 11-12') BBIQ	127

3.1.1 Reticuline 8



Reticuline **8** is an important precursor in the biosynthesis of various isoquinoline alkaloids that has been discussed in chapter 2 (Section 2.6, page 33). It was obtained as a pale brown amorphous powder with $[\alpha]_D^{25} +30.0^\circ$ ($c=0.20$, CHCl_3). The UV spectrum exhibited an absorption maximum at λ_{max} 285 nm which suggested the presence of a benzylisoquinoline moiety (Sangster & Stuart, 1965). The IR spectrum revealed absorption at ν_{max} 3349 cm^{-1} due to the OH stretching vibration. The EIMS (Figure 3.2) showed a pseudo-molecular ion peak $[\text{M}+\text{H}]^+$ at m/z 330.1720 corresponding to a molecular formula of $\text{C}_{19}\text{H}_{23}\text{NO}_4$ (calcd. for $\text{C}_{19}\text{H}_{24}\text{NO}_4$, 330.1705).

The $^1\text{H-NMR}$ spectrum (Figure 3.3) displayed signals corresponding to five aromatic protons, two O-CH_3 groups, one N-CH_3 group, one $\text{CH}_2\text{-CH}_2\text{-N}$ group, one shielded methine proton, and one isolated methylene group. The signals in the aromatic region were ascribed to the singlets of H-5 (δ_{H} 6.52) and H-8 (δ_{H} 6.36) of ring A, and the three protons of ring C with a AMX spin system forming a doublet of doublets (dd) ($J=8.2$ Hz, 2.0 Hz) centered at H-6' (δ_{H} 6.57) *ortho*-coupled to H-5' (δ_{H} 6.71, d , $J=8.2$ Hz) and *meta*-coupled to H-2' (δ_{H} 6.77, d , $J=2.0$ Hz). The two methoxyl signals were present at δ_{H} 3.83 and δ_{H} 3.84. The former was attached to C-6, while the latter to C-4'. A singlet, typical of an *N*-methyl group, appeared at δ_{H} 2.45. Subsequently, H-1 resonated as a dd

($J=6.1, 14.0$ Hz) at δ_{H} 3.68, while, $\text{H}_{\text{A}-\alpha}$ resonated as a *dd* ($J=14.0$ Hz, 6.1 Hz) at δ_{H} 3.04 and $\text{H}_{\text{B}-\alpha}$ as a broad doublet ($J=14.0$ Hz) at δ_{H} 2.74. The other aliphatic protons appeared as multiplets in the region between δ_{H} 2.55–3.20.

The aliphatic protons that appear as multiplets were assigned based on the COSY spectrum (Figure 3.5) which showed cross peaks between $\text{CH}_2\text{-3}/\text{CH}_2\text{-4}$ and $\text{CH}_2\text{-}\alpha/\text{CH-1}$. The correlation between $\text{H-5'}/\text{H-6'}$ belonging to the vicinal aromatic protons was also observed in the COSY spectrum.

The ^{13}C NMR (Figure 3.4) and HSQC (Figure 3.6) spectra showed 19 carbon signals comprising five sp^2 methine carbons (C-5, C-8, C-2', C-5', C-6'), seven sp^2 quaternary carbons (C-4a, C-8a, C-6, C-7, C-1', C-3', C-4'), three sp^3 methylene carbons (C-3, C-4, C- α), one sp^3 methine carbon (C-1), two methoxyl groups (6-OCH₃, 4'-OCH₃) and one *N*-CH₃ group. Among the seven sp^2 quaternary carbons, four of them were oxygenated (C-6, C-7, C-3', C-4') and appeared more downfield compared to the others. The sp^3 methine carbon (C-1) appeared more deshielded at δ_{C} 64.6 indicating the presence of an *N*-methyl group adjacent to it. Another significant feature was the sp^2 methine carbon, C-6' which resonated in the deshielded region at δ_{C} 121.0 in comparison to C-5, C-8, C-2' and C-5'.

The HMBC analysis showed the following cross peaks centered at C- α ; H-1 to C- α , H-2', H-6' to C- α . These correlations confirmed the connectivity between ring C and ring B through a methylene group C- α . In addition, the correlations of H-8 to C-4a and H-5 to C-8a proved that ring B and ring A are fused together via the C-4a-C-8a junction. The full assignments of all the cross peaks in order to construct this alkaloid are shown in Figure 3.7.

Based on the spectral data and upon comparison with literature (Table 3.2), the above alkaloid was assigned as (+)-reticuline **8** (Castro et al., 1985).

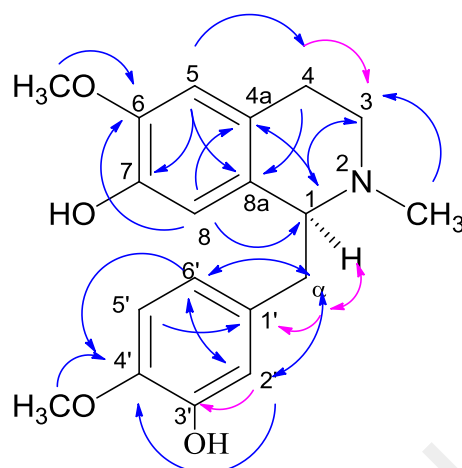


Figure 3.1: ^1H - ^{13}C Correlations Observed in the HMBC spectrum of Reticuline **8**

Table 3.2: ^1H and ^{13}C -NMR Data of Reticuline **8** in CDCl_3

Position	Unit	^1H - NMR 8 CDCl_3 , 400 MHz, δ (J , Hz)	^1H - NMR CDCl_3 , 360 MHz, δ (J) (Castro et al., 1985)	^{13}C - NMR 8 CDCl_3 , 100 MHz, δ	^{13}C - NMR CDCl_3 , 100 MHz, δ (Castro et al., 1985)
1	CH	3.68 (<i>dd</i> , 14.0, 6.1)		64.6	64.5
3	CH ₂	α 3.18 (<i>m</i>) β 2.78 (<i>m</i>)		46.8	46.8
4	CH ₂	α 2.82 (<i>m</i>) β 2.57 (<i>m</i>)		24.9	25.8
4a	C			125.1	124.9
5	CH	6.52 (<i>s</i>)	6.54 (<i>s</i>)	110.7	113.7
6	C			145.4	145.8
6-OMe	O-CH ₃	3.83 (<i>s</i>)	3.85 (<i>s</i>)	55.9	55.9
7	C			143.5	143.3
8	CH	6.36 (<i>s</i>)	6.39 (<i>s</i>)	113.8	110.5
8a	C			129.8	132.9
α	CH ₂	α 3.04 (<i>dd</i> , 14.0, 6.1) β 2.74 (<i>d</i> , 14.0)		41.0	40.9
1'	C			133.0	129.8
2'	CH	6.77 (<i>d</i> , 2.0)	6.77 (<i>d</i>)	115.7	110.5
3'	C			145.1	145.2
4'	C			145.3	145.6
4'-OMe	O-CH ₃	3.84 (<i>s</i>)	3.85 (<i>s</i>)	55.9	55.9
5'	CH	6.71 (<i>d</i> , 8.2)	6.73 (<i>d</i>)	110.5	113.7
6'	CH	6.57 (<i>dd</i> , 8.2, 2.0)	6.60 (<i>dd</i>)	121.0	120.8
2-NMe	N-CH ₃	2.45 (<i>s</i>)	2.47 (<i>s</i>)	42.4	42.4

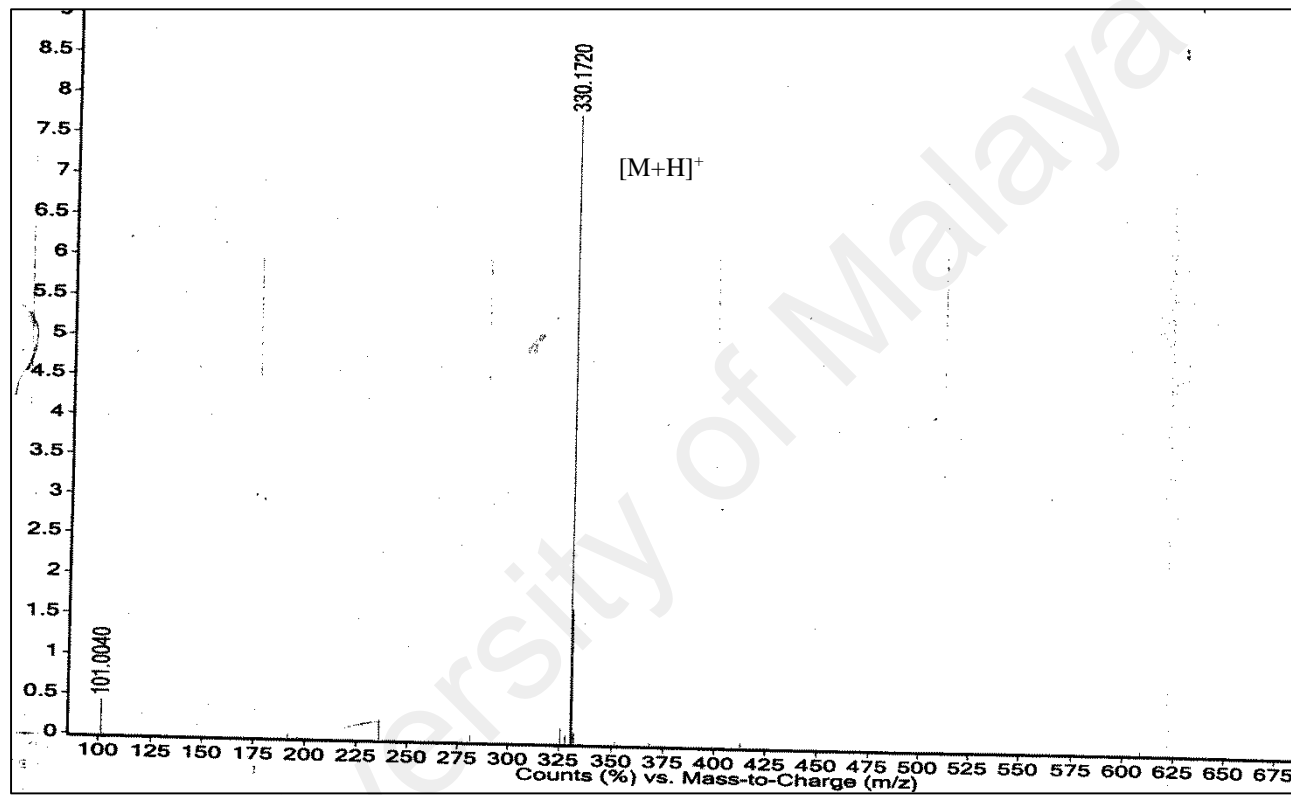


Figure 3.2: LCMS Spectrum of Reticuline 8

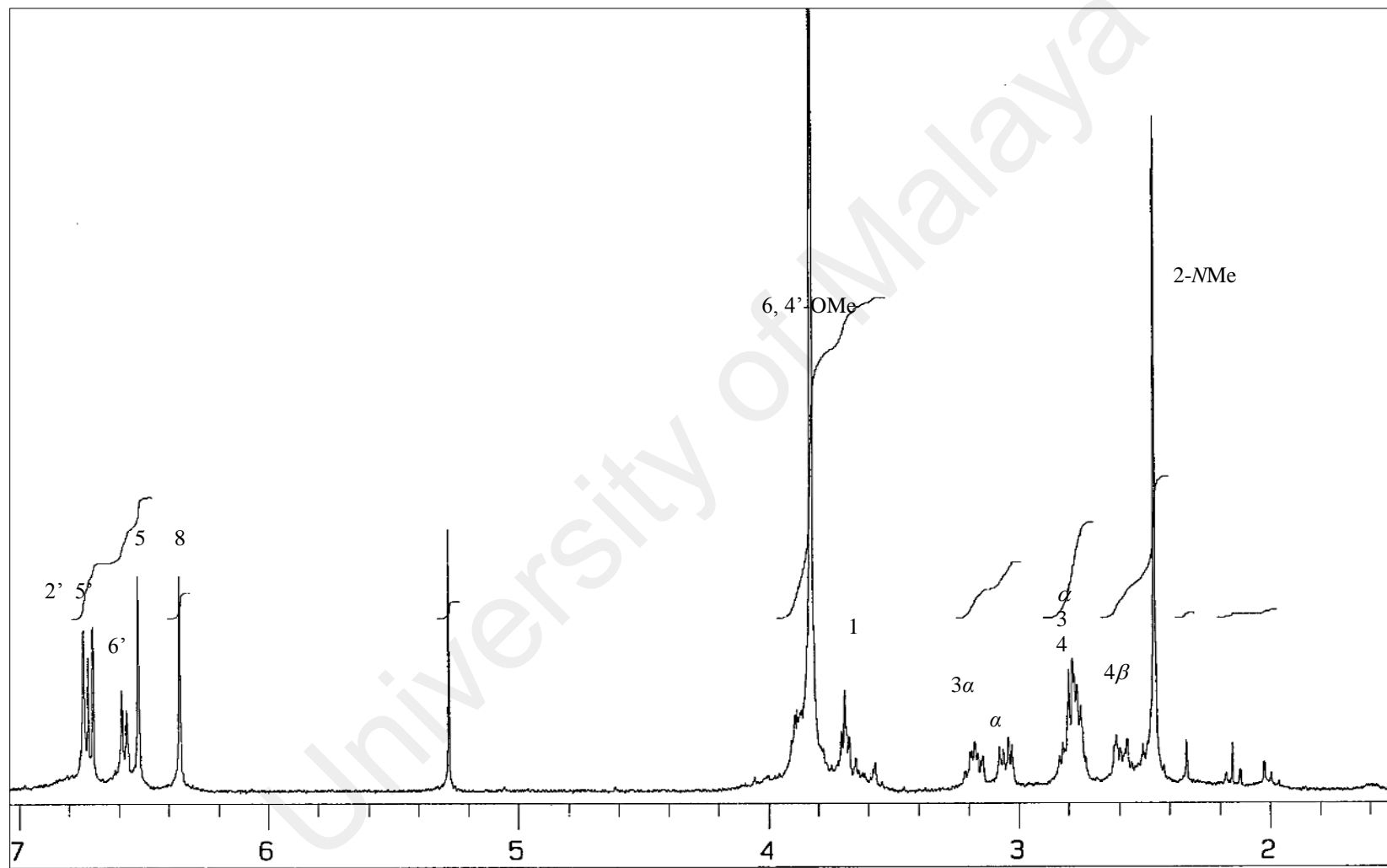


Figure 3.3: ^1H NMR Spectrum of Reticuline 8

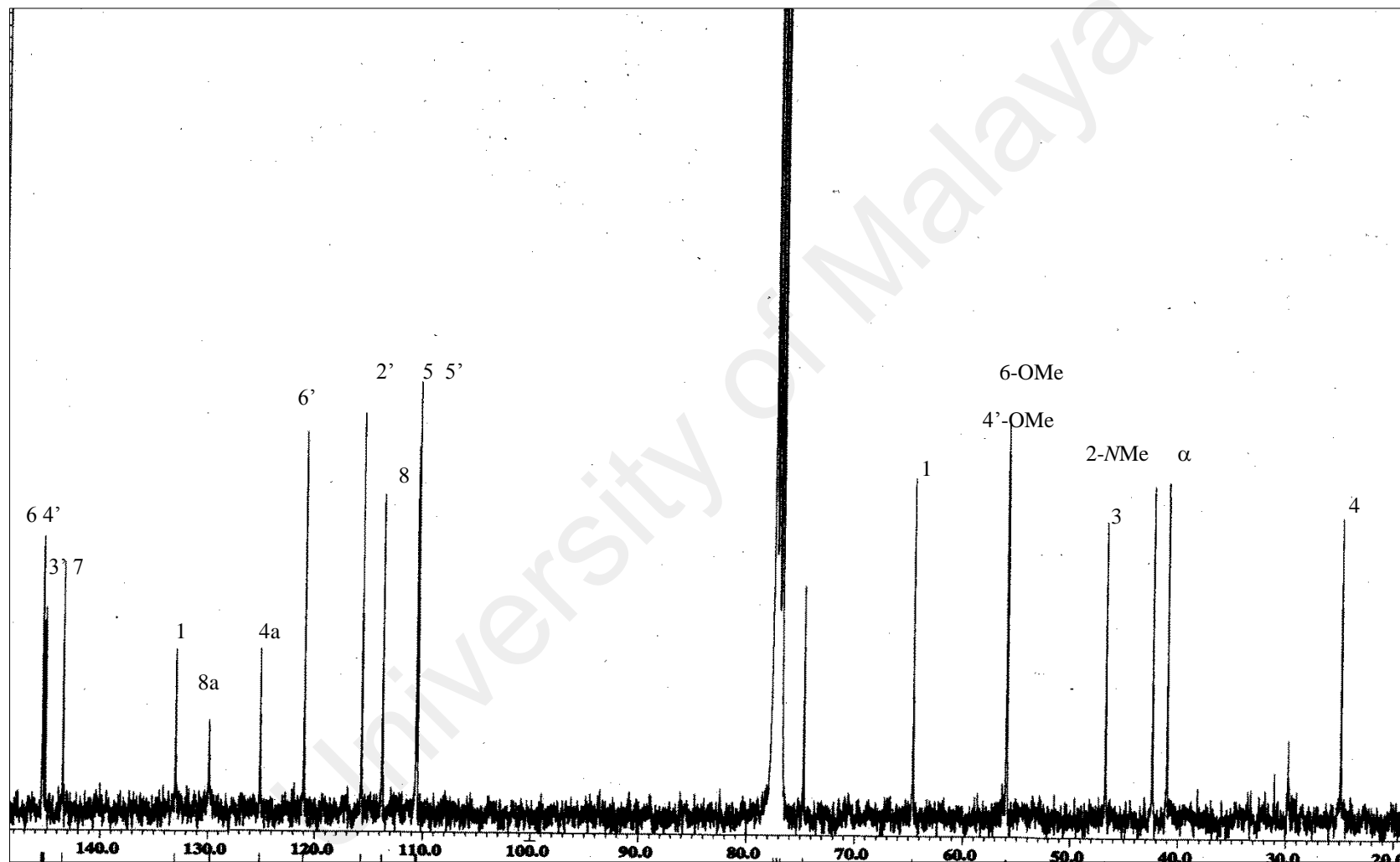


Figure 3.4: ^{13}C NMR Spectrum of Reticuline 8

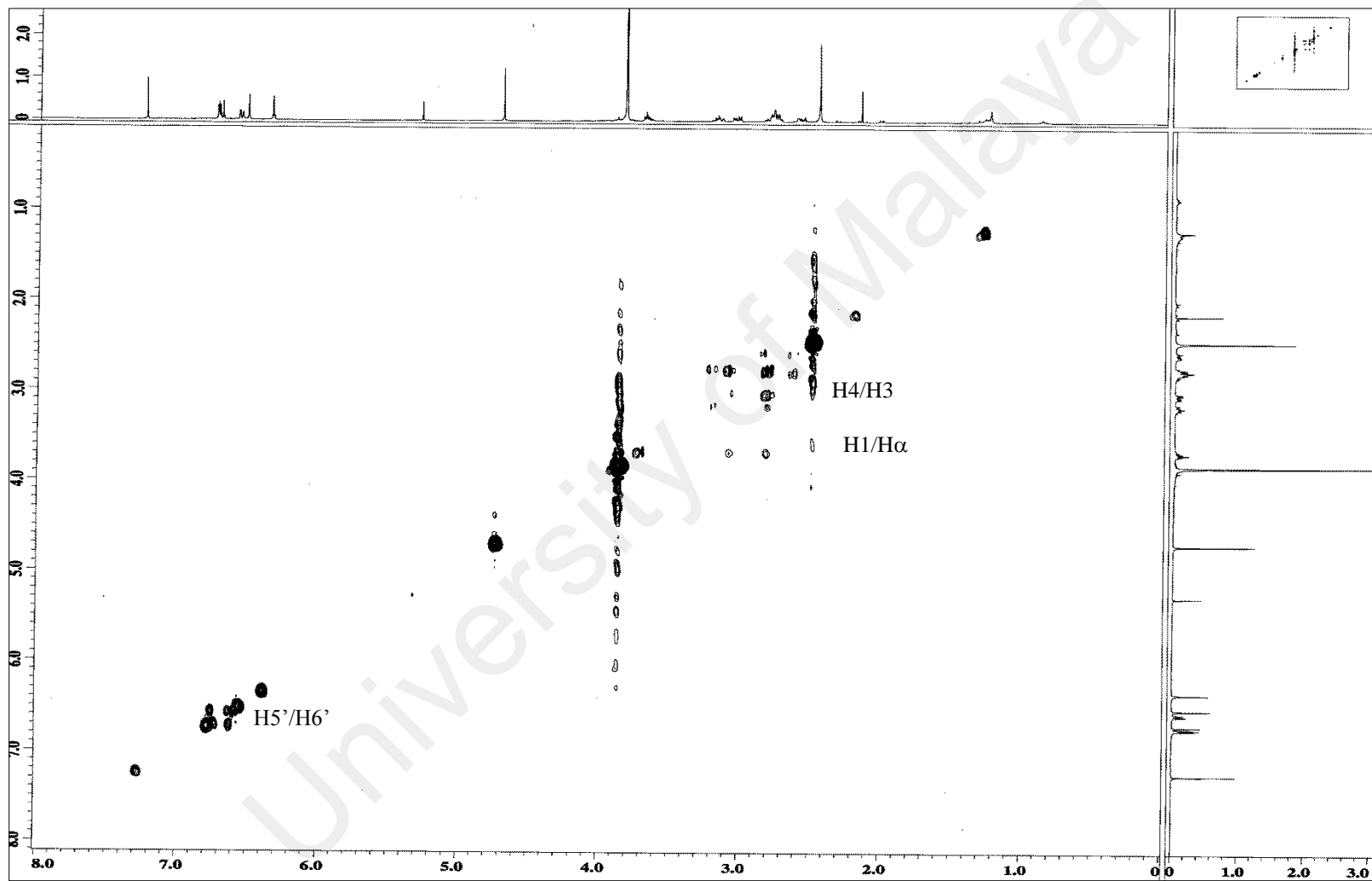


Figure 3.5: COSY Spectrum of Reticuline 8

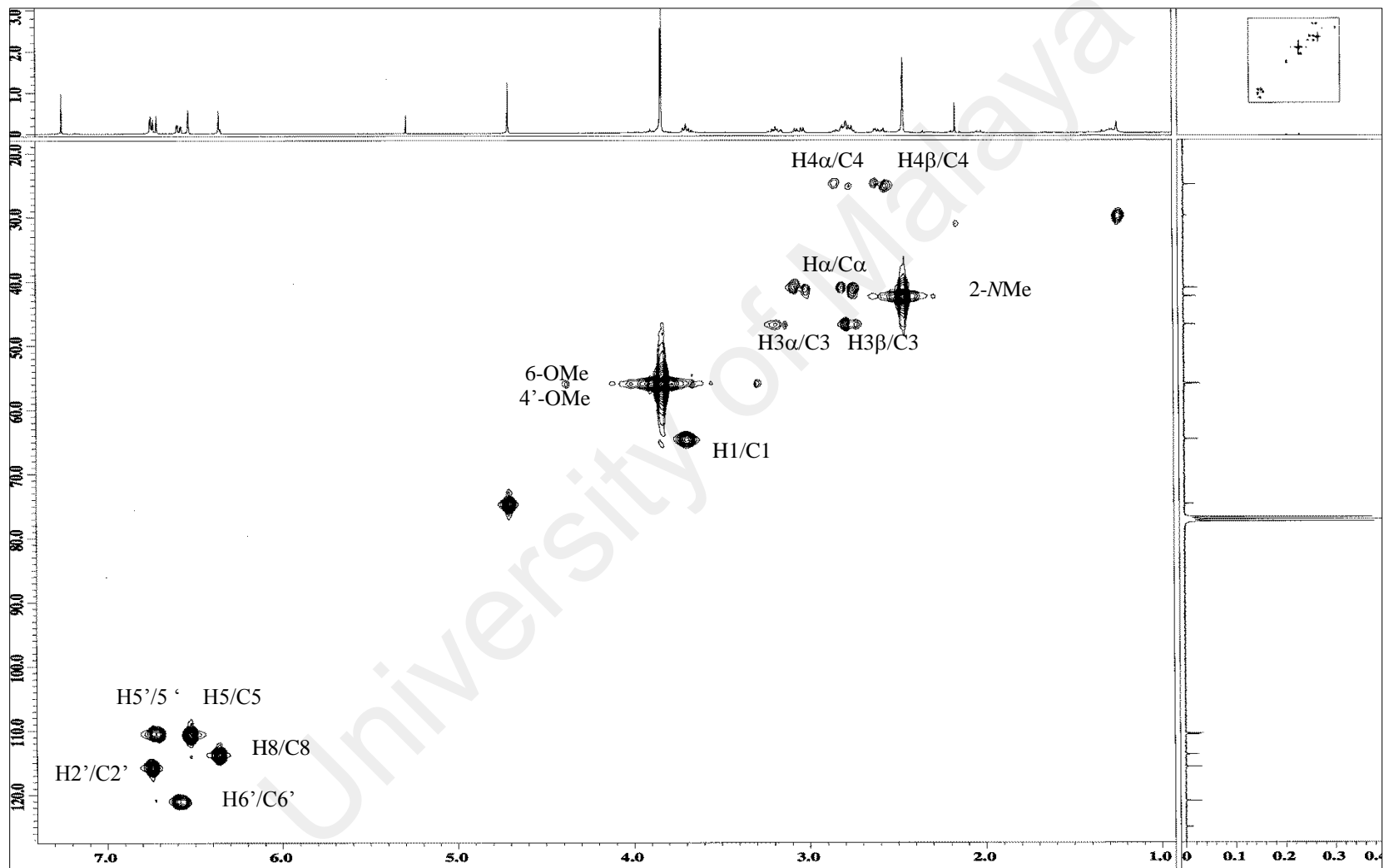


Figure 3.6: HSQC Spectrum of Reticuline 8

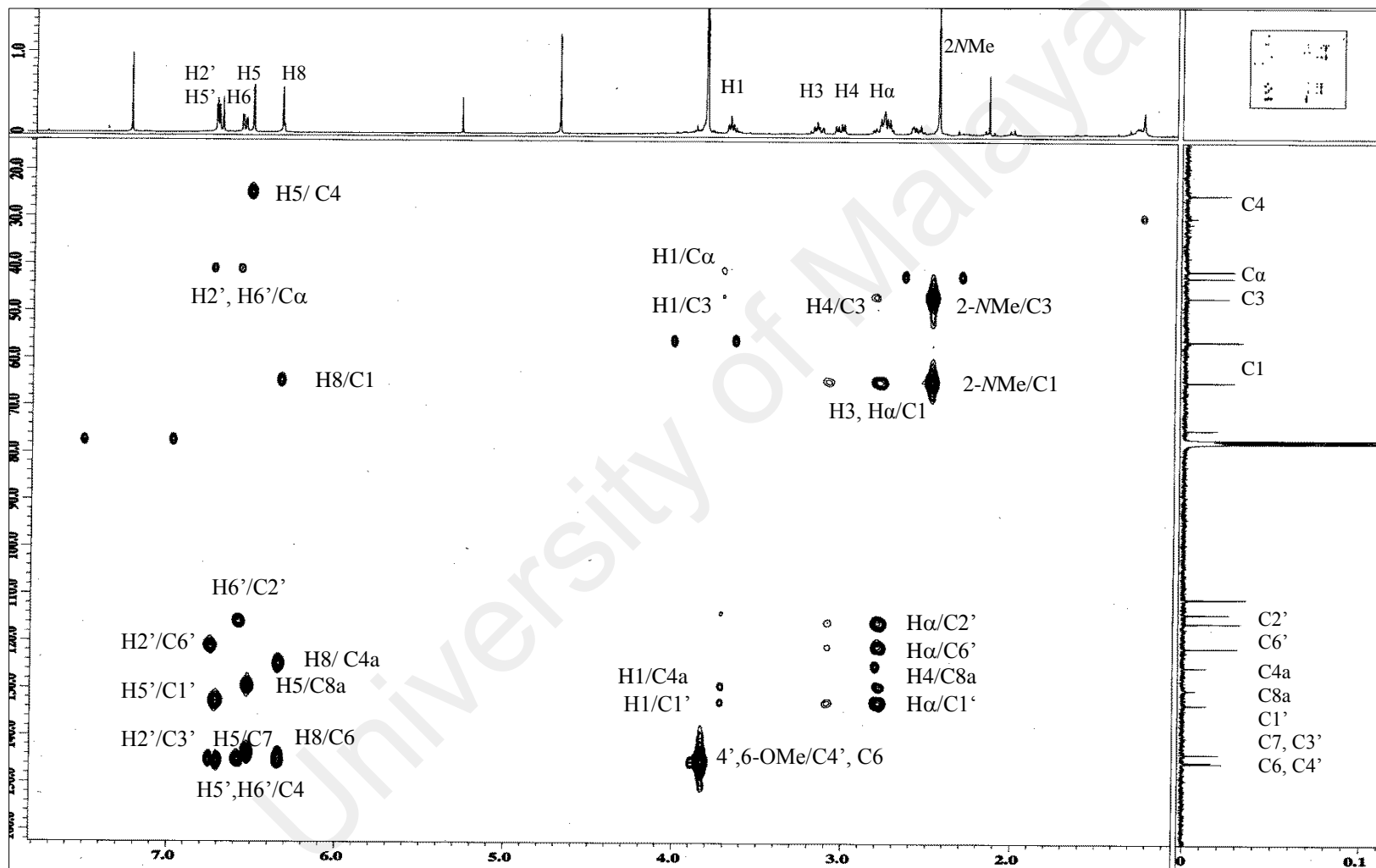
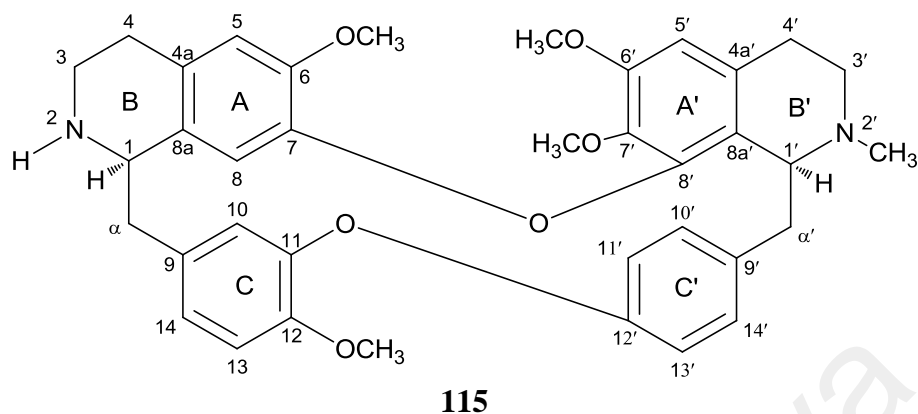


Figure 3.7: HMBC Spectrum of Reticuline 8

3.1.2 2-Norobaberine 115



2-Norobaberine **115** was afforded as a yellow amorphous solid with $[\alpha]_D^{25} +130.0^\circ$ ($c=0.1$, MeOH). Its molecular formula was confirmed as $C_{37}H_{40}N_2O_6$ from the ESIMS spectrum (Figure 3.9) which showed a pseudo-molecular ion peak $[M+H]^+$ at m/z 609.2921 (calcd. for $C_{37}H_{41}N_2O_6$, 609.2965) with 19 degree of unsaturation based on its molecular formula. Its UV spectrum was indicative of a bisbenzylisoquinoline (BBIQ) chromophore, with absorption maxima at λ_{max} 212 and 284 nm (Gibson & Turnbull, 1980). The IR spectrum showed absorption bands at ν_{max} 1266 cm^{-1} (phenyl ethers), 1640 and 1514 cm^{-1} (aromatic ring) and 3306 cm^{-1} (N-H) stretching vibrations.

The 1H NMR spectrum (Figure 3.10) showed the presence of ten aromatic signals, four O-CH₃ signals, one N-CH₃ signal, two methine protons, two CH₂-CH₂-N groups and two sets of isolated methylene protons. The ten aromatic signals were present as: three singlets assigned to H-5 (δ_H 6.37), H-5' (δ_H 6.38) and H-8 (δ_H 6.70), three signals forming an AMX spin system with H-14 appearing as a doublet of doublets (dd , $J=8.1$ Hz, 1.6 Hz) at δ_H 6.83 which was *ortho*-coupled to H-13 (δ_H 6.80, d , 8.1 Hz) and *meta*-coupled to H-10 (δ_H 5.58, d , 1.6 Hz) and four dd representing an AA'BB' spin system at H-10' (δ_H 6.87, 8.2 Hz, 2.0 Hz), H-11' (δ_H 6.31, 8.2 Hz, 2.5 Hz), H-13' (δ_H 6.99, 8.2 Hz, 2.5 Hz) and H-14' (δ_H 7.50, 8.2 Hz, 2.0 Hz). The spectrum also displayed four

singlets at δ_{H} 3.23, δ_{H} 3.64, δ_{H} 3.79 and δ_{H} 3.91 corresponding to the methoxyl groups attached to C-7', C-6, C-6' and C-12, while the singlet at δ_{H} 2.71 was assigned to the *N*'-methyl group. The chemical shift for the 7'-methoxyl protons was more shielded than the others due to the presence of the bulky substituents. Other prominent peaks of an AX spin system were observed at δ_{H} 3.27 ($J=14.0, 3.0$ Hz), δ_{H} 2.86 and δ_{H} 3.38 ($J=14.6, 5.0$ Hz), δ_{H} 2.86 ($J=14.6$ Hz) supporting the presence of the two geminal protons, H- α' and H- α respectively. The downfield signal of H-1' which was adjacent to the H- α' appeared as a broad doublet ($J=5.0$ Hz) at δ_{H} 4.27. The main difference between 2-norobaberine **115** and its close isomer 2'-norobaberine **116** (Figure 3.8) was due to the signals of H-1' and H-1. For 2-norobaberine **115**, the chemical shifts of both H-1 (δ_{H} 4.33, *brs*) and H-1' (δ_{H} 4.27, *d*, 5.0 Hz) differed only by 0.06 ppm. Meanwhile, for 2'-norobaberine **116**, the difference was more significant between these two protons with H-1 being more shielded at δ_{H} 3.65, while H-1' was more deshielded at δ_{H} 4.70 (Schiff Jr, 1991; Tantisewie et al., 1989).

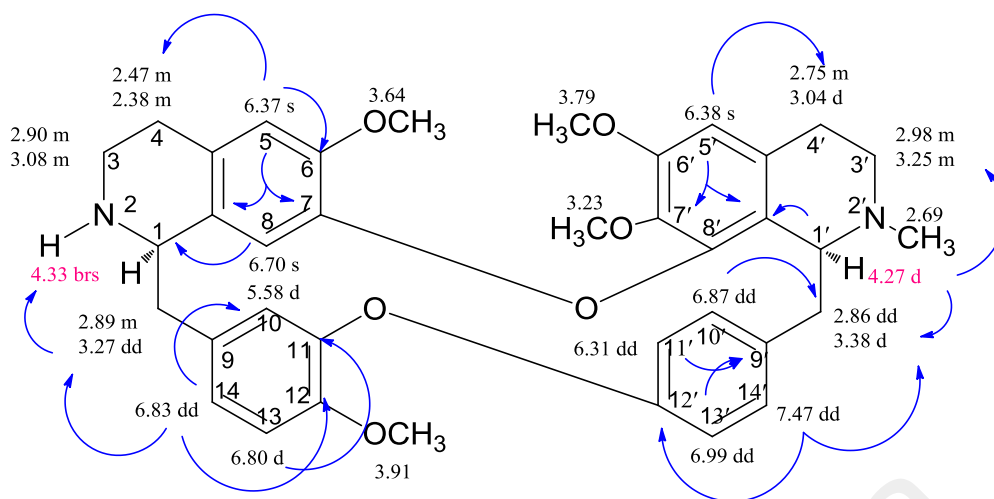
The ^{13}C NMR (Figure 3.11) and HSQC spectra (Figure 3.13) showed the presence of 37 carbon signals inclusive of ten sp^2 methines, fourteen sp^2 quaternary carbons, six sp^3 methylenes, two sp^3 methines, four methoxyl groups and one *N*-CH₃ group. Ten sp^2 methine carbons in the aromatic region which resonated at a higher field at δ_{C} 110.9, 116.0, 115.9, 111.8, 123.3, 105.8, 131.2, 120.9, 122.4 and 128.0 were assigned to C-5, C-8, C-10, C-5', C-13, C-8 and C-10, respectively. The signals of the fourteen sp^2 quaternary carbons which were observed at δ_{C} 130.6, 127.3, 128.4, 127.3, 122.4, 139.1 and lower field at 137.3, 144.1, 147.3, 147.6, 148.6, 149.7, 151.7, 151.9 were assigned to C-4a, C-8a, C-9, C-4a', C-8a', C-9' and C-7', C-7, C-12, C-8', C-6', C-11, C-6, C-12' respectively. The higher chemical shifts were attributed to the presence of the oxygenated substituents; ether and OCH₃. The methylene carbons; C-3, C- α , C-4 and C-3', C-4', C- α' resonated at δ_{C} 42.2, 38.9, 29.4 and 45.3, 39.9, 24.9 respectively. Two

methine carbons at δ_C 54.8 and 61.8 were ascribed to C-1 and C-1'. The *N*-methyl peak was observed at δ_C 41.8.

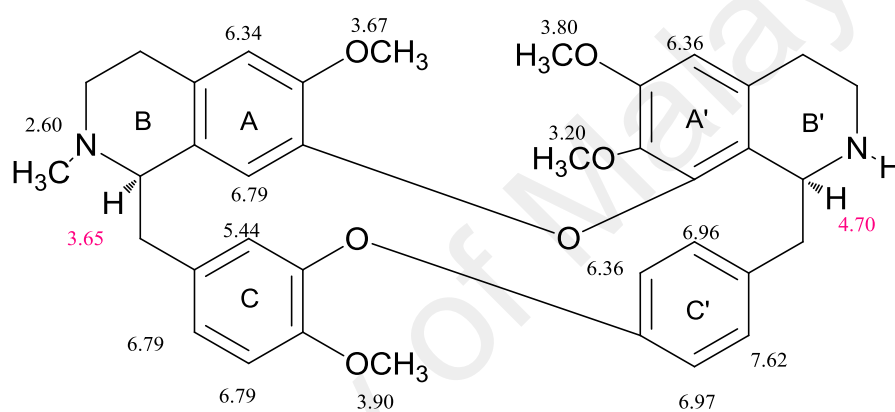
The COSY spectrum (Figure 3.12) showed the correlations of the following vicinal protons; H-13'/H-14', H-10'/H-11', H-14/H-13, H-3/H-4 and H-3'/H-4'.

The HMBC correlations for **115** are shown in Figure 3.14 to establish the full assignment of the position of the methoxyl groups and the linkage between the two benzylisoquinoline (BIQ) moieties which define the type of the BBIQ. The HMBC spectrum aided in the placement of the methoxyl groups by exhibiting the following correlations; 6-OCH₃/C-6, 6'-OCH₃/C-6', 7'-OCH₃/C-7', 12-OCH₃/C-12. The other quaternary carbons, C-7, C-8' (ring A-A'), C-11, C-12' (ring C-C') were involved in the ethereal linkage between the two BIQs at C-7-O-C-8' and C-11-O-C-12' which suggested it belonged to the type VI BBIQ alkaloid (Guinaudeau et al., 1986).

The presence of the two chiral carbons C-1 and C-1' at δ_C 54.8 and 61.8, respectively suggested that this structure could give rise to four different configurations; 'anti' for (1*R*, 1'*R*), (1*S*, 1'*S*) dimers or 'syn' for (1*R*, 1'*S*), (1*S*, 1'*R*) dimers. The positive optical rotation value suggested that the structure was assumed to have either a (1*R*, 1'*S*) or (1*R*, 1'*R*) configuration. The fact that H-10 resonated upfield at δ_H 5.58 was indicative that this alkaloid belonged to the 'syn' configuration. Therefore, the configuration of C-1 and C-1' was determined as (1*R*, 1'*S*) based on the positive sign of its optical rotation and the 'syn' configuration characteristics. Complete ¹H and ¹³C-NMR assignments of (+)-2-norobaberine **115** together with the literature values (Table 3.3) (Tantisewie et al., 1989) confirmed without a doubt the identity of the BBIQ was type VI, (1*R*, 1'*S*)-(+)-2-norobaberine **115**. (+)-2-norobaberine was isolated from *Stephania erecta* Craib by (Likhitwitayawuid et al., 1993) and was reported to exhibit antiplasmodial and cytotoxic activities.



115



116

Figure 3.8: ^1H NMR and HMBC Correlations of (+)-2-norobaberine **115** and (+)-2'-norobaberine **116**

Table 3.3: ¹H, ¹³C-NMR and HMBC Data of 2-norobaberine **115**

Position	Unit	¹ H- NMR 115 CDCl ₃ , 600 MHz δ (J, Hz)	¹ H- NMR CDCl ₃ , 360 MHz (Tantisewie & Ruchirawat, 1992) δ	¹³ C- NMR 115 CDCl ₃ , 100 MHz δ	HMBC (¹ H- ¹³ C)
1	CH	4.33 (<i>brs</i>)	4.23	54.8	α
3	CH ₂	α 3.08 (<i>m</i>) β 2.90 (<i>m</i>)		42.2	
4	CH ₂	α 2.47 (<i>m</i>) β 2.38 (<i>m</i>)		29.4	3
4a	C			130.6	
5	CH	6.37 (<i>s</i>)	6.37	110.9	4,6,7,8a
6	C			151.7	
6-OMe	O-CH ₃	3.64 (<i>s</i>)	3.64	56.0	
7	C			144.1	
8	CH	6.70 (<i>s</i>)	6.69	116.0	1,4a,6, 7
8a	C			127.3	
α	CH ₂	α 3.27 (<i>dd</i> , 14.0, 3.0) β 2.89 (<i>m</i>)		38.9	
9	C			128.4	
10	CH	5.58 (<i>d</i> , 1.6)	5.61	115.9	α , 12, 14
11	C			149.7	
12	C			147.3	
12-OMe	O-CH ₃	3.91 (<i>s</i>)	3.92	56.3	
13	CH	6.80 (<i>d</i> , 8.1)	6.81	111.8	9,11
14	CH	6.83 (<i>dd</i> , 8.1, 1.6)	6.81	123.3	α , 10, 12
1'	CH	4.27 (<i>d</i> , 5.0)	4.23	61.8	α' , 3', 8a'
N'-Me	N'-CH ₃	2.71 (<i>s</i>)	2.69	41.8	α' , 3'
3'	CH ₂	α 3.25 (<i>m</i>) β 2.98 (<i>m</i>)		45.3	
4'	CH ₂	α 3.04 (<i>m</i>) β 2.75 (<i>d</i> , 3.0)		24.9	3', 4a'
4a'	C			127.3	
5'	CH	6.38 (<i>s</i>)	6.36	105.8	4',6',7',8a'
6'	C			148.6	
6'-OMe	O-CH ₃	3.79 (<i>s</i>)	3.79	55.1	
7'	C			137.3	
7'-OMe	O-CH ₃	3.23 (<i>s</i>)	3.23	60.5	
8'	C			147.6	
8a'	C			122.4	
α'	CH ₂	α 3.38 (<i>d</i> , 14.6) β 2.86 (<i>dd</i> , 14.6, 5.0)		39.9	1',8a', 9', 10', 14'
9'	C			139.1	
10'	CH	6.87 (<i>dd</i> , 8.2, 2.0)	6.87	131.2	α'
11'	CH	6.31 (<i>dd</i> , 8.2, 2.5)	6.31	120.9	9'
12'	C			151.9	
13'	CH	6.99 (<i>dd</i> , 8.2, 2.5)	6.99	122.4	9', 11', 12'
14'	CH	7.50 (<i>dd</i> , 8.2, 2.0)	7.47	128.0	α' , 10', 12'

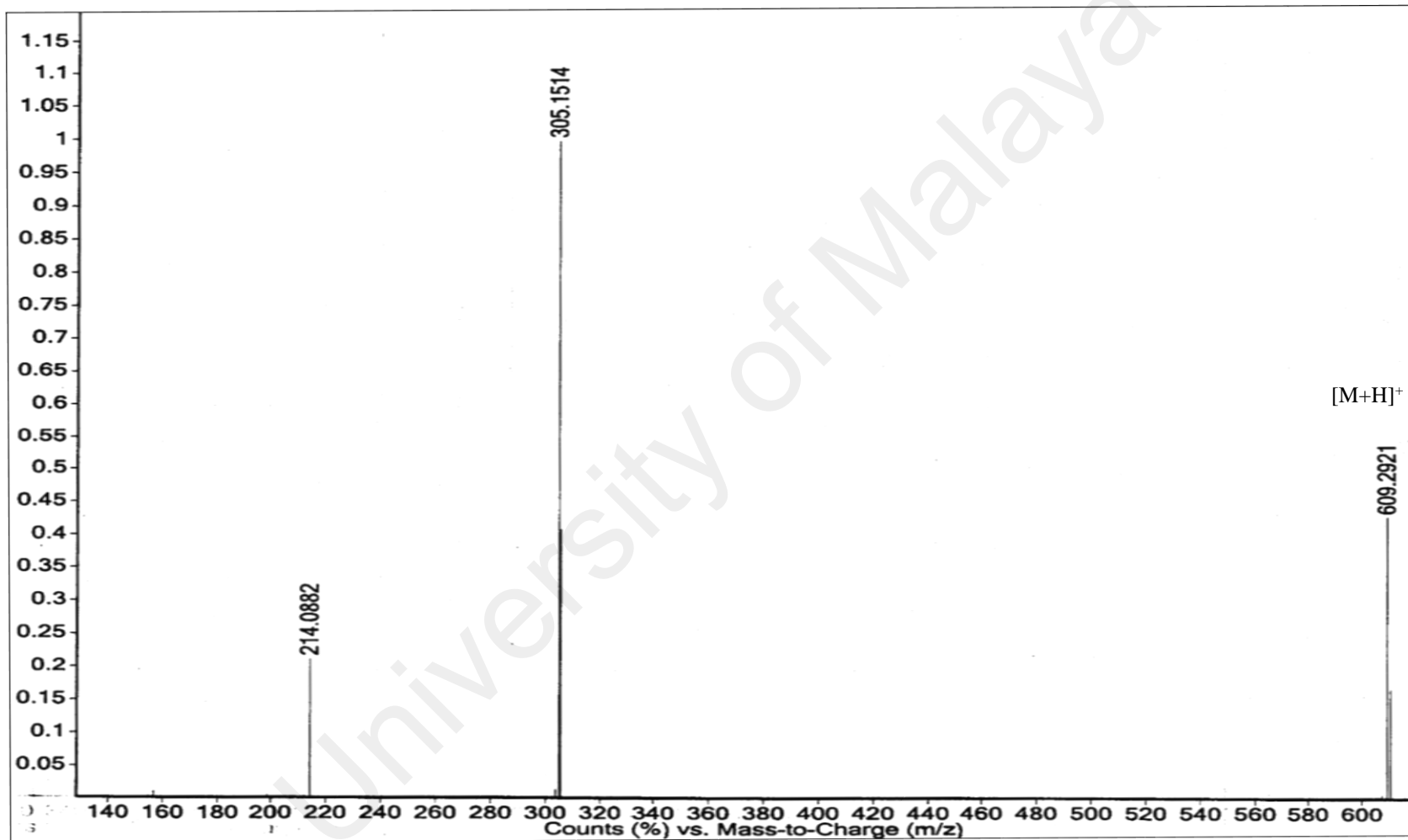


Figure 3.9: LCMS Spectrum of 2-norobaberine **115**

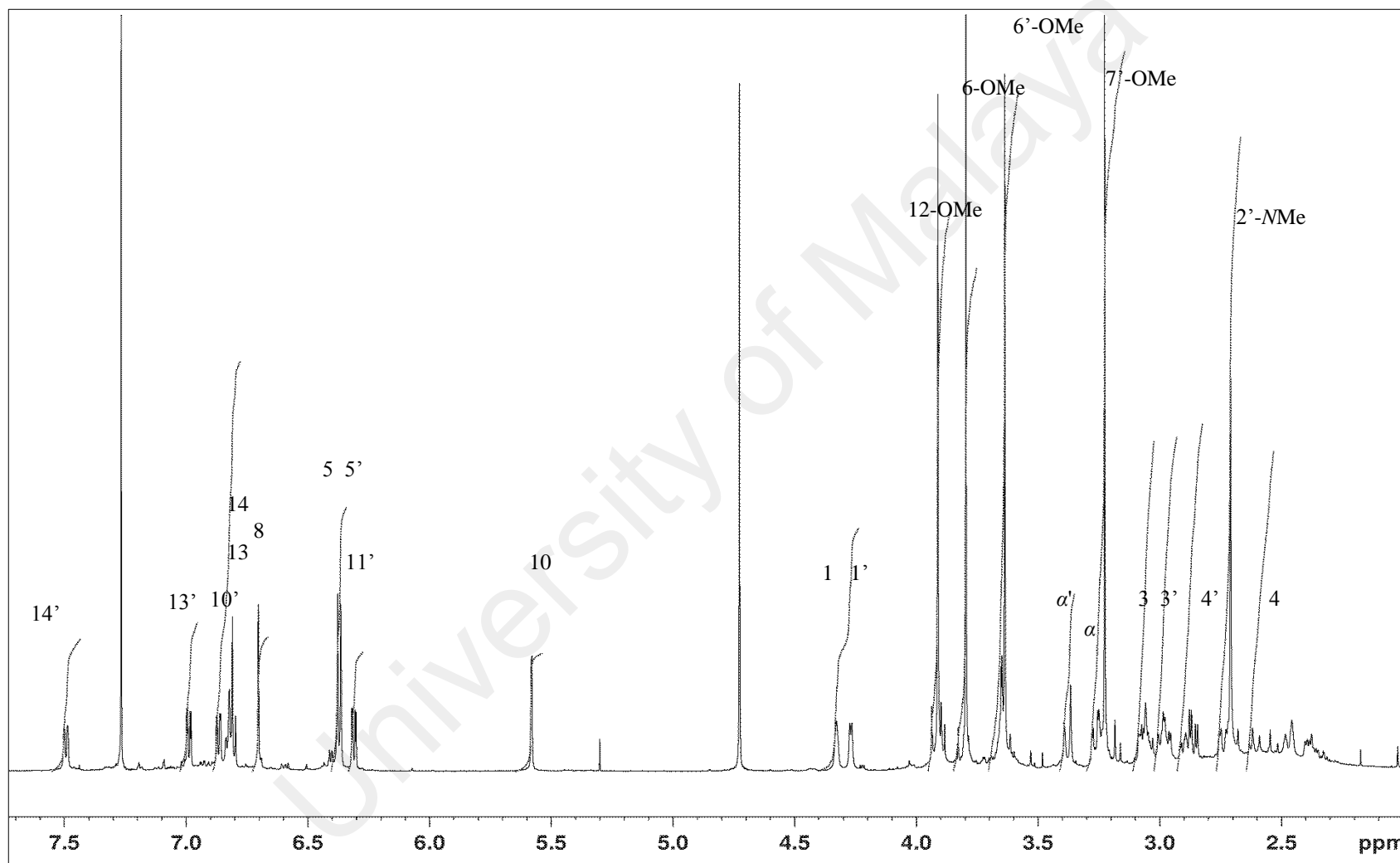


Figure 3.10: ¹H NMR Spectrum of 2-norobaberine **115**

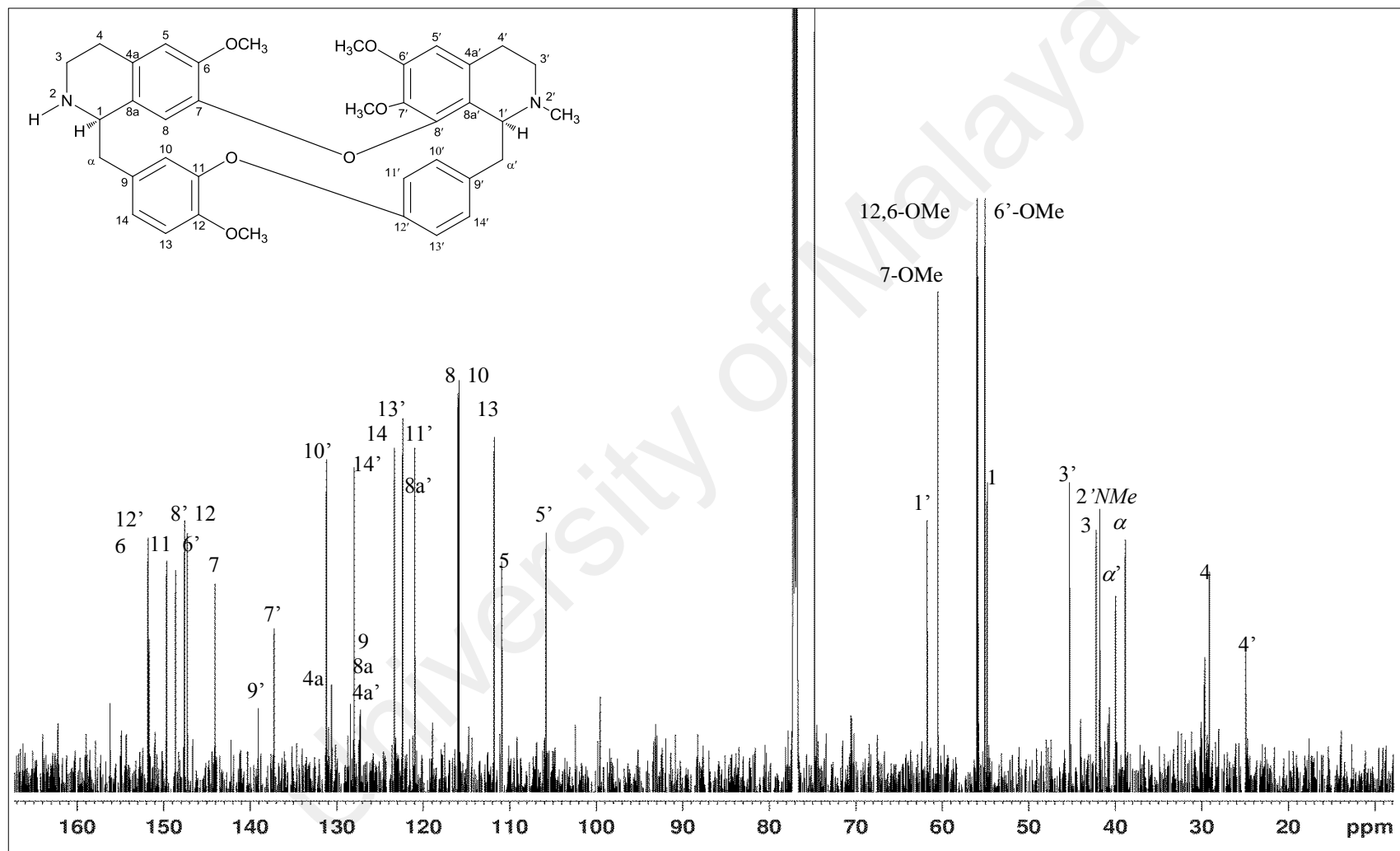


Figure 3.11: ^{13}C NMR Spectrum of 2-norobaberine **115**

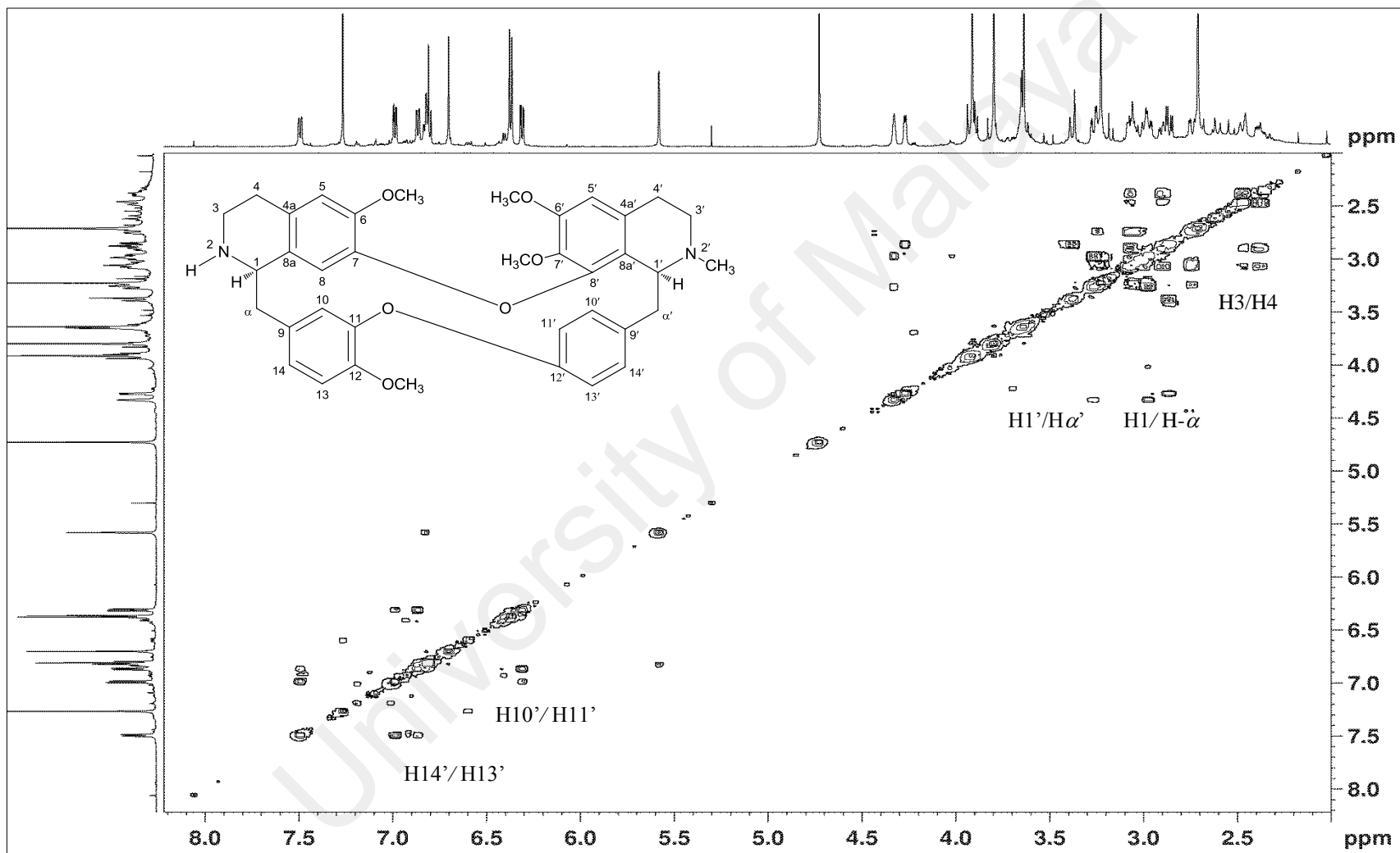


Figure 3.12: COSY Spectrum of 2-norobaberine **115**

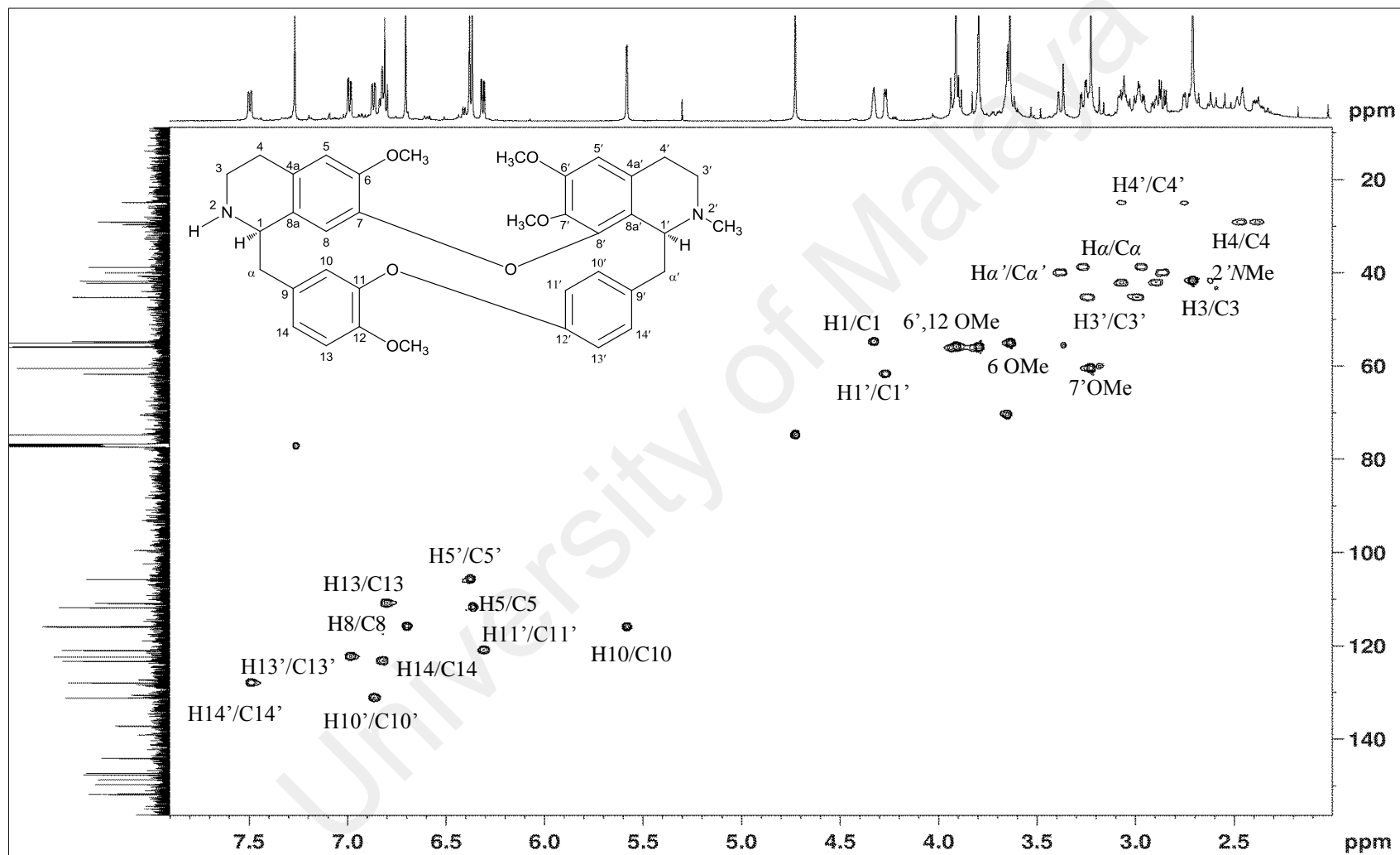


Figure 3.13: HSQC Spectrum of 2-norobaberine **115**

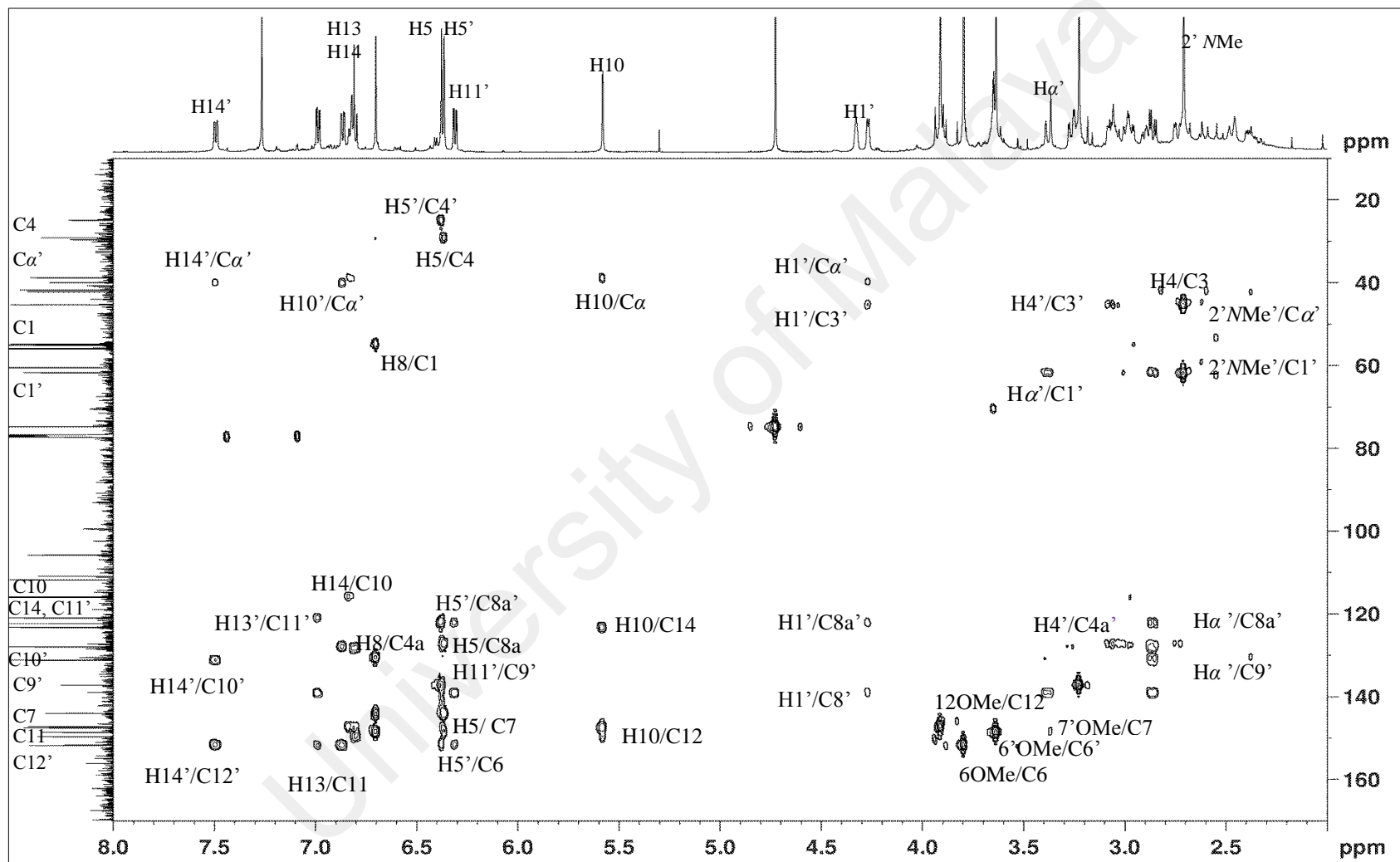
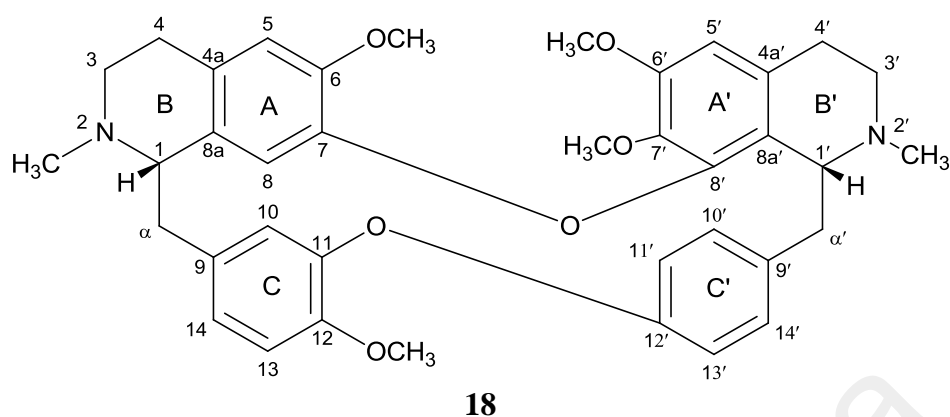


Figure 3.14: HMBC Spectrum of 2-norobaberine **115**

3.1.3 Gyrolidine **18**

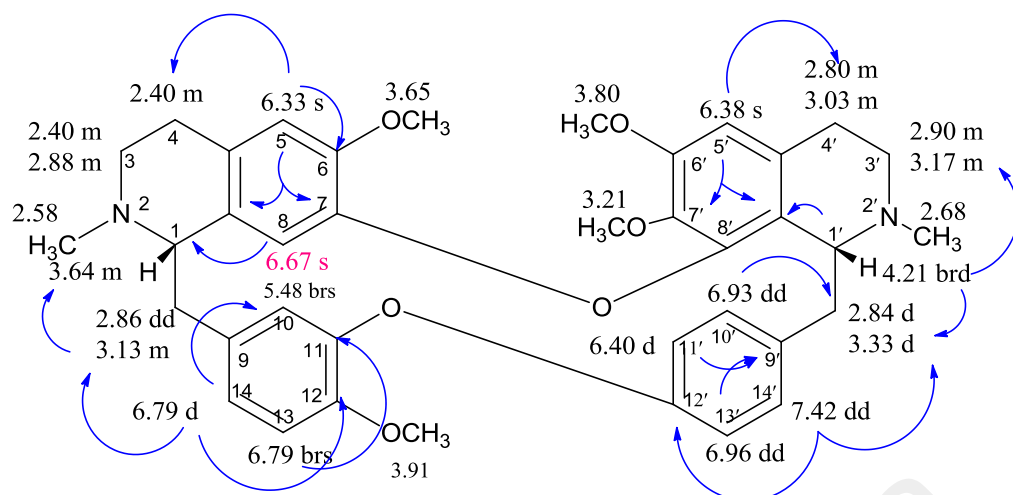


Gyrolidine **18** was isolated as a yellow amorphous powder with $[\alpha]_D^{25} -53.0^\circ$ ($c = 0.02$, MeOH). The ESIMS spectrum exhibited the pseudo-molecular ion peak $[M+H]^+$ at m/z 623.3100 suggesting a molecular formula of $C_{38}H_{42}N_2O_6$ (calcd. for $C_{38}H_{43}N_2O_6$, 623.3121). IR spectrum implied the presence of phenyl ethers (ν_{\max} 1268 cm^{-1}) and aromatic rings at 1510 and 1637 cm^{-1} .

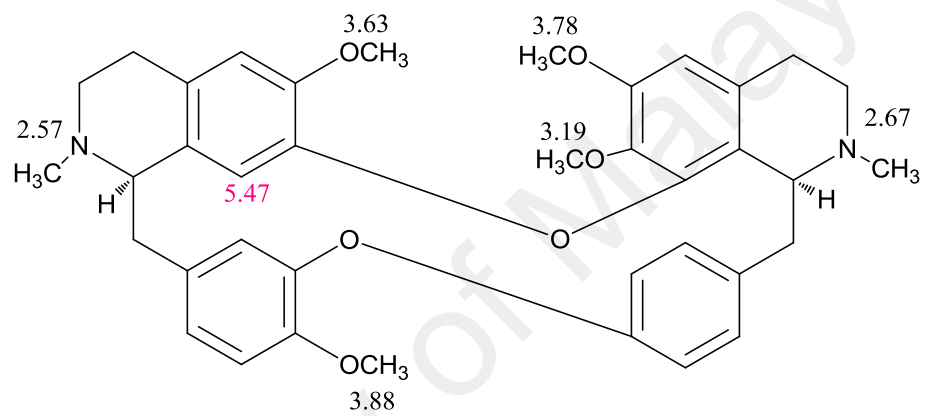
Analysis of the ^1H (Figure 3.16) and ^{13}C NMR (Figure 3.17) spectra indicated that gyrolidine **18** was structurally related to 2-norobaberine **115**. However, **18** revealed an additional *N*-methyl signal that resonated as a singlet at δ_{H} 2.58 and δ_{C} 43.7 assignable to *N*-2. The relatively upfield H-1 in **18** as compared to the corresponding atom in **115** might due to the decreasing inductive effect by the nitrogen atom attached to the methyl group which is an electron donating group. The disappearing of intense *N*-H stretching at ν_{\max} 3306 cm^{-1} in IR spectrum **115** further verified the structure only contain tertiary amine groups.

The additional cross peak of 2- NCH_3 to C-3 and C-1, further supported the presence of the *N*- CH_3 group in ring B as can be seen in 2D NMR spectrum in Appendix A (Figure A1 and A2).

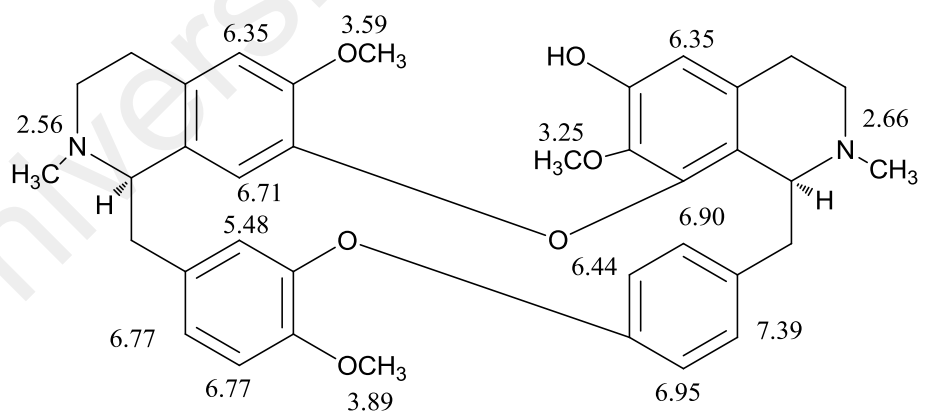
The enantiomer of gyrolidine **18** is (+)-obaberine **62** (Figure 3.15) (Lu & Wang, 1977). It has an 'anti' configuration with a shielded aromatic proton at H-8. The negative optical rotation value suggested a structure with either the (1*S*, 1'*R*) or (1*S*, 1'*S*) configuration. However, H-10 at δ_{H} 5.48 which was shielded and H-8 (δ_{H} 6.67) which was deshielded upon comparison with **62**, proved that it belonged to the 'syn' configuration (1*S*, 1'*R*). Therefore, the identity of this alkaloid was confirmed as (1*S*, 1'*R*) (-)-gyrolidine **18** (Table 3.4) (Chalandre et al., 1986) by analysis of the 1D (¹H-NMR, ¹³C-NMR), 2D (COSY, HSQC, HMBC) and by comparing it with its close isomer; (-)-gyrocarpine **117** (Chalandre et al., 1986). Gyrolidine **18** was isolated previously from *Gyrocarpus americanus* Jacq. (Chalandre et al., 1986).



18



62



117

Figure 3.15: ¹H NMR and HMBC Correlations of (-)-Gyrolidine **18**, (+)-Obaberine **62** and (-)-Gyrocarpine **117**.

Table 3.4: ¹H, ¹³C-NMR and HMBC Data of Gyrolidine **18**

Position	Unit	¹ H- NMR 18 CDCl ₃ , 400 MHz δ (J, Hz)	¹ H- NMR CDCl ₃ , 360 MHz (Chalandre et al., 1986) δ	¹³ C- NMR 18 CDCl ₃ , 100 MHz δ	HMBC (¹ H- ¹³ C)
1	CH	3.64 (<i>brs</i>)		63.9	<i>N</i> -CH ₃ , 4a
<i>N</i> -Me	<i>N</i> -CH ₃	2.58 (<i>s</i>)	2.57	43.7	
3	CH ₂	2.88 (<i>m</i>) 2.40 (<i>m</i>)		51.0	
4	CH ₂	2.40 (<i>m</i>)		28.7	
4a	C			130.9	
5	CH	6.33 (<i>s</i>)	6.36	110.9	4,6,7,8a
6	C			148.3	
6-OMe	O-CH ₃	3.65 (<i>s</i>)		54.9	
7	C			143.8	
8	CH	6.67 (<i>s</i>)	6.65	116.7	1,4a,6,7
8a	C			127.7	
α	CH ₂	3.13 (<i>m</i>) 2.86 (<i>dd</i> , 14.6, 3.6)		37.5	
9	C			130.9	
10	CH	5.48 <i>brs</i>	5.47	116.5	α, 11,12,14
11	C			149.0	
12	C			146.6	
12-OMe	O-CH ₃	3.91 (<i>s</i>)	3.89	55.9	
13	CH	6.79 (<i>brs</i>)	6.78	110.7	9,11
14	CH	6.79 (<i>d</i> , 8.0)	6.78	123.5	α, 11
1'	CH	4.21 (<i>brd</i> , 5.6)		61.4	3',8',8a', α'9'
<i>N'</i> -Me	<i>N'</i> -CH ₃	2.68 (<i>s</i>)	2.66	42.2	1',3'
3'	CH ₂	3.17 (<i>m</i>) 2.90 (<i>m</i>)		45.3	4',4a'
4'	CH ₂	3.03 (<i>m</i>) 2.80 (<i>m</i>)		25.6	
4a'	C			127.2	
5'	CH	6.38 (<i>s</i>)		105.8	4',6',7',8a'
6'	C			151.6	
6'-OMe	O-CH ₃	3.80 (<i>s</i>)	3.79	56.0	
7'	C			137.0	
7'-OMe	O-CH ₃	3.21 (<i>s</i>)	3.19	60.4	
8'	C			147.5	
8'a	C			127.7	
α'	CH ₂	3.33 (<i>brd</i> , 14.6) 2.84 (<i>dd</i> , 14.6, 5.6)		39.5	1',8a', α' ,9',10',14'
9'	C			139.0	
10'	CH	6.93 (<i>dd</i> , 8.3, 2.0)		131.4	α',9',11',12',14'
11'	CH	6.40 (<i>d</i> , 8.3)		121.1	10'
12'	C			152.2	
13'	CH	6.96 (<i>dd</i> , 8.3, 2.0)		122.2	9',11'
14'	CH	7.42 (<i>dd</i> , 8.3, 2.0)		127.8	α',10',12'

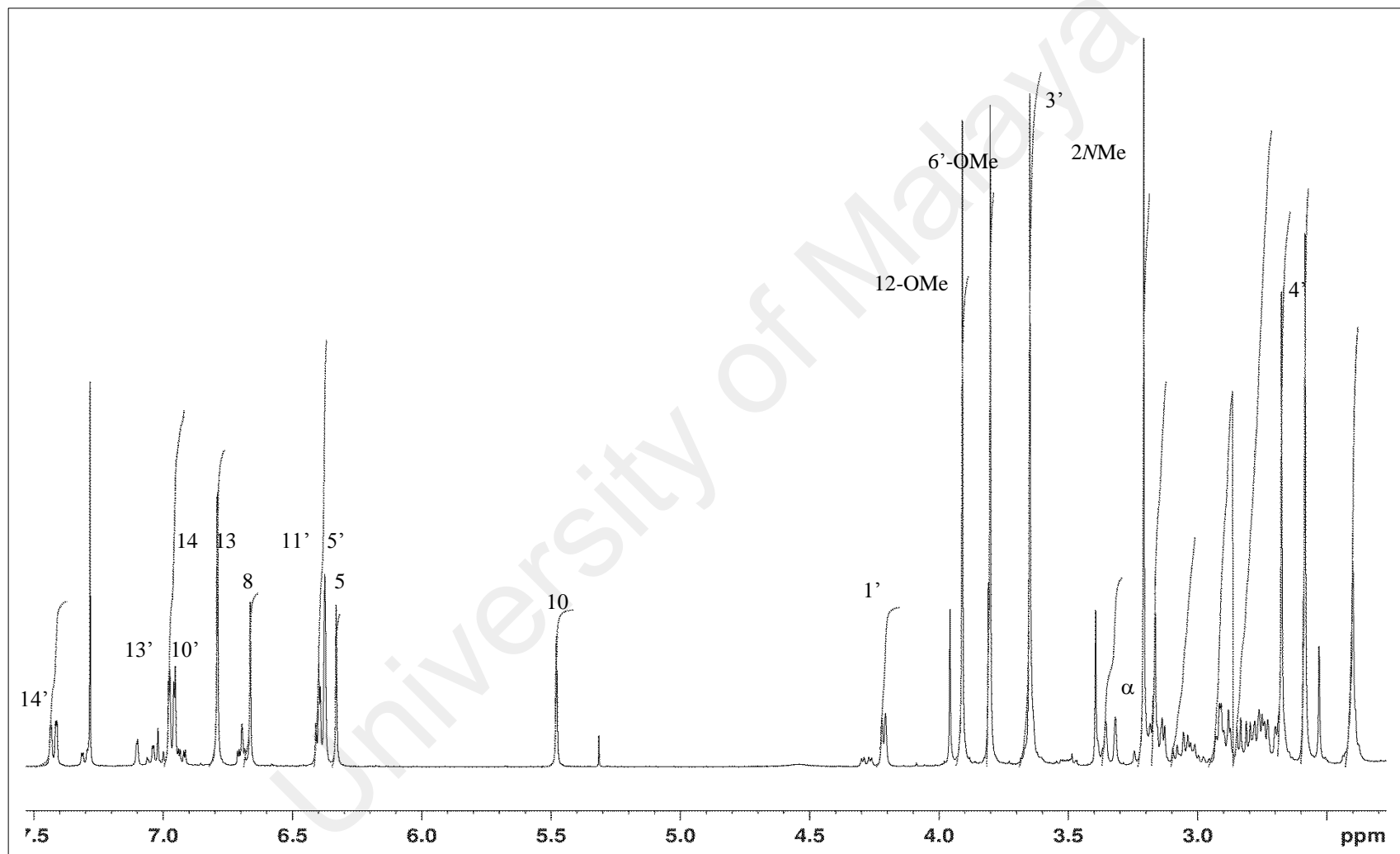


Figure 3.16: ¹H NMR Spectrum of Gyrolidine **18**

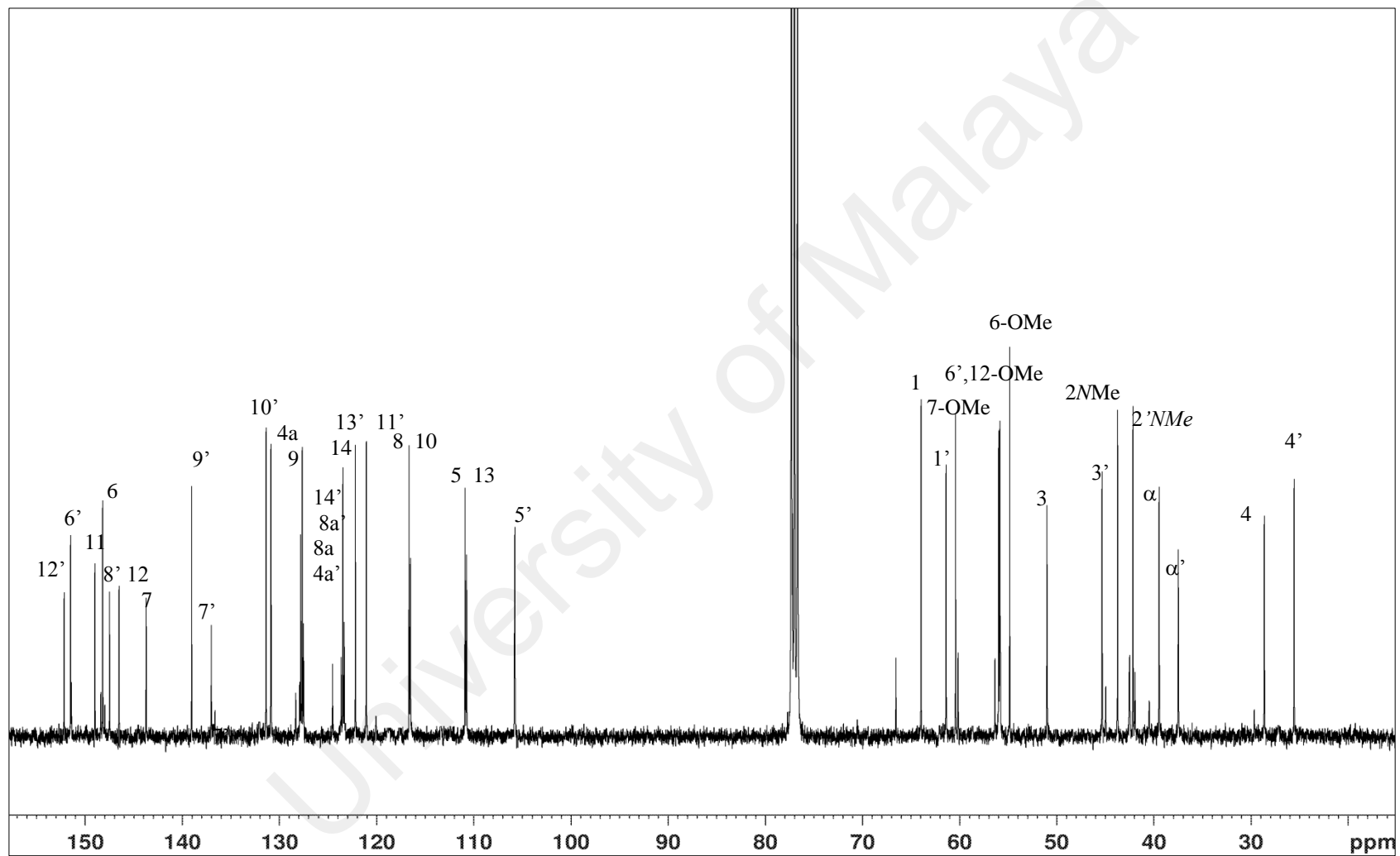
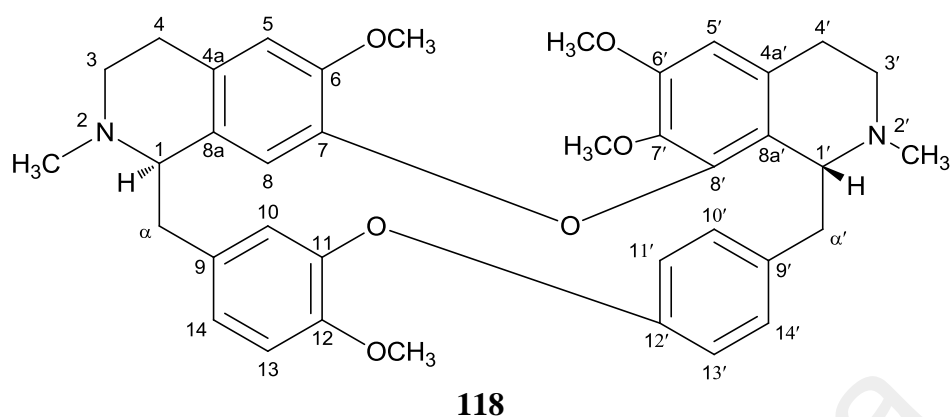


Figure 3.17: ^{13}C NMR Spectrum of Gyrolidine **18**

3.1.4 *O*-methyllimacusine **118**



O-methyllimacusine **118** $[\alpha]_D^{25} +90.0^\circ$ ($c = 0.11$, CHCl_3) was purified as a colourless amorphous powder. The EIMS spectrum exhibited a pseudo-molecular ion peak $[\text{M}+\text{H}]^+$ at m/z 623.3071 which suggested a molecular formula of $\text{C}_{38}\text{H}_{42}\text{N}_2\text{O}_6$ (calcd. for $\text{C}_{38}\text{H}_{43}\text{N}_2\text{O}_6$, 623.3121). The UV and IR spectra of **118** were similar to those of gyrolidine **18**.

The ^1H NMR spectrum (Figure 3.18) of *O*-methyllimacusine **118** possessed the same aromatic substitution pattern as **18**. However, the ^1H chemical shift of *O*-methyllimacusine **118** significantly differed from that of **18** with H-10 resonating at δ_{H} 6.65 (d , $J=1.6$ Hz) instead of δ_{H} 5.48 and the H-8 singlet being more shielded at δ_{H} 6.41 instead of δ_{H} 6.67. Another characteristic peak was the two *N*-Me singlets ascribed to *N*-2 and *N*-2' which resonated very close to each other at δ_{H} 2.55 and 2.54 differing only by 0.02 ppm, instead of δ_{H} 2.58 and 2.66, respectively.

The position of the three methoxys groups, was established in the similar manner as was carried out for **115** and further confirmed using NOESY experiment (Figure 3.20); H-5 (δ_{H} 6.46)/ 6-OCH₃ (δ_{H} 3.43), H-5' (δ_{H} 6.41)/ 6'-OCH₃ (δ_{H} 3.86), and H-13 (δ_{H} 6.95)/ 12-OCH₃ (δ_{H} 3.96). The shielded signal at δ_{H} 3.02 was assigned to 7'-OCH₃.

The positive sign of the specific optical rotation of *O*-methyllimacusine **118** suggested that the structure was assumed to have either a (1*R*, 1'*S*) or (1*R*, 1'*R*) configuration. The ethereal linkages of type VI bisbenzylisoquinoline and the deshielded H-10 at δ_{H} 6.65 when compared with the corresponding atom in **18** (δ_{H} 5.48) ascertained that it belonged to the *anti*-configuration. Comparison of the observed data (Table 3.5), ^{13}C NMR spectrum (Figure 3.19), LCMS and 2D NMR spectrum that supplemented in Appendix A (Figure A3-A5) with the literature values confirmed that the alkaloid is indeed (1*R*, 1'*R*) (+)-*O*-methyllimacusine **118** (Chalandre et al., 1986; Dute et al., 1988).

Table 3.5: ¹H, ¹³C-NMR and HMBC Data of *O*-methyllimacusine **118**

Position	Unit	¹ H- NMR 118 CDCl ₃ , 400 MHz δ (J, Hz)	¹ H- NMR CDCl ₃ , 360 MHz (Dute et al., 1988) δ	¹³ C- NMR 118 100 MHz δ	HMBC (¹ H- ¹³ C)
1	CH	3.48 (<i>m</i>)	3.49	65.5	<i>α</i> , 3, 4a, 8, 9
2	<i>N</i> -CH ₃	2.55 (<i>s</i>)	2.56	42.2	1, 3
3	CH ₂	<i>α</i> 3.05 (<i>m</i>) <i>β</i> 2.74 (<i>m</i>)		46.4	
4	CH ₂	<i>α</i> 2.81 (<i>m</i>) <i>β</i> 2.63 (<i>m</i>)		26.3	3
4a	C			127.6	
5	CH	6.46 (<i>s</i>)	6.40	112.5	4,6,7,8a
6	C			149.3	
6	O-CH ₃	3.43 (<i>s</i>)	3.43	56.4	
7	C			144.5	
8	CH	6.41 (<i>s</i>)	6.45	120.5	1,6,7
8a	C			131.2	
<i>α</i>	CH ₂	<i>α</i> 2.81 (<i>d</i> , 13.4) <i>β</i> 2.51 (<i>m</i>)		40.6	9, 10, 14
9	C			133.9	
10	CH	6.65 (<i>d</i> , 1.6)	6.65	120.2	<i>α</i> , 11,12,14
11	C			148.6	
12	C			148.8	
12	O-CH ₃	3.96 (<i>s</i>)	3.96	56.3	12
13	CH	6.95 (<i>d</i> , 8.0)	6.96	112.8	9,11
14	CH	6.98 (<i>dd</i> , 8.0, 1.6)	6.99	123.5	<i>α</i> , 12
1'	CH	4.27 (<i>d</i> , 12.0)	4.30	60.4	<i>α</i> ' , 4'
2'	<i>N</i> '-CH ₃	2.54 (<i>s</i>)	2.56	41.5	1',3'
3'	CH ₂	<i>α</i> 3.53 (<i>m</i>) <i>β</i> 2.98 (<i>m</i>)		44.2	
4'	CH ₂	<i>α</i> 2.99 (<i>m</i>) <i>β</i> 2.76 (<i>m</i>)		22.9	3'
4a'	C			121.1	
5'	CH	6.41 (<i>s</i>)	6.40	106.7	4', 4a', 6',7',8a'
6'	C			152.1	
6'	O-CH ₃	3.80 (<i>s</i>)	3.77	56.0	6
7'	C			137.9	
7'	O-CH ₃	3.02 (<i>s</i>)	3.02	59.8	7
8'	C			149.0	
8a'	C			127.5	
<i>α</i> '	CH ₂	<i>α</i> 3.30 (<i>d</i> , 12.0) <i>β</i> 2.85 (<i>m</i>)		43.8	1',8a', <i>α</i> ' ,9',10',14'
9'	C			136.0	
10'	CH	6.82 (<i>dd</i> , 8.3, 2.0)	6.81	131.7	9', 12'
11'	CH	6.84 (<i>dd</i> , 8.3, 2.0)		120.4	10'
12'	C			155.5	
13'	CH	7.13 (<i>dd</i> , 8.3, 2.0)	7.13	121.5	11',12'
14'	CH	7.35 (<i>d</i> , 8.3)	7.36	130.2	<i>α</i> ' ,10',12'

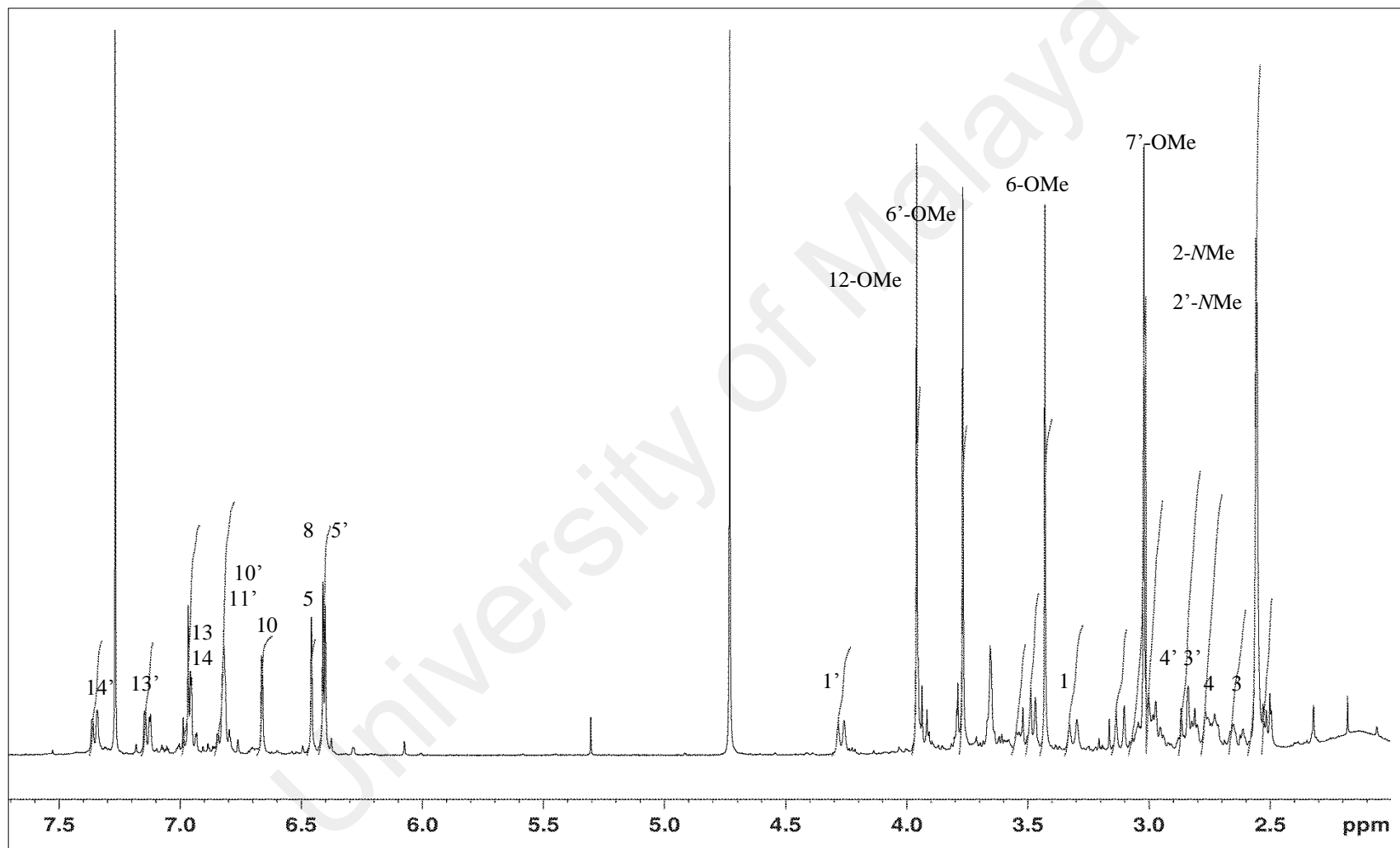


Figure 3.18: ^1H NMR Spectrum of *O*-methyllicmacusine **118**

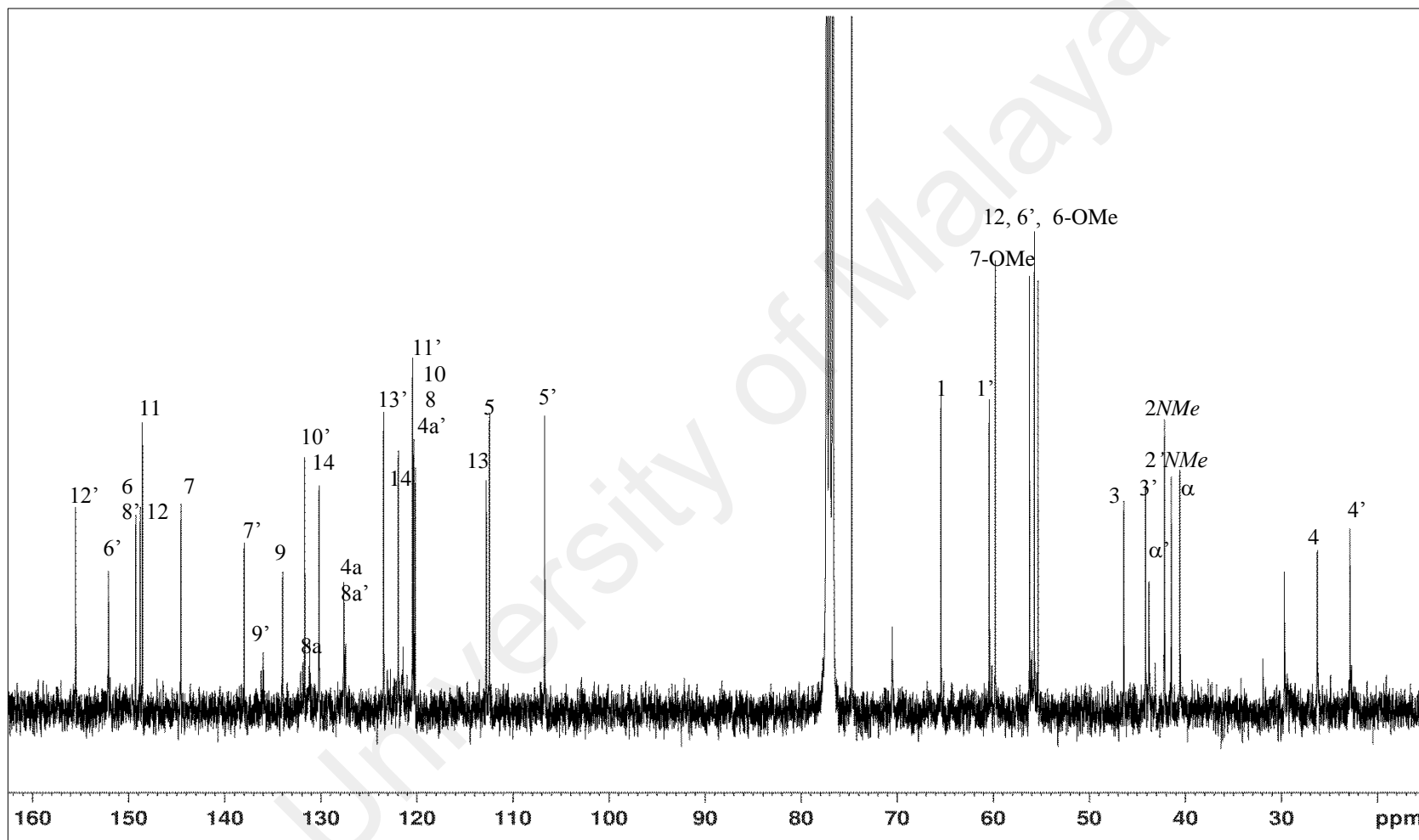


Figure 3.19: ^{13}C NMR Spectrum of *O*-methyllicmacusine **118**

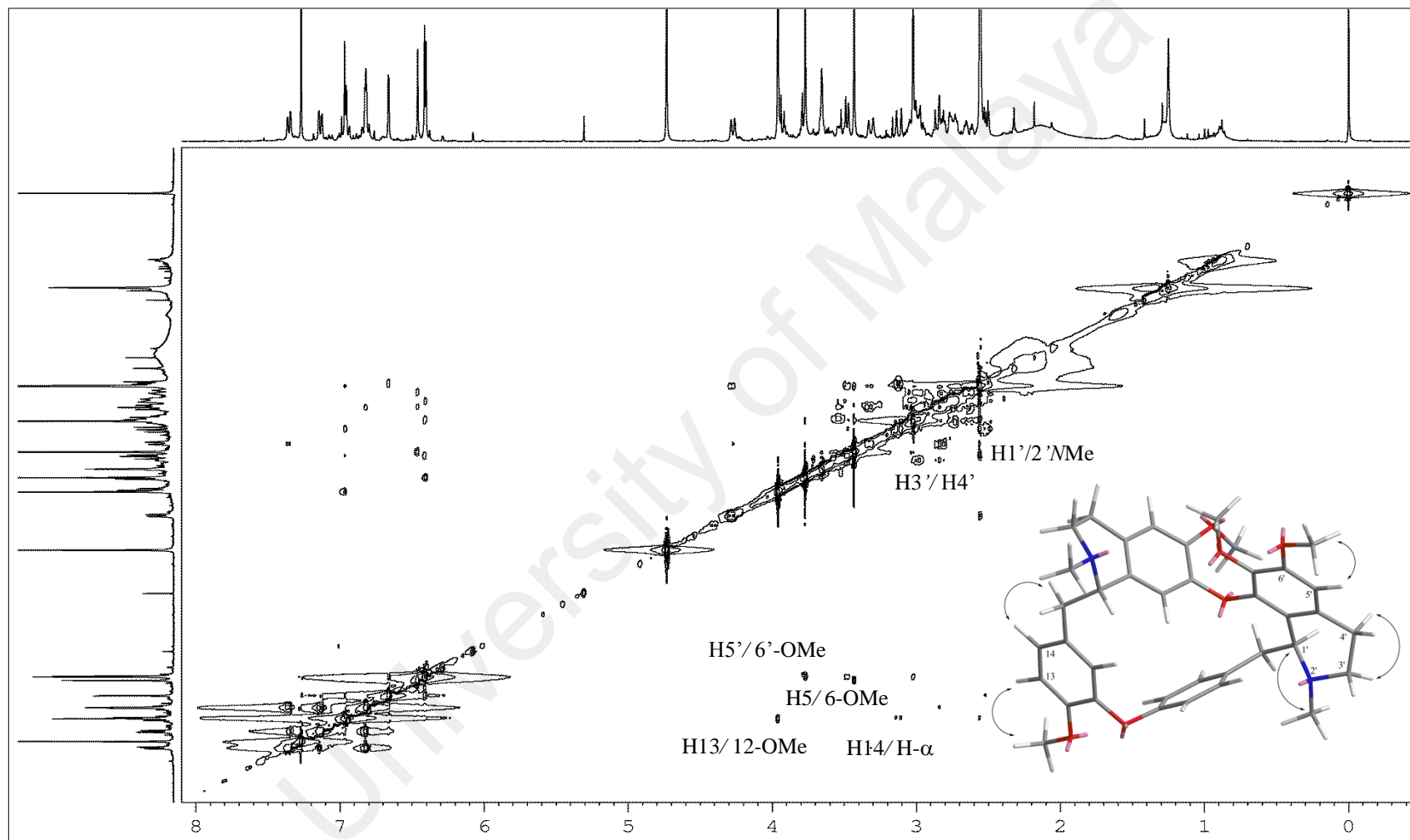
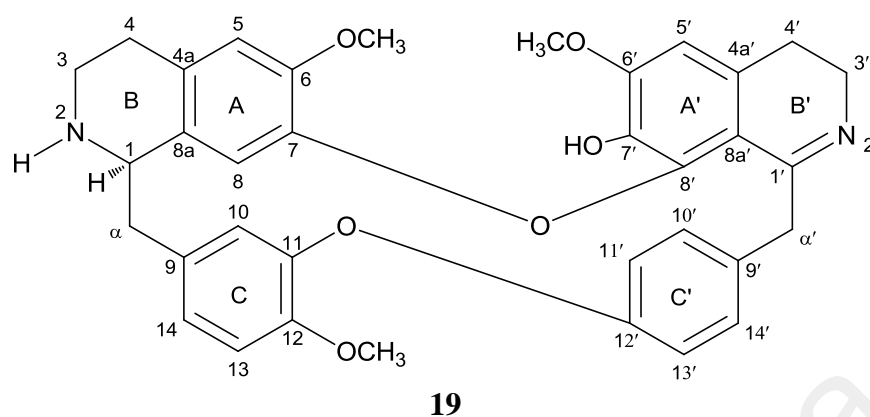


Figure 3.20 NOESY Spectrum of *O*-methyllicacusine **118**

3.1.5 3', 4'-Dihydronorstephasubine **19**



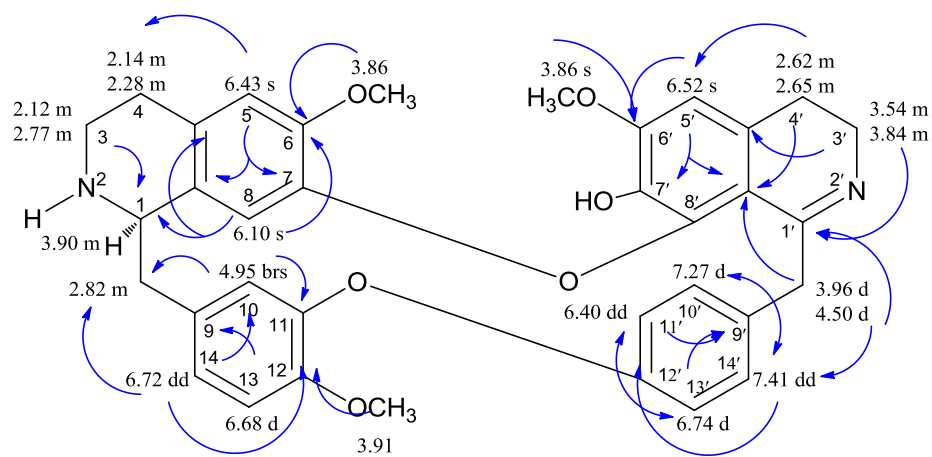
3', 4'- Dihydronorstephasubine **19** was purified as a brown amorphous solid with $[\alpha]_D^{25} +30.0^\circ$ ($c = 0.5$, MeOH). The EIMS spectrum showed a pseudo-molecular ion peak $[M+H]^+$ at m/z 579.2535, corresponding to the molecular formula of $C_{35}H_{34}N_2O_6$ (calcd. for $C_{35}H_{35}N_2O_6$, 579.2495), with 20 degrees of unsaturation. The UV absorption at λ_{max} 203 and 286 nm were consistent with the presence of a bisbenzylisoquinoline chromophore (Gibson & Turnbull, 1980). Its IR spectrum revealed absorption bands due to phenyl ether groups (1260 cm^{-1}), aromatic rings and dihydroisoquinoline imine groups ($1510, 1604\text{ cm}^{-1}$) and a hydroxyl group (3600 cm^{-1}) (Patra et al., 1986).

The ^1H (Figure 3.22) and ^{13}C (Figure 3.23) NMR spectroscopic data of 3', 4'-dihydronorstephasubine **19** were similar to those of 2-norobaberine **115**, except for the following two differences; the absence of the OCH_3 singlet at δ_{H} 3.23 led to the assumption that the methoxyl group at C-7' was replaced by a hydroxyl substituent in **19** and the presence of the deshielded geminal methylene protons $\text{H}_{\text{A}-\alpha'}$ and $\text{H}_{\text{B}-\alpha'}$ at δ_{H} 3.96 and δ_{H} 4.50 respectively, that appeared as doublet ($J=13.7\text{ Hz}$) in comparison with **115**. The above signals suggesting that the benzylic methylene was adjacent to an imine group. Furthermore, the signals of the aromatic protons assignable to H-10 and H-8 shifted to the shielded region at δ_{H} 4.95 and δ_{H} 6.10, instead of resonating at δ_{H} 5.58 and δ_{H} 6.70 respectively, as in that of **115**. This shift could be due to the presence of the

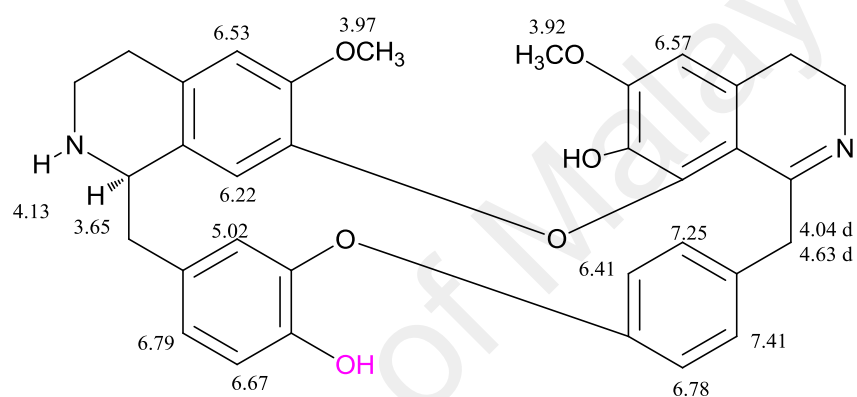
imine function in ring B' which was corroborated by the absence of the H-1' signal and the generation of a quaternary carbon at δ_C 165.1 (C-1'). This was further supported by the presence of an absorption band at ν_{\max} 1604 cm^{-1} in the IR spectrum corresponding to the C=N stretching (Namli & Turhan, 2006).

The HMBC spectrum showed correlations between H- α' and C-1' (δ_C 165.1), which in turn coupled to H-3' and H-4', thus confirming the position of the imine group in the molecule.

The presence of the shielded H-10 signal at δ_H 4.95 (Figure 3.21) was similar to that of pangkorimine **69** (δ_H 5.02), proving that the structure of 3', 4'-dihydronorstephasubine **19** also belonged to type VI BBIQ. The stereochemistry at C-1 was assigned as the *R* configuration based on its positive optical rotation. Upon comparison of the structural data; 1D-NMR and 2D-NMR (Appendix A (Figure A6-A9)) with literature value, this alkaloid is indeed (+) - 3', 4'-dihydronorstephasubine **19** (Mukhtar et al., 2009).



19



69

Figure 3.21: ^1H NMR and HMBC Correlations of (+) - 3', 4'- dihydronorstephasubine **19** and Pangkorimine **69**.

Table 3.6: ¹H, ¹³C-NMR and HMBC Data of 3',4'-dihydronorstephasubine **19**

Position	Unit	¹ H- NMR 19 CDCl ₃ , 400 MHz δ (J, Hz)	¹ H- NMR pangkorimine 69 (Schiff Jr, 1991) δ	¹³ C- NMR 19 100 MHz δ	HMBC (¹ H- ¹³ C)
1	CH	3.90 (<i>m</i>)	4.13	54.5	
3	CH ₂	2.12 (<i>m</i>) 2.77 (<i>m</i>)		41.2	1, 4a
4	CH ₂	2.14 (<i>m</i>) 2.28 (<i>m</i>)		29.4	4a
4a	C			130.2	
5	CH	6.43 (<i>s</i>)	6.53	112.7	4, 6, 7, 8a
6	C			148.0	
6-OMe	O-CH ₃	3.86 (<i>s</i>)	3.97	56.2	6
7	C			145.5	
8	CH	6.10 (<i>s</i>)	6.22	112.5	1,4a,6,7
8a	C			127.0	
α	CH ₂	2.77-2.82 (<i>m</i>)		38.6	
9	C			127.9	
10	CH	4.95 (<i>brs</i>)	5.02	116.9	α, 11, 12, 14
11	C			150.5	
12	C			147.0	
12-OMe	O-CH ₃	3.91 (<i>s</i>)		55.9	12
13	CH	6.68 (<i>d</i> , 8.6)		110.8	9,11
14	CH	6.72 (<i>dd</i> , 8.6, 2.0)	6.67	122.6	α, 10, 12
1'	CH			165.1	
3'	CH ₂	3.60 (<i>m</i>) 3.84 (<i>m</i>)		46.7	1', 4a'
4'	CH ₂	2.65 (<i>m</i>)		27.0	4a', 8a'
4a'	C			131.5	
5'	CH	6.52 (<i>s</i>)	6.57	105.9	4',6',7',8a'
6'	C			150.9	
6'-OMe	O-CH ₃	3.86 (<i>s</i>)	3.92	56.2	6'
7'	C			136.1	
8'	C			142.0	
8'a	C			131.5	
α'	CH ₂	3.96 (<i>d</i> , 13.7) 4.50 (<i>d</i> , 13.7)	4.04 (<i>d</i> , 13.6) 4.63 (<i>d</i> , 13.6)	44.7	1', 8a', 9', 10', 14'
9'	C			135.3	
10'	CH	7.27 (<i>d</i> , 8.6)	7.25	132.1	12', 14', α'
11'	CH	6.40 (<i>dd</i> , 8.6, 2.0)	6.41	121.9	9', 12', 13'
12'	C			152.6	
13'	CH	6.74 (<i>d</i> , 8.6)	6.78	122.4	9', 11'
14'	CH	7.41 (<i>d</i> , 8.6)	7.41	128.8	α', 10', 12'

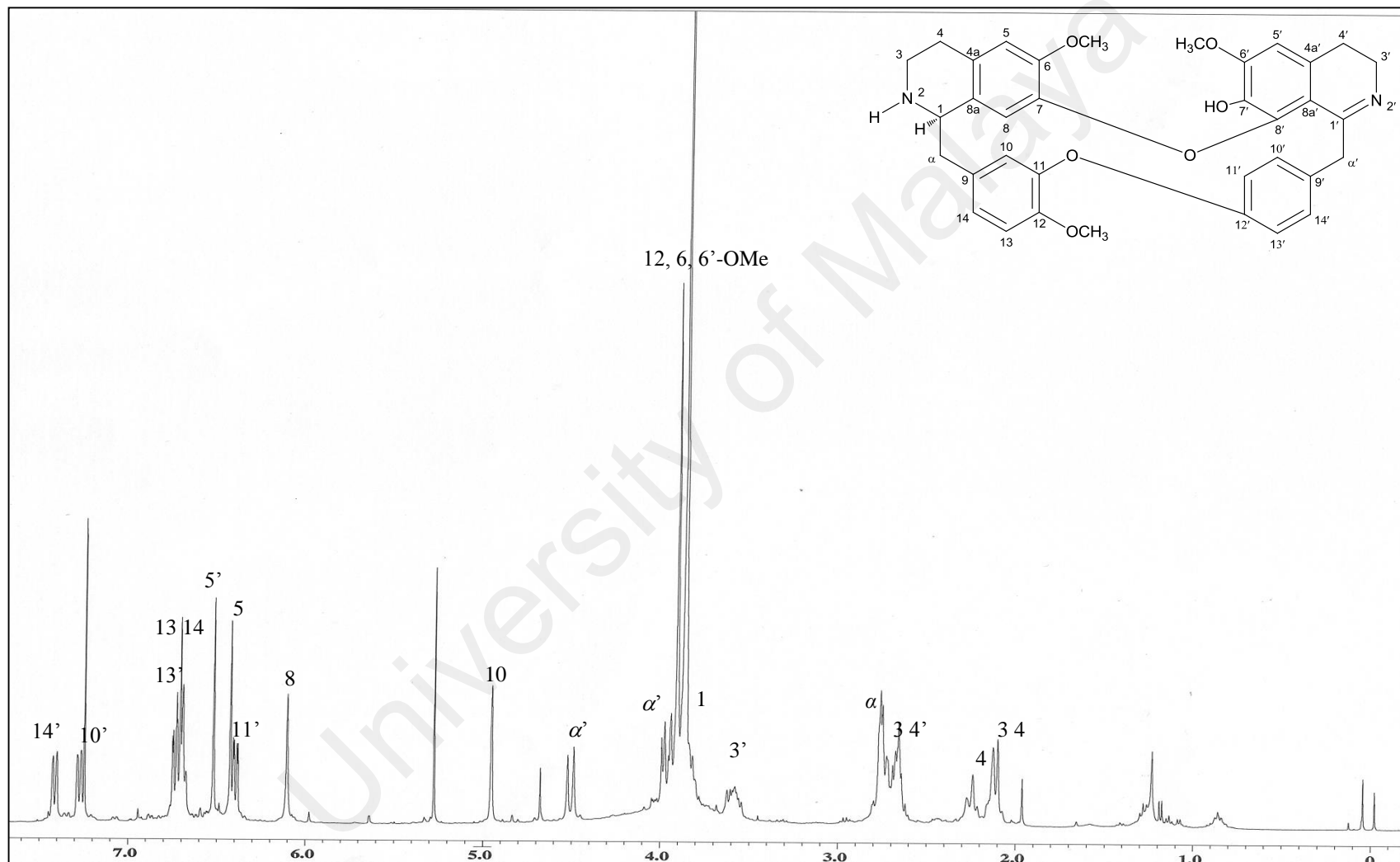


Figure 3.22: ¹H NMR Spectrum of 3',4'-dihydronorstephasubine **19**

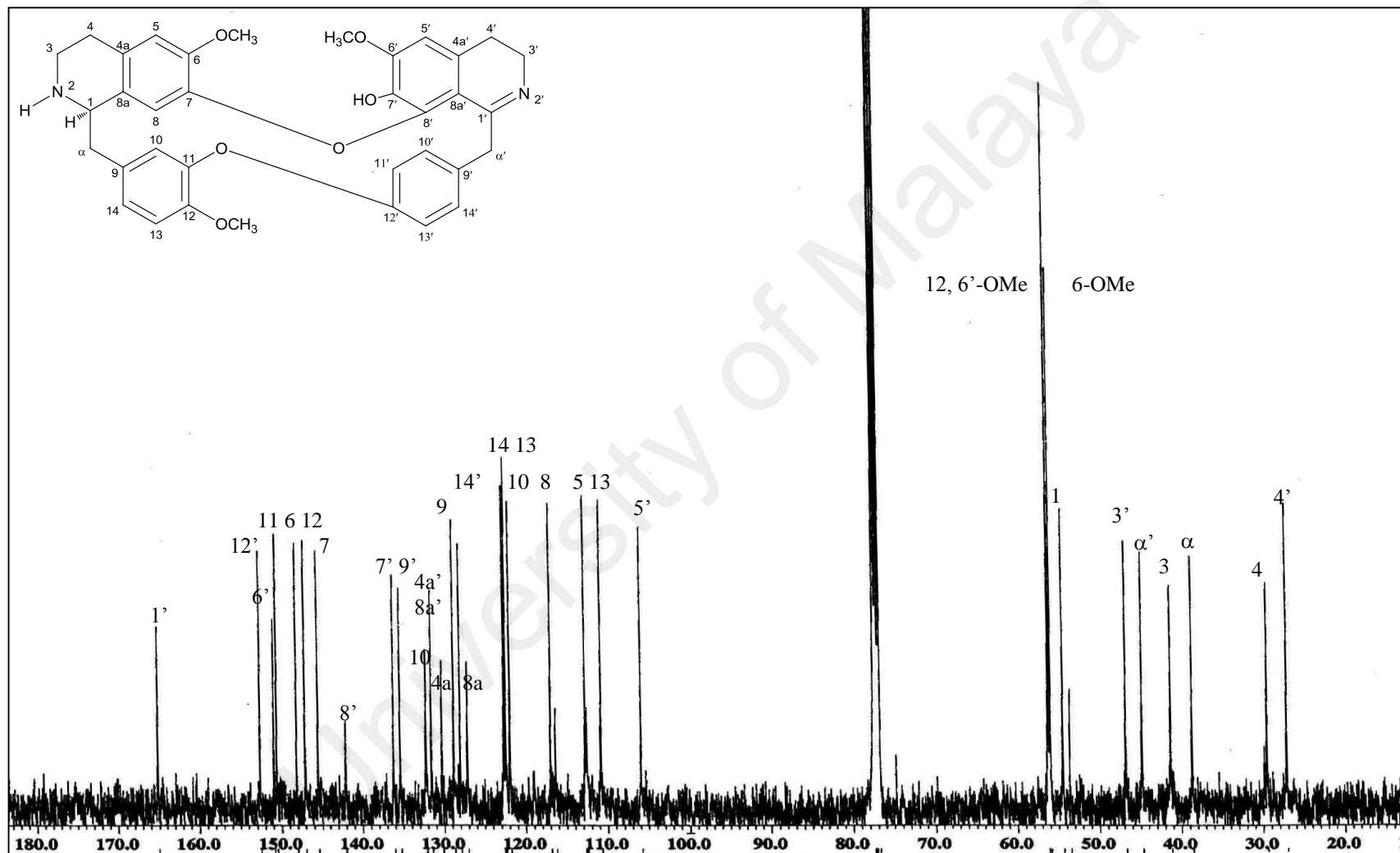
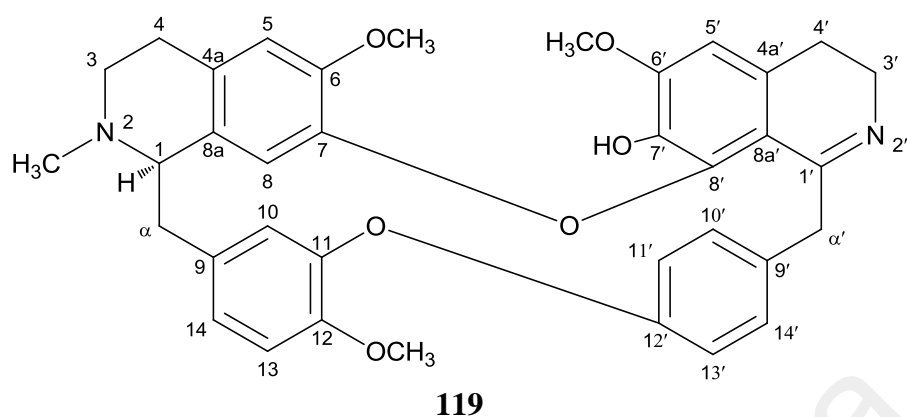


Figure 3.23: ¹³C NMR Spectrum of 3',4'-dihydronorstephasubine 19

3.1.6 3', 4'-Dihydrostephasubine **119**



3', 4'-Dihydrostephasubine **119** was afforded as a dark brown amorphous powder with $[\alpha]_D^{25} +50.0^\circ$ ($c = 0.5$, MeOH). The positive electrospray mass spectrum displayed a pseudo-molecular ion peak $[M+H]^+$ at m/z 593.2622, compatible with the molecular formula $C_{36}H_{36}N_2O_6$ (calcd. for $C_{36}H_{37}N_2O_6$, 593.2652). The NMR spectroscopic data (Table 3.7) of **119** were similar to those of **19**, thus implying that **119** was also a BBIQ bearing an imine function with a structure closely resembling that of **19** (Kanyinda et al., 1997; Namli & Turhan, 2006; Shamma, 1972).

However for 3', 4'-dihydrostephasubine **119**, the additional resonances at δ_H 2.64 and δ_C 41.4 in its 1H (Figure 3.25) and ^{13}C NMR (Figure 3.26) spectra respectively indicated the presence of an *N*-CH₃ group at *N*-2. The position of the *N*-CH₃ group on the left side of the dimer was proven from the HMBC correlations (Appendix A -Figure A11) of H-3 and H-1 to *N*-CH₃ (δ_C 41.5). The placement of methoxyl and hydroxyl groups were established in the similar manner as was done for alkaloid **19**.

Through analysis of all the data obtained and comparison with literature values indicated that the alkaloid was (+)-3', 4'-dihydrostephasubine **119** (Figure 3.24) which was isolated previously from *Stephania hernandifolia* (Willd.) Walp (Patra et al., 1986). The retention factor of **119** ($R_f = 0.81$) was higher than that of **19** ($R_f = 0.71$) with the

same skeleton due to the additional *N*-CH₃ group which rendered the molecule being less polar (Sun et al., 2000).

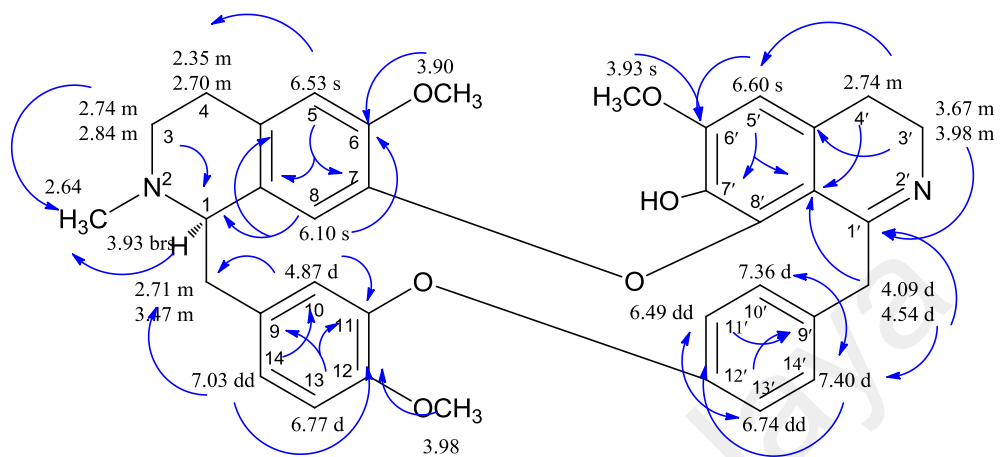


Figure 3.24: ¹H NMR and HMBC Correlations of (+)-3', 4'-dihydrostephasubine **119**

Table 3.7: ^1H and ^{13}C -NMR Data of 3',4'-dihydrostephasubine **119**

Position	Unit	^1H - NMR CDCl ₃ , 400 MHz (δ (Hz))	^1H - NMR (δ (Hz)) (Patra et al., 1988) (270MHz, CDCl ₃)	^{13}C - NMR 100MHz (δ)
1	CH	3.93 (<i>brs</i>)	3.59	63.0
2	N-CH ₃	2.64 (<i>s</i>)	2.51	41.4
3	CH ₂	2.74 (<i>m</i>)		47.1
		2.84 (<i>m</i>)		
4	CH ₂	2.35 (<i>m</i>)		22.9
		2.70 (<i>m</i>)		
4a	C			127.0
5	CH	6.53 (<i>s</i>)	6.51	111.7
6	C			148.5
6-OMe	O-CH ₃	3.90 (<i>s</i>)	3.88	55.9
7	C			145.0
8	CH	6.10 (<i>s</i>)	6.10	113.0
8a	C			122.6
α	CH ₂	2.71 (<i>m</i>)		37.6
		3.47 (<i>m</i>)		
9	C			132.0
10	CH	4.87 (<i>d</i> , 1.5)	4.91	116.6
11	C			150.0
12	C			146.9
12-OMe	O-CH ₃	3.98 (<i>s</i>)	3.95	55.9
13	CH	6.77 (<i>d</i> , 8.3)	6.73	111.1
14	CH	7.03 (<i>dd</i> , 8.3, 1.5)	6.84	123.5
1'	C			165.1
2'	N'-CH ₃			
3'	CH ₂	3.67 (<i>m</i>)		46.0
		3.98 (<i>m</i>)		
4'	CH ₂	2.74 (<i>m</i>)		26.9
4a'	C			131.9
5'	CH	6.60 (<i>s</i>)	6.60	106.0
6'	C			150.0
6'-OMe	O-CH ₃	3.93 (<i>s</i>)	3.91	56.3
7'	C			135.6
8'	C			140.5
8'a	C			134.6
α'	CH ₂	4.09 (<i>d</i> , 13.9)	4.08	44.2
		4.54 (<i>d</i> , 13.9)	4.52	
9'	C			134.6
10'	CH	7.36 (<i>d</i> , 8.3)	7.36	132.1
11'	CH	6.49 (<i>dd</i> , 8.3, 2.0)	6.48	121.9
12'	C			152.7
13'	CH	6.74 (<i>dd</i> , 8.3, 2.0)	6.77	122.5
14'	CH	7.38 (<i>d</i> , 8.3)	7.40	128.3

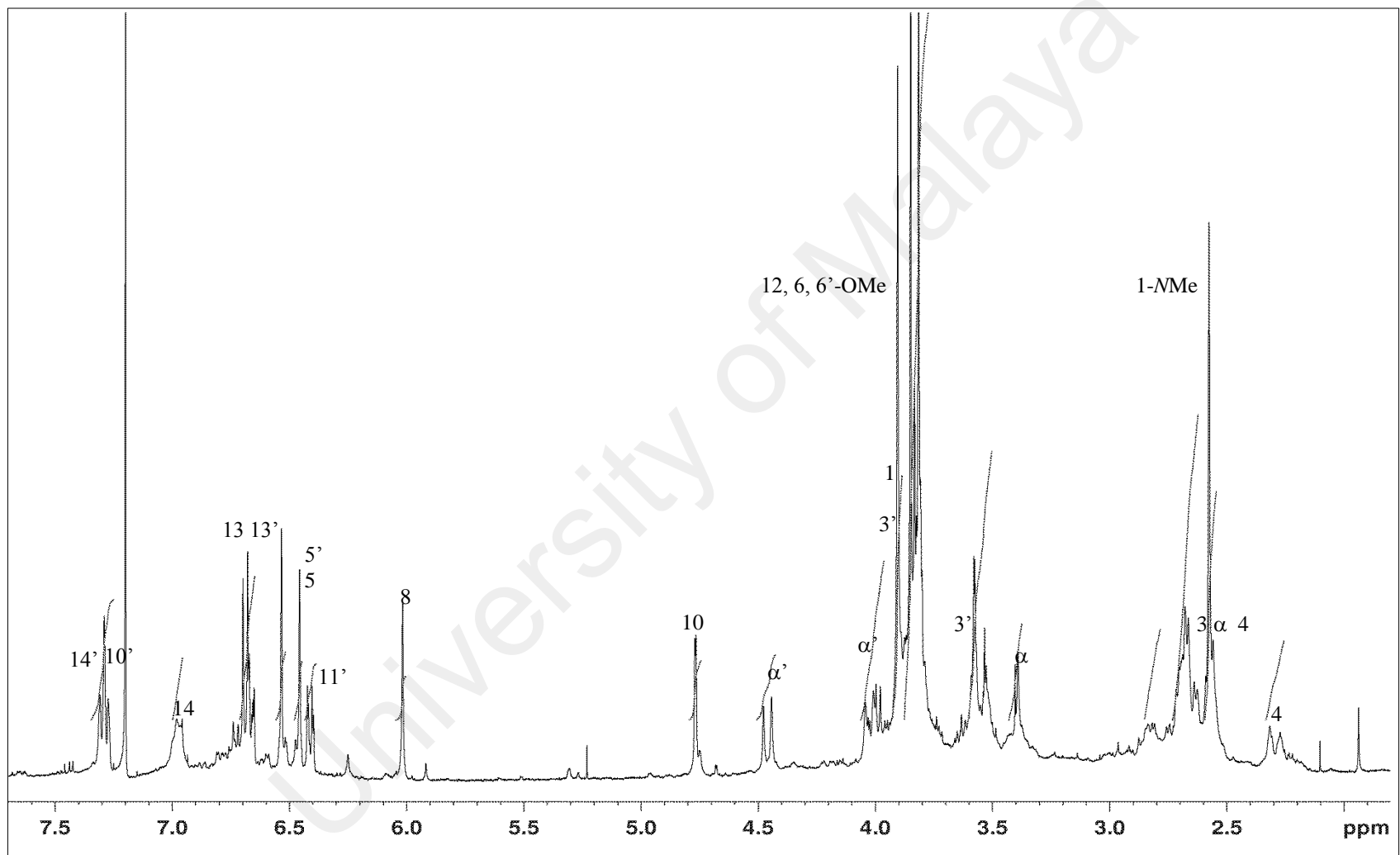


Figure 3.25: ¹H NMR Spectrum of 3',4'-dihydrostephasubine **119**

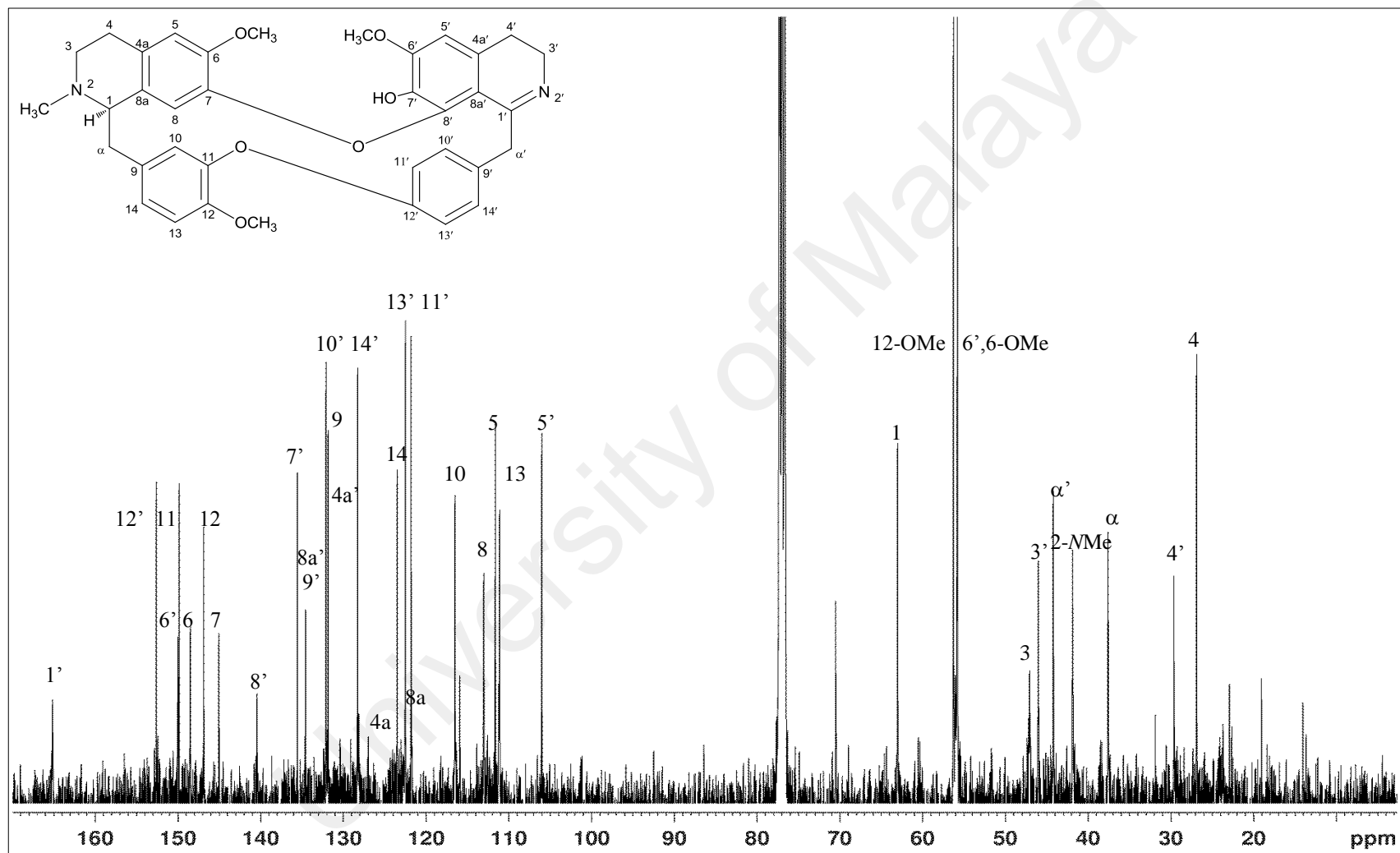
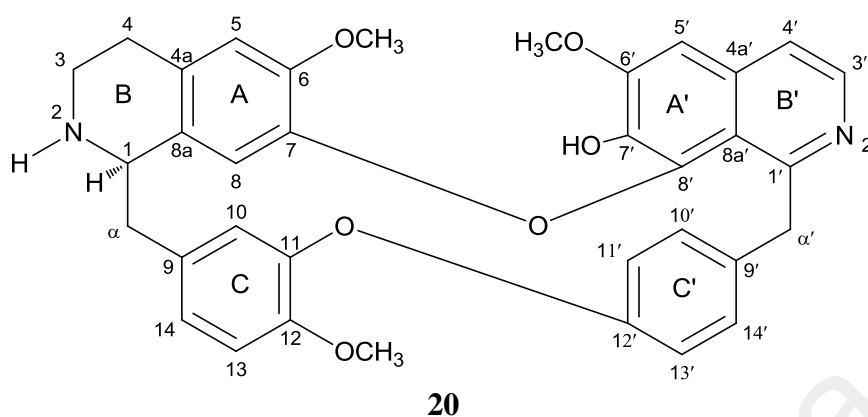


Figure 3.26: ^{13}C NMR Spectrum of 3',4'-dihydrostephasubine **119**

3.1.7 Norstephasubine **20**



Norstephasubine **20** was obtained as a pale yellow amorphous solid with $[\alpha]_D^{25} +310.0^\circ$ ($c=1.0, \text{MeOH}$). The UV spectrum displayed absorptions maxima at λ_{max} 244, 286 and 338 nm which suggested the presence of a bisbenzylisoquinoline moiety (Kanyinda et al., 1997; Shamma, 1972). Its IR spectrum revealed absorption bands due to phenyl ether groups ($1223, 1259 \text{ cm}^{-1}$), aromatic rings with dihydroisoquinoline imine groups ($1432, 1512, 1606 \text{ cm}^{-1}$) and a hydroxyl group (3400 cm^{-1}) (Patra et al., 1986). The ESIMS spectrum revealed a pseudo-molecular ion peak $[\text{M}+\text{H}]^+$ at m/z 577.2371 (calcd. for $\text{C}_{35}\text{H}_{33}\text{N}_2\text{O}_6$, 577.2339) suggesting a molecular formula of $\text{C}_{35}\text{H}_{32}\text{N}_2\text{O}_6$, corresponding to 21 degrees of unsaturation.

Norstephasubine **20** displayed similar ^1H (Figure 3.27) and ^{13}C NMR (Figure 3.28) spectral features with those of **19**. However, the only difference was the presence of a dihydroisoquinoline imine group in ring B' which was inferred from the existence of a pair of vicinal protons at δ_{H} 8.43 (H-3') and δ_{H} 7.47 (H-4') appearing as a pair of doublets with a small coupling constant of 5.6 Hz. The downfield shift in the resonances of $\text{H}_{\text{A}-\alpha'}$ and $\text{H}_{\text{B}-\alpha'}$ to δ_{H} 5.36 and δ_{H} 4.51, respectively upon comparison with the corresponding atoms in **19**, thus suggested that the benzylic methylene was adjacent to ring B' bearing the dihydroisoquinoline imine functionality.

The downfield signal at δ_c 157.0, δ_c 140.4 and δ_c 119.0 corresponding to C-1', C-3', and C-4' in the ^{13}C NMR spectrum further proved the observed functionality in ring B'. Upon comparison of the HMBC spectrum of norstephasubine **20** with **19**, a mark similarity was notified from the correlations of H-3' and H- α' to C-1' (δ_c 157.0) which enable the placement of the imine group. Meanwhile, the additional correlation between H-3' and H-5' to C-4' (δ_c 119.0) verified the dihydroisoquinoline imine group in ring B'. The same substituents could be characterized in both compounds; **20** and **19** by further supported by 2D NMR spectra supplemented in Appendix A (Figure A12-A14).

The positive optical rotation sign and spectroscopic data evidence were consistent with those isolated from *Stephania suberosa* Forman found in the literatures, thus confirming the identity of (+)-norstephasubine **20** (Table 3.8) (Patra et al., 1986; Tantisewie & Ruchirawat, 1992).

Table 3.8: ^1H , ^{13}C -NMR and HMBC Data of Norstephasubine **20**

Position	Unit	^1H - NMR CDCl_3 , 400 MHz (δ (Hz)) Norstephasubine 20	^1H - NMR (δ (Hz)) (Patra et al., 1986)	^{13}C -NMR 100 MHz (δ)	HMBC (^1H - ^{13}C)
1	CH	4.09 (<i>m</i>)	4.02 (<i>m</i>)	54.6	
3	CH ₂	2.90 (<i>m</i>) 2.55 (<i>m</i>)		41.5	
4	CH ₂	2.38 (<i>m</i>) 2.20 (<i>m</i>)		29.7	
4a	C			129.8	
5	CH	6.56 (<i>s</i>)	6.53 (<i>s</i>)	112.4	4,6,7,8a
6	C			147.5	
6-OMe	O-CH ₃	4.05 (<i>s</i>)	4.02 (<i>s</i>)	56.1	
7	C			144.6	
8	CH	6.04 (<i>s</i>)	6.02 (<i>s</i>)	110.9	1,4a,6,7
8a	C			127.9	
α	CH ₂	2.73 (<i>m</i>) 2.70 (<i>m</i>)		38.6	10, 14, 9
9	C			127.9	
10	CH	4.88 (<i>d</i> , 2.0)	4.87 (<i>d</i>)	116.6	α , 11, 12, 14
11	C			150.4	
12	C			146.9	
12-OMe	O-CH ₃	3.88 (<i>s</i>)	3.88 (<i>s</i>)	55.9	
13	CH	6.72 (<i>d</i> , 8.3)	6.73 (<i>d</i>)	110.8	9, 11, 12
14	CH	6.65 (<i>dd</i> , 8.3, 2.0)	6.71 (<i>dd</i>)	122.6	α , 12, 9
1'	C			157.0	
3'	CH	8.43 (<i>d</i> , 5.6)	8.41 (<i>d</i>)	140.4	1', 4', 4a'
4'	CH	7.47 (<i>d</i> , 5.6)	7.46 (<i>d</i>)	119.0	4a', 3', 5'
4a'	C			133.4	
5'	CH	6.97 (<i>s</i>)	6.93 (<i>s</i>)	101.6	4', 6', 8a'
6'	C			151.3	
6'-OMe	O-CH ₃	4.04 (<i>s</i>)	4.03 (<i>s</i>)	56.3	
7'	C			135.7	
8'	C			145.2	
8'a	C			137.0	
α'	CH ₂	5.36 (<i>d</i> , 13.6) 4.51 (<i>d</i> , 13.6)	5.35 (<i>d</i>) 4.50 (<i>d</i>)	45.3	1', 9', 10'
9'	C			137.6	
10'	CH	7.09 (<i>d</i> , 8.3)	7.09 (<i>dd</i>)	129.2	α' , 12', 14'
11'	CH	6.65 (<i>dd</i> , 8.3, 2.0)	6.66 (<i>dd</i>)	122.6	9', 12', 13'
12'	C			152.3	
13'	CH	6.43 (<i>dd</i> , 8.3, 2.0)	6.43 (<i>dd</i>)	121.9	9', 11', 12'
14'	CH	7.37 (<i>d</i> , 8.3)	7.37 (<i>dd</i>)	127.8	α' , 10', 12'

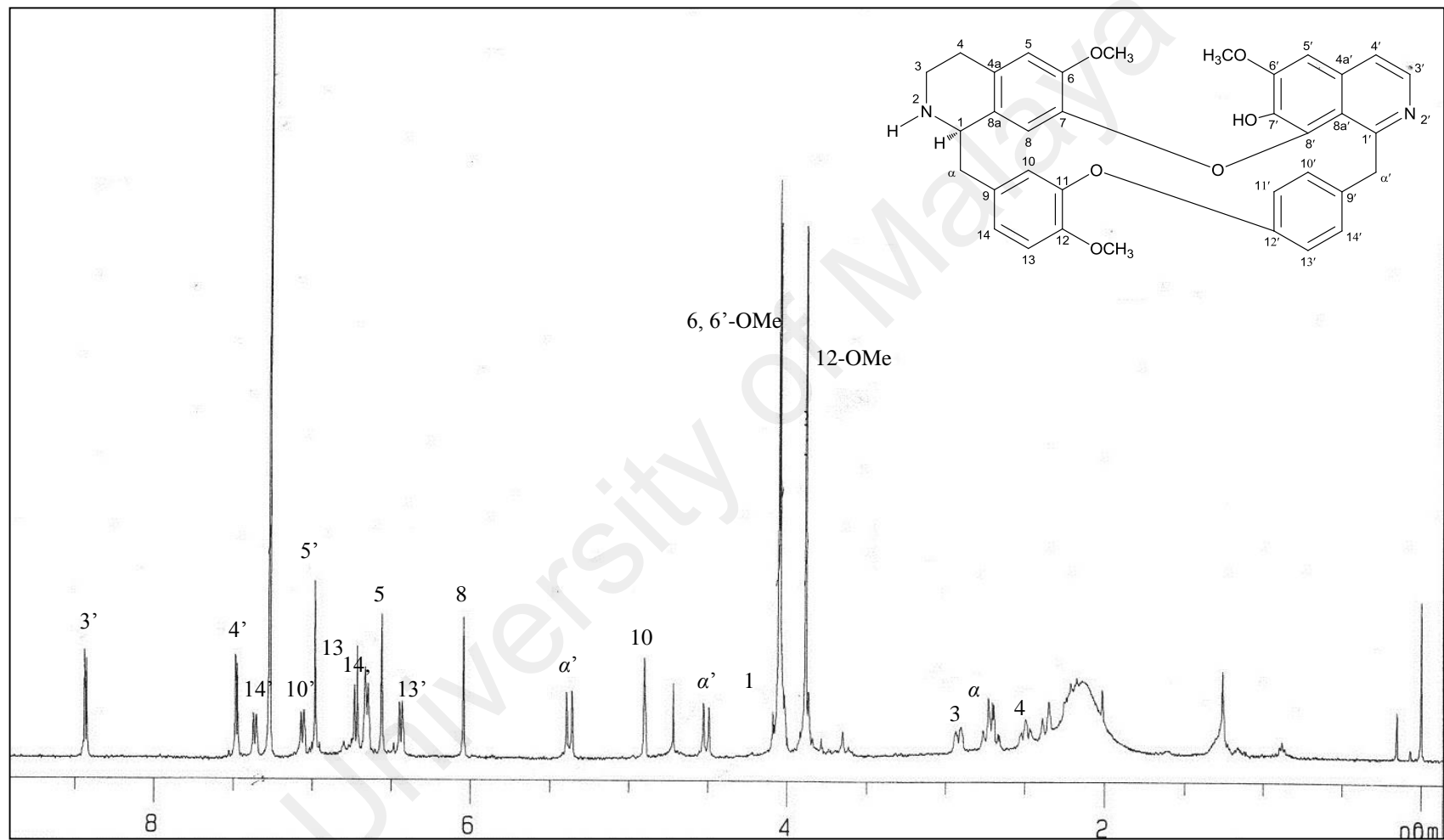


Figure 3.27: ¹H NMR Spectrum of Norstephasubine **20**

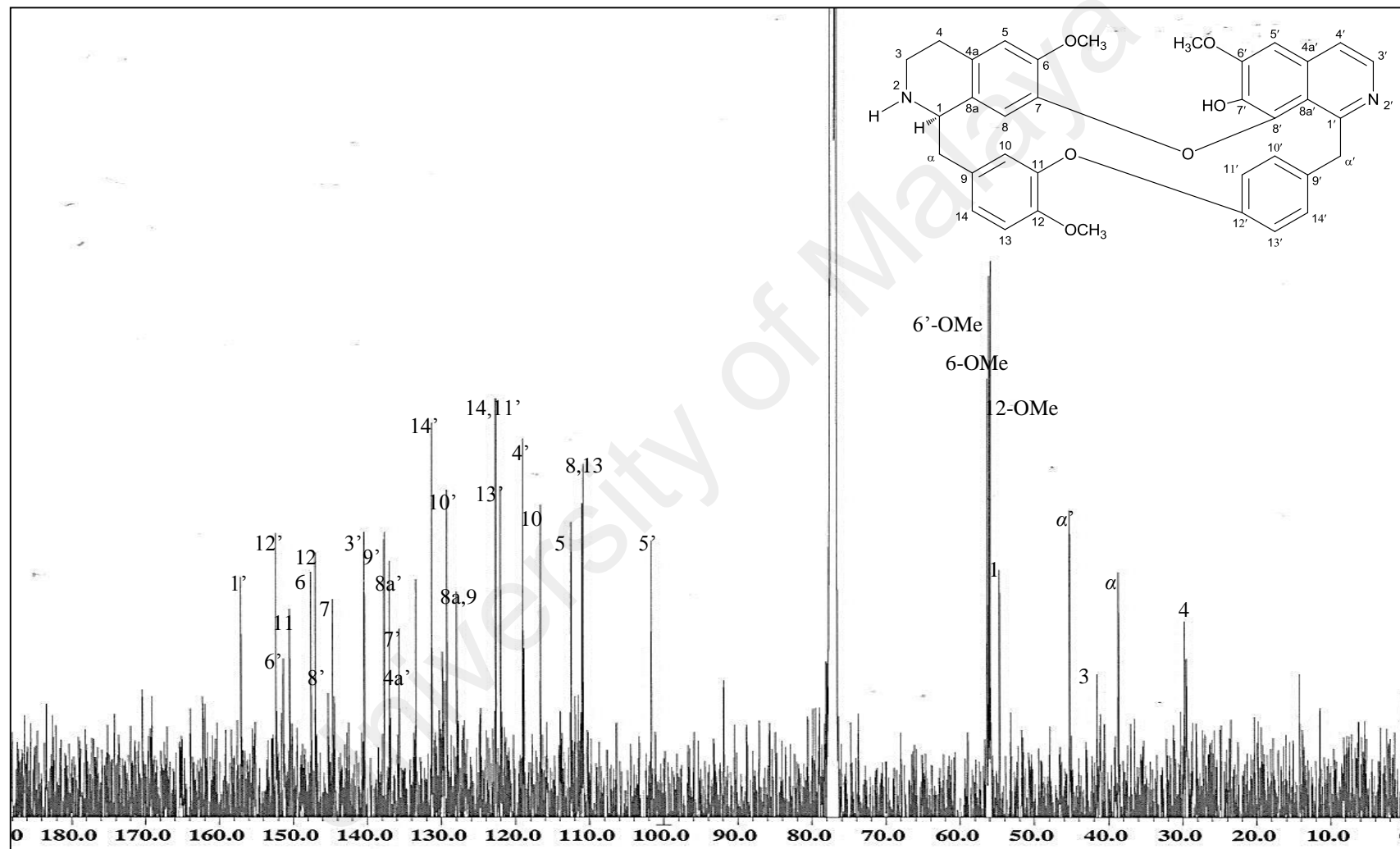
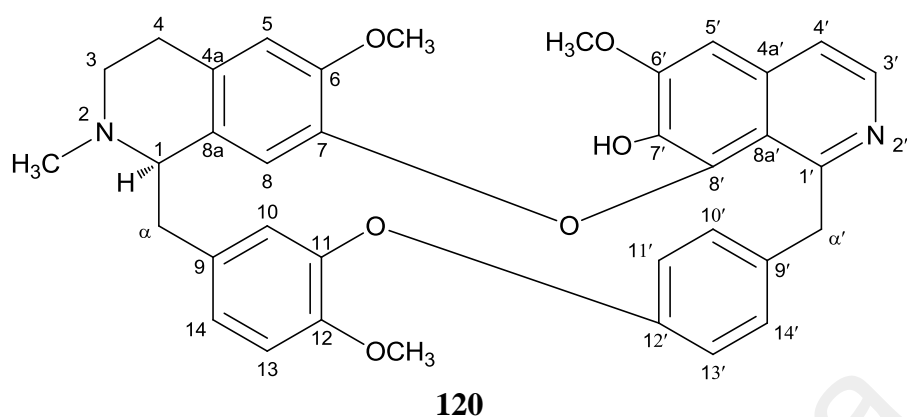


Figure 3.28: ^{13}C NMR Spectrum of Norstephasubine 20

3.1.8 Stephasubine 120



Stephasubine **120**, $[\alpha]_D^{25} +350.0^\circ$ ($c = 1.0$, MeOH) was isolated as a brown amorphous solid. ESIMS spectrum (showed a pseudo-molecular ion peak $[M+H]^+$ at m/z 591.2449 which suggested the molecular formula of $C_{36}H_{34}N_2O_6$ (calcd. for $C_{36}H_{35}N_2O_6$, 591.2495).

Significant resemblances were observed between the UV, IR, 1H NMR (Figure 3.30), ^{13}C NMR (Figure 3.31) spectra of stephasubine **120** and norstephasubine **20**, which in turn confirmed a close structural relationship between both these alkaloids. However, the additional presence of the resonances at δ_H 2.52 and δ_C 43.0 in the 1H and ^{13}C NMR spectra of **120**, was due to the N - CH_3 group at N -2. The placement of the N - CH_3 group on the left side of the dimer was deduced from the HMBC correlations (Figure 3.28) of 2 - NCH_3 to C-1 (δ_C 63.2) and C-3 (δ_C 48.8).

The stereochemistry at C-1 was assigned as R -configuration based on the comparison of its optical rotation value with the reported data in the literature. On the basis of the aforementioned data (Table 3.9) and also upon confirmation by supplemented spectra of LCMS (Figure A15) and 2D NMR (Figure A16-17) the structure of stephasubine **120** was established. The retention factor of **120** ($R_f = 0.44$) was higher compared to that of **20** ($R_f = 0.27$) with an identical skeleton due the additional N - CH_3 group which made

the molecule less polar (Sun et al., 2000). Previously, stephasubine **120** was isolated from *Stephania hernandifolia* (Willd.) Walp (Patra et al., 1988) and *Stephania suberosa* Forman. (Patra et al., 1986).

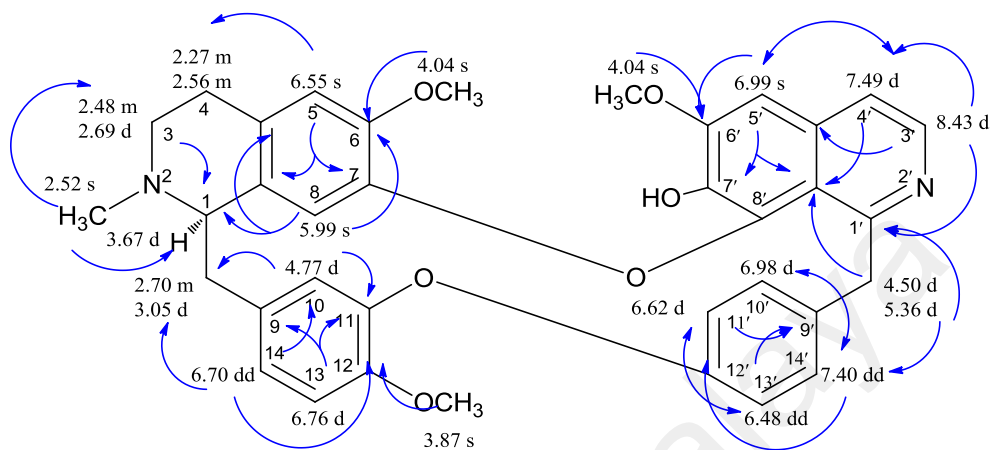


Figure 3.29: ¹H NMR and HMBC Correlations of (+)-Stephasubine **120**

University of Madras

Table 3.9: ^1H and ^{13}C -NMR Data of Stephasubine **120**

Position	Unit	^1H - NMR CDCl ₃ , 400 MHz Stephasubine 120 δ (J, Hz)	^1H - NMR CDCl ₃ 270 MHz (Patra et al., 1988) δ (J)	^{13}C -NMR 100 MHz (δ)
1	CH	3.67 (<i>d</i> , 11.0)	3.60 (<i>m</i>)	63.2
2	N-CH ₃	2.52 (<i>s</i>)	2.51 (<i>s</i>)	43.0
3	CH ₂	2.69 (<i>d</i> , 9.1) 2.48 (<i>m</i>)		48.8
4	CH ₂	2.56 (<i>m</i>) 2.27 (<i>m</i>)		29.7
4a	C			129.6
5	CH	6.55 (<i>s</i>)	6.54 (<i>s</i>)	111.5
6	C			147.4
6-OMe	O-CH ₃	4.04 (<i>s</i>)	4.05 (<i>s</i>)	56.3
7	C			144.0
8	CH	5.99 (<i>s</i>)	5.95 (<i>s</i>)	111.5
8a	C			135.2
α	CH ₂	3.05 (<i>d</i> , 11.0) 2.70 (<i>m</i>)		37.8
9	C			128.7
10	CH	4.77 (<i>d</i> , 1.4)	4.84 (<i>brs</i>)	116.6
11	C			149.7
12	C			146.3
12-OMe	O-CH ₃	3.87 (<i>s</i>)	3.86 (<i>s</i>)	55.8
13	CH	6.76 (<i>d</i> , 8.0)	6.71 (<i>brs</i>)	110.8
14	CH	6.70 (<i>dd</i> , 8.0, 1.4)	6.71 (<i>brs</i>)	122.6
1'	C			156.9
3'	CH ₂	8.43 (<i>d</i> , 5.5)	8.45 (<i>d</i>)	140.4
4'	CH ₂	7.49 (<i>d</i> , 5.5)	7.47 (<i>d</i>)	118.9
4a'	C			133.5
5'	CH	6.99 (<i>s</i>)	7.00 (<i>s</i>)	101.7
6'	C			150.9
6'-OMe	O-CH ₃	4.04 (<i>s</i>)	4.05 (<i>s</i>)	56.3
7'	C			137.3
8'	C			146.3
8a'	C			118.8
α'	CH ₂	5.36 (<i>d</i> , 14.0) 4.50 (<i>d</i> , 14.0)	5.36 (<i>d</i>) 4.49 (<i>d</i>)	45.0
9'	C			136.9
10'	CH	6.98 (<i>d</i> , 8.0)	7.03 (<i>dd</i>)	128.7
11'	CH	6.62 (<i>d</i> , 8.0)	6.65 (<i>dd</i>)	123.0
12'	C			152.5
13'	CH	6.48 (<i>dd</i> , 8.2, 2.4)	6.49 (<i>dd</i>)	122.0
14'	CH	7.40 (<i>d</i> , 8.2)	7.43 (<i>dd</i>)	131.1

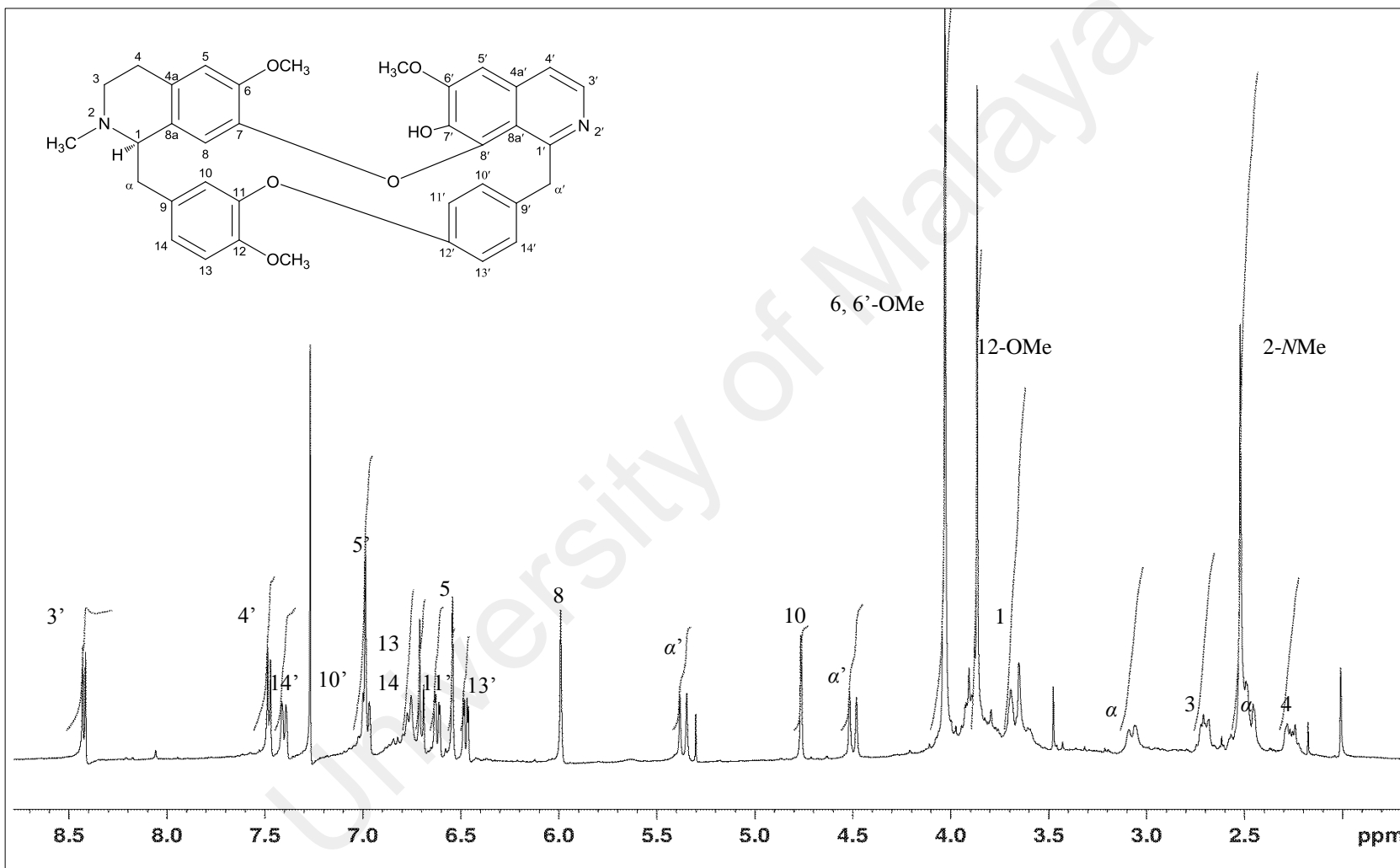


Figure 3.30: ¹H NMR Spectrum of Stephasubine **120**

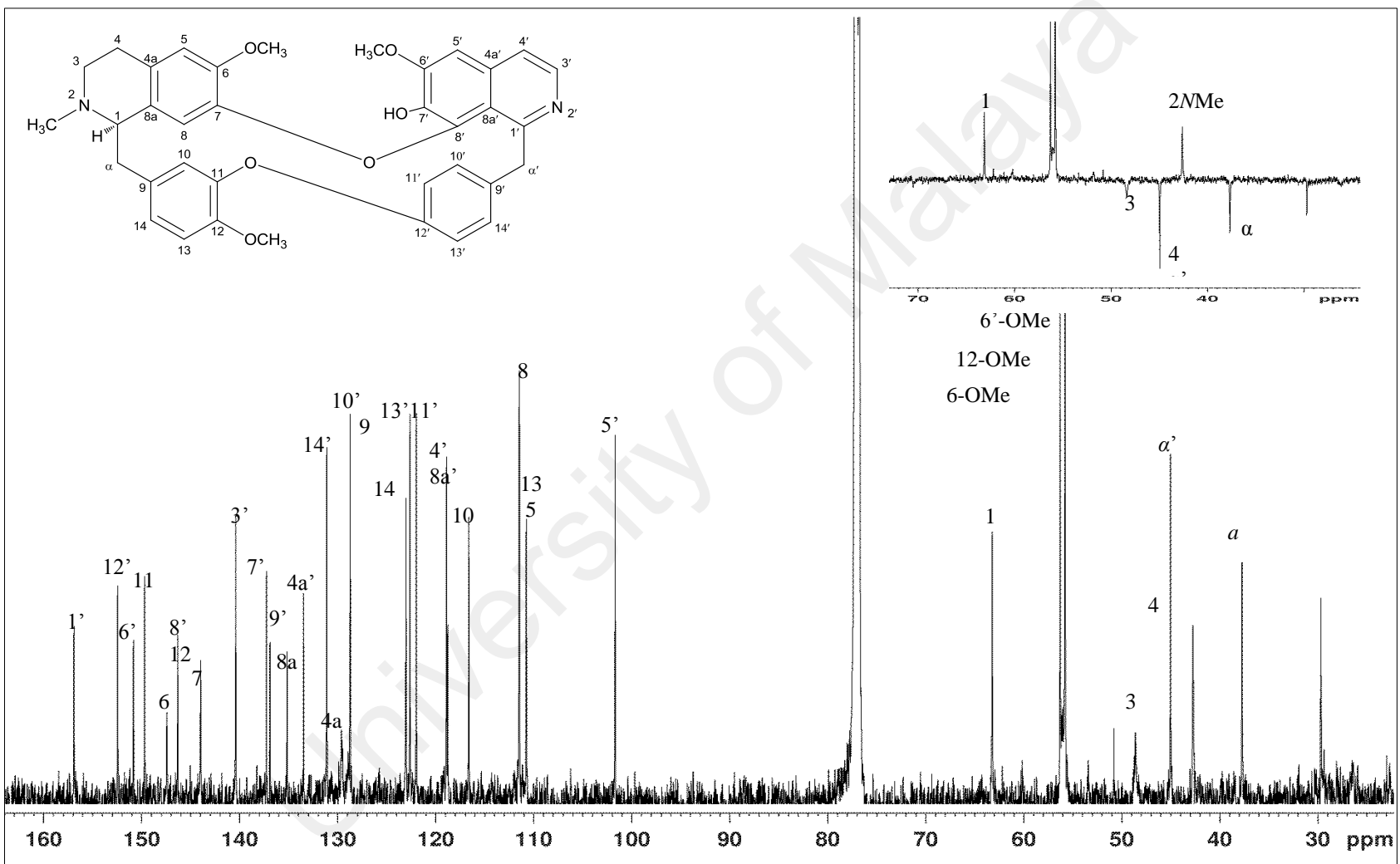
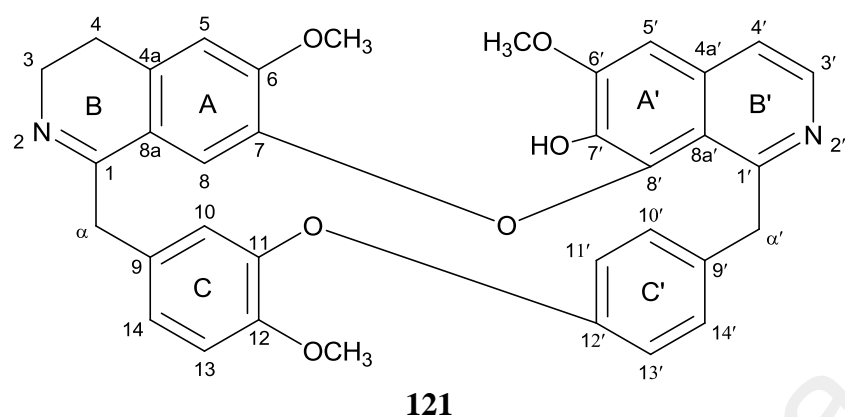


Figure 3.31: ^{13}C NMR Spectrum (inset: DEPT spectrum) of Stephasubine 120

3.1.9 Stephasubimine 121



Stephasubimine **121** was afforded as an optically inactive brownish amorphous solid. HRESI⁺ showed a [M+H]⁺ peak at *m/z* 575.2164 corresponding to the molecular formula of C₃₅H₃₁N₂O₆ (575.2182 calcd. for C₃₅H₃₂N₂O₆) with 22 degrees of unsaturation, thus suggesting the presence of a new imine group in ring B when compared to norstephasubine **20**.

The similarities between the UV, IR, ¹H (Figure 3.33) and ¹³C NMR (Figure 3.34) spectra of stephasubimine **121** and **20** validate the possibility of both alkaloids possessing the same skeleton. The only difference was the presence of an imine group in ring B of **121** which was further verified by the absence of the methine proton at δ_H 4.09 (H-1) which in turn gave rise to the quaternary carbon C-1 (δ_C 169.5) in stephasubimine **121**.

The HMBC correlations for stephasubimine **121** were shown in appendix A (Figure A20). The positions of Δ^{1'-N'} and Δ^{1-N} double bonds were confirmed by the HMBC correlations of H-3' (δ_H 8.44) and H-α' (2H, δ_H 5.37, 4.53) to C-1' on right hand side of the dimer and H-8 (δ_H 6.53) and H-α (δ_H 3.65) to C-1 on the other hand. Therefore, peak at δ_C 169.5 and δ_C 157.3 were assignable to C-1 and C-1' respectively, thus confirming the imine function in ring B and the dihydroisoquinoline imine function in ring B'.

All the additional information to confirm that stephasubimine **121** was a type VI bisbenzylisoquinoline, which was previously isolated from *Stephania suberosa* Forman (Patra et al., 1986) can be seen in appendix A (Figure A18-A20). The NMR and HMBC data are presented in Table 3.10.

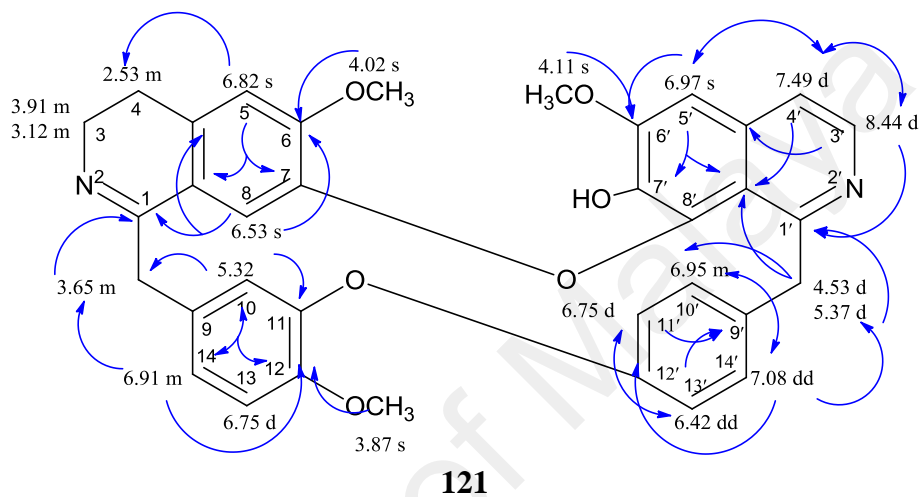


Figure 3.32: ^1H NMR and HMBC Correlations of Stephasubimine **121**

Table 3.10: ^1H , ^{13}C -NMR and HMBC Data of Stephasubimine **121**

Position	Unit	^1H - NMR CDCl ₃ , 400 MHz Stephasubimine 121 δ (<i>J</i> , Hz)	^1H - NMR CDCl ₃ , 270 MHz (Patra et al., 1986) δ (<i>J</i>)	^{13}C -NMR 100 MHz δ	HMBC (^1H - ^{13}C)
1	C			169.5	
3	CH ₂	3.91 (<i>m</i>) 3.12 (<i>m</i>)	3.81 (<i>m</i>) 3.11 (<i>m</i>)	45.4	
4	CH ₂	2.53 (<i>m</i>)	2.47 (<i>m</i>)	29.7	
4a	C			134.6	
5	CH	6.82 (<i>s</i>)	6.50 (<i>s</i>)	110.9	4, 7, 8a
6	C			152.4	
6-OMe	O-CH ₃	4.02 (<i>s</i>)	4.02 (<i>s</i>)	56.3	6
7	C			144.9	
8	CH	6.53 (<i>s</i>)	6.81 (<i>s</i>)	114.1	1,4a,6
8a	C			127.9	
α	CH ₂	3.65 (<i>m</i>)		40.1	1
9	C			129.5	
10	CH	5.32 (<i>d</i> , 1.2)	5.37 (<i>d</i>)	115.6	α , 11, 12, 14
11	C			150.1	
12	C			146.8	
12-OMe	O-CH ₃	3.87 (<i>s</i>)	3.88 (<i>s</i>)	55.9	12
13	CH	6.75 (<i>d</i> , 8.1)	6.74 (<i>d</i>)	111.9	9, 11
14	CH	6.91 (<i>m</i>)	6.82 (<i>dd</i>)	121.7	α , 10, 12
1'	C			157.3	
3'	CH	8.44 (<i>d</i> , 5.6)	8.45 (<i>d</i>)	140.5	1', 4', 4a'
4'	CH	7.49 (<i>d</i> , 5.6)	7.49 (<i>d</i>)	119.1	4a', 3', 5'
4a'	C			133.5	
5'	CH	6.97 (<i>s</i>)	6.96 (<i>s</i>)	101.2	4', 6', 7', 8a'
6'	C			150.9	
6'-OMe	O-CH ₃	4.11 (<i>s</i>)	4.11 (<i>s</i>)	56.4	6'
7'	C			136.1	
8'	C			135.4	
8a'	C			118.3	
α'	CH ₂	5.37 (<i>d</i> , 13.9) 4.53 (<i>d</i> , 13.9)	5.40 (<i>d</i>) 4.54 (<i>d</i>)	45.4	1', 8a', 9', 10'
9'	C			137.9	
10'	CH	6.95 (<i>m</i>)	6.97 (<i>dd</i>)	129.5	α' , 12', 14'
11'	CH	6.75 (<i>d</i> , 8.2, 2.4)	6.75 (<i>dd</i>)	122.7	9', 13'
12'	C			152.9	
13'	CH	6.42 (<i>dd</i> , 8.2, 2.4)	6.42 (<i>dd</i>)	122.1	9', 11'
14'	CH	7.08 (<i>dd</i> , 8.2, 2.4)	7.10 (<i>dd</i>)	130.8	α' , 10', 12'

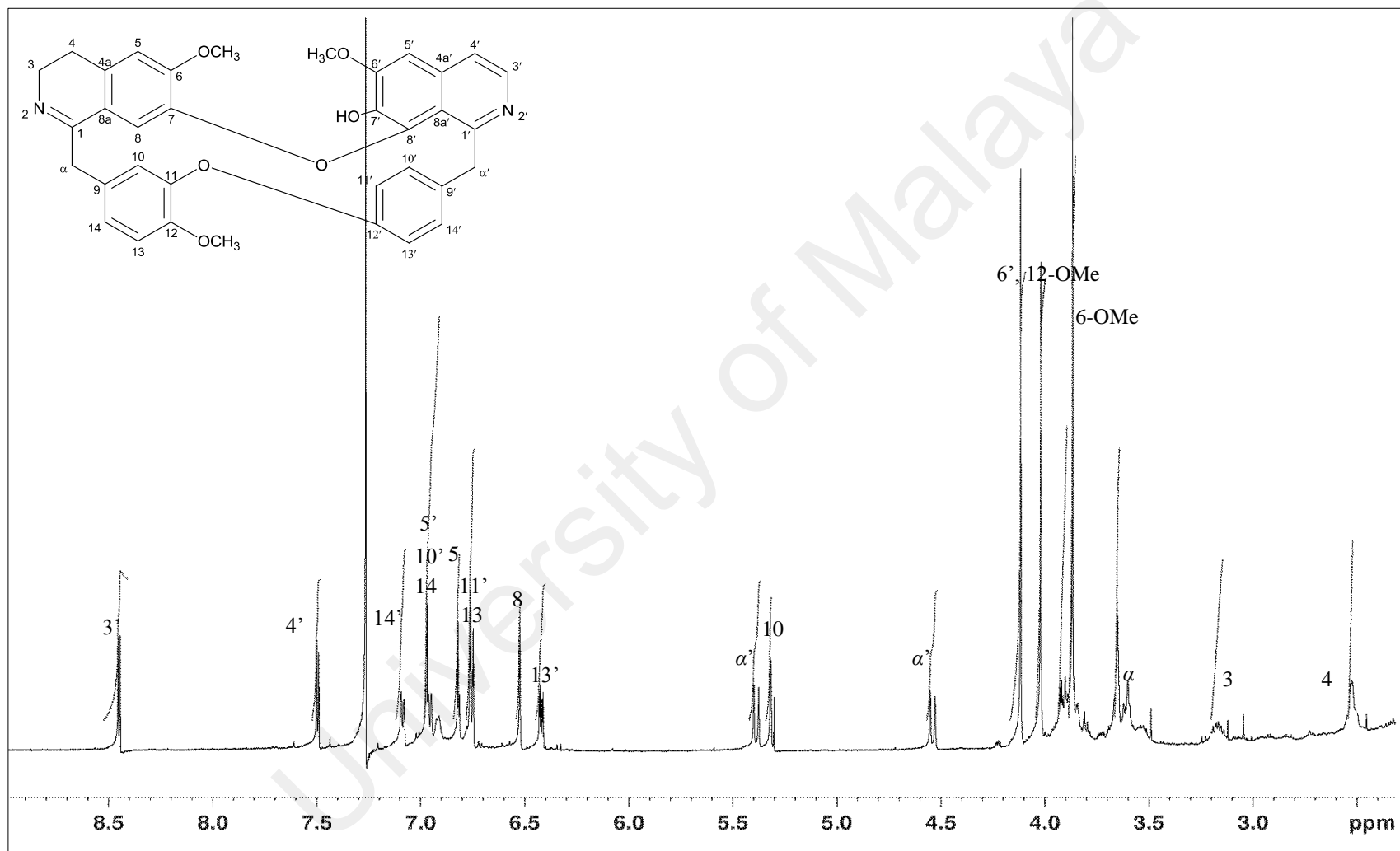


Figure 3.33: ^1H NMR Spectrum of Stephasubimine **121**

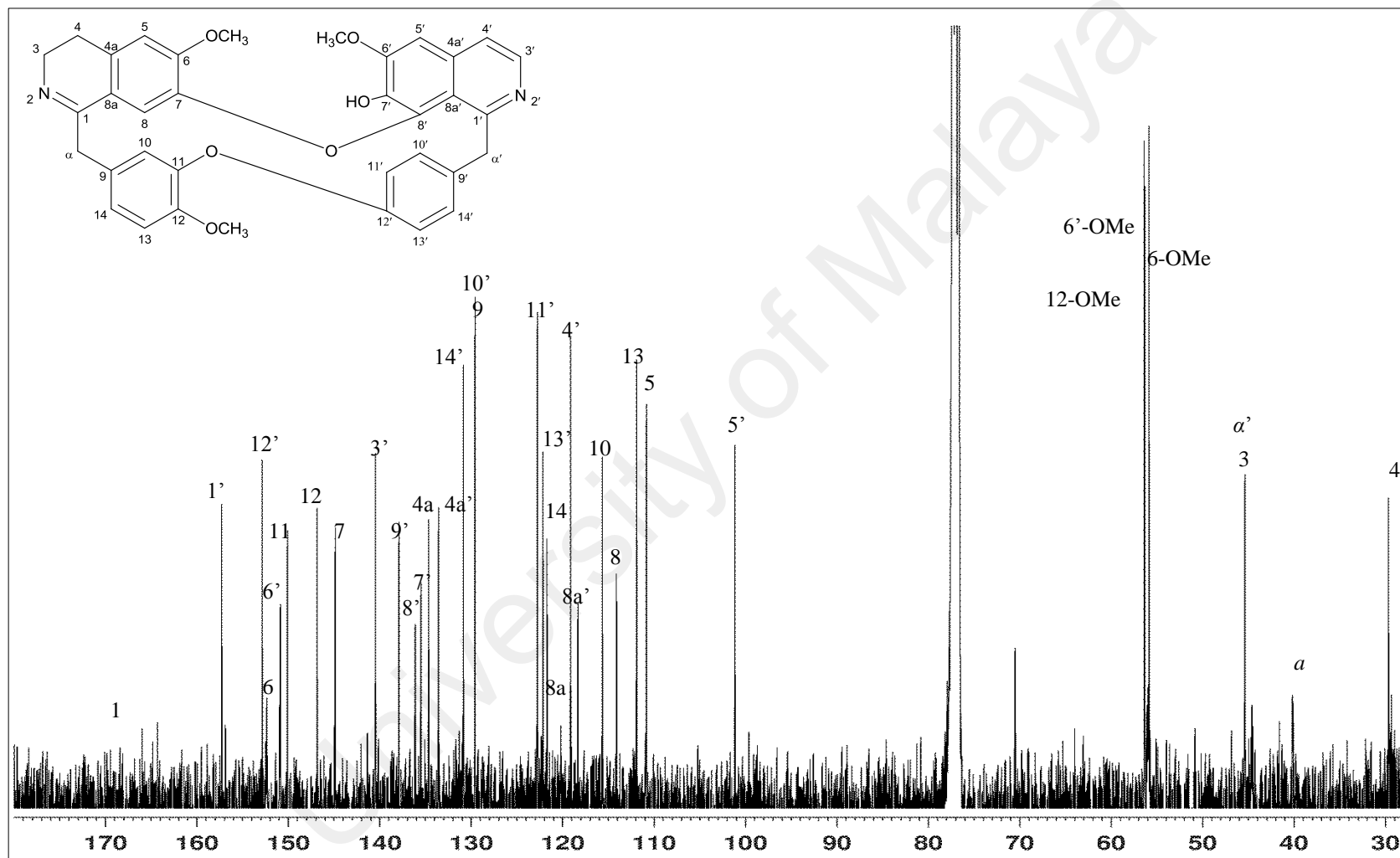
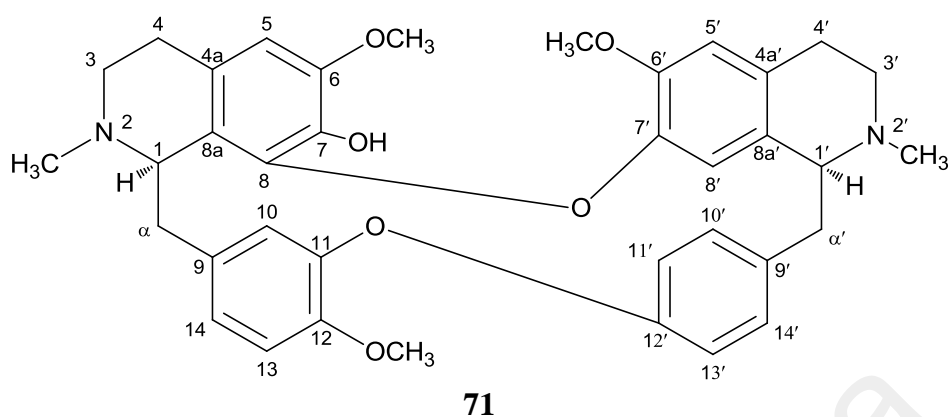


Figure 3.34: ^{13}C NMR Spectrum of Stephasubimine 121

3.1.10 Thalrugosine 71



Thalrugosine **71** was purified as a yellow amorphous powder with $[\alpha]_D^{25} +118.0^\circ$ ($c = 1.1$, MeOH). The UV spectrum revealed absorptions maxima at λ_{\max} 244 and 286 nm, while its IR spectrum implied the presence of hydroxyl, aromatic rings and phenyl ether groups at ν_{\max} 3349 cm^{-1} , 1515, 1635 cm^{-1} and 1230, 1260 cm^{-1} respectively. The ESIMS spectrum exhibited a pseudo-molecular ion peak $[M+H]^+$ at m/z 609.2930 suggesting a molecular formula of $\text{C}_{37}\text{H}_{40}\text{N}_2\text{O}_6$ (calcd. for $\text{C}_{37}\text{H}_{41}\text{N}_2\text{O}_6$, 609.2965).

The $^1\text{H-NMR}$ spectrum (Figure 3.36) showed the presence of ten aromatic signals, three O-CH₃ signals, two N-CH₃, two CH₂-CH₂-N groups, two shielded methine protons, and two sets of isolated none equivalent methylene groups. The signals at H-10 (δ_{H} 6.15, *brs*), H-13 (δ_{H} 6.75, *d*, 8.1 Hz) and H-14 (δ_{H} 6.75, *d*, 8.1 Hz) were assigned to the protons of the 1, 3, 4-trisubstituted in ring C. Ring C' on the other hand was a para-disubstituted aromatic ring (AA'BB' spin system) with its signal resonating as four set of *dd*; H-10' (δ_{H} 6.37, $J = 8.3$ Hz, 2.0 Hz), H-11' (δ_{H} 6.67, $J = 8.3$ Hz, 2.5 Hz), H-13' (δ_{H} 6.98, $J = 8.3$ Hz, 2.5 Hz) and H-14' (δ_{H} 7.30, $J = 8.3$ Hz, 2.0 Hz). The remaining signals at δ_{H} 6.28, 6.67 and 6.04 were attributed to the signals of H-5, H-5', and H-8' respectively. The three methoxyl groups appeared as singlets at δ_{H} 3.73 (6-OCH₃), 3.79 (6'-OCH₃), and 3.86 (12-OCH₃) in the $^1\text{H-NMR}$ spectrum.

Analysis of the ^1H NMR spectrum indicated the signature of type VIII bisbenzylisoquinoline with a *syn*-configuration. The signature peak was ascribed to the two *N*-CH₃ signals that appeared at distinctly different positions at δ_{H} 2.33 (*2N*-CH₃) and δ_{H} 2.58 (*2N'*-CH₃), varying by 0.25 ppm. For type VI BBIQs such as **118**, the difference in the chemical shift between the above mentioned two peaks was only 0.02 ppm. Typically, the presence of a broad singlet at δ_{H} 6.15 (H-10), a shielded singlet at δ_{H} 6.04 (H-8') and the presence of a shielded *dd* at δ_{H} 6.37 (H-10') in the ^1H NMR spectrum indicated a type VIII BBIQ. The H-1' methine proton that appeared as multiplet at δ_{H} 3.89 was obscured due to the 12-OCH₃ signal.

The ^{13}C NMR (Figure 3.37) and HSQC (Figure 3.39) spectra of thalrugosine **71** revealed a total of thirty-seven carbons. The presence of a shielded carbon at δ_{C} 121.6 belonging to C-8' is the signature of a type VIII BBIQ, in comparison to a type VI BBIQ, whereby its C-8' resonates at δ_{C} 149.0 as for **118**. The COSY spectrum showed the correlation the following vicinal protons: H-13'/H-14', H-10'/H-11', H-3/H-4 and H-3'/H-4'.

The diaryl ether bridges in a type VIII BBIQ was between C-8-O-C-7' and C-11-O-C-12'. This was deduced from the following 3J (H, C) correlations; H-5 to C-8, H-5' to C7' and H-13 to C-11 and H-10', H-14' to C-12' as inferred from the HMBC spectrum (Figure 3.40).

The positive optical rotation value suggested **71** of having either the (1*R*, 1'*S*) or (1*R*, 1'*R*) configuration. The nature of the type VIII BBIQ with shielded H-8' and H-10' at δ_{H} 6.04 and δ_{H} 6.37 respectively, proposed that it belonged to the '*syn*' configuration (1*R*, 1'*S*). Extensive analysis of all spectroscopic data (Table 3.11) and comparison with its enantiomer (-)-limacine **123**, eventually led to the identification of the alkaloid as type VIII BBIQ, (1*R*,1'*S*) (+)-thalrugosine **71** (Lin et al., 1993) (+)-Thalrugosine was

previously isolated from *Stephania cephalantha* Hayata and was reported to be active against herpes simplex virus (HSV) (Nawawi et al., 1999).

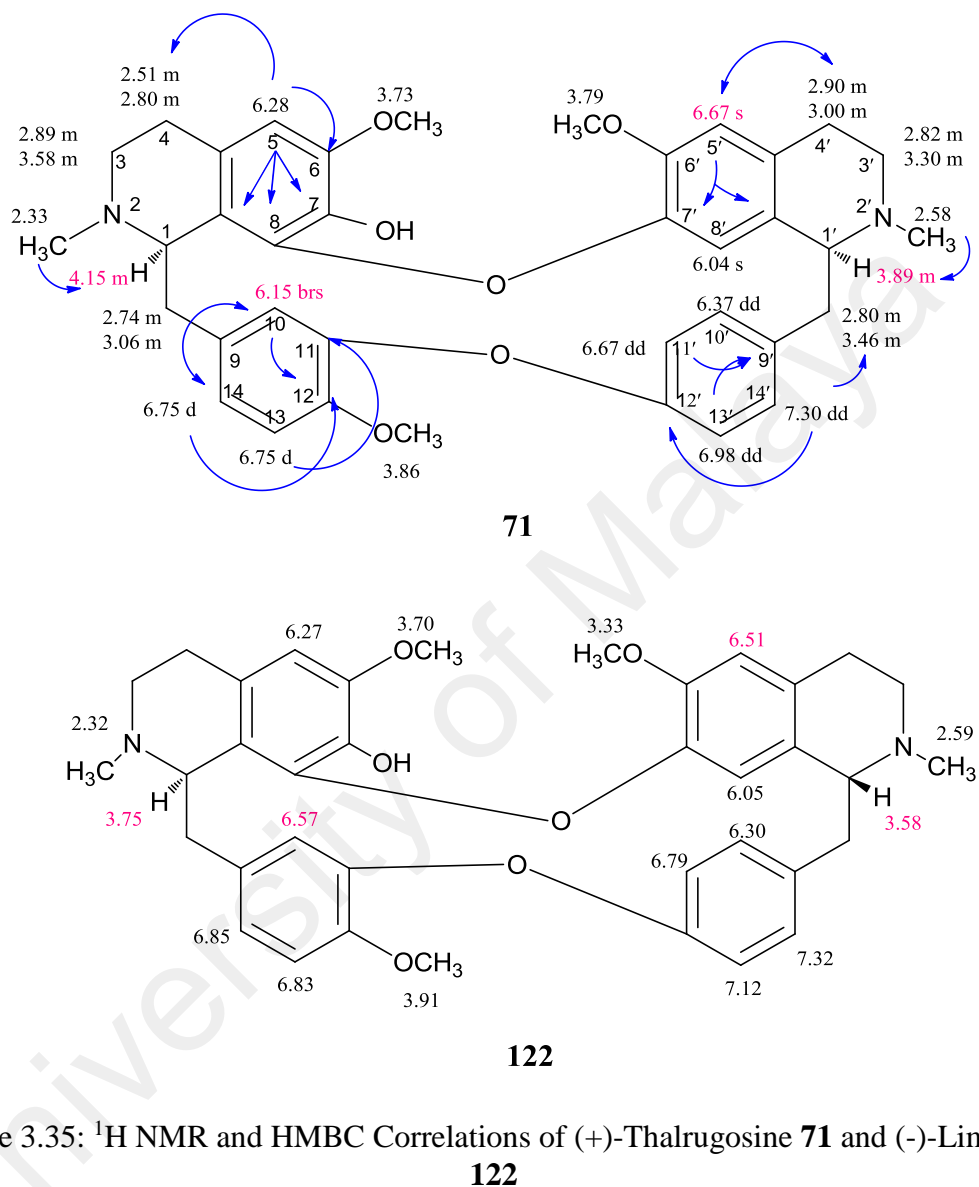


Table 3.11: ¹H and ¹³C-NMR Data of Thalrugosine **71**.

Position	Unit	¹ H- NMR CDCl ₃ , 400 MHz Thalrugosine 71 δ (<i>J</i> , Hz)	¹ H- NMR CDCl ₃ 500 MHz (Lin et al., 1993) δ	¹ H- NMR Limacine 122 (Lin et al., 1993)	¹³ C- NMR CDCl ₃ , 100 MHz 71 δ	¹³ C- NMR CDCl ₃ , 100 MHz (Lin et al., 1993) δ
1	CH	4.15 (<i>m</i>)	3.98	3.75	60.8	60.1
2	<i>N</i> -CH ₃	2.33 (<i>s</i>)	2.28	2.32	42.1	42.1
3	CH ₂	<i>α</i> 3.58 (<i>m</i>) <i>β</i> 2.89 (<i>m</i>)	3.21 2.74	3.49 2.85	46.2	43.7
4	CH ₂	<i>α</i> 2.80 (<i>m</i>) <i>β</i> 2.51 (<i>m</i>)	2.79 2.32	2.90 2.39	23.6	22.3
4a	C				122.7	122.1
5	CH	6.28 (<i>brs</i>)	6.32	6.27	106.7	107.4
6	C				146.9	146.8
6-OMe	O-CH ₃	3.73 (<i>s</i>)	3.72	3.70	56.1	55.8
7	C				135.7	136.3
8	C				143.5	144.2
8a	C				126.3	124.2
<i>α</i>	CH ₂	<i>α</i> 3.06 (<i>m</i>) <i>β</i> 2.74 (<i>m</i>)	2.90 2.61	2.69 2.57	38.7	39.0
9	C				132.0	133.1
10	CH	6.15 (<i>brs</i>)	6.26	6.57	114.7	114.7
11	C				150.3	150.1
12	C				147.7	146.5
12-OMe	O-CH ₃	3.86 (<i>s</i>)	3.88	3.91	56.1	56.1
13	CH	6.75 (<i>d</i> , 8.1)	6.76	6.83	112.0	111.4
14	CH	6.75 (<i>d</i> , 8.1)	6.60	6.85	122.5	121.8
1'	CH	3.89 (<i>m</i>)	3.58	3.58	64.7	64.9
2'	<i>N'</i> -CH ₃	2.58 (<i>s</i>)	2.45	2.59	42.6	42.9
3'	CH ₂	<i>α</i> 3.30 (<i>m</i>) <i>β</i> 2.82 (<i>m</i>)	3.31 2.74	3.49 2.83	45.5	45.8
4'	CH ₂	<i>α</i> 3.00 (<i>m</i>) <i>β</i> 2.90 (<i>m</i>)	2.90 2.88	2.94 2.72	24.5	25.4
4a'	C				129.3	130.6
5'	CH	6.67 (<i>s</i>)	6.70	6.51	112.0	112.8
6'	C				150.1	148.9
6'-OMe	O-CH ₃	3.79 (<i>s</i>)	3.86	3.33	56.2	55.9
7'	C				143.6	143.2
8'	CH	6.04 (<i>s</i>)	6.04	6.05	121.6	121.2
8a'	C				129.7	130.7
<i>α</i> '	CH ₂	<i>α</i> 3.46 (<i>dd</i> , 13.0, 4.6) <i>β</i> 2.80 (<i>m</i>)	3.18 2.76	3.22 2.75	38.4	37.9
9'	C				133.9	135.2
10'	CH	6.37 (<i>dd</i> , 8.3, 2.0)	6.41	6.30	132.0	131.9
11'	CH	6.67 (<i>dd</i> , 8.3, 2.5)	6.80	6.79	122.7	122.8
12'	C				154.8	154.4
13'	CH	6.98 (<i>dd</i> , 8.3, 2.5)	7.02	7.12	122.6	122.5
14'	CH	7.30 (<i>dd</i> , 8.3, 2.0)	7.28	7.32	130.5	129.9

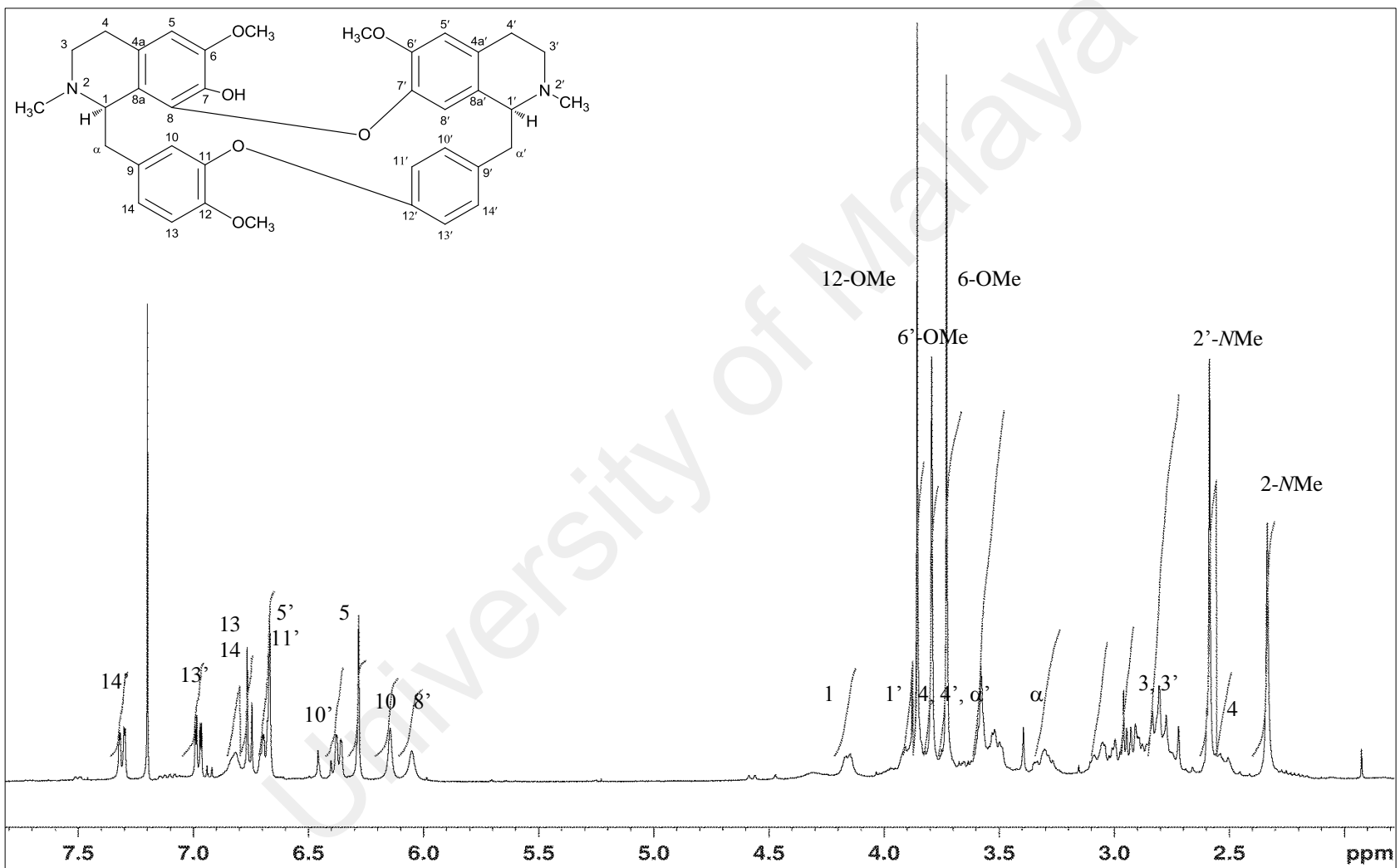


Figure 3.36: ¹H NMR Spectrum of Thalrugosine 71

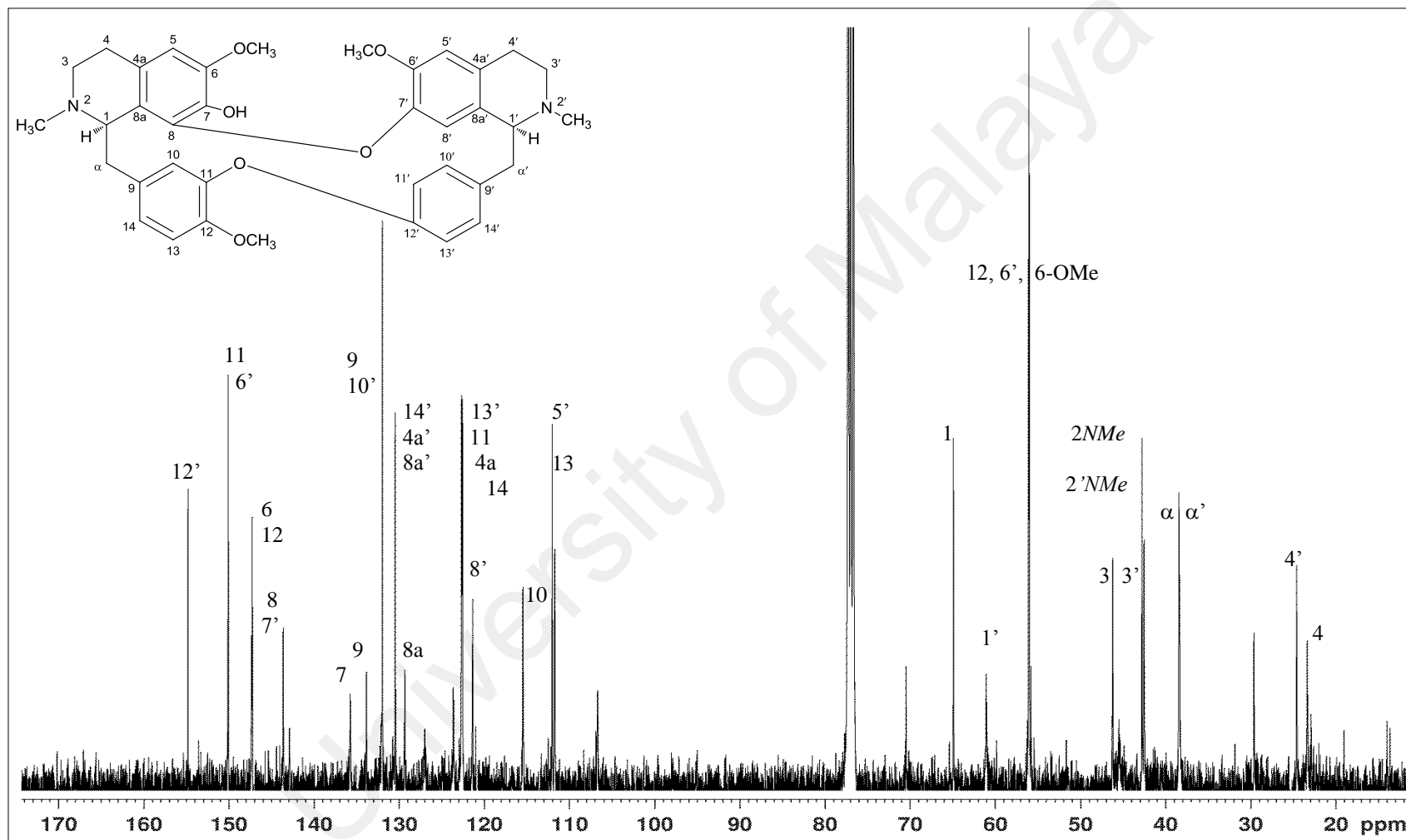


Figure 3.37: ^{13}C NMR Spectrum of Thalrugosine 71

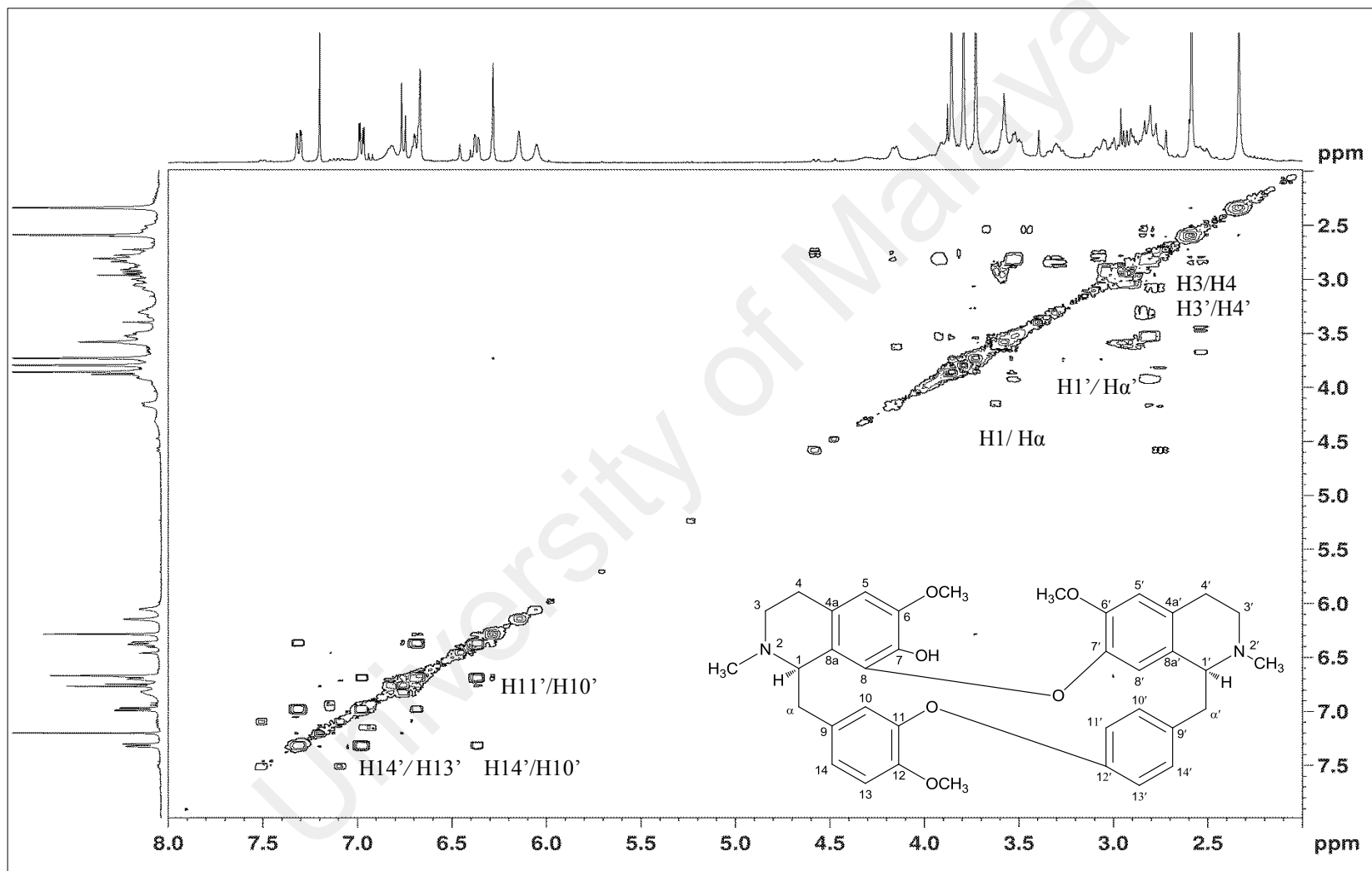


Figure 3.38: COSY Spectrum of Thalrugosine **71**

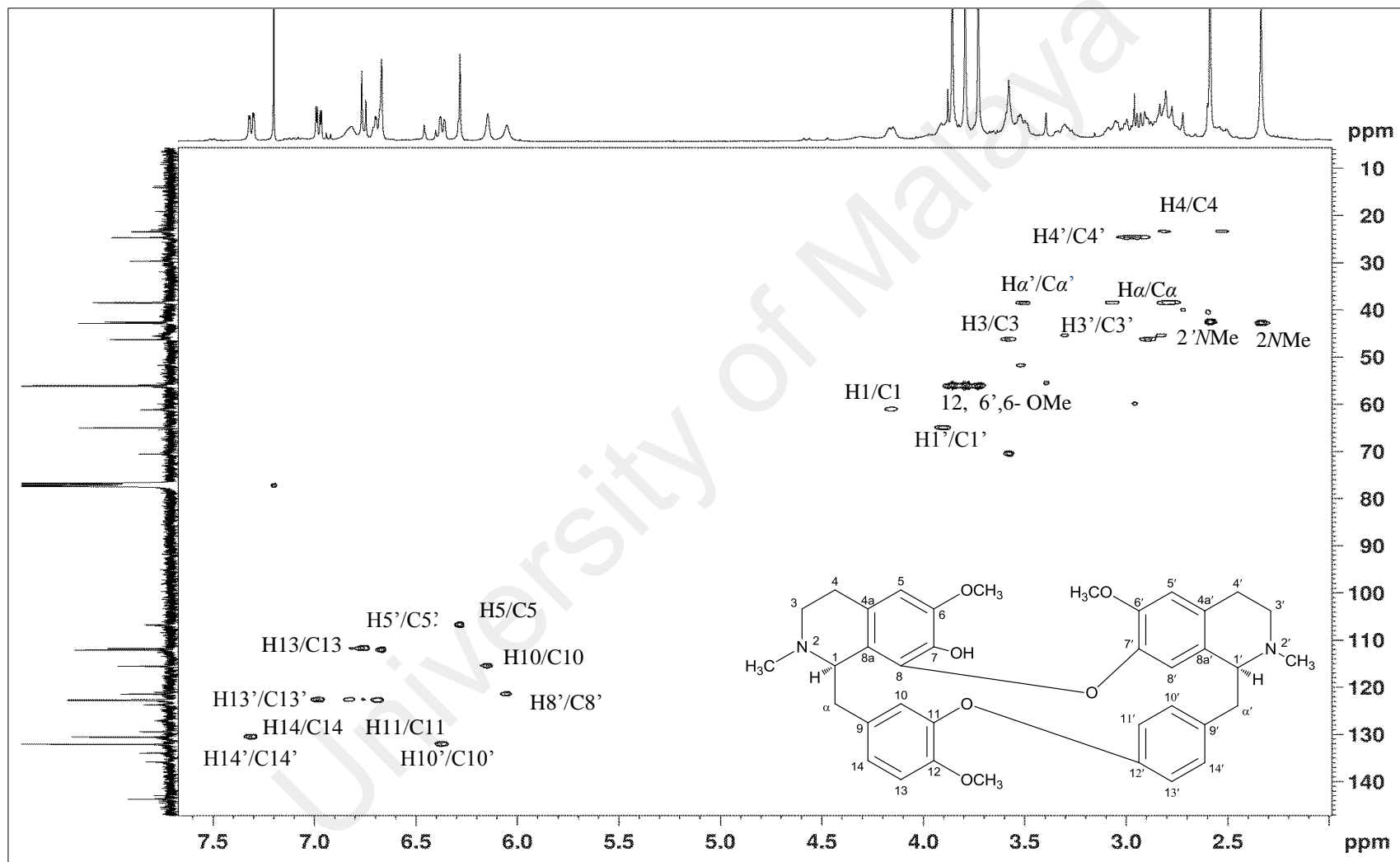


Figure 3.39: HSQC Spectrum of Thalrugosine 71

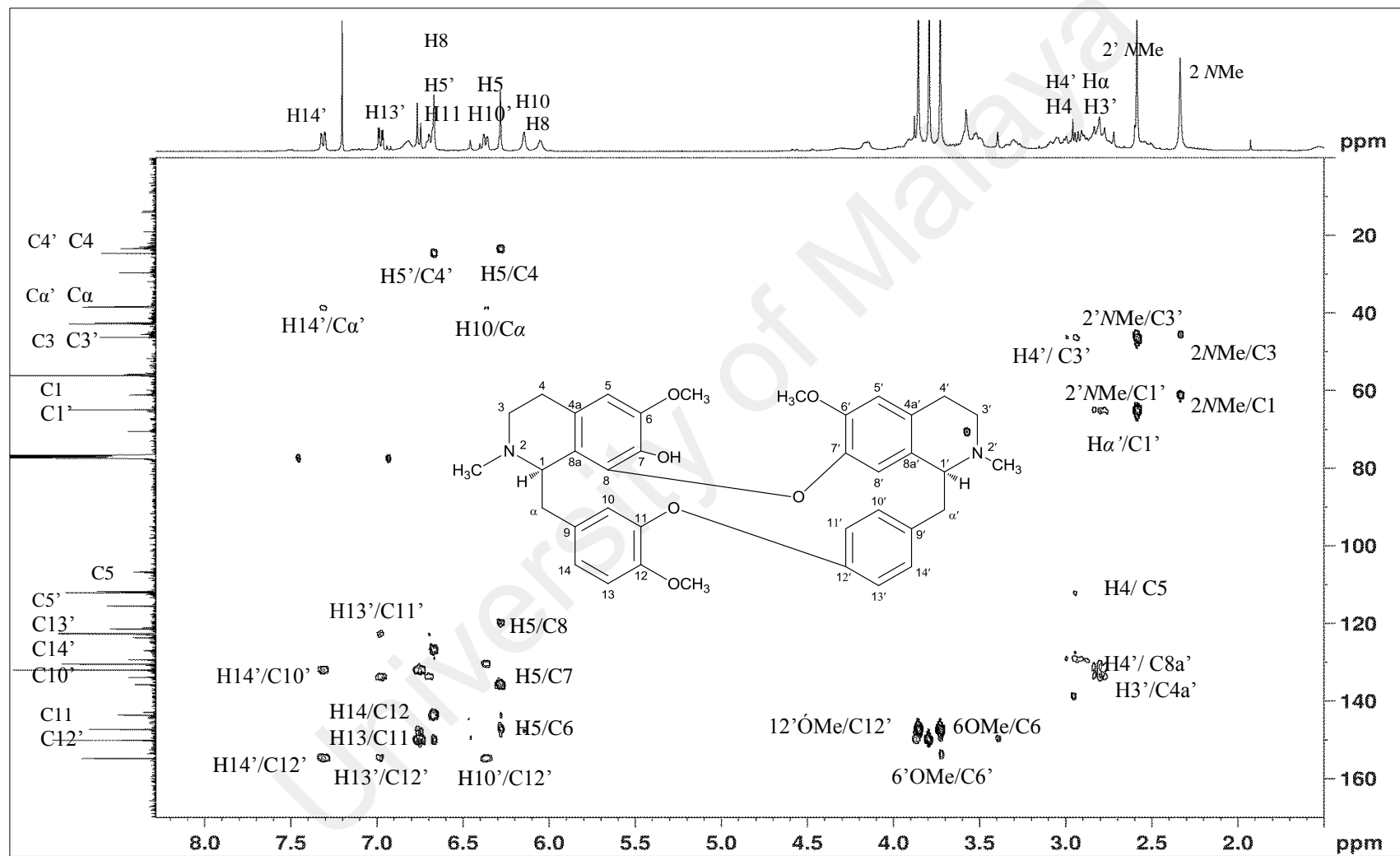
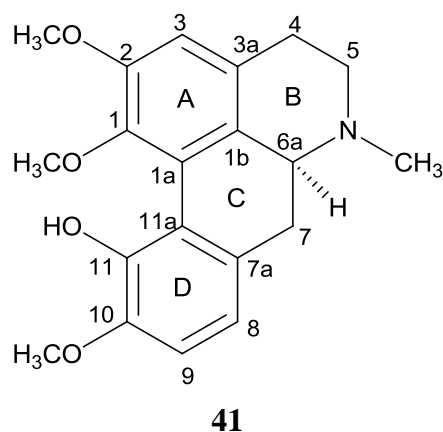


Figure 3.40: HMBC Spectrum of Thalrugosine 71

3.1.11 Isocorydine 41



Isocorydine **41** was isolated as a brownish amorphous solid with $[\alpha]_D^{25} +220^\circ$ ($c=1.30$, CHCl_3). The HREIMS spectrum (Figure 3.42) revealed a pseudo-molecular ion peak $[\text{M}+\text{H}]^+$ at m/z 342.1720, corresponding to the molecular formula of $\text{C}_{20}\text{H}_{24}\text{O}_4\text{N}$ (calcd. for $\text{C}_{20}\text{H}_{25}\text{O}_4\text{N}$, 342.1705). The UV spectrum was characteristic of a 1, 2, 10, 11-tetrasubstituted aporphine type alkaloid, with absorption maxima at λ_{max} 270 and 310 nm (Sangster & Stuart, 1965). In the IR spectrum, an absorption band due to the OH group (3180 cm^{-1}) and aromatic system (1594 and 1552 cm^{-1}) were observed.

The $^1\text{H-NMR}$ spectrum (Figure 3.43) exhibited signals corresponding to three aromatic protons, three O-CH₃ groups, one N-CH₃ group, one methine proton and three methylene groups. H-3 appeared as a singlet at δ_{H} 6.63, while the two vicinal protons H-8 and H-9, appeared as a pair of doublets ($J=8.1$ Hz) at δ_{H} 6.77 and 6.78. The aliphatic protons; H-4, H-5, H-6a and H-7 resonated between δ_{H} 2.39-3.11. The *dd* at δ_{H} 2.80 ($J=13.1, 3.4$ Hz) was assigned to H-6a, while its neighbouring H-7 α and H-7 β resonated as a multiplet and triplet ($J=13.1$ Hz) respectively at δ_{H} 2.93 and δ_{H} 2.39. A singlet was observed at δ_{H} 2.50, indicating the presence of an N-Me group in ring B. The singlets at δ_{H} 3.63, 3.82, 3.84 were respectively assured to the 1-OCH₃, 2-OCH₃ and 10-OCH₃ methoxyl groups. The 1-OCH₃ signal was rather shielded compared to those of 2-OCH₃ and 10-OCH₃, since the protons of the former were forced to place themselves on top of

ring A where the electron density was high (anisotropic effect). The presence of a hydroxyl group at C-11 was evident from the broad OH peak at δ_{H} 8.75.

The ^{13}C -NMR spectrum (Figure 3.44) of isocorydine **41** revealed a total of twenty carbons signals; three sp^2 methine carbons, nine sp^2 quaternary carbons, three sp^3 methylene carbons, one sp^3 methine carbon, three methoxyl groups and one N-CH_3 group. The presence of the methoxyl groups was inferred from the peaks at δ 62.89, 56.16 and 55.89 respectively assigned to 1-O $\underline{\text{C}}\text{H}_3$, 10-O $\underline{\text{C}}\text{H}_3$ and 2-O $\underline{\text{C}}\text{H}_3$.

The H-9/C-7a and H-7/C-11a crosspeaks as inferred from the HMBC spectrum (Figure 3.46) indicated that ring D was fused to ring C at the C-11a-C-7a junction. Additionally, the cross peaks between H-5/C-6a and H-7/C-1b confirmed the attachment of ring C and ring B via the C-6a-C-1b junction. The complete arrangement of ring B and ring A can be observed from the cross peaks between H-3/C-4 and H-3/C-1b. 11-OH signal at δ_{H} 8.75 which coupled to C-10, C-11 and C-11a established the position of the hydroxyl group in ring D.

Considering all these data (Table 3.12), together with the literature values as well as the positive optical rotation value, the chiral carbon 6a with an *S*-configuration confirmed the identity of (+)-isocorydine **41** (Ferreira et al., 2010).

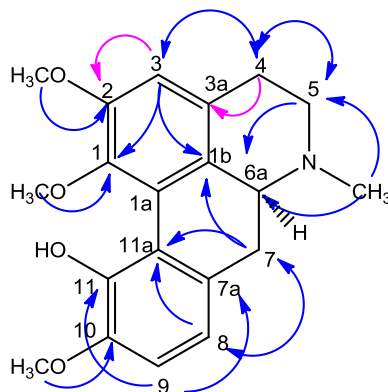


Figure 3.41: ^1H - ^{13}C Correlations Observed in HMBC Spectrum of isocorydine **41**

Table 3.12: ^1H and ^{13}C -NMR Data of Isocorydine **41**

Position	Unit	^1H - NMR CDCl ₃ , 600 MHz Isocorydine 41 δ (<i>J</i> , Hz)	^1H - NMR CDCl ₃ , 500 MHz (Ferreira et al., 2010)	^{13}C - NMR 100 MHz Isocorydine 41 δ	^{13}C - NMR (Ferreira et al., 2010) δ
1	C			142.2	142.2
1-OMe	O-CH ₃	3.63 (<i>s</i>)	3.64	62.1	62.1
1a	C			125.9	125.9
1b	C			129.2	129.3
2	C			151.3	151.3
2-OMe	O-CH ₃	3.82 (<i>s</i>)	3.84	55.9	55.9
3	CH	6.63 (<i>s</i>)	6.63	111.2	111.1
3a	C			129.9	129.9
4	CH ₂	α 3.11 (<i>ddt</i> , 22.2, 11.2, 6.0) β 2.64 (<i>dd</i> , 16.3, 3.4)	3.11 2.64	29.3	29.4
5	CH ₂	α 2.96 (<i>m</i>) β 2.43 (<i>ddd</i> , 22.2, 11.2, 3.4)	2.94 2.41	52.8	52.7
6	<i>N</i> -CH ₃	2.46 (<i>s</i>)		43.9	43.9
6a	CH	2.80 (<i>dd</i> , 13.1, 3.4)	2.80	62.9	62.9
7	CH ₂	α 2.93 (<i>m</i>) β 2.39 (<i>t</i> , 13.1)	2.97 2.37	35.6	35.9
7a	C			130.2	130.2
8	CH	6.77 (<i>d</i> , 8.1)	6.76	118.9	118.9
9	CH	6.78 (<i>d</i> , 8.1)	6.79	111.0	110.9
10	C			149.4	149.5
10-OMe	O-CH ₃	3.84 (<i>s</i>)	3.85	56.2	56.2
11	C			144.0	144.0
11a	C			120.2	120.2

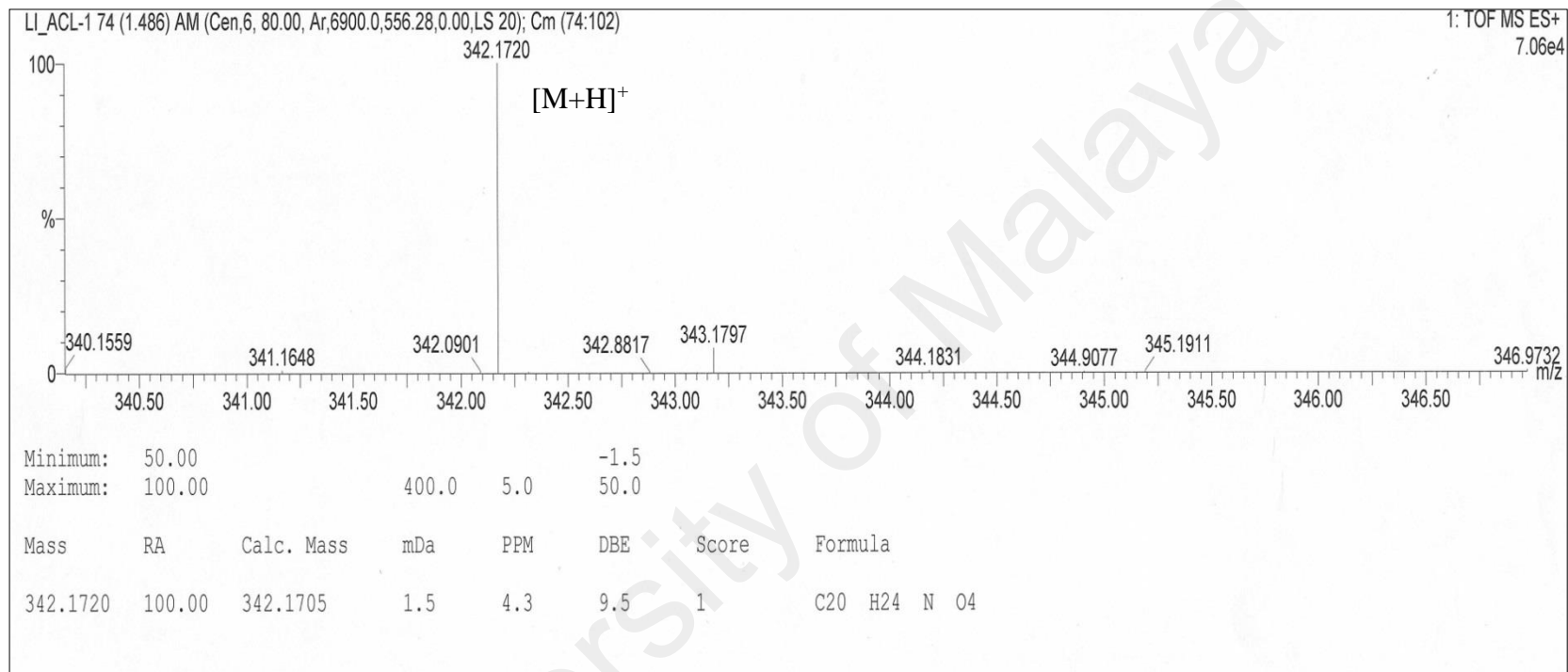


Figure 3.42: HREIMS Spectrum of Isocorydine **41**

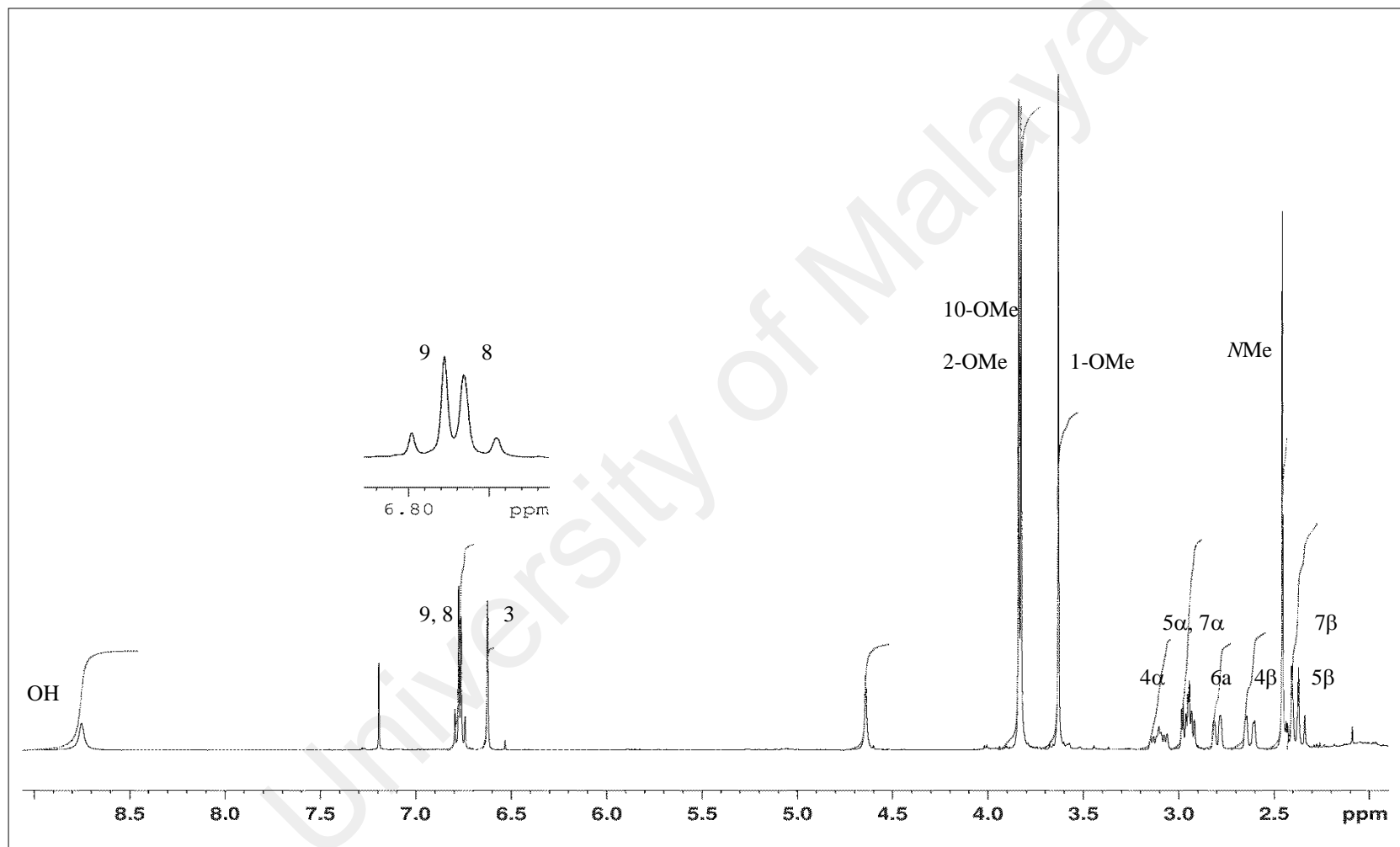


Figure 3.43: ^1H NMR Spectrum of Isocorydine **41**

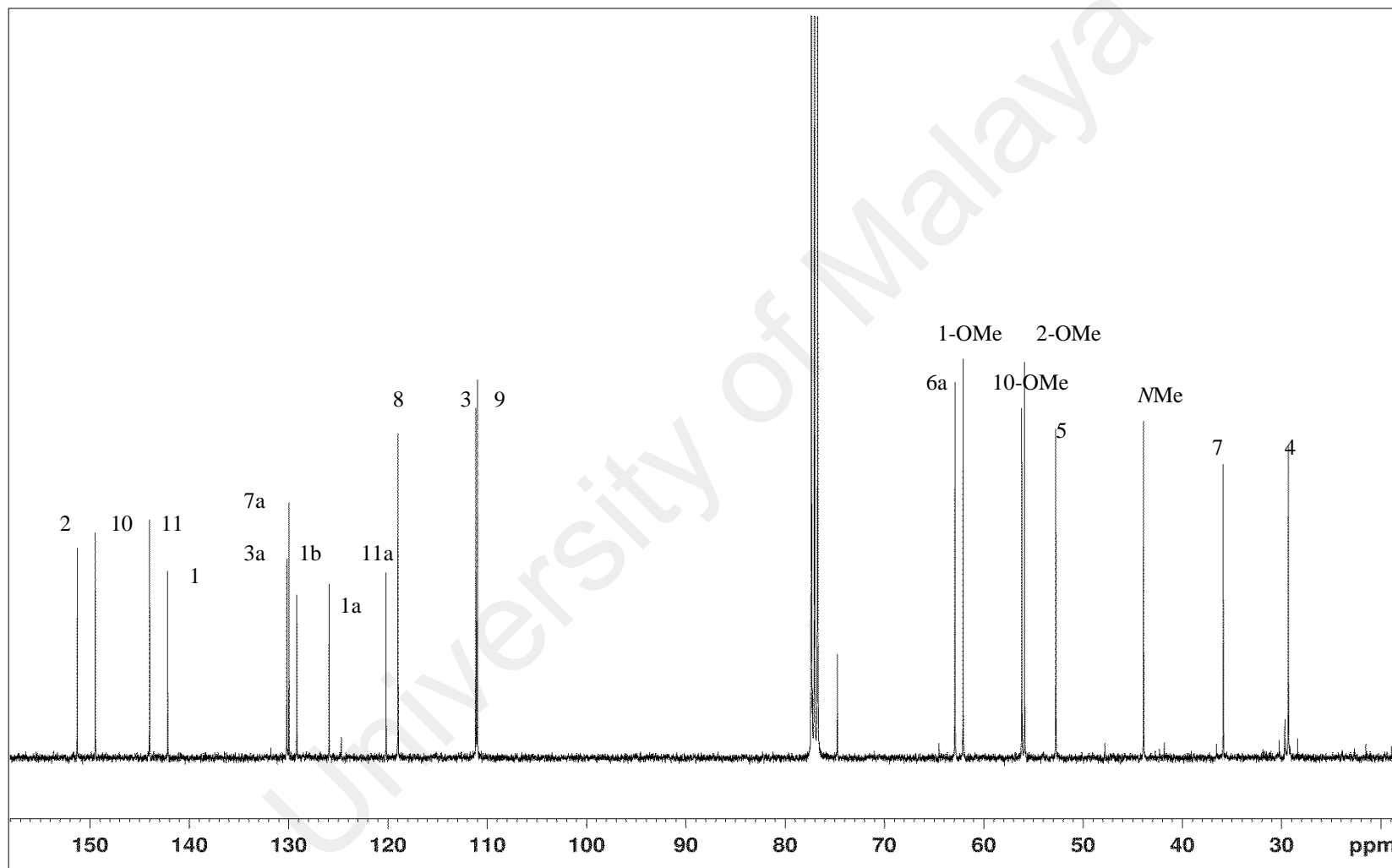


Figure 3.44: ^{13}C NMR Spectrum of Isocorydine **41**

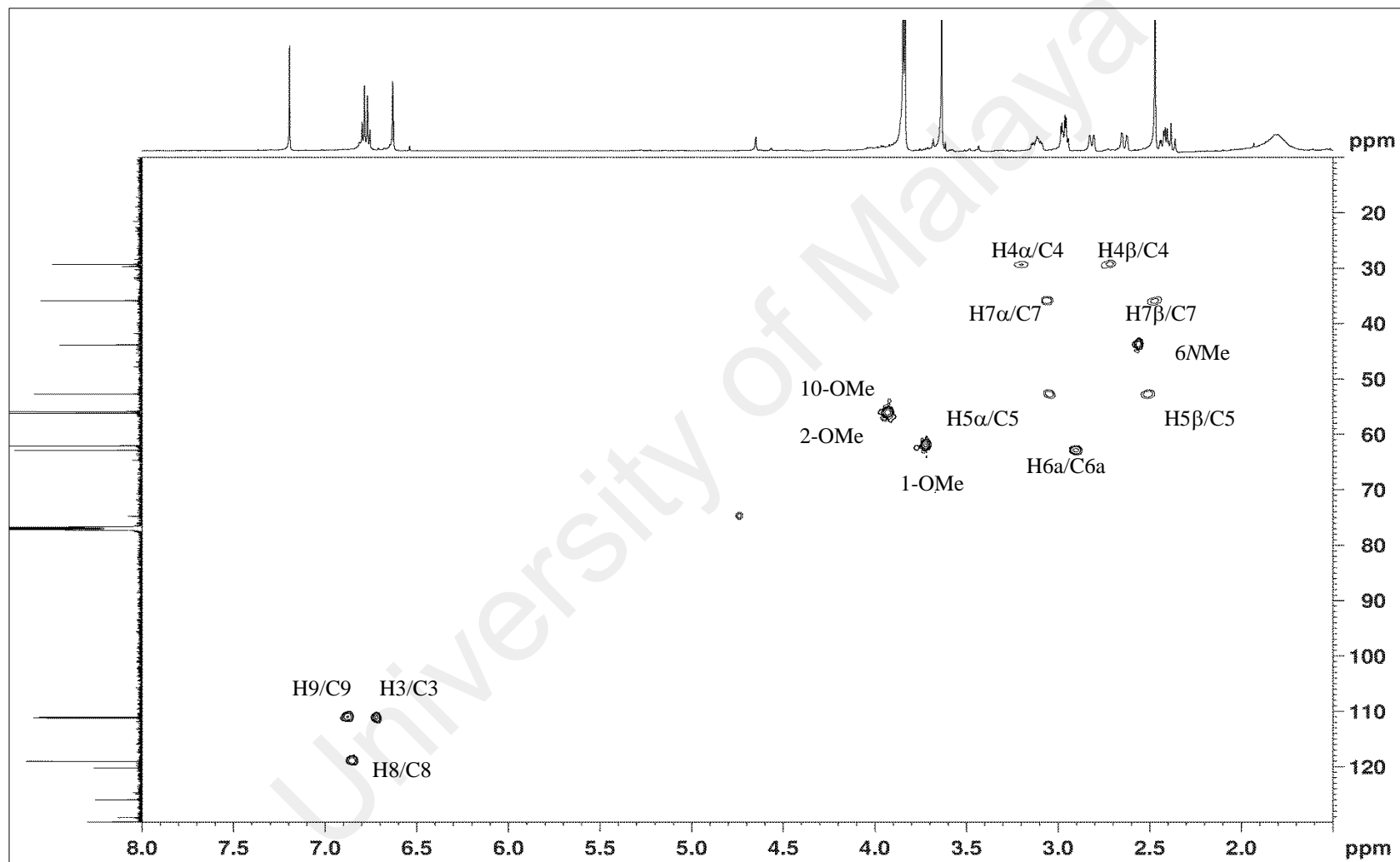


Figure 3.45: HSQC Spectrum of Isocorydine **41**

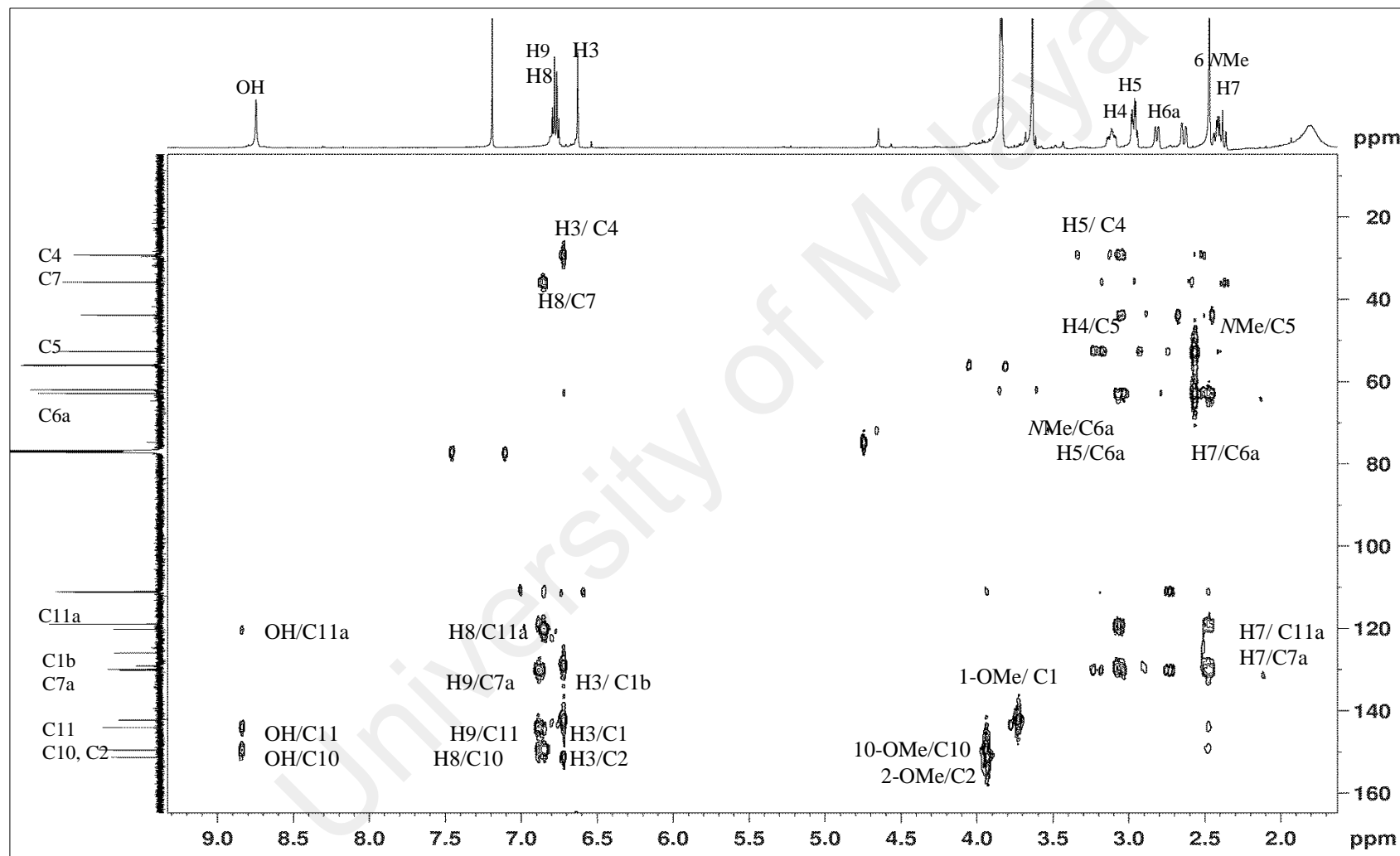
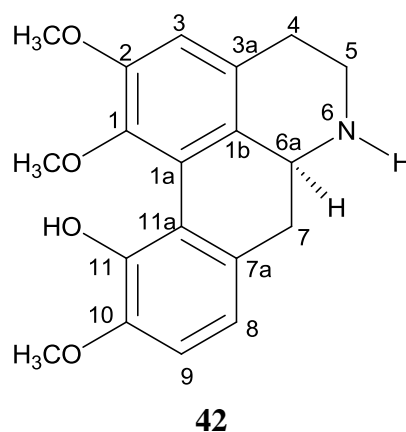


Figure 3.46: HMBC Spectrum of Isocorydine 41

3.1.12 Norisocorydine **42**



Norisocorydine **42** was afforded as a dark brownish amorphous powder with $[\alpha]_D^{25} +178^\circ$ ($c=1.20$, CHCl_3) indicating that it has an *S*-configuration similar to **41**. The HRESIMS spectrum revealed a pseudo-molecular ion peak $[\text{M}+\text{H}]^+$ at m/z 328.1538 (calcd. for $\text{C}_{19}\text{H}_{23}\text{NO}_4$, 328.1549), corresponding to the molecular formula of $\text{C}_{19}\text{H}_{22}\text{NO}_4$. Broad absorption peak at ν_{max} 3314 cm^{-1} indicated of the presence of OH and NH groups in the IR spectrum.

Similar spectroscopic features were observed for the UV, ^1H (Figure 3.48) and ^{13}C NMR (Figure 3.49) spectra of isocorydine **41** and norisocorydine **42**. Nonetheless, a significant differences was the absence of the 6*N*-Me signal at δ_{H} 2.46 and δ_{C} 43.9 which was apparent in **41** but was absent in **42**. H-5 appeared more deshielded (δ_{H} 3.49, 3.03) compared to H-4 (δ_{H} 3.20, 2.82) in the ^1H -NMR spectrum due to the electron withdrawing effect of the more electronegative neighbouring *N*-atom (6-NH). The presence of broad absorption band peak at ν_{max} 3314 cm^{-1} further proved the nitrogen atom belong to the secondary amine (6-NH). The COSY spectrum revealed the exact position of aliphatic proton between $\text{CH}_2\text{-5}/\text{CH}_2\text{-4}$ and $\text{CH}_2\text{-7}/\text{CH-6a}$.

The retention factor of norisocorydine **42** ($R_f = 0.37$) was lower than **20** ($R_f = 0.58$) with the same aporphine skeleton because the nitrogen atom in **42** was demethylated

which resulted in the molecule being more polar (Betts, 1990). The assignments of the structure were confirmed by 1D (Table 3.13) and 2D NMR (Appendix A-Figure A21-A23) spectral data and literature review. As a result, the author deduced that alkaloid was indeed (+)-norisocorydine **42** (Ferreira et al., 2010).

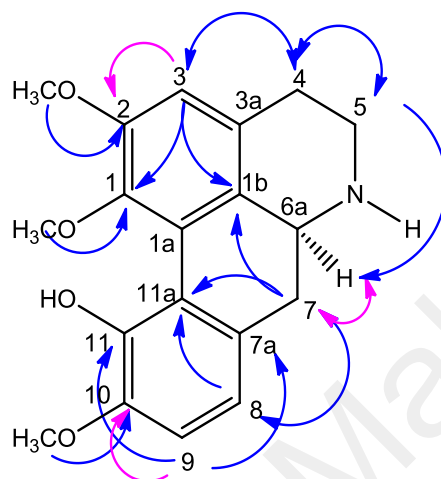


Figure 3.47: ^1H - ^{13}C Correlations Observed in HMBC Spectrum of Norisocorydine **42**

Table 3.13: ^1H and ^{13}C -NMR Data of Norisocorydine **42**

Position	Unit	^1H - NMR CDCl ₃ , 400 MHz Norisocorydine 42 δ (J, Hz)	^1H - NMR CDCl ₃ , 500 MHz (Ferreira et al., 2010)	^{13}C - NMR 100 MHz 42 δ	^{13}C - NMR (Ferreira et al., 2010) δ
1	C			142.4	142.8
1-OMe	O-CH ₃	3.74 (s)	3.66	62.2	61.9
1a	C			125.9	126.0
1b	C			128.4	128.3
2	C			151.2	152.5
2-OMe	O-CH ₃	3.93 (s)	3.84	55.9	56.0
3	CH	6.74 (s)	6.66	111.7	111.2
3a	C			128.9	129.2
4	CH ₂	α 3.20 (ddt, 20.1, 12.2, 6.2) β 2.82 (dd, 16.4, 4.0)	3.35 2.80	28.3	26.8
5	CH ₂	α 3.49 (dd, 12.2, 6.2) β 3.03 (ddd, 20.1, 12.2, 4.0)	3.59 3.02	42.9	41.6
6a	CH	3.79 (dd, 13.2, 4.0)	3.85	53.9	53.6
7	CH ₂	α 2.94 (dd, 13.2, 4.0) β 2.73 (t, 13.2)	3.07 2.90	37.4	36.0
7a	C			129.5	127.7
8	CH	6.83 (d, 8.1)	6.76	119.9	119.5
9	CH	6.87 (d, 8.1)	6.79	111.2	111.5
10	C			149.6	149.9
10-OMe	O-CH ₃	3.93 (s)	3.84	56.1	56.0
11	C			144.3	144.4
11a	C			120.2	119.7

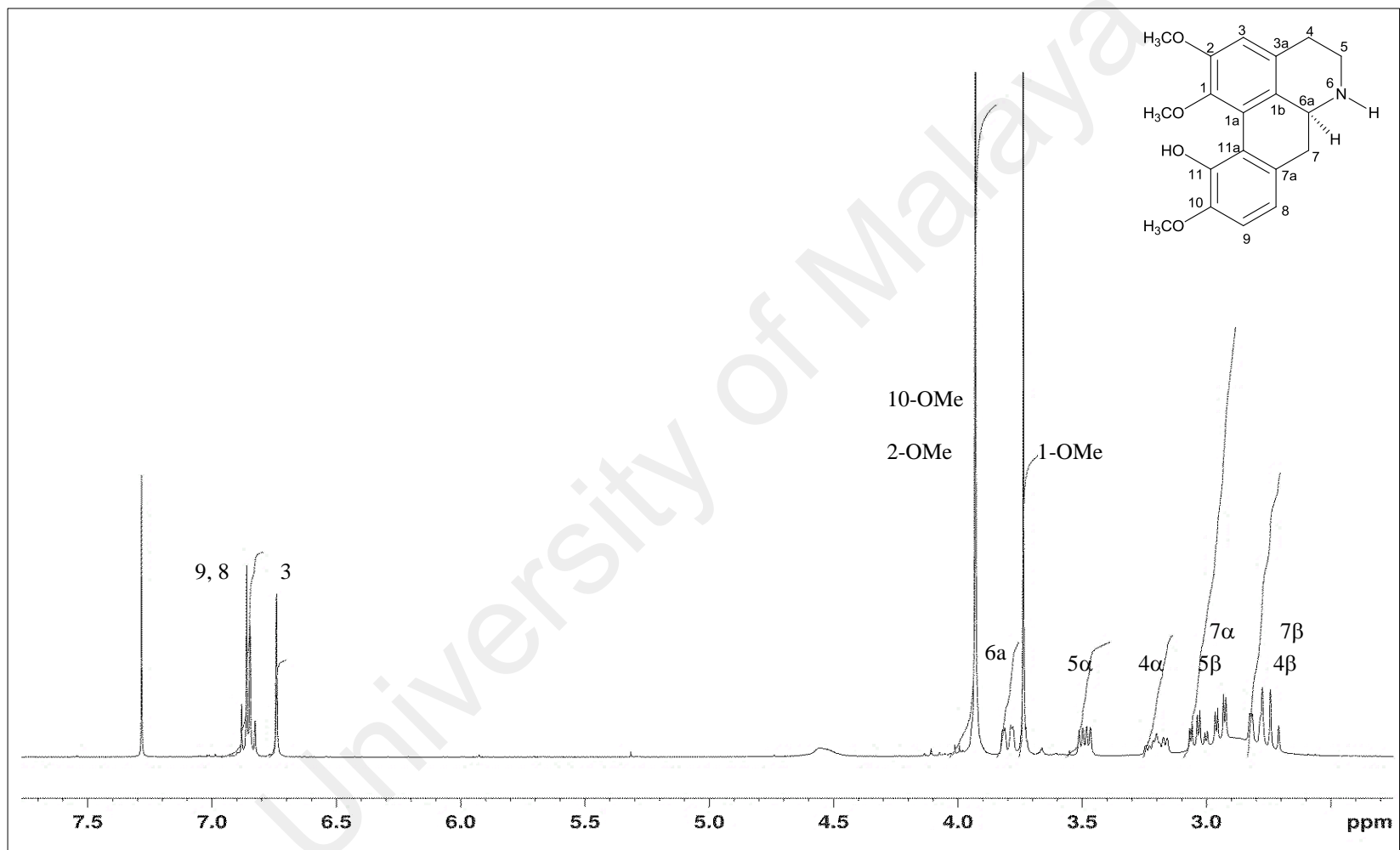


Figure 3.48: ¹H NMR Spectrum of Norisocorydine 42

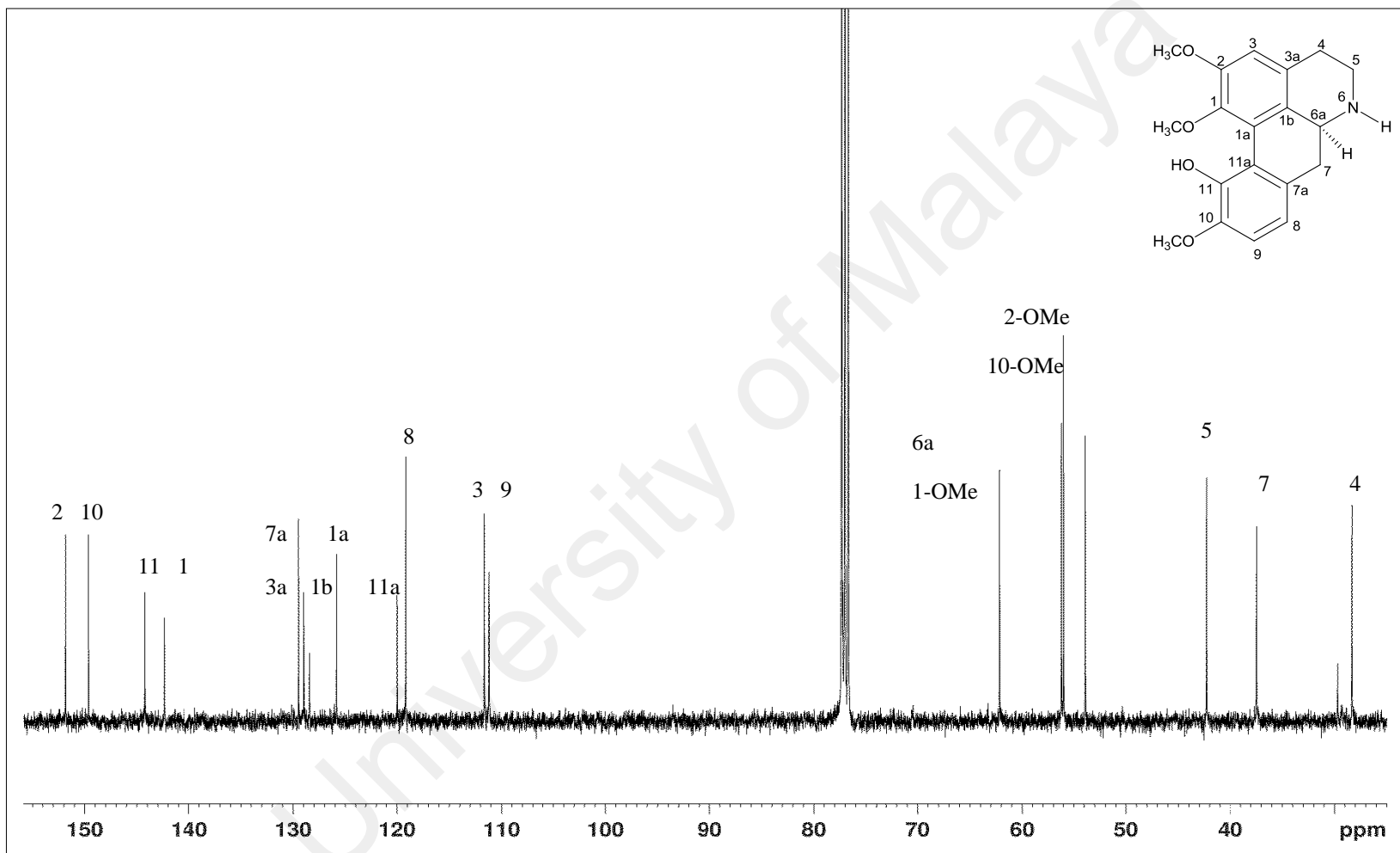
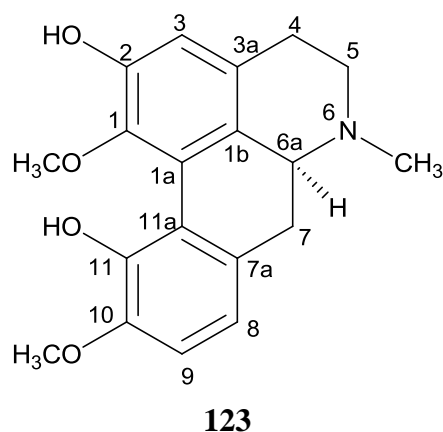


Figure 3.49: ^{13}C NMR Spectrum of Norisocorydine 42

3.1.13 *N*-methyl lindcarpine **123**



N-methyl lindcarpine **123**, $[\alpha]_D^{25} +160.0^\circ$ ($c = 0.50$, CHCl_3) was afforded as a yellowish amorphous solid. The EIMS showed a molecular ion peak $[\text{M}+\text{H}]^+$ at m/z 328.1538, suggesting a molecular formula of $\text{C}_{19}\text{H}_{21}\text{NO}_4$ (calcd. for $\text{C}_{19}\text{H}_{22}\text{NO}_4$, 328.1549).

The UV, IR, ^1H NMR (Figure 3.50) and ^{13}C NMR (Figure 3.51) spectra of *N*-methyl lindcarpine **123** were almost identical to those of isocorydine **41**, with the only difference was the absence of the methoxyl group attached to C-2. Only two singlet signals were observed at δ_{H} 3.58 and δ_{H} 3.85 in the ^1H NMR spectrum, indicating the presence of 1-OCH₃ and 10-OCH₃ respectively. The 1-OCH₃ signal was rather shielded compared to 10-OCH₃, since the protons of the former were forced to place themselves on top of ring A where the electron density was high (anisotropic effect). C-2 in **123** bore a hydroxyl group instead. The stereochemistry of C-6a for **123** was the same as for **41**.

Based on literature survey and experimental data (Table 3.14), it could be proposed that it is a known alkaloid, namely (+)-*N*-methyl lindcarpine **123** (Karimova et al., 1978).

Table 3.14: ^1H and ^{13}C -NMR Data of *N*-methyllindcarpine **123**.

Position	Unit	^1H - NMR CDCl ₃ , 400 MHz <i>N</i> -methyllindcarpine 123 δ (<i>J</i> , Hz)	^1H - NMR (Karimova et al., 1978)	^{13}C - NMR 100 MHz 123 δ
1	C			141.2
1-OMe	O-CH ₃	3.58 (<i>s</i>)	3.58 (<i>s</i>)	62.4
1a	C			124.8
1b	C			129.8
2	C			149.5
3	CH	6.69 (<i>s</i>)	6.55 (<i>s</i>)	114.7
3a	C			130.5
4	CH ₂	2.41 (<i>m</i>) 2.97 (<i>m</i>)	2.60-3.00 (<i>m</i>)	29.7
5	CH ₂	2.99-3.06 (<i>m</i>)	2.60-3.00 (<i>m</i>)	45.5
6	<i>N</i> -CH ₃	2.45 (<i>s</i>)	2.48 (<i>s</i>)	31.1
6a	CH	3.60 (<i>m</i>)		52.3
7	CH ₂	2.36-2.42 (<i>m</i>) 2.60 (<i>m</i>)	2.60-3.00 (<i>m</i>)	38.7
7a	C			130.0
8	CH	6.78 (<i>d</i> , 8.0)	6.78 (<i>s</i>)	119.5
9	CH	6.78 (<i>d</i> , 8.0)	6.78 (<i>s</i>)	111.3
10	C			148.2
10-OMe	O-CH ₃	3.85 (<i>s</i>)	3.85 (<i>s</i>)	56.2
11	C			143.6
11a	C			120.0

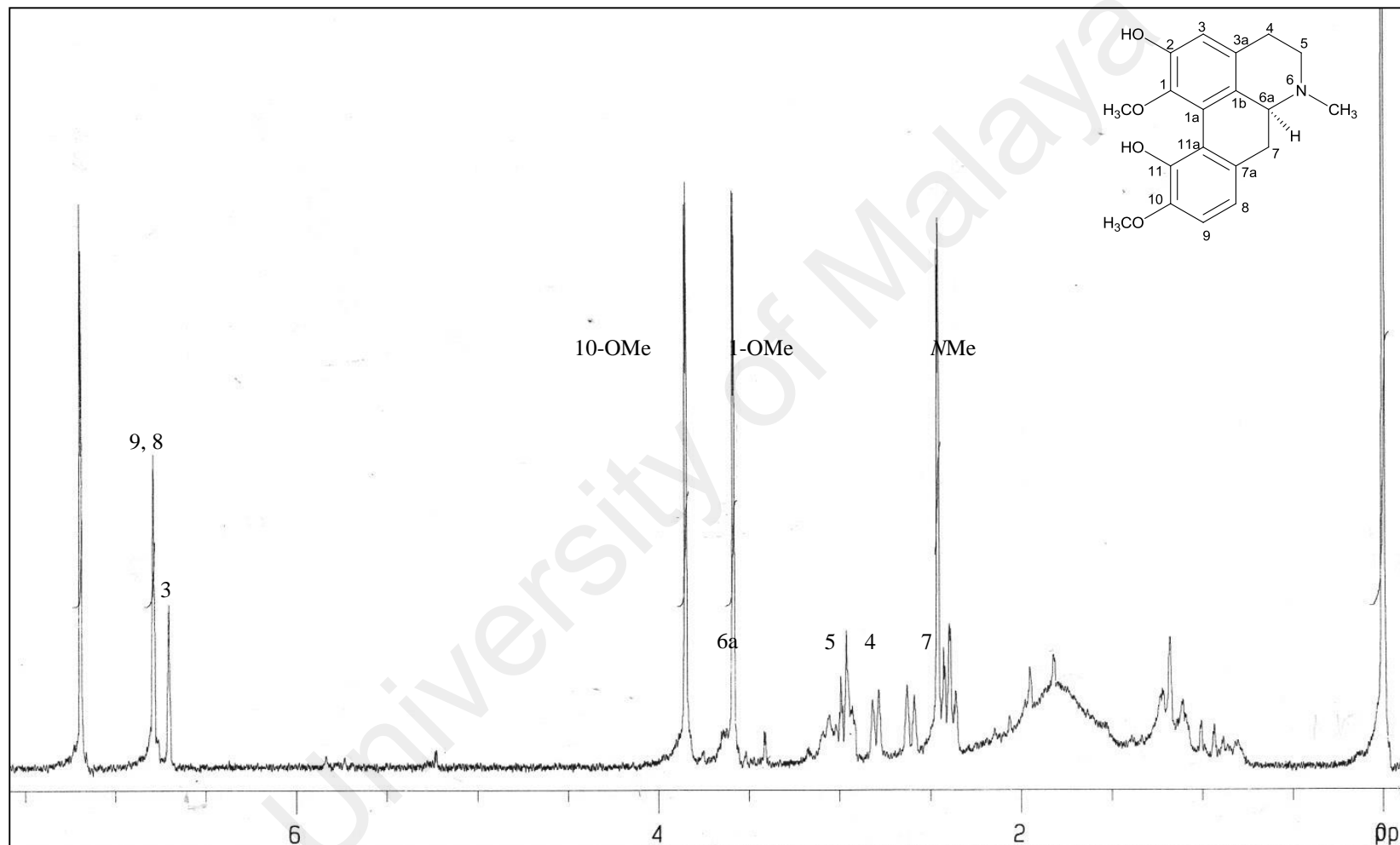


Figure 3.50: ^1H NMR Spectrum of *N*-methylindcarpine **123**

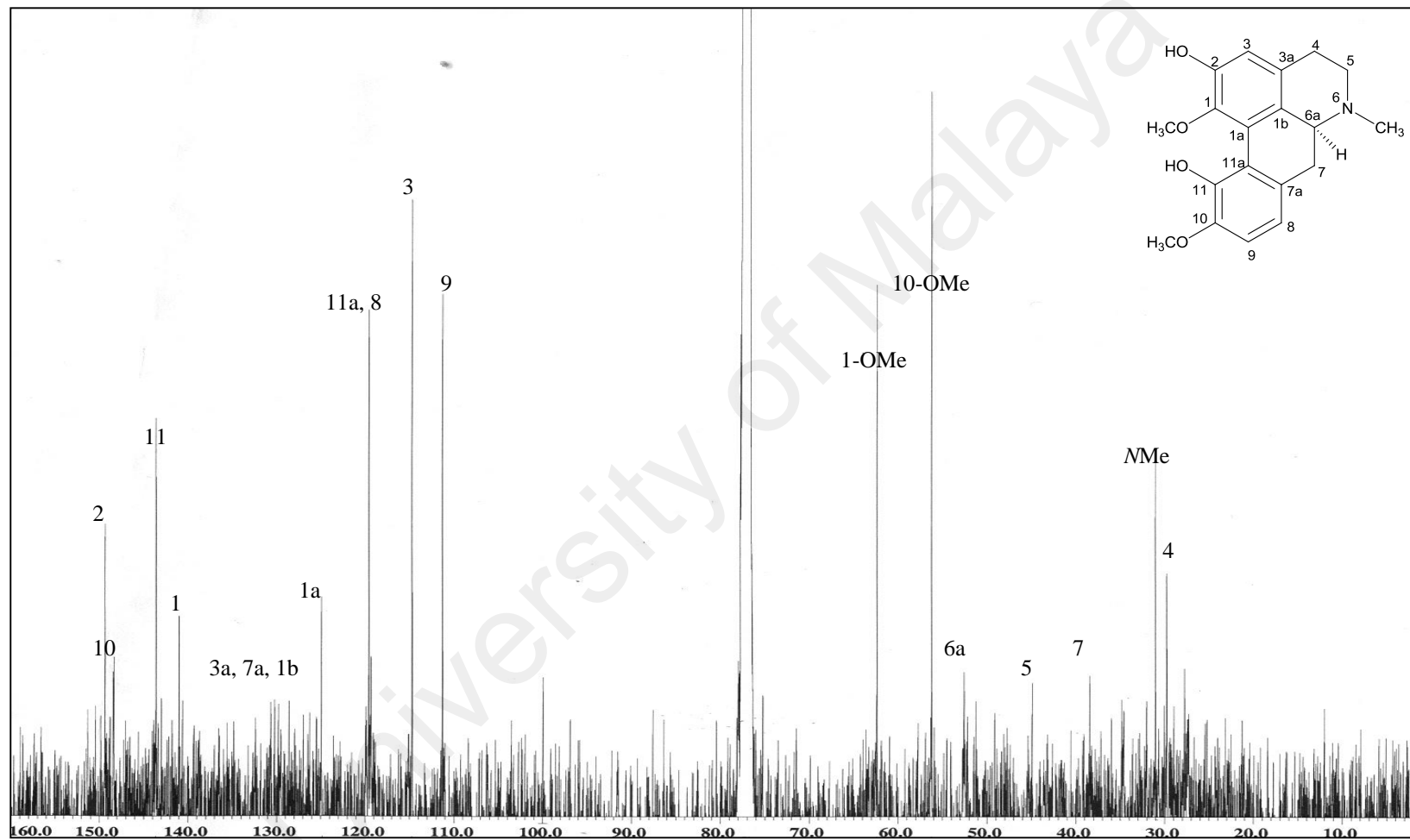
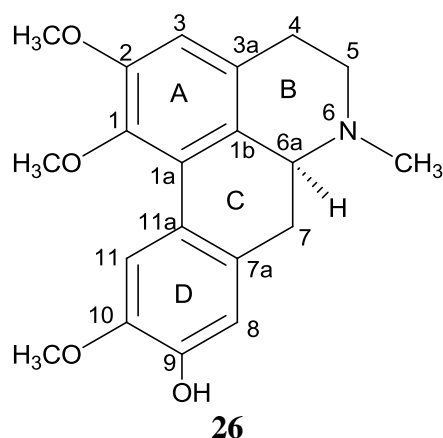


Figure 3.51: ^{13}C NMR Spectrum of *N*-methylindcarpine **123**

3.1.14 *N*-methyllaurotetanine **26**



N-methyllaurotetanine **26** was isolated as a dark brown amorphous powder with $[\alpha]_D^{25} +80.0^\circ$ ($c = 0.50$, CHCl_3). Its HRESIMS spectrum (Figure 3.52) which showed a pseudo-molecular ion peak $[\text{M}+\text{H}]^+$ at m/z 342.1716 (calcd. for $\text{C}_{20}\text{H}_{25}\text{NO}_4$, 342.1705) proposed a molecular formula of $\text{C}_{20}\text{H}_{24}\text{NO}_4$. The IR spectrum revealed absorptions at ν_{max} 3395 and 1603 cm^{-1} due to the OH and aromatic rings stretching vibration. In the UV spectrum, absorption maxima were observed at λ_{max} 215, 285 and 305 nm with equal intensity, thus indicating that this alkaloid belonged to a aporphine which is substituted at positions 1, 2, 9, 10 (Sangster & Stuart, 1965).

Analysis of the $^1\text{H-NMR}$ spectrum (Figure 3.53) suggested that the alkaloid has a different substitution aromatic pattern in its ring D when compared to isocorydine **41**. In the aromatic region, the spectrum displayed three singlets at δ_{H} 6.60 (H-3), δ_{H} 6.82 (H-8) and δ_{H} 8.06 (H-11) which indicated that C-2, C-9 and C-10 were substituted. The 1-OCH_3 signal resonated at δ_{H} 3.66 and was found to be rather shielded compared to 2-OCH_3 (δ_{H} 3.89) and 10-OCH_3 (δ_{H} 3.90). This was due to the fact that the protons of the former were forced to place themselves on top of ring A, where the electron density was high, thus causing the 1-OCH_3 to be sterically hindered (anisotropic effect). The $N\text{-CH}_3$

group resonated as a singlet at δ_{H} 2.72. The COSY spectrum showed cross peaks between CH₂-5/CH₂-4 which indicated that those protons were adjacent to each others.

Based on the ¹³C NMR spectrum (Figure 3.54) and HSQC (Figure 3.55) correlations, a total of 20 carbon signals comprising three sp² methine (C-3, C-8, C-11), nine sp² quaternary carbons (C-1, C-1a, C-1b, C-2, C-3a, C-7a, C-9, C-10, C-11a), three sp³ methylene carbons (C-4, C-5, C-7), one sp³ methine carbon (C-6a), three methoxyl groups (1-OCH₃, 2-OCH₃, 10-OCH₃) and one *N*-CH₃ group. The downfield signal for the quaternary carbons at δ_{C} 144.2, 151.9, 144.8 and 145.3 which were assigned to C-1, C-2, C-9 and C-10 respectively, suggested that they were oxygenated.

The HMBC spectrum (Figure 3.56) showed cross peaks between H-11/C-7a and H-8/C-11a indicating that ring D was fused to ring C at the C-11a-C-7a junction. Furthermore, the connectivity of ring C with ring B was observed via the correlation between H-5/C-6a and H-7/C-1b. Ring A and B are fused through the C-3a-C-1b junction based on the H-3/C-4 and H-3/C-1b correlations.

The positive optical rotation value and comparison with literature values (Table 3.15), certified that the alkaloid was a 1, 2, 9, 10-tetrasubstituted aporphine, (+)-*N*-methyllaurotetanine **26** (Chang et al., 2001; C. Y. Chen et al., 1997; Johns et al., 1967).

Table 3.15: ^1H , ^{13}C -NMR and HMBC Data of *N*Me-laurotetanine **26**.

Position	Unit	^1H - NMR CDCl ₃ , 400 MHz <i>N</i> Me-laurotetanine 26 δ (<i>J</i> , Hz)	^1H - NMR CD ₃ OD, 400 MHz (Chang et al., 2001)	^{13}C - NMR 100 MHz (δ) <i>N</i> Me- laurotetanine 26	HMBC (^1H - ^{13}C)
1	C			144.2	
1-OCH ₃	O-CH ₃	3.66 (<i>s</i>)	3.56	60.2	1
1a	C			127.1	
1b	C			128.9	
2	C			151.9	
2-OCH ₃	O-CH ₃	3.89 (<i>s</i>)	3.88	55.8	2
3	CH	6.60 (<i>s</i>)	6.58	110.3	1, 1b, 2, 4
3a	C			127.2	
4	CH ₂	α 3.38 (<i>m</i>) β 2.85 (<i>m</i>)		29.2	1b, <i>N</i> CH ₃ , 5
5	CH ₂	α 3.28 (<i>dd</i> , 6.2, 17.3) β 2.85 (<i>m</i>)		53.3	3a, 6a
<i>N</i> -CH ₃	<i>N</i> -CH ₃	2.72 (<i>s</i>)	2.74	44.0	5, 6a
6a	CH	3.38 (<i>m</i>)		62.6	
7	CH ₂	α 3.03 (<i>dd</i> , 13.9, 4.0) β 2.74 (<i>t</i> , 13.9)		34.3	1b, 8, 11a
7a	C			130.2	
8	CH	6.82 (<i>s</i>)	6.75	113.9	7, 10, 11a
9	C			144.8	
10	C			145.3	
10-OCH ₃	O-CH ₃	3.90 (<i>s</i>)	3.85	56.1	10
11	CH	8.06 (<i>s</i>)	7.96	111.2	1a, 7a, 9
11a	C			124.0	

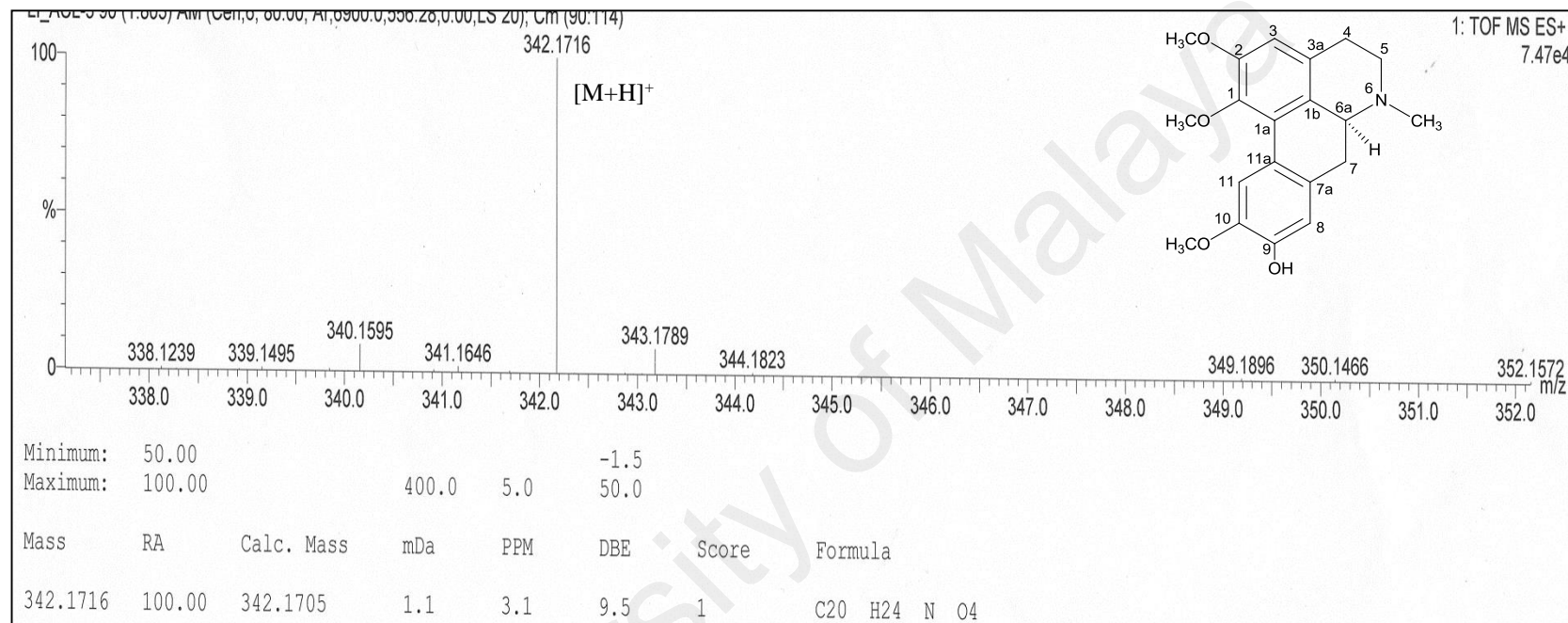


Figure 3.52: HREIMS Spectrum of *N*-methyl-laurotetanine **26**

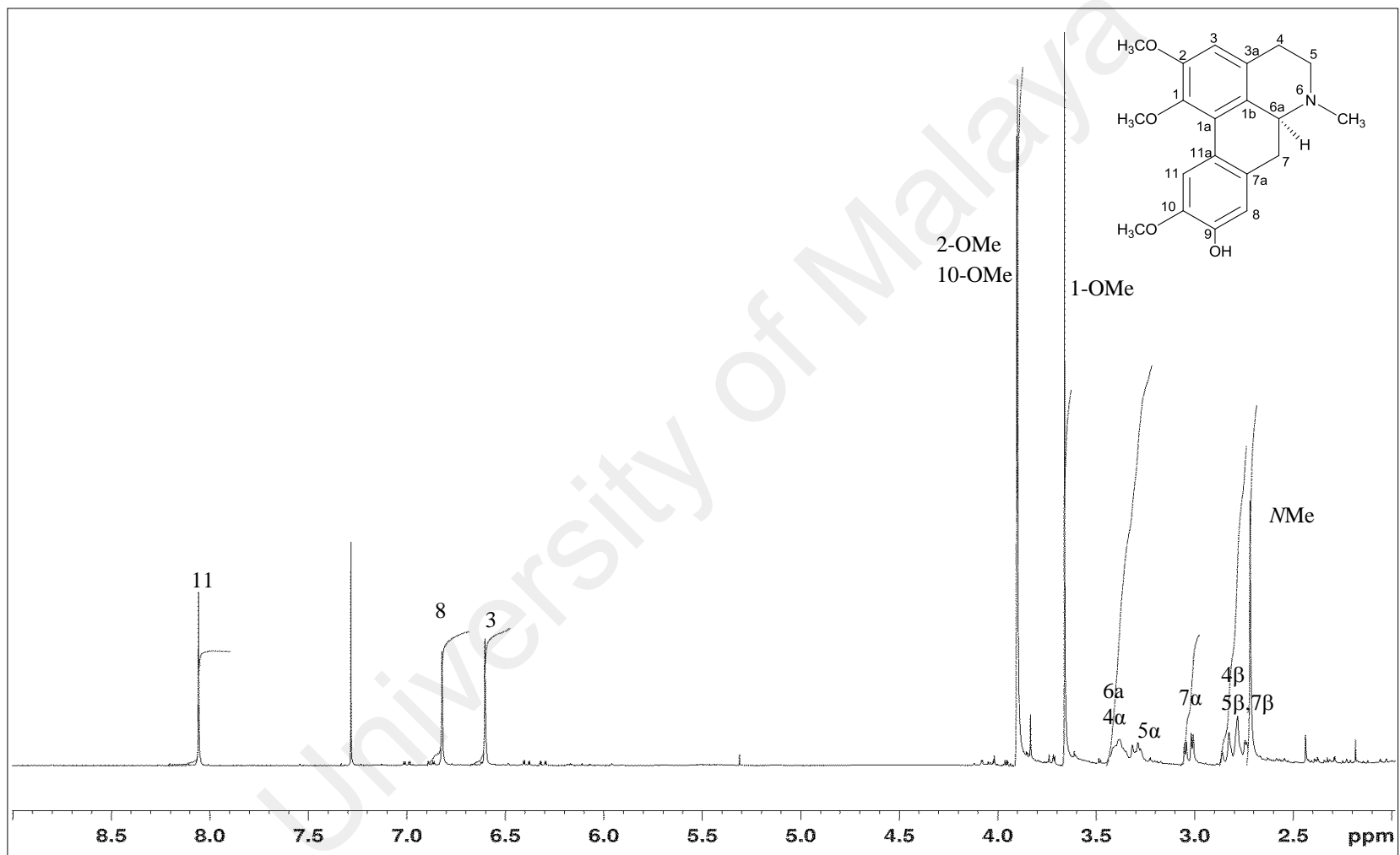


Figure 3.53: ^1H NMR Spectrum of *N*-methylaurotetanine **26**

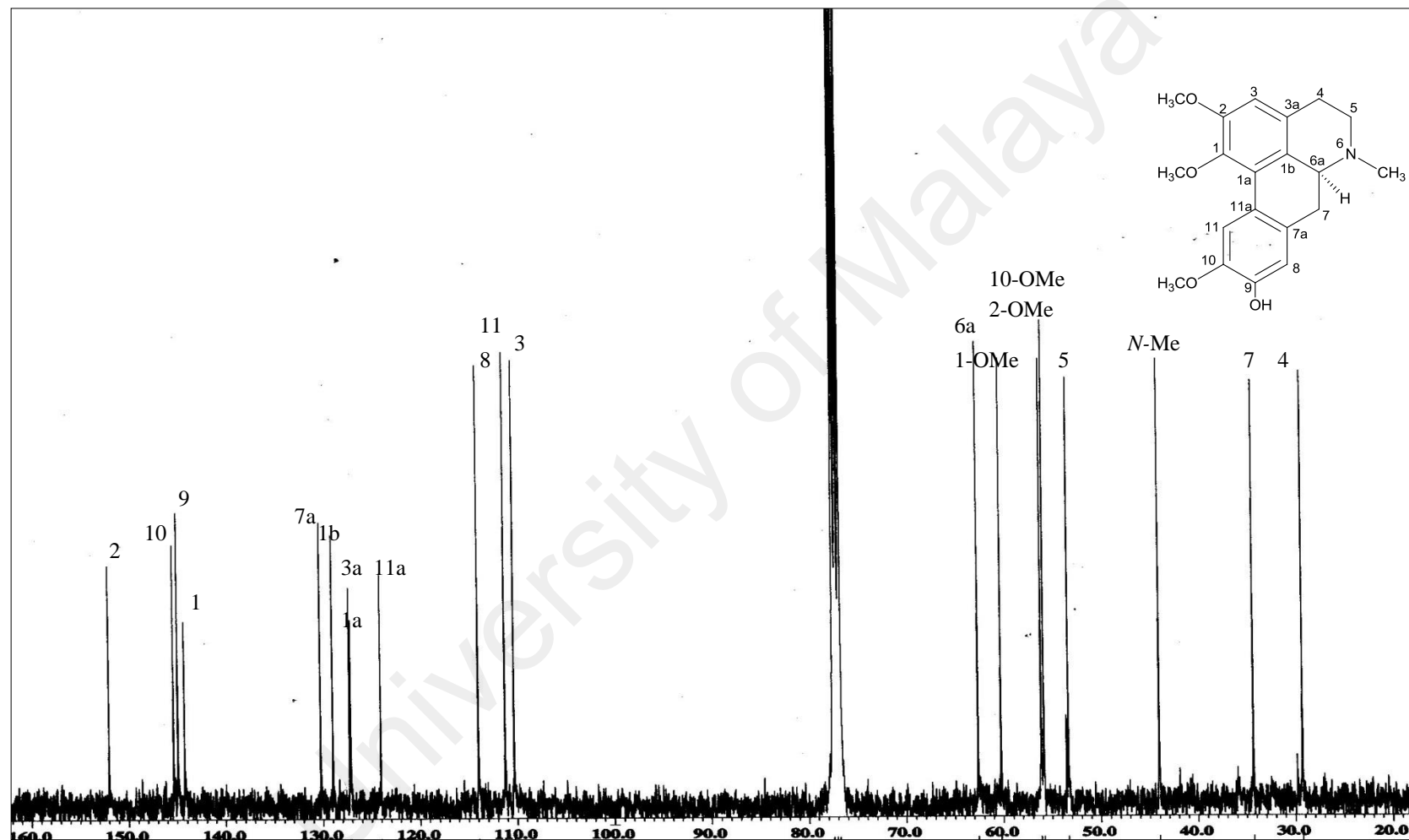


Figure 3.54: ^{13}C NMR Spectrum of *N*-methylaurotetanine 26

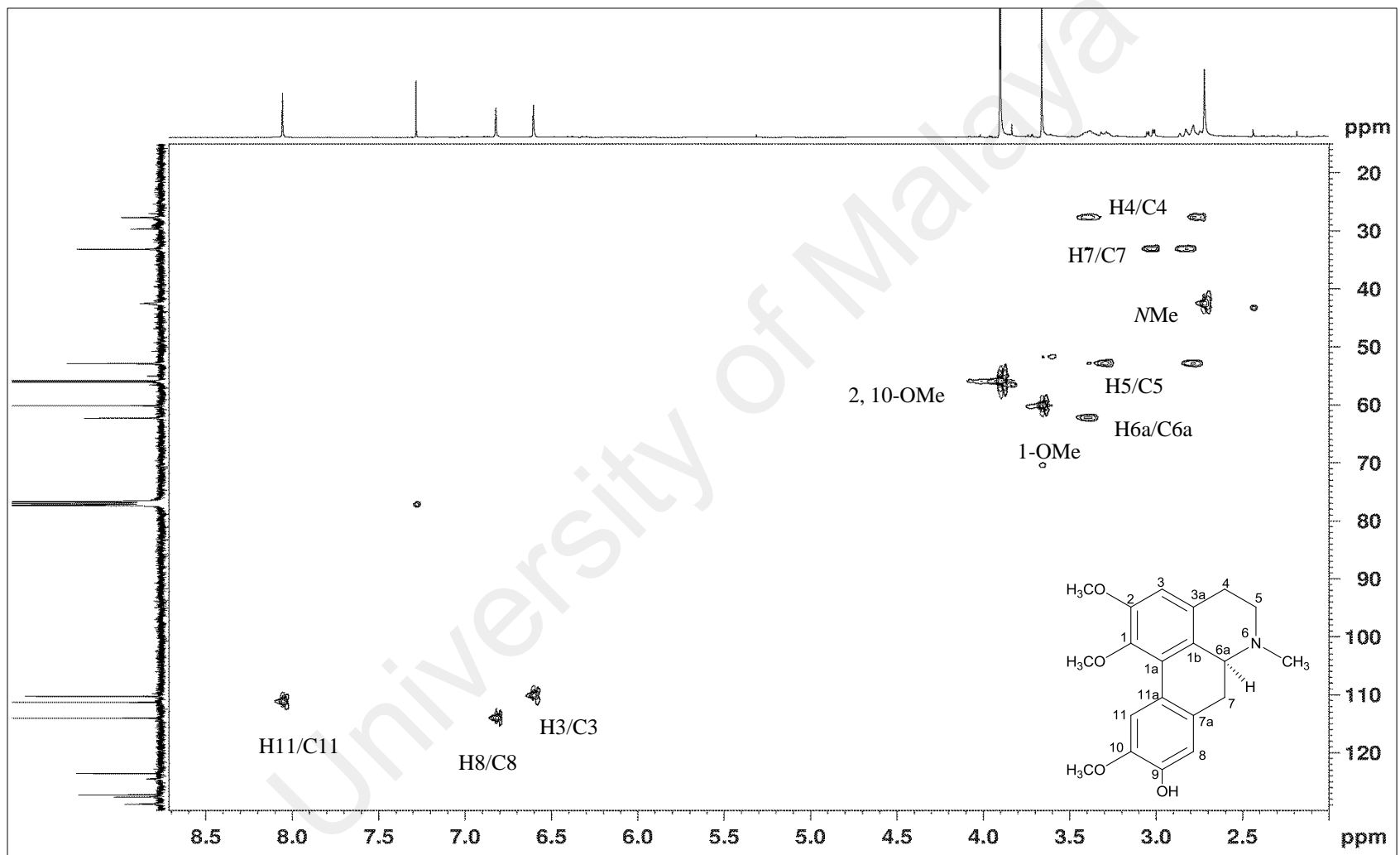


Figure 3.55: HSQC Spectrum of *N*-methyllaurotetanine 26

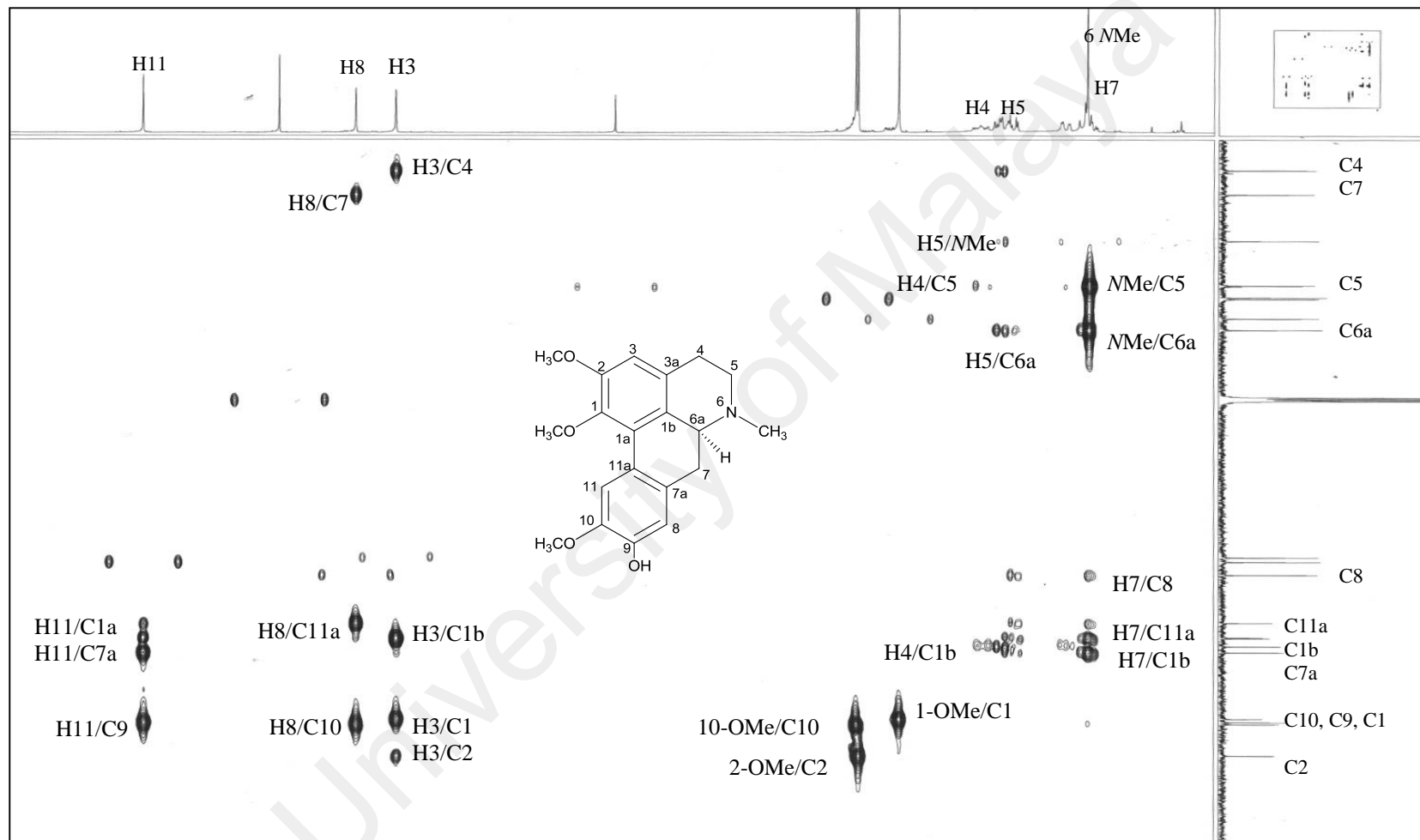
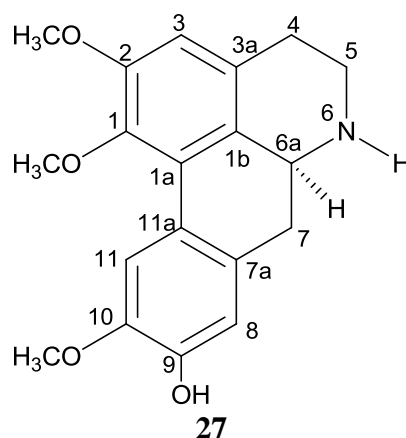


Figure 3.56: HMBC Spectrum of *N*-methyl-laurotetanine **26**

3.1.15 Laurotetanine **27**



Laurotetanine **27** was found in both species *Alseodaphne corneri* and *Dehaasia longipedicelata*. It was obtained as a pale brown amorphous powder with $[\alpha]_D^{25} +120.0^\circ$ ($c = 0.50$, CHCl_3), hence indicating that the absolute configuration at C-6a was *S*. The positive electrospray mass spectrum displayed a pseudo-molecular ion peak $[\text{M}+\text{H}]^+$ at m/z 328.1566, compatible with the molecular formula of $\text{C}_{19}\text{H}_{21}\text{NO}_4$ (calcd. for $\text{C}_{19}\text{H}_{22}\text{NO}_4$, 328.1549). The physical characteristic as well as the UV-vis and IR spectral data of laurotetanine **27** also pointed to a 1, 2, 9, 10-tetrasubstituted aporphine moiety bearing hydroxyl group (Sangster & Stuart, 1965).

The ^1H NMR (Figure 3.58) spectrum of laurotetanine **27** was identical to that of *N*-methyllaurotetanine **26**, except for the lack of the *N*- CH_3 signal that resonated at δ_{H} 2.72. In addition, the signal of H-6a that appeared at δ_{H} 3.28 in **26** shifted downfield to δ_{H} 3.81 ($J=13.9$ Hz) in **27**, indicating the presence of an *NH* group adjacent to the methine H-6a proton. Furthermore, the absence of the signal at δ_{C} 44.0 belong to *N*- CH_3 in the ^{13}C -NMR spectrum (Figure 3.59) of **27** and the apparent of IR absorption at ν_{max} 3330 cm^{-1} thus confirmed the presence of secondary amine group as 6-NH.

The R_f value of laurotetanine **27** ($R_f = 0.24$) was lower than **26** ($R_f = 0.55$) due to the lack of the *N*-methyl group in laurotetanine **27** which rendered the molecule being more hydrophilic. The relatively high polarity of the 1, 2, 9, 10-tetrasubstituted aporphine **27** in comparison with the 1, 2, 10, 11-tetrasubstituted aporphine **41** was deduced based on purification of these alkaloids whereby the former eluted in later fractions at 27-31 while the latter eluted between fractions 17-22 in column chromatography (Scheme 7.1, page 255) (Betts, 1990). Hence, the alkaloid can be deduced to be 1, 2, 9, 10-tetrasubstituted aporphine alkaloid. Complete assignment of the ^1H , ^{13}C NMR was achieved by the aid of 2D NMR spectra in appendix A (Figure A25-A26). The spectral data (Table 3.16) were in full agreement with the literature values confirmed that it is laurotetanine **27** (Babcock & Segelman, 1974).

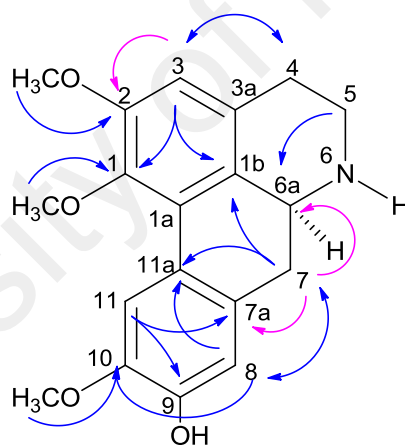


Figure 3.57: ^1H - ^{13}C Correlations Observed in HMBC Spectrum of Laurotetanine **27**

Table 3.16: ^1H , ^{13}C -NMR and HMBC Data of Laurotetanine **27**.

Position	Unit	^1H - NMR CDCl ₃ , 400 MHz Laurotetanine 27 δ (<i>J</i> , Hz)	^1H - NMR CDCl ₃ , 400MHz (Babcock & Segelman, 1974) δ	^{13}C - NMR 100 MHz Laurotetanine 27 δ	HMBC (^1H - ^{13}C)
1	C			144.3	
1- OCH ₃	O-CH ₃	3.64 (<i>s</i>)	3.70	60.3	1
1a	C			126.8	
1b	C			128.6	
2	C			152.2	
2- OCH ₃	O-CH ₃	3.86 (<i>s</i>)	3.91	55.9	2
3	CH	6.58 (<i>s</i>)	6.61	110.8	1, 1b, 2, 4
3a	C			128.9	
4	CH ₂	α 3.00 (<i>m</i>) β 2.65 (<i>dd</i> , 16.4, 5.6)		29.0	1b, 3
5	CH ₂	α 3.37 (<i>d</i> , 5.6) β 3.00 (<i>m</i>)		43.1	3a, 6a
6a	CH	3.81 (<i>d</i> , 13.9)		53.8	
7	CH ₂	2.75 (<i>d</i> , 13.9)		36.6	8, 6a, 7a, 11a
7a	C			129.8	
8	CH	6.78 (<i>s</i>)	6.80	113.9	7, 10, 11a
9	C			144.9	
10	C			145.4	
10- OCH ₃	O-CH ₃	3.87 (<i>s</i>)	3.91	56.1	10
11	CH	8.06 (<i>s</i>)	8.08	111.3	1a, 7a, 9
11a	C			124.0	

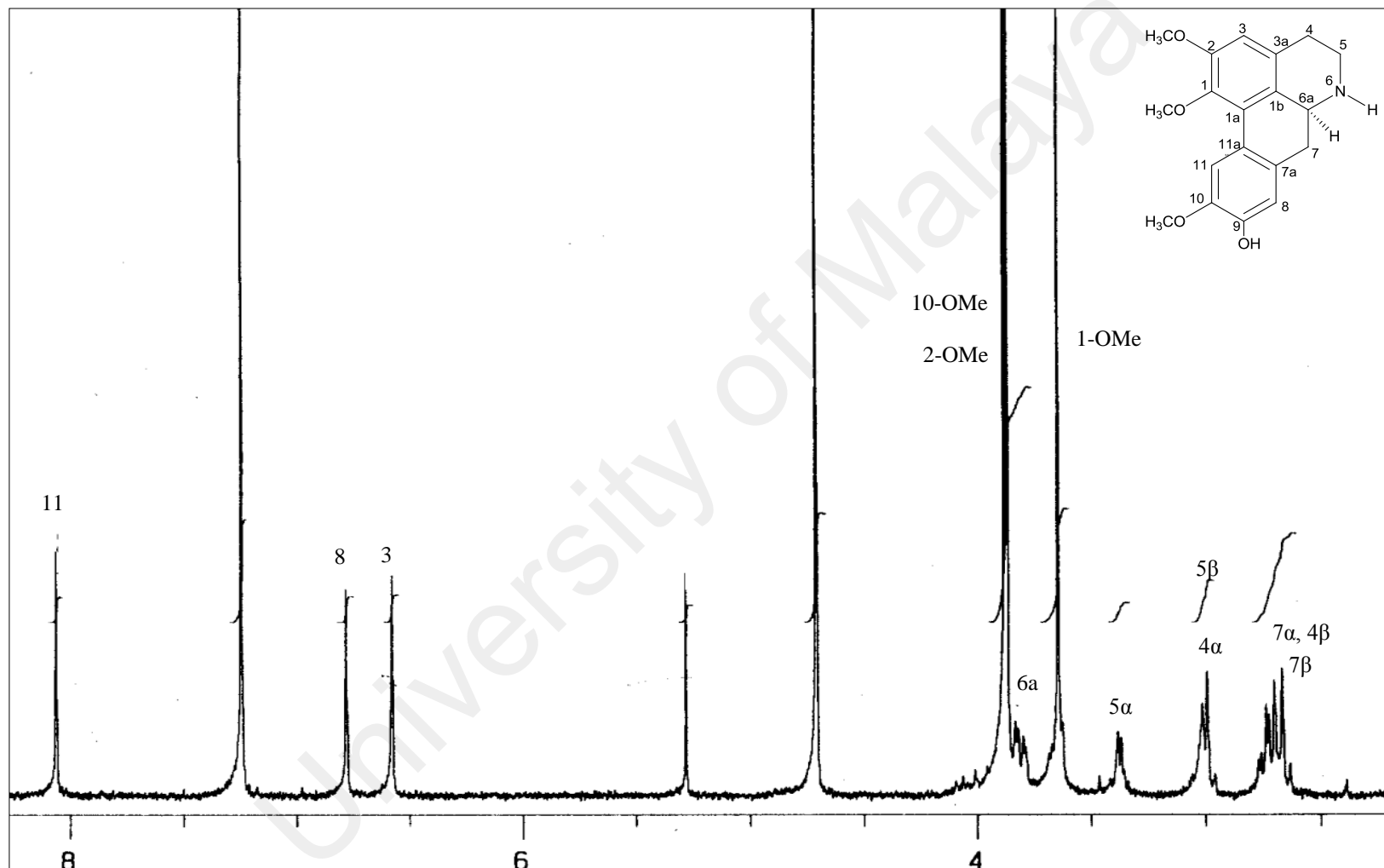


Figure 3.58: ^1H NMR Spectrum of Laurotetanine 27

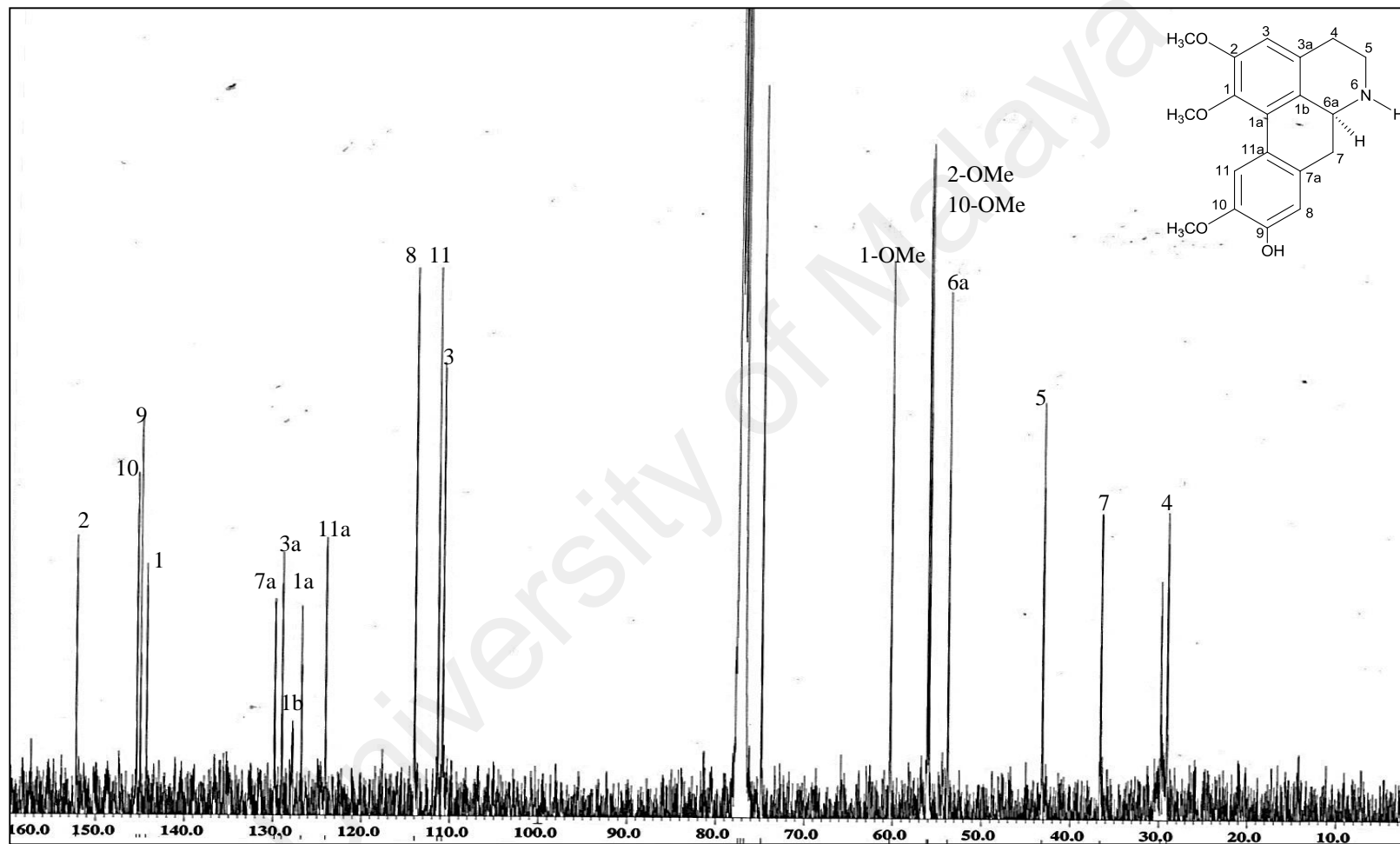
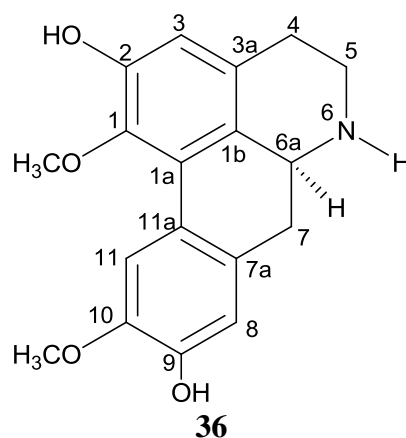


Figure 3.59: ^{13}C NMR Spectrum of Laurotetanine 27

3.1.16 Norboldine 36



Norboldine **36** was purified by using HPLC technique (Figure 7.1, page 252) to give a light violet amorphous solid with $[\alpha]_D^{25} +70^\circ$ ($c=0.7$, MeOH). The ESI⁺ mass spectrum showed a pseudo-molecular ion peak $[M+H]^+$ at m/z 314.1446, corresponding to the elemental formula of C₁₈H₁₉NO₄ (calcd. for C₁₈H₂₀NO₄, 314.1392).

The UV, IR, ¹H (Figure 3.60) and ¹³C NMR (Figure 3.61) spectra showed considerable similarities with that of laurotetanine **27** indicating that the two structures are closely related to one another. However, for **36**, C-2 attach to hydroxyl group instead of a methoxyl group.

The actual distribution of OH and OMe substituents were determined by using HMBC spectrum. The correlation of H-3 to C-1 and C-2, H-11 to C-9 and H-8 to C-10 thus proving the oxygenation pattern for the ring A was 1-methoxyl-2-hydroxyl and for ring D was 9-hydroxyl-10-methoxyl.

Detailed analysis of LCMS and 2D NMR spectra (Appendix A; Figure A27-A29) and comparing the 1D NMR data (Table 3.17) with the literature values (Guinaudeau et al., 1994) confirmed the identity of the alkaloid as (+)-norboldine **36**.

Table 3.17: ^1H and ^{13}C -NMR Data of Norboldine **36**.

Position	Unit	^1H - NMR CD ₃ OD, 400 MHz Norboldine 36 δ (<i>J</i> , Hz)	^1H - NMR (DMSO- D ₆)/(CD ₃ OD) (Guinaudeau et al., 1994) δ	^{13}C - NMR CD ₃ OD, 100 MHz Norboldine 36 δ	^{13}C - NMR (Guinaudeau et al., 1994) (CD ₃ OD) δ
1	C			143.9	144.4
1-OMe	O-CH ₃	3.59 (<i>s</i>)	3.55 (<i>s</i>)	59.1	60.3
1a	C			126.2	127.6
1b	C			119.4	126.6
2	C			151.1	150.9
3	CH	6.64 (<i>s</i>)	6.49 (<i>s</i>)	114.2	115.5
3a	C			126.3	130.0
4	CH ₂	α 3.18 (<i>m</i>) β 2.89 (<i>m</i>)		24.7	28.8
5	CH ₂	α 3.65 (<i>m</i>) β 3.31 (<i>m</i>)		41.3	43.7
6a	CH	4.16 (<i>dd</i> , 3.7, 13.7)	3.51 (<i>dd</i>)	53.2	54.8
7	CH ₂	α 2.93 (<i>m</i>) β 2.81 (<i>t</i> , 13.7)		32.8	36.7
7a	C			126.7	130.3
8	CH	6.74 (<i>s</i>)	6.66 (<i>s</i>)	114.6	115.8
9	C			146.4	147.2
10	C			147.0	147.8
10-OMe	O-CH ₃	3.84 (<i>s</i>)	3.76 (<i>s</i>)	55.2	56.6
11	CH	7.87 (<i>s</i>)	7.87 (<i>s</i>)	111.5	112.8
11a	C			122.8	124.8

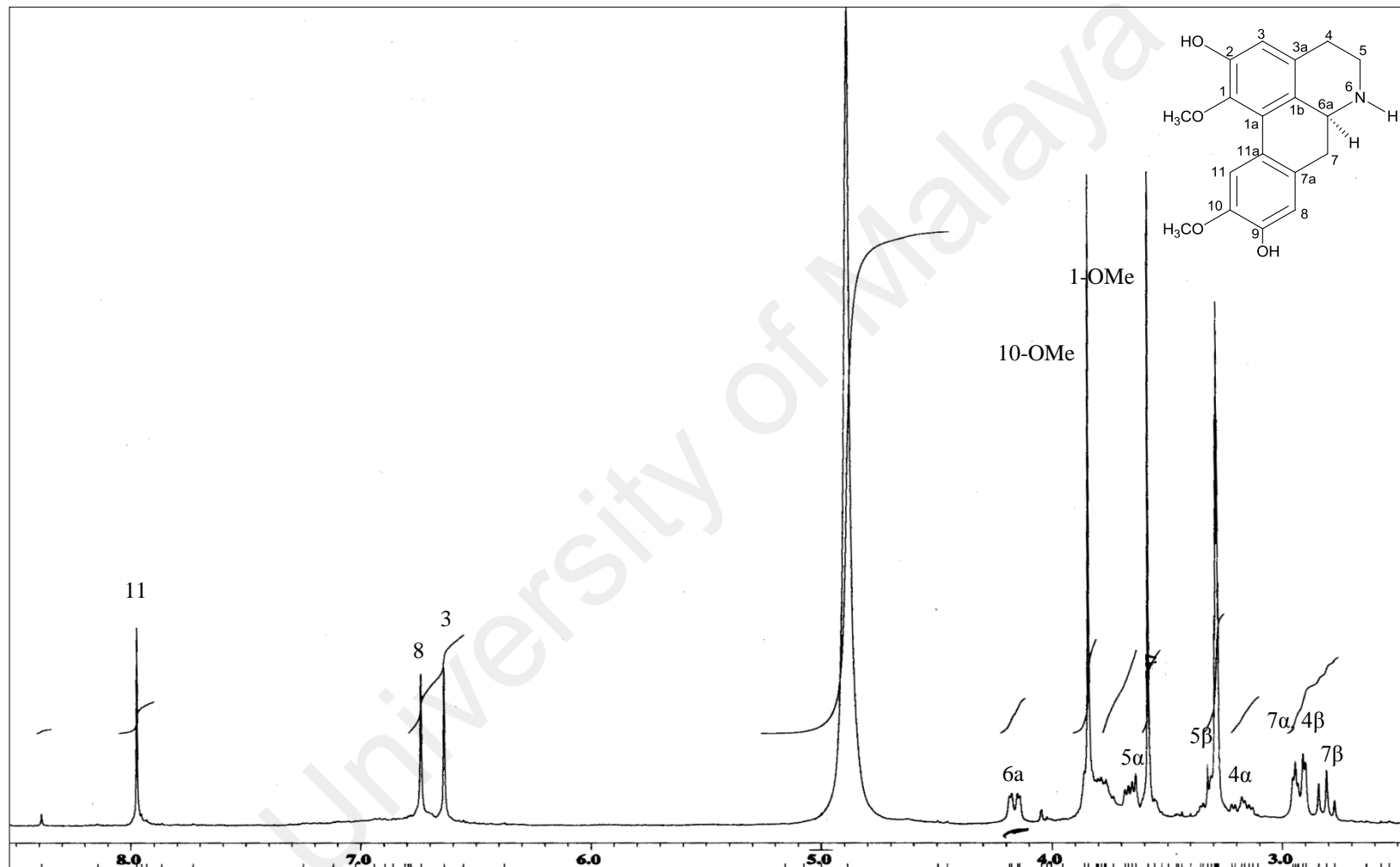


Figure 3.60: ^1H NMR Spectrum of Norboldine **36**

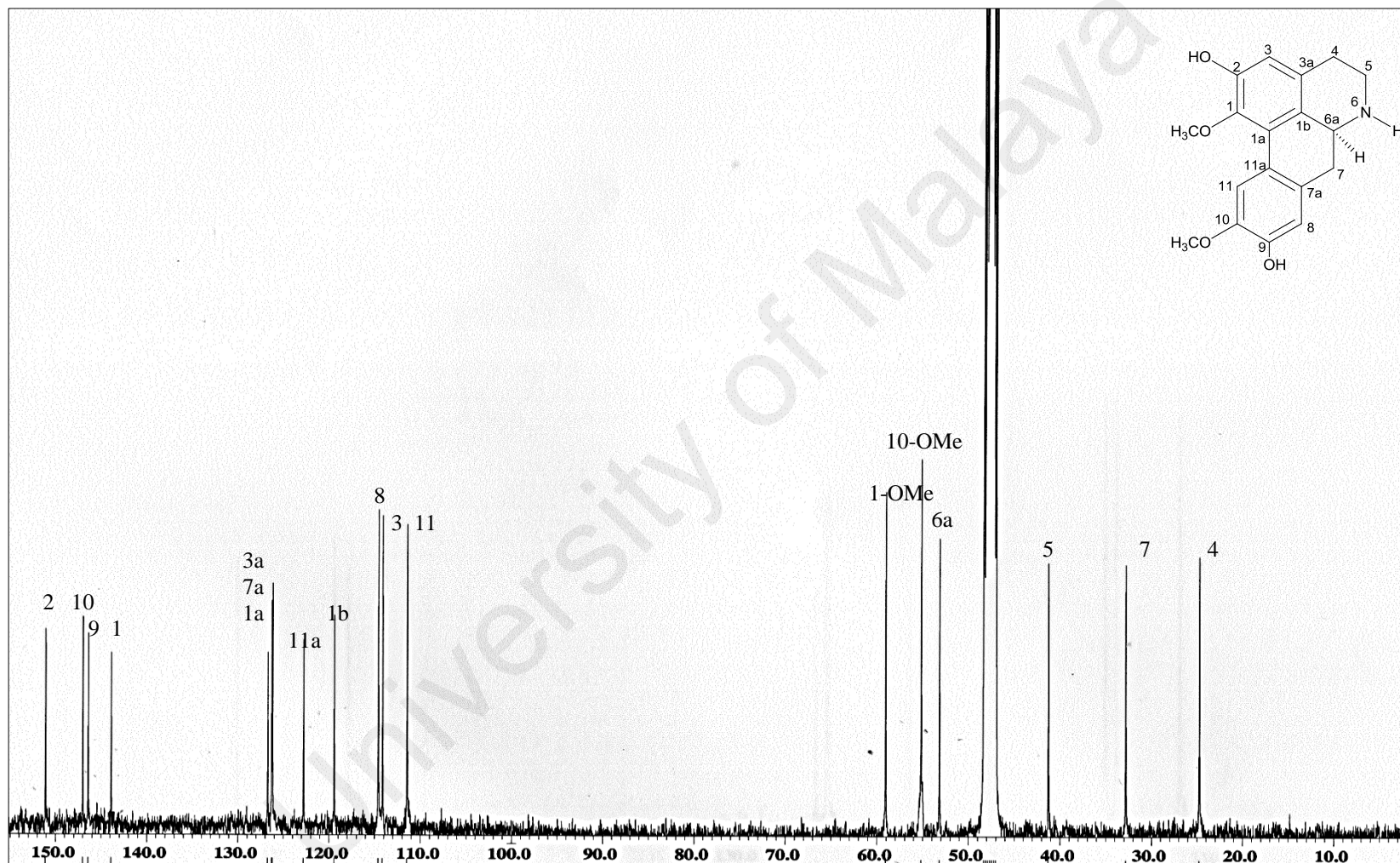
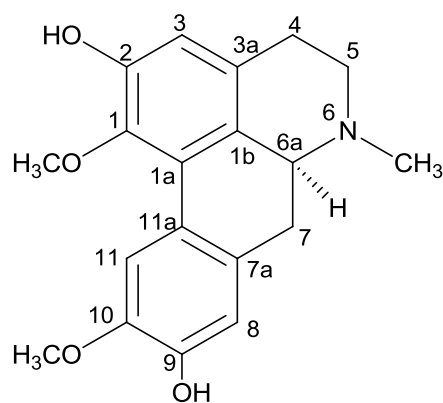


Figure 3.61: ^{13}C NMR Spectrum of Norboldine 36

3.1.17 Boldine **37**



37

Boldine **37** was purified as dark violet amorphous powder and showed a pseudo-molecular ion peak $[M+H]^+$ at m/z 328.1523 for a formula of $C_{19}H_{21}NO_4$ (calcd. for $C_{19}H_{22}NO_4$, 328.1549). The positive optical rotation, $[\alpha]_D^{25} +125.0^\circ$ ($c=1.40$, MeOH) was similar to that norboldine **36**, hence, the stereochemistry also pointed to the same configuration. The UV and NMR spectroscopic data of boldine **37** and **36** were almost identical.

Close inspection between the 1H (Figure 3.62) and ^{13}C (Figure 3.63) NMR spectra of **36** and **37** revealed that the only difference between these two alkaloids was due to the additional signal at δ_H 2.45 and δ_C 44.0 in the spectra of **37**. This led to the assumption that the hydrogen which was initially bonded to *N*-6 in **36** was replaced by a methyl group in **37**.

Extensive analysis of all spectroscopic data established enabled the complete assignment of all the 1H and ^{13}C signals of alkaloid, which eventually led to the identification of the compound as (+)-boldine **37** (Yan et al., 1999).

Table 3.18: ^1H and ^{13}C -NMR Data of Boldine **37**.

Position	Unit	^1H - NMR CDCl ₃ , 400 MHz Boldine 37 δ (<i>J</i> , Hz)	^1H - NMR (acetone-D ₆) (Yan et al., 1999) δ	^{13}C - NMR 100 MHz Boldine 37 δ	^{13}C - NMR (acetone-D ₆) (Yan et al., 1999) δ
1	C			144.2	143.8
1-OMe	O-CH ₃	3.52 (<i>s</i>)	3.58 (<i>s</i>)	60.2	
1a	C			127.1	127.3
1b	C			128.9	125.7
2	C			151.9	150.3
3	CH	6.56 (<i>s</i>)	6.57 (<i>s</i>)	110.3	114.7
3a	C			127.2	129.6
4	CH ₂	2.48- 3.00 (<i>m</i>)		29.2	28.8
5	CH ₂	2.90- 3.00 (<i>m</i>)		53.3	53.7
6	<i>N</i> -CH ₃	2.45 (<i>s</i>)	2.53 (<i>s</i>)	44.0	
6a	CH	3.00 (<i>m</i>)		62.6	63.3
7	CH ₂	2.48- 2.58 (<i>m</i>)		34.3	34.2
7a	C			130.2	130.3
8	CH	6.75 (<i>s</i>)	6.79 (<i>s</i>)	113.9	115.7
9	C			144.8	146.9
10	C			145.3	147.1
10-OMe	O-CH ₃	3.84 (<i>s</i>)	3.85 (<i>s</i>)	56.1	
11	CH	7.82 (<i>s</i>)	7.96 (<i>s</i>)	111.2	112.4
11a	C			124.0	124.0

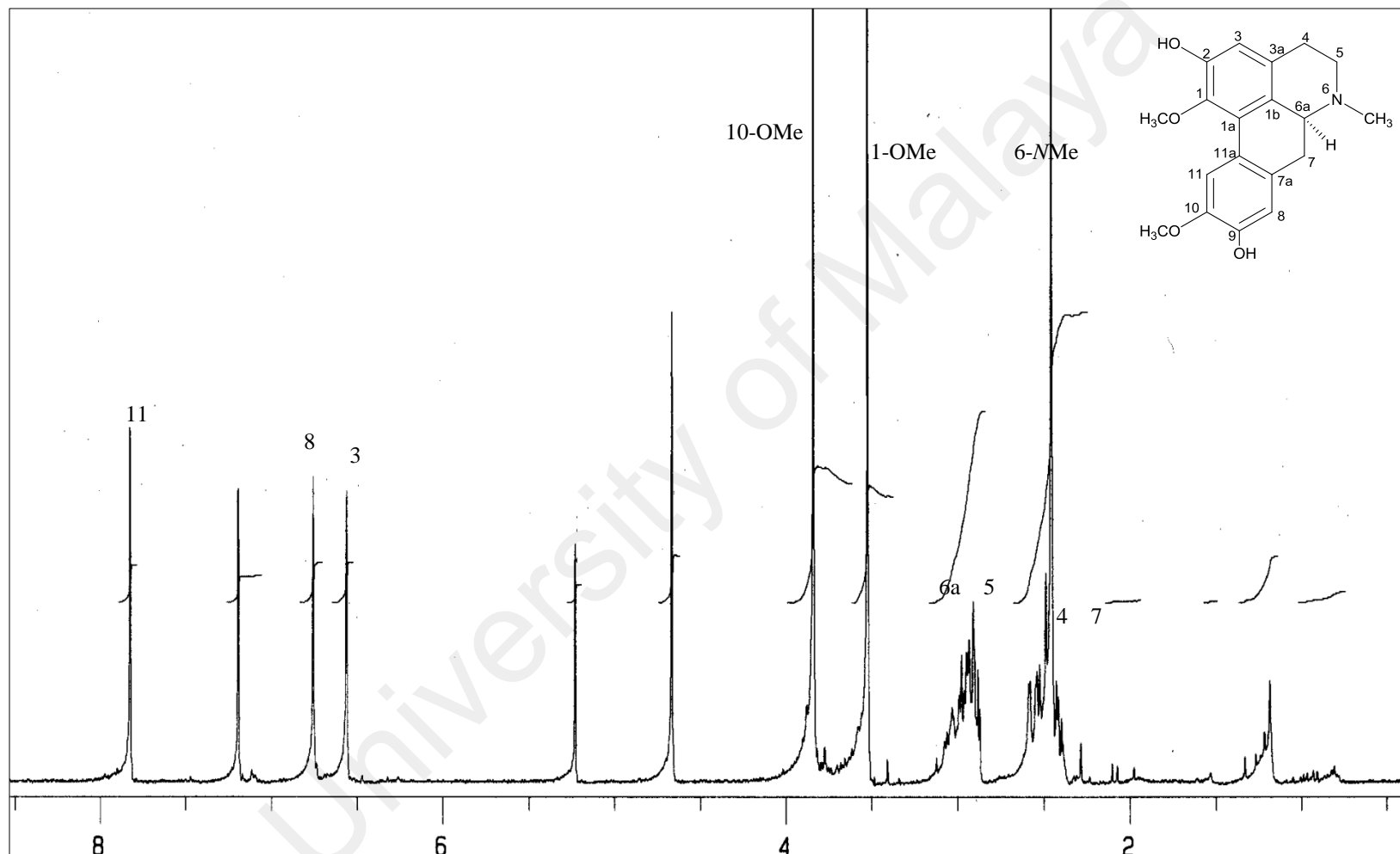


Figure 3.62: ^1H NMR Spectrum of Boldine 37

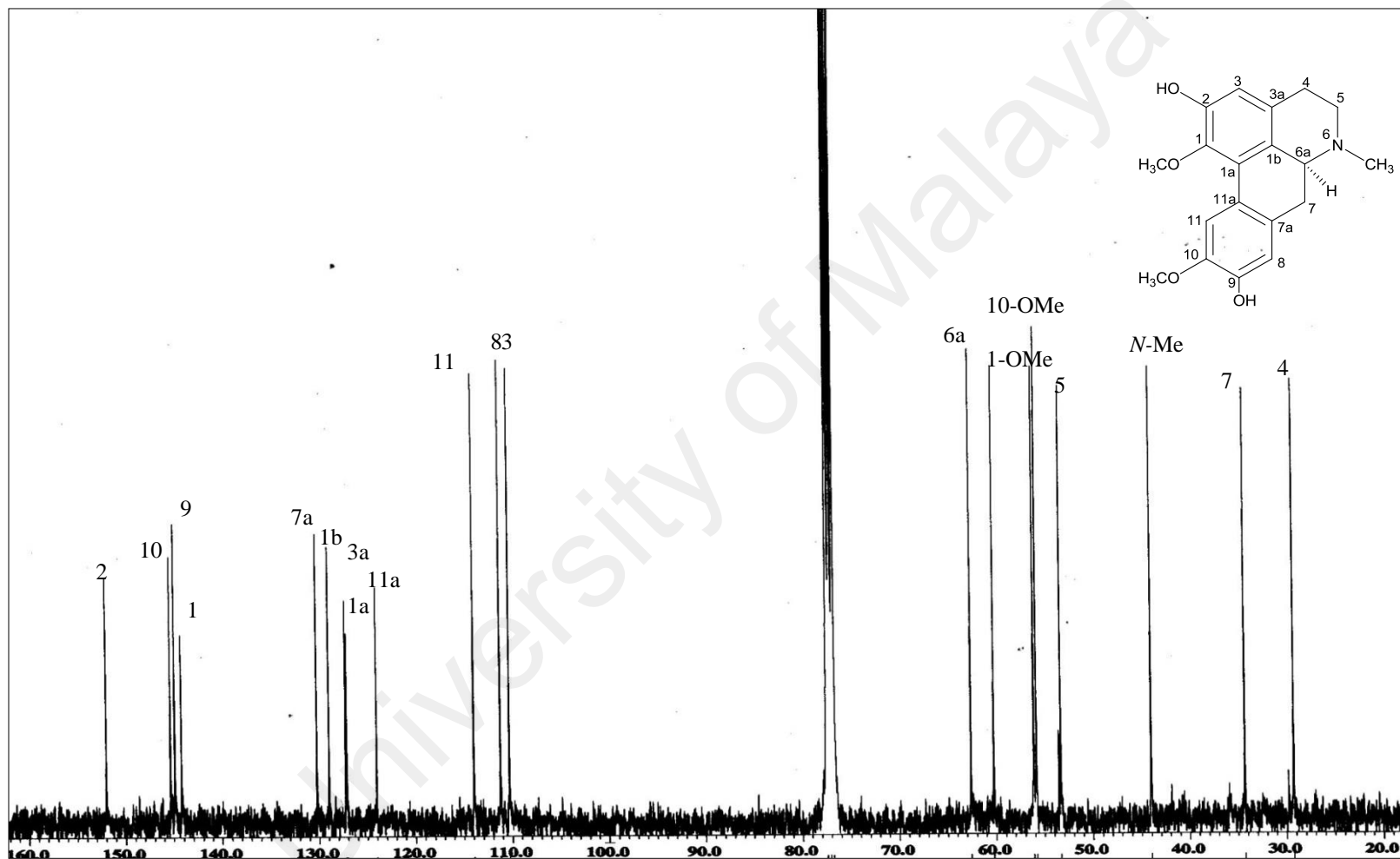
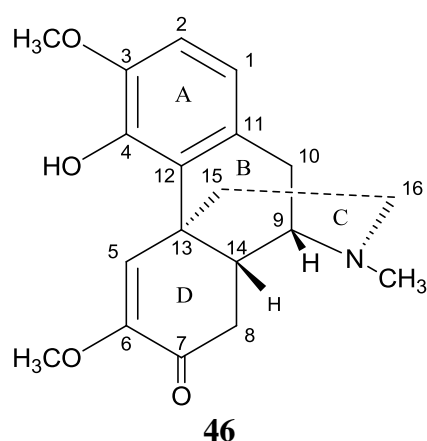


Figure 3.63: ^{13}C NMR Spectrum of Boldine **37**

3.1.18 Milonine 46



Milonine **46**, $[\alpha]_D^{25} +60.0^\circ$ ($c = 0.50$, MeOH), was afforded as a purple-reddish amorphous solid. The EIMS showed pseudo-molecular ion peak $[M+H]^+$ at m/z 330.1728 which was agreeable with the molecular formula of $C_{19}H_{23}NO_4$ (calcd. for 330.1705, $C_{19}H_{24}NO_4$). Its UV spectrum exhibited absorption maxima at λ_{\max} 210 and 264 nm, indicating the characteristic of α , β -unsaturated carbonyl chromophore (Dvorackova et al., 1975; Kashiwaba et al., 1996; Sangster & Stuart, 1965). Absorption bands at ν_{\max} 3506, 1682, 1614 and 1582 cm^{-1} in the IR spectrum (Figure 3.65) suggested the existence of hydroxyl (OH), carbonyl (C=O) and aromatic ring (C=C) groups respectively.

In the ^1H NMR spectrum (Figure 3.66), signals of two aromatic protons, one olefinic proton, one $N\text{-CH}_3$ group, two $O\text{-CH}_3$ groups and aliphatic signals were observed. Vicinal aromatic protons H-1 and H-2 of ring A appeared as doublets ($J=8.3$ Hz) at δ_{H} 6.61 and δ_{H} 6.68. A singlet olefinic proton corresponding to H-5 resonated more deshielded at δ_{H} 7.65 due to the anisotropic effect from ring A. In addition, the presence of three sets of resonances belonging to H-9, H-10 α and H-10 β were observed. These signals are typical for a morphinandienone skeleton. H-9 appeared as a doublet ($J= 5.6$ Hz) at δ_{H} 2.80. H-10 α resonated as a doublet ($J=17.6$ Hz) while its geminal partner H-

10 β , resonated as *dd* ($J=17.6, 5.6$ Hz) at δ_{H} 2.70. Two signals at δ_{H} 3.34 (H-8) and δ_{H} 2.44 (H-14) are characteristic of a 8, 14-dihydromorphinandienone skeleton (isosinomenine type).

The ^{13}C -NMR and DEPT (Figure 3.67) spectra of milonine **46** exhibited 19 signals comprising one carbonyl, three sp^2 methine carbons, five sp^2 quaternary carbons, one sp^3 quaternary carbon, four sp^3 methylene carbons, two sp^3 methine carbons, two methoxyl groups and one $N\text{-CH}_3$ group. The signals at δ_{C} 144.3, 150.4 and 142.6 were respectively assigned to C-3, C-6 and C-4, implying that they were oxygenated. The signal at δ_{C} 194.5 was assigned to α, β -unsaturated carbonyl ketone (C-7) in ring D. Furthermore, the presence of sp^3 carbons; C-8 (δ_{C} 40.6), C-13 (δ_{C} 38.9) and C-14 (δ_{C} 37.4) suggested that 8, 14-dihydromorphinandienone moiety was present which was further supported by the COSY correlation between CH_2 -8 and CH-14 as seen in Figure 3.68. The HMBC spectrum (Figure 3.69) showed cross peaks between H-8 and H-14 with C-7, thus confirming the aforementioned moiety.

Finally, the linkages between the four different rings were assigned with the aid of the HMBC spectrum. The cross peaks between H-5 and C-14 and H-8 with C-13 further confirmed that rings B and ring D were fused via C-13-C-14 junction. The cross peaks between H-15 and C-5 inferred that ring C was connected to ring D through C-13. The cross peaks between H-10 with C-11 and H-1 with C-12 confirmed that ring B was fused to ring A through the C11-C12 junction.

Comparison of the spectral data (Table 3.19) with the literature values confirmed that the alkaloid was (+)-milonine **46** (De Freitas et al., 1995).

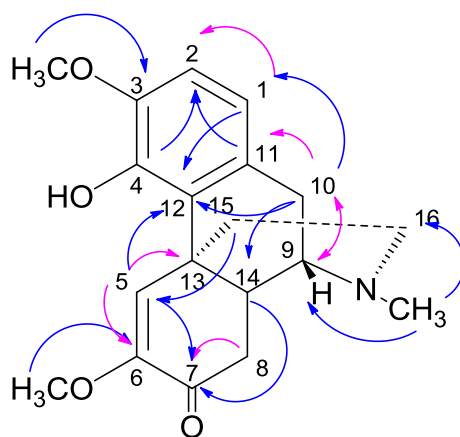


Figure 3.64: ^1H - ^{13}C Correlations Observed in HMBC Spectrum of Milonine **46**

Table 3.19: ^1H and ^{13}C -NMR Data of Milonine **46**.

Position	Unit	^1H - NMR CDCl ₃ , 400 MHz Milonine 46 δ (<i>J</i> , Hz)	^1H - NMR Pyridine D ₆ (De Freitas et al., 1995) δ (<i>J</i>)	^{13}C - NMR 100 MHz Milonine 46 δ	^{13}C - NMR Pyridine D ₆ (De Freitas et al., 1995) δ
1	CH	6.61 (<i>d</i> , 8.3)	6.79 (<i>d</i>)	118.9	119.9
2	CH	6.68 (<i>d</i> , 8.3)	6.93 (<i>d</i>)	109.5	109.5
3	C			144.3	147.2
3-OMe	OCH ₃	3.83 (<i>s</i>)	3.78 (<i>s</i>)	55.8	56.7
4	C			142.6	145.7
5	CH	7.65 (<i>s</i>)	8.34 (<i>s</i>)	123.3	125.5
6	C			150.4	152.0
6-OMe	OCH ₃	3.58 (<i>s</i>)	3.65 (<i>s</i>)	54.4	55.1
7	C=O			194.5	194.5
8	CH ₂	H α 3.34 (<i>dd</i> , 17.6, 13.6) H β 2.65 (<i>d</i> , 17.6)	3.65 (<i>dd</i>)	40.6	40.6
9	CH	2.80 (<i>d</i> , 5.6)	2.81 (<i>brd</i>)	56.2	57.5
10	CH ₂	H α 3.02 (<i>d</i> , 17.6) H β 2.70 (<i>dd</i> , 17.6, 5.6)	3.11 (<i>d</i>) 2.76 (<i>dd</i>)	27.3	28.6
11	C			130.9	132.3
12	C			125.8	128.3
13	C			38.9	38.9
14	CH	2.44 (<i>m</i>)	2.41 (<i>m</i>)	37.4	42.2
15	CH ₂	1.90 (<i>m</i>)	2.22 (<i>m</i>)	31.7	33.2
16	CH ₂	2.39 (<i>m</i>)	2.42 (<i>m</i>)	46.3	47.6
NCH ₃	NCH ₃	2.28 (<i>s</i>)	2.28 (<i>s</i>)	42.3	43.3

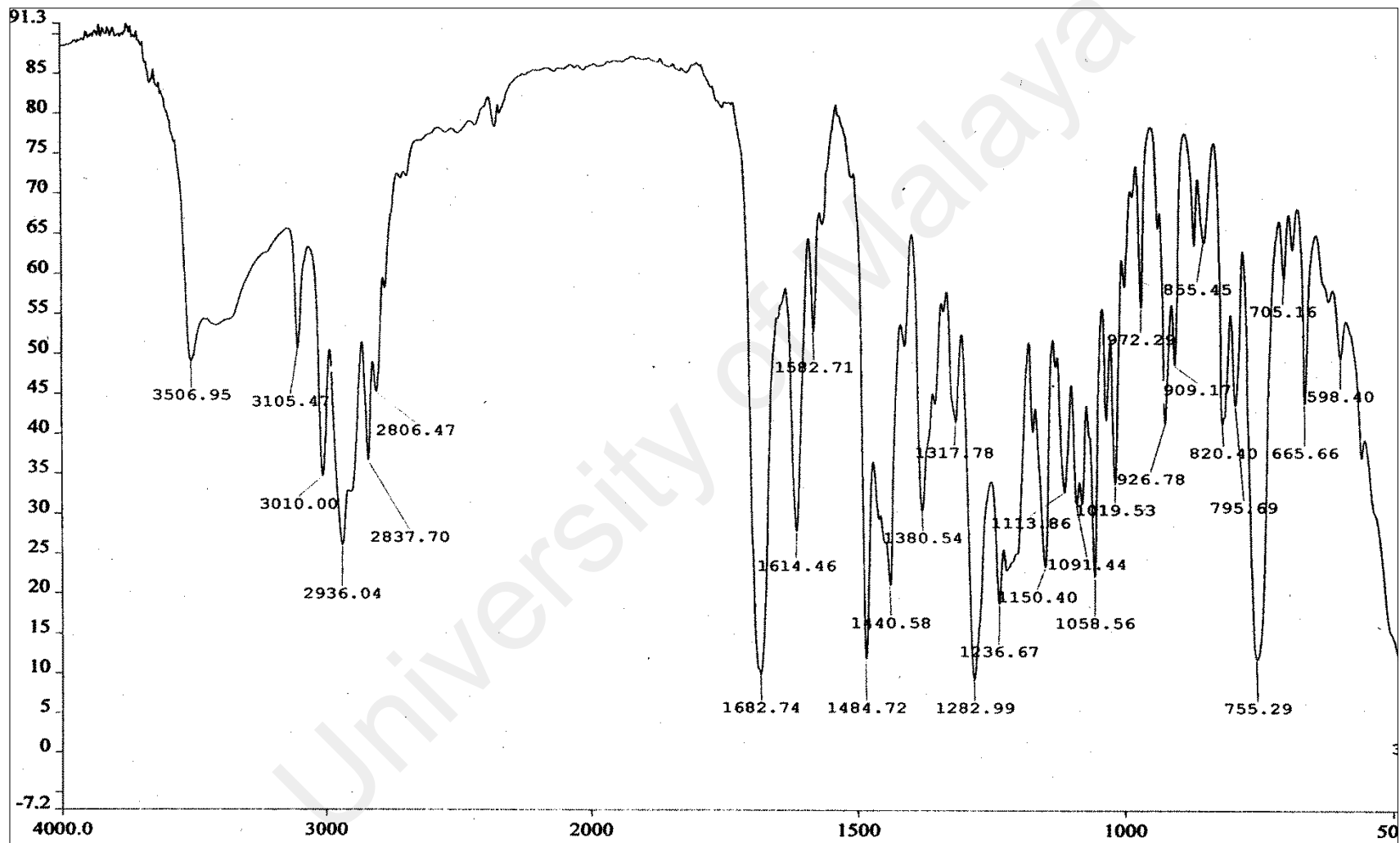


Figure 3.65: IR Spectrum of Milonine 46

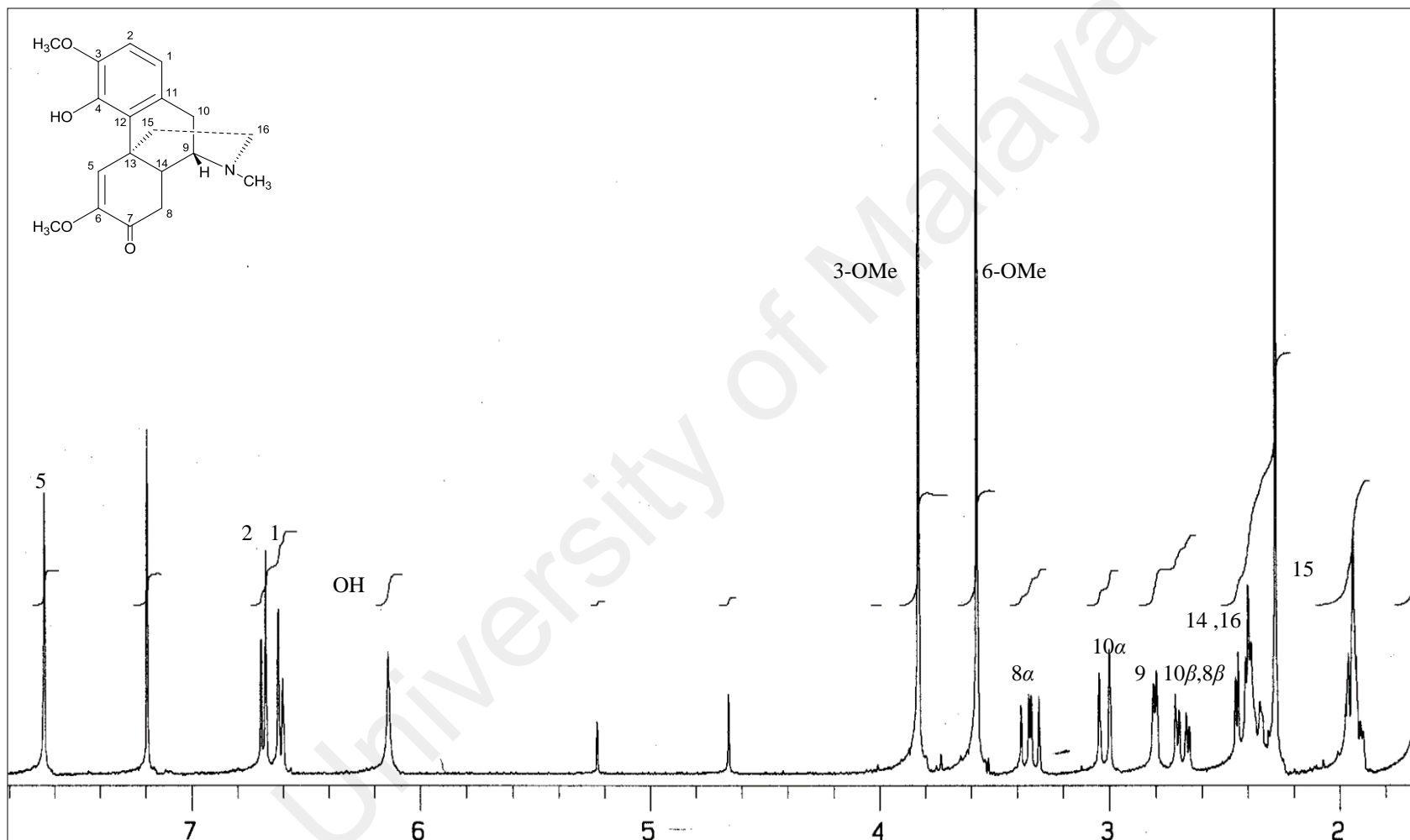


Figure 3.66: ¹H NMR Spectrum of Milonine 46

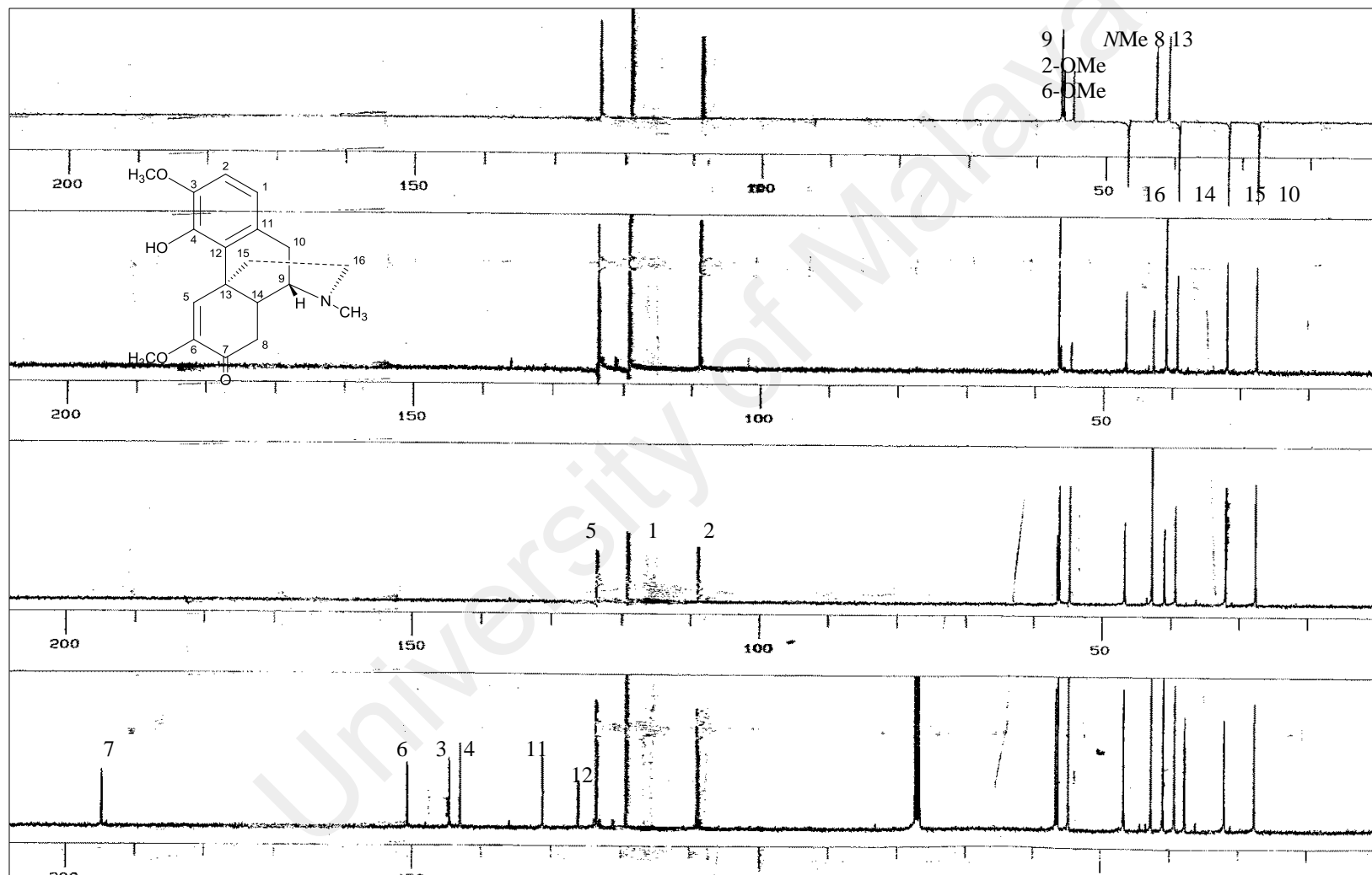


Figure 3.67: DEPT NMR Spectrum of Milonine 46

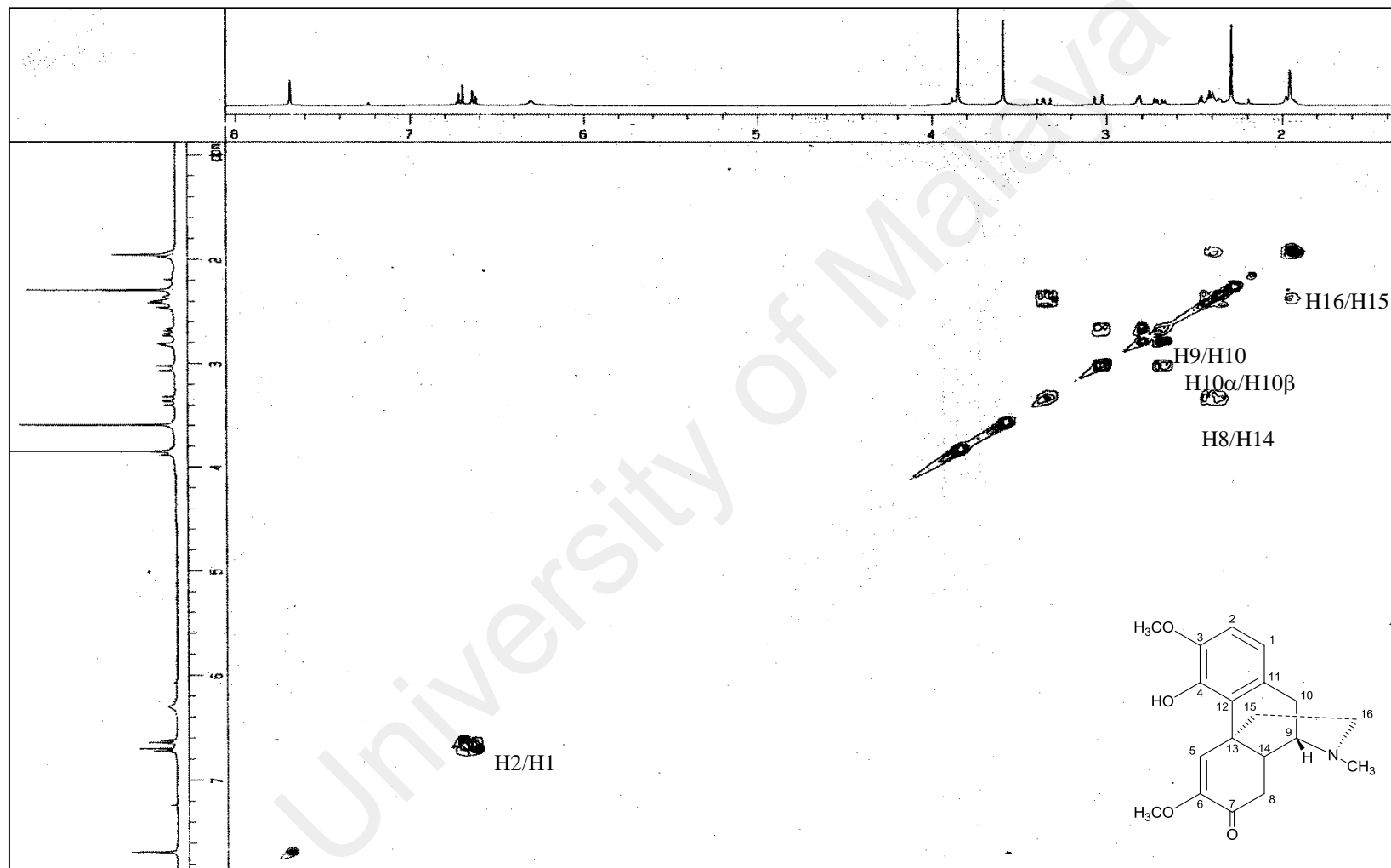


Figure 3.68: COSY Spectrum of Milonine **46**

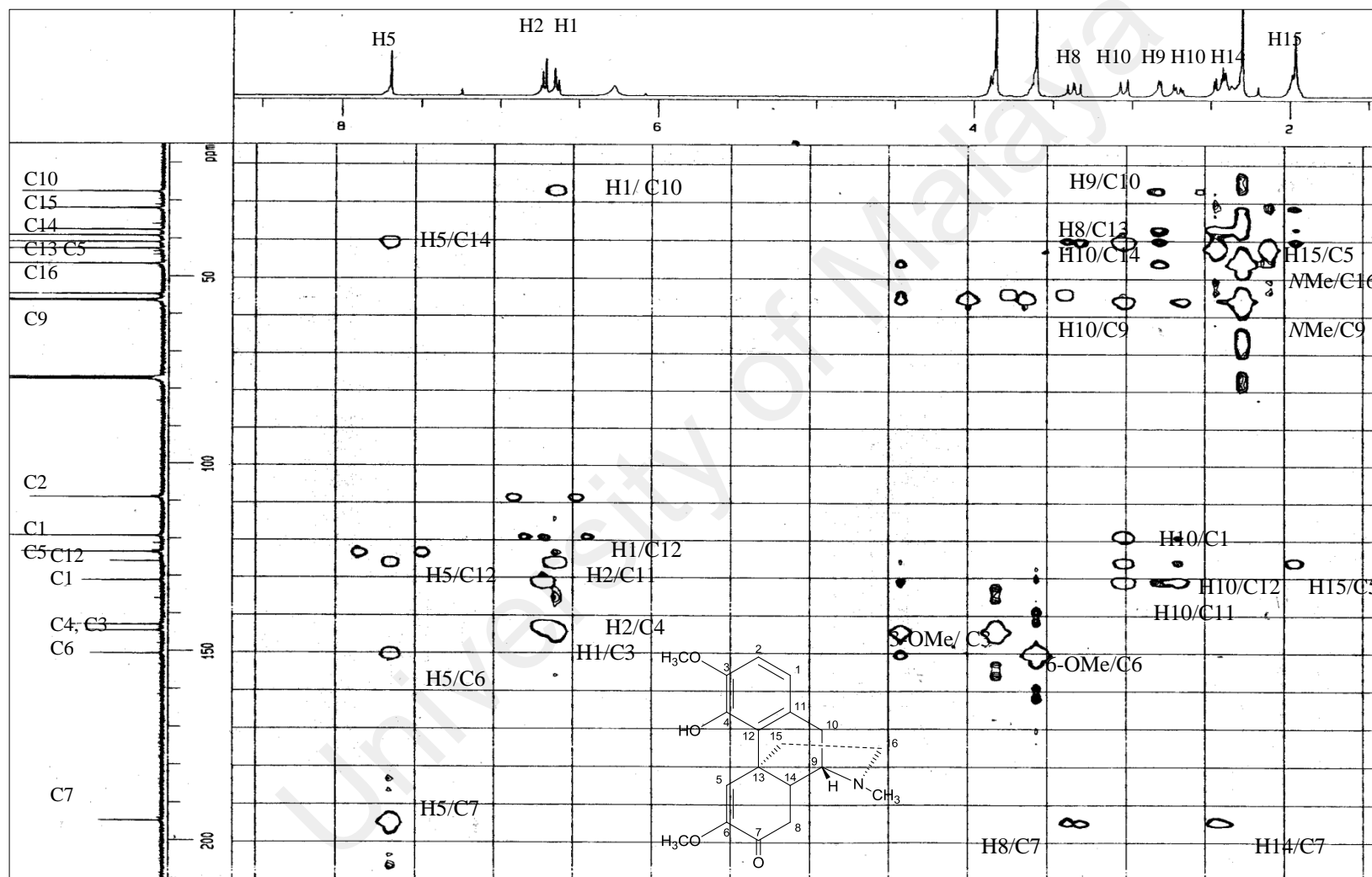
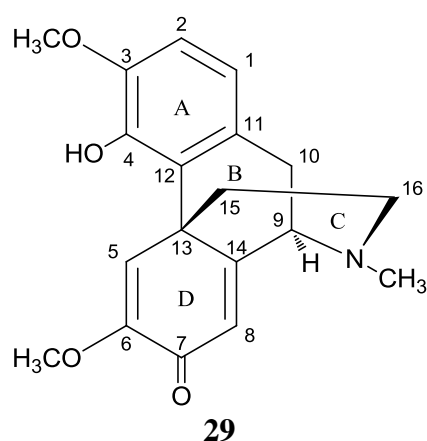


Figure 3.69: HMBC Spectrum of Milonine 46

3.1.19 Sinoacutine 29



Sinoacutine **29** was isolated as colourless amorphous powder. The EIMS spectrum showed a pseudo-molecular ion peak $[M+H]^+$ at m/z 328.1530 which was compatible to a molecular formula of $C_{20}H_{23}NO_4$, (calcd. for $C_{20}H_{24}NO_4$, 328.1549). The UV spectrum showed maxima at λ_{max} 245 and 293 nm which indicated the existence of the conjugated system in the structure (Blasko & Cordell, 1988). Its IR spectrum suggested the presence of hydroxyl (3410 cm^{-1}), α , β -unsaturated carbonyl (1676 cm^{-1}) and aromatic ring ($1582, 1615\text{ cm}^{-1}$). The C-9 chiral carbon was determined to have an *R*-configuration based on the negative optical rotation value, $[\alpha]_D^{25} -10.0^\circ$ ($c=0.10$, $CHCl_3$).

Analysis of the 1H (Figure 3.71) and ^{13}C NMR (Figure 3.72) spectra corroborated that sinoacutine **29** was a morphinandienone type alkaloid structurally related to milonine **46**. The evident difference in those structures can be seen by additional olefinic proton in ring D when compared to **46**. This olefinic proton, H-8 resonated at δ_H 6.32 and δ_C 122.4 in the the **29** spectra. It was further supported by the C-14 (δ_C 122.4) that acts as quaternary carbon. The presence of three sets of significance morphinandienone characteristic peak corresponding to H-9, H-10 α and H-10 β were also noticed. H-9 appeared as a doublet ($J= 5.2$ Hz) at δ_H 3.67. H-10 α resonated as a doublet ($J= 17.3$ Hz) and its geminal partner H-10 β , displayed as *dd* ($J=17.3, 5.2$ Hz) at

δ_H 2.99. The non-split pattern between both H-9 and H-10 signals; $J_{9,10\alpha} = 0$ Hz, suggested that the dihedral angle between these protons were in the approximately 90° as shown in Figure 3.70. Hence, the structure can be deduced to be sinoacutine **29** and the spectral data were in full agreement with the literature values reported by (Kashiwaba et al., 1996).

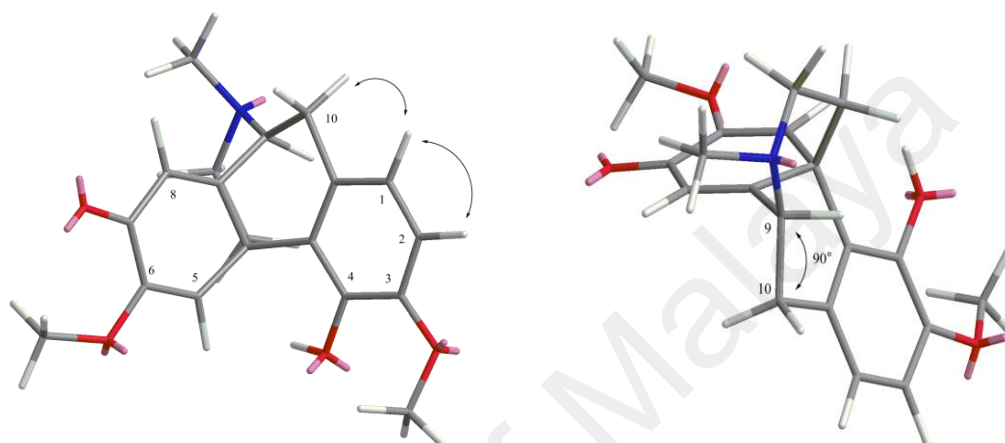


Figure 3.70: NOESY Correlation of Sinoacutine **29**

Table 3.20: ^1H and ^{13}C -NMR Data of Sinoacutine **29**

Position	Unit	^1H - NMR CDCl ₃ , 400 MHz Sinoacutine 29 δ (J, Hz)	^1H - NMR (Kashiwaba et al., 1996)	^{13}C - NMR Sinoacutine 29 100 MHz δ	^{13}C - NMR (Kashiwaba et al., 1996) δ
1	CH	6.65 (<i>d</i> , 8.3)	6.67 (<i>d</i>)	118.9	118.5
2	CH	6.74 (<i>d</i> , 8.3)	6.75 (<i>d</i>)	109.5	109.5
3	C			145.4	145.0
3-OMe	OCH ₃	3.87 (<i>s</i>)	3.89 (<i>s</i>)	56.4	56.3
4	C			143.4	143.0
5	CH	7.51 (<i>s</i>)	7.55 (<i>s</i>)	120.5	120.5
6	C			151.0	150.9
6-OMe	OCH ₃	3.73 (<i>s</i>)	3.75 (<i>s</i>)	54.9	54.8
7	C=O			181.6	181.5
8	CH	6.32 (<i>s</i>)	6.33 (<i>s</i>)	122.4	122.2
9	CH	3.70 (<i>d</i> , 5.2)	3.69 (<i>d</i>)	61.1	61.0
10	CH ₂	α 3.35 (<i>d</i> , 17.3) β 2.99 (<i>dd</i> , 17.3, 5.2)	3.33 (<i>d</i>) 2.98 (<i>dd</i>)	32.7	32.6
11	C			129.8	129.8
12	C			124.0	124.0
13	C			43.7	43.7
14	C			161.6	161.6
15	CH ₂	1.77 (<i>ddd</i> , 12.5, 3.0, 1.8)	1.77 (<i>m</i>)	37.8	37.8
16	CH ₂	2.61 (<i>dd</i> , 12.5, 3.0) 2.51 (<i>m</i>)	2.61 (<i>dd</i>) 2.49 (<i>ddd</i>)	47.1	47.0
NCH ₃	NCH ₃	2.45 (<i>s</i>)	2.45 (<i>s</i>)	41.7	41.7

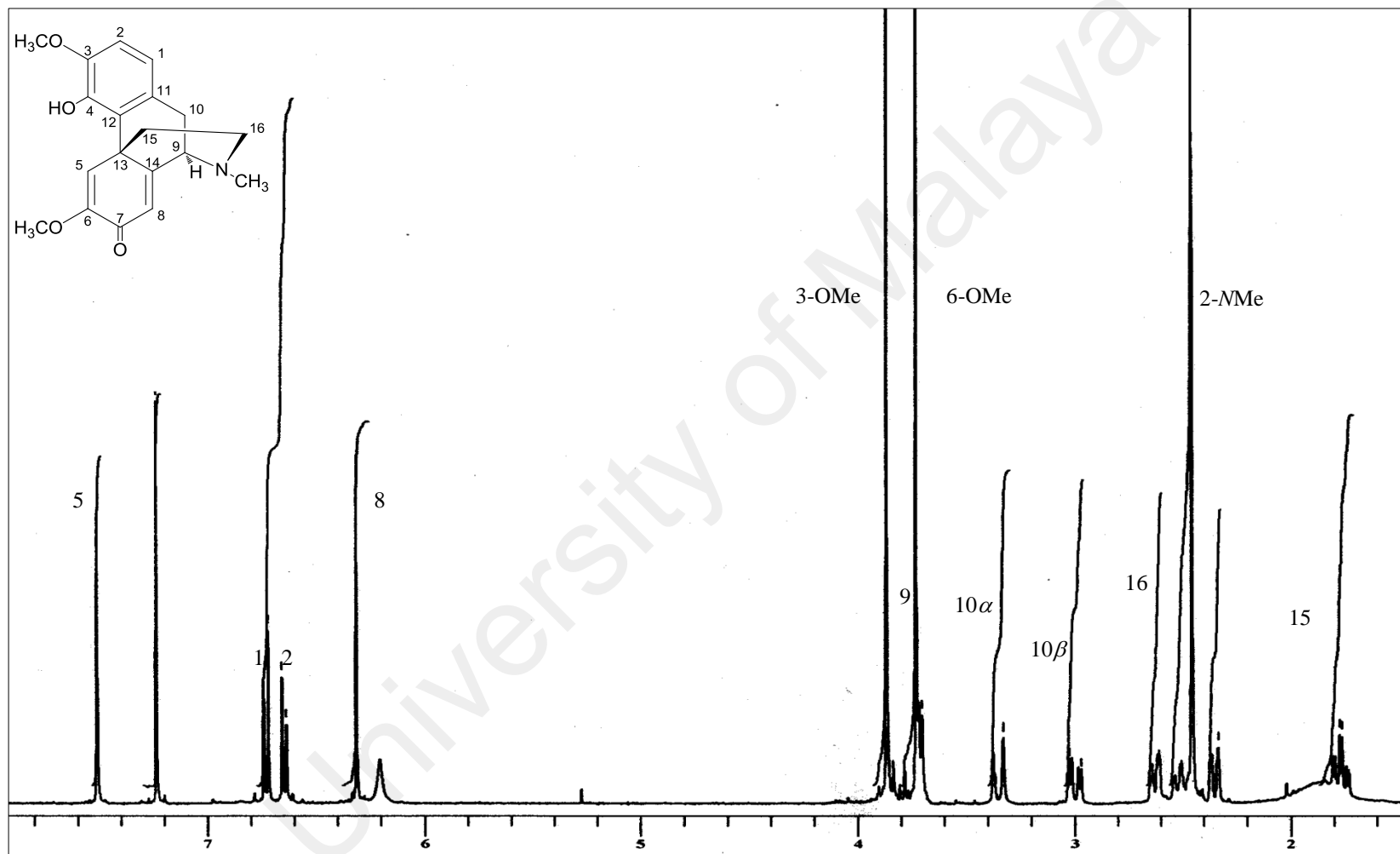


Figure 3.71: ¹H NMR Spectrum of Sinoacutine 29

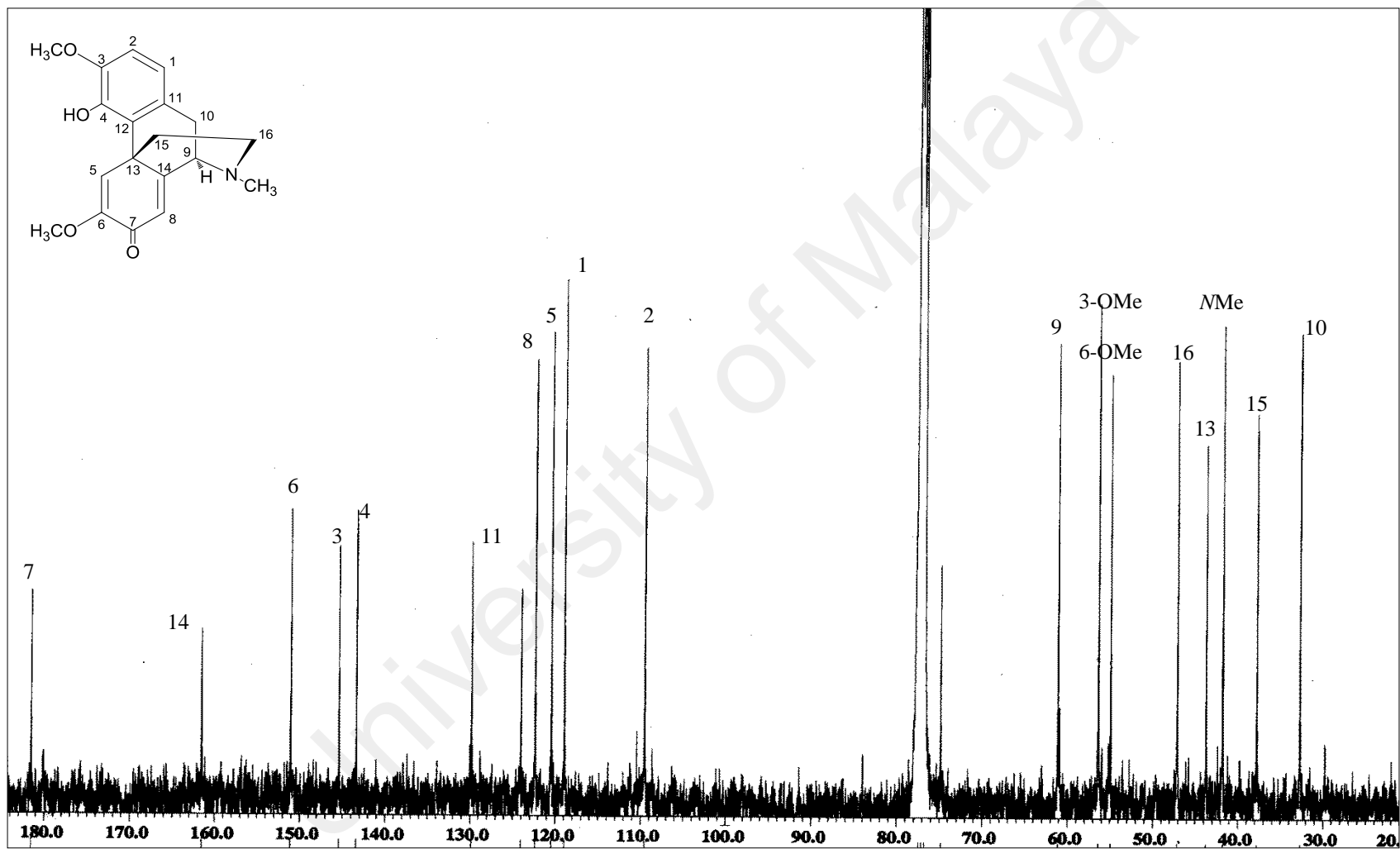
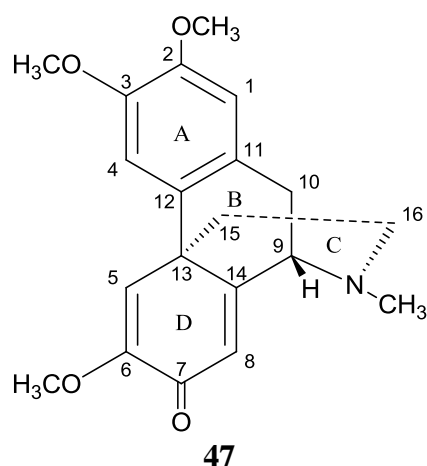


Figure 3.72: ¹³C NMR Spectrum of Sinoacutine 29

3.1.20 Sebiferine 47



Sebiferine **47** was purified as a light yellow crystal with $[\alpha]_D^{25} +10.0^\circ$ ($c=0.10$, CHCl_3). The sharp absorption peaks at 1666, 1645, 1617 cm^{-1} proved the presence of a cross-conjugated cyclohexadienone group in the IR spectrum (Figure A30) (Bartley et al., 1994). The positive ESI-MS revealed a pseudo-molecular ion peak $[\text{M}+\text{H}]^+$ at m/z 342.1730 proposing the molecular formula of $\text{C}_{20}\text{H}_{23}\text{NO}_4$ (calcd. for $\text{C}_{20}\text{H}_{24}\text{NO}_4$, 342.1705).

Aside from similar typical signal of morphinandienone skeleton as in **29**, the ^1H NMR (Figure 3.73) spectrum of **47** depicted two singlets aromatic signals corresponding to H-1 (δ_{H} 6.60) and H-4 (δ_{H} 6.78) in ring A and two singlets olefinic protons; H-5 (δ_{H} 6.33) and H-8 (δ_{H} 6.30) in ring D. The presence of an upfield H-5 signal resonating at δ_{H} 6.33 instead of δ_{H} 7.51 in **29**, due to the absence of the anisotropic effect from ring A. Three methoxyl singlets at δ_{H} 3.86, δ_{H} 3.84 and δ_{H} 3.78 situated at different position at C-2, C-3 and C-6 respectively in comparison with **29**. No absorption band over ν_{max} 3000 cm^{-1} showed that the absence of hydroxyl group in **47**.

The appearance of the sp^3 quaternary carbon (C-13) and conjugated ketonic carbonyl (C-7) in ^{13}C NMR spectrum (Figure 3.74) was confirmed by the resonance at δ_{C} 42.3 and δ_{C} 181.0 respectively.

The ^1H - ^1H COSY spectrum (Appendix A: Figure A31) revealed the connectivity of aliphatic protons. The correlation was traced out starting with geminally coupled C-10 sp^3 methylene protons and vicinal coupled with sp^3 methine proton of C-9. Further connectivity can be seen by correlation of two group sp^3 methylene protons C-16 with C-15.

The spectroscopic data (Table 3.21) obtained were consistent with those found in the literature (Bartley et al., 1994; Roblot et al., 1984), thus proved the identity of (+)-sebiferine **47**.

University of Malaysia

Table 3.21: ^1H and ^{13}C -NMR Data of Sebiferine **47**.

Position	Unit	^1H - NMR CDCl ₃ , 400 MHz Sebiferine 47 δ (<i>J</i> , Hz)	^1H - NMR (Roblot et al., 1984) δ (<i>J</i>)	^{13}C - NMR 100 MHz Sebiferine 47 δ	^{13}C - NMR (Roblot et al., 1984) δ
1	CH	6.61 (<i>s</i>)	6.60 (<i>s</i>)	110.5	110.2
2	C			148.4	147.8
2-OMe	OCH ₃	3.86 (<i>s</i>)	3.85 (<i>s</i>)	55.9	55.7
3	C			148.1	148.1
3-OMe	OCH ₃	3.84 (<i>s</i>)	3.87 (<i>s</i>)	56.3	56.1
4	CH	6.78 (<i>s</i>)	6.78 (<i>s</i>)	108.6	108.5
5	CH	6.33 (<i>s</i>)	6.33 (<i>s</i>)	118.8	118.7
6	C			151.5	151.2
6-OMe	OCH ₃	3.78 (<i>s</i>)	3.79 (<i>s</i>)	55.2	54.9
7	C=O			181.0	180.7
8	CH	6.30 (<i>s</i>)	6.31 (<i>s</i>)	122.4	121.9
9	CH	3.67 (<i>d</i> , 6.2)	3.69 (<i>d</i>)	60.9	60.7
10	CH ₂	α 3.40 (<i>d</i> , 18.0) β 3.02 (<i>dd</i> , 18.0, 6.2)	3.34 (<i>d</i>) 3.04 (<i>dd</i>)	32.8	32.5
11	C			128.8	128.6
12	C			130.0	129.8
13	C			42.3	42.1
14	C			161.8	161.6
15	CH ₂	α 1.91 (<i>ddd</i> , 12.5, 6.4) β 1.83 (<i>m</i>)	1.93 (<i>m</i>) 1.83 (<i>m</i>)	41.2	41.0
16	CH ₂	2.55-2.58 (<i>m</i>)	2.57- 2.58 (<i>m</i>)	45.8	45.5
NMe	NCH ₃	2.44 (<i>s</i>)	2.46 (<i>s</i>)	41.8	41.6

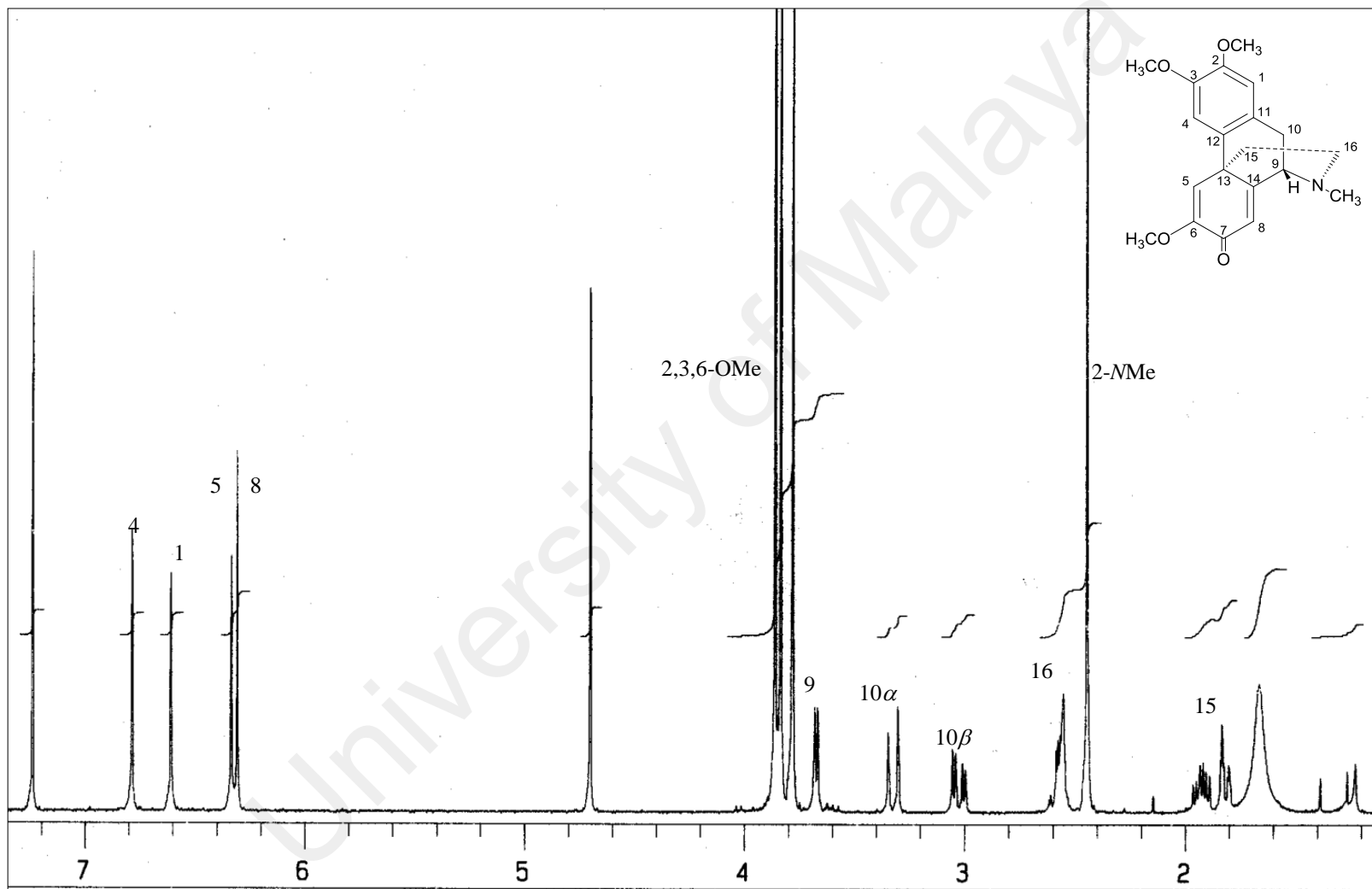


Figure 3.73: ¹H NMR Spectrum of Sebiferine 47

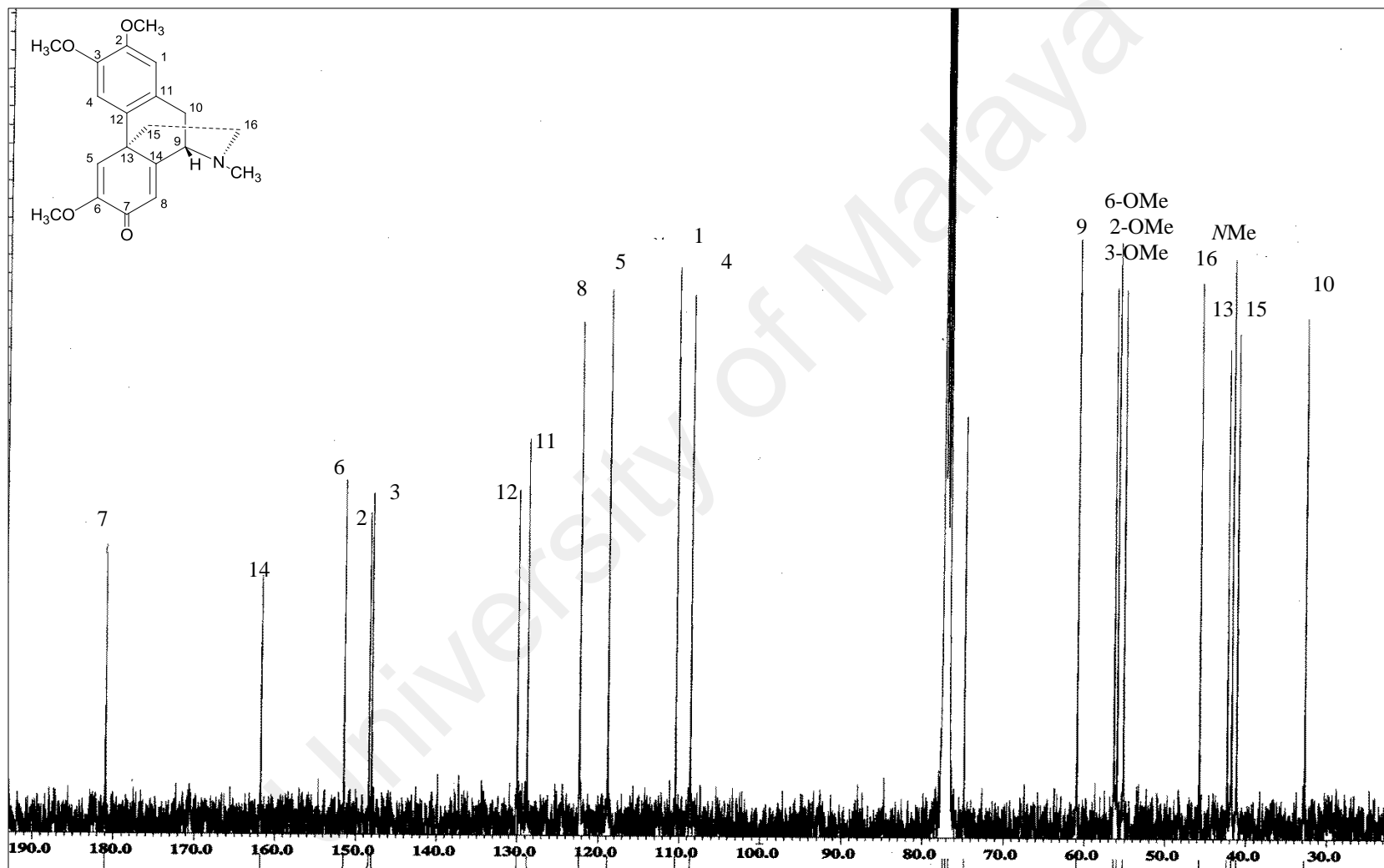
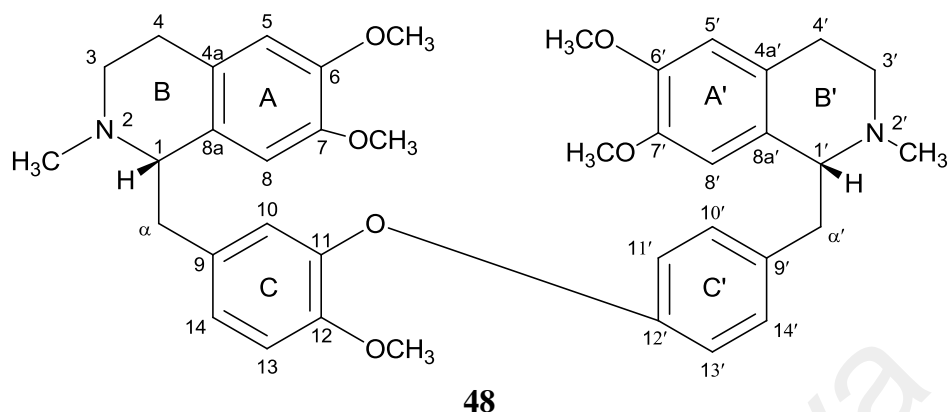


Figure 3.74: ^{13}C NMR Spectrum of Sebiferine 47

3.1.21 *O-O*-dimethylgrisabine **48**



O-O-dimethylgrisabine **48** was obtained as a brownish amorphous powder with $[\alpha]_D^{25}$ -35.0° ($c=0.002$, CHCl_3). The UV spectrum showed absorption maxima at λ_{max} 296 nm which is typical of a bisbenzylisoquinoline conjugated moiety. The ESIMS spectrum revealed a typical type I bisbenzylisoquinoline (BBIQ) with only 1% of the height of the base peak at m/z 639.3432 (calcd. for $\text{C}_{39}\text{H}_{47}\text{N}_2\text{O}_6$, 639.3434), suggesting a molecular formula of $\text{C}_{39}\text{H}_{46}\text{N}_2\text{O}_6$. The mass spectrum of **48** also showed a base peak ion at m/z 206 corresponding to the tetrahydroisoquinoline, thus indicating that this skeleton belonged to the type I BBIQ that only has a single tail-to-tail ether bridge. No intense absorption peak at ν_{max} 3400 indicated that the structure consist only tertiary amine group.

Investigation of the ^1H NMR spectrum (Figure 3.75) indicated the presence of eleven aromatic protons, five O- CH_3 groups, two *N*- CH_3 groups, two $\text{CH}_2\text{-CH}_2\text{-N}$ groups, and two sets of isolated none equivalent methylene groups. The typical of ABX and AA'BB' spin systems for ring C and ring C' were similar to those of 2-norobaberine **115**. Three aromatic protons in ring C (ABX system) resonated as doublet doublet ($J=8.3, 2.0$ Hz) centered at H-14 (δ_{H} 6.75) that *ortho*-coupled with H-13 (δ_{H} 6.80, $d, J=8.3$ Hz) and *meta*-coupled with H-10 (δ_{H} 6.66, $brd, J=2.0$ Hz) and four aromatic protons in ring C' (AA'BB') resonated as two set of doublet that have similar chemical

environment with $J = 8.5$ Hz coupling constant at $\delta_{\text{H}} 6.93$ and $\delta_{\text{H}} 6.71$ belong to H-10', H-14' and H-11', H-13' respectively. The significant features of type I BBIQ was the singlets at $\delta_{\text{H}} 5.96$, $\delta_{\text{H}} 6.00$, $\delta_{\text{H}} 6.45$ and $\delta_{\text{H}} 6.48$ ascribed to H-8', H-8', H-5' and H-5 of rings A and A'.

The ^{13}C NMR spectrum (Figure 3.76) revealed thirty-nine carbons belonging to eleven sp^2 methine carbons (C-5, C-8, C-10, C-13, C-14, C-5', C-8', C-10', C-11', C-13', C-14'), thirteenth sp^2 quaternary carbons (C-4a, C-6, C-7, C-8a, C-9, C-11, C-12, C-4a', C-6', C-7', C-8a', C-9', C-12'), six sp^3 methylene carbons (C- α , C-3, C-4, C- α' , C-3', C-4'), two sp^3 methine carbons (C-1, C-1'), five methoxyl groups (6-OCH₃, 6'-OCH₃, 7-OCH₃, 7'-OCH₃, 12-OCH₃) and two *N*-CH₃ groups (2-NCH₃, 2'-NCH₃) groups. The signature signal of type I BBIQ was the presence of superimposed carbons as followed; C-1 ($\delta_{\text{C}} 64.9$) and C-1' ($\delta_{\text{C}} 64.8$), C-3 ($\delta_{\text{C}} 46.9$) and C-3' ($\delta_{\text{C}} 46.8$), C- α ($\delta_{\text{C}} 40.4$) and C- α' ($\delta_{\text{C}} 40.6$), and C-4 ($\delta_{\text{C}} 25.5$) and C-4' ($\delta_{\text{C}} 25.4$). Therefore, this indicated there was no ether linkage connecting ring A-A' like in 2-norobaberine **115**. The substituents attributable to 6-OCH₃, 6'-OCH₃ and 7-OCH₃, 7'-OCH₃ appeared as singlets at $\delta_{\text{C}} 55.8$ and $\delta_{\text{C}} 55.7$ respectively.

The upper part of the isoquinoline moiety that comprised ring A and ring B was connected to ring C via C- α based on the cross peaks between H-14, H-10 with C- α , and H- α with C-1. Meanwhile, ring A' and ring B' were linked to ring C' via methylene C- α' based on the cross peak of H-14', H-10' with C- α' and H- α' with C-1'. Lastly, *O-O*-dimethylgrisabine **48** was constructed from the connecting of two benzyloisoquinoline units via a single diaryl ether bridge between C-11 and C-12' based on the following 3J (H, C) correlations; H-13/C-11 and H-14'/C-12'. Only one ether bridge was found showed it belong to type I BBIQ. The ether bridges located between C-11-O-C-12'

On the basis of the above evidence and upon comparison with the literature values (Table 3.22), it is concluded that this alkaloid could be none other than (-)-*O-O*-dimethylgrisabine **48** (Ahmad & Cava, 1977; Damas et al., 1985)

Table 3.22: ^1H and ^{13}C -NMR Data of *O-O*-dimethylgrisabine **48**.

Position	Unit	^1H - NMR CDCl ₃ , 400 MHz <i>O-O</i> -dimethylgrisabine 48 δ (J, Hz)	^1H - NMR CDCl ₃ , 100MHz 48 δ	^{13}C - NMR CDCl ₃ , 100 MHz (Damas et al., 1985) δ
1	CH	3.63 (<i>dd</i> , 13.6, 5.4)	64.8	63.9
<i>N</i> -Me	<i>N</i> -CH ₃	2.41 (<i>s</i>)	42.7	43.7
3	CH ₂	3.07 (<i>m</i>) 2.76 (<i>m</i>)	46.9	51.0
4	CH ₂	3.03 (<i>m</i>) 2.54 (<i>m</i>)	25.5	28.7
4a	C		126.0	130.9
5	CH	6.48 (<i>s</i>)	111.2	110.9
6	C		147.3	148.3
6-OMe	O-CH ₃	3.72 (<i>s</i>)	55.8	54.9
7	C		146.4	143.8
7-OMe	O-CH ₃	3.54 (<i>s</i>)	55.7	54.9
8	CH	6.00 (<i>s</i>)	110.9	116.7
8a	C		128.1	127.7
α	CH ₂	2.99 (<i>dd</i> , 13.6, 5.4) 2.65 (<i>m</i>)	40.4	37.5
9	C		132.9	130.9
10	CH	6.66 (<i>d</i> , 2.0)	122.5	116.5
11	C		144.6	149.0
12	C		149.8	146.6
12-OMe	O-CH ₃	3.76 (<i>s</i>)	56.2	55.9
13	CH	6.80 (<i>d</i> , 8.3)	112.5	110.7
14	CH	6.76 (<i>dd</i> , 8.3, 2.0)	126.1	123.5
1'	CH	3.58 (<i>m</i>)	64.9	61.4
<i>N</i> '-Me	<i>N</i> '-CH ₃	2.45 (<i>s</i>)	42.6	42.2
3'	CH ₂	3.14 (<i>m</i>) 2.72 (<i>m</i>)	46.8	45.3
4'	CH ₂	3.03 (<i>m</i>) 2.50 (<i>m</i>)	25.4	25.6
4a'	C		126.0	127.2
5'	CH	6.45 (<i>s</i>)	111.2	105.8
6'	C		147.3	151.6
6'-OMe	O-CH ₃	3.74 (<i>s</i>)	55.8	56.0
7'	C		146.3	137.0
7'-OMe	O-CH ₃	3.51 (<i>s</i>)	55.7	60.4
8'	CH	5.96 (<i>s</i>)	111.0	147.5
8'a	C		128.0	127.7
α'	CH ₂	3.09 (<i>m</i>) 2.70 (<i>m</i>)	40.6	39.5
9'	C		133.8	139.0
10'	CH	6.93 (<i>d</i> , 8.5)	130.8	131.4
11'	CH	6.71 (<i>d</i> , 8.5)	116.8	121.1
12'	C		156.4	152.2
13'	CH	6.71 (<i>d</i> , 8.5)	116.8	122.2
14'	CH	6.93 (<i>d</i> , 8.5)	130.8	127.8

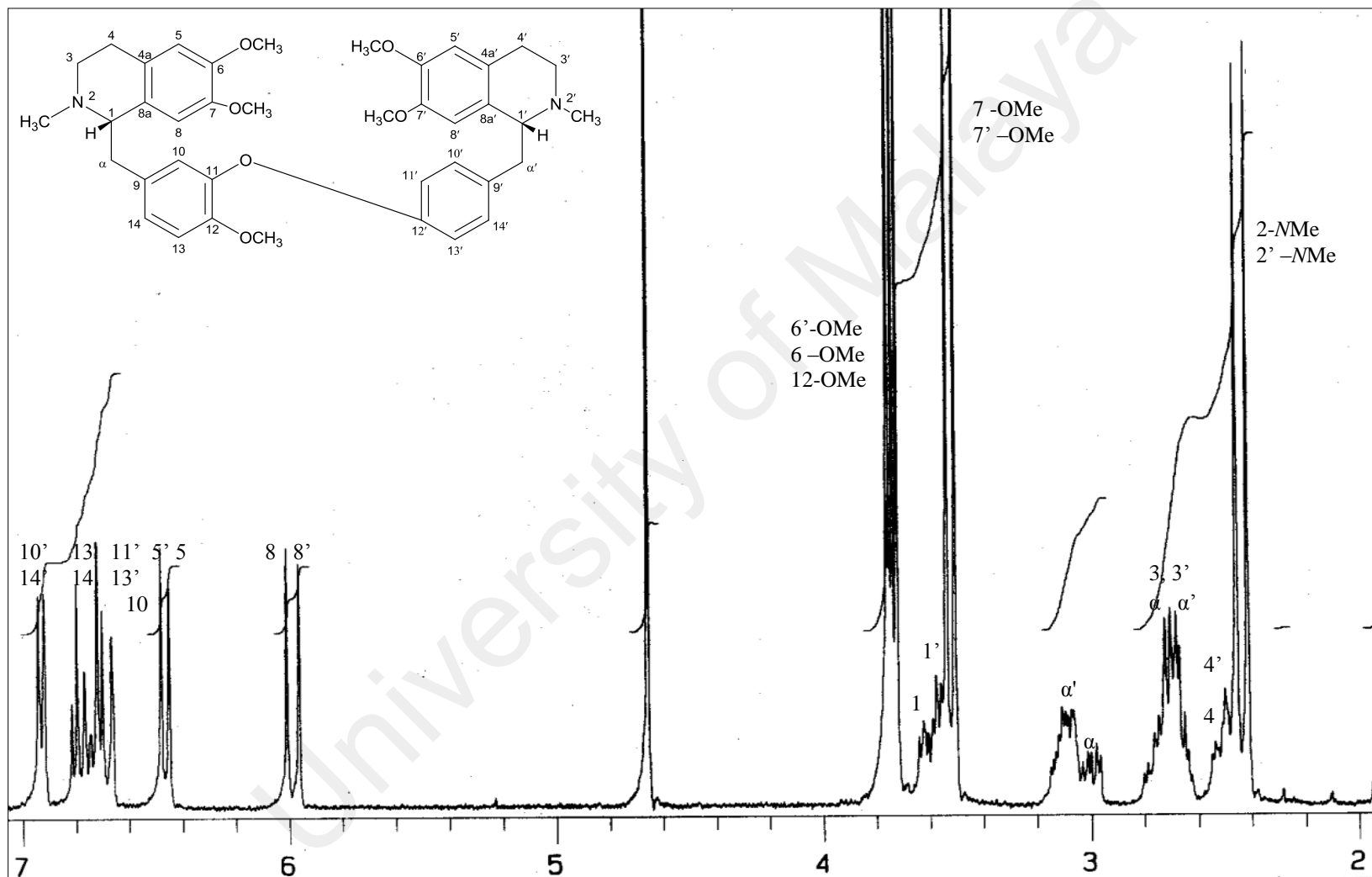


Figure 3.75: ¹H NMR Spectrum of *O-O*-dimethylgrisabine 48

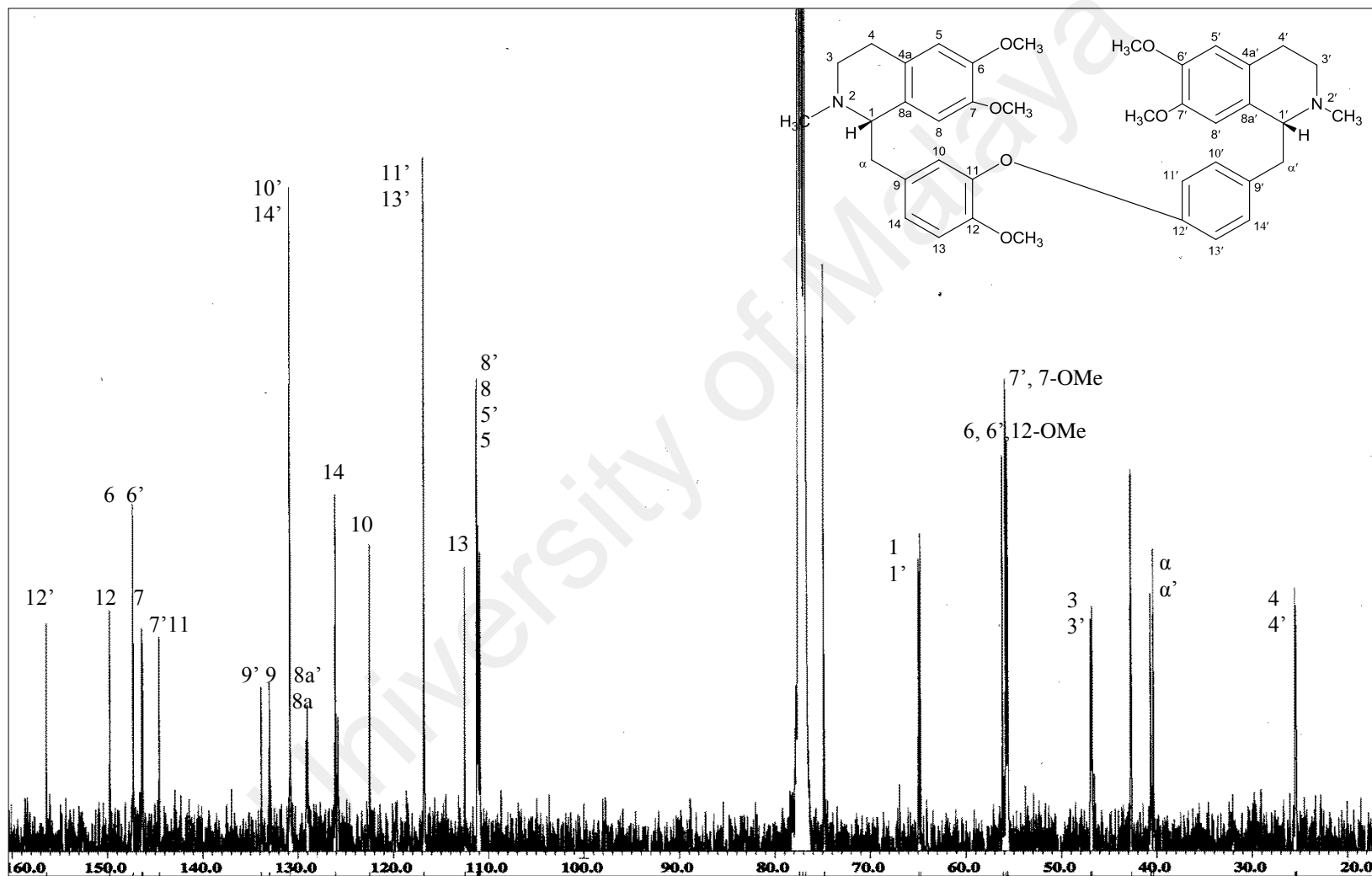


Figure 3.76: ^{13}C NMR Spectrum of *O-O*-dimethylgrisabine **48**

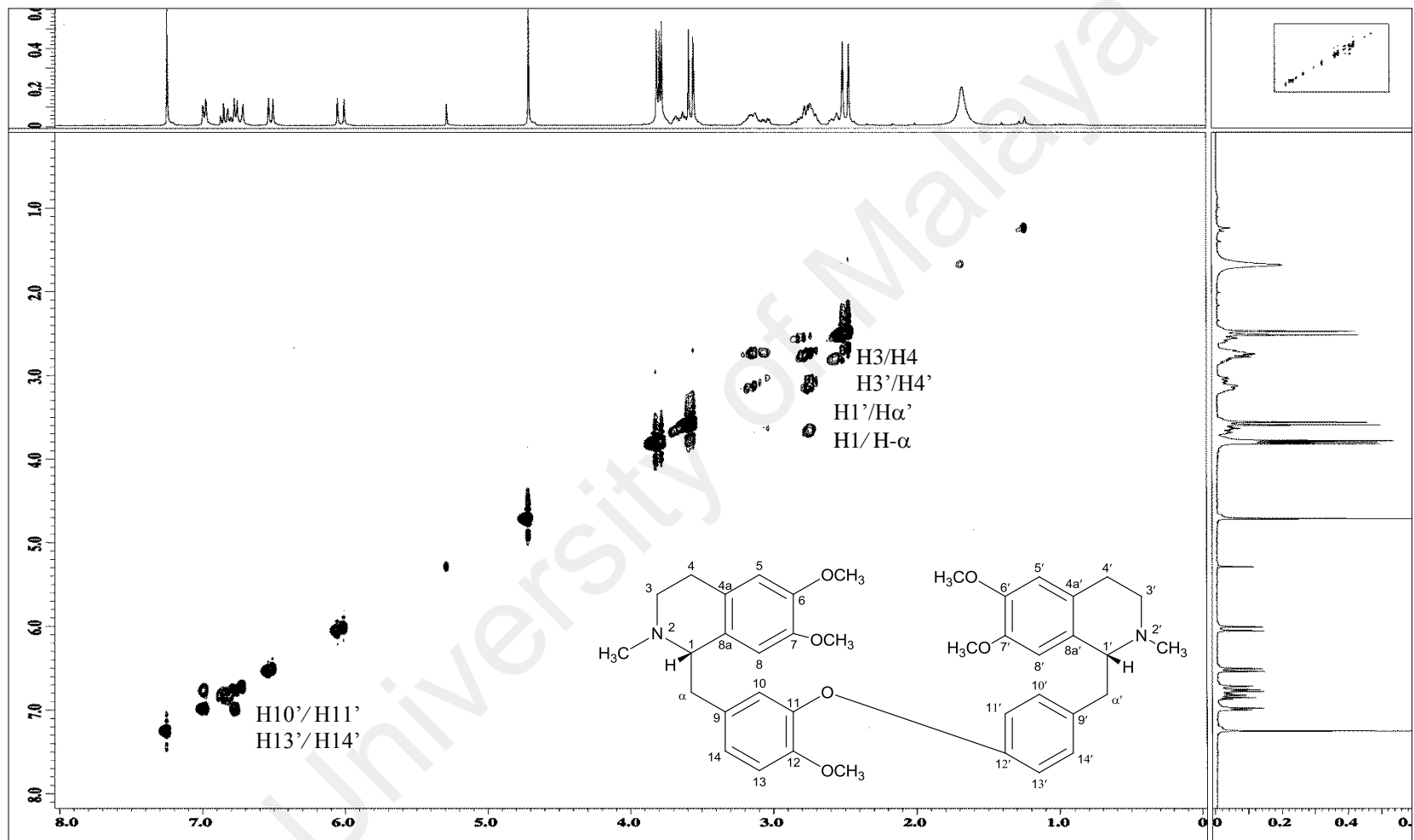
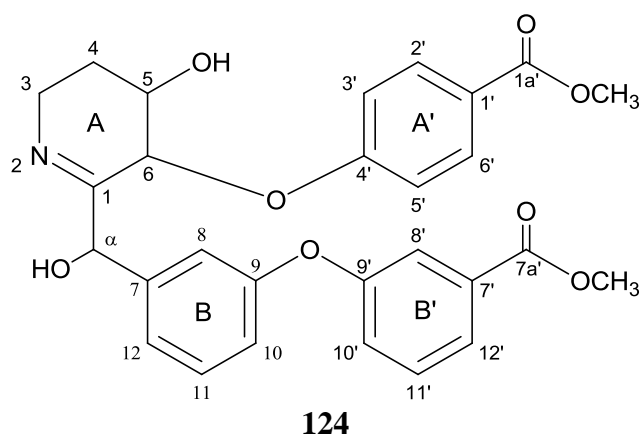


Figure 3.77: COSY Spectrum of *O,O*-dimethylgrisabine **48**

3.1.22 Cornerin A 124



Cornerin A **124** was purified as brownish amorphous solid. The IR spectrum exhibited an absorption band at 1260, 1733 and 3400 cm^{-1} that was characteristic of the C-O-C stretching, an ester group and hydroxyl group respectively. The EIMS showed a pseudo-molecular ion peak $[\text{M}+\text{H}]^+$ at m/z 506.3329 giving a potential molecular formula of $\text{C}_{28}\text{H}_{27}\text{NO}_8$ (calcd. for $\text{C}_{28}\text{H}_{28}\text{NO}_8$, 506.1815).

^1H NMR spectrum Figure 3.80 showed the presence of twelve aromatic protons, two O- CH_3 and one $\text{CH}_2\text{-CH}_2\text{-N}$ groups and additional aliphatic protons. H-11 in ring B resonated as doublet doublet (δ_{H} 7.63, $J= 8.2, 8.0$ Hz) that *ortho*-coupled with H-12 (δ_{H} 8.32, *dt*, $J= 8.0, 2.7, 1.3$ Hz) and H-10 (δ_{H} 8.40, *ddd*, $J= 8.2, 2.3, 1.1$ Hz). Meanwhile, H-8 resonated as triplet ($J=2.0$ Hz) indicated that it was *meta*-coupled with H-10 and H-12. The remaining four aromatic protons in ring B' showed similar splitting pattern and chemical shift as in ring B. The spectrum also established two set of doublet ($J= 8.5$ Hz) at δ_{H} 7.15, 7.13 and δ_{H} 6.81, 6.80 belong to H-2', H-6' and H-3', H-5' respectively, therefore indicated the presence of a *para*-disubstituted benzene ring system. Two methoxyl singlets at δ_{H} 3.73 and 3.93 referring to methoxyl groups attached to C-1a' and C-7a' respectively.

The ^{13}C NMR spectrum (Figure 3.81) revealed twenty-eight carbons in the structure which belong to twelve sp^2 methines (C-2', C-3', C-5', C-6', C-8, C-10, C-11, C-12, C-8', C-10', C-11', C-12'), nine sp^2 quaternary carbons (C-1, C-1a', C-1', C-4', C-7, C-7', C-9, C-9', C-7a'), three sp^3 methine (C-5, C-6, C- α), two sp^3 methylenes (C-3, C-4) and two methoxyl (1a'-OCH₃, 7a'-OCH₃) carbon signals. In addition, the presence of carbonyl group attached to C-1a' and C-7a' were shown at δ_{C} 159.2 and δ_{C} 165.1 respectively.

The NOESY spectrum (Figure 3.82) showed correlations between H-10/H-11, H-12/H-11, H-10'/H-11', H-12'/H-11', H-2'/H-3', H-6'/H-5'.

The location of ester group attached in ring A' was identified by cross peaks of 1a'-OCH₃ with C1a' (δ_{C} 159.2) in HMBC spectrum (Figure 3.84). Extra quaternary carbon was assigned to C-4' and C-6 for the placement of diaryl ether bridges between C-4'-O-C-6 (rings A-A') by correlation of H-2', H-6' with C-4' and H-5 with C-6. The proposed connection between ring A and ring B was via CH-OH attach to C- α (δ_{C} 70.5). Furthermore, the correlation between H-11 to quaternary carbon C-9 (ring B) and H-11' to quaternary carbon C-9' (ring B') demonstrated another diaryl ether bridges situated at C-9-O-C-9'. The placement of another ester groups in ring B' was identified by correlation between 7a' and C-7a' OCH₃ with C7a' (δ_{C} 165.1).

In depth analysis of spectroscopic data pointed out that this alkaloid is a new isoquinoline that possibly resulted from biochemical oxidation of benzyltetrahydroisoquinoline units (Wu et al., 1980). It is a new compound, thus named as cornerin A. The NMR assignments of **124** were presented in Table 3.23.

Table 3.23: ^1H , ^{13}C -NMR and HMBC Data of Cornerin A **124**

Position	Unit	^1H - NMR 124 CDCl ₃ , 400 MHz (δ (Hz))	^{13}C - NMR 124 (δ)	HMBC (^1H - ^{13}C)
1	C		165.1	
3	CH ₂	3.55 (<i>m</i>)	39.7	
4	CH ₂	2.20-1.18 (<i>m</i>)	29.7	
5	CH	3.58 (<i>m</i>)	70.5	
6	CH	3.58 (<i>m</i>)	70.5	
α	CHOH	3.58 (<i>m</i>)	70.5	
7	C		130.4	
8	CH	8.84 (<i>t</i> , 2.0, 1.8)	125.1	
9	C		158.0	
10	CH	8.40 (<i>ddd</i> , 8.2, 2.3, 1.1)	127.9	8
11	CH	7.63 (<i>dd</i> , 8.2, 8.0)	129.8	7, 9
12	CH	8.32 (<i>dt</i> , 8.0, 2.7, 1.3)	135.7	8
1'	C		129.7	
1a'	C=O		159.2	
1a'-OMe	O-CH ₃	3.73 (<i>s</i>)	52.8	1a'
2'	CH	7.15 (<i>d</i> , 8.5)	130.4	1', 4'
3'	C	6.81 (<i>d</i> , 8.5)	114.1	5'
4'	C		159.2	
5'	C	6.80 (<i>d</i> , 8.5)	114.1	3'
6'	C	7.13 (<i>d</i> , 8.5)	130.4	1', 4'
7a'	C=O		165.1	
7a'-OMe	O-CH ₃	3.93 (<i>s</i>)	55.3	7a'
7'	C		130.4	
8'	CH	8.81 (<i>t</i> , 2.0, 1.8)	124.6	
9'	C		158.0	
10'	CH	8.37 (<i>ddd</i> , 8.2, 2.3, 1.1)	127.4	8'
11'	CH	7.60 (<i>dd</i> , 8.2, 8.0)	129.6	7', 9'
12'	CH	8.30 (<i>dt</i> , 8.0, 2.7, 1.3)	135.3	8'

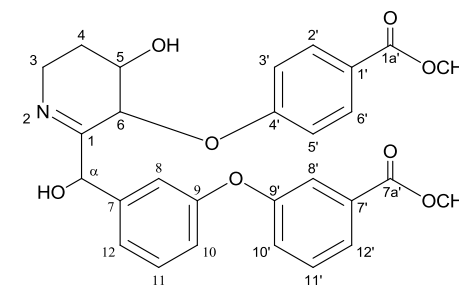
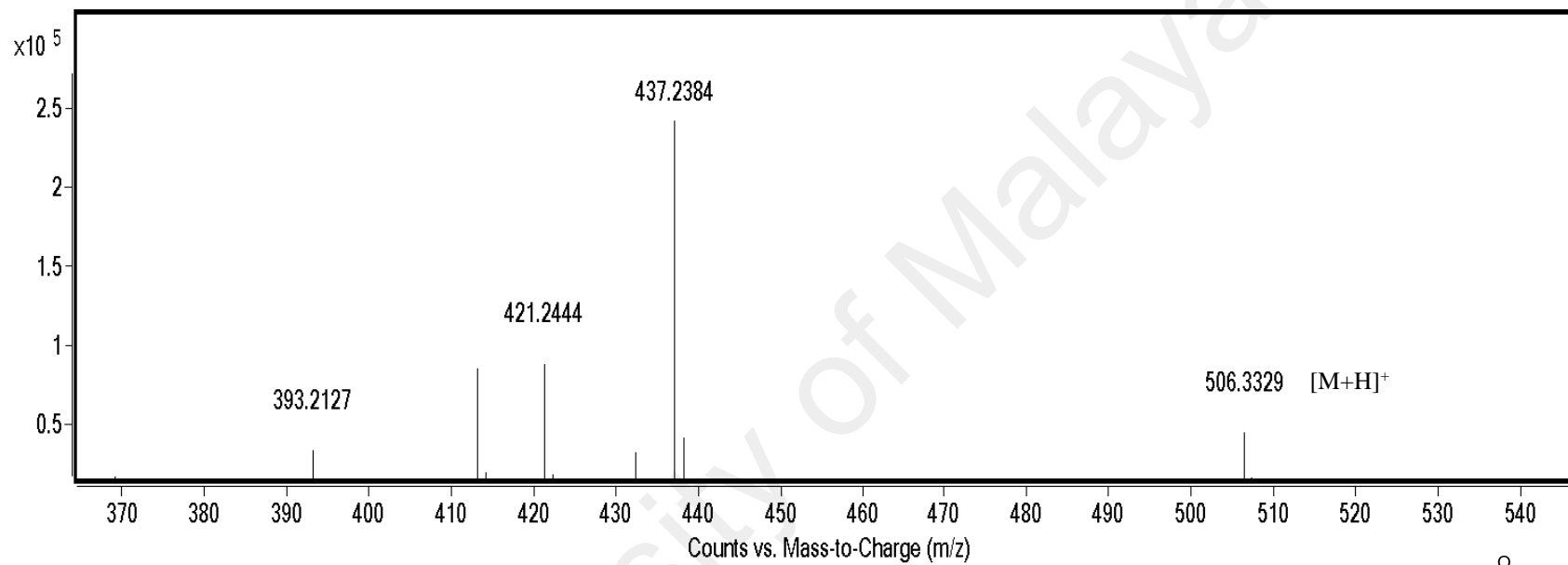


Figure 3.78: EIMS Spectrum of Cornerin A 124

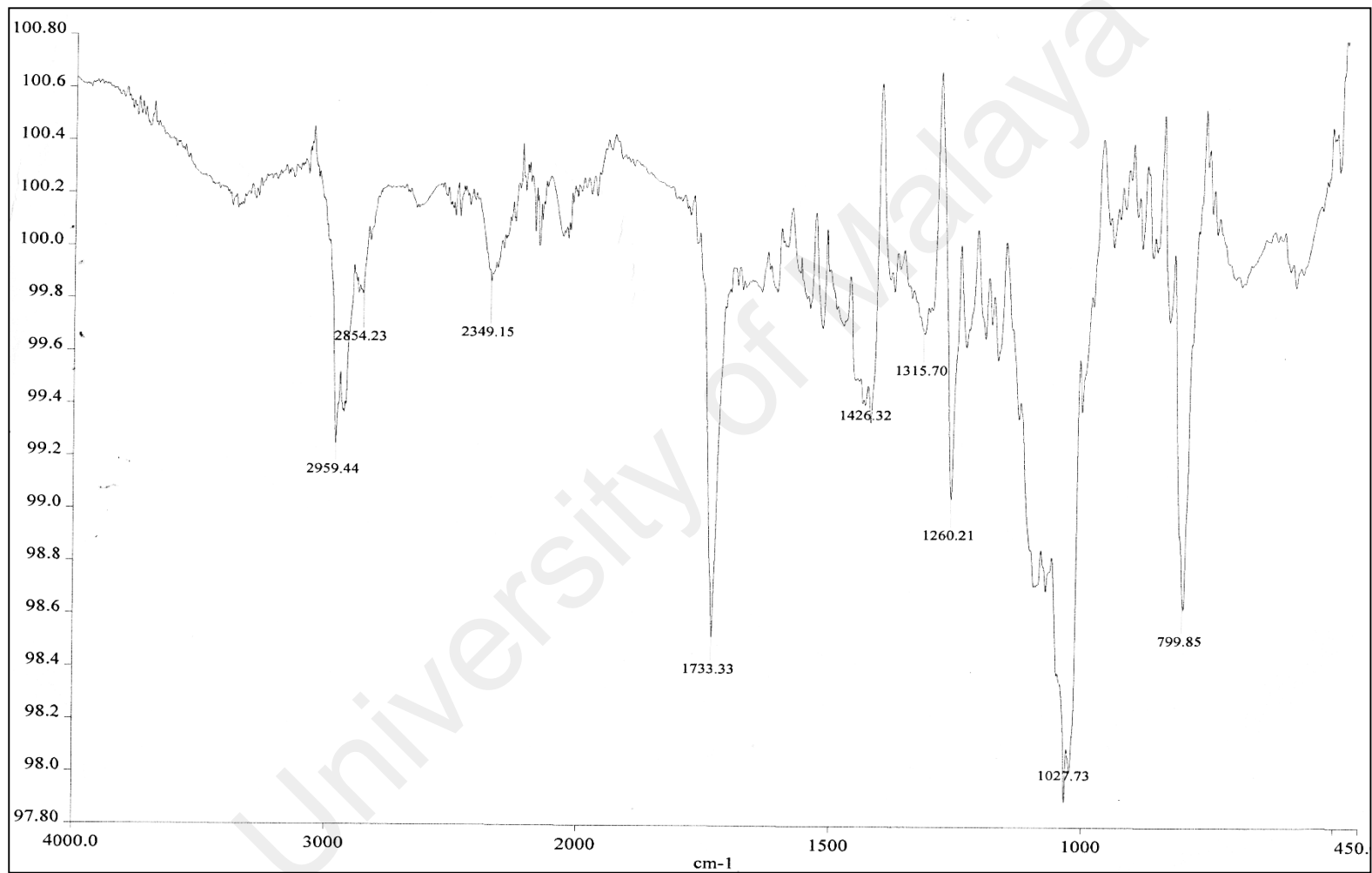


Figure 3.79: Infrared Spectrum of Cornerin A **124**

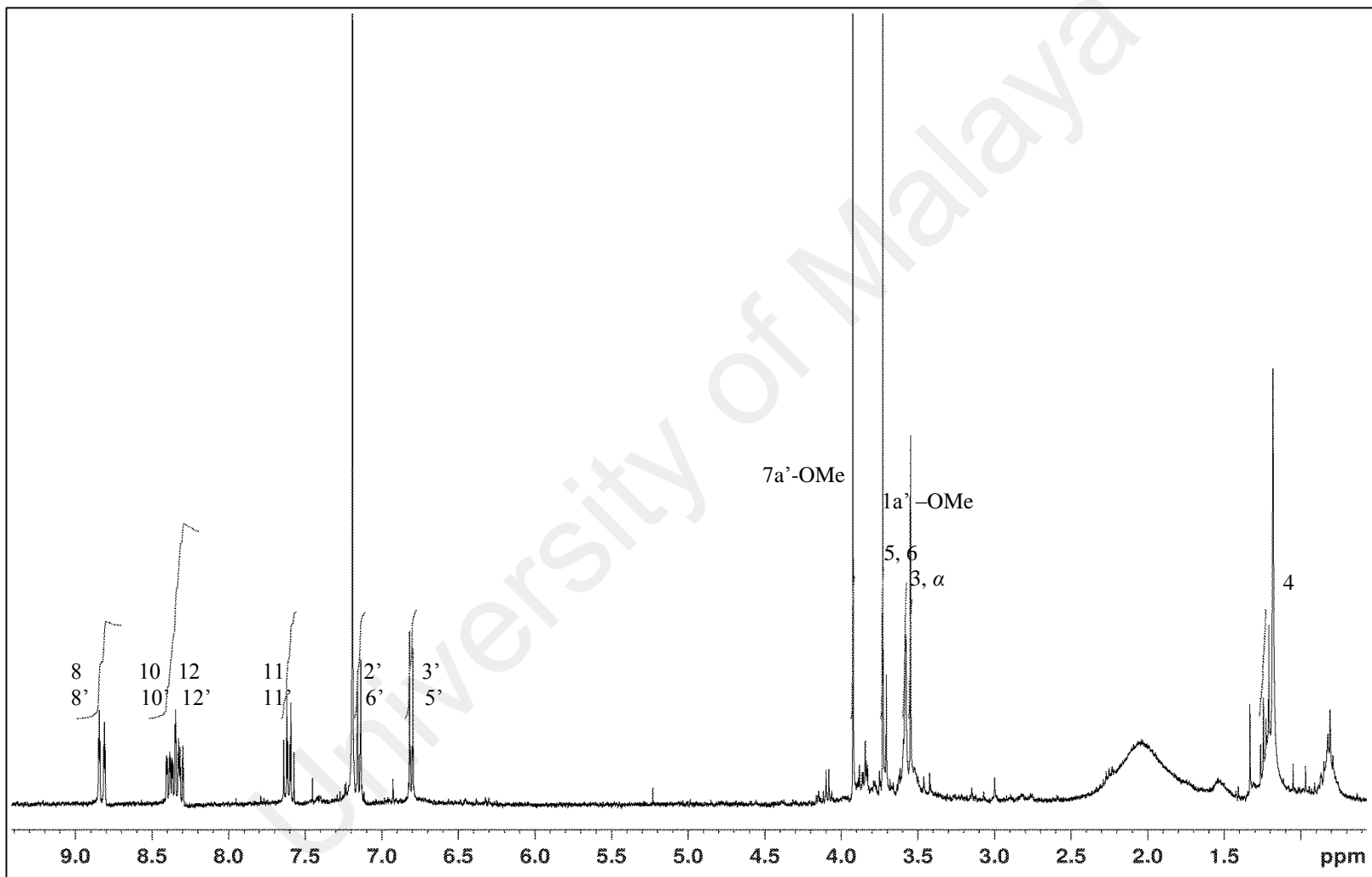


Figure 3.80: ¹H NMR Spectrum of Cornerin A 124

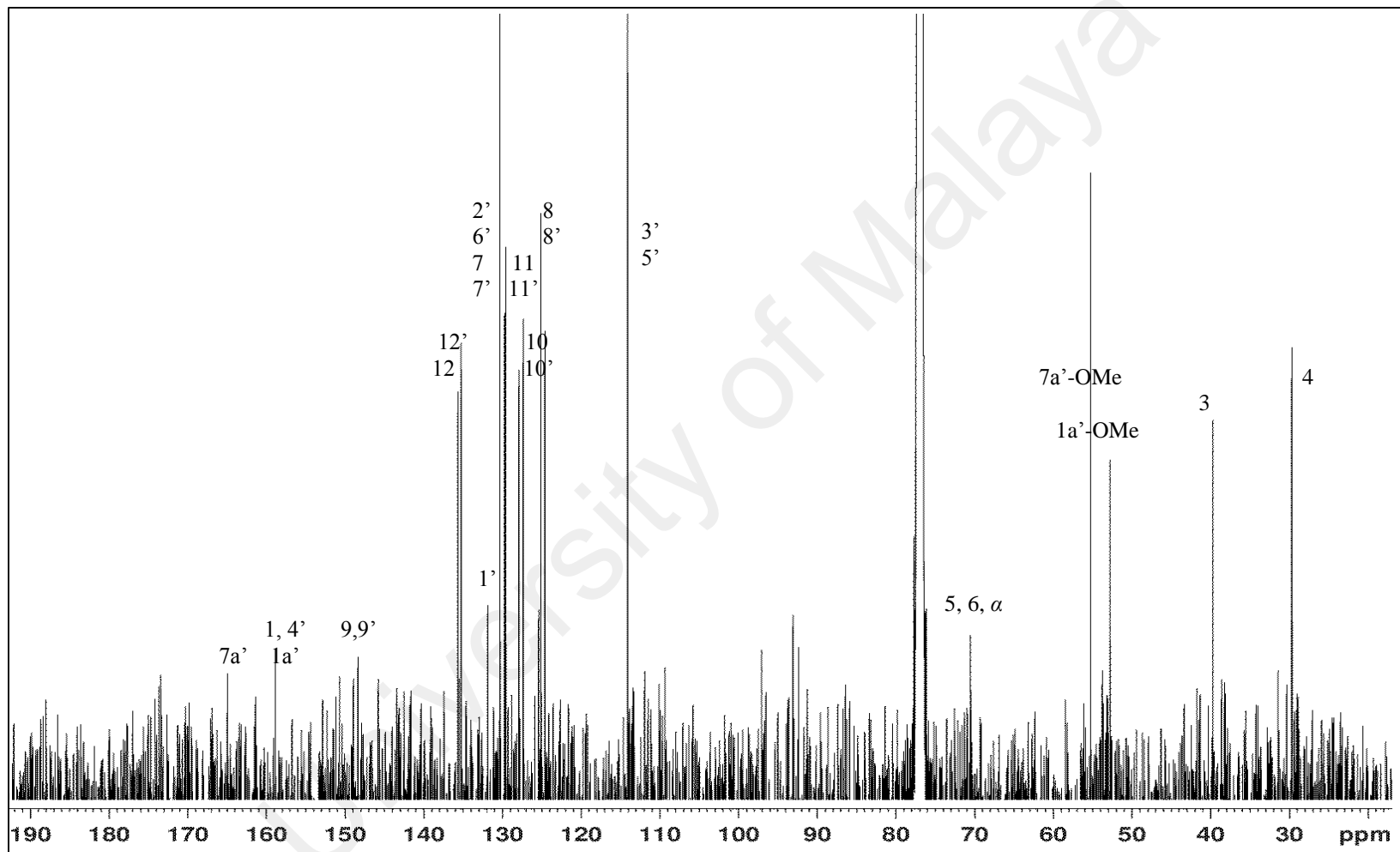


Figure 3.81: ^{13}C NMR Spectrum of Cornerin A 124

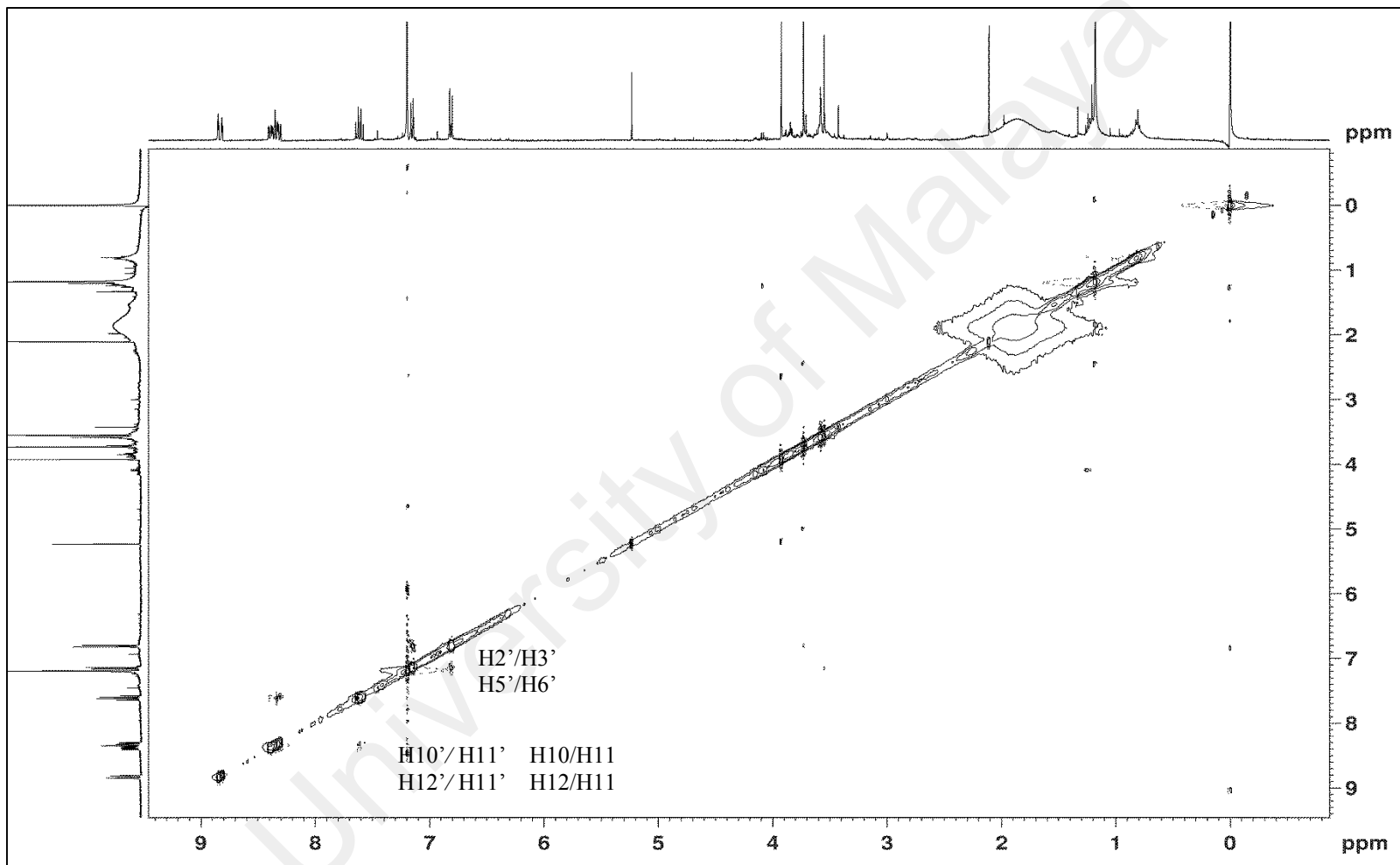


Figure 3.82: NOESY Spectrum of Cornerin A 124

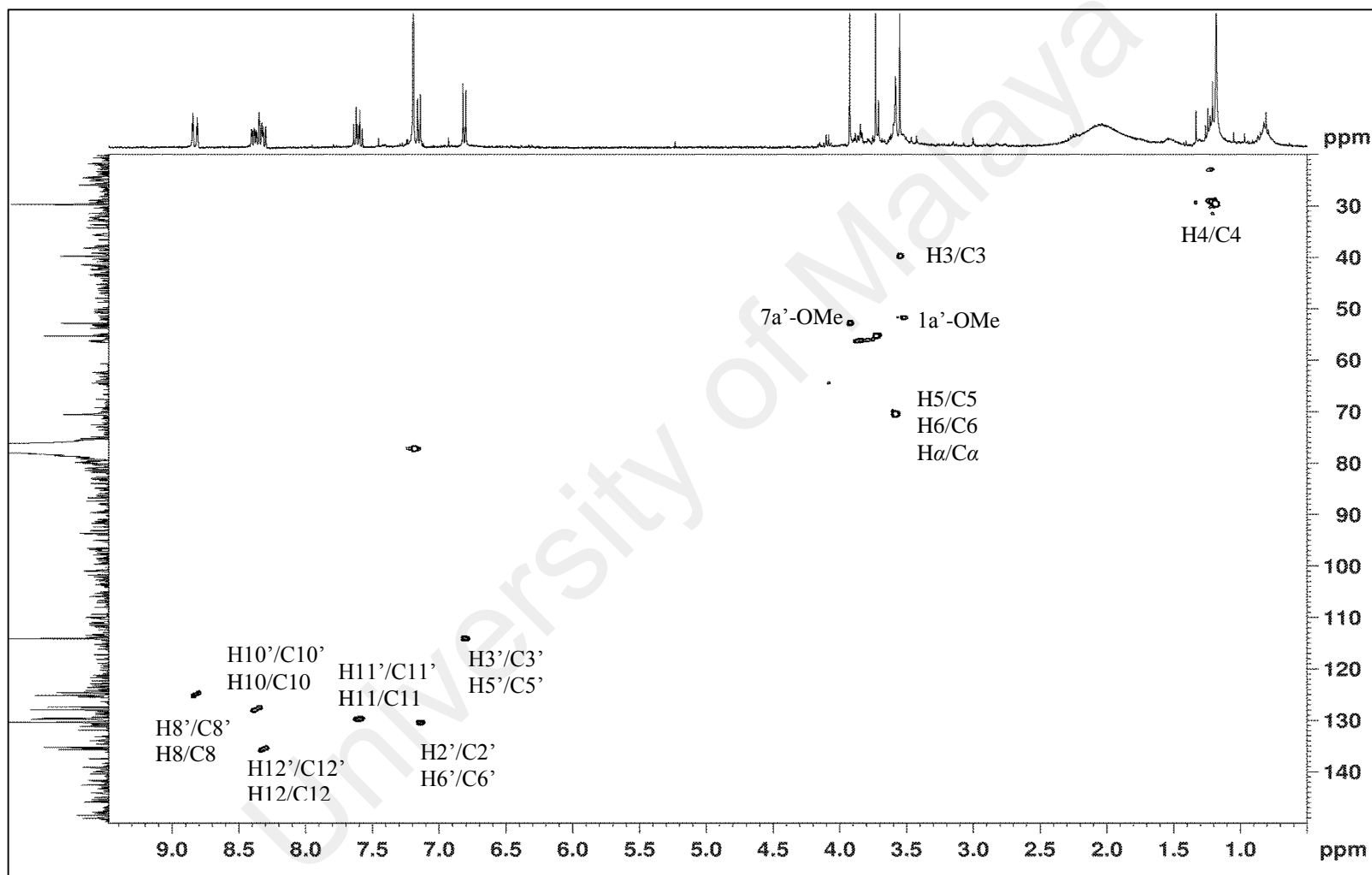


Figure 3.83: HSQC Spectrum of Cornerin A 124

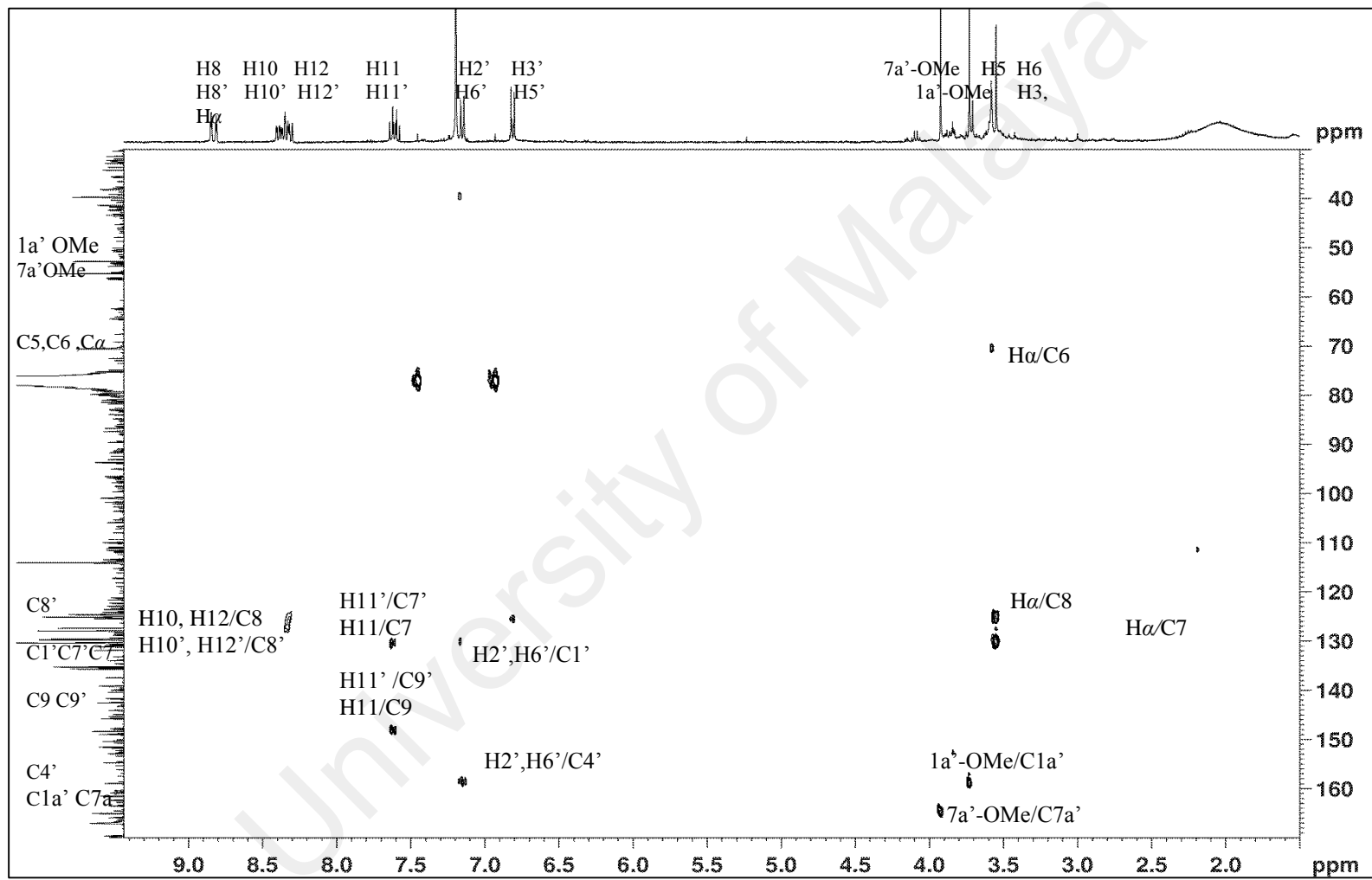


Figure 3.84: HMBC Spectrum of Cornerin A 124

CHAPTER 4: BIOACTIVITY

4.1 Introduction

Vectors are insects that carry infectious agents such as viruses, protozoa and bacteria. Examples of vectors include mosquitoes, fleas, tick and sand flies. Often or known as vector-borne diseases, they carry and transmit numerous diseases to humans. More than one billion people are infected and more than one million people die annually from vector-borne disease. Mosquitoes have become the main vectors for diseases, for example *Aedes* mosquitoes are responsible for dengue, West Nile virus and Chikungunya. Meanwhile, *Culex* mosquitoes transmit Japanese Encephalitis (JE), filariasis disease and *Anopheles* mosquitoes carry malaria infection as shown in Figure 4.1 (WHO, 2014). There are over 3000 mosquito species worldwide with 434 species detected in Malaysia. Out of these species, 75 belong to *Anopheles* mosquito with 9 detected to be vectors of malaria in Malaysia (Rahman et al., 1997).




Mosquitoes	Diseases vector
 <i>Aedes</i>	Dengue, West Nile virus and Chikungunya
 <i>Culex</i>	Japanese Encephalitis (JE), filariasis
 <i>Anopheles</i>	Malaria

Figure 4.1: Vector-borne Disease from Mosquito.

Malaysia lies within the equatorial zone with suitable temperatures and humidity for the development, reproduction, and survival rate of mosquitoes. Malaria is a parasitic protozoa disease from *Plasmodium* that triggers fever, chills and flu-like illness after seven days after being bitten by mosquito. Until now, there is no commercially available vaccine against malaria.

Malaria is caused by the infection of the red blood cells with parasites from genus *Plasmodium*. Most cases of severe malaria were caused by *Plasmodium falciparum*, followed by *P. vivax*, *P. knowlesi*, *P. malariae* and *P. ovale*. In 2013, World Health Organization (WHO) estimated 198 million cases were reported with 584,000 deaths globally. Malaria is considered endemic throughout tropical and subtropical countries (WHO, 2014). Among that, 3850 cases were reported with 14 deaths in Malaysia for malaria transmitted by *Anopheles leucosphyrus* mosquitoes (William et al., 2013; Yusof et al., 2014). Reduction in the number of malaria cases has been observed and achieved in Malaysia. Malaysia is in the pre-elimination phase of malaria control and aims to be malaria-free by 2020. However, a significant increase in *P. knowlesi* (Figure 4.2) cases has been observed in Malaysia between 2004 and 2011 and this trend threatens malaria elimination (Barber et al., 2012; Yusof et al., 2014). Chloroquine **126**, an antimalarial drug was first used in Peninsular Malaysia in 1963. After approximately 10 years of used, mutation within parasite *P. falciparum* conferred the resistance toward chloroquine (Health, 2014). The current drug, artemisinin **128**, is also nowadays become redundant and no effect toward parasites strain in 4 countries; Cambodia, Myanmar, Thailand and Vietnam (WHO, 2013). Historically, the majority of the antimalarial drugs have been derived from plants; example artemisinin **128**, isolated from the Chinese herb *Artemisia annua* and quinine **125** from *Cinchona pubescens* (Newman & Cragg, 2007). The evaluation of discovery on antimalarial drug derived from plants with its mechanism of action will be further discussed in section 4.4.

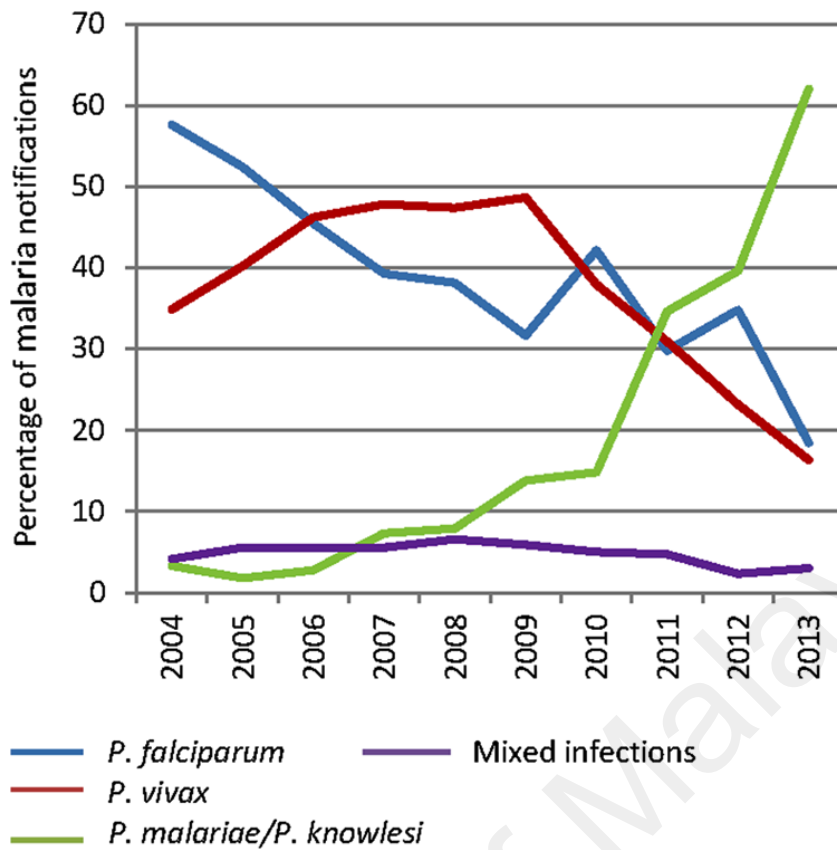
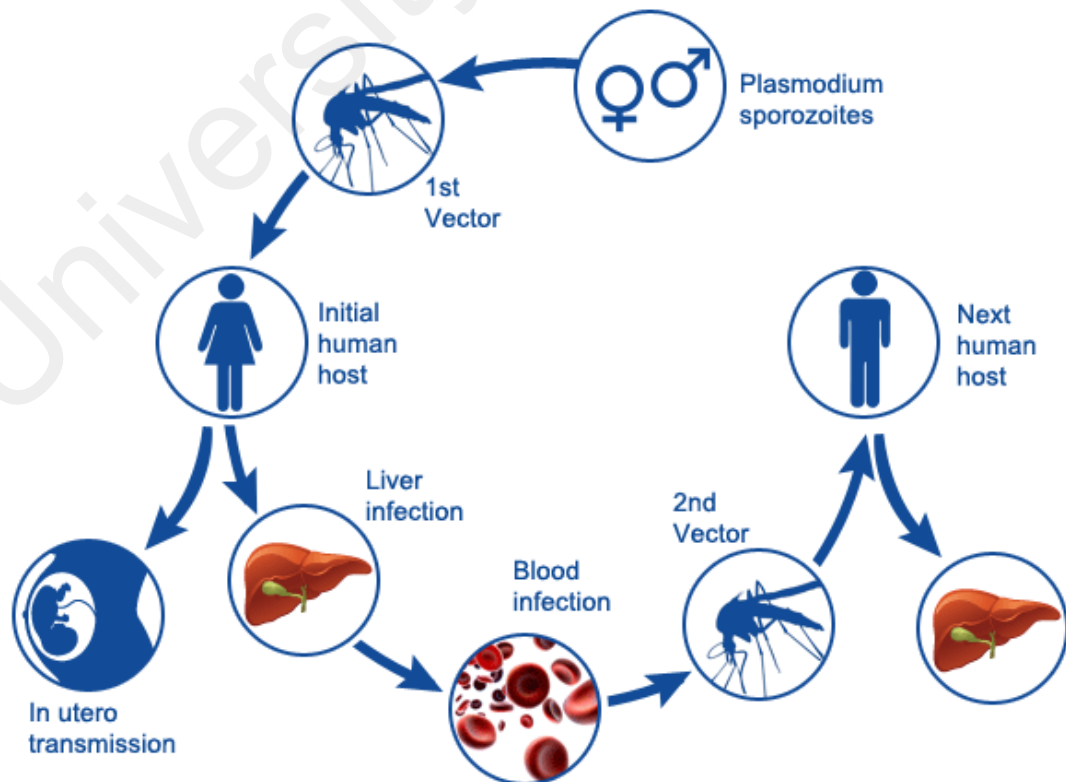


Figure 4.2: Percentage of Malaria Based on *Plasmodium* Parasite, 2004-2013.

4.2 Life Cycle of Malaria



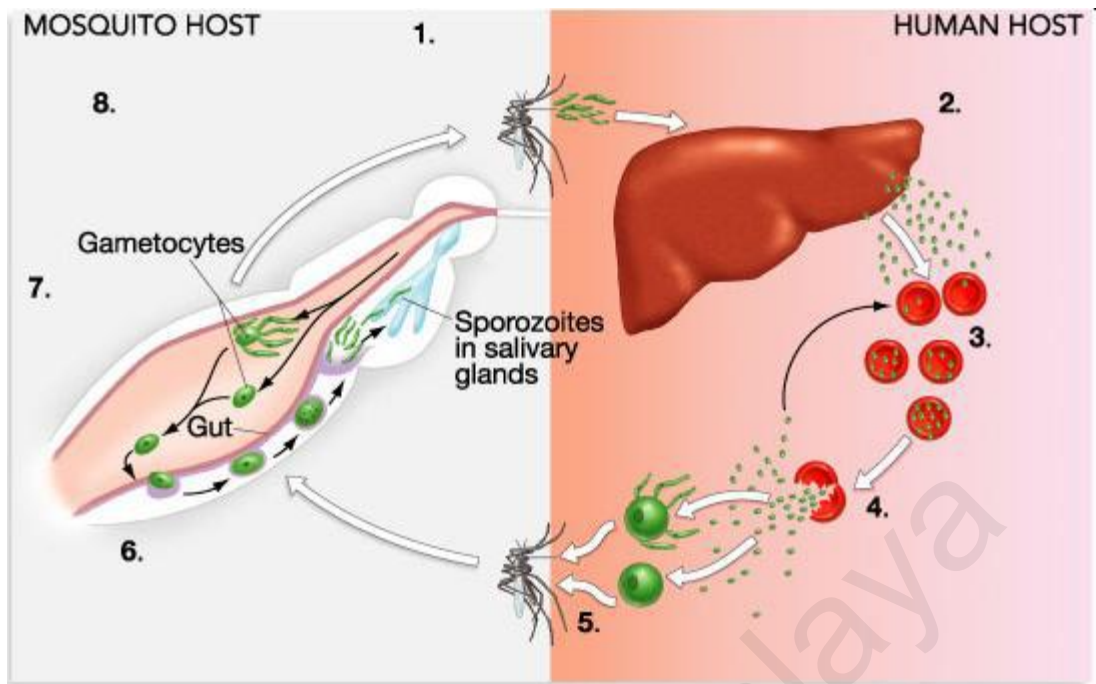


Figure 4.3: Life Cycle of Malaria Transmission (Malaria, 2015)

It is important to know the transmission of the malaria parasite (Figure 4.3) in order to determine the suitable treatment based on the interaction of parasites in the human host. The life cycle of mosquitoes are divided into several stages; liver stage, blood stage, transmission stage and also mosquito stage. At first, *Plasmodium* sporozoites are introduced into the host's skin from mosquito saliva. The sporozoites in a blood vessel will infect the liver within 30 minutes and start replicating. Drugs that can target liver stage such as primaquine are important to prevent a disease from developing and to provide 'radical cure' for *Plasmodium vivax* and *Plasmodium ovale*. After 5 to 10 days, the liver cell will burst and merozoites will invade the red blood cells and develop rapidly, causing symptomatic high fevers. At the blood stage, drugs such as chloroquine are used to control the symptoms of the disease and mortality. The parasite will experience several cycles of asexual reproduction in the transmission cycle and will differentiate into male and female gamocytes. Next, the gamocytes will fuse to form zygote that further develops into new sporozoites. New sporozoites in mosquitoes will

infect humans for next cycle onwards. Drugs that target the transmission and mosquito stage are essential to prevent the infection of other humans (Biamonte et al., 2013).

4.3 Oxidative Stress

Oxidation is a process where chemical substances take oxygen or lose electrons in our metabolism. Oxygen is the ultimate electron acceptor in electron flow system that produces energy in the form of ATP. In the meantime, if electron flow becomes uncoupled (transferred of unpaired electron), it will generate free radicals, also known as reactive oxygen species (ROS). ROS comprise of free radicals such as superoxide anion radicals ($O_2\cdot^-$), hydroxyl radicals (OH \cdot), nitric oxide radical (NO \cdot) and non-free radical species such as hydrogen peroxide (H_2O_2) and singlet oxygen (1O_2) (Greve et al., 1999; Yang et al., 2009). Excessive production of ROS may lead to many diseases such as Alzheimers, Parkinson, arthritis, aging, cancer and malaria (Pracheta et al., 2011). During malaria infection, ROS are produced and may lead to erythrocyte membrane damage and also contribute towards anaemia in host (Kremsner et al., 2000). Besides that, malaria infection also induces the generation of hydroxyl radical (OH \cdot) in the liver that cause oxidative stress and apoptosis. It was proven in publication by (Atamna & Ginsburg, 1993) that erythrocytes infected with *P.falciparum* produce about twice as much OH radicals and H_2O_2 compared to normal erythrocytes (Percario et al., 2012).

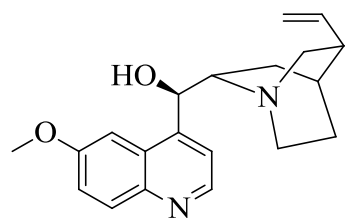
The human body has its own antioxidant system to protect itself from free radicals. However, some ROS still escape to cause damage specifically in acute malaria disease. In order to minimize damage to the human body, synthetic antioxidants such as BHA, BHT and ebselen are used in many products today (Augustyniak et al., 2010). The disadvantages of synthetic antioxidants are that it causes damage to the liver and may be carcinogenic to our body. Hence, natural origin antioxidants as an alternative are

considered much safer and less toxic to protect the human body from free radicals and retard the progress of chronic diseases.

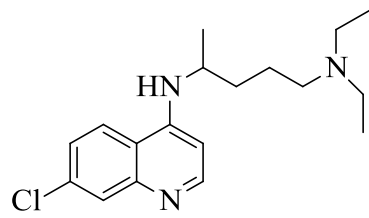
4.4 Drugs Used in the Malaria Treatment

(Bero et al., 2009) has found that natural products have been lead compounds for new malaria drugs over the last period. *In-vitro* screening has been successful in detecting 25,000 pure compounds belonging to different skeletons potent against the parasite with $IC_{50} \leq 1 \mu\text{M}$. However, only 300 compounds potent for antimalarial activities have been isolated from plants used in traditional medicine. Among those compounds which were suggested to be active in malaria, only a few skeletons (Figure 4.4) have been clearly evaluated to be active in patients and animal models. Among the compounds listed, six belong to alkaloid structures, namely; quinine **125**, chloroquine **126**, cryptolepine **130**, strictosamide **132**, protopine **133** and febrifugine **134**.

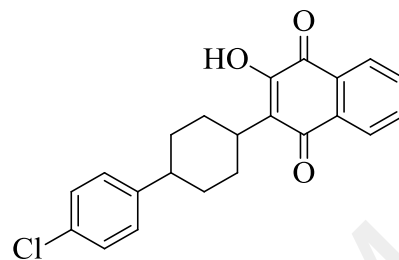
The oldest and effective antimalarial drug since 1820 for malaria is quinine **125**, which was isolated from the bark of *Cinchona pubescens*. Quinine **125** served as a lead structure for the derivatives and synthesis of several antimalarial drugs such as chloroquine **126**, atovaquone **127** and mefloquine. In 2006, it is no longer recommended by WHO as a first-line treatment for malaria, and it should be used only when artemisinin are not available. Artemisinin **128** was first isolated from the leaves of the sweet wormwood (*Artemisia annua*) in 1971. Treatments comprising of an artemisinin derivative (artemisinin-combination therapies, ACTs) are now standard treatment worldwide for malaria disease against parasite, *P. falciparum*. Chemically, artemisinin **128** structure consists of sesquiterpene lactone with an unusual peroxide bridge. This peroxide bridge is believed to be responsible for the drug's mechanism of action. The first signs that the *P. falciparum* is not killed by artemisinin **128** drugs can be seen in Cambodian patients with longer times for their fever to clear. This constant threat of



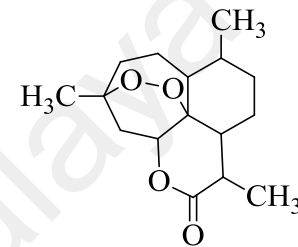
125



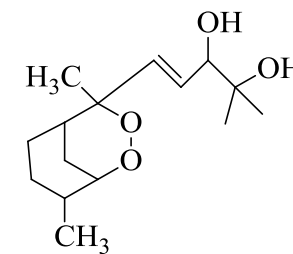
126



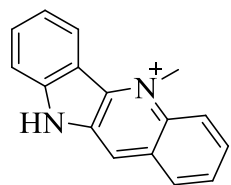
127



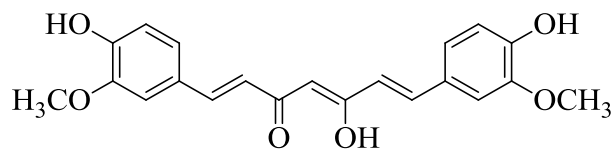
128



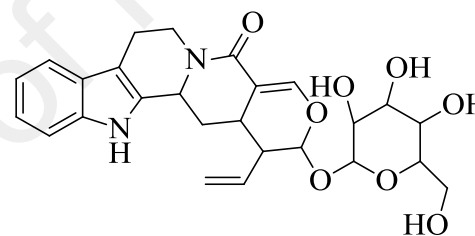
129



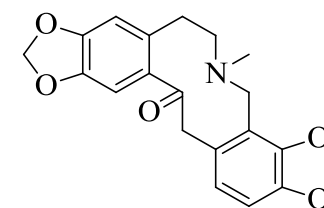
130



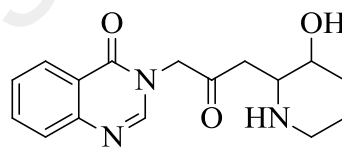
131



132



133



134

Figure 4.4: Structures Natural/ Naturally Derived Compounds from Plants Discovered in Antimalarial Drug Research

resistance showed that new classes of antimalarial are needed in order to kill the parasites.

The postulated mechanism of action for quinine **125** is hemazoin polymerization parasite inhibition to treat malaria. Whereas, artemisinin **128** and yingzhaosu A **129** have been shown to exert antiplasmodial activity by free radical activation in the presence of free ferrous ion liberated in erythrocytes by parasite digestion of haemoglobin. The phenolic compounds, curcumin **131** act as an antioxidant and utilize antiplasmodial activity by elevating the red blood cell oxidation and inhibiting the parasite protein synthesis and also counteract the oxidative damage induced by the malaria parasite.

(Wells, 2011) has reported that according to WHO, the combination therapy of drugs to eliminate disease is that one compound should protect the other against resistance. Both compounds, therefore, need to have anti-parasitic activities and different mechanism mode of actions against parasite resistance. The advantage goes to natural product extracts that tend to have two or more such components which act as monotherapy. Making the most of the aforementioned mechanism of action can influence the discovery of new antimalarial agents.

Generally, a large number of plants worldwide show strong antioxidant activities. However, antioxidant properties of *Alseodaphne corneri* and *Dehaasia longipedicellata* have not been studied before. Here, we report the antiplasmodial activities together with antioxidant activities and cytotoxicity towards normal cell line of alkaloids isolated from both plants.

4.5 Antiplasmodial Activities

4.5.1 Antiplasmodial Assay

The *in-vitro* antiplasmodial assay is focused on the compounds ability to affect parasite growth in red cells. In order to evaluate the preliminary activity of potential antimalarial agents, *in vitro* antiplasmodial activity were developed against *P.falciparum* strain K1 and FcB1 which is resistant to chloroquine. Chloroquine diphosphate (purity 98.0%) was purchased from Sigma Chemicals and used as positive controls. It has been used as the standard antimalarial drug for curative, suppressive and prophylactic antiplasmodial assessment because of its established activity on *Plasmodium*. The screening is based on the ability to culture *P.falciparum* in human erythrocytes *in vitro*. It was maintained in continuous culture as described by (Trager & Jensen, 1976) with some modification (Makler & Hinrichs, 1993). The synchronization of the malaria culture to one stage is by (Lambros & Vanderberg, 1979).

Antiplasmodial activity was evaluated using Histidine-Rich Protein II (HRPII) assay by enzyme linked immunosorbent assay (Noedl et al., 2005). Micro titration techniques were used to measure the activity of samples over a wide range of concentrations. All tests were performed in duplicate. Crude extract was dissolved in DMSO to produce a stock solution of 20 mg/ml. The stock solutions were subsequently diluted with deionized water at 20 concentrations of two-fold dilutions into two 96-well microtiter plates. 10 μ l of each concentration was transferred into another 96-well microtiter plates. 200 μ l of parasitized red blood cell suspension (1% parasitemia) were added to it. The mixtures were incubated for 24 hours at 37 °C and were subsequently cooled at - 20 °C to lyse the red blood cells. The plates were allowed at room temperature, and 20 μ l of the blood suspension was dispensed into a new microtiter plate containing 100 μ l MALSTAT reagent, 20 μ l nitroblue tetrazolium and phenazine ethanosulphate mixture.

Absorbance was measured with an ELISA plate reader at 780 nm. The percentage inhibition at each concentration was determined and the mean of IC₅₀ values of parasite sustainability was calculated using analysis. IC₅₀ values defined as the concentration of the alkaloids causing 50% inhibition of parasite growth relative to untreated control (Adjalley et al., 2010; Chan et al., 2004).

4.5.2 Results

The result showed a potent *in vitro* antiplasmodial of the crude CH₂Cl₂ bark extract of *A. corneri* and *D. longiepedicellata* with an IC₅₀ value of 2.78 µg/ml and 1.30 µg/mL respectively, against K1 resistant strain of *plasmodium falciparum*. Therefore, twelve alkaloids with sufficient amount were then subjected to *in vitro* antiplasmodial evaluation against a chloroquine resistant strain (K1) and two isolated alkaloids against FcB1 strain of *P.falciparum*. Six alkaloids namely; (-)-gyrolidine **18**, (+)-norstephasubine **20**, (+)-laurotetanine **27**, (+)-2-norobaberine **115**, (+)-*O*-methyllimacusine **118**, and (+)-stephasubine **120** were isolated from the bark of *A. corneri*, while (+)-isocorydine **41** and (+)-norisocorydine **42** were isolated from the leaves of *A. corneri*. Another six alkaloids isolated from *D. longiepedicellata* were; (+)-reticuline **8**, (+)-norboldine **36**, (+)-boldine **37**, (+)-milonine **46**, (+)-sebiferine **47** and (-)-*O-O*-dimethylgrisabine **48**. IC₅₀ values (dose required to inhibit the parasite survival by 50%) for each alkaloids with range 10-100 µM for active compounds is shown in Table 4.1.

The alkaloids isolated from the bark of *A. corneri* exhibited antiplasmodial activity against K1 with (+)-norstephasubine **20** being the most potent showing an IC₅₀ value of 0.116 µM, followed by (+)-laurotetanine **27** with an IC₅₀ value of 0.189 µM. The other alkaloids showed good activities ranging from 0.666-1.315 µM. The antiplasmodial activity against the chloroquine-resistant strain of *P. falciparum* FcB1 demonstrated that

(+)-isocorydine **41** and (+)-norisocorydine **42** isolated from the leaves of *A. corneri* exhibited good antiplasmodial activity.

Among the six alkaloids evaluated for their antiplasmodial activity from bark of *D. longipedicellata*, (-)-*O-O*-dimethylgrisabine **48** clearly showed the most potent *in vitro* antiplasmodial activity with an IC₅₀ value of 0.031 μM that was slightly better than the positive control chloroquine (0.090 μM). In addition, (+)-milonine **46** also displayed a strong inhibition capacity with an IC₅₀ value of 0.097 μM, followed by; (+)-boldine **37**, (+)-norbaldine **36**, (+)-sebiferine **47**, and (+)-reticuline **8**.

Table 4.1: Antiplasmodial Activities of Isolated Alkaloids.

Alkaloids	IC ₅₀ (K1) μM	IC ₅₀ (FcB1) μM
(-)-gyrolidine 18	0.666	
(+)-norstephasubine 20	0.116	
(+)-laurotetanine 27	0.189	
(+)-2-norobaberine 115	0.743	
(+)- <i>O</i> -methyllimacusine 118	1.193	
(+)-stephasubine 120	1.315	
(+)-isocorydine 41		51.3
(+)-norisocorydine 42		19.8
(+)-reticuline 8	30.40	
(+)-norbaldine 36	9.284	
(+)-boldine 37	2.602	
(+)-milonine 46	0.097	
(+)-sebiferine 47	22.46	
(-)- <i>O-O</i> -dimethylgrisabine 48	0.031	
Chloroquine diphosphate	0.090	0.078

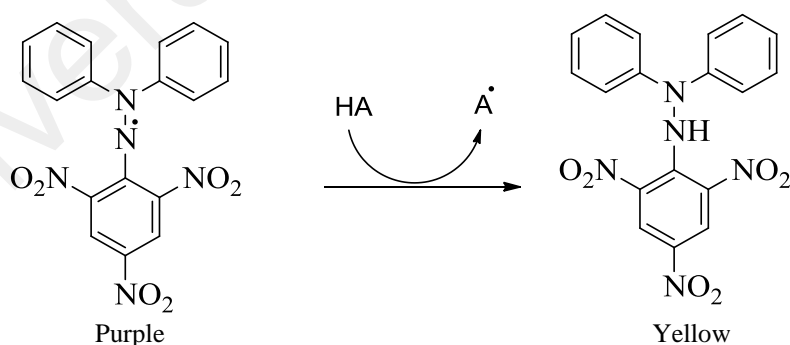
4.6 Antioxidant Activities

Many studies in the recent years have focused on natural antioxidants such as ascorbic acid and α-tocopherol compared to synthetic antioxidants (Choi et al., 2000). It

is known that the mechanism of antioxidant actions in biological system is very complex and several factors may interfere in the system. Given this complexity, three different methods have been used for assessing the antioxidant activities for alkaloids isolated from the bark and leaves of *A. corneri* and bark of *D. longipedicellata* using 1,1-diphenyl-2-picrylhydrazyl (DPPH), ferric reducing power assay (FRAP) and metal chelating assay.

4.6.1 DPPH

The free radical scavenging activity of alkaloids were measured in terms of hydrogen or electron donating ability using DPPH radical as described by (Shimada et al., 1992) with a slight modification. 40 μL of alkaloids at different concentrations (0.05- 2.0 mg/ml) were mixed with 200 μL of 50 μM DPPH solution in ethanol. The mixture was shaken vigorously and incubated for 15 min in the dark at room temperature. The decrease in absorbance was measured at 517 nm with a microplate reader (Tecan Sunrise, Austria) using UV-VIS spectrophotometer. The scavenging reaction between DPPH radical and the antioxidant compound (H-A) can be written as:



A purple colour stable free radical DPPH that contains an odd electron is reduced to α, α -diphenyl- β -picryl hydrazine and gives a yellow colour when accepting hydrogen donated by antioxidant compounds (H-A). The degree of discoloration indicates the scavenging abilities of the antioxidant compounds. The percentage of scavenging of DPPH was calculated using the following equation:

$$\text{DPPH scavenging effect (\%)} = \frac{A^{\circ} - A_1}{A^{\circ}} \times 100$$

Equation 4.1

Where A° is the absorbance of the control reaction and A_1 is the absorbance in the presence of the alkaloid. BHA (Sigma, purity 99.0%) and ascorbic acid were used as standard reference for alkaloids **41, 42** and **18, 20, 27, 36, 37, 46, 47, 48, 118, 119, 120** respectively. The concentration of alkaloids required to scavenge 50% of DPPH radical was estimated from the graph plotted against the percentage inhibition and compared with the standard. All the tests were performed in triplicate, and the results were expressed as μM .

4.6.2 Ferric Reducing Antioxidant Power Assay (FRAP)

The reducing power was determined using the method of (Oyaizu, 1986). The alkaloids (**47, 46, 37, 36, 19, 48, 27, 18, 118, 20, 120**) (0.5 mL) dissolved in ethanol at different concentrations (0, 50, 100, 150, 200 $\mu\text{g/mL}$) were mixed with 0.5 mL phosphate buffer (0.2 M, pH 6.6) and potassium ferricyanide [$\text{K}_3\text{Fe}(\text{CN})_6$] (0.5 mL, 1%). The mixture was then incubated at 50 °C for 20 min. A portion of trichloroacetic acid (0.5 mL, 10%) was added to the mixture, which was then centrifuged for 10 min at 3000 rpm (1000 g). The upper layer of solution (0.5 mL) was mixed with distilled water (0.5 mL) and FeCl_3 (0.1 mL, 0.1%) for 10 min, and then the absorbance was measured at 700 nm in a spectrophotometer. The reducing power activity was expressed as percentage of absorbance (Equation 4.2) compared with EDTA.

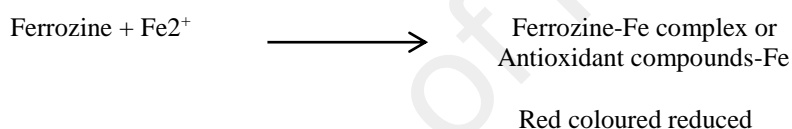
$$(\%) \text{ inhibition} = 100 - \left[\left(\frac{A_1}{A^{\circ}} \right) \times 100 \right]$$

Equation 4.2

4.6.3 Metal Chelating Activity Assay

The chelation of ferrous ions was determined according to the method of (Dinis et al., 1994) by measuring the formation of the Fe^{2+} -ferrozine complex based on the

method described by (Decker & Welch, 1990). Compounds at different concentrations (50-800 $\mu\text{g/mL}$) were mixed with 120 μL distilled water and 10 μL FeCl_2 (2 mM) in a 96-well microplate. Ferrozine (5 mM, 20 μL) was added to the mixture to initiate reaction. The reaction mixture was incubated at room temperature for 20 min and was measured at absorbance 562 nm along with EDTA- Na_2 (5-80 $\mu\text{g/mL}$) as a standard metal chelator for alkaloids **41, 42** and BHA as a standard for alkaloids **18, 20, 27, 36, 37, 46, 47, 48, 118, 119, 120**. Ethanol (100 μL) was used as a control; blank without ferrozine (20 μL of distilled water instead of ferrozine). Ferrozine can form a complex with ferrous ions (Fe^{2+}) giving a red coloured complex. The antioxidant compounds act as chelating agents and capture free ferum before ferrozine and interfere with the formation of ferrous-ferrozine complex as summarized below:



The percent inhibition of Fe^{2+} -ferrozine complex was calculated according to the following equation:

$$\text{Ferrous ion chelating activity (\%)} = \frac{A_{\text{control}} - A_{\text{sample or standard}}}{A_{\text{control}}} \times 100 \quad \text{Equation 4.3}$$

The concentration of extract or pure compounds required to chelate 50 % of the Fe^{2+} ion (IC_{50}) was calculated from the graph against the percentage of inhibition. All the tests were performed in triplicate, and the results were expressed as ferrous ion chelating activity μM .

4.6.4 Results

Similar alkaloids that have been evaluated for antiplasmodial activity also have been tested for their antioxidant activities against DPPH, FRAP and metal chelating assays (Table 4.2).

Alkaloids **18**, **20**, **27**, **115**, **118**, and **120** isolated from the bark of *A. corneri* showed significant antioxidant activities in all three assays (DPPH, FRAP, metal chelating). Norstephasubine **20** and laurotetanine **27** showed high scavenging activity of DPPH, FRAP, metal chelating with an IC₅₀ value of 130.42 μM, 74.25 %, IC₅₀ value of 104.58 μM and latter with an IC₅₀ value of 131.72 μM, 89.22 %, IC₅₀ value of 153.25 μM respectively. The high antioxidant activity of (+)-laurotetanine **27** and (+)-norstephasubine **20** may be due to the hydroxyl group that could donate the electron to the free radicals and possess the ability to chelate metal (ferum). (+)-Isocorydine **41** and (+)-norisocorydine **42** that was isolated from the leaves of *A. corneri* also exhibited antioxidant activities in DPPH and metal chelating assays.

Interestingly, alkaloids **8**, **36**, **37**, **47**, **46** and **48** that was isolated from *D. longipedicellata* also showed positive results towards antioxidant activities. (-)-*O-O*-dimethylgrisabine **48** showed a high scavenging activity of free radical DPPH with an IC₅₀ value of 28.75 μM comparable to the standard; BHA (77.73 μM). IC₅₀ values of free radical DPPH, metal chelating and percentage of FRAP for each alkaloids were shown in Table 4.2.

Table 4.2: Antioxidant Activities of Isolated Alkaloids.

Alkaloids	IC ₅₀ DPPH Activity (μ M)	% FRAP	IC ₅₀ Metal Chelating Activity (μ M)
(-)-gyrolidine 18	280.95	41.32	252.14
(+)-norstephasubine 20	130.42	74.25	104.58
(+)-laurotetanine 27	131.72	89.22	153.25
(+)-2-norobaberine 115	254.95	51.50	351.80
(+)- <i>O</i> -methyllimacusine 118	265.09	65.87	263.32
(+)-stephasubine 120	233.82	94.01	338.44
(+)-sebiferine 47	313.62	45.69	542.92
(+)-isocorydine 41	229.06		87.76
(+)-norisocorydine 42	93.13		124.00
(+)-reticuline 8	153.70	87.43	325.33
(+)-norboldine 36	254.68	52.10	500.51
(+)-boldine 37	137.13	34.37	786.61
(+)-milonine 46	176.50	27.39	651.52
(-)- <i>O-O</i> -dimethylgrisabine 48	28.75	44.31	100.59
EDTA (Standard)		83.74	
EDTA-Na (Standard)			25.49
BHA (Standard)	26.46		108.73
Ascorbic acid (Standard)	77.73		

4.7 Cytotoxic Activities

4.7.1 Cytotoxic Assay

The alkaloids were evaluated for cytotoxic activity against three types of cancer cell lines; lung (A549), skin (A375), pancreatic (BxPC-3); and one normal cell line, pancreatic (hTERT-HPNE). Cell lines were cultured in DMEM media supplemented with 2 mM L-glutamine, 10% fetal bovine serum, 50 μ g/mL gentamicin and 10% Penicillin-Streptomycin (Pen Strep), maintained in a 37 °C humid atmosphere of 5% CO₂ cell incubator.

Cells were plated into 96-well microplates and maintained in the cell incubator for 24 h. Then, 100 μ L of samples were introduced in triplicates to a final concentration of 0.1 – 200 μ M. Drug standards were also introduced to a final concentration of 0.03 – 2000

μM (cisplatin). Cells were further incubated for 48 h and cell viability was determined using MTS assay kit (CellTiter 96[®] AQueous One Solution, Promega) according to the manufacturer protocol. Microplates were returned to the incubator for 1–2 h and absorbance of the formazan product was read on a microplate reader at 490 nm with 690 nm as the background wavelength (Infinite 200, Tecan, Mannedorf, Switzerland). IC_{50} of samples and drug standards were determined using dose-response curves, and statistical analysis using student's T-test ($p < 0.05$) was performed in Prism 5.02 software (GraphPad Software Inc., La Jolla, CA, USA).

4.7.2 Results

In an effort to minimize the side-effects, the National Cancer Institute (Boyd & Paull, 1995) have been exploring the vast resource of natural products for potent and selective anticancer and antiplasmodial, but as yet, the success rate of discovering such molecules have remained very low. In addition to antiplasmodial and antioxidant, certain isolated alkaloids that have enough yield (**8**, **36**, **37**, **47**, **46** and **48**) from the bark of *D. longipedicellata* were also tested for cytotoxicity against a few cancer cell lines and normal cell line (Table 4.3). All of the isolated alkaloids showed no potency against lung (A549) cancer cells and weak cytotoxicity against skin (A375) cancer cells with IC_{50} values below $100.0 \mu\text{M}$ for (+)-norboldine **36** ($82.9 \pm 9.7 \mu\text{M}$) and (-)-*O-O*-dimethylgrisabine **48** ($82.9 \pm 8.7 \mu\text{M}$). However, for pancreatic cancer cells (BxPC-3), great potency was shown by (+)-norboldine **36** with IC_{50} of $27.1 \pm 1.0 \mu\text{M}$. The same alkaloids were tested against normal pancreatic cells (hTERT-HPNE) and no cytotoxicity was observed. Therefore it proves that all the isolated alkaloids, particularly boldine **37** and (-)-*O-O*-dimethylgrisabine **48** were safe to normal pancreatic cell lines.

Table 4.3: Cytotoxicity Activities of Isolated Alkaloids.

Alkaloids	A549 IC ₅₀ (μM)	A375 IC ₅₀ (μM)	BxPC-3 IC ₅₀ (μM)	hTERT- HPNE IC ₅₀ (μM)
(+)-reticuline 8	>200.0	97.6 ± 6.6	82.6 ± 0.8	>200.0
(+)-norboldine 36	>200.0	82.9 ± 9.7	27.1 ± 1.0	>200.0
(+)-boldine 37	117.6 ± 0.07	112.5 ± 3.5	45.5 ± 2.9	>200.0
(+)-milonine 46	>200.0	>200.0	>200.0	>200.0
(+)-sebiferine 47	>200.0	>200.0	93.4 ± 5.6	>200.0
(-)- <i>O-O</i> -dimethylgrisabine 48	>200.0	82.9 ± 8.7	>200.0	>200.0
Cisplatin	17.5 ± 1.8	35.9 ± 5.2	26.9 ± 0.9	24.7 ± 0.4

4.8 Discussion

The results indicated a positive correlation for (-)-*O-O*-dimethylgrisabine **48**, (+)-norstephasubine **20** and (+)-laurotetanine **27** that possessed antiplasmodial together with antioxidant property. These two properties, upon co-existence, are beneficial to the patients, since the host can be protected by the antioxidant activity while the *plasmodium* can be killed through the antiplasmodial property. Alkaloids that have ability to inhibit parasite survival and stimulate the immune systems of malaria patients have potential to reduce or prevent cerebral malaria (Ye & Rossan, 2013). The antiplasmodial property of the isolated alkaloids is comparable to chloroquine. Chloroquine is considered an antimalarial drug since 1940. Its mechanism of action is still unclear but in general its antiplasmodial action is expressed through its accumulation in the acidic food vacuole of the parasite via pH trapping and inhibition of hemazoin formation, thus, killing the *plasmodium* parasite (Teixeira et al., 2014). The BBIQ skeletons are more active than aporphine in both activities; antiplasmodial and antioxidant, this might be due to the presence of two nitrogen atoms in BBIQ as compared to only one nitrogen atom in aporphine. Recently, the combination of BBIQ alkaloids (tetrandrine **94**) and chloroquine is effective against *P. falciparum* strain in

Aotus monkey and increase the antimalarial potency of chloroquine (Ye & Rossan, 2013). The aporphine alkaloid; **27**, **37** and **36** belonging to type 1, 2, 9, 10 tetrasubstituted possessed the highest antiplasmodial activity in comparison with **41** and **42** that belong to type 1, 2, 10, 11 tetrasubstituted aporphine. These results suggest that the position and number of the substituents (OH/OCH₃) could play a significant role in the antiplasmodial and antioxidant activities of an aporphine (Wright et al., 2000).

Plasmodium parasite invades the host haemoglobin as a source of amino acids for its own survival. During this process, the host haemoglobin is destroyed and liberates free electron and free heme. Free electron is formed from the oxidation of iron bound in haemoglobin Fe²⁺ to Fe³⁺ (Wilson & Britigan, 1998). The release of free electrons will produce free radicals called reactive oxygen species (ROS). Generation of ROS is associated with oxidative stress and it is highly toxic to the host cell that will lead to haemolysis or cell damage. *Plasmodium* parasites from malaria infection are synergistic to high levels of oxidative stress (Percario et al., 2012). A study conducted with 100 Gabonese children with severe *P.falciparum* malaria verified the increase of ROS during acute malaria (Kremsner et al., 2000). Therefore, the presence of alkaloids that possess antioxidant activity will prevent the oxidative damage to the hosts due to the ability of the hydroxyl groups which can chelate iron and donate electrons to free radicals in the ROS (Musonda et al., 2004). In addition, free heme will also be released during haemoglobin destruction. This free heme eventually will convert to hemazoin. Hemazoin is important for the survival of *Plasmodium* parasites. The potent antioxidant alkaloids are able to bind to the toxic free heme and thus prevent the formation of hemazoin (Biagini et al., 2003; Greve et al., 1999; Yang et al., 2009). Thus, the synergism between antimalarial and antioxidant are advantageous in improving the suppression of malaria infection, slowing down the emergence of drug resistance and include additive therapy that lessens damage to the host.

CHAPTER 5: ACID-BASE EQUILIBRIA

5.1 Introduction

According to Bronsted-Lowry theory, acid is a substance that can lose a proton and a base is a substance that can accept a proton. A state of chemical equilibrium exists when acids are in equilibrium with their conjugate base forms present in medium. In general definition, pK_a is property of the molecule itself; pH is property of the medium (solvent or blood) (Kohlmann, 2003). Every living organism has internal mechanisms for maintaining the pH level of their blood. The blood flow in the human body has a physiological pH between 7.35 and 7.45. The nature of aporphine structure is amphoteric and consisting of amine group that acts as basic nitrogen and methoxyphenolic functions that could give an acidic proton. Many important drugs or natural products have nitrogen atom and phenolic function in their structures such as acetaminophen **135** ($pK_a = 9.5$), morphine **136** ($pK_a = 10.2, 9.1$) and levorphanol **137** ($pK_a = 10.5$) (Research, 2016; Troy et al., 2006) (Figure 5.1). Aporphine structure that contain both nitrogen atom and phenols might be the reason for various interesting biological activities; smooth muscle relaxant (Mustafa et al., 1995), antibacterial and cytotoxic activities (Wei et al., 2012). By comparison with drugs mentioned above, the pK_a of these aporphines could be estimated to be around 9.1-10.5 (Liptak et al., 2002).

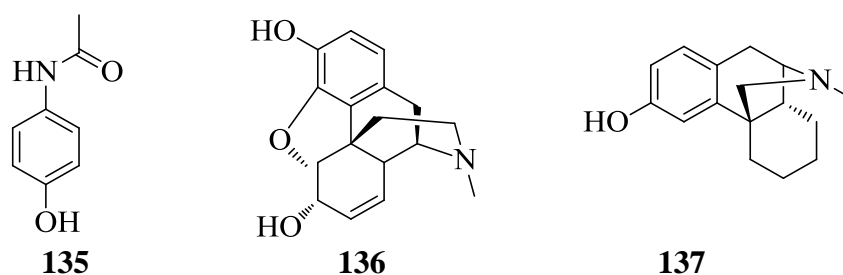


Figure 5.1: Structure of Drugs Consist of Nitrogen Atom and Phenolic Function

Studies of acid dissociation constant of alkaloids are important physicochemical parameters which can provide information about interaction of alkaloids (drugs) at the active site in terms of solubility, stability, activity and absorption. Drugs mainly consist of weak acids or weak bases that can exist in ionized or non-ionized form (or mixture of both) that may be active in one form but not in another. As an example, salicylic acid has antibacterial activity in non-ionized form but no activity in ionized form. Accordingly, these substances require an acidic environment to function effectively as an antibacterial agents (Troy et al., 2006). In addition, an acidic or basic pH could either enhance or reduce the ionization of these drugs by its pH gradient across the membrane. As we can see, drugs in non-ionized form are more soluble in lipid and can diffuse readily across the cell membrane. In contrast, the ionized drugs usually are less able to penetrate the lipid membrane because of their low lipid solubility (Brunton et al., 2011). Therefore, stability (or instability) of an alkaloid structure may result from gain or loss of a proton (hydrogen ion) in a structure which can be made by electronic rearrangement that will reduce (or increase) the reactivity of certain drugs (Troy et al., 2006). Rates of absorption of a variety of drugs are related to their ionization constant and in many cases may be predicted quantitatively on the basis of this relationship.

The importance of pH studies can be seen as early as the learning of science by dipping pieces of pH paper into various medium to measure acidity and basicity. Recently, the measurement of the pH study has been elevated by using more sophisticated techniques such as potentiometric titration, UV/vis spectroscopy, NMR spectroscopy, conductivity, calorimeter, capillary zone electrophoresis and software computational prediction. Among these techniques, the UV-vis spectroscopic method is used in this study due to its high sensitivity (detection limits can be reached with concentrations of substances as low as 10^{-6} M). Moreover, aporphine alkaloids fulfilled the important requirements of this method, which requires it to have a chromophore in

proximity to the ionization centre so that the protonated and deprotonated species show satisfactory spectral differences (Avdeef et al., 1999). The same approach was also employed in this work to determine the acid-base behaviour of the alkaloids against varying pH and temperature dependence (Kuntworbe et al., 2013). These parameters are also important in selecting appropriate acidic or basic reagents in drug delivery studies (Kilic, 2010). Another importance of this research is to determine the effect of temperature of alkaloid in certain circumstances. At high temperatures, alkaloids move faster and have a chance to collide and produce a reaction with low activation energy or in other words increasing temperature results in an increase of rate of reaction. Along with an increase in temperature, the molecules would change forms which lead to disruption of hydrogen bonds that maintain the structure of the folded protein alkaloid. When this happens, the proteins unfold, and the shape of the structure could change, thus resulting in the loss of activity. One of the symptoms of malaria is fever, which will result in an increase in body temperature to 40°C. This can cause changes in enzyme catalysis reaction rate and also change the shape of molecules which could result in the 'adminstrated drug' no longer being active (Bender, 2007). Thus, it is important to study the effect of temperature on alkaloids in the range of 30-50°C.

Previously in chapter 4, we have described that malaria disease is caused by the *plasmodium* which posses acidic food vacuole. This organelle is vital to the organism as it is involved in the digestion of the host haemoglobin. This digestion occurs at the acidic food vacuole which gives hemazoin. Basic natural products such as alkaloids are helpful in inhibiting the formation of hemazoin by reducing the acidity of food vacoule. In order to unravel the potential relationship between the acid-base properties of an alkaloid and its antiplasmodial activity, it is crucial to determine its ionization constant (K_a).

5.2 Experimental

5.2.1 Reagents and Materials

Boldine **37**, Isocorydine **41** and Norisocorydine **42** (Table 5.1) were chosen as the substance in acid-base equilibria study due to the highest yield throughout plant investigation and also the structure of this alkaloid is one of the important classes of Lauraceae family. The stock solutions of alkaloids were prepared in appropriate working concentration in acetonitrile for calculation of intensity absorbance between 1.00- 2.00, in order to increase sensitivity by maximize the signal and minimize the noise.

Table 5.1: The List of Alkaloids Studied in Acid-base Equilibria.

Alkaloids	Aporphine type	Working concentration
Boldine 37	1, 2, 10, 11-substituents	2.00×10^{-4} M
Isocorydine 41	1, 2, 10, 11-substituents	2.00×10^{-4} M
Norisocorydine 42	1, 2, 9,10-substituents	2.00×10^{-4} M

All other chemicals were obtained from Acros, Merck and Sigma, as reagent grade materials (Table 5.2). All stock and buffer solutions were prepared in deionized water.

Table 5.2: List of Chemicals Used in the Acid-base Equilibria.

Chemical	Manufacturer	Purity
Hydrochloric acid fuming 37%	Merck	-
Sodium hydroxide pellets	Merck	≥ 99%
Sodium chloride	J.Kollin	≥ 99.3%
Sodium formate	Merck	≥ 99%
Sodium acetate anhydrous	Fisher Scientific	≥ 99%
2-Morpholinoethanesulfonic acid monohydrate (MES)	Merck	≥ 99%
MOPS	Sigma	≥ 99.5%
Tris (hydroxymethyl)aminomethane	Sigma-Aldrich	≥ 99.8%
Glycine	Merck	≥ 99.7%

The alkaloids are not appreciably soluble in water; therefore the stock solutions of the alkaloids were prepared in an appropriate volume of acetonitrile. The experiment was performed in a mixture of acetonitrile-water (2% v/v acetonitrile). Solvent mixture of

acetonitrile and water was chosen because it has low toxicity and does not affect the stability of alkaloids (Thomas, 2011). HCl and NaOH of various concentrations were used to cover the strongly acidic and basic regions. Buffer solutions of glycine, formate, acetate, MES, MOPS and TRIS were used to guard the pH ranges from 3.0 to 11.0 (Table 5.3). The preparation of these buffers followed the standard method published by (Perrin & Dempsey, 1974).

Table 5.3: The List of Buffer Solution and its pH Range.

Buffer	pH range
Formate	3.0-4.0
Acetate	4.0-5.0
MES	5.5-6.5
MOPS	6.5-7.5
TRIS	7.5-8.5
Glycine	9.0-10.0

5.2.2 Instrumentation

Studies for the determination of acid dissociation constant of the compounds were carried out by using a Shimadzu 1650 PC UV/vis double beam Spectrophotometer equipped with multicell compartment and peltier-controlled temperature. Quartz cells with 1 cm path length were used both as reference and blank sample. The pH of the solutions was measured by Mettler Toledo Model S40 digital pH meter with an accuracy of ± 0.01 units. The meter was equipped with a combined pH electrode with ATC temperature detector filled with a solution of 3M KCl and was standardized using standard aqueous buffers (pH 4.01, 7.00 and 9.21 at 35°C).

5.2.3 pH Measurement

The experimental reaction mixtures were prepared by diluting the appropriate amount of the stock solutions of each alkaloid **37**, **41** and **42** in a pre-prepared buffer solution to give the alkaloid concentration of 2.00×10^{-4} M. The ionic strength was

maintained at 0.10 M with NaCl at 35°C. Deionized water and pure acetonitrile were used to prepare the solutions of 2% v/v acetonitrile. The UV/vis spectra were monitored from 190 nm to 400 nm for each alkaloid. The reference cell contained deionized water or acetonitrile, for measurements done in 2% v/v acetonitrile, respectively. The temperature of the sample was maintained in a thermostated waterbath. While the spectrum was running, the pH of the sample was measured at an appropriate temperature using a pH electrode. It was attached to a digital pH meter equipped with an automatic temperature probe. The electrode was calibrated at the same temperature as the sample using standard buffers of known pH at the sample temperature.

5.2.4 Acid and Bases

Acids are in equilibrium with their conjugate base forms. One of these species will be charged and the equilibrium ratio, therefore, could determine the extent to which the molecule is ionized in solution (Troy et al., 2006).



Thus, the expression for acid dissociation constant shows that the equilibrium constant,

$$K_a = \frac{[A^{-}][H^{+}]}{[HA]} \quad \text{Equation 5.2}$$

Taking logarithm of both sides of the equation provides,

$$\log K_a = \log[A^{-}] + \log[H^{+}] - \log[HA] \quad \text{Equation 5.3}$$

Multiplying both sides of the equation by -1 and substitute pK_a for $-\log K_a$ and pH for $-\log[H^{+}]$ gives,

$$pK_a = pH + \log \frac{[HA]}{[A^{-}]} \quad \text{Equation 5.4}$$

This Henderson-Hasselbalch equation gives the relationship between pK_a of an acid and the ratio of its acid form to conjugate base form at given pH.

In general,

$$pK_a = pH + \log \frac{[acid\ form]}{[conjugate\ base\ form]} \quad \text{Equation 5.5}$$

Or,

$$pK_a = pH + \log \frac{[non\ ionized]}{[ionized]} \quad \text{Equation 5.6}$$

5.2.5 Determination of Acidity Constants

The acidity constants of the acids depend upon the ratio of the non-ionized species to its ionized species (cation or anion). The ratio of this two species depends solely upon the pH at which the solution is optically measured. If it is assumed that Beer Lambert's law is obeyed for both species, the observed absorbance A_{obs} , at a particular wavelength will be equal to the sum of the absorbance of the ionized species, A_{S^-} , and the absorbance of the non-ionized species, A_{SH} (Equation 5.7).

$$A_{obs} = A_{S^-} + A_{SH} \quad \text{Equation 5.7}$$

Thus,

$$A_{obs} = (\epsilon_{S^-} \times \ell \times C_{S^-}) + (\epsilon_{SH} \times \ell \times C_{SH}) \quad \text{Equation 5.8}$$

Where ϵ_{S^-} and ϵ_{SH} are the molar extinction coefficients of the ionized and non-ionized species, respectively; ℓ is the pathlength of the cell which is constant throughout the experiment; and C_{S^-} and C_{SH} are the concentrations of the ionized and non-ionized species, respectively. For the mixture of ionized and non-ionized species of the substrate, the concentration of its particular species, C_{S^-} is equal to $F_{S^-} [X]_0$, where F_{S^-} is the fraction of the ionised species, C_{SH} is equal to $F_{SH} [X]_0$, where F_{SH} is the fraction of the non-ionised species and $[X]_0$ is the initial molar concentration of the substrate.

Since, the path length of the cell is constant, *i.e.* 1 cm throughout the study, therefore the observed absorbance is:

$$A_{obs} = (\epsilon_{S^-} \times 1 \times F_{S^-}[X]_0) + (\epsilon_{SH} \times 1 \times F_{SH}[X]_0) \quad \text{Equation 5.9}$$

$$= (\epsilon_{S^-}F_{S^-} + \epsilon_{SH} F_{SH}) [X]_0 \quad \text{Equation 5.10}$$

Whereas, the fractions of the ionized and non-ionized species are given by:

$$F_{S^-} = \frac{[S^-]}{[S^-] + [SH]} = \frac{K_a}{[H^+] + K_a} \quad \text{Equation 5.11}$$

$$F_{SH} = \frac{[SH]}{[SH] + [S^-]} = \frac{[H^+]}{K_a + [H^+]} \quad \text{Equation 5.12}$$

Substitution of Equation 5.11 and Equation 5.12 into Equation 5.10 results in:

$$A_{obs} = \frac{\epsilon_{S^-}K_a + \epsilon_{SH}[H^+]}{[H^+] + K_a} [X]_0 \quad \text{Equation 5.13}$$

Thus, the parameters of K_a , ϵ_{S^-} , and ϵ_{SH} could be determined from the plot of A_{obs} vs. pH, where the pH is equal to the activity of $[H^+]$. Furthermore, $[X]_0$ is the initial concentration of the substrate used. The pK_a values determined by using equation below:

$$pK_a = -\log K_a \quad \text{Equation 5.14}$$

5.2.6 Temperature Variation and Acid Base Equilibria

In addition, temperature variations also influence the effective mobility of the alkaloids via its degree of ionisation as can be seen in Table 5.5. Norisocorydine **42** showed that the increase in the temperature could lead to a decrease in its pK_a values. This can be exemplified by the van't Hoff equations where;

$$\frac{d(\ln K)}{d\left(\frac{1}{T}\right)} = \frac{\Delta H^\circ}{R} \quad \text{Equation 5.15}$$

$$\frac{d(pK_a)}{dT} = \frac{\Delta H^\circ}{2.303 RT^2} \quad \text{Equation 5.16}$$

ΔH° is assumed to be constant and independent of temperature. When the dissociation is exothermic ($\Delta H^\circ < 0$), the pK_a will increase with increasing temperature, and when it is endothermic ($\Delta H^\circ > 0$), the pK_a will decrease. The experimental data are in agreement with the Le Chatelier's principle which is the addition of heat to a reaction will favour the endothermic direction of a reaction as this reduces the amount of heat produced in the equilibrium system (Clausen et al., 2002; Ferrari & Cutler, 1987; Shields & Seybold, 2013).

5.3 Results

5.3.1 Acid Dissociation Equilibria

The general mechanism for the dissociation equilibria of alkaloids **37**, **41** and **42** have been proposed as shown in Figure 5.2 and Figure 5.3. There were two acid dissociation constant (K_a) values were predicted for boldine **37** (Figure 5.2), while only one K_a value for isocorydine **41** and norisocorydine **42** (Figure 5.3). In brief, both mechanisms indicate that aporphine protons tend to dissociate from phenolic proton of the phenolic groups.

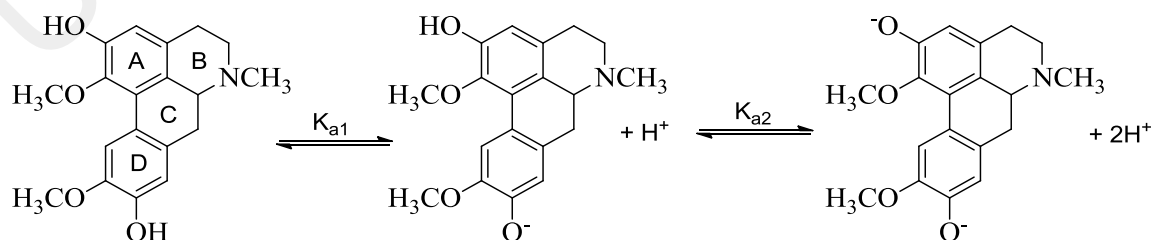


Figure 5.2: General Acid-base Equilibria for Boldine **37**

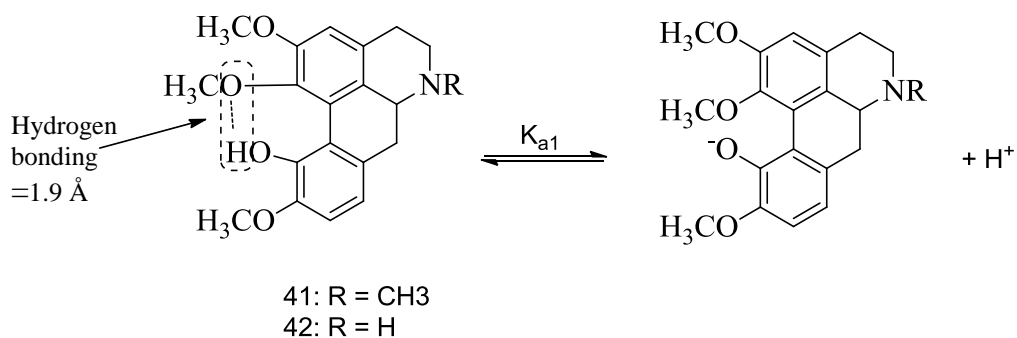


Figure 5.3: General Acid-base Equilibria for Isocorydine **41**, Norisocorydine **42**.

5.3.2 Electronic Spectra

Figure 5.4 depicted the UV-vis spectra of alkaloids **37**, **41** and **42** in 2% v/v acetonitrile. The UV-vis spectra of isocorydine **41** and norisocorydine **42**, each with a hydroxyl group at position 11, were similar to each other at all ranges and were characterized by three bands that showed maxima at A1, B1 (246 nm), A2, B2 (270 nm) and A3, B3 (300 nm). Meanwhile, boldine **37** that is unsubstituted at position 11 was characterized by five bands which showed maxima at C1 (253 nm), C2 (274 nm), C3 (282 nm), C4 (302 nm) and C5 (315 nm), with bands C3, C4 and C5 having equal intensity. In this case, the shapes of the curves and the intensities of the maxima were reliant on the position of the substituents in ring D (Sangster & Stuart, 1965).

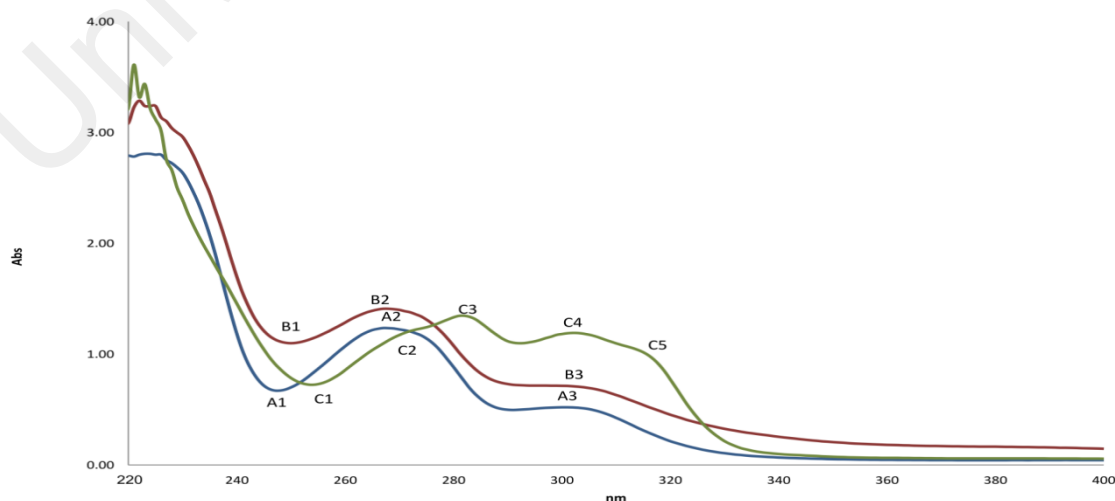


Figure 5.4: The UV Absorption of 2.0×10^{-4} M Isocorydine **41** (blue), Norisocorydine **42** (red), Boldine **37** (green) in Acetonitrile.

The UV-vis spectra at different pH ranges were monitored in 2% v/v acetonitrile for alkaloids **41**, **42** and **37** to determine the K_a values as shown in Figure 5.5, Figure 5.6, and Figure 5.7 respectively. A wavelength called ‘analytical wavelength’ is chosen at which the greatest difference between the absorbance of the two species is observed. Isocorydine **41** and norisocorydine **42** exhibited no substantial shifts in their wavelengths and changes in their shapes within the pH range of 1.0 to 10.0 (inset Figure 5.5, Figure 5.6). Thus, it remained in its neutral form in the acidic medium in which no monocation species was detected (Sun et al., 1996). However, spectral differences were observed at 338 nm as a result of changes in the pH from 10.0 to 13.5. As a result of dissociation of the alkaloids in alkaline medium, the UV-vis spectra of isocorydine **41**, norisocorydine **42** had undergone substantial bathochromic effect to A3, B3 as shown in Figure 5.4 and Figure 5.5. Meanwhile, in Figure 5.7, broad absorption bands between 290 and 350 nm, indicated the spectral change of boldine **37** with pH as a result of the presence of two acid-base equilibria in the solution. The analytical wavelength was observed to be at 295 nm and 332 nm. These two bands of boldine **37** remained in their neutral forms in the acidic medium in which no monocation was detected. Nevertheless, the C3, C4, C5 bands amended hyper chromic and bathochromic effects in the alkaline medium between pH 9.0 to 11.0 as shown inset Figure 5.6.

The inset of each Figure 5.4 and Figure 5.5 revealed the substantial changes of the absorbance within pH 11.0 –12.0 for **41** and **42**, and inset of Figure 5.6 showed two substantial changes of the absorbance at 295 and 332 nm between pH 10.0-11.0 and 9.0–10.0 respectively for **37**. Thus, this indicated the existence of equilibrium between the ionic species and the neutral species of the alkaloids. In conjugation with that, a good S-shaped curve was constructed using the absorbance (Abs)-pH relation for each alkaloid, thus obeying **Equation 5.13**. The calculated data associated with low residual errors of the absorbance are supplemented in Appendix B. Absorbance at a specific

wavelength was recorded and the acidity constants (pK_a , K_a) were calculated using Basica Programme (Appendix C) (Khan, 2006).

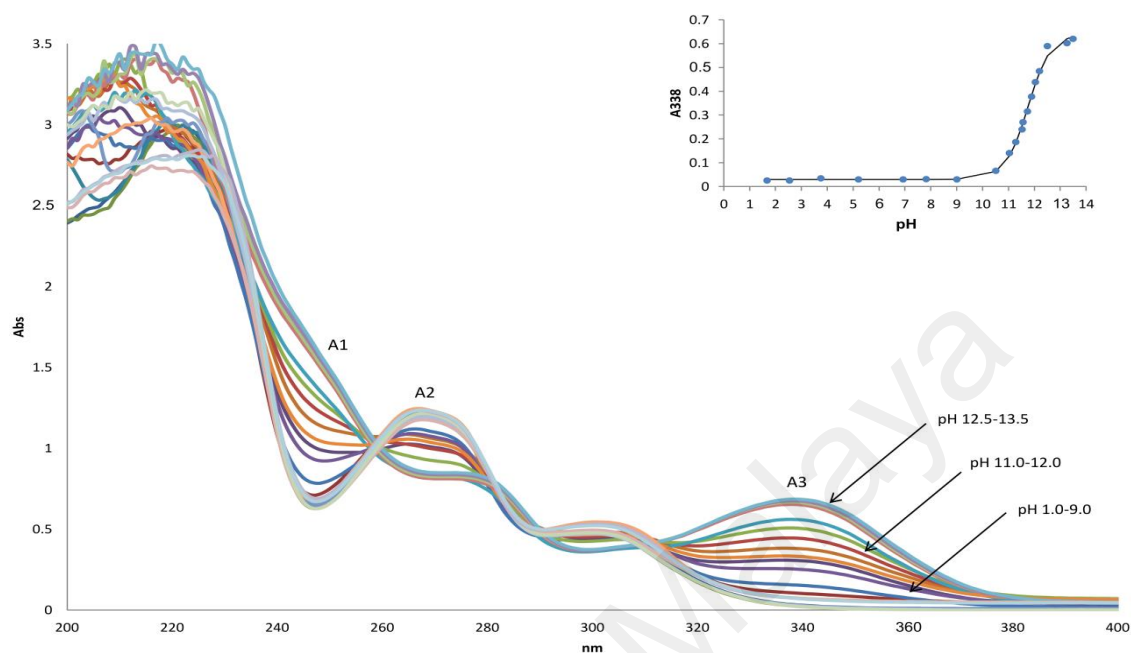


Figure 5.5: The UV Absorption Spectra of 2×10^{-4} M Isocorydine **41** in 2% v/v Acetonitrile at pH 1-13.5. Inset Shows the pH-dependence of the Absorbance at 338 nm.

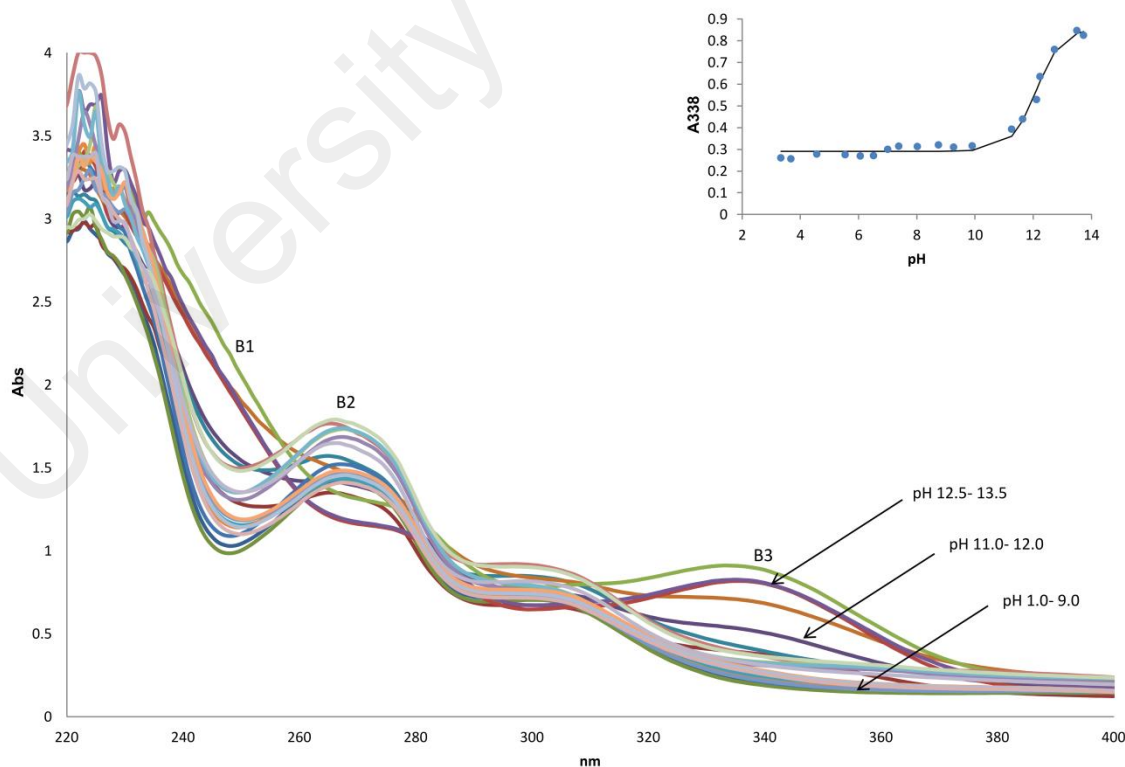


Figure 5.6: The UV Absorption Spectra of 2×10^{-4} M Norisocorydine **42** in 2% v/v Acetonitrile at pH 1-13.5. Inset Shows the pH-dependence of the Absorbance at 338nm.

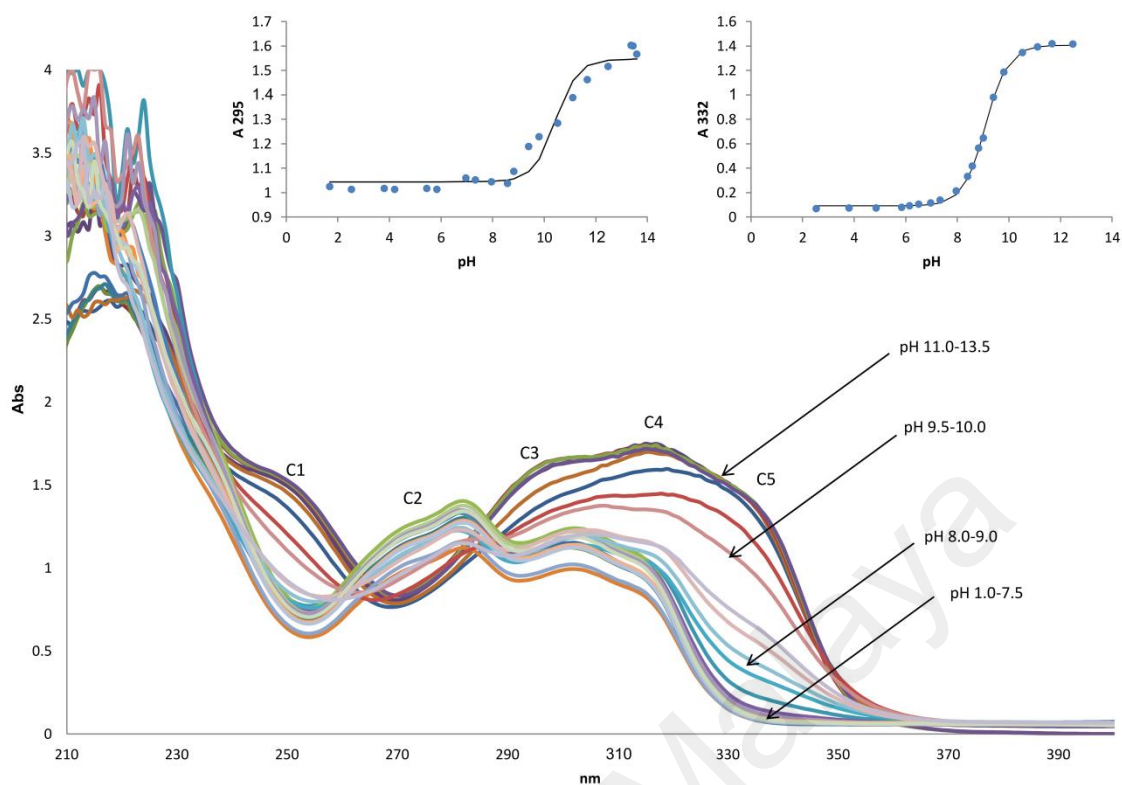


Figure 5.7: The UV absorption Spectra of 2×10^{-4} M Boldine **37** in 2% v/v Acetonitrile at pH 1-13.5. Inset Shows the pH-dependence of the Absorbance at 295 and 332 nm.

The calculated values are given in Table 5.4 for all of the alkaloids that have been studied at 35°C. The values for isocorydine **41** (pK_a 11.75) and norisocorydine **42** (pK_a 12.11) were essentially similar. This could be expected based on their similar structural features with the only difference in the methylation of *N*-2 in isocorydine **41**. Meanwhile, boldine **37** that has a different value and position of substituent compared to both alkaloids gave much lower value (pK_a 9.12, 10.44). The pK_a values for these three alkaloids can be compared to methoxyphenol that has pK_a values around 9.29-10.50 (Liptak et al., 2002).

These differences could be related to the steric factor since isocorydine **41** and norisocorydine **42** are hydroxyl substituted at position 11, while boldine **37** is substituted at position 2 and 9 instead. Steric effects can influence the pK_a value by distorting the molecular structure from planarity or otherwise disrupting the electronic

system of the acid (Shields & Seybold, 2013). The intramolecular hydrogen bonding between the 1-OCH₃ group in ring A and the 11-OH group in ring D (Figure 5.3) could be the reason as to why isocorydine **41** and norisocorydine **42** showed higher pK_a values as compared to that of boldine **37**. This may be due to the fact that proton attached to the oxygen is not free to be released as H⁺, since it is occupied in hydrogen bonding with the oxygen of the methoxyl group at C-1. This type of intramolecular hydrogen bonding was not observed in boldine **37** due to the absence of 11-OH group as in skeleton (De Heer et al., 1999). This O-H distance has been calculated from model to be approximately 1.9 Å, which makes hydrogen bonding possible (Baarschers et al., 1964). Boldine **37**, on the other hand exhibited two pK_a values due to the presence of two hydroxyl groups; 2-OH and 9-OH, in its ring A and D respectively (Figure 5.2). The lower pK_a values of the latter could have resulted from the intersystem crossing of electrons between rings D to A via resonance of the electron donating 9-OH group. As for the 2-OH group, its higher pK_a values may be due to the absence of the intersystem crossing of electrons between ring A to D via resonance because the 2-OH group in ring A acts as an electron acceptor (Das, 2001). The additional pK_a values of boldine **37** at 9.57 and 9.56 belonging to the absorbance at 312 and 253 nm respectively (Table 5.4) may be referred to the mean value of the two ionization constants corresponding to the 2-OH and 9-OH groups.

Table 5.4: Values of Ionization Constant for Alkaloids **37**, **41**, **42** (2×10^{-4} M) in 2% v/v Acetonitrile, $I = 0.1$ M (NaCl), at 35°C.

Alkaloids	λ /nm	K_a^a (M)	pK_a^b	$10^{-2} E_{SH}^a$ (M ⁻¹ cm ⁻¹)	$10^{-2} E_S^a$ (M ⁻¹ cm ⁻¹)
Boldine 37	332	$(7.61 \pm 0.3) \times 10^{-10}$	9.12	11.5 ± 0.8^c	141.0 ± 0.8^c
	312	$(2.68 \pm 0.5) \times 10^{-10}$	9.57	96.2 ± 1.4	116.7 ± 1.7
	295	$(3.59 \pm 1.2) \times 10^{-11}$	10.44	104.4 ± 1.5	154.6 ± 2.2
	274	$(6.19 \pm 1.5) \times 10^{-10}$	9.21	113.6 ± 1.1	77.4 ± 1.6
	253	$(2.74 \pm 0.5) \times 10^{-10}$	9.56	64.5 ± 1.2	132.0 ± 2.1
Isocorydine 41	338	$(1.77 \pm 0.1) \times 10^{-12}$	11.75	2.9 ± 0.5	64.0 ± 0.9
	270	$(2.24 \pm 0.3) \times 10^{-12}$	11.65	119.1 ± 0.6	78.4 ± 1.1
	246	$(1.75 \pm 0.02) \times 10^{-12}$	11.76	63.9 ± 0.9	161.9 ± 1.8
norisocorydine 42	338	$(7.72 \pm 1.1) \times 10^{-13}$	12.11	29.1 ± 0.7	85.5 ± 1.9
	270	$(7.63 \pm 5.2) \times 10^{-13}$	12.12	141.0 ± 2.5	99.5 ± 5.2
	246	$(1.02 \pm 0.5) \times 10^{-12}$	11.99	115.2 ± 2.7	193.1 ± 6.3

^a calculated from equation 5.7

^b calculated from $pK_a = (-\log K_a)$

^c errors limits are standard deviations.

In addition, temperature variations also influence the effective mobility of the alkaloids via its degree of ionisation as can be seen in Table 5.5. Norisocorydine **42** showed that the increase in the temperature could leads to a decrease in its pK_a values. As a conclusion to the Le Chatelier principle, a graph of pK_a versus $(1/T)$ was plotted. This gave a straight line with a regression value of 0.97, indicating that the acid dissociation was temperature dependant (Figure 5.7). Figure 5.8 shows UV absorption spectra of 2×10^{-4} M norisocorydine **42** in 2% v/v acetonitrile at pH 12.0 for different temperature.

Table 5.5: Values of Ionization Constant for Norisocorydine **42** ($2 \times 10^{-4}\text{M}$) in 2% v/v Acetonitrile, $I = 0.1 \text{ M}$ (NaCl), at 30- 50 °C.

T / °C	K_a^a (M)	pK_a^b	$10^{-2} E_{SH}^a$ ($\text{M}^{-1}\text{cm}^{-1}$)	$10^{-2} E_S^a$ ($\text{M}^{-1}\text{cm}^{-1}$)
30	$(5.80 \pm 0.86) \times 10^{-13}$	12.24	23.2 ± 0.7^c	80.0 ± 1.6
35	$(7.72 \pm 1.08) \times 10^{-13}$	12.11	29.1 ± 0.7	85.5 ± 1.9
40	$(10.14 \pm 1.45) \times 10^{-13}$	11.99	22.9 ± 0.7	81.5 ± 1.8
45	$(14.41 \pm 2.11) \times 10^{-13}$	11.84	22.8 ± 0.7	82.4 ± 2.1
50	$(19.43 \pm 3.09) \times 10^{-13}$	11.71	22.8 ± 0.8	81.5 ± 2.2

- ^a calculated from equation 5.7
^b calculated from $pK_a = (-\log K_a)$
^c errors limits are standard deviations.

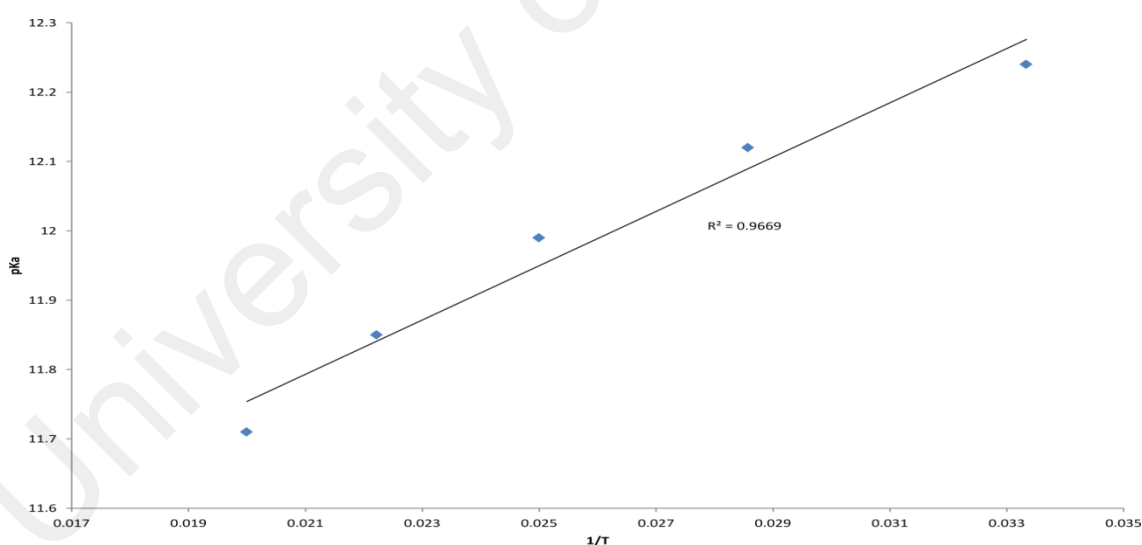


Figure 5.8: Graph of pK_a of Norisocorydine **42** ($2 \times 10^{-4}\text{M}$) in Water/acetonitrile, $I = 0.1 \text{ M}$ (NaCl) versus Different Temperature (30 – 50°C).

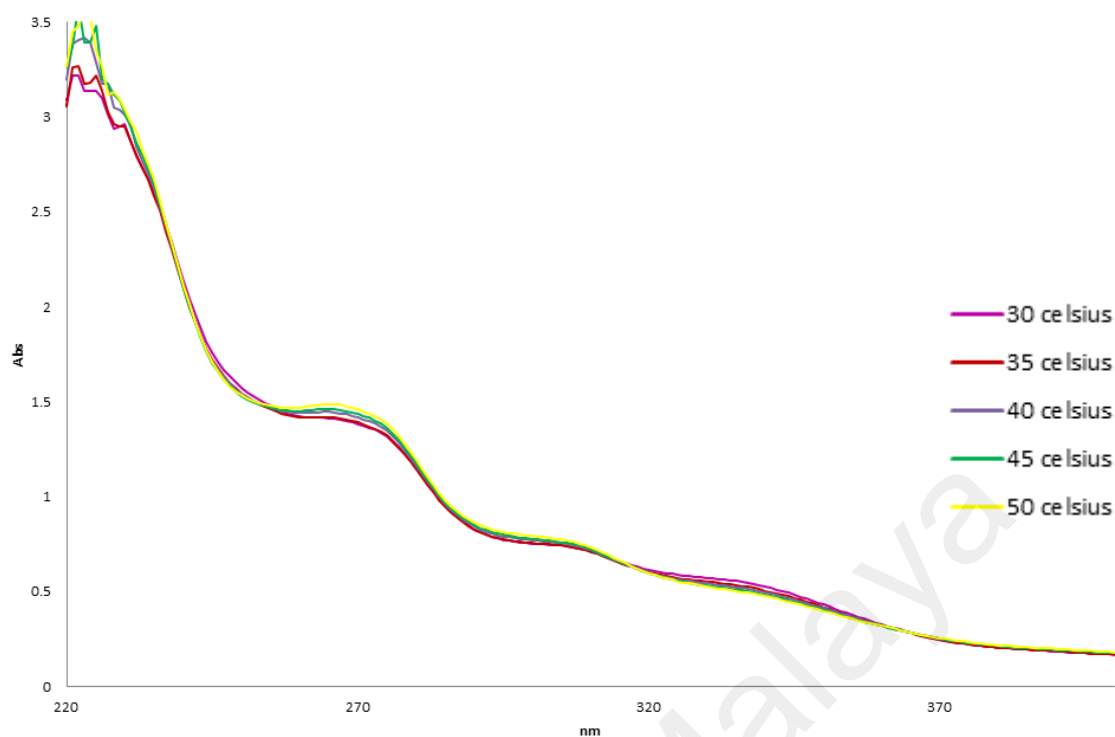


Figure 5.9: The UV Absorption Spectra of 2×10^{-4} M Norisocorydine **42** in 2% v/v Acetonitrile at pH 12.0 for Different Temperature (30-50°C).

5.4 Discussion

It is well known that acidic food vacuole in *Plasmodium* is a special organelle for the digestion of the host haemoglobin, as well as a storage site for hemazoin. It is also the site of action of many antimalarial drugs with a pH around 5.5 (Saliba et al., 2003). Therefore, it is important to find molecules that can cross the erythrocyte and parasite membranes to neutralize the parasite acidic food vacuole. Phenolic aporphine alkaloids are amphoteric and more stable in acidic rather than in alkaline medium. In acidic and physiological pH medium, the aporphines or alkaloids exist as non-ionized molecules therefore its basic nitrogen can donate its electron to neutralize acidic parasite food vacuole via pH trapping. Once protonated, they are trapped in the food vacuole resulting in the increased drug accumulation at the target site, and hence enhancing antiplasmodial activity (Kaur et al., 2010). Usually the majority of important drugs belong to the class of weak acids or weak bases as they can be present in solution as

both the non-ionized and ionized species. As an example for alkaloids, the antimalarial drug chloroquine has pK_a values around 8.35 and 10.4 (Adegoke et al., 2006). Therefore, the transmembrane distribution of a weak electrolyte is influenced by its pK_a and the pH gradient across the membrane. The pK_a is the pH at which half of the drug concentration (weak acid or base electrolyte) is in its ionized form (Brodie et al., 1960; Brunton et al., 2011).

The similar pattern of UV-vis spectra (Figure 5.9) of norisocorydine **42** for all different range of temperature, 30-50 °C, showed that the alkaloid structure is stable within the cited temperature range.

University of Malaya

CHAPTER 6: CONCLUSION

Two Malaysian plants from the Lauraceae family; *Alseodaphne corneri* (KL5641) and *Dehaasia longipedicellata* (KL 5634) have been thoroughly studied for their alkaloidal content. Phytochemical investigation of the bark and the leaves of *A. corneri* led to the isolation and characterization of three types of alkaloids; bisbenzylisoquinolines (BBIQ), benzylisoquinolines (BIQ) and aporphines. Nine BBIQs were isolated from the bark of *A. corneri*, in which eight were classified as type VI BBIQ, namely; 2-norobaberine **115**, gyrolidine **18**, *O*-methyllimacusine **118**, 3', 4'-dihydronorstephasubine **19**, 3', 4'-dihydo-stephasubine **119**, norstephasubine **20**, stephasubine **120** and stephasubimine **121**, together with one type VIII BBIQ; thalrugosine **71** and one new benzyltetrahydroisoquinoline alkaloid; cornerin A **124**. Studies of the leaves of *A. corneri* yielded five aporphines; *N*-methyllaurotetanine **26**, laurotetanine **27**, *N*-methyllindcarpine **123**, isocorydine **41** and norisocorydine **42**. The bark and the leaves of *D. longipedicellata* (KL 5634) yielded four different types of alkaloids; morphinandienones, aporphines, BIQs and BBIQs. In total eight alkaloids were isolated from this plant; sinoacutine **29**, milonine **46** and sebiferine **47** were morphinandienones, laurotetanine **27**, norboldine **36** and boldine **37** were aporphines, *O*-*O*-dimethylgrisabine **48** was a type I BBIQ. Reticuline **8**, a BIQ and laurotetanine **27** were afforded from both plants. The results showed that majority of alkaloids isolated from *A. corneri* belong to BBIQ skeleton which is rare skeleton, whereby only 7% of all isolated from Lauraceae belong to this skeleton. Furthermore, this is the first time; type VIII BBIQ skeleton, has been isolated from *Alseodaphne* plant. On the other hand, majority alkaloid isolated from *D. longipedicellata* belong to morphinandienone also another rare skeleton, whereby, only 6% of all alkaloid isolated from Lauraceae belong to this skeleton. The structure of all the isolated alkaloids were elucidated by extensive

spectroscopic methods; 1D-NMR, 2D-NMR, UV, IR, MS and upon comparison with literature data.

Both species showed positive response to antiplasmodial, antioxidant (DPPH, FRAP, metal chelating) and cytotoxic activities. The results showed potent *in vitro* antiplasmodial activity of the crude CH₂Cl₂ bark extract of *A. corneri* and *D. longipedicellata* with IC₅₀ values of 2.78 µg/ml and 1.30 µg/ml, respectively, against the K1 resistant strain of *P. falciparum*. Evaluation of bioactivities afforded that three alkaloids; two BBIQ and one aporphine showed potent antiplasmodial activities; norstephasubine **20** (0.116 µM), *O-O*-dimethylgrisabine **48** (0.031 µM) and laurotetanine **27** (0.189 µM). **48** had a higher potency with a lower IC₅₀ value compared to the antimalarial drug, chloroquine, 0.090 µM. Antioxidant properties of a drug are beneficial to the host (human) as it could help as an additive therapy to reduce the side effects of malaria disease. Thus, these alkaloids have also been tested for their antioxidant activities. **20**, **27** and **48** showed high DPPH scavenging and metal chelating activities in comparison to the standards. **48** showed the highest scavenging activity with an IC₅₀ value of 28.75 µM when compared to the standard, BHA (77.73 µM). Furthermore, the most potent alkaloid, **48** apart from being potent antiplasmodial and antioxidant agents, is also not toxic towards normal pancreatic cell line, which makes it a good candidate for the drug development of malarial compounds. The BBIQ alkaloids were found to be more active than aporphine in both activities, which could be due to the two nitrogen atom in their former as compared to one in the latter. Three of the bioactive and highest yield alkaloids; boldine **37**, isocorydine **41** and norisocorydine **42** were studied for acid dissociation constant using UV-vis spectrophotometry. The UV-vis spectra of all of the alkaloids remained unchanged in acidic condition; however substantial bathochromic shifts were observed due to the deprotonation of the phenolic protons in basic condition. The *pK_a* values of **41** and **42** were 11.75 and 12.11,

respectively. Meanwhile, **37** gave two pK_a values of 9.12 and 10.44. Therefore, the pK_a values are substantially dependent on the position of the substituents. Moreover, all alkaloids showed pK_a values above the physiological pH; thereby all of them will not ionize at the physiological pH, thus permitting the basic nitrogen to be protonated and accumulated within the acidic food vacuole of *Plasmodium* via pH trapping. Subsequently, acidic food vacuoles that have been neutralized by the alkaloids would result in the enhancement of the antiplasmodial activity. Interestingly, these alkaloids also possessed antioxidant activities that will prevent oxidative damage to the host by binding to free heme and neutralizing the electrons produced during the *P.falciparum* mediated haemoglobin destruction in the host. Among all of the alkaloids, **37** showed comparable antiplasmodial and antioxidant activities and it is also not toxic to normal pancreatic cell line with pK_a values near to chloroquine. In conclusion, this study showed that alkaloids having pK_a values above the physiological pH, together with the antioxidant property are beneficial for the enhancement of the antiplasmodial activity. Therefore, one may suggest that *O-O*-dimethylgrisabine **48** and boldine **37** as potential candidates for the further development of antimalarial drugs that causes less damage to the host.

6.1 Future work

The most active compounds belong to BBIQ skeleton. These skeletons possess two nitrogen atoms that might be the active site for the bioactivities of antiplasmodial and antioxidant. These nitrogen atoms also might act as basic nitrogen to reduce acidic food vacuole. Thereby, the dissociation constant studies for BBIQ skeleton are necessary to further confirm their potency as antiplasmodial agents. The results also can be compared with aporphine structure and further analysis and comparison can be done between different isoquinoline skeleton of alkaloids.

CHAPTER 7: EXPERIMENTAL

7.1 Plant Material

The plant materials were collected and identified by Mr Teo Leong Eng, Mr Din Mat Nor and Mr. Rafly Syamsir from the phytochemical group of the Department of Chemistry, Faculty of Science, University of Malaya. They were deposited at the Herbarium of the Department of Chemistry, University of Malaya, Kuala Lumpur, Malaysia. The plant species and their respective localities are shown in Table 7.1.

Table 7.1: Plant Species and Locality

Voucher specimen	Species	Part of plant	Locality and date of collection
KL 5641	<i>Alseodaphne corneri</i>	Leaves and bark	Kenderong Reserve Forest, Gerik, Perak, Malaysia. 31 Mac 2009
KL 5634	<i>Dehaasia longipedicellata</i>	Leaves and bark	Sungai Tekam Reserve Forest, Jerantut, Pahang, Malaysia. 19 February 2009

7.2 Instrumentation

The 1D- and 2D-NMR spectra were recorded in deuterated chloroform (CDCl_3) on a JEOL LA, JEOL ECA FT NMR, BRUKER Advance III NMR spectrometers (400 or 600 Mhz for ^1H and 100 MHz for ^{13}C). Chemical shifts reported in ppm or δ scale and the coupling constant are given in Hz.

The ESIMS and LCMS-IT-TOF spectra were obtained from Agilent Technologies 6530 Accurate-Mass Q-TOF LC/MS with ZORBAX Eclipse XDB-C18 Rapid Resolution HT 4.6 mm i.d x 50mm x 1.8 μm column.

IR spectra were recorded on a Perkin Elmer Spectrum FTIR Spectrometer RXI with spectroscopic chloroform as the solvent. A Jasco P-1020 was used to record the optical rotation.

The UV spectra were obtained using a Shimadzu UV-250 Ultraviolet-Visible Spectrometer. Solvent used was methanol or acetonitrile, while the wavelength in which the spectrum was recorded is between 200-400 nm.

7.3 Solvent

All solvents were of AR grade. Those used for bulk extraction were distilled prior to usage. The solvents used were hexane, dichloromethane, methanol, ammonia solution and hydrochloric acid.

7.4 Chromatography

Purification processes were performed using various chromatography techniques in manner of classical or modern techniques.

7.4.1 Thin Layer Chromatography (TLC)

Aluminium supported silica gel 60 F₂₅₄ plates were used for visualized isolated compounds based on the spot of TLC. TLC spots were visualized under ultra-violet light (245-365 nm) using the model UVGL-58 after spraying with the Dragendorff's reagent.

7.4.2 Column Chromatography (CC)

Silica gel 60, 70-230 mesh ASTM (Mersk 7734) was used for column chromatography. A slurry of silica gel 60 (approximately ratio of 30:1, silica gel: sample) in dichloromethane solvent was poured into a glass column of appropriate size.

The crude extract was initially dissolved in minimum amount of solvent and loaded on top of the packed column. The extract was eluted with gradient solvent system at a certain flow rate.

7.4.3 Preparative Thin Layer Chromatography (PTLC)

PTLC silica gel 60 F₂₅₄ glass plates of size 20x20 cm were used for separation of compounds that cannot be separated by conventional column. UV Light Model UVGL-58 was used to examine bands on the PTLC.

7.4.4 Recycle High Performance Liquid Chromatography (RHPLC)

Recycle HPLC was performed on LC-908W-C60. Chromatographic analysis and separations were performed on a JAIGEL GS320 (21.5 mm ID, 500 mm L, 13 mm) size exclusion column using methanol as the solvent.

7.4.5 High Performance Liquid Chromatography (HPLC)

HPLC was performed on WATERS equipped with Binary Gradient Module (Waters 2545), System fluidics Organizer (Waters SFO), and Photoiodide Array Detector (190-600nm, Waters 2998) and sample manager (Waters 2767). Chromatographic analysis and separations were performed on CHROMALITH semiprep RP18-encapped HPLC column. The samples were eluted at a flow rate of 4 mL/min.

7.5 Reagents

Mayer's and Dragendorff's reagent were used to identify the presence of the alkaloids and alkaloids spotting (TLC).

7.5.1 Mayer's Reagent (Potassium Mercuric Iodide)

1.4 g mercuric iodide in 60 ml distilled water was mixed with solution of 5.0 g potassium iodide in 10 ml distilled water. The mixture was then made up to 100 ml solution. The positive result was indicated by the formation of white precipitate when the aqueous layer (acidified) was treated with 2-3 drops of Mayer's reagent.

7.5.2 Dragendorff's Reagent (Potassium Bismuth Iodide)

Bismuth (III) nitrate (0.85 g) was added in a mixture glacial acetic acid (10 ml) and distilled water (40 ml) for solution A. While for solution B; Potassium iodide (8.0 g) was dissolved in distilled water (20 ml). To prepare the stock solution, solution A and B was mixed with equal volumes. The stock solution (20 ml) was then diluted in the mixture acetic acid (20) ml and distilled water (60 ml) for spray agent. A positive result was indicated by the formation of orange spots.

7.6 Extraction of the Bark

Plant extraction was carried out by cold percolation. Dried grounded bark samples (*Alseodaphne corneri* and *Dehaasia longipedicellata*) were initially defatted with hexane (17 L) for three days at room temperature. Then, the hexane extract was filtered and dried on the rotary evaporator. The plant material or residue after hexane extraction were dried and then later moistened with 25% ammonia solution and left for 2 hours. They were then re-extracted with dichloromethane (CH_2Cl_2) (17 L) for three days and the CH_2Cl_2 extract was dried using a rotary evaporator to obtain CH_2Cl_2 crude extract. The hexane crude was obtained as a yellowish residue while the CH_2Cl_2 crude was obtained as dark brown residue. The yields of the crudes extracts of each plant are given in Table 7.2.

7.7 Extraction of the Leaves

An extraction method for leaves was similar to bark but with additional acid-base extraction for CH₂Cl₂ extract. The CH₂Cl₂ extract was concentrated to about 500 ml by using rotary evaporator. Then, 5% HCl (under ice-bath condition) was added to give two layers of organic and aqueous phase. Then, the mixture was subjected to the separating funnel. The organic layer (below) was removed and the aqueous layer was monitored with Mayer's reagent test. Then, the aqueous layer further basified with NH₃ solution until pH 11 (under ice-bath condition). Then, the mixture was transfer to separating funnel. This time, the organic layer of CH₂Cl₂ was taken and further washed with distilled water and dried with sodium sulphate anhydrous. Finally, the organic solution was concentrated using rotary evaporator to give CH₂Cl₂ crude. The yields of the crude alkaloid from leaves extract of *A. corneri* are given in Table 7.2.

Table 7.2: Yield of Crude Extracted from Plants.

Species	Part of plant	Amount (kg)	Yield of crude (g)	Percentage yield (%)
<i>A. corneri</i>	Leaves	1.5	Hexane: 10.3	0.69
			CH ₂ Cl ₂ : 22.0	1.47
			CH ₂ Cl ₂ : 4.67	0.31
			(After acid base extraction)	
	Bark	2.0	Hexane: 13.5	0.68
			CH ₂ Cl ₂ : 40.0	2.00
<i>D. longipedicellata</i>	Leaves	1.5	Hexane: 17.7	1.18
			CH ₂ Cl ₂ : 32.7	2.18
	Bark	2.5	Hexane: 6.5	0.26
			CH ₂ Cl ₂ : 18.7	0.75

7.8 Isolation and Purification

The CH₂Cl₂ crude was subjected to column chromatography using silica gel (0.04-0.063mm; 6 x 65 cm) as the stationary phase. The solvent used was CH₂Cl₂ with increasing portion of methanol (gradient eluent system) act as mobile phase. Solvent

system used for column chromatography separation of CH₂Cl₂ crude of *A. corneri* and *D. longipedicellata* were shown in Table 7.3.

Solvent system CH₂Cl₂ : MeOH (CH₃OH)

Table 7.3: Solvent Systems for the Isolation and Purification of CH₂Cl₂ Crude Alkaloid.

Dichloromethane (CH ₂ Cl ₂)	:	MeOH (CH ₃ OH)
100	:	0
99	:	1
98	:	2
96	:	4
95	:	5
94	:	6
92	:	8
90	:	10
80	:	20
0	:	100

The fractions collected were grouped into a series of fractions, monitored with TLC and the fraction with similar compounds was then combined. Each series were then treated separately to isolate and purify its alkaloid content by PTLC and small column chromatography. Certain fractions were separated using HPLC and recycled HPLC to purify the alkaloids. Conditions that have been used to purify the alkaloids using parameters and solvent system are showed in Table 7.4 (HPLC) and Table 7.5 (RHPLC). Figure 7.1 show the chromatogram for isolation of norboldine **36**. Figure 7.2 show the chromatogram for purification of gyrolidine **18** and stephasubimine **122**.

Table 7.4: HPLC Solvent System of Fraction from *D. longipedicellata* for Norboldine

36

Time (min)	Flow rate (mL/min)	% B2 (Acetonitrile (ACN) + 0.1% formic acid (FA))	% A2 (H ₂ O+ 0.1% formic acid)
0	2.5	80	20
5	2.5	80	20
45	2.5	00	100
50	2.5	00	100
51	2.5	80	20
60	2.5	80	20

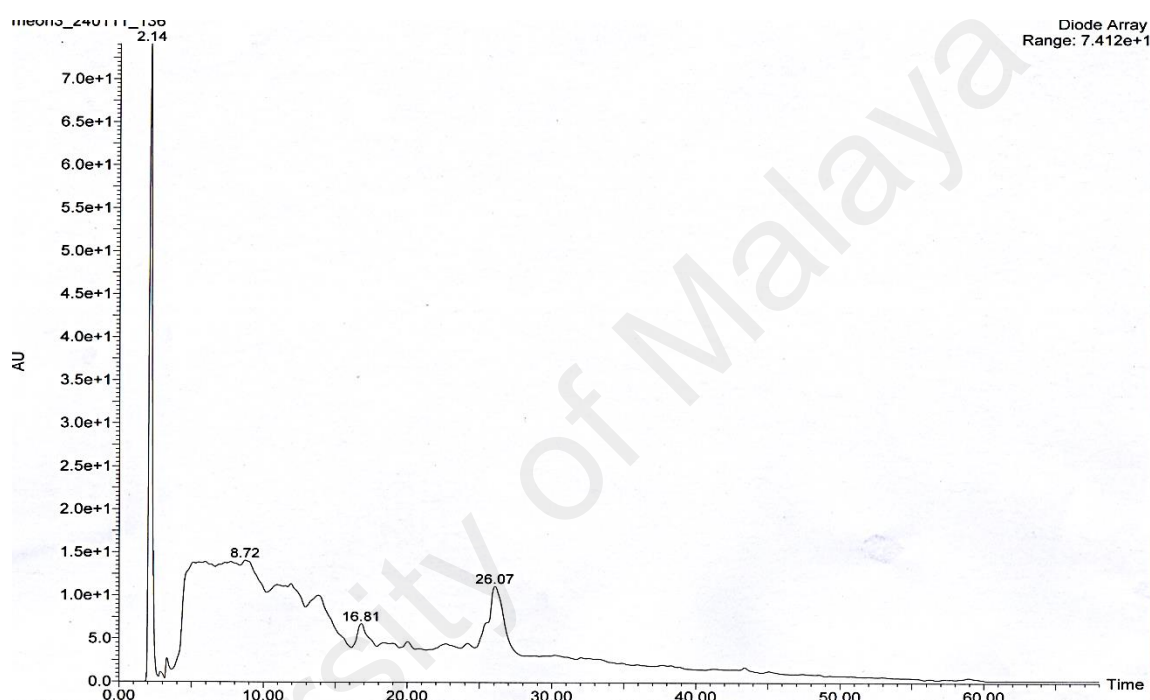


Figure 7.1: HPLC Chromatogram of Fraction 61-140 from *D. longipedicellata* for Norboldine **36**

Table 7.5: RHPLC Solvent System of Fraction from *A. corneri* for Gyrolidine **18** and Stephasubimine **122**.

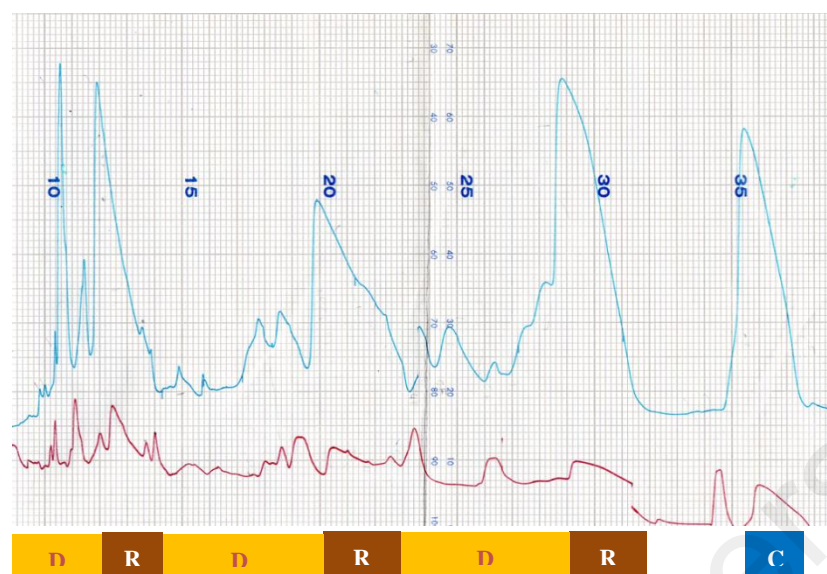
Three recycles in a duration of 40 min. afforded gyrolidine **18** with retention times of 35 min

Time (min)	Flow rate (mL/min)	% Methanol
0	4.0	100
40	4.0	100

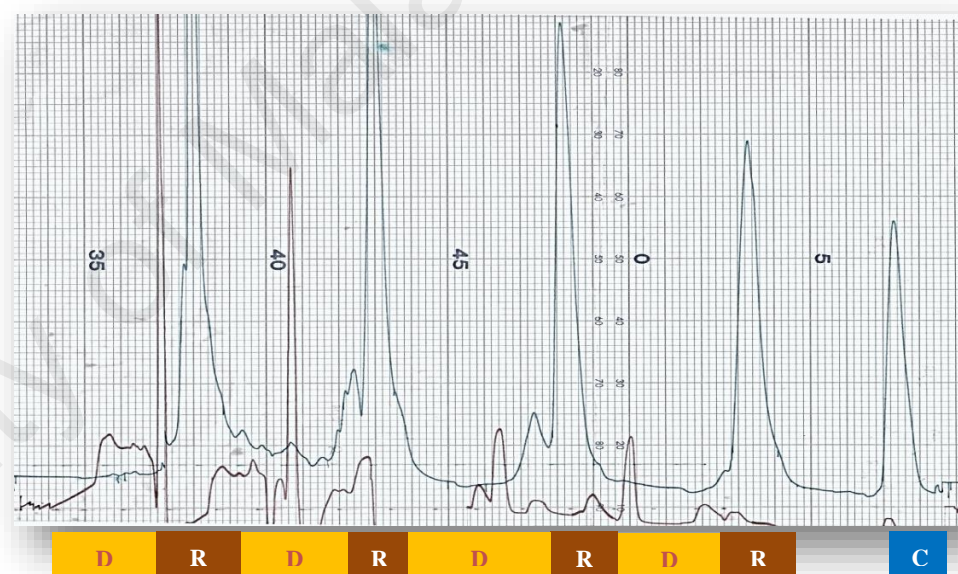
Eleven recycles in a duration of 60 min. yielded stephasubimine **121** with retention times of 57 min

Time (min)	Flow rate (mL/min)	% Methanol
0	4.0	100
60	4.0	100

A:



B:



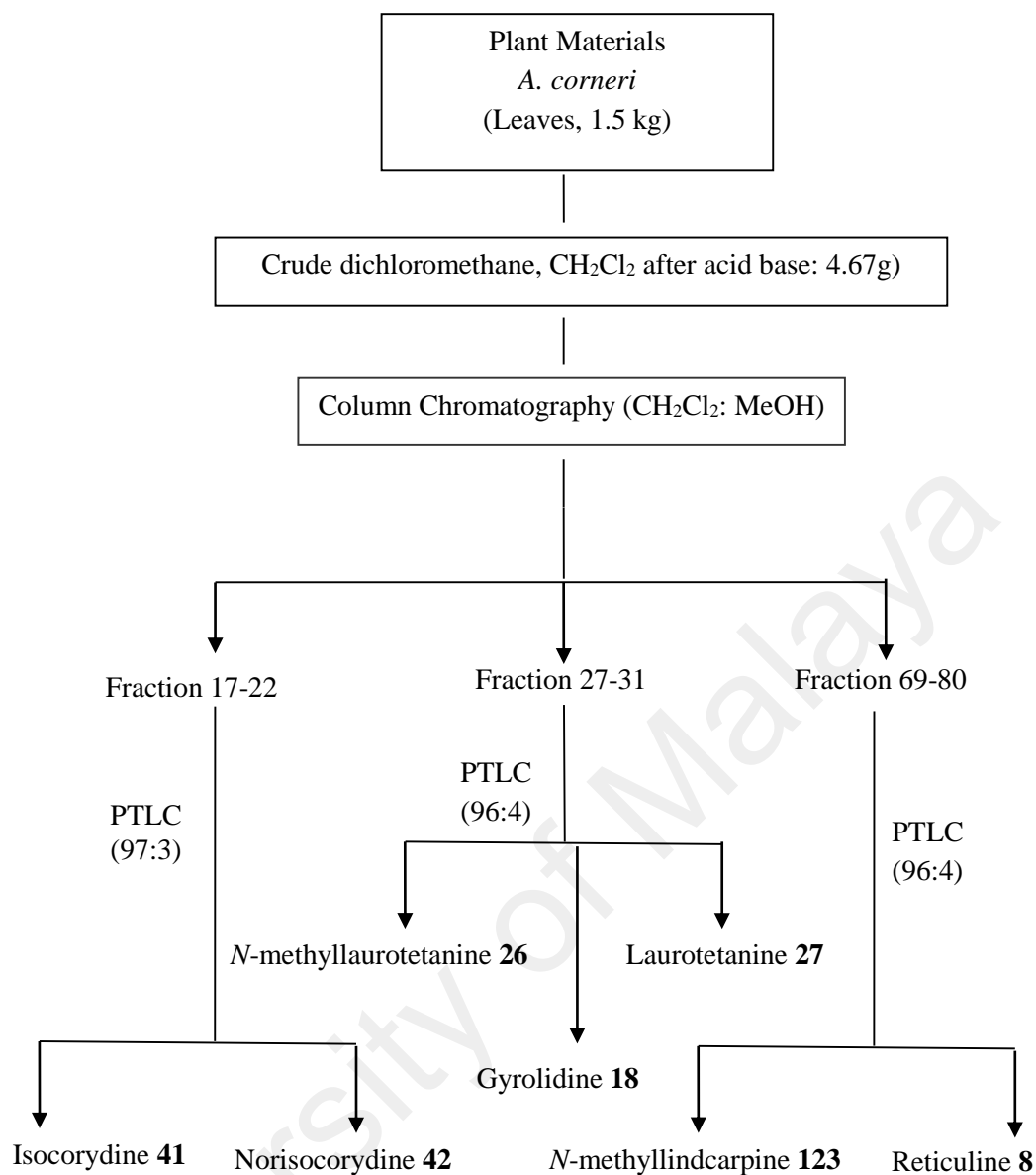
Column: size exclusion
Solvent: Methanol
Flow rate: 4.0ml/min

R Recycled area
D Drained area
C Collected area

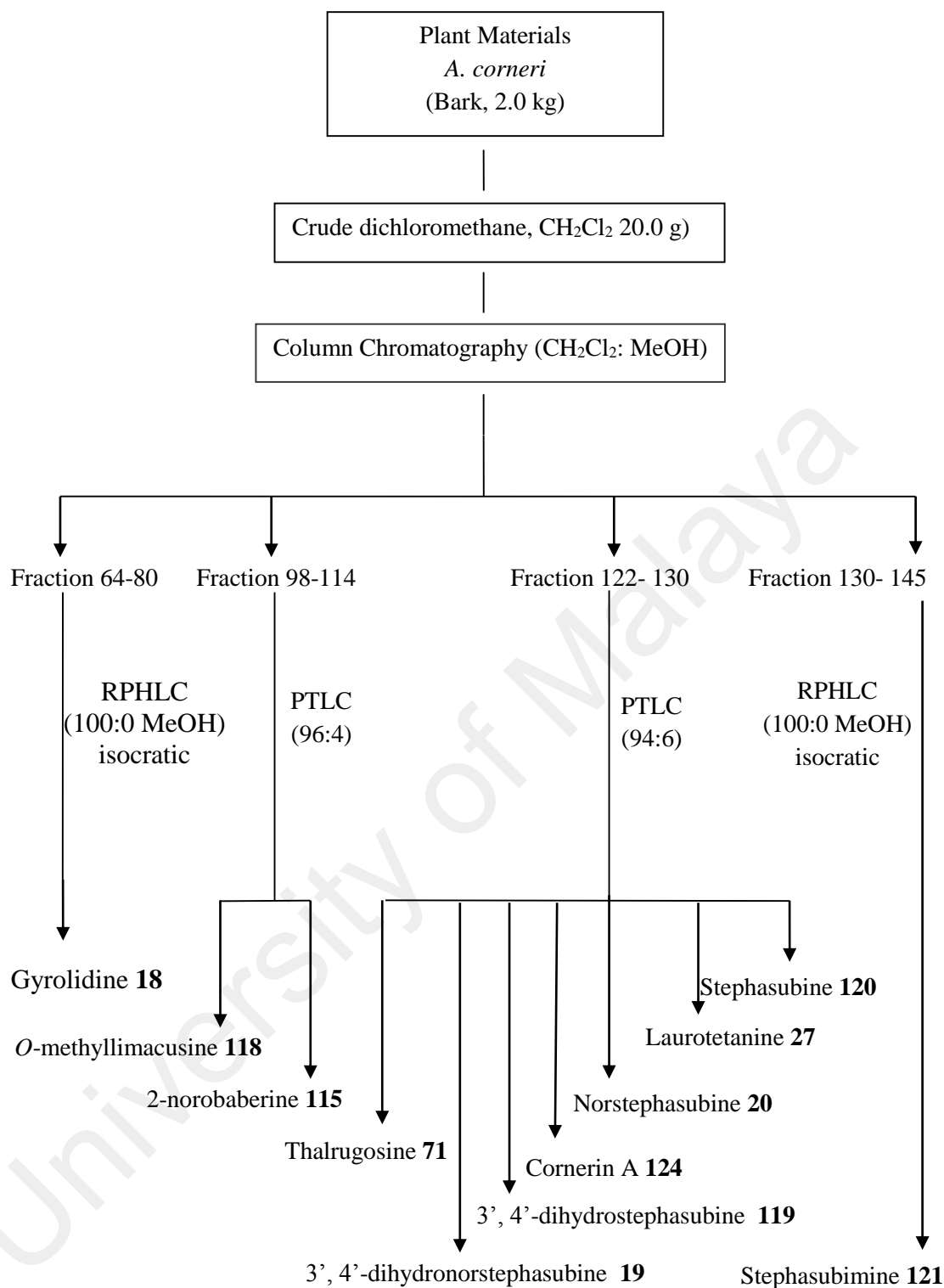
Figure 7.2: RHPLC Chromatogram of Fraction from *A. corneri* for A (Gyrolidine **18**) and B (Stephasubimine **121**)

Structural identification of the isolated compounds were carried out by using spectroscopic methods such as 1D NMR (^1H , ^{13}C , DEPT), 2D NMR (COSY, HSQC, HMBC, NOESY), UV, IR, and LCMS. The optical rotations for the optically active compounds were also determined.

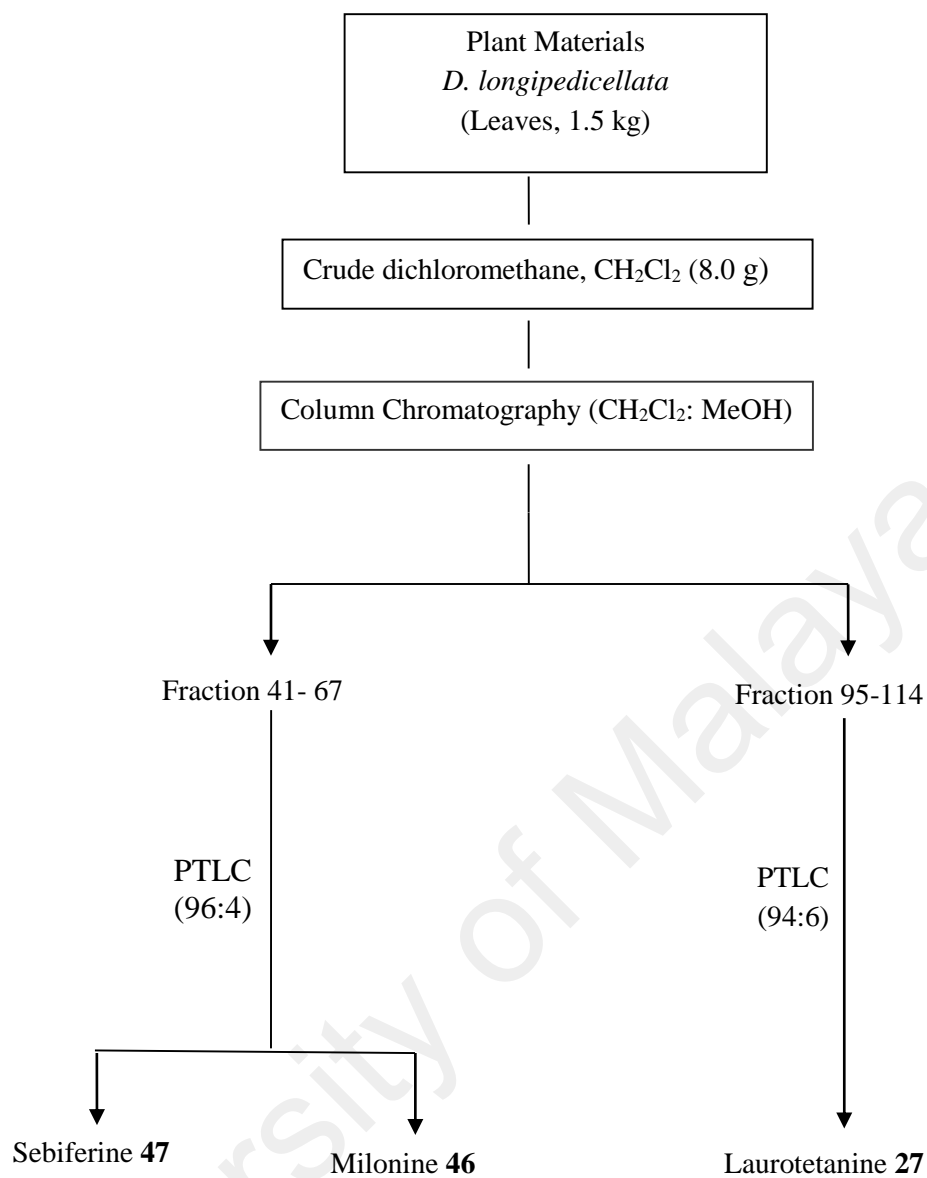
The isolation of alkaloids from *Alseodaphne corneri* are summarized in the flow diagram shown in Scheme 7.1 (leaves) and Scheme 7.2 (bark), whereas alkaloids isolated from *D. longipedicellata* are shown in Scheme 7.4 (leaves) and Scheme 7.3 (bark). The list of alkaloids isolated from the leaves and bark of *A. corneri* are shown in Table 7.6 and Table 7.7 respectively. Table 7.8 and Table 7.9 showed alkaloids isolated from the leaves and bark of *D. longipedicellata*.



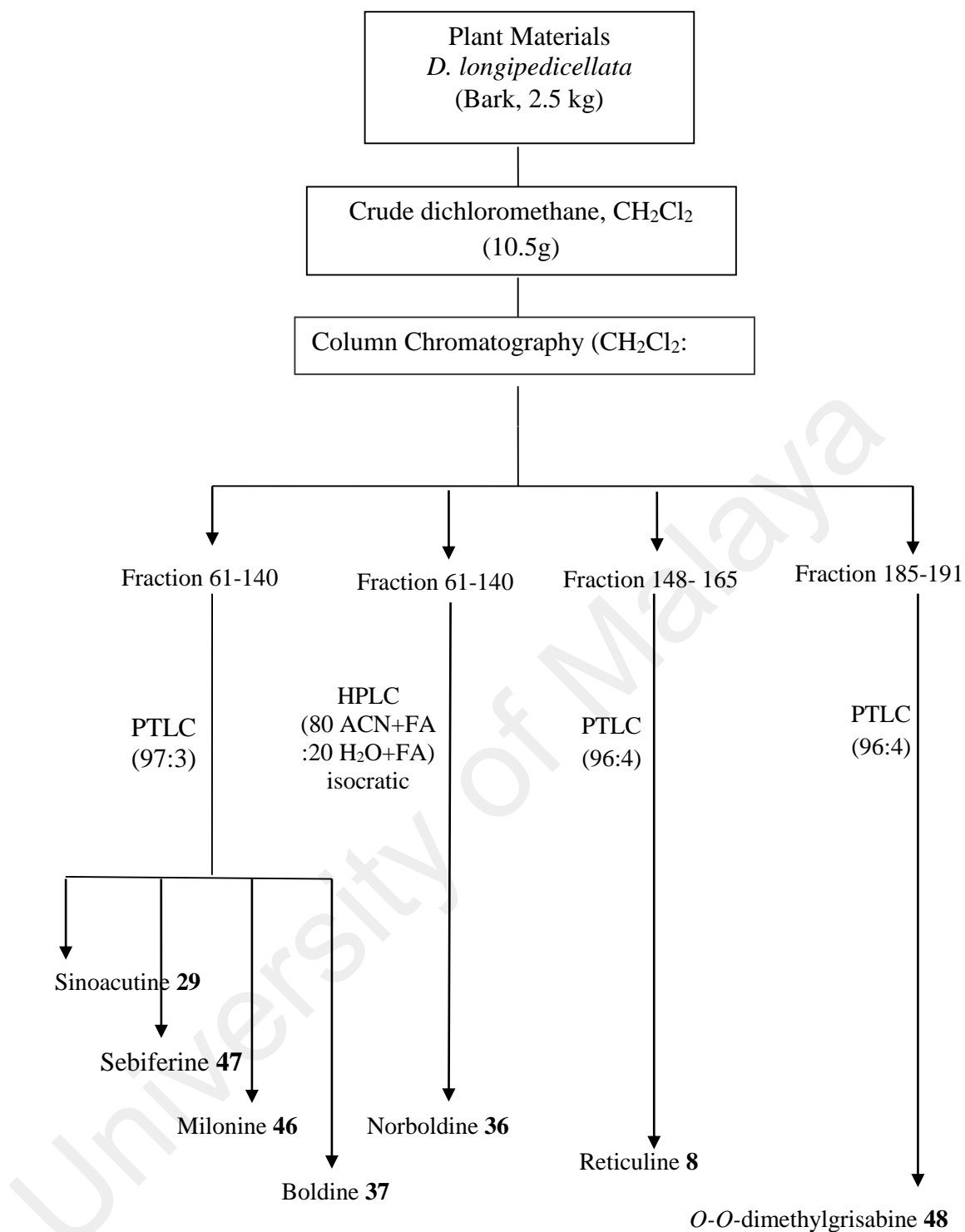
Scheme 7.1: Isolation of Alkaloids from the Leaves of *Alseodaphne corneri* Kosterm.



Scheme 7.2: Isolation of Alkaloids from the Bark of *Aseodaphne corneri* Kosterm.



Scheme 7.3: Isolation of Alkaloids from the Leaves of *Dehaasia longipedicellata*



Scheme 7.4: Isolation of Alkaloids from the Bark of *Dehaasia longipedicellata*

Table 7.6: List of Eluent and Fractions of Respective Alkaloids from the Leaves of *Alseodaphne corneri* Kosterm

Alkaloid isolated	Eluent CH ₂ Cl ₂ : MeOH	Fraction	Rf	Weight (mg)
Isocorydine 41	97 : 3	17-22	0.58	10.5
Norisocorydine 42	96 : 4	17-22	0.37	12.8
<i>N</i> -Methyl Laurotetanine 26	96 : 4	27-31	0.55	4.0
Gyrolidine 18	96 : 4	27-31	0.34	7.0
Laurotetanine 27	96 : 4	27-31	0.24	3.5
<i>N</i> -methyl lindcarpine 123	96 : 4	69-80	0.81	3.4
Reticuline 8	96 : 4	69-80	0.51	2.8

Table 7.7: List of Eluent and Fractions of Respective Alkaloids from the Bark of *Alseodaphne corneri* Kosterm

Alkaloid isolated	Eluent MeOH (RHPLC- isocratic)	Fraction	Rt	Weight (mg)
Gyrolidine 18	100	64-80	35.0 min	14.1
Stephasubimine 121	100	130-145	57.0 min	3.5
Alkaloid isolated	Eluent CH ₂ Cl ₂ : MeOH	Fraction	Rf	Weight (mg)
<i>O</i> -methyllimacusine 118	96 : 4	98-114	0.50	13.2
2-norobaberine 115	96 : 4	98-114	0.45	9.7
Thalrugosine 71	94 : 6	122-130	0.89	2.1
3', 4'-dihydrostephasubine 119	94 : 6	122-130	0.81	2.3
3', 4'-dihydronorstephasubine 19	94 : 6	122-130	0.71	3.7
Cornerin A 124	94 : 6	122-130	0.60	1.8
Stephasubine 120	94 : 6	122-130	0.44	10.0
Laurotetanine 27	94 : 6	122-130	0.35	6.0
Norstephasubine 20	94 : 6	122-130	0.27	12.0

Table 7.8: List of Eluent and Fractions of Respective Alkaloids from the Leaves of *Dehaasia longipedicellata*

Alkaloid isolated	Eluent CH ₂ Cl ₂ : MeOH	Fraction	Rf	Weight (mg)
Sebiferine 47	96 : 4	41-67	0.48	17.7
Milonine 46	96 : 4	41-67	0.42	27.7
Laurotetanine 27	94 : 6	95-114	0.51	2.5

Table 7.9: List of Eluent and Fractions of Respective Alkaloids from the Bark of *Dehaasia longipedicellata*

Alkaloid isolated	Eluent CH ₂ Cl ₂ : MeOH	Fraction	Rf	Weight (mg)
Sinoacutine 29	97 : 3	61-140	0.65	5.0
Sebiferine 47	97 : 3	61-140	0.58	20.0
Milonine 46	97 : 3	61-140	0.42	17.0
Boldine 37	97 : 3	61-140	0.33	10.0
Reticuline 8	96 : 4	148-165	0.38	11.5
<i>O-O</i> -dimethylgrisabine 48	96 : 4	185-191	0.83	8.0

Alkaloid isolated	Eluent ACN+FA: H ₂ O +FA	Fraction	Rt	Weight (mg)
Norbaldine 36	80: 20	61-140	2.00 min	12.2

7.9 Physical and Spectral Data of the Isolated Compounds

Reticuline 8

Reticuline	: C ₁₉ H ₂₃ NO ₄
UV λ_{\max} nm	: 285
IR ν_{\max} cm ⁻¹	: 3349
$[\alpha]_D^{25}$: +30.0° (c=0.20, CHCl ₃)
Mass spectrum m/z	: 330.1720 [M+H] ⁺
¹ H NMR (CDCl ₃) δ ppm	: see Table 3.2
¹³ C NMR (CDCl ₃) δ ppm	: see Table 3.2

2-norobaberine 115

2-norobaberine	: C ₃₇ H ₄₀ N ₂ O ₆
UV λ_{\max} nm	: 212 and 284
IR ν_{\max} cm ⁻¹	: 1266, 1514, 1640, 3306
$[\alpha]_D^{25}$: +130.0°(c=0.10, MeOH)
Mass spectrum m/z	: 609.2921 [M+H] ⁺
¹ H NMR (CDCl ₃) δ ppm	: see Table 3.3
¹³ C NMR (CDCl ₃) δ ppm	: see Table 3.3

Gyrolidine 18

Gyrolidine	: C ₃₈ H ₄₂ N ₂ O ₆
UV λ_{\max} nm	: 244 and 286
IR ν_{\max} cm ⁻¹	: 1268, 1510, 1637
$[\alpha]_D^{25}$: -53.0.0°(c=0.02, MeOH)
Mass spectrum m/z	: 623.3100 [M+H] ⁺

^1H NMR (CDCl_3) δ ppm	: see Table 3.4
^{13}C NMR (CDCl_3) δ ppm	: see Table 3.4

***O*-methyllimacusine 118**

<i>O</i> -methyllimacusine	: $\text{C}_{38}\text{H}_{42}\text{N}_2\text{O}_6$
UV λ_{max} nm	: 286
IR ν_{max} cm^{-1}	: 1269, 1508, 1607
$[\alpha]_D^{25}$: +90.0 (c=0.11, CHCl_3)
Mass spectrum m/z	: 623.3071 $[\text{M}+\text{H}]^+$
^1H NMR (CDCl_3) δ ppm	: see Table 3.5
^{13}C NMR (CDCl_3) δ ppm	: see Table 3.5

3', 4'-dihydronorstephasubine 19

3', 4'-dihydronorstephasubine	: $\text{C}_{35}\text{H}_{34}\text{N}_2\text{O}_6$
UV λ_{max} nm	: 203, 286
IR ν_{max} cm^{-1}	: 1260, 1510, 1604, 3600
$[\alpha]_D^{25}$: +30.0 (c=0.5, MeOH)
Mass spectrum m/z	: 579.2535 $[\text{M}+\text{H}]^+$
^1H NMR (CDCl_3) δ ppm	: see Table 3.6
^{13}C NMR (CDCl_3) δ ppm	: see Table 3.6

3', 4'-dihydrostephasubine 119

3', 4'-dihydrostephasubine	: $\text{C}_{36}\text{H}_{36}\text{N}_2\text{O}_6$
UV λ_{max} nm	: 203, 286
IR ν_{max} cm^{-1}	: 1220, 1260, 1460, 1510, 1605, 3610

$[\alpha]_D^{25}$: +50.0 (c=0.5, MeOH)
Mass spectrum m/z	: 593.2622 [M+H] ⁺
¹ H NMR (CDCl ₃) δ ppm	: see Table 3.7
¹³ C NMR (CDCl ₃) δ ppm	: see Table 3.7

Norstephasubine 20

Norstephasubine	: C ₃₅ H ₃₂ N ₂ O ₆
UV λ _{max} nm	: 244, 286, 338
IR ν _{max} cm ⁻¹	: 1223, 1259, 1432, 1512, 1606, 3400
$[\alpha]_D^{25}$: +310.0 (c=1.0, MeOH)
Mass spectrum m/z	: 577.2371 [M+H] ⁺
¹ H NMR (CDCl ₃) δ ppm	: see Table 3.8
¹³ C NMR (CDCl ₃) δ ppm	: see Table 3.8

Stephasubine 120

Stephasubine	: C ₃₆ H ₃₄ N ₂ O ₆
UV λ _{max} nm	: 244, 286, 338
IR ν _{max} cm ⁻¹	: 1232, 1261, 1514, 1637, 3306
$[\alpha]_D^{25}$: +350.0 (c=1.0, MeOH)
Mass spectrum m/z	: 591.2449 [M+H] ⁺
¹ H NMR (CDCl ₃) δ ppm	: see Table 3.9
¹³ C NMR (CDCl ₃) δ ppm	: see Table 3.9

Stephasubimine 121

Stephasubimine	: C ₃₅ H ₃₁ N ₂ O ₆
UV λ_{\max} nm	: 242, 281, 323
IR ν_{\max} cm ⁻¹	: 1229, 1260, 1506, 1602, 2933, 3392
$[\alpha]_D^{25}$: -
Mass spectrum m/z	: 575.2164 [M+H] ⁺
¹ H NMR (CDCl ₃) δ ppm	: see Table 3.10
¹³ C NMR (CDCl ₃) δ ppm	: see Table 3.10

Thalrugosine 71

Thalrugosine	: C ₃₇ H ₄₀ N ₂ O ₆
UV λ_{\max} nm	: 244, 286
IR ν_{\max} cm ⁻¹	: 1230, 1260, 1515, 1635, 3349
$[\alpha]_D^{25}$: +118.0 (c=1.1, MeOH).
Mass spectrum m/z	: 609.2930 [M+H] ⁺
¹ H NMR (CDCl ₃) δ ppm	: see Table 3.11
¹³ C NMR (CDCl ₃) δ ppm	: see Table 3.11

Isocorydine 41

Isocorydine	: C ₂₀ H ₂₄ O ₄ N
UV λ_{\max} nm	: 270, 310
IR ν_{\max} cm ⁻¹	: 1552, 1594, 3180
$[\alpha]_D^{25}$: +120.0 (c=0.30, CHCl ₃)
Mass spectrum m/z	: 342.1720 [M+H] ⁺
¹ H NMR (CDCl ₃) δ ppm	: see Table 3.12

^{13}C NMR (CDCl_3) δ ppm : see **Table 3.12**

Norisocorydine 42

Norisocorydine : $\text{C}_{19}\text{H}_{22}\text{NO}_4$

UV λ_{max} nm : 270, 310

IR ν_{max} cm^{-1} : 1580, 1624, 3314

$[\alpha]_D^{25}$: +178.0 ($c=1.20$, CHCl_3)

Mass spectrum m/z : 328.1538 $[\text{M}+\text{H}]^+$

^1H NMR (CDCl_3) δ ppm : see **Table 3.13**

^{13}C NMR (CDCl_3) δ ppm : see **Table 3.13**

***N*-methyllindcarpine 123**

N-methyllindcarpine : $\text{C}_{19}\text{H}_{21}\text{NO}_4$

UV λ_{max} nm : 270, 310

IR ν_{max} cm^{-1} : 1600, 1652, 3314

$[\alpha]_D^{25}$: +160.0 ($c=0.50$, CHCl_3)

Mass spectrum m/z : 328.1538 $[\text{M}+\text{H}]^+$

^1H NMR (CDCl_3) δ ppm : see **Table 3.14**

^{13}C NMR (CDCl_3) δ ppm : see **Table 3.14**

***N*-methyllaurotetanine 26**

N-methyllaurotetanine : $\text{C}_{20}\text{H}_{24}\text{NO}_4$

UV λ_{max} nm : 215, 285, 305

IR ν_{max} cm^{-1} : 1603, 3395

$[\alpha]_D^{25}$: +80.0 ($c=0.50$, CHCl_3)

Mass spectrum m/z	: 342.1716 [M+H] ⁺
¹ H NMR (CDCl ₃) δ ppm	: see Table 3.15
¹³ C NMR (CDCl ₃) δ ppm	: see Table 3.15

Laurotetanine 27

Laurotetanine	: C ₁₉ H ₂₁ NO ₄
UV λ _{max} nm	: 215, 285, 305
IR ν _{max} cm ⁻¹	: 1590, 1614, 3330
[α] _D ²⁵	: +120.0 (c=0.50, CHCl ₃)
Mass spectrum m/z	: 328.1566 [M+H] ⁺
¹ H NMR (CDCl ₃) δ ppm	: see Table 3.16
¹³ C NMR (CDCl ₃) δ ppm	: see Table 3.16

Norboldine 36

Norboldine	: C ₁₈ H ₁₉ NO ₄
UV λ _{max} nm	: 282, 305
IR ν _{max} cm ⁻¹	: 1595, 1620, 3162, 3584
[α] _D ²⁵	: +70.0 (c=0.7, MeOH)
Mass spectrum m/z	: 314.1446 [M+H] ⁺
¹ H NMR (CDCl ₃) δ ppm	: see Table 3.17
¹³ C NMR (CDCl ₃) δ ppm	: see Table 3.17

Boldine 37

Boldine	: C ₁₉ H ₂₁ NO ₄
UV λ _{max} nm	: 282, 305
IR ν _{max} cm ⁻¹	: 1603, 1641, 3327

$[\alpha]_D^{25}$: +125.0 (c=1.40, MeOH)
Mass spectrum m/z	: 328.1523 [M+H] ⁺
¹ H NMR (CDCl ₃) δ ppm	: see Table 3.18
¹³ C NMR (CDCl ₃) δ ppm	: see Table 3.18

Milonine 46

Milonine	: C ₁₉ H ₂₃ NO ₄
UV λ _{max} nm	: 210, 264
IR ν _{max} cm ⁻¹	: 1582, 1614, 1682, 3506
$[\alpha]_D^{25}$: +60.0 (c=0.50, MeOH)
Mass spectrum m/z	: 330.1728 [M+H] ⁺
¹ H NMR (CDCl ₃) δ ppm	: see Table 3.19
¹³ C NMR (CDCl ₃) δ ppm	: see Table 3.19

Sinoacutine 29

Sinoacutine	: C ₂₀ H ₂₃ NO ₄
UV λ _{max} nm	: 229, 272
IR ν _{max} cm ⁻¹	: 1582, 1615, 1676, 3410
$[\alpha]_D^{25}$: -10.0 (c=0.10, CHCl ₃)
Mass spectrum m/z	: 328.1530 [M+H] ⁺
¹ H NMR (CDCl ₃) δ ppm	: see Table 3.20
¹³ C NMR (CDCl ₃) δ ppm	: see Table 3.20

Sebiferine 47

Sebiferine	: C ₁₉ H ₂₂ NO ₄
UV λ_{\max} nm	: 209, 238, 280
IR ν_{\max} cm ⁻¹	: 1518, 1617, 1645, 1666, 2936
$[\alpha]_D^{25}$: +10.0 (c=0.10, CHCl ₃)
Mass spectrum m/z	: 342.1730 [M+H] ⁺
¹ H NMR (CDCl ₃) δ ppm	: see Table 3.21
¹³ C NMR (CDCl ₃) δ ppm	: see Table 3.21

O-O-dimethylgrisabine 48

<i>O-O</i> -dimethylgrisabine	: C ₃₉ H ₄₆ N ₂ O ₆
UV λ_{\max} nm	: 296
IR ν_{\max} cm ⁻¹	: 1226, 1610, 2930
$[\alpha]_D^{25}$: -35.0 (c=0.002, CHCl ₃)
Mass spectrum m/z	: 639.3432 [M+H] ⁺
¹ H NMR (CDCl ₃) δ ppm	: see Table 3.22
¹³ C NMR (CDCl ₃) δ ppm	: see Table 3.22

Cornerin A 124

Cornerin A	: C ₂₈ H ₂₇ NO ₈
IR ν_{\max} cm ⁻¹	: 1260, 1733, 3400
Mass spectrum m/z	: 506.3329 [M+H] ⁺
¹ H NMR (CDCl ₃) δ ppm	: see Table 3.23
¹³ C NMR (CDCl ₃) δ ppm	: see Table 3.23

REFERENCES

- Abdur, R. M., & Aftaf, N. M. (1988). Chemical investigation of a medicinal plant *Dehaasia kurzii*. II. Isolation of alkaloidal components. *Chittagong University Studies, Part 2, 12*(1), 11-16.
- Abdur, R. M., & Anwar, H. M. (1987). Chemical investigation of a rare medicinal plant *Dehaasia kurzii*; separation and identification of a hydrocarbon n-nonacosane. *Chittagong Univ. Stud., Part 2, 11*(1-2), 131-135.
- Adegoke, O. A., Babalola, C. P., Oshitade, O. S., & Famuyiwa, A. A. (2006). Determination of the physicochemical properties of pyronaridine - a new antimalarial drug. *Pakistan Journal of Pharmaceutical Sciences, 19*(1), 1-6.
- Adjalley, S. H., Lee, M. C. S., & Fidock, D. A. (2010). A Method for Rapid Genetic Integration into *Plasmodium falciparum* Utilizing Mycobacteriophage Bxb1 Integrase. *Methods in molecular biology (Clifton, N.J.)*, 634, 87-100.
- Ahmad, R., & Cava, M. P. (1977). Grisabine and grisabutine, new bisbenzylisoquinoline alkaloids from *Abuta grisebachii*. *The Journal of organic chemistry*, 42(13), 2271-2273.
- Ali, M. K., Badman, T., Bertzky, B., Engels, B., Hughes, A., & Shi, Y. (2013). *Terrestrial biodiversity and the World Heritage List : identifying broad gaps and potential candidate sites for inclusion in the natural World Heritage network* (M. K. Ali, T. Badman, B. Bertzky, B. Engels, A. Hughes, & Y. Shi Eds.). Gland, CH : IUCN ; Cambridge, UK: IUCN publication.
- Aniszewski, T. (2007). *Alkaloids - Secrets of Life: Alkaloid Chemistry, Biological Significance, Applications and Ecological Role*. University of Eastern Finland, Joensuu, Finland: Elsevier Science, 1-15.
- Atamna, H., & Ginsburg, H. (1993). Origin of reactive oxygen species in erythrocytes infected with *Plasmodium falciparum*. *Molecular and biochemical parasitology*, 61(2), 231-241.
- Atta-Ur-Rahman, Pervin, A., & Abdur, R. M. (1990). Isolation and structural studies on the alkaloids of *Dehaasia kurzii*. *Fitoterapia, LXII*(3), 261-265.
- Augustyniak, A., Bartosz, G., Cipak, A., Duburs, G., Horakova, L., Luczaj, W., et al. (2010). Natural and synthetic antioxidants: an updated overview. *Free Radic Res*, 44(10), 1216-1262.

- Avdeef, A., Box, K. J., Comer, J. E. A., Gilges, M., Hadley, M., Hibbert, C., et al. (1999). PH-metric log *P* 11. p*K*_a determination of water-insoluble drugs in organic solvent–water mixtures. *Journal of pharmaceutical and biomedical analysis*, 20(4), 631-641.
- Baarschers, W. H., Arndt, R. R., Pachler, K., Weisbach, J. A., & Douglas, B. (1964). Nuclear magnetic resonance study of aporphine alkaloids. *Journal of the Chemical Society*, 4778-4782.
- Babcock, P. A., & Segelman, A. B. (1974). Alkaloids of *Lindera benzoin* (L.) Blume (Lauraceae) I: Isolation and identification of laurotetanine. *Journal of pharmaceutical sciences*, 63(9), 1495-1496.
- Barber, B., William, T., Dhararaj, P., Anderios, F., Grigg, M., Yeo, T., et al. (2012). Epidemiology of *Plasmodium knowlesi* malaria in north-east Sabah, Malaysia: family clusters and wide age distribution. *Malaria Journal*, 11(1), 401.
- Bartley, J. P., Baker, L. T., & Carvalho, C. F. (1994). Alkaloids of *Stephania bancroftii*. *Phytochemistry*, 36(5), 1327-1331.
- Barton, D., Kirby, A., & Kirby, G. (1968). Phenol oxidation and biosynthesis. Part XVII. Investigations on the biosynthesis of sinomenine. *Journal of the Chemical Society C: Organic*, 929-936.
- Bender, D. A. (2007). *Introduction to Nutrition and Metabolism, Fourth Edition*. University College London, UK: Taylor & Francis, 13-42.
- Bero, J., Frédérich, M., & Quetin-Leclercq, J. (2009). Antimalarial compounds isolated from plants used in traditional medicine. *Journal of Pharmacy and Pharmacology*, 61(11), 1401-1433.
- Betts, T. J. (1990). Chromatographic evaluation of boldine and associated alkaloids in boldo. *Journal of Chromatography A*, 511, 373-378.
- Biagini, G. A., Bray, P. G., Spiller, D. G., White, M. R. H., & Ward, S. A. (2003). The digestive food vacuole of the malaria parasite is a dynamic intracellular Ca²⁺ store. *Journal of Biological Chemistry*, 278(30), 27910-27915.
- Biamonte, M. A., Wanner, J., & Le Roch, K. G. (2013). Recent advances in malaria drug discovery. *Bioorganic & medicinal chemistry letters*, 23(10), 2829-2843.
- Blasko, G., & Cordell, G. A. (1988). Morphinandienone alkaloids. *Heterocycles*, 27(5), 1269-1300.

- Böhlke, M., Guinaudeau, H., Angerhofer, C. K., Wongpanich, V., Soejarto, D. D., Farnsworth, N. R., et al. (1996). Costaricine, a new antiplasmodial bisbenzylisoquinoline alkaloid from *Nectandra salicifolia* trunk bark. *Journal of natural products*, 59(6), 576-580.
- Bowsher, C., Steer, M. W., & Tobin, A. K. (2008). *Plant Biochemistry* (1 ed.). New York, USA: Garland Science, 335-337.
- Boyd, M. R., & Paull, K. D. (1995). Some practical considerations and applications of the National Cancer Institute in vitro anticancer drug discovery screen. *Drug Development Research*, 34(2), 91-109.
- Brodie, B. B., Kurz, H., & Schanker, L. S. (1960). The importance of dissociation constant and lipid-solubility in influencing the passage of drugs into the cerebrospinal fluid. *Journal of Pharmacology and Experimental Therapeutics*, 130(1), 20-25.
- Brunton, L., Chabner, B., & Knollman, B. (2011). *Goodman and Gilman's The Pharmacological Basis of Therapeutics, Twelfth Edition* (12 ed.). China: McGraw-Hill Education, 17-39.
- Bun, S. S., Laget, M., Chea, A., Ollivier, E., & Elias, R. (2009). Cytotoxic activity of alkaloids isolated from *Stephania rotunda* in vitro cytotoxic activity of cepharanthine. *Phytotherapy Research*, 23(4), 587-590.
- Cao, Z. F. (1996). Scavenging effect of tetrandrine of active oxygen radicals. *Planta medica*, 62(5), 413-414.
- Castro, C. O., López, V. J., & Vergara, G. A. (1985). Aporphine alkaloids from *Phoebe pittieri*. *Phytochemistry*, 24(1), 203-204.
- Cavalcanti da Silva, E., Rayol, C. D., Medeiros, P. L., Figueiredo, R. C. B. Q., Piuvezan, M. R., Brabosa-Filho, J. M., et al. (2012). Antileishmanial activity of warifteine: a bisbenzylisoquinoline alkaloid isolated from *Cissampelos sympodialis* Eichl. (Menispermaceae). *The Scientific World Journal*, 516408, 516405 pp.
- Chalandre, M.-C., Bruneton, J., Cabalion, P., & Guinaudeau, H. (1986). Alcaloïdes de *Gyrocarpus americanus*. *Journal of natural products*, 49(1), 101-105.
- Chan, K.-L., Choo, C.-Y., Abdullah, N. R., & Ismail, Z. (2004). Antiplasmodial studies of *Eurycoma longifolia* Jack using the lactate dehydrogenase assay of *Plasmodium falciparum*. *Journal of ethnopharmacology*, 92(2-3), 223-227.

- Chang, Y. C., Chen, C. Y., Chang, F. R., & Wu, Y. C. (2001). Alkaloids from *Lindera glauca*. *Journal of the Chinese Chemical Society*, 48(4), 811-815.
- Charles, A., Joseph, M., & Ramani, A. (2013). Phytochemical Analysis of *Alseodaphne Semecarpifolia* Leaf Extract by GCMS. *Asian Journal of Pharmaceutical and Clinical Research*, 6(4).
- Charles, A., Joseph, M., & Ramani, V. A. (2012). In vitro antioxidant potential of *Alseodaphne semecarpifolia* leaf extract. *European Journal of Experimental Biology*, 2(2), 354-357.
- Charles, A., & Ramani, A. (2011). Phytochemical screening and antimicrobial resistance of *Alseodaphne semecarpifolia* nees. *Journal of Chemical and Pharmaceutical Research*, 3(5), 205-211.
- Chen, C.-K., Chen, C.-S., Chen, C.-H., & Lee, S.-S. (2007). Isoquinoline alkaloids from the leaves of *Dehaasia hainanensis*. *Natural Product Communications*, 2(1), 75-78.
- Chen, C.-K., Lee, S.-S., & Chen, C.-H. (2003). Chemical constituents from *Dehaasia triandra*. III. Bisbenzylisoquinoline alkaloids from the leaves and their conformational analysis. *Chinese Pharmaceutical Journal (Taipei, Taiwan)*, 55(1), 35-47.
- Chen, C. Y., Chang, F. R., & Wu, Y. C. (1997). The constituents from the stems of *Annona cherimola*. *Journal of the Chinese Chemical Society*, 44(3), 313-319.
- Choi, H.-S., Song, H. S., Ukeda, H., & Sawamura, M. (2000). Radical-Scavenging Activities of Citrus Essential Oils and Their Components: Detection Using 1,1-Diphenyl-2-picrylhydrazyl. *Journal of Agricultural and Food Chemistry*, 48(9), 4156-4161.
- Clausen, A., Dowling, T., & Bicker, G. (2002). Description of the retention behavior and chromatographic measurement of the change in pKa with temperature of a diastereomeric pair of isoleucine derivatives. *Journal of Liquid Chromatography and Related Technologies*, 25(5), 705-715.
- Cordell, G. A. (2013). Fifty years of alkaloid biosynthesis in Phytochemistry. *Phytochemistry*, 91, 29-51.
- Cordell, G. A. (2014). Phytochemistry and traditional medicine—The revolution continues. *Phytochemistry Letters*, 10(0), xxviii-xl.

- Corner, E. J. H. (1951). *Wayside Trees of Malaya* (Vol. 1). Malaysia: Malaysian Nature Society, 334-338.
- Cortes, S. d. F., Alencar, J. L. d., Thomas, G., & Filho, J. M. B. (1995). Spasmolytic action of warifteine a bisbenzylisoquinoline alkaloid isolated from the root bark of *Cissampelos sympodialis* Eichl. (Menispermaceae). *Phytotherapy Research*, 9, 579-583.
- Custodio, D. L., & Florencio da Veiga Junior, V. (2014). Lauraceae alkaloids. *RSC Advances*, 4(42), 21864-21890.
- Damas, P., Bruneton, J., Fournet, A., & Guinaudeau, H. (1985). 2-Norlimacusine, new bisbenzylisoquinoline isolated from *Sciadotenia eichleriana*. *Journal of natural products*, 48(1), 69-71.
- Das, T. N. (2001). Absorption Spectra, pKa, and Reduction Potential of Phenoxy Radical from 4,4'-Biphenol in Aqueous Medium. *Journal of Physical Chemistry A*, 105(24), 5954-5959.
- De Freitas, M. R., De Alencar, J. L., Da-Cunha, E. V. L., Barbosa-Filho, J. M., & Gray, A. I. (1995). Milonine, an 8, 14-dihydromorphinandienone alkaloid from leaves of *Cissampelos sympodialis*. *Phytochemistry*, 40(5), 1553-1555.
- De Heer, M. I., Korth, H.-G., & Mulder, P. (1999). Poly Methoxy Phenols in Solution: O-H Bond Dissociation Enthalpies, Structures, and Hydrogen Bonding. *Journal of Organic Chemistry*, 64(19), 6969-6975.
- Decker, E. A., & Welch, B. (1990). Role of ferritin as a lipid oxidation catalyst in muscle food. *Journal of Agricultural and Food Chemistry*, 38(3), 674-677.
- Dewick, P. M. (2009). *Medicinal Natural Products: A Biosynthetic Approach* (3 ed.). Chennai, India: John Wiley & Sons, Ltd, 311-420.
- Dhillon, I., Kaushik, A., & Kaushik, J. J. (2009). Anti-inflammatory and effect on central nervous system of *Alseodaphne andersonii* in experimental animal models. *The pharmaceutical research*, 2, 8-15.
- Dinis, T. C. P., Madeira, V. M. C., & Almeida, L. M. (1994). Action of phenolic derivatives (acetaminophen, salicylate, and 5-aminosalicylate) as inhibitors of membrane lipid peroxidation and as peroxy radical scavengers. *Archives of Biochemistry and Biophysics*, 315(1), 161-169.

- Dute, P., Chalandre, M.-C., Cabalion, P., & Bruneton, J. (1988). (+)-auroramine and (+)-maroumine, new seco-bis-benzyl-isoquinoline dimers from *Gyrocarpus americanus*. *Phytochemistry*, 27(2), 655-657.
- Dvorackova, S., Hruban, L., Preininger, V., & Santavy, F. (1975). Ultraviolet and Infrared-Spectra of Alkaloids with a Cyclohexadienone or Cyclohexenone Ring. *Heterocycles*, 3(7), 575-613.
- Environment, M. o. N. R. a. (2014). *5th Report to Convention on Biological Diversity*. Putrajaya, Malaysia: Government of Malaysia.
- Ferrari, V., & Cutler, D. J. (1987). Temperature dependence of the acid dissociation constants of chloroquine. *Journal of pharmaceutical sciences*, 76(7), 554-556.
- Ferreira, M. L. R., de Pascoli, I. C., Nascimento, I. R., Zukerman-Schpector, J., & Lopes, L. M. X. (2010). Aporphine and bisaporphine alkaloids from *Aristolochia lagesiana* var. *intermedia*. *Phytochemistry*, 71(4), 469-478.
- Gibson, E. P., & Turnbull, J. H. (1980). The luminescence of bisbenzyltetrahydroisoquinoline alkaloids. The berbamine and oxyacanthine alkaloids. *Journal of the Chemical Society, Perkin Transactions* 2(11), 1696-1700.
- Gottlieb, O. R. (1972). Plant chemosystematics and phylogeny. III. Chemosystematics of the Lauraceae. Review. *Phytochemistry*, 11(5), 1537-1570.
- Greve, B., Lehman, L. G., Lell, B., Luckner, D., Schmidt-Ott, R., & Kremsner, P. G. (1999). High oxygen radical production is associated with fast parasite clearance in children with *Plasmodium falciparum* malaria. *The Journal of infectious diseases*, 179(6), 1584-1586.
- Guinaudeau, H., Freyer, A. J., & Shamma, M. (1986). Spectral characteristics of the bisbenzylisoquinoline alkaloids. *Natural Product Reports*, 3(5), 477-488.
- Guinaudeau, H., Lebœuf, M., & Cavé, A. (1994). Aporphinoid alkaloids, V. *Journal of natural products*, 57(8), 1033-1135.
- Gupta, P., & Bhagat, M. (2010). Immunomodulatory activities of aqueous extract of *Alseodaphne andersonii* in mice. *International Journal of Medical Sciences (India)*, 2(2), 177-180.
- Hadi, A. H. A., Mukhtar, M. R., Wee, K. C., Abd Azziz, S. S. S., & Awang, K. (2008). Alkaloids isolated from *Dehaasia candolleana* (Meisn.) Kosterm. *Malaysian Journal of Science*, 27(2), 115-121.

- Haitao, C., Lian, L., & Pengfei, T. (1999). Chemical constituents of *Alseodaphne hainanensis*. *Zhongcaoyao*, 31(10), 725-727.
- Hasan, C. M., Rahman, P., Karim, A., Jabbar, A., Gray, A. I., & Waterman, P. G. (1987). Boldine from the stem bark of *Dehaasia kurzii*. *Fitoterapia*, 58(6), 430.
- Health, M. o. (2014). *Guidelines of Malaria in Malaysia*. Malaysia: Ministry of Health Malaysia.
- Hossan, S., Agarwala, B., Sarwar, S., Karim, M., Jahan, R., & Rahmatullah, M. (2010). Traditional use of medicinal plants in Bangladesh to treat urinary tract infections and sexually transmitted diseases. *Ethnobotany Research and Applications*, 8, 061-074.
- Jackman, L. M., Trewella, J. C., Moniot, J. L., Shamma, M., Stephens, R. L., Wenkert, E., et al. (1979). The Carbon-13 NMR Spectra of Aporphine Alkaloids. *Journal of natural products*, 42(5), 437-449.
- Jackson, A. H., & Martin, J. A. (1966). Steric effects in the mass spectra of aporphine alkaloids. *Journal of the Chemical Society C: Organic*(0), 2181-2183.
- Janssen, R. H. A. M., Lousberg, R. J. J. C., Wijkens, P., Kruk, C., & Theuns, H. G. (1989). Assignment of proton and carbon-13 NMR resonances of some isoquinoline alkaloids. *Phytochemistry*, 28(10), 2833-2839.
- Johns, S. R., Lamberton, J. A., & Sioumis, A. A. (1967). 1-Benzyl-1,2,3,4-tetrahydroisoquinoline alkaloids from *Alseodaphne archboldiana*. *Australian Journal of Chemistry*, 20(8), 1729-1735. doi: <http://dx.doi.org/10.1071/CH9671729>
- Johns, S. R., Lamberton, J. A., & Sioumis, A. A. (1967). Laurotetanine and *N*-methyllaurotetanine from *Palmeria fengeriana*. *Australian Journal of Chemistry*, 20(8), 1787.
- Julia, S., Soepadmo, E., & Yahud, W. (2009). Problem in the generic delimitation between *Alseodaphne*, *Dehaasia*, *Nothaphoebe* (Lauraceae) in Borneo. *Blumea*, 54(1-3), 192-197.
- Kalita, G. J., Rout, S., Mishra, R. K., & Sarma, P. (2015). Traditionally used medicinal Plants of Bajali Sub-division, Barpeta District, Assam. *Journal of Medicinal Plants Studies*, 3(2), 08-17.

- Kanyinda, B., Vanhaelen-Fastre, R., Vanhaelen, M., & Ottinger, R. (1997). Two New Isochondodendrine-Type Alkaloids from the Roots of *Anisocycla jollyana*. *Journal of natural products*, 60(11), 1121-1124.
- Karimova, S. U., Israilov, I. A., Yunusov, M. S., & Yunusov, S. Y. (1978). Structure of Glaufine. *Chemistry of Natural Compounds*, 14(6), 699-699.
- Kashiwaba, N., Morooka, S., Kimura, M., Ono, M., Toda, J., Suzuki, H., et al. (1996). New Morphinane and Hasubanane Alkaloids from *Stephania cepharantha*. *Journal of natural products*, 59(5), 476-480.
- Kashiwada, Y., Aoshima, A., Ikeshiro, Y., Chen, Y.-P., Furukawa, H., Itoigawa, M., et al. (2005). Anti-HIV benzyloquinoline alkaloids and flavonoids from the leaves of *Nelumbo nucifera*, and structure-activity correlations with related alkaloids. *Bioorganic & medicinal chemistry*, 13(2), 443-448.
- Kaur, K., Jain, M., Reddy, R. P., & Jain, R. (2010). Quinolines and structurally related heterocycles as antimalarials. *European journal of medicinal chemistry*, 45(8), 3245-3264.
- Kaushik, A., Parcha, V., Kaushik, J. J., Rawat, M. S., & Gaim, D. (2010). Antifungal activity of leaf extracts of *Alseodaphne andersonii* against different pathogenic fungal cultures. *Pharmacologyonline*, 1, 352-355.
- Khan, M. N. (2006). *Micellar Catalysis*. Univeristy of Malaya, Kuala Lumpur: CRC Press, 1-439.
- Kilic, H. (2010). Electronic absorption study on acid-base equilibria for some pyrimidine derivatives containing semi- and thiosemicarbazone moiety. *Spectrochimica Acta, Part A: Molecular and Biomolecular Spectroscopy*, 75A(2), 728-733.
- Kohlmann, F. J. (2003). *What is it pH and how is it measured*. USA: Hach Company.
- Kremsner, P. G., Greve, B., Lell, B., Luckner, D., & Schmid, D. (2000). Malarial anemia in African children associated with high oxygen-radical production. *Lancet*, 355(9197), 40-41.
- Kumar, S. (2014). Alkaloidal Drugs - A Review. *Asian Journal of Pharmaceutical Science & Technology*, 4(3), 107-119.
- Kuntworbe, N., Alany, R. G., Brimble, M., & Al-Kassas, R. (2013). Determination of pK_a and forced degradation of the indoloquinoline antimalarial compound cryptolepine hydrochloride. *Pharm Dev Technol*, 18(4), 866-876.

- Lambros, C., & Vanderberg, J. P. (1979). Synchronization of *Plasmodium falciparum* erythrocytic stages in culture. *The Journal of parasitology*, 65(3), 418-420.
- Lee, S.-S., Chang, S.-M., & Chen, C.-H. (2001). Chemical constituents from *Alseodaphne andersonii*. *Journal of natural products*, 64(12), 1548-1551.
- Lee, S.-S., Chen, C.-K., & Chen, C.-H. (1996). Chemical constituents from *Dehaasia triandra*. II. Five new alkaloids, secoxanthoplanine, dehydroisocorydione, 11, 8'-O-bisisocorydine, (8, 8'-R)- and (8, 8'-S)-bisisocorydine, isolated from the leaves. *Tetrahedron*, 52(19), 6561-6568.
- Lee, S.-S., Chen, C.-K., Chen, I.-S., & Chen, C.-H. (1996). Chemical constituents from *Dehaasia triandra*. 1. Three new alkaloids, isocorydione, norisocorydione, and dehatriline, from the leaves. *Journal of natural products*, 59(1), 55-58.
- Likhitwitayawuid, K., Angerhofer, C. K., Cordell, G. A., & Pezzuto, J. M. (1993). Traditional medicinal plants of Thailand. XX. Cytotoxic and antimalarial bisbenzylisoquinoline alkaloids from *Stephania erecta*. *Journal of natural products*, 56(1), 30-38.
- Lin, L.-Z., Shieh, H.-L., Angerhofer, C. K., Pezzuto, J. M., Cordell, G. A., Xue, L., et al. (1993). Cytotoxic and antimalarial bisbenzylisoquinoline alkaloids from *Cyclea barbata*. *Journal of natural products*, 56(1), 22-29.
- Liptak, M. D., Gross, K. C., Seybold, P. G., Feldgus, S., & Shields, G. C. (2002). Absolute pKa determinations for substituted phenols. *Journal of the American Chemical Society*, 124(22), 6421-6427.
- Lu, S. T., Tsai, I. L., & Leou, S. P. (1989). Studies on the alkaloids of Formosan lauraceous plants. Part 31. Alkaloids of *Dehaasia triandra*. *Phytochemistry*, 28(2), 615-620.
- Lu, S. T., & Wang, E. C. (1977). Studies on the alkaloids of Formosan Lauraceous plants. XXIII. Alkaloids of *Dehaasia triandra* Merr. (1). Isolation of isocorydine and obaberine. *Taiwan Yaoxue Zazhi*, 29(1-2), 49-53.
- Mahiou, V., Roblot, F., Fournet, A., & Hocquemiller, R. (2000). Bisbenzylisoquinoline alkaloids from *Guatteria boliviana* (Annonaceae). *Phytochemistry*, 54(7), 709-716.
- Mahmud, Z., Khan, M. N., Lajis, N. H., & Toia, R. F. (1992). Perakensol: A phenanthrenoid isolated from *Alseodaphne perakensis*. *Journal of natural products*, 55(4), 533-535.

- Makler, M. T., & Hinrichs, D. J. (1993). Measurement of the lactate dehydrogenase activity of *Plasmodium falciparum* as an assessment of parasitemia. *The American journal of tropical medicine and hygiene*, 48(2), 205-210.
- Malaria, T. (2015). Malaria Transmission. Retrieved 28 august 2015, 2015, from www.euroclinix.co.uk.
- Marsaioli, A. J., Rúveda, E. A., & de AM Reis, F. (1978). ¹³C NMR spectral analysis of some isoquinoline alkaloids. *Phytochemistry*, 17(9), 1655-1658.
- Marshall, S. J., Russell, P. F., Wright, C. W., Anderson, M. M., Phillipson, J. D., Kirby, G. C., et al. (1994). *In vitro* antiplasmodial, antiamebic, and cytotoxic activities of a series of bisbenzylisoquinoline alkaloids. *Antimicrobial agents and chemotherapy*, 38(1), 96-103.
- Mukhtar, M. R., Hadi, A. H. A., Litaudon, M., & Awang, K. (2004). Morphinandienone alkaloids from *Dehaasia longipedicellata*. *Fitoterapia*, 75(7-8), 792-794.
- Mukhtar, M. R., Nafiah, M. A., & Awang, K. (2009). α' -oxoperakensimines A-C, new bisbenzylisoquinoline alkaloids from *Alseodaphne perakensis* (Gamble) Kosterm. *Heterocycles*, 78(8), 2085-2092.
- Mukhtar, M. R., Nafiah, M. A., Awang, K., Hadi, A. H. A., & Weng, N. S. (2008). 2, 7-Dihydroxy-3, 6-dimethoxyphenanthrene from *Dehaasia longipedicellata*. *Acta Crystallographica Section E: Structure Reports Online*, 64(6), 1135.
- Mukhtar, M. R., Zahari, A., Nafiah, M. A., Hamid A. Hadi, A., Thomas, N. F., Arai, H., et al. (2009). 3',4'-Dihydronorstephasubine, a new bisbenzylisoquinoline from the bark of *Alseodaphne corneri*. *Heterocycles*, 78(10), 2571-2578.
- Musonda, C. C., Taylor, D., Lehman, J., Gut, J., Rosenthal, P. J., & Chibale, K. (2004). Application of multi-component reactions to antimalarial drug discovery. Part 1: Parallel synthesis and antiplasmodial activity of new 4-aminoquinoline Ugi adducts. *Bioorganic & medicinal chemistry letters*, 14(15), 3901-3905.
- Mustafa, M., Mohamad, R., Din, L., & Wahid, S. (1995). Smooth muscle relaxant activities of compounds isolated from malaysian medicinal plants on rat aorta and guinea-pig ileum. *Phytotherapy Research*, 9(8), 555-558.
- Naaz, H., Singh, S., Pandey, V. P., Singh, P., & Dwivedi, U. N. (2013). Anti-cholinergic alkaloids as potential therapeutic agents for Alzheimer's disease : An *in silico* approach. *Indian Journal of Biochemistry & Biophysics*, 50, 120-125.

- Nafiah, M. A., Mukhtar, M. R., Omar, H., Ahmad, K., Morita, H., Litaudon, M., et al. (2011). *N*-Cyanomethylnorboldine: A New Aporphine Isolated from *Alseodaphne perakensis* (Lauraceae). *Molecules*, 16(4), 3402-3409.
- Namli, H., & Turhan, O. (2006). Background defining during the imine formation reaction in FT-IR liquid cell. *Spectrochimica Acta Part A: Molecular and Biomolecular Spectroscopy*, 64A(1), 93-100.
- Nawawi, A. a., Ma, C.-M., Nakamura, N., Hattori, M., Kurokawa, M., Shiraki, K., et al. (1999). Anti-herpes simplex virus activity of alkaloids isolated from *Stephania cepharantha*. *Biological & Pharmaceutical Bulletin*, 22(3), 268-274.
- Newman, D. J., & Cragg, G. M. (2007). Natural Products as Sources of New Drugs over the Last 25 Years. *Journal of natural products*, 70(3), 461-477.
- Ng, F. S. P. (1989). *Tree Flora of Malaya* (Vol. 4). Forest Research Institute Malaysia: Longman Malaysia Sdn Bhd, 98.
- Ng, F. S. P. (1989). *Tree flora of Malaya; a manual for foresters* (Vol. 3). Forest Research Institute Malaysia: Longman Malaysia Sdn Bhd, 98-139.
- Noedl, H., Bronnert, J., Yingyuen, K., Attlmayr, B., Kollaritsch, H., & Fukuda, M. (2005). Simple histidine-rich protein 2 double-site sandwich enzyme-linked immunosorbent assay for use in malaria drug sensitivity testing. *Antimicrobial agents and chemotherapy*, 49(8), 3575-3577.
- Oh, J., Bowling, J. J., Carroll, J. F., Demirci, B., Başer, K. H. C., Leininger, T. D., et al. (2012). Natural product studies of U.S. endangered plants: Volatile components of *Lindera melissifolia* (Lauraceae) repel mosquitoes and ticks. *Phytochemistry*, 80, 28-36.
- Ong, C. Y., Ling, S. K., Ali, R. M., Chee, C. F., Samah, Z. A., Ho, A. S. H., et al. (2009). Systematic analysis of *in vitro* photo-cytotoxic activity in extracts from terrestrial plants in Peninsula Malaysia for photodynamic therapy. *Journal of Photochemistry and Photobiology, B: Biology*, 96(3), 216-222.
- Oyaizu, M. (1986). Antioxidative Activities of Products of Browning Reaction Prepared from Glucosamine. *The Japanese Journal of Nutrition and Dietetics*, 44(6), 307-315.
- Parcha, V., Kaushik, A., Kaushik, J., Rawat, M., & Biswas, S. (2007). Evaluation of Antimicrobial Potential of *Alseodaphne andersonii*. Leaf Extracts against Pathogenic Bacteria. *Pharmaceutical biology*, 45(1), 60-63.

- Parvin, R., Ilias, M., M., H. C., & Abdul, J. (1988). Cytotoxic and antimicrobial activities of alkaloids from *Dehaasia kurzii* King stem bark. *Bangladesh Journal of Botany*, 17(1), 25-31.
- Patra, A., Freyer, A. J., Guinaudeau, H., Shamma, M., Tantisewie, B., & Pharadai, K. (1986). The bisbenzylisoquinoline alkaloids of *Stephania suberosa*. *Journal of natural products*, 49(3), 424-427.
- Patra, A., Mandal, T. K., Mukhopadhyay, P. K., & Ranu, B. C. (1988). (+)-3', 4'-dihydrostephasubine, a bisbenzylisoquinoline alkaloid from *Stephania hernandifolia*. *Phytochemistry*, 27(2), 653-655.
- Pelletier, S. W. (1970). *Chemistry of the alkaloids*. New York, United States of America: Van Nostrand Reinhold Company, 795.
- Percario, S., Moreira, D. R., Gomes, B. A. Q., Ferreira, M. E. S., Goncalves, A. C. M., Laurindo, P. S. O. C., et al. (2012). Oxidative stress in malaria. *International Journal of Molecular Sciences*, 13, 16346-16372.
- Perrin, D., & Dempsey, B. (1974). *Buffers for pH and Metal Ion Control*. University of California, USA: Chapman and Hall, 4-93.
- Philipson, J. D., Roberts, M. F., & Zenk, M. H. (1985). *The chemistry and biology of isoquinoline alkaloids*. Germany: Springer Verlag, 213-228.
- Pracheta, S. V., Paliwal, R., & Sharma, S. (2011). Preliminary phytochemical screening and *in vitro* antioxidant potential of hydro-ethanolic extract of *Euphorbia neriifolia* Linn. *International Journal of PharmTech Research*, 3(1), 124-132.
- Rahman, W. A., Che'rus, A., & Ahmad, A. H. (1997). Malaria and *Anopheles* mosquitos in Malaysia. *Southeast Asian Journal of Tropical Medicine and Public Health*, 28(3), 599-605.
- Rahmatullah, M., Hasan, A., Parvin, W., Moniruzzaman, M., Khatun, A., Khatun, Z., et al. (2012). Medicinal plants and formulations used by the Soren clan of the Santal tribe in Rajshahi district, Bangladesh for treatment of various ailments. *African Journal of Traditional, Complementary and Alternative Medicines*, 9(3), 350-359.
- Rahmatullah, M., Mollik, A. H., Ali, M., Abbas, M. H. B., Jahan, R., Chowdhury, M. H., et al. (2011). An ethnomedicinal survey of Vitbilia village in Sujanager sub-district of Pabna district, Bangladesh. *American-Eurasian Journal of Sustainable Agriculture*, 10(1), 106-111.

- Rathbun, J. Y., Droniou, M. E., Damoiseaux, R., Haworth, K. G., Henley, J. E., Exline, C. M., et al. (2015). Novel Arenavirus Entry Inhibitors Discovered by Using a Minigenome Rescue System for High-Throughput Drug Screening. *Journal of virology*, 89(16), 8428-8443.
- Research, C. I. o. H. (2016). Drug and drug target database. Retrieved 12 april 2016, 2016, from <http://www.drugbank.ca/>
- Ridley, H. N. (1967). *The flora of the Malay Peninsula* (Vol. 3). Amsterdam, Holland: A. Asher & Co.
- Roblot, F., Hocquemiller, R., & Cave, A. (1984). Etude des morphinane-dienones: 13C et 1H RMN de la sébiférine et d'alcaloïdes apparentés. *Bulletin de la Société chimique de France*(3-4), II. 139-II. 141.
- Said, I. M., Latiff, A., Partridge, S. J., & Phillipson, J. D. (1991). Alkaloids from *Dehaasia incrassata*. *Planta medica*, 57(4), 389.
- Sakurai, Y., Kolokoltsov, A. A., Chen, C.-C., Tidwell, M. W., Bauta, W. E., Klugbauer, N., et al. (2015). Two-pore channels control Ebola virus host cell entry and are drug targets for disease treatment. *Science*, 347(6225), 995-998.
- Saliba, K. J., Allen, R. J., Zissis, S., Bray, P. G., Ward, S. A., & Kirk, K. (2003). Acidification of the malaria parasite's digestive vacuole by a H⁺-ATPase and a H⁺-pyrophosphatase. *Journal of Biological Chemistry*, 278(8), 5605-5612.
- Sangster, A. W., & Stuart, K. L. (1965). Ultraviolet spectra of alkaloids. *Chemical Reviews*, 65(1), 69-130.
- Sarker, S. D., Nahar, L., Sarker, S. D., & Nahar, L. (2007). *Natural Product Chemistry*. West Sussex, England: John Wiley & Sons, Ltd., 283-370.
- Saxena, S., Pant, N., Jain, D., & Bhakuni, R. (2003). Antimalarial agents from plant sources. *Current Science*, 85(9), 1314-1329.
- Schiff Jr, P. L. (1991). Bisbenzylisoquinoline alkaloids. *Journal of natural products*, 54(3), 645-749.
- Schroeder, C. A. (1976). Some useful plants of the botanical family Lauraceae. *California Avocado Society Yearbook*, 59, 30-34.

- Serck, C. H., Hack-Seang, K., Rak, M. K., Youngsoo, K., Kyung, L. H., Kyung, C. Y., et al. (2000). Anti-inflammatory effects of fangchinoline and tetrandrine. *Journal of ethnopharmacology*, 69(2), 173-179.
- Shamma, M. (1972). *The isoquinoline alkaloids: chemistry and pharmacology* (Vol. 25). New York and London: Academic Press, 594.
- Shamma, M., & Moniat, J. L. (1978). *Isoquinoline alkaloids research, 1972-1977* (1 ed.). New York: Plenum Press, 27-176.
- Shields, G. C., & Seybold, P. G. (2013). *Computational Approaches for the Prediction of pKa Values*. Boca raton, USA: CRC Press, 99-104.
- Shimada, K., Fujikawa, K., Yahara, K., & Nakamura, T. (1992). Antioxidative properties of xanthan on the autoxidation of soybean oil in cyclodextrin emulsion. *Journal of Agricultural and Food Chemistry*, 40(6), 945-948.
- Smolnycki, W. D., Moniot, J. L., Hindenlang, D. M., Miana, G. A., & Shamma, M. (1978). Srilankine: a 4-hydrokylated aporphine. *Tetrahedron Letters*, 19(47), 4617-4620.
- Suau, R., Cuevas, A., Garcia, A. I., Rico, R., & Cabezudo, B. (1991). Isoquinoline alkaloids from Platycapnos. *Phytochemistry*, 30(10), 3315-3317.
- Sun, S.-W., Kuo, C.-H., Lee, S.-S., & Chen, C.-K. (2000). Determination of bisbenzylisoquinoline alkaloids by high-performance liquid chromatography (II). *Journal of Chromatography A*, 891(1), 189-194.
- Sun, S.-W., Lee, S.-S., & Huang, H.-M. (1996). Determination of lauraceous aporphine alkaloids by high-performance liquid chromatography. *Journal of pharmaceutical and biomedical analysis*, 14(8-10), 1383-1387.
- Suyanto, S., Sardi, I., Buana, Y., & van Noordwijk, M. (2009). *Analysis of local livelihoods from past to present in the Central Kalimantan ex-mega rice project area*. World Agroforestry Centre, Bogor.
- Tamez, P. A., Lantvit, D., Lim, E., & Pezzuto, J. M. (2005). Chemosensitizing action of cepharanthine against drug-resistant human malaria, *Plasmodium falciparum*. *Journal of ethnopharmacology*, 98(1-2), 137-142. doi: <http://dx.doi.org/10.1016/j.jep.2005.01.015>
- Tantisewie, B., Amurrio, S., Guinaudeau, H., & Shamma, M. (1989). New bisbenzylisoquinolines from *Stephania pierrii*. *Journal of natural products*, 52(4), 846-851.

- Tantisewie, B., & Ruchirawat, S. (1992). Alkaloids from the plants of Thailand. *Alkaloids (Academic Press)*, 41, 1-40.
- Teik, N. L., Lien-Chai, C., Yu-Tseng, L., & Chun-Ching, L. (2006). Antiproliferative and apoptotic effects of tetrandrine on different human hepatoma cell lines. *The American journal of Chinese medicine*, 34(01), 125-135.
- Teixeira, C. t., Vale, N., Pérez, B., Gomes, A., Gomes, J. R. B., & Gomes, P. (2014). "Recycling" Classical Drugs for Malaria. *Chemical Reviews*, 114(22), 11164-11220.
- Thakur, B. K., Anthwal, A., Rawat, D. S., Rawat, B., Rashmi, & Rawat, M. S. M. (2012). A Review on Genus *Alseodaphne*: Phytochemistry and Pharmacology. *Mini-Reviews in Organic Chemistry*, 9(4), 433-445.
- Thomas, G. (2011). *Medicinal Chemistry: An Introduction* (2 ed.). West Sussex, England: Wiley, 30-70.
- Tomita, M., Furukawa, H., Kikuchi, T., Kato, A., & Ibuka, T. (1966). Studies on the Alkaloids of Menispermaceous Plants. CCXX. Mass Spectra of Benzylisoquinoline Alkaloids. *Chemical & Pharmaceutical Bulletin*, 14(3), 232-237.
- Trager, W., & Jensen, J. B. (1976). Human malaria parasites in continuous culture. *Science*, 193(4254), 673-675.
- Troy, D. B., Remington, J. P., & Beringer, P. (2006). *Remington: The Science and Practice of Pharmacy*. Philadelphia, USA: Lippincott Williams & Wilkins, 1095-1249.
- Vongsombath, C., Pålsson, K., Björk, L., Borg-Karlson, A.-K., & Jaenson, T. G. T. (2012). Mosquito (Diptera: Culicidae) Repellency Field Tests of Essential Oils From Plants Traditionally Used in Laos. *Journal of Medical Entomology*, 49(6), 1398-1404.
- Wei, Z., Jin, F. H., Lv, W.-W., Zhao, Q.-C., & Shi, G.-B. (2012). Antibacterial, antifungal and cytotoxic isoquinoline alkaloids from *Litsea cubeba*. *Molecules*, 17(11), 12950-12960.
- Wells, T. N. C. (2011). Natural products as starting points for future anti-malarial therapies: going back to our roots. *Malaria Journal*, 10(Suppl 1), S3.
- Whitmore, T. C., & Ng, F. S. P. (1989). *Tree flora of Malaya: a manual for foresters*. Forest Research Institute Malaysia: Longman, 109-111.

- WHO. (2013). *World Malaria Report 2013* (W. H. Organization Ed.). Geneva: World Health Organization.
- WHO. (2014). A global brief on vector-borne diseases.
- WHO. (2014). *World Malaria Report 2014* (W. H. Organization Ed.). Geneva: World Health Organization.
- William, T., Rahman, H., Jelip, J., Ibrahim, M., Menon, J., Grigg, M., et al. (2013). Increasing incidence of *Plasmodium knowlesi* malaria following control of *P. falciparum* and *P. vivax* Malaria in Sabah, Malaysia. *PLoS neglected tropical diseases*, 7, e2026.
- Wilson, M. E., & Britigan, B. E. (1998). Iron acquisition by parasitic protozoa. *Parasitology Today*, 14(9), 348-353.
- Winterstein, E., & Tier, G. (1910). *Die Alkaloide*. Berlin: Bornträger: Eine Monographie dermatürlichen
- Wong, T.-M., Wu, S., Yu, X.-C., & Li, H.-Y. (2000). Cardiovascular actions of Radix *Stephaniae Tetrandrae*: a comparison with its main component, tetrandrine. *Acta Pharmacologica Sinica*, 21(12), 1083-1088.
- Wright, C. W., Marshall, S. J., Russell, P. F., Anderson, M. M., Phillipson, J. D., Kirby, G. C., et al. (2000). *In vitro* antiplasmodial, antiamoebic, and cytotoxic activities of some monomeric isoquinoline alkaloids. *Journal of natural products*, 63(12), 1638-1640.
- Wu, W.-N., Beal, J. L., & Doskotch, R. W. (1980). Alkaloids of *Thalictrum*. XXXIII. Isolation and characterization of alkaloids from the root of *Thalictrum alpinum*. *Journal of natural products*, 43(3), 372-381.
- Wu, W.-N., & Moyer, M. D. (2004). API-ionspray MS and MS/MS study on the structural characterization of bisbenzylisoquinoline alkaloids. *Journal of pharmaceutical and biomedical analysis*, 34(1), 53-66.
- Yan, X., Wei, X., Xie, H., Liu, M., & Zhang, F. (1999). Aporphine alkaloids of *Litsea rotundifolia* and *L. rotundifolia* var. *oblongifolia*. *Journal of Tropical and Subtropical Botany*, 8(4), 324-328.
- Yang, M. H., Yoon, K. D., Chin, Y.-W., Park, J. H., & Kim, J. (2009). Phenolic compounds with radical scavenging and cyclooxygenase-2 (COX-2) inhibitory activities from *Dioscorea opposita*. *Bioorganic & medicinal chemistry*, 17(7), 2689-2694.

- Ye, Z., & Rossan, R. N. (2013). Effective treatment with a tetrandrine/chloroquine combination for chloroquine-resistant *falciparum malaria* in Aotus monkeys. *Malaria Journal*, 12, 117.
- Yusof, R., Lau, Y., Mahmud, R., Fong, M., Jelip, J., Ngian, H., et al. (2014). High proportion of knowlesi malaria in recent malaria cases in Malaysia. *Malaria Journal*, 13(1), 168.
- Zenk, M. H. (1991). Chasing the enzymes of secondary metabolism: plant cell cultures as a pot of gold. *Phytochemistry*, 30(12), 3861-3863.
- Zenk, M. H., & Juenger, M. (2007). Evolution and current status of the phytochemistry of nitrogenous compounds. *Phytochemistry*, 68(22-24), 2757-2772.
- Zhang, F., Liu, M., Li, Y., Mai, L., & Lu, R. (1988). Alkaloids of *Alseodaphne hainanensis* Merr. *Zhiwu Xuebao*, 30(2), 183-186.
- Zuguang, Y., & Knox, V. D. (1989). Selective antimalarial activity of tetrandrine against chloroquine resistant *Plasmodium falciparum*. *Biochemical and biophysical research communications*, 159(1), 242-248.

LIST OF PUBLICATIONS AND PAPERS PRESENTED

Publications and Journals

1. Azeana Zahari, Abdulwali Ablat, Noridayu Omer, Mohd Azlan Nafiah, Yasodha Sivasothy, Jamaludin Mohamad, Mohammad Niyaz Khan, Khalijah Awang. Ultraviolet-visible study on acid-base equilibria of aporphine alkaloids with antiplasmodial and antioxidant activities from *Alseodaphne corneri* and *Dehaasia longipedicellata*. Scientific Report. Sci Rep. 2016, 6, 21517.
2. Azeana Zahari, Abdulwali Ablat, Yasodha Sivasothy, Jamaludin Mohamad, Muhammad I. Choudhary, Khalijah Awang. Bisbenzylisoquinoline alkaloids from *Alseodaphne corneri* Kosterm possessing *in vitro* antiplasmodial with antioxidant activities. Asian Pacific Journal of Tropical Medicine, 2016, 9 (4), 328-332.
3. Azeana Zahari, Foo Kit Cheah, Jamaludin Mohamad, Syazreen Nadia Sulaiman, Marc Litaudon, Kok Hoong Leong, Khalijah Awang. Antiplasmodial and Antioxidant Isoquinoline Alkaloids from *Dehaasia longipedicellata*. Planta Medica, 2014, 80 (07), 599-603.
4. Ayu Afiqah Nasrullah, Azeana Zahari, Jamaludin Mohamad, Khalijah Awang. Antiplasmodial Alkaloids from the Bark of *Cryptocarya nigra* (Lauraceae). Molecules, 2013, 18 (7), 8009-8017.
5. Syazreen Nadia Sulaiman, Mat Ropi Mukhtar, A. Hamid A. Hadi, Khalijah Awang, Hazrina Hazni, Azeana Zahari, Marc Litaudon, Kazumasa Zaima, Hiroshi Morita. Lancifoliaine, a New Bisbenzylisoquinoline from the Bark of *Litsea lancifolia*, Molecules, 2011, 16 (4), 3119-3127.

Presentations in Conferences/Congress/Meeting:

Poster presentation:

1. Azeana Zahari, Jamaludin Mohamad, Khalijah Awang. Antiplasmodial and Antioxidant Isoquinoline Alkaloids from *Dehaasia longipedicellata*. 9th Mathematics and Physical Sciences Graduate Congress (MPSGC). 8th-10th January 2014. University of Malaya (UM), Kuala Lumpur, Malaysia.

Oral Presentation:

2. Azeana Zahari, Adlin Afzan, Mat Ropi Mukhtar, A. Hamid A. Hadi, Khalijah Awang. Antiplasmodial from the bark of *Alseodaphne corneri*. 8th Mathematics and Physical Sciences Graduate Congress (MPSGC). 8th – 10th disember 2012. Chulalongkorn University (CU), Thailand.

Meeting:

3. Azeana Zahari, The black seed (*Nigella Sativa*) ‘A cure for every illness’. The 8th Scientific meeting the black seed (*Nigella Sativa*). 30th April 2014. University of Malaya, Malaysia.

APPENDIX

Appendix A	Title	Page
Figure A1	HSQC Spectrum of Gyrolidine 18	290
Figure A2	HMBC Spectrum of Gyrolidine 18	291
Figure A3	LCMS Spectrum of <i>O</i> -methyllimacusine 118	292
Figure A4	HSQC Spectrum of <i>O</i> -methyllimacusine 118	293
Figure A5	HMBC Spectrum of <i>O</i> -methyllimacusine 118	294
Figure A6	LCMS Spectrum of 3',4'-dihydronorstephasubine 19	295
Figure A7	NOESY Spectrum of 3',4'-dihydronorstephasubine 19	296
Figure A8	HSQC Spectrum of 3',4'-dihydronorstephasubine 19	297
Figure A9	HMBC Spectrum of 3',4'-dihydronorstephasubine 19	298
Figure A10	HSQC Spectrum of 3',4'-dihydrostephasubine 119	299
Figure A11	HMBC Spectrum of 3',4'-dihydrostephasubine 119	300
Figure A12	NOESY Spectrum of Norstephasubine 20	301
Figure A13	HSQC Spectrum of Norstephasubine 20	302
Figure A14	HMBC Spectrum of Norstephasubine 20	303
Figure A15	LCMS Spectrum of Stephasubine 120	304
Figure A16	HSQC Spectrum of Stephasubine 120	305
Figure A17	HMBC Spectrum of Stephasubine 120	306
Figure A18	LCMS Spectrum of Stephasubimine 121	307
Figure A19	HSQC Spectrum of Stephasubimine 121	308
Figure A20	HMBC Spectrum of Stephasubimine 121	309
Figure A21	LCMS Spectrum of Norisocorydine 42	310
Figure A22	HSQC Spectrum of Norisocorydine 42	311
Figure A23	HMBC Spectrum of Norisocorydine 42	312
Figure A24	COSY Spectrum of <i>N</i> -methyllindcarpine 123	313
Figure A25	HSQC Spectrum of Laurotetanine 27	314
Figure A26	HMBC Spectrum of Laurotetanine 27	315
Figure A27	LCMS Spectrum of Norboldine 36	316
Figure A28	HSQC Spectrum of Norboldine 36	317
Figure A29	HMBC Spectrum of Norboldine 36	318
Figure A30	IR Spectrum of Sebiferine 47	319
Figure A31	COSY Spectrum of Sebiferine 47	320

Appendix B	Title	Page
	Table B1: The values of observed absorbance (A_{obs}) at 246 nm as a function of pH for ionization of Isocorydine 41 in 2% v/v acetonitrile.	321
	Table B2: The values of observed absorbance (A_{obs}) at 270 nm as a function of pH for ionization of Isocorydine 41 in 2% v/v acetonitrile.	322
	Table B3: The values of observed absorbance (A_{obs}) at 338 nm as a function of pH for ionization of Isocorydine 41 in 2% v/v acetonitrile.	323
	Table B4: The values of observed absorbance (A_{obs}) at 246 nm as a function of pH for ionization of Norisocorydine 42 in 2% v/v acetonitrile.	325
	Table B5: The values of observed absorbance (A_{obs}) at 270 nm as a function of pH for ionization of Norisocorydine 42 in 2% v/v acetonitrile.	326
	Table B6: The values of observed absorbance (A_{obs}) at 338 nm as a function of pH for ionization of Norisocorydine 42 in 2% v/v acetonitrile.	327
	Table B7: The values of observed absorbance (A_{obs}) at 253 nm as a function of pH for ionization of Boldine 37 in 2% v/v acetonitrile.	329
	Table B8: The values of observed absorbance (A_{obs}) at 274 nm as a function of pH for ionization of Boldine 37 in 2% v/v acetonitrile.	330
	Table B9: The values of observed absorbance (A_{obs}) at 295 nm as a function of pH for ionization of Boldine 37 in 2% v/v acetonitrile.	331
	Table B10: The values of observed absorbance (A_{obs}) at 312 nm as a function of pH for ionization of Boldine 37 in 2% v/v acetonitrile.	332
	Table B11: The values of observed absorbance (A_{obs}) at 332 nm as a function of pH for ionization of Boldine 37 in 2% v/v acetonitrile.	333
	Figure B1: pH-Absorbance curves of Isocorydine 41 in 2% v/v acetonitrile at 246 nm, 270 nm, and 338 nm.	324
	Figure B2: pH-Absorbance curves of Norisocorydine 42 in 2% v/v acetonitrile at 246 nm, 270 nm, and 338 nm.	328
	Figure B3: pH-Absorbance curves of Boldine 37 in 2% v/v acetonitrile at 253 nm, 274 nm, 295 nm, 312 nm and 332 nm.	334
Appendix C		
	Nonlinear least squares computer in BASICA programme	335

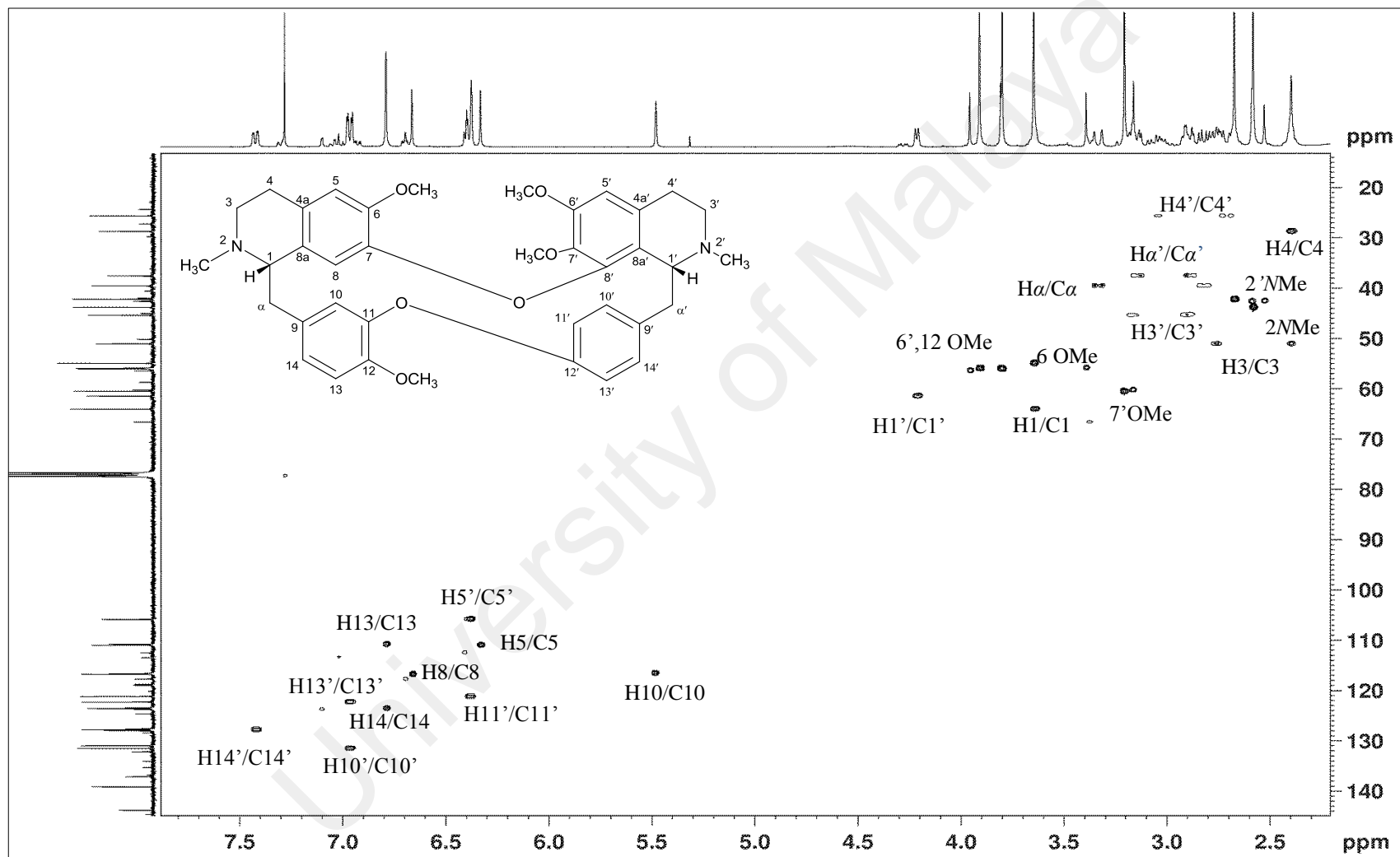


Figure A1: HSQC Spectrum of Gyrolidine 18

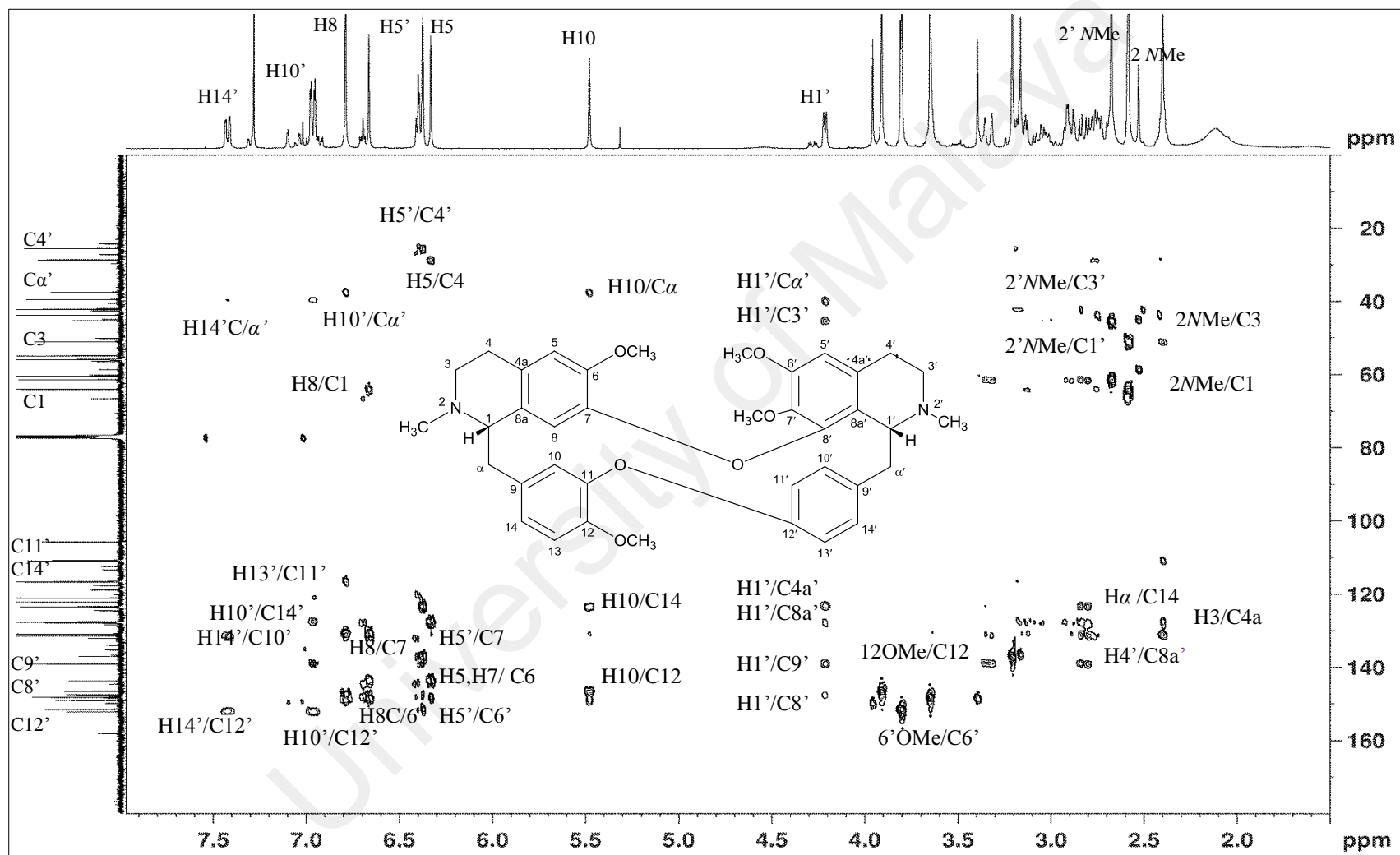


Figure A2 : HMBC Spectrum of Gyrolidine 18

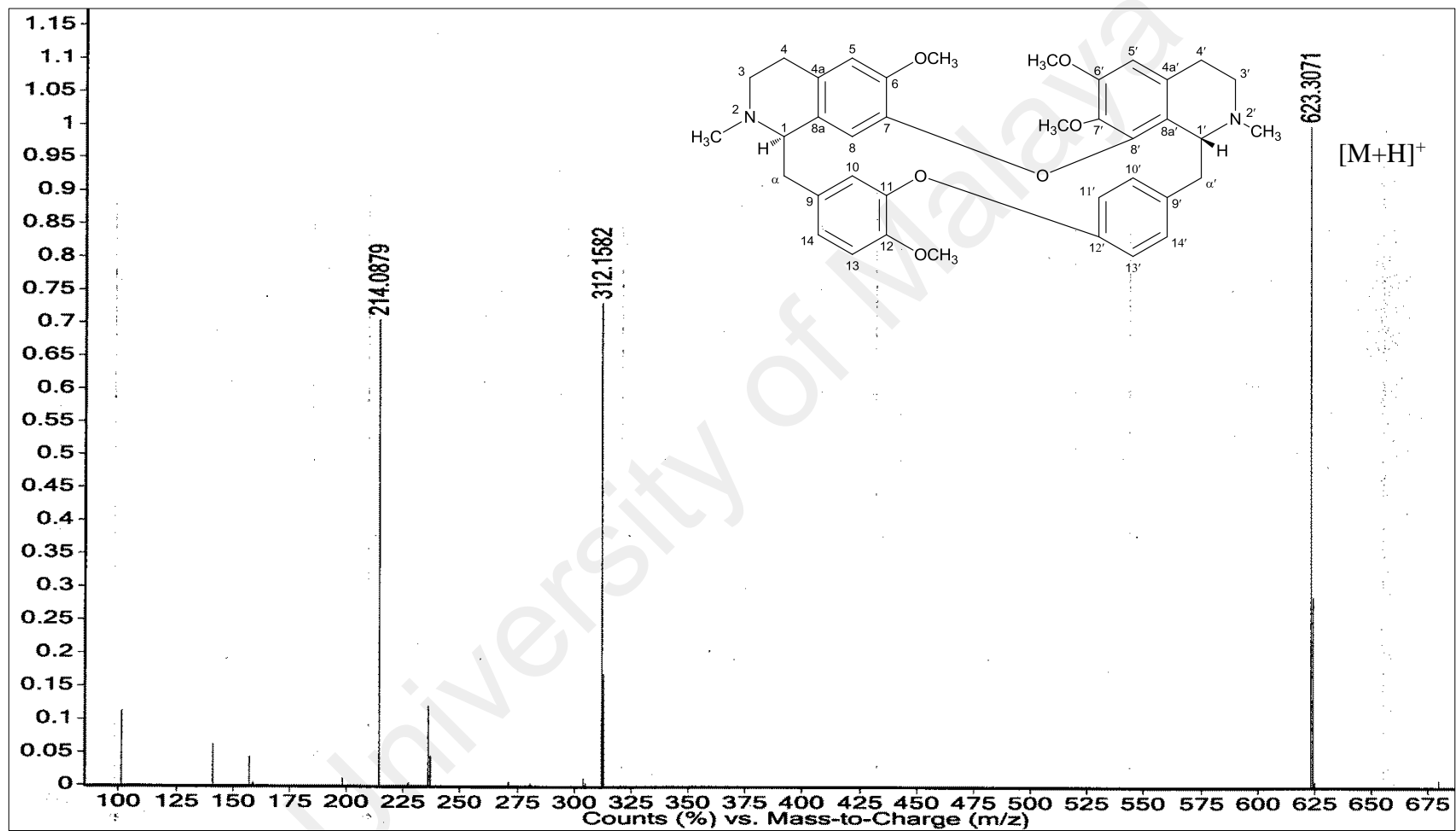


Figure A3: LCMS Spectrum of *O*-methyllicacusine **118**

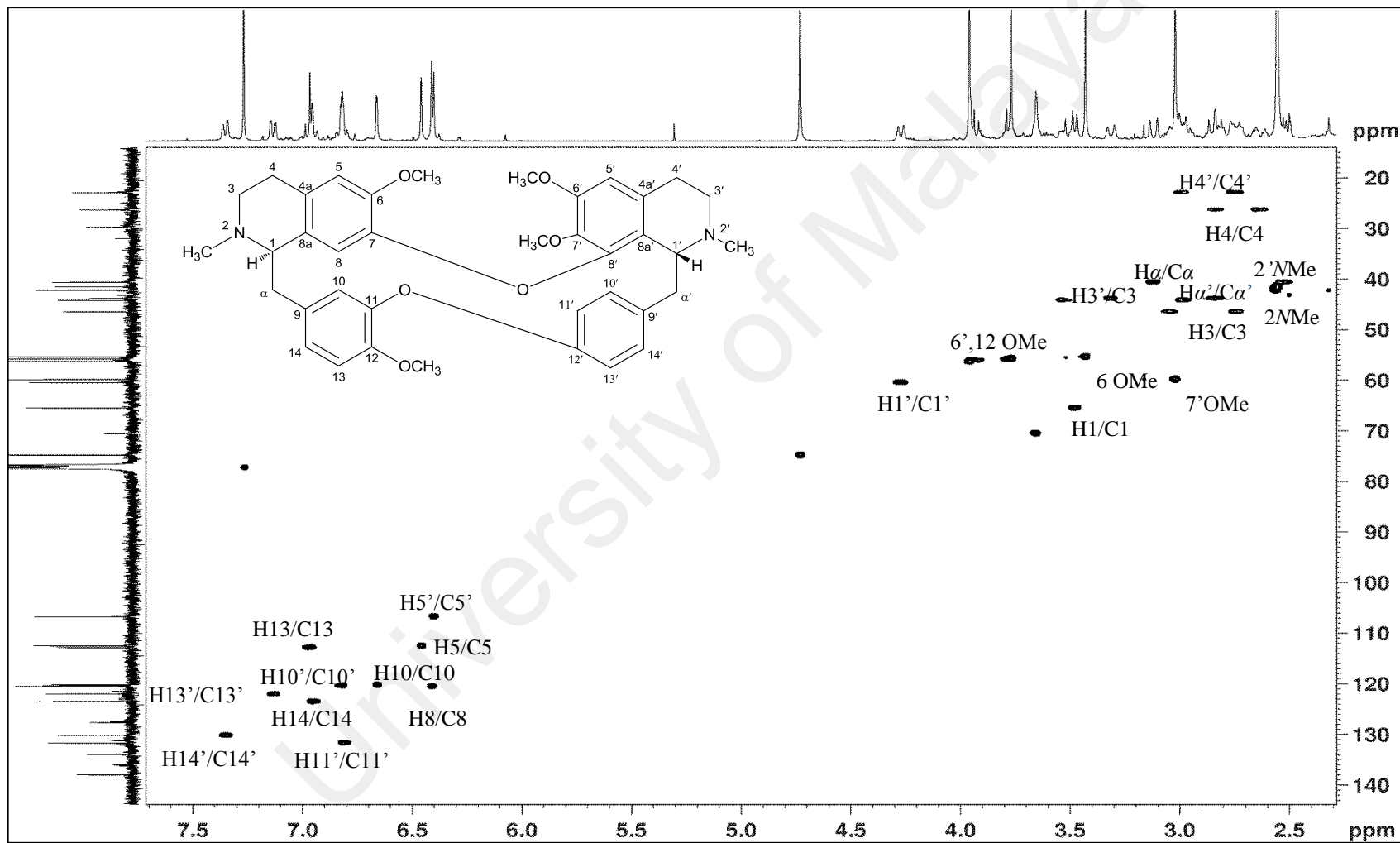


Figure A4: HSQC Spectrum of *O*-methyllicmacusine 118

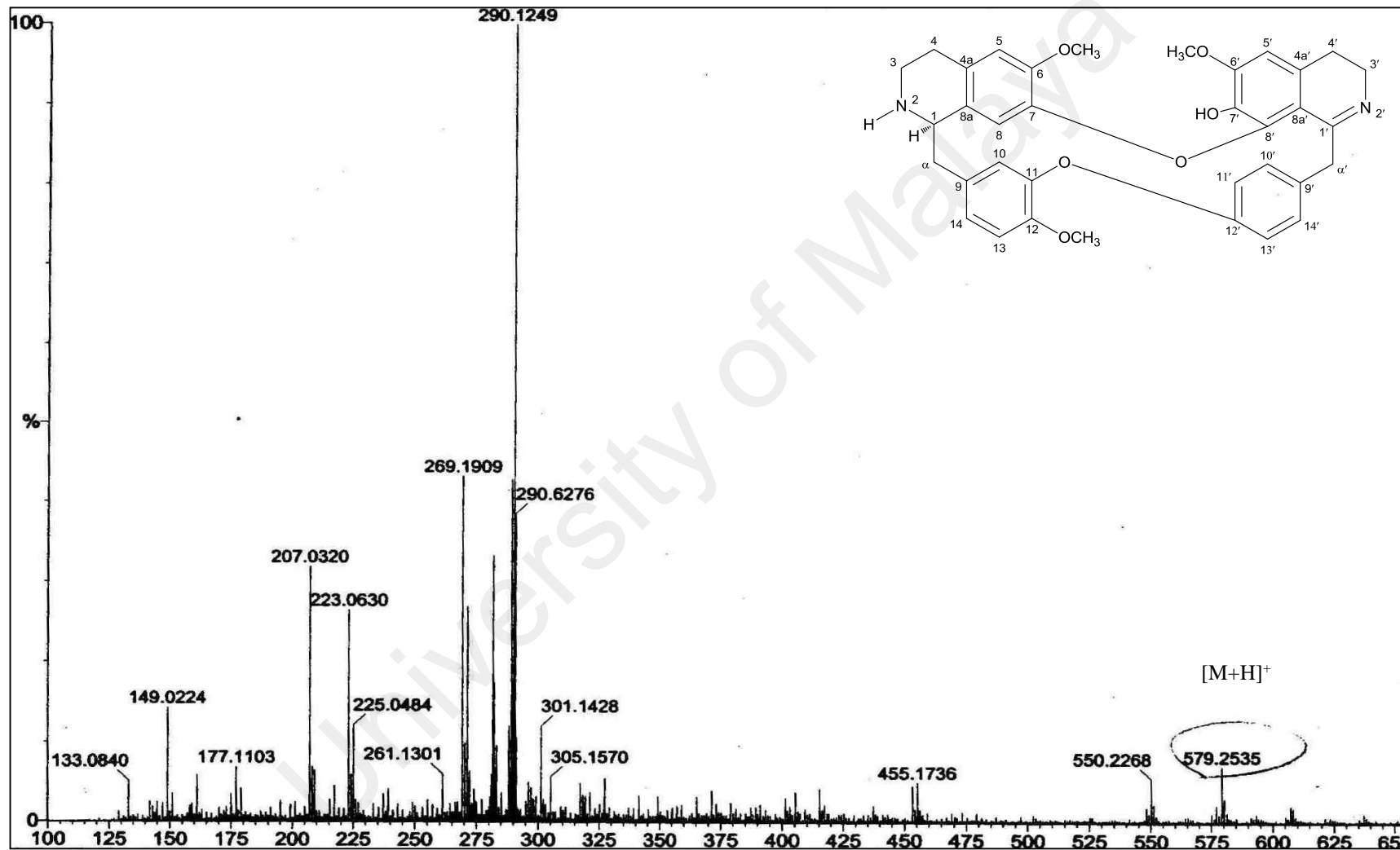


Figure A6: LCMS Spectrum of 3',4'-dihydronorstephasubine **19**

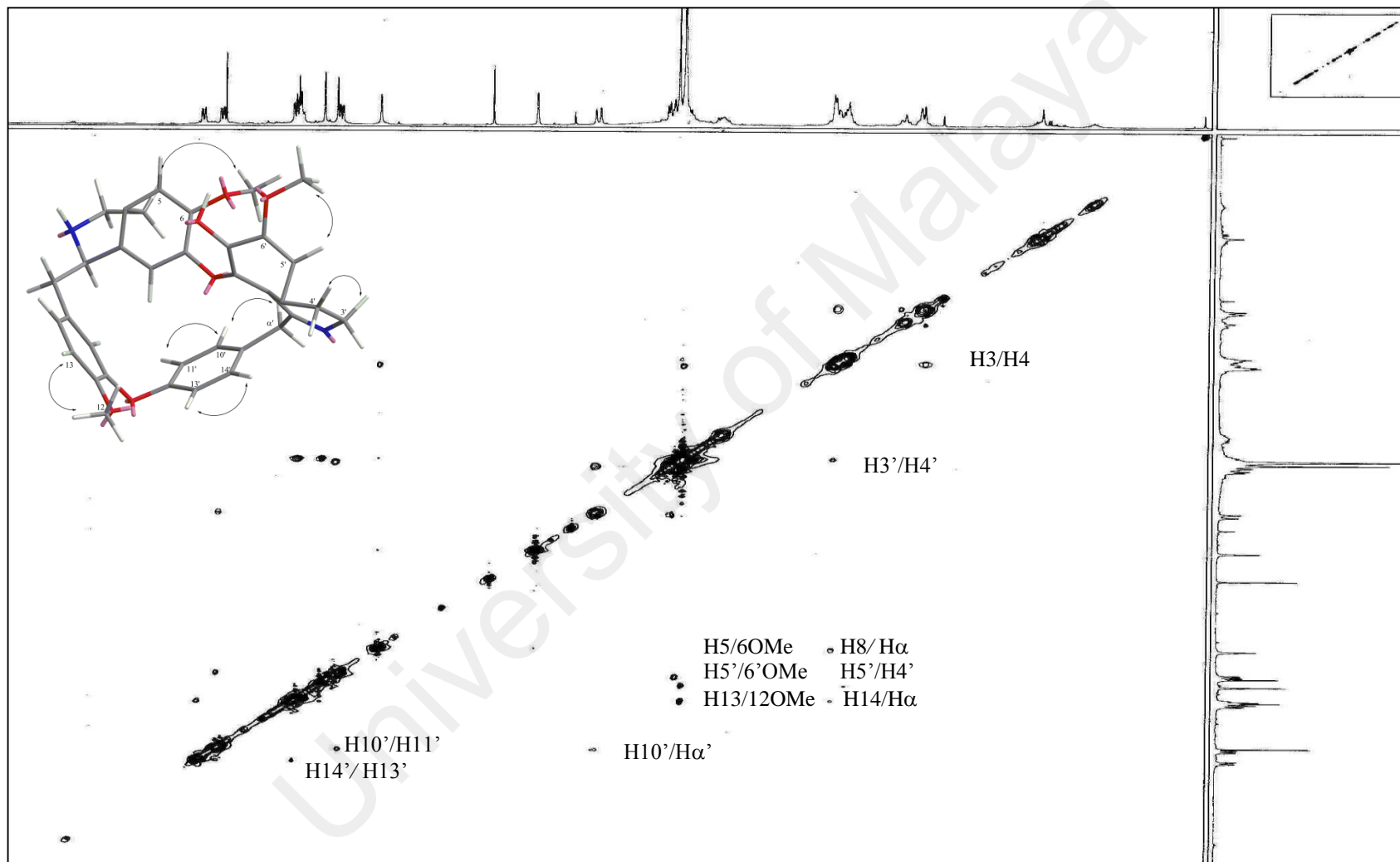


Figure A7: NOESY Spectrum of 3',4'-dihydronorstephasubine **19**

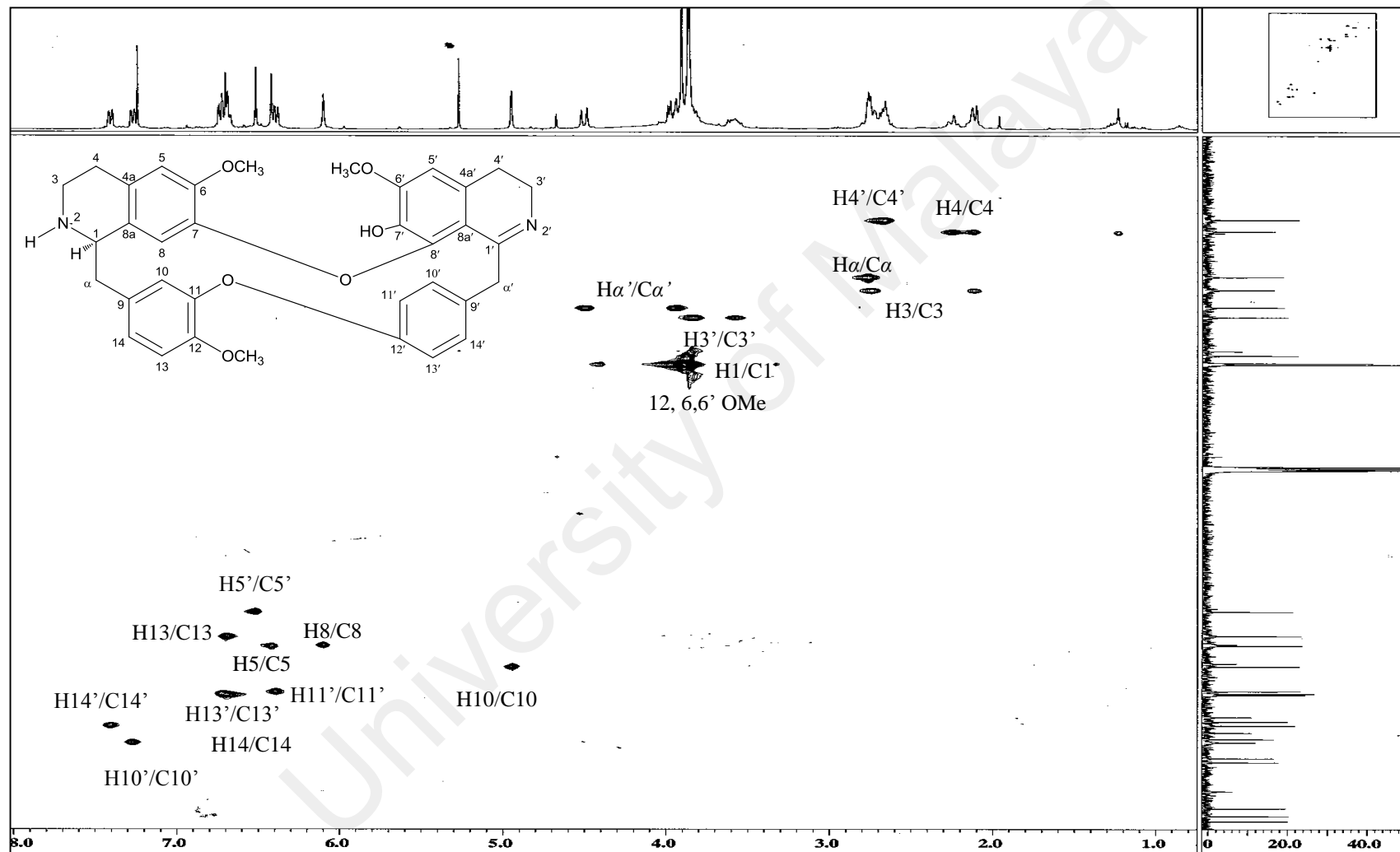


Figure A8: HSQC Spectrum of 3',4'-dihydronorstephasubine **19**

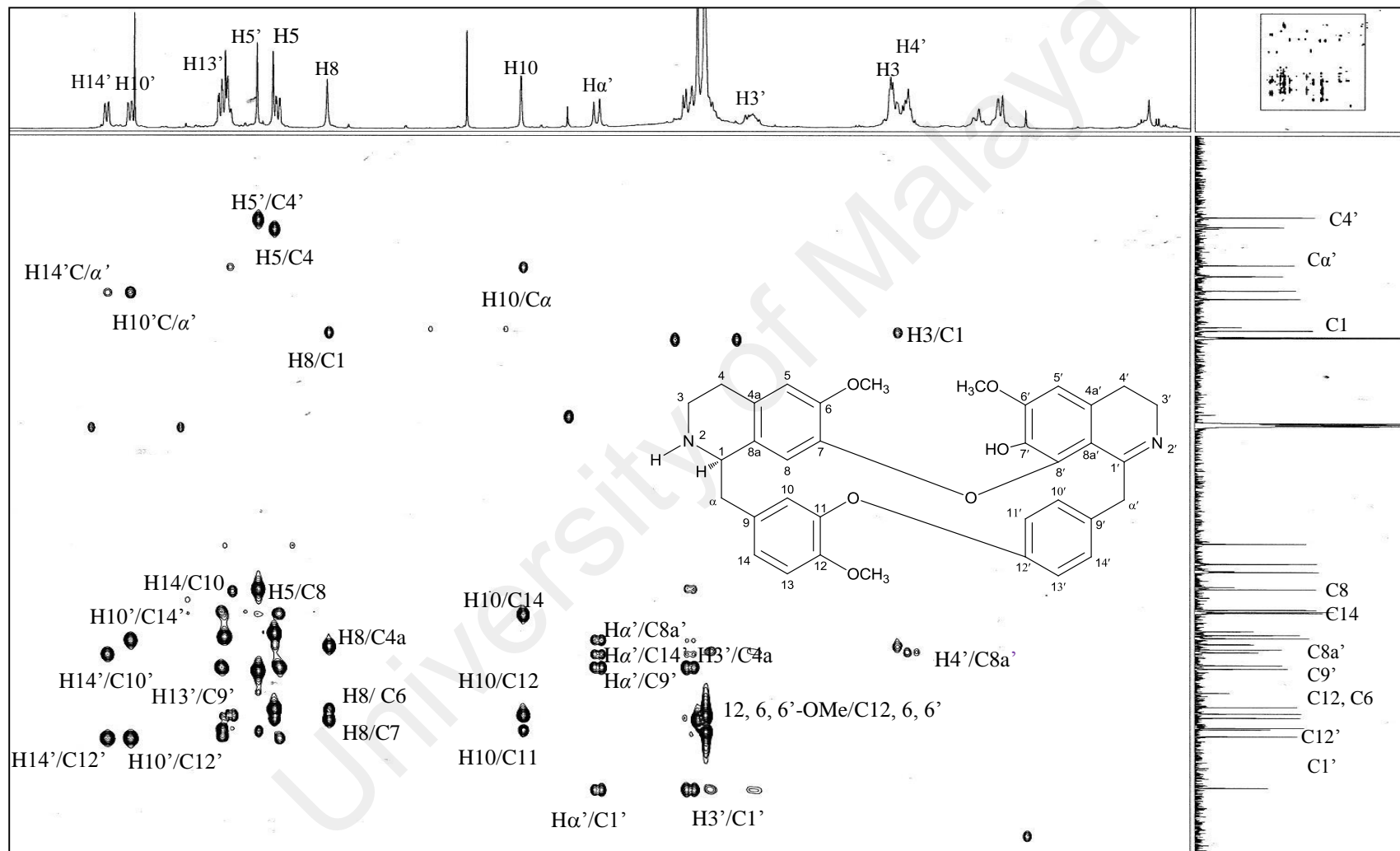


Figure A9: HMBC Spectrum of 3',4'-dihydronorstephasubine **19**

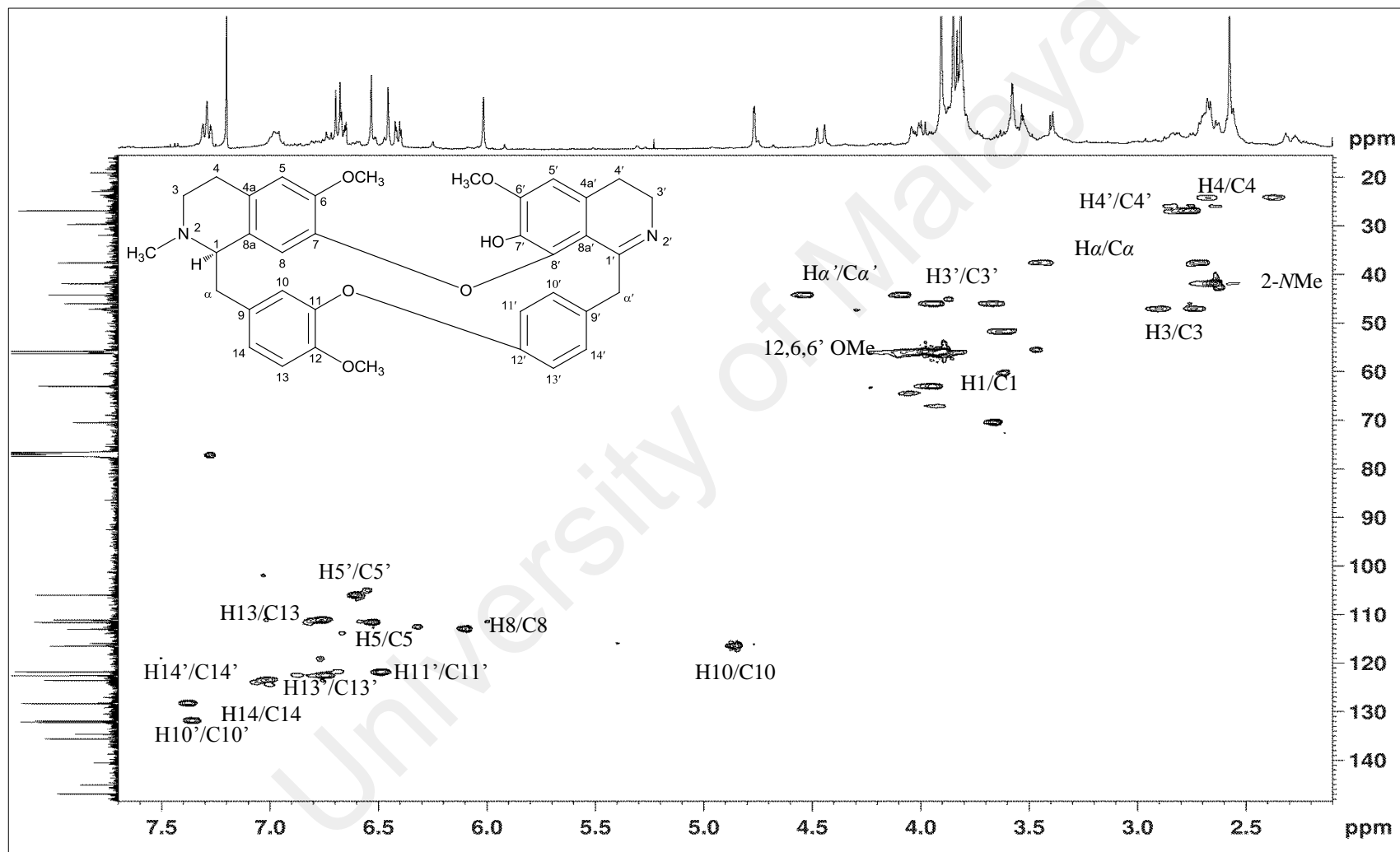


Figure A10: HSQC Spectrum of 3',4'-dihydrostephasubine **119**

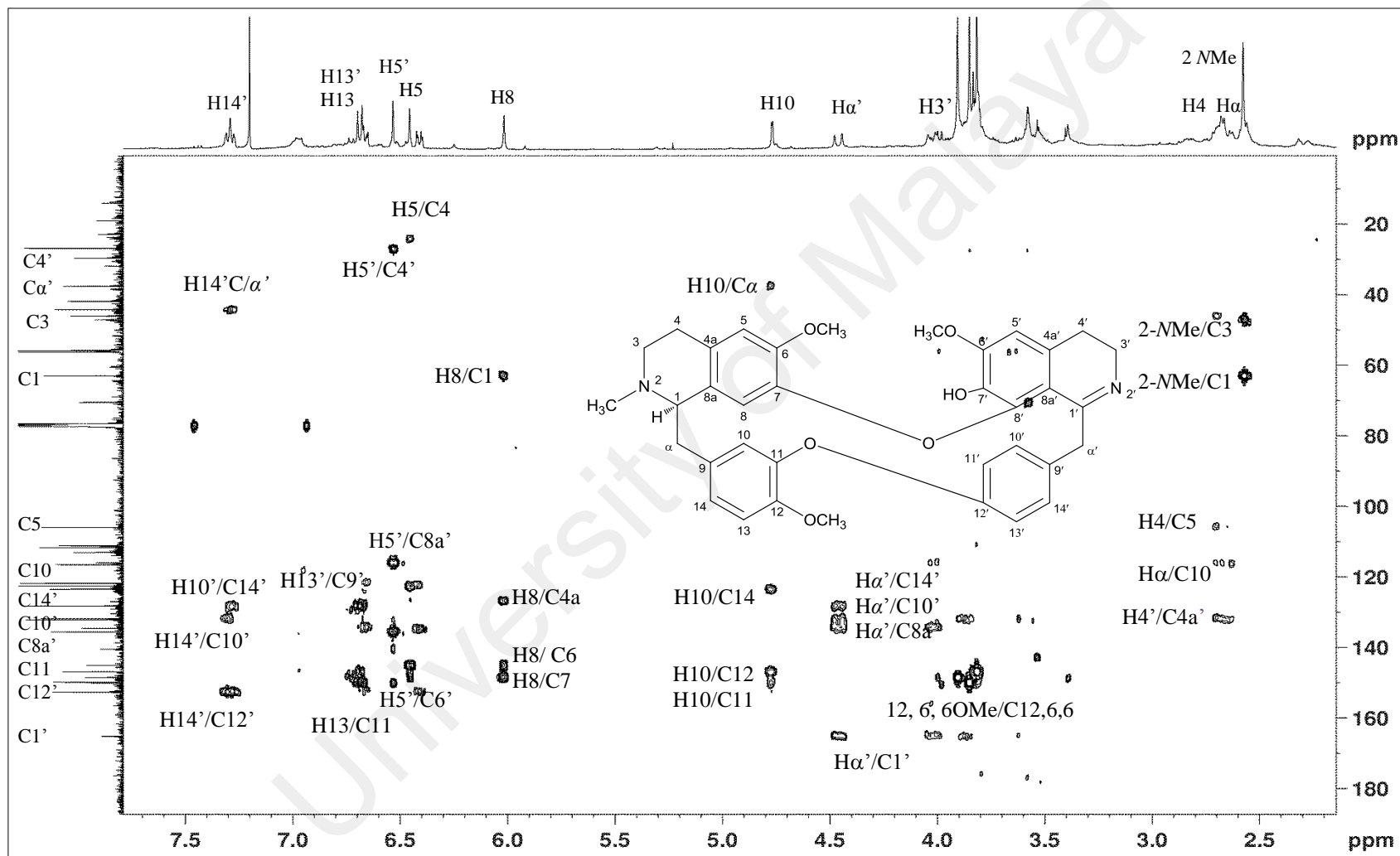


Figure A11: HMBC Spectrum of 3',4'-dihydrostephasubine **119**

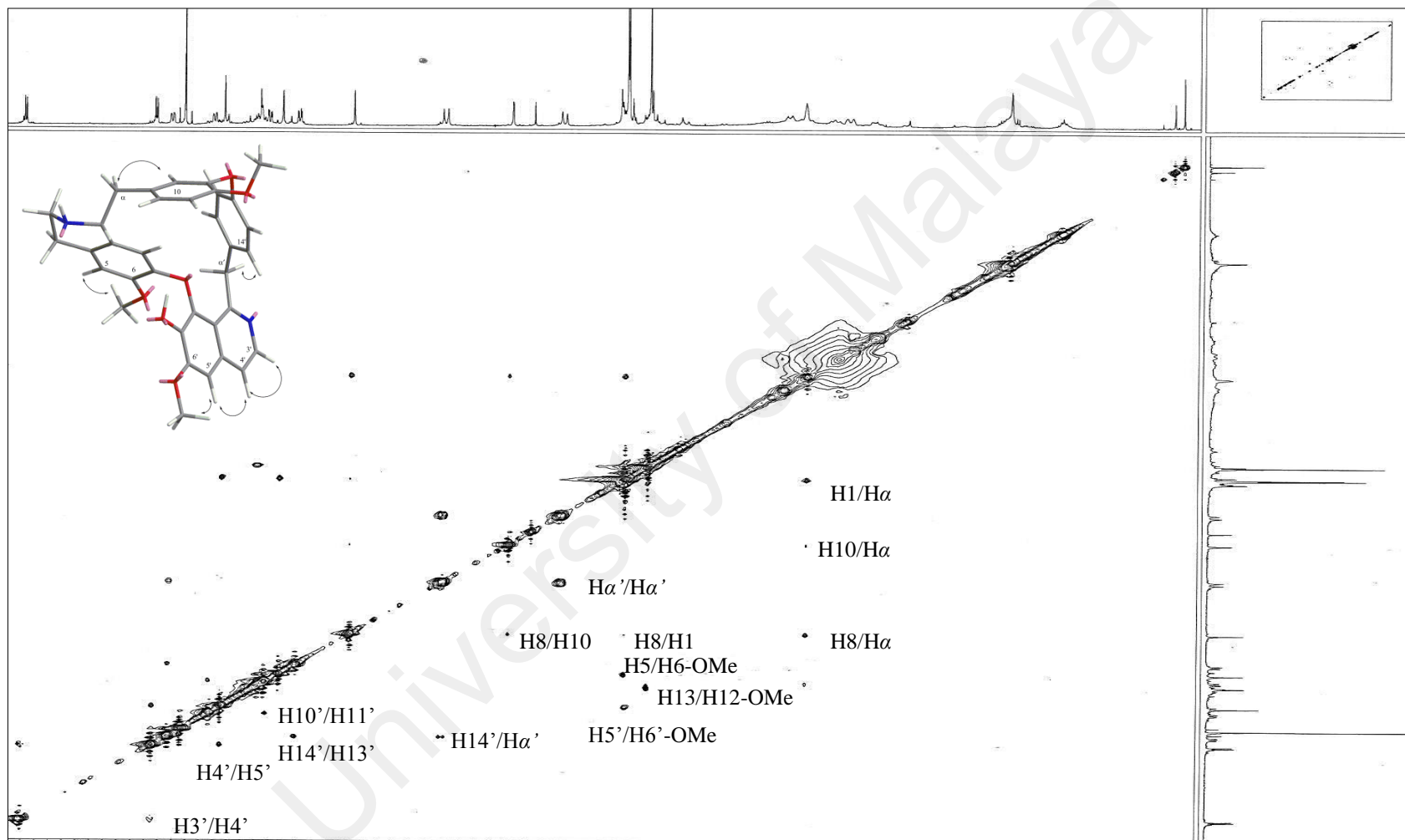


Figure A12: NOESY Spectrum of Norstephasubine **20**

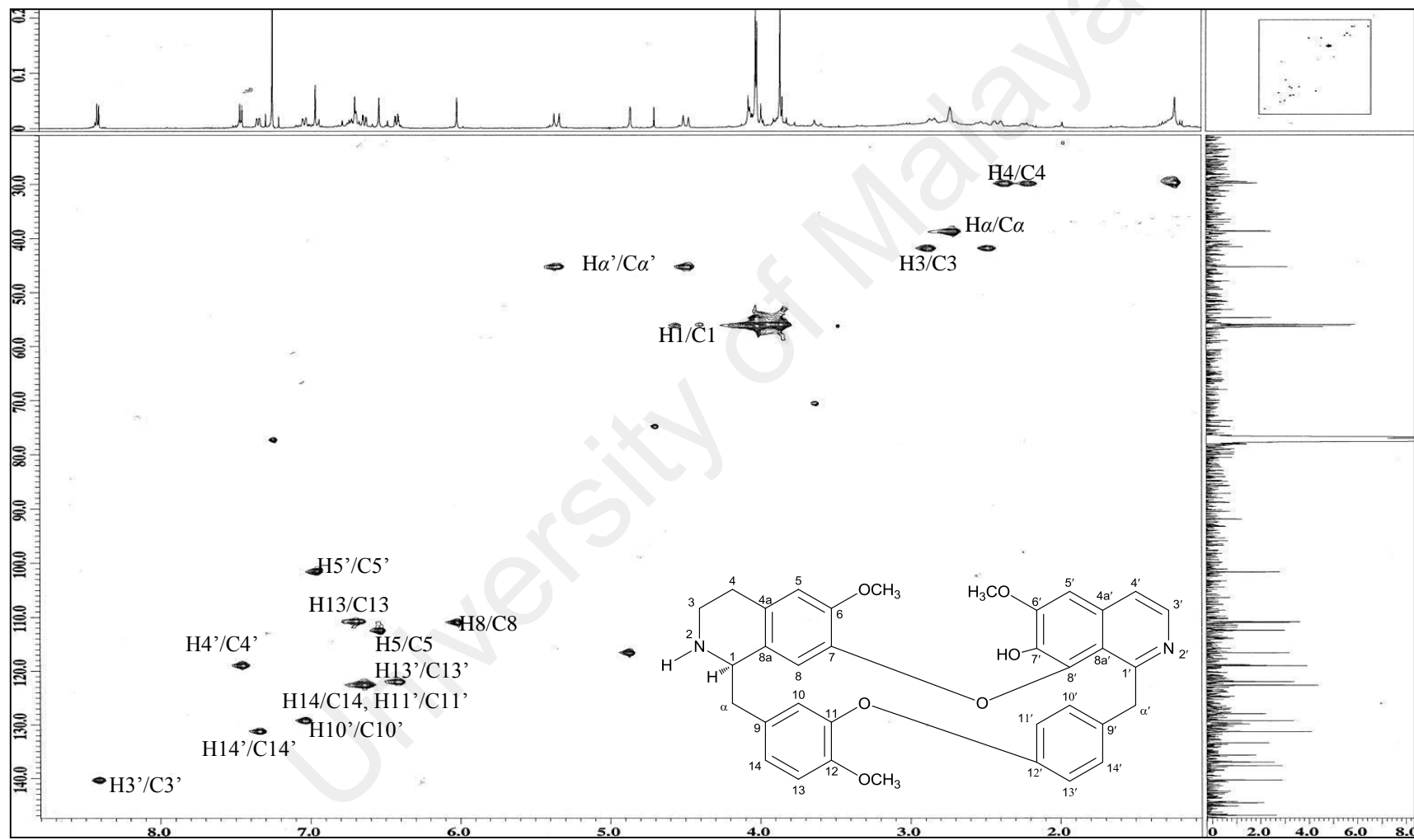


Figure A13: HSQC Spectrum of Norstephasubine **20**

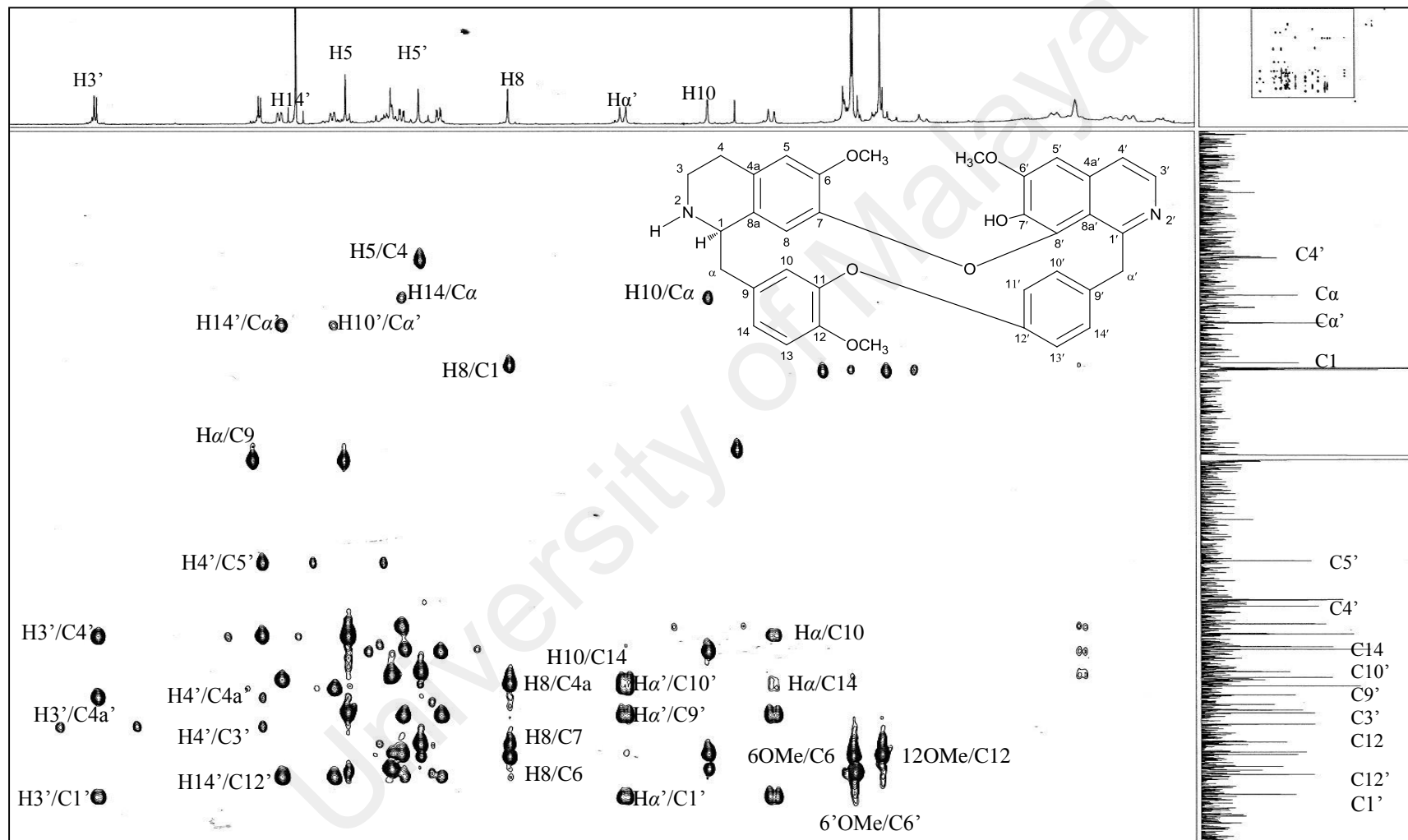


Figure A14: HMBC Spectrum of Norstephasubine 20

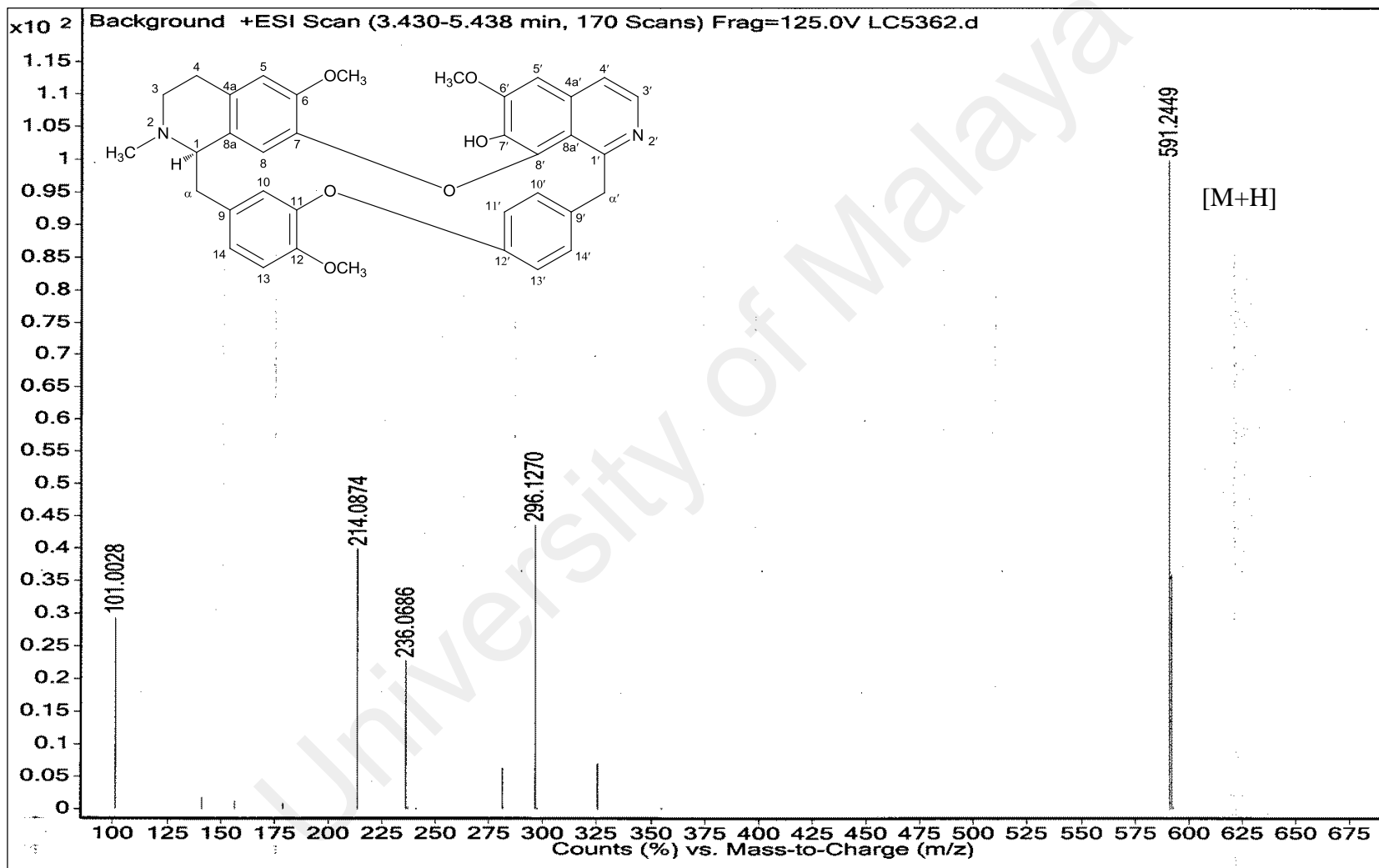


Figure A15: LCMS Spectrum of Stephasubine 120

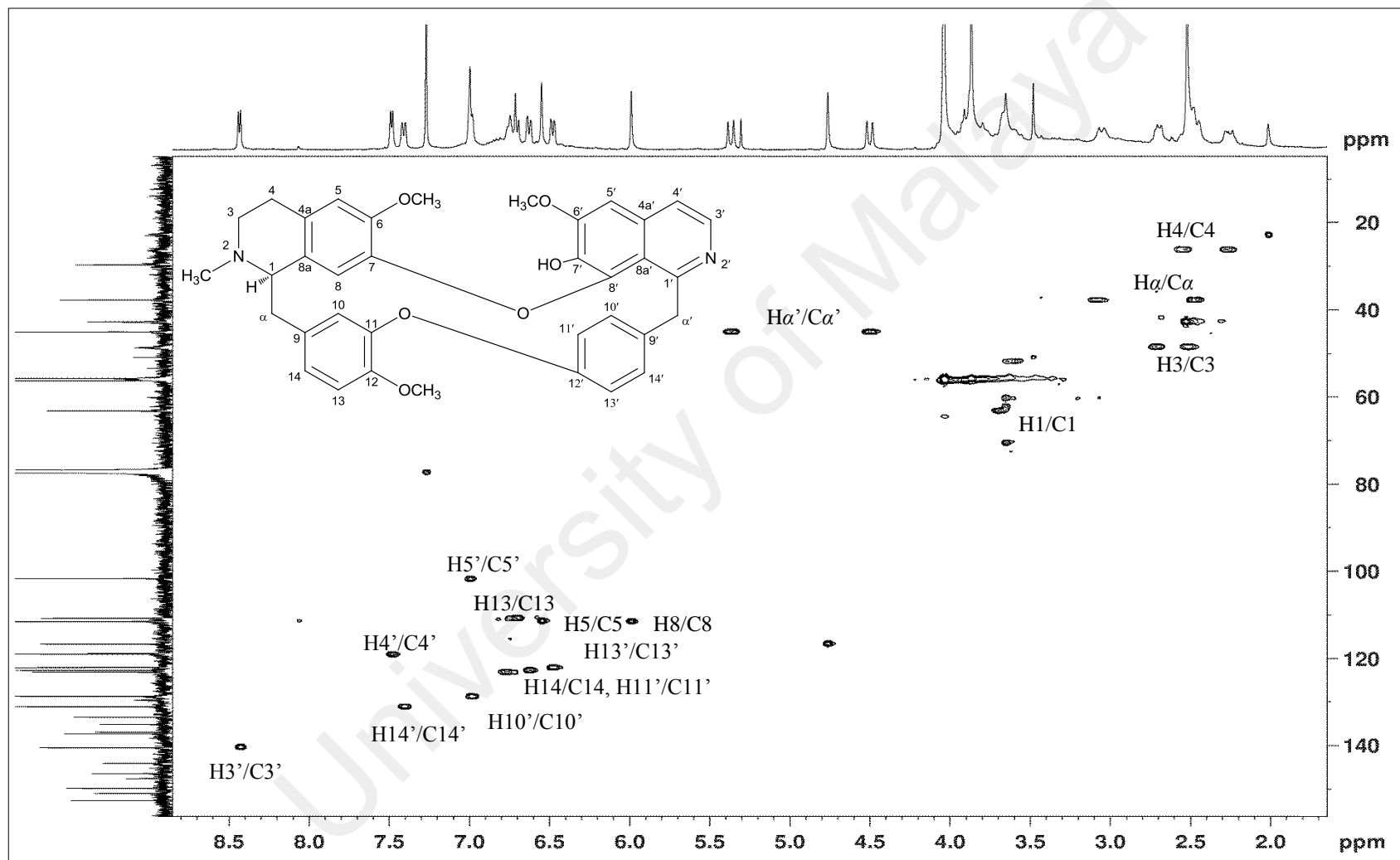


Figure A16: HSQC Spectrum of Stephasubine 120

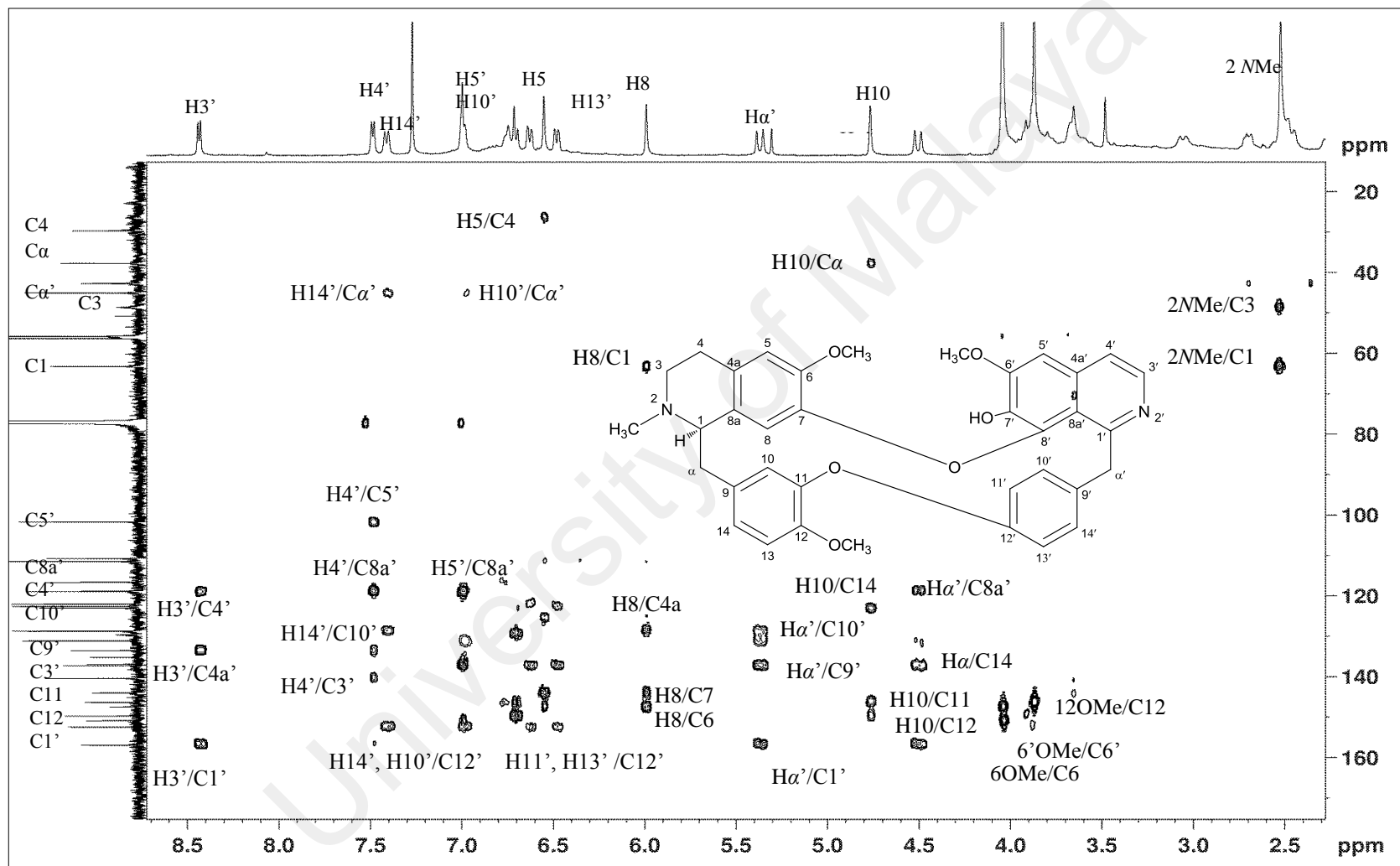


Figure A17: HMBC Spectrum of Stephasubine 120

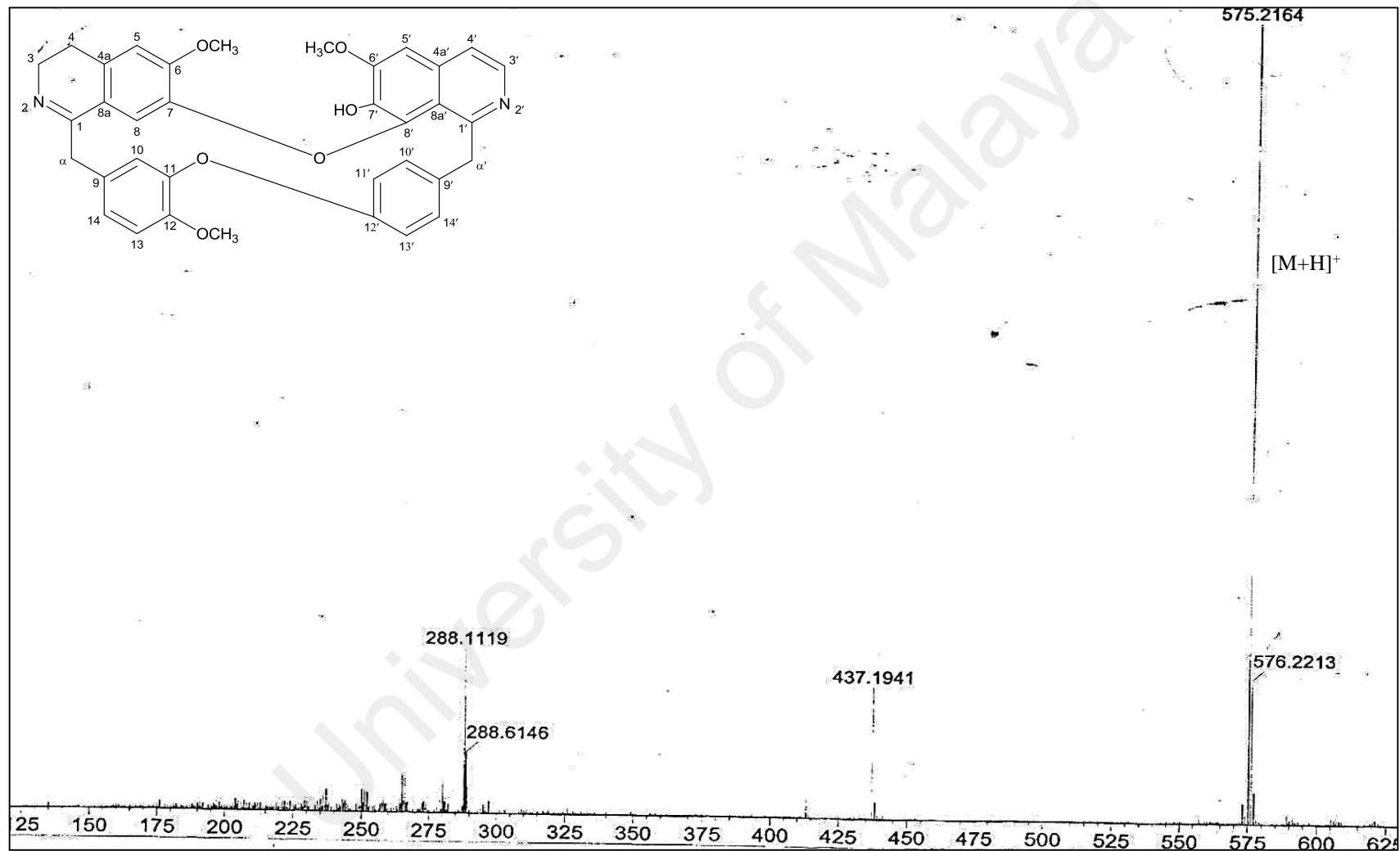


Figure A18: LCMS Spectrum of Stephasubimine 121

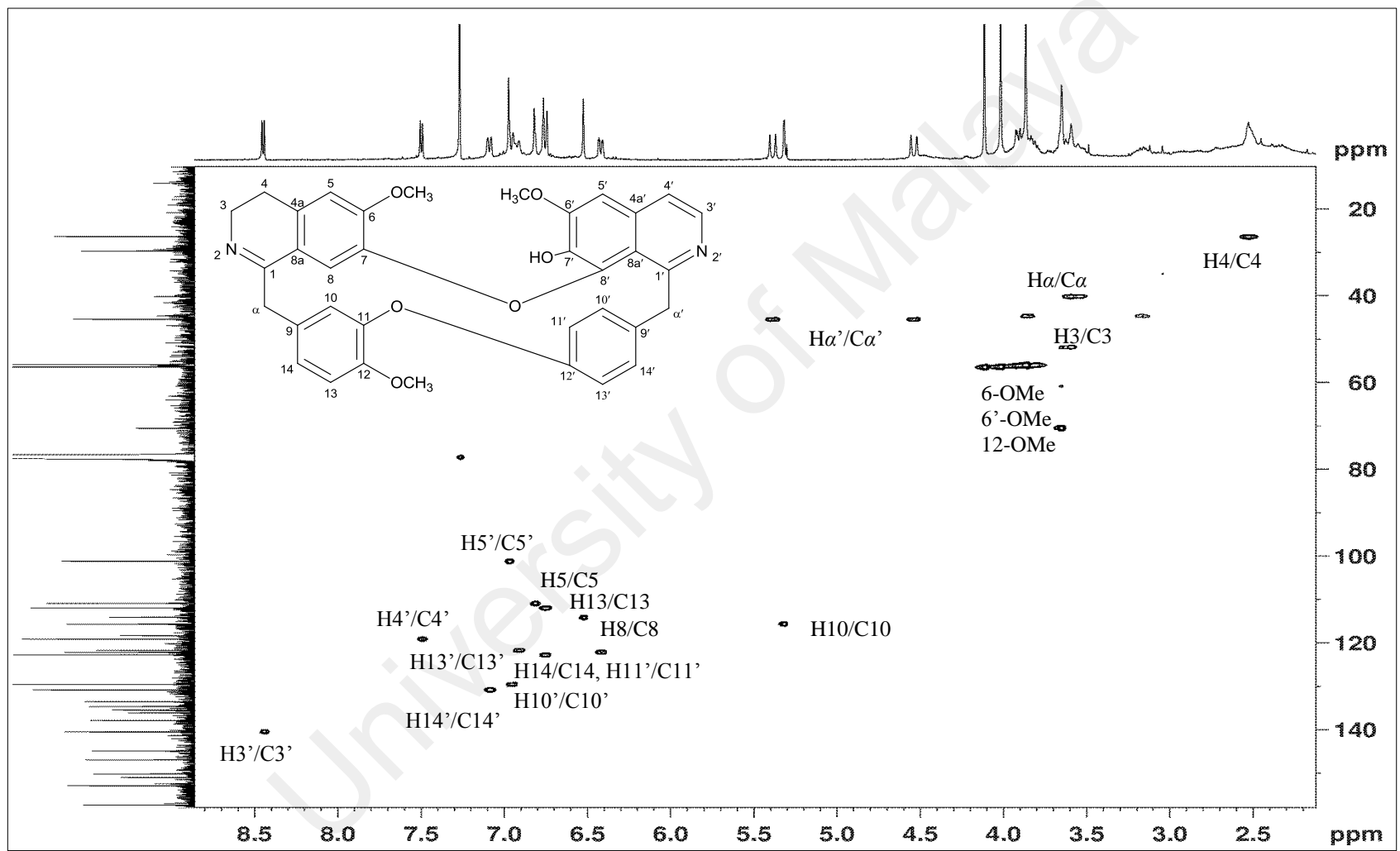


Figure A19: HSQC Spectrum of Stephasubimine 121

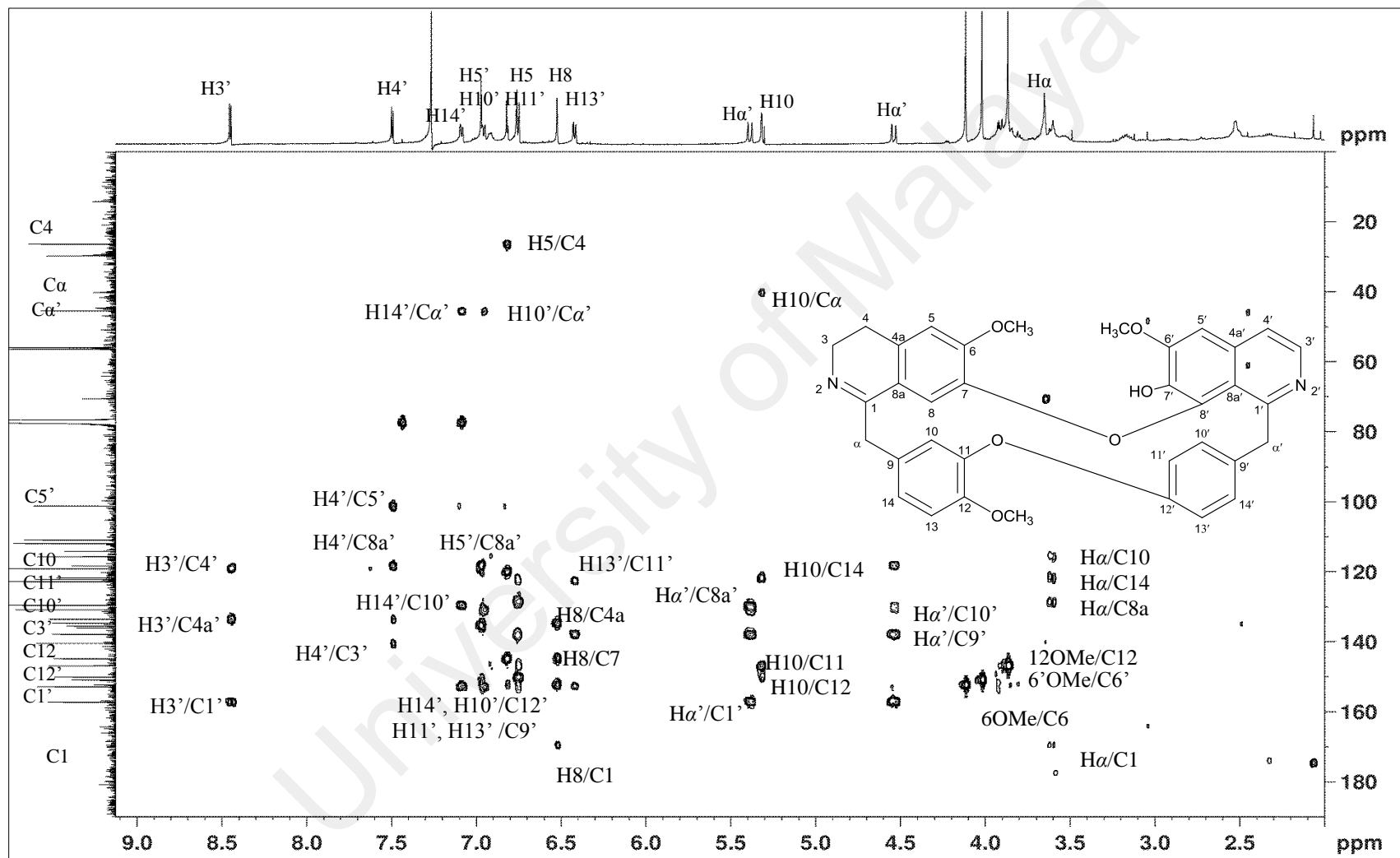


Figure A20: HMBC Spectrum of Stephasubimine **121**

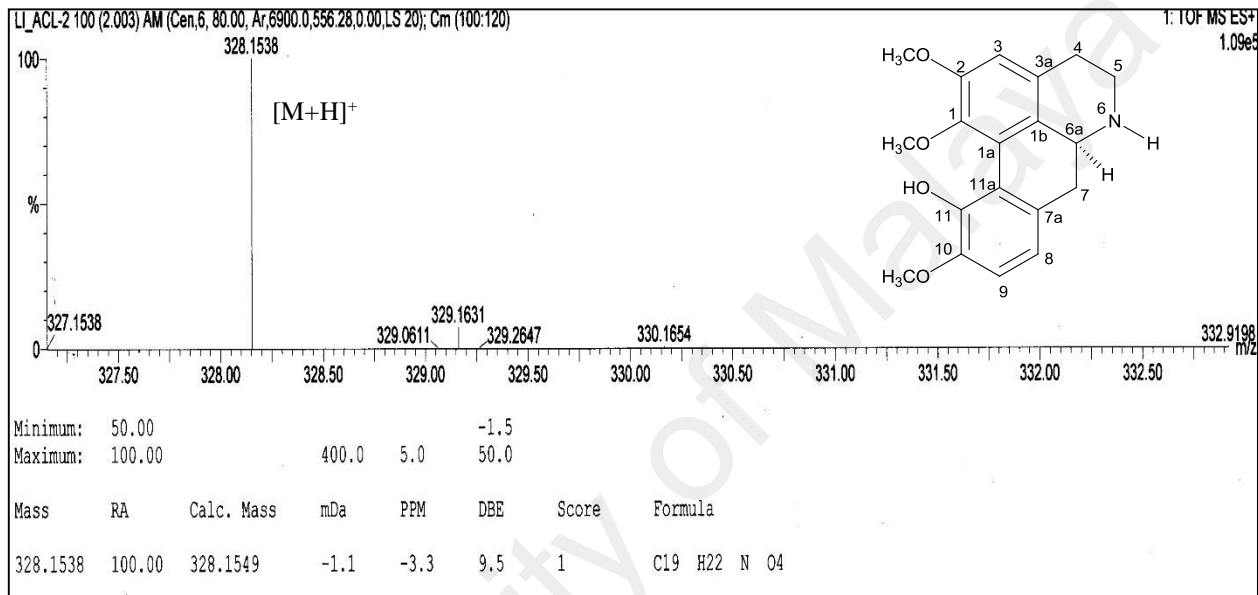


Figure A21: HREIMS Spectrum of Norisocorydine 42

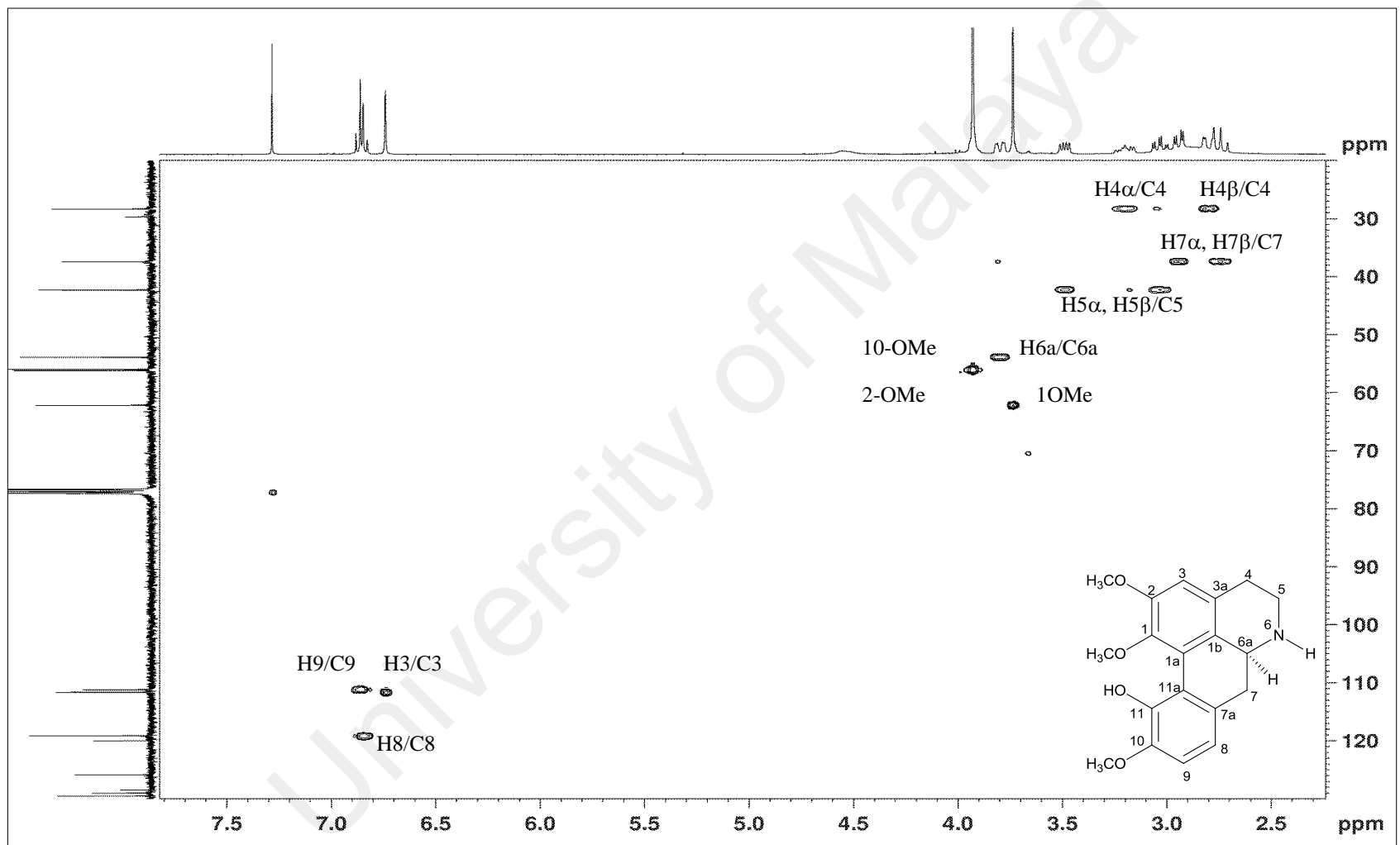


Figure A22: HSQC Spectrum of Norisocorydine 42

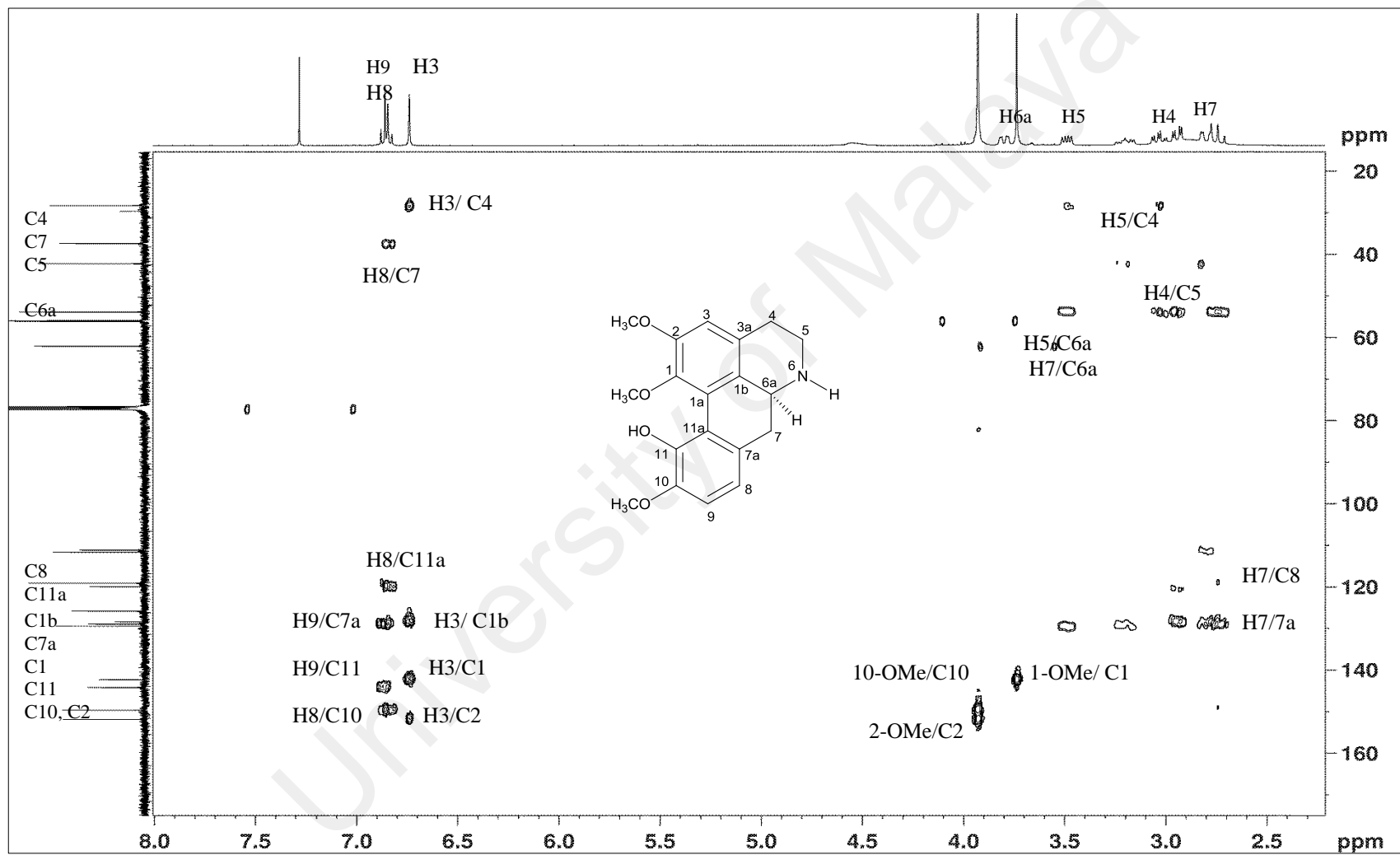


Figure A23: HMBC Spectrum of Norisocorydine **42**

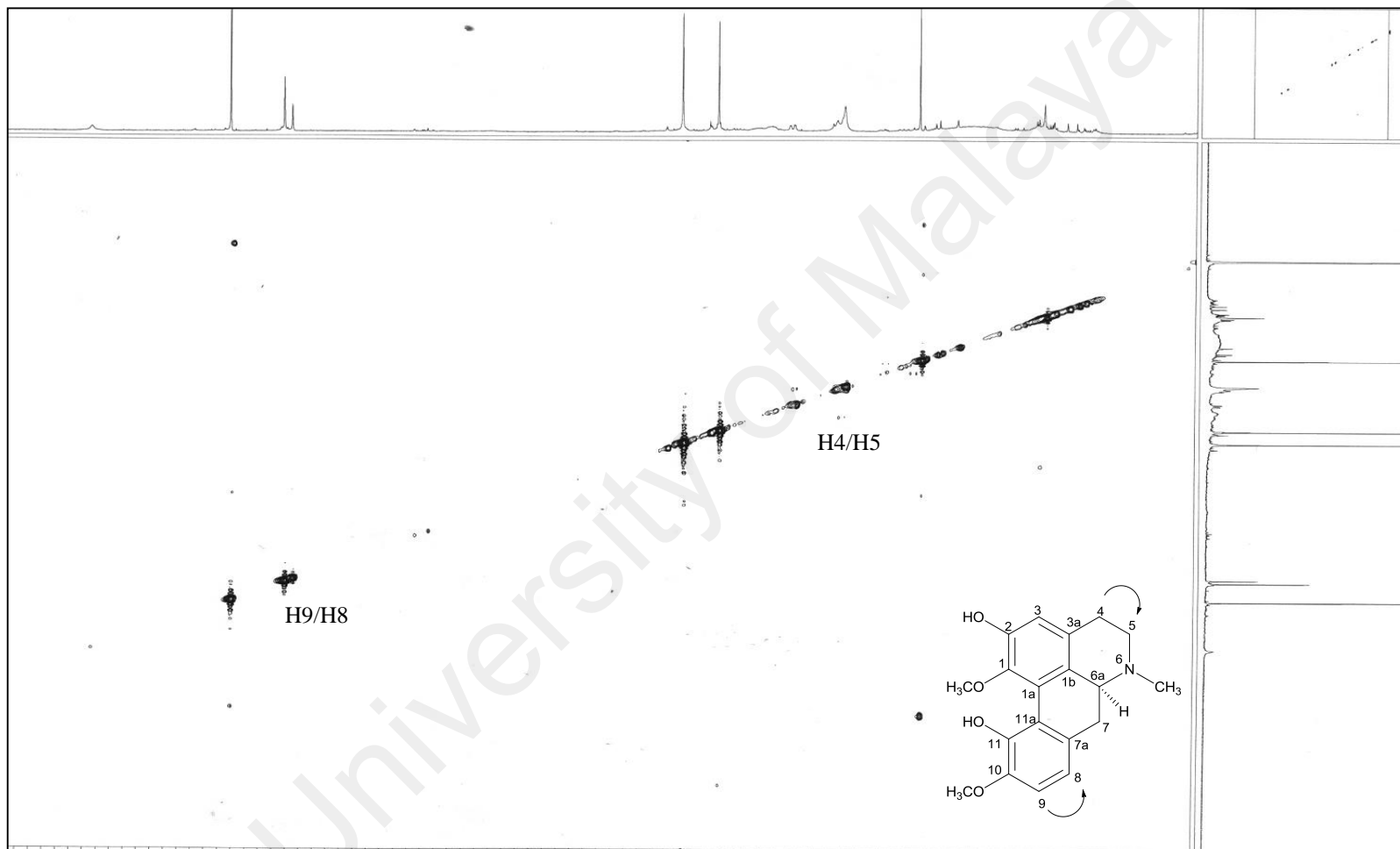


Figure A24: COSY Spectrum of *N*-methylindocarpine **123**

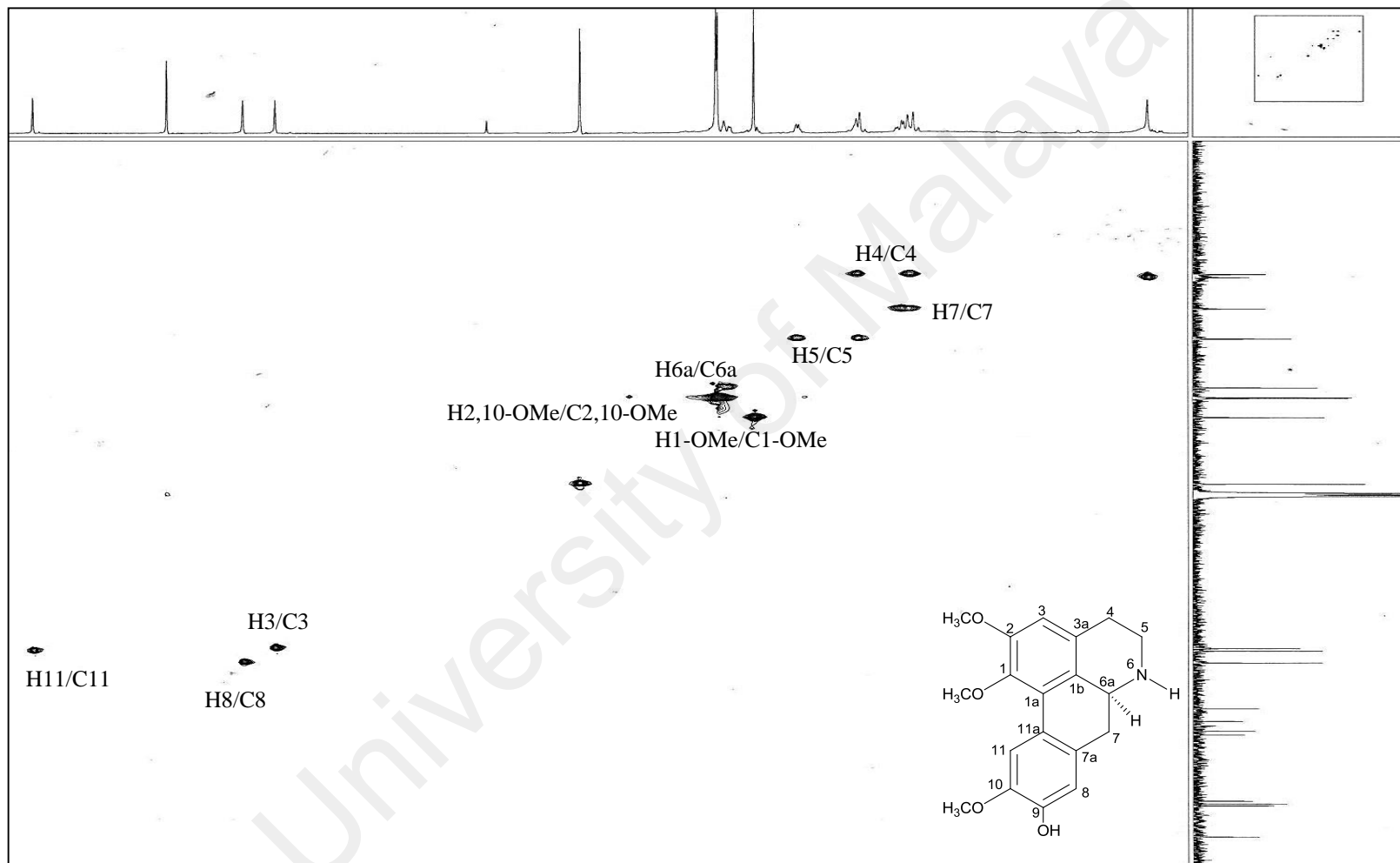


Figure A25: HSQC Spectrum of Laurotetanine 27

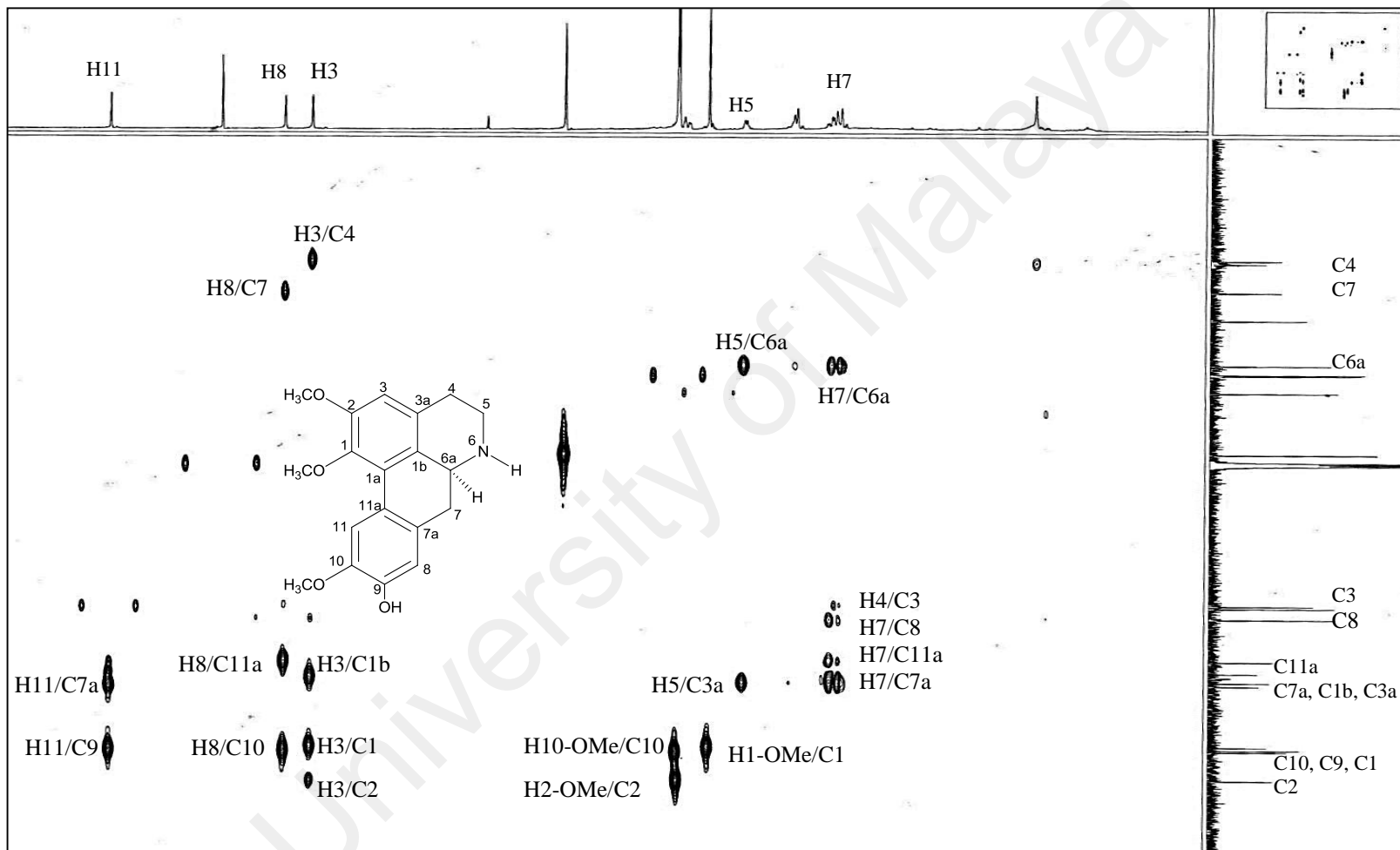


Figure A26: HMBC Spectrum of Laurotetanine **27**

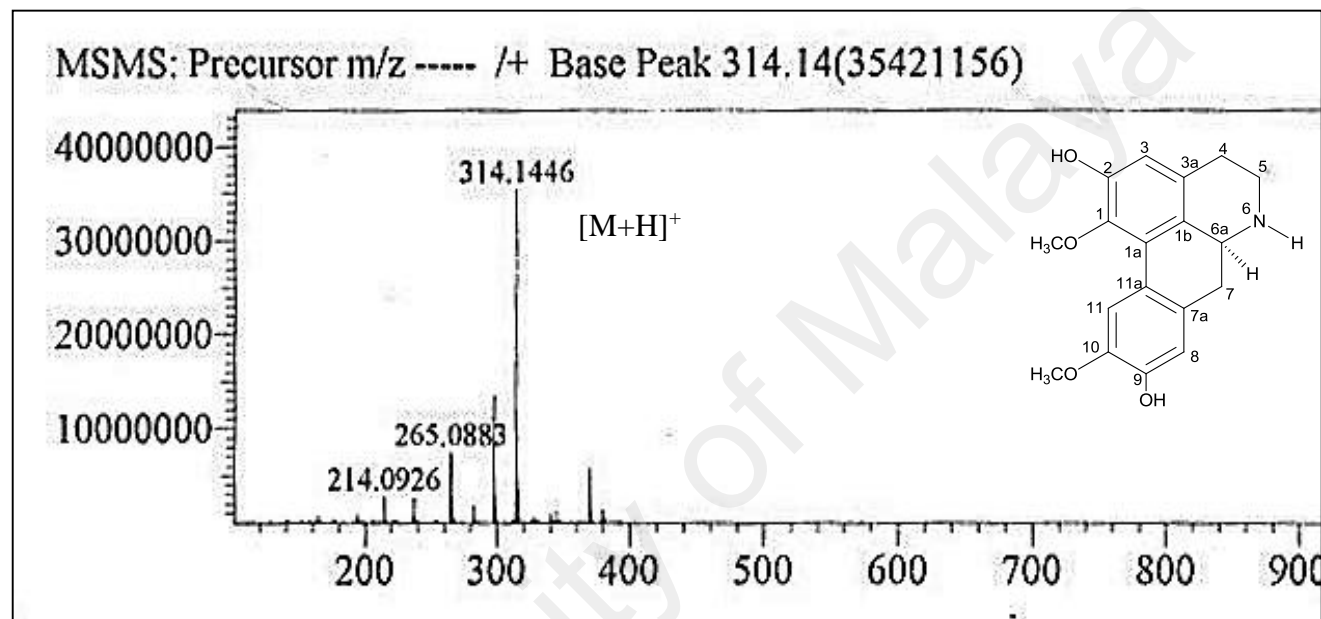


Figure A27: LCMS Spectrum of Norboldine **36**

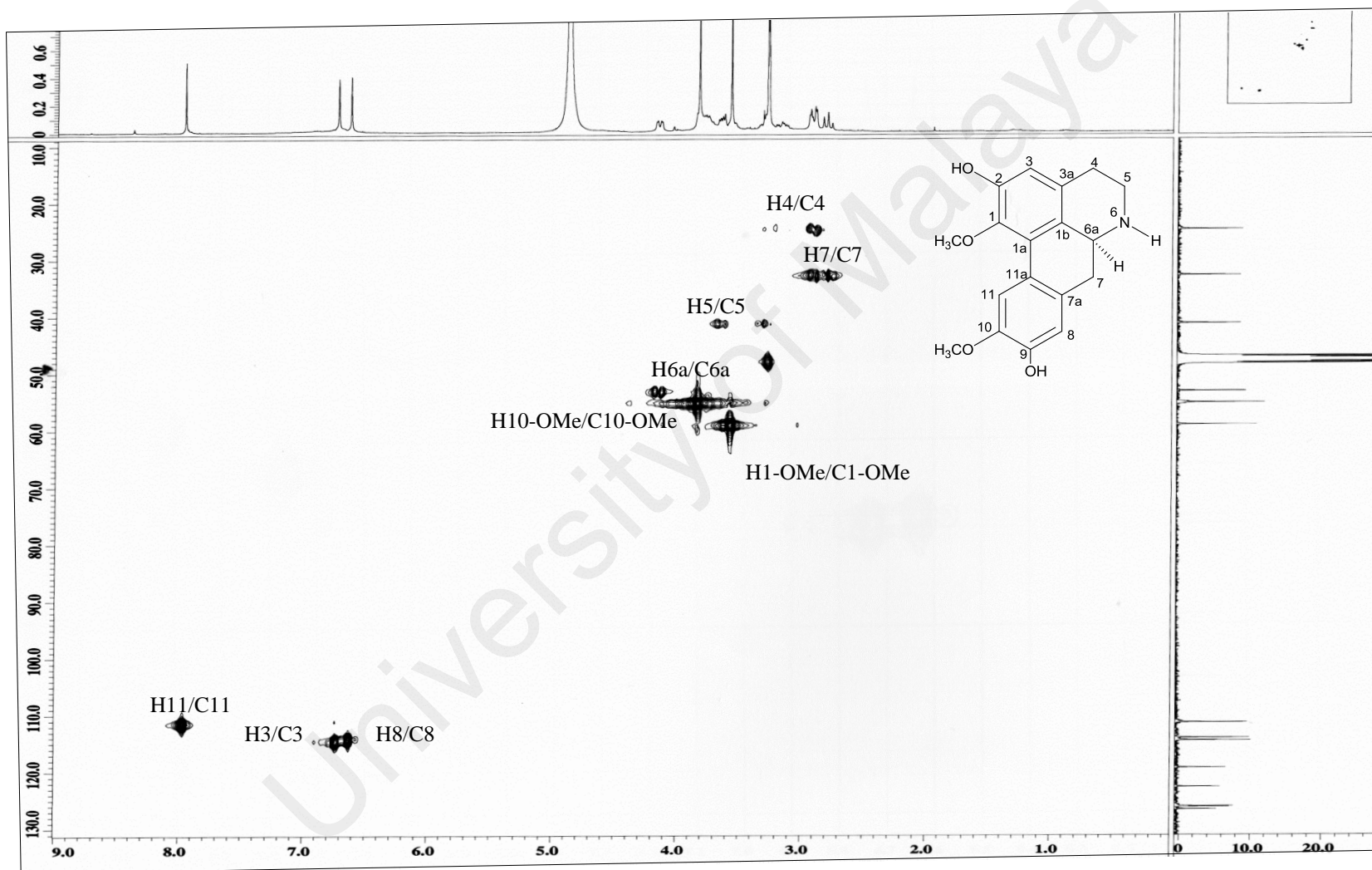


Figure A28: HSQC Spectrum of Norboldine **36**

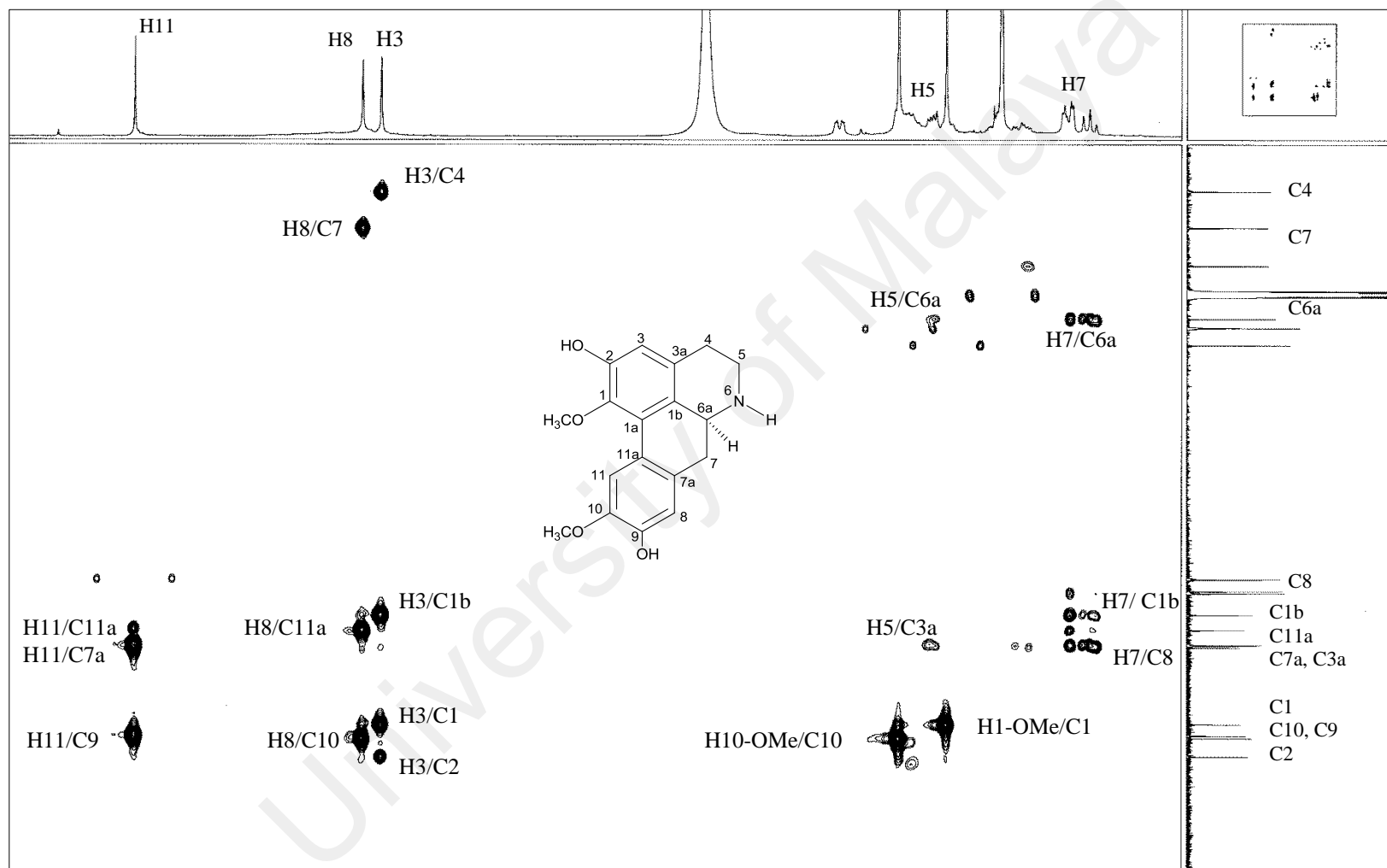


Figure A29: HMBC Spectrum of Norboldine **36**

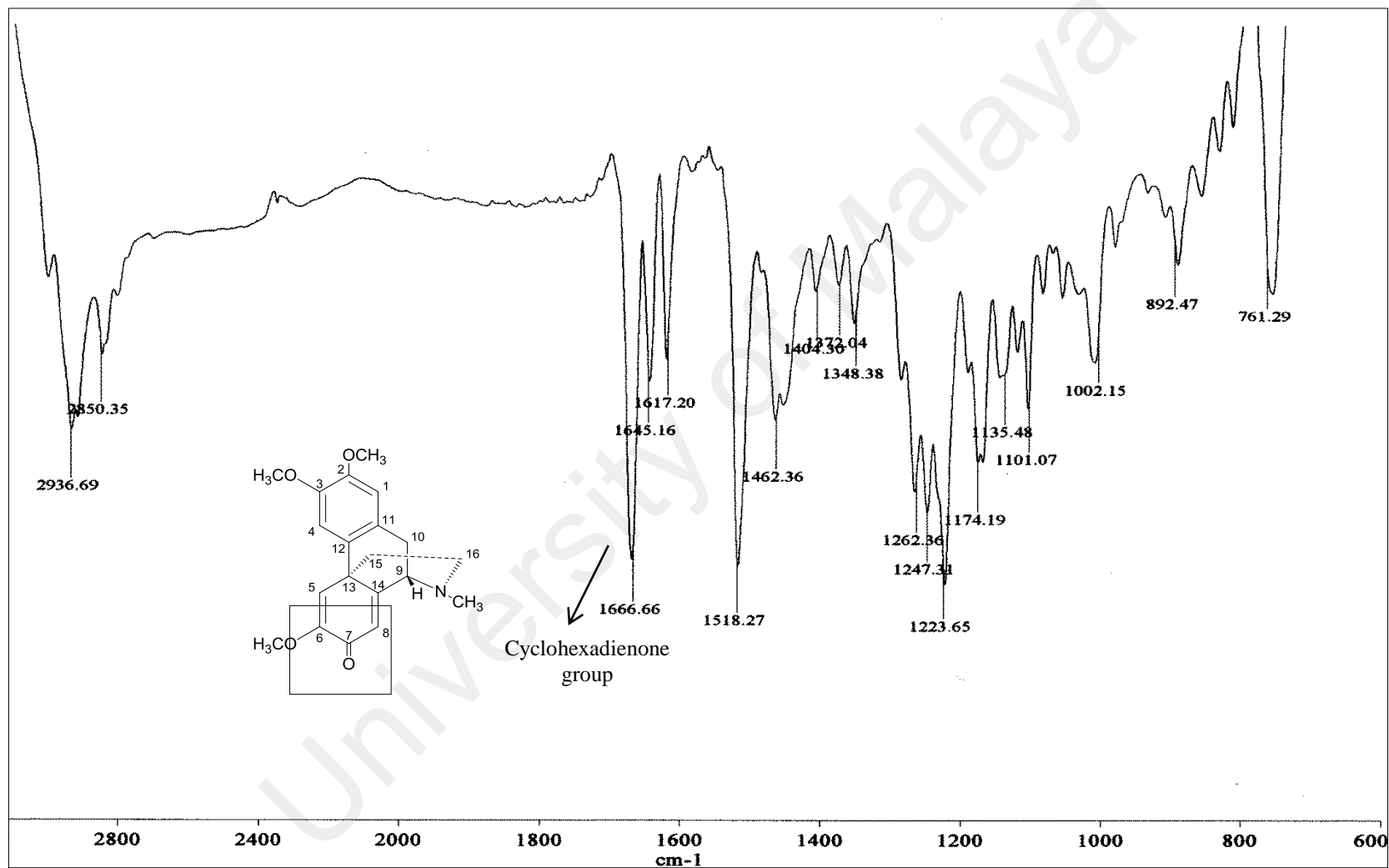


Figure A30: IR Spectrum of Sebiferine 47

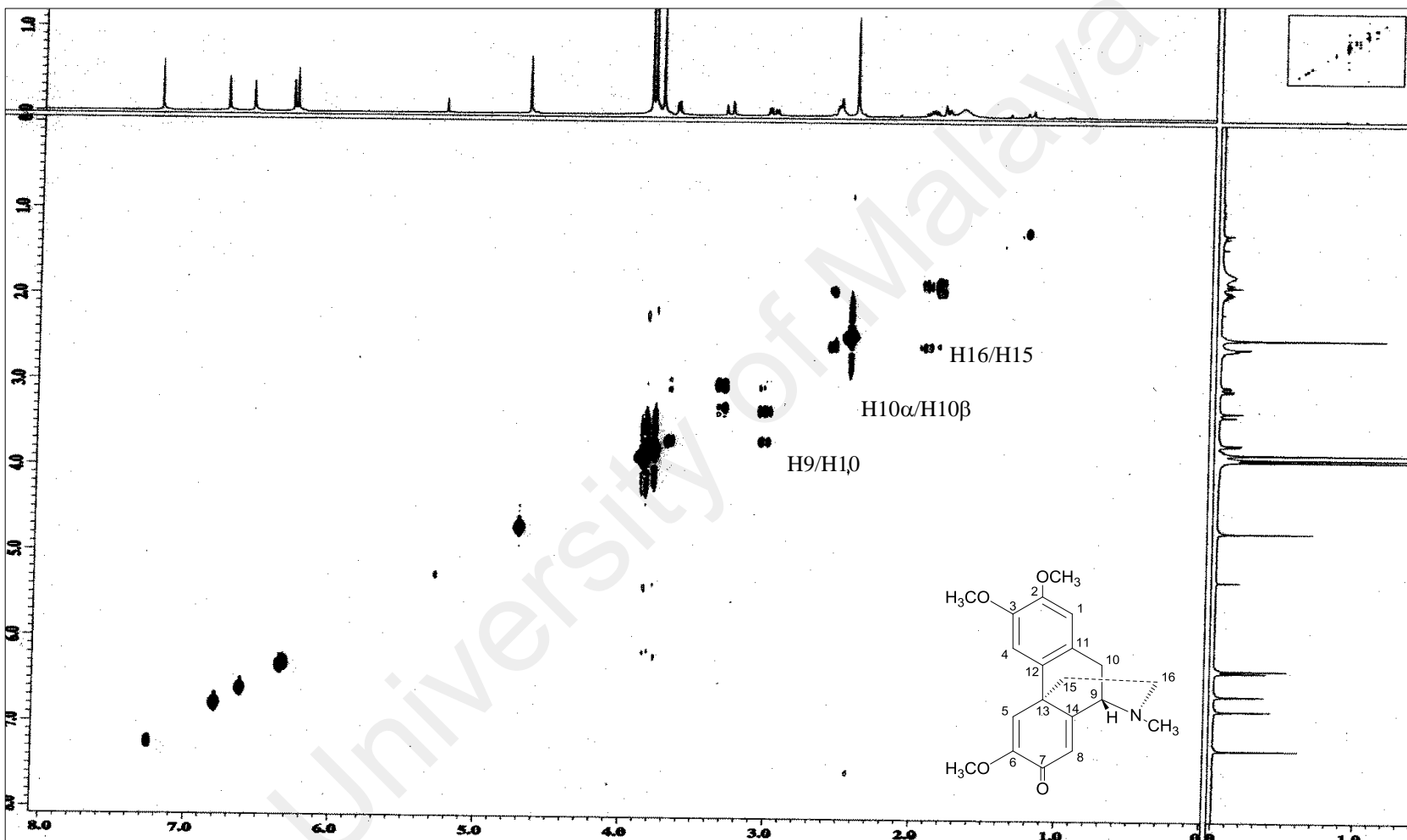


Figure A31: COSY Spectrum of Sebiferine 47

Appendix B

Table B1: The values of observed absorbance (A_{obs}) at 246 nm as a function of pH for ionization of Isocorydine **41** in 2% v/v acetonitrile.

pH	A_{obs}	A_{calc}	%RE
13.50	1.578	1.602	-1.55
13.27	1.548	1.591	-2.76
12.51	1.550	1.473	4.99
12.20	1.376	1.360	1.17
12.04	1.295	1.284	0.86
11.89	1.211	1.204	0.58
11.74	1.117	1.120	-0.26
11.56	1.019	1.020	-0.11
11.53	0.959	1.004	-4.71
11.28	0.880	0.884	-0.49
11.04	0.780	0.797	-2.17
10.52	0.675	0.693	-2.63
7.82	0.663	0.639	3.60
6.93	0.643	0.639	0.62
5.21	0.639	0.639	-0.002
4.12	0.639	0.639	-0.002
3.75	0.638	0.639	-0.16
2.55	0.636	0.639	-0.47
1.68	0.644	0.639	0.77
0.81	0.654	0.639	2.29

$$K_a = (1.750 \pm 0.019) \times 10^{-12}$$

$$10^{-2} E_{\text{SH}} = 63.90 \pm 0.89$$

$$10^{-2} E_{\text{S-}} = 161.99 \pm 1.81$$

Table B2: The values of observed absorbance (A_{obs}) at 270 nm as a function of pH for ionization of Isocorydine **41** in 2% v/v acetonitrile.

pH	A_{obs}	A_{calc}	%RE
13.6	0.794	0.789	0.68
13.5	0.777	0.790	-1.64
12.51	0.838	0.833	0.54
11.89	0.926	0.933	-0.73
11.74	0.991	0.967	2.47
11.04	1.084	1.111	-2.46
10.52	1.153	1.163	-0.84
9.01	1.181	1.190	-0.74
7.82	1.175	1.191	-1.33
6.93	1.181	1.191	-0.82
5.21	1.187	1.191	-0.31
3.75	1.220	1.191	2.41
2.55	1.200	1.191	0.78
1.68	1.211	1.191	1.68

$$K_a = (2.24 \pm 0.3) \times 10^{-12}$$

$$10^{-2} E_{\text{SH}} = 119.07 \pm 0.63$$

$$10^{-2} E_{\text{S}^-} = 78.4 \pm 1.1$$

Table B3: The values of observed absorbance (A_{obs}) at 338 nm as a function of pH for ionization of Isocorydine **41** in 2% v/v acetonitrile.

pH	A_{obs}	A_{calc}	%RE
13.50	0.620	0.629	-1.43
13.27	0.602	0.622	-3.25
12.51	0.589	0.549	6.82
12.20	0.484	0.479	0.99
12.04	0.438	0.432	1.35
11.89	0.377	0.383	-1.47
11.74	0.315	0.330	-4.85
11.56	0.270	0.268	0.68
11.53	0.240	0.258	-7.58
11.28	0.187	0.183	1.95
11.04	0.140	0.129	8.10
10.52	0.066	0.063	4.09
9.01	0.030	0.031	-2.13
7.82	0.031	0.030	4.49
6.93	0.030	0.030	1.51
5.21	0.030	0.030	1.54
3.75	0.034	0.030	13.13
2.55	0.025	0.030	-18.15
1.68	0.025	0.030	-18.15

$$K_a = (1.769 \pm 0.098) \times 10^{-12}$$

$$10^{-2} E_{\text{SH}} = 2.95 \pm 0.47$$

$$10^{-2} E_{\text{s-}} = 63.95 \pm 0.91$$

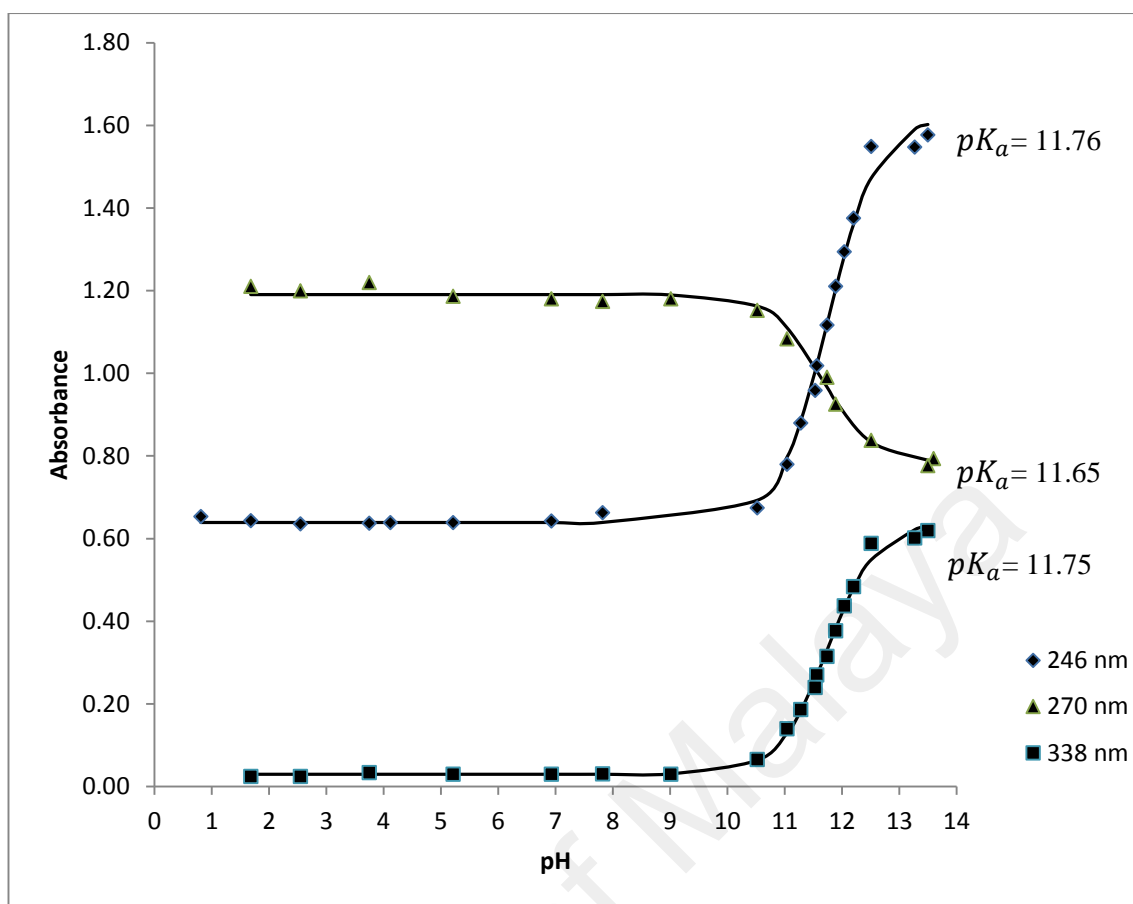


Figure B1: pH-Absorbance curves of Isocorydine **41** in 2% v/v acetonitrile at 246 nm, 270 nm, and 338 nm.

Table B4: The values of observed absorbance (A_{obs}) at 246 nm as a function of pH for ionization of Norisocorydine **42** in 2% v/v acetonitrile.

pH	A_{obs}	A_{calc}	%RE
13.73	1.922	1.917	0.24
13.51	1.928	1.909	1.01
12.74	1.819	1.814	0.29
12.12	1.508	1.600	-6.08
11.26	1.423	1.274	10.45
9.91	1.313	1.158	11.78
9.27	1.228	1.153	6.08
8.02	1.117	1.152	-3.13
7.39	1.061	1.152	-8.56
6.52	1.182	1.152	2.55
6.07	1.144	1.152	-0.69
5.55	1.170	1.152	1.55
4.57	1.072	1.152	-7.45
3.68	1.109	1.152	-3.86
3.33	1.044	1.152	-10.33

$$K_a = (1.02 \pm 0.47) \times 10^{-12}$$

$$10^{-2} E_{\text{SH}} = 115.18 \pm 2.72$$

$$10^{-2} E_{\text{S}^-} = 193.13 \pm 6.26$$

Table B5: The values of observed absorbance (A_{obs}) at 270 nm as a function of pH for ionization of Norisocorydine **42** in 2% v/v acetonitrile.

pH	A_{obs}	A_{calc}	%RE
13.73	0.998	1.000	-0.20
13.51	1.017	1.010	0.69
12.74	1.069	1.070	-0.09
12.12	1.221	1.200	1.72
11.26	1.318	1.360	-3.19
9.91	1.469	1.410	4.02
9.27	1.418	1.410	0.56
6.52	1.477	1.410	4.54
6.07	1.448	1.410	2.62
5.55	1.485	1.410	5.05
3.68	1.301	1.410	-8.38
3.33	1.297	1.410	-8.71

$$K_a = (7.63 \pm 5.22) \times 10^{-13}$$

$$10^{-2} E_{\text{SH}} = 141 \pm 2.52$$

$$10^{-2} E_{\text{S}^-} = 99.46 \pm 5.18$$

Table B6: The values of observed absorbance (A_{obs}) at 338 nm as a function of pH for ionization of Norisocorydine **42** in 2% v/v acetonitrile.

pH	A_{obs}	A_{calc}	%RE
13.73	0.824	0.8415	-2.13
13.51	0.847	0.8331	1.63
12.74	0.760	0.7473	1.67
12.24	0.634	0.6141	3.14
12.12	0.529	0.5754	-8.77
11.64	0.439	0.4332	1.32
11.26	0.392	0.3606	8.01
9.91	0.316	0.2947	6.74
9.27	0.310	0.2920	5.81
8.75	0.320	0.2914	8.93
8.02	0.312	0.2912	6.66
7.39	0.314	0.2912	7.27
7.01	0.300	0.2912	2.94
6.52	0.270	0.2912	-7.84
6.07	0.269	0.2912	-8.24
5.55	0.275	0.2912	-5.88
4.57	0.277	0.2912	-5.11
3.68	0.256	0.2912	-13.74
3.33	0.260	0.2912	-11.99

$$K_a = (7.72 \pm 1.08) \times 10^{-13}$$

$$10^{-2} E_{\text{SH}} = 29.11 \pm 0.72$$

$$10^{-2} E_{\text{s-}} = 85.5 \pm 1.88$$

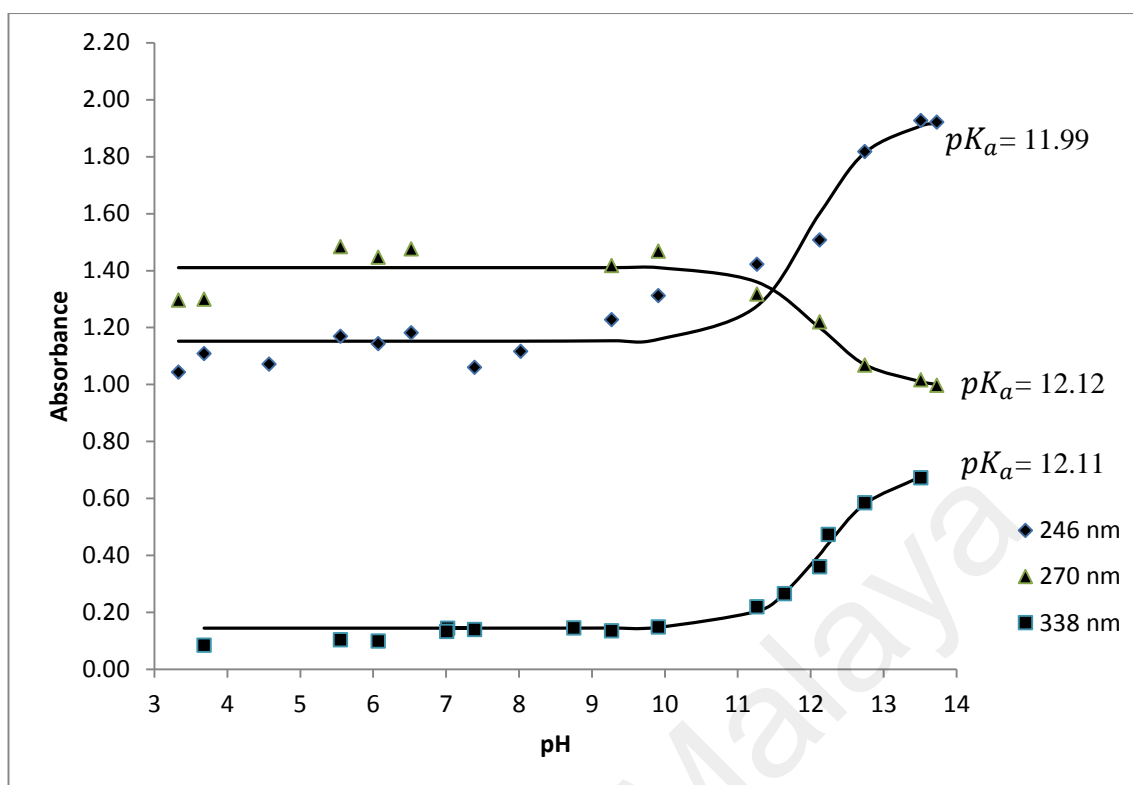


Figure B2: pH-Absorbance curves of Norisocorydine **42** in 2% v/v acetonitrile at 246 nm, 270 nm, and 338 nm.

Table B7: The values of observed absorbance (A_{obs}) at 253 nm as a function of pH for ionization of Boldine **37** in 2% v/v acetonitrile.

pH	A_{obs}	A_{calc}	%RE
12.48	1.358	1.320	2.811
11.68	1.356	1.316	2.983
11.11	1.291	1.302	-0.858
10.53	1.186	1.255	-5.826
9.80	1.033	1.073	-3.918
9.40	0.944	0.921	2.441
8.83	0.791	0.751	5.047
8.58	0.739	0.709	4.034
8.40	0.698	0.689	1.299
7.96	0.712	0.662	7.041
7.34	0.686	0.649	5.334
6.97	0.670	0.647	3.418
5.85	0.612	0.646	-5.475
5.45	0.618	0.645	-4.438
4.85	0.613	0.645	-5.284
4.21	0.619	0.645	-4.261
3.80	0.622	0.645	-3.758
2.53	0.619	0.645	-4.261

$$K_a = (2.74 \pm 0.5) \times 10^{-10}$$

$$10^{-2} E_{\text{SH}} = 64.5 \pm 1.2$$

$$10^{-2} E_{\text{S}^-} = 132 \pm 2.1$$

Table B8: The values of observed absorbance (A_{obs}) at 274 nm as a function of pH for ionization of Boldine **37** in 2% v/v acetonitrile.

pH	A_{obs}	A_{calc}	%RE
12.48	0.815	0.774	5.04
11.68	0.793	0.775	2.28
11.11	0.763	0.778	-2.00
10.53	0.743	0.790	-6.36
9.80	0.841	0.848	-0.79
9.40	0.934	0.916	1.97
9.01	0.958	0.996	-3.93
8.83	1.050	1.029	1.97
8.58	1.068	1.067	0.07
7.96	1.168	1.117	4.37
7.34	1.174	1.131	3.62
6.97	1.175	1.134	3.47
5.85	1.107	1.136	-2.63
5.45	1.111	1.136	-2.27
4.21	1.108	1.136	-2.55
2.53	1.113	1.136	-2.09
1.69	1.126	1.136	-0.92
0.80	1.126	1.136	-0.92

$$K_a = (6.19 \pm 1.5) \times 10^{-10}$$

$$10^{-2} E_{\text{SH}} = 113.6 \pm 1.1$$

$$10^{-2} E_{\text{S}^-} = 77.4 \pm 1.6$$

Table B9: The values of observed absorbance (A_{obs}) at 295 nm as a function of pH for ionization of Boldine **37** in 2% v/v acetonitrile.

pH	A_{obs}	A_{calc}	%RE
13.59	1.566	1.546	1.27
13.44	1.600	1.546	3.38
13.37	1.602	1.546	3.50
12.48	1.516	1.542	-1.71
11.68	1.462	1.519	-3.89
11.11	1.388	1.457	-4.98
10.53	1.284	1.320	-2.78
9.80	1.228	1.137	7.43
9.40	1.188	1.086	8.62
8.83	1.086	1.056	2.76
8.58	1.037	1.051	-1.34
7.96	1.044	1.046	-0.17
7.34	1.051	1.045	0.62
6.97	1.059	1.044	1.39
5.85	1.012	1.044	-3.17
5.45	1.016	1.044	-2.77
4.21	1.012	1.044	-3.17
3.80	1.016	1.044	-2.77
2.53	1.013	1.044	-3.07
1.69	1.024	1.044	-1.96

$$K_a = (3.59 \pm 1.2) \times 10^{-11}$$

$$10^{-2} E_{\text{SH}} = 104.4 \pm 1.5$$

$$10^{-2} E_{\text{S}^-} = 154.6 \pm 2.2$$

Table B10: The values of observed absorbance (A_{obs}) at 312 nm as a function of pH for ionization of Boldine **37** in 2% v/v acetonitrile.

pH	A_{obs}	A_{calc}	%RE
13.59	1.696	1.667	1.69
13.44	1.712	1.667	2.61
13.77	1.713	1.667	2.67
12.48	1.676	1.666	0.57
11.68	1.668	1.662	0.37
11.11	1.601	1.648	-2.91
10.53	1.495	1.597	-6.86
9.80	1.366	1.406	-2.89
9.40	1.288	1.246	3.25
8.83	1.118	1.070	4.25
8.58	1.051	1.027	2.24
7.96	1.025	0.979	4.49
7.34	1.011	0.966	4.43
5.85	0.950	0.962	-1.29
5.45	0.949	0.962	-1.39
4.85	0.940	0.962	-2.35
4.21	0.940	0.962	-2.35
3.80	0.942	0.962	-2.14
2.53	0.930	0.962	-3.45
1.69	0.934	0.962	-3.01

$$K_a = (2.68 \pm 0.5) \times 10^{-10}$$

$$10^{-2} E_{\text{SH}} = 96.2 \pm 1.4$$

$$10^{-2} E_{\text{S}^-} = 166.7 \pm 1.7$$

Table B11: The values of observed absorbance (A_{obs}) at 332 nm as a function of pH for ionization of Boldine **37** in 2% v/v acetonitrile

pH	A_{obs}	A_{calc}	%RE
12.48	1.414	1.408	0.45
11.68	1.417	1.405	0.87
11.11	1.390	1.395	-0.37
10.53	1.345	1.360	-1.11
9.80	1.184	1.185	-0.10
9.40	0.978	0.964	1.45
9.01	0.645	0.681	-5.56
8.83	0.564	0.554	1.78
8.58	0.417	0.405	2.92
8.40	0.331	0.322	2.68
7.96	0.213	0.198	6.81
7.34	0.137	0.136	0.92
6.97	0.114	0.124	-8.49
6.50	0.105	0.118	-12.06

$$K_a = (7.61 \pm 0.27) \times 10^{-10}$$

$$10^{-2} E_{\text{SH}} = 11.5 \pm 0.8$$

$$10^{-2} E_{\text{S}^-} = 141 \pm 0.8$$

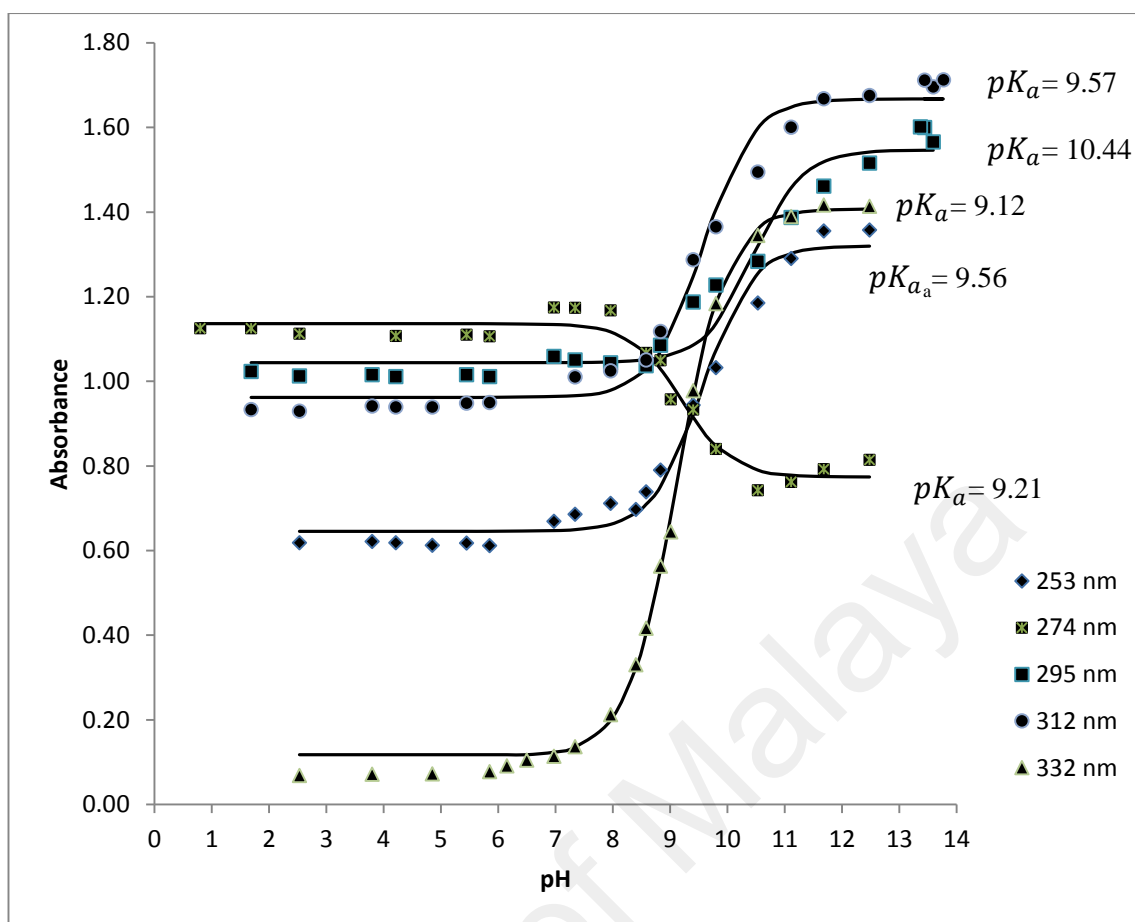


Figure B3: pH-Absorbance curves of Boldine **37** in 2% v/v acetonitrile at 253 nm, 274 nm, 295 nm, 312 nm and 332 nm.

Appendix C

Nonlinear least squares computer in BASICA programme.

```
30 PRINT "NO. OF PARAMETERS = ";
40 INPUT N
50 PRINT "NO. OF POINTS";
60 INPUT K
70 DIM J(K,N),L(N,K),E(K,1),C(K,1),O(K,2),B(K,1),V(1,K),W(N,1)
80 DIM M(N,N),X(N,1),T(N,1),U(1,1),F(N,N),S(N,1)
90 PRINT "NN =";
100 INPUT NN
105 PRINT "value of cmc =";
106 INPUT C1
190 FOR I=1 TO K
210 READ Z1
215 O(I,1) = 10^(-Z1)
220 NEXT I
230 FOR I= 1 TO K
250 READ Z2
255 O(I,2) = Z2
260 NEXT I
270 PRINT "INITIAL GUESS VALUE OF A1 =";
280 INPUT A1
290 PRINT "INITIAL GUESS VALUE OF A2 =";
294 INPUT A2
295 IF N=2 THEN 310
296 PRINT "INITIAL GUESS VALUE OF A3 =";
297 INPUT A3
298 IF N=3 THEN 310
```

```

299 PRINT "INITIAL GUESS VALUE OF A4 =";
300 INPUT A4
302 IF N=4 THEN 310
304 PRINT "INITIAL GUESS VALUE OF A5 =";
306 INPUT A5
310 PRINT "INITIAL CONC. OF SUBS. =";
320 INPUT X0
322 PRINT "value of kw =";
323 INPUT KW
330 T(1,1)=A1
340 T(2,1)=A2
342 IF N=2 THEN 360
346 T(3,1)=A3
350 IF N=3 THEN 360
352 T(4,1)=A4
354 IF N=4 THEN 360
356 T(5,1)=A5
360 PRINT "TOTAL # OF ITERATION =:
370 INPUT K2
380 DATA 6.08,6.33,6.8,7.43,7.73,8.1,8.17,8.26,8.43,8.57,8.83,9,9.15,9.38,9.56,9
.78,9.9,10.11
381 DATA .845,.855,.832,.905,1.05,1.179,1.334,1.294,1.465,1.587,1.721,1.824,1.92
3,2.07,2.131,2.192,2.25,2.21
382 DATA .000145,.000156,.00015
400 PRINT"ERROR CHECK =";
410 INPUT E0
420 PRINT"TOTAL # OF ITERATION ="K2
421 PRINT"ERROR CHECK ="E0

```

```

430 GOSUB 722
440 A1=T(1,1)
450 A2=T(2,1)
452 IF N=2 THEN 470
454 A3=T(3,1)
456 IF N=3 THEN 470
458 A4=T(4,1)
460 IF N=4 THEN 470
464 A5=T(5,1)
470 FOR I=1 TO K
471 V(1,I)=E(I,1)
472 NEXT I
480 U(1,1)=0!
481 FOR I=1 TO K
482 U(1,1)=U(1,1)+V(1,I)*E(I,1)
483 NEXT I
490 FOR I=1 TO N
500 S(I,1)=SQR(U(1,1)*F(I,I)/(K-N))
510 NEXT I
520 PRINT"ITERATION # ="K1
530 PRINT"A1  ="T(1,1);"STD. ="S(1,1)
540 PRINT"A2  ="T(2,1);"STD. ="S(2,1)
550 IF N=2 THEN 590
560 PRINT"A3  ="T(3,1);"STD. ="S(3,1)
570 IF N=3 THEN 590
580 PRINT"A4  ="T(4,1);"STD. ="S(4,1)
585 IF N=4 THEN 590
587 PRINT"A5  ="T(5,1);"STD. ="S(5,1)

```

```

590 PRINT"LEAST SQ. VALUE ="U(1,1)
600 PRINT"-----"
610 FOR I=1 TO N
620 IF ABS(W(I,1)/T(I,1))<E0 THEN 640
630 IF ABS(W(I,1)/T(I,1))>E0 THEN 660
640 NEXT I
641 PRINT"DO YOU WANT LSQ";
642 INPUT Y9
650 GOTO 680
660 K1=K1+1
670 IF K1<K2 THEN 430
680 PRINT"TIME      Aobs      Acalcd    % Res. Error"
690 FOR I=1 TO K
700 PRINT O(I,1),O(I,2),C(I,1),100*(O(I,2)-C(I,1))/O(I,2)
710 NEXT I
720 STOP
722 IF NN>2 THEN 792
730 FOR I=1 TO K
740 J(I,1)=(X0/(O(I,1)+A1))*(A3-((A2*O(I,1)+A3*A1)/(O(I,1)+A1)))
750 J(I,2)=X0*O(I,1)/(O(I,1)+A1)
760 IF N=2 THEN 785
765 J(I,3)=X0*A1/(A1+O(I,1))
770 IF N=3 THEN 785
774 J(I,4)=
776 IF N=4 THEN 785
778 J(I,5)=
785 C(I,1)=((A1*A3+A2*O(I,1))/(A1+O(I,1)))*X0
789 E(I,1)=O(I,2)-C(I,1)

```

```

790 NEXT I
791 GOTO 800
792 FOR I=1 TO K
793 J(I,1)=1/(A2+O(I,1))
794 J(I,2)=-A1/((A2+O(I,1))^2)
796 C(I,1)=A1/(A2+O(I,1))
797 E(I,1)=O(I,2)-C(I,1)
798 NEXT I
800 FOR I=1 TO K
801 FOR M=1 TO N
802 L(M,I)=J(I,M)
803 NEXT M
804 NEXT I
806 FOR I=1 TO N
807 FOR J=1 TO N
808 F(I,J)=0!
809 X(I,1)=0!
810 W(I,1)=0!
811 NEXT J
812 NEXT I
813 FOR M=1 TO N
814 FOR JJ=1 TO N
815 FOR I=1 TO K
816 F(M,JJ)=L(M,I)*J(I,JJ) + F(M,JJ)
817 NEXT I
818 NEXT JJ
819 NEXT M
820 FOR KK=1 TO N

```

```

825 FOR J= 1 TO N-1
830 M(KK,J)=F(KK,J+1)/F(KK,1)
840 NEXT J
845 M(KK,N)=1/F(KK,1)
850 IF KK=1 THEN 890
855 I=1
860 R1=F(I,1)
865 FOR J=1 TO N-1
870 M(I,J)=F(I,J+1)-R1*M(KK,J)
875 NEXT J
880 M(I,N)=-R1*M(KK,N)
885 IF KK=2 THEN 915
890 I=2
895 R2=F(I,1)
896 FOR J=1 TO N-1
897 M(I,J)=F(I,J+1)-R2*M(KK,J)
900 NEXT J
905 M(I,N)=-R2*M(KK,N)
910 IF KK=3 THEN 955
915 IF N=2 THEN 1004
920 I=3
925 R3=F(I,1)
930 FOR J=1 TO N-1
935 M(I,J)=F(I,J+1)-R3*M(KK,J)
940 NEXT J
945 M(I,N)=-R3*M(KK,N)
950 IF KK=4 THEN 990
955 IF N=3 THEN 1004

```



```

960 I=4
965 R4=F(I,1)
970 FOR J=1 TO N-1
975 M(I,J)=F(I,J+1)-R4*M(KK,J)
980 NEXT J
983 M(I,N)=-R4*M(KK,N)
986 IF KK=5 THEN 1004
990 IF N=4 THEN 1004
992 I=5
994 R5=F(I,1)
996 FOR J=1 TO N-1
998 M(I,J) =F(I,J+1)-R5*M(KK,J)
1000 NEXT J
1002 M(I,N)=-R5*M(KK,N)
1004 FOR I=1 TO N
1006 FOR J=1 TO N
1008 F(I,J)=M(I,J)
1010 NEXT J
1012 NEXT I
1014 NEXT KK
1020 FOR M=1 TO N
1030 FOR I=1 TO K
1040 X(M,1)=X(M,1)+L(M,I)*E(I,1)
1050 NEXT I
1060 NEXT M
1070 FOR MM=1 TO N
1080 FOR I=1 TO N
1090 W(MM,1)=W(MM,1)+F(MM,I)*X(I,1)

```

1100 NEXT I

1110 NEXT MM

1120 FOR I=1 TO N

1130 $T(I,1)=T(I,1)+W(I,1)$

1140 NEXT I

1150 RETURN

1160 END

University of Malaya

9th Mathematics and Physical Sciences Graduate Congress

Faculty of Science
University of Malaya

8-10 Jan 2014



Hosted By

Participating Universities:



Antiplasmodial And Antioxidant Isoquinoline Alkaloids From *Dehaasia longipedicellata*

*Azeana Zahari^a, Jamaludin Mohamad^b, Khalijah Awang^a.

^aDepartment of Chemistry, Faculty of Science, University of Malaya, 50603, Lembah Pantai, Kuala Lumpur
^bInstitute of Biology, Faculty of Science, University of Malaya, 50603, Lembah Pantai, Kuala Lumpur.

Abstract. *Dehaasia longipedicellata* crude extract exhibited strong antiplasmodial activity against the growth of *Plasmodium falciparum* K1 isolate (resistant strain). Phytochemical studies led to the isolation of six alkaloids; two morphinandieneones; (+)-sebiferine 1, (-)-milonine 2, two aporphines; (-)-boldine 3, (-)-norboldine 4, one benzylisoquinoline; (-)-reticuline 5, one bisbenzylisoquinoline; (-)-O-O-dimethylgrisabine 6. Their structures were determined on the basis of 1D and 2D NMR, MS, IR, UV, LCMS and comparison with literature values. Antiplasmodial activity was determined for all isolated compounds and showed potent to moderate antiplasmodial activity with IC₅₀ values ranging from 0.03 to 7.60 µg/ml with (-)-O-O-dimethylgrisabine 6 and (-)-milonine 2 being the two most potent with IC₅₀ values of 0.020 and 0.052 respectively that were comparable to the standard, chloroquine. Compounds were also assessed for antioxidant activities with good to low activity having DPPH (IC₅₀= 18.4 - 107.3 µg/ml), reducing power (27.4 - 44.3 %) and metal chelating activity (IC₅₀= 6.43 to 257.2 µg/ml). (-)-O-O-dimethylgrisabine 6 exhibited a potent antioxidant activity of 44.3 % reducing power, DPPH and metal chelating activity with IC₅₀ values of 18.38 and 64.3 µg/ml respectively, thus it may be considered as a good reductant with the ability to chelate metal and preventing pro oxidant activity.

Keywords: Lauraceae, *Dehaasia longipedicellata*, antiplasmodial, antioxidant



Chulalongkorn University
จุฬาลงกรณ์มหาวิทยาลัย
Pillar of the Kingdom

Abstract Book

The 8th Mathematics and Physical Science
Graduate Congress

Connect Science

Connect ASEAN

8 - 10 December 2012

Faculty of Science
Chulalongkorn University, Thailand

Participating Universities :



ANTIPLASMODIAL ALKALOIDS FROM THE BARK OF *ALSEODAPHNE* *CORNERI*

Azeana Zahari¹, Adlin Afzan², Mat Ropi Mukhtar¹, A.Hamid A.Hadi¹, Khalijah Awang¹

¹Department of Chemistry, Faculty of Science, University of Malaya, 50603 Kuala Lumpur, Malaysia.

²Herbal Medicine Research Center, Institute for Medicinal Research, Jalan Pahang, 50588, Kuala Lumpur, Malaysia
email: ezianna@gmail.com

Abstract

Alseodaphne is a small genus of trees that belongs to the family of Lauraceae is widely distributed in India, southern China and Malaysia. Most of the trees are excellent timbers especially from the southern of India, Ceylon and Malaysia. Many species of *Alseodaphne* are recognized by the local with names such as *medang kunyit*, *medang tanduk*, *medang kapas* and many more. *Alseodaphne corneri* the species from the family Lauraceae, has been known to produce various new alkaloids structure as well as alkaloids of medicinal value. A phytochemical study on the leaves of *Alseodaphne corneri* which belongs to the family of Lauraceae was performed. Chemical studies on the leaves has yielded six known compounds; gyrolidine, *O*-methylrepandine, 2-norobaberine, stephasubine, norstephasubine and fangchinoline. Isolation and structural elucidation of the alkaloids were performed via spectral methods namely 1D: ¹H, ¹³C NMR and 2D: COSY, HMQC, HMBC and IR, UV, MS. The results of crude dichloromethane of this plant give good activity towards antiplasmodial activity.

Keywords: *Alseodaphne corneri*, gyrolidine, *O*-methylrepandine, 2-norobaberine, stephasubine, norstephasubine, fangchinoline



Kingdom of Saudi Arabia
Ministry of Higher Education



Taibah University
College of Medicine



In collaboration with The International Commission on Scientific Signs of Qur'an and Sunnah

Certificate of Attendance

MABL Eajaz Chair for Scientific Miracles in Prophetic Medicine Award

Attended the The Eighth Scientific meeting

The black seed (Nigella Sativa) "A cure for every illness"

Wednesday, 30th April, 2014- The First of Rajab, 1435

Accredited by the Saudi Council for Health Specialties by 8 CME HRs (2014/42195)



General Supervisor of MABL Eajaz chair

Prof Bassem Yousef Sheikh